Thioredoxin reductase from barley: Structure, recognition of thioredoxin, protein engineering and catalytic mechanism

Kirkensgaard, Kristine Groth

Publication date:
2011

Document Version
Publisher's PDF, also known as Version of record

Thioredoxin reductase from barley: Structure, recognition of thioredoxin, protein engineering and catalytic mechanism

PhD thesis

2011

Kristine Groth Kirkensgaard

Enzyme and Protein Chemistry (EPC),
Department of Systems Biology,
Technical University of Denmark (DTU)

Supervisors:

Prof. Birte Svensson, EPC, Department of Systems Biology, DTU

Assoc. Prof. Per Hägglund, EPC, Department of Systems Biology, DTU

Prof. Anette Henriksen, Carlsberg laboratory

Preface

The present thesis represents the results of my PhD study carried out in the Enzyme and Protein Chemistry group, Department of Systems Biology, Technical University of Denmark (DTU) for the period of August 2007 to August 2011 under supervision of Prof. Birte Svensson and Associate Prof. Per Hägglund. Parts of the PhD study involving crystallography and homology modelling has taken place at Carlsberg Laboratories, under supervision of Prof. Anette Henriksen.

This project was funded by a DTU PhD stipend and supported by the Centre for Advanced Food Studies (LMC) and by a grant from The Danish Council for Technology and Innovation (FTP, grant number 274-08-0413).

The study included a five month period spent at Commonwealth Scientific and Industrial Research Organisation (CSIRO) in the department of Plant Industry in Canberra, Australia, under supervision of Dr. Frank Gubler. Part of this period was not financed by the PhD stipend but instead supported by scholarships from the Oticon Foundation and Otto Mønsted Foundation.

The work has resulted in the following manuscripts:

Kirkensgaard, K.G., Hägglund, P., Finnie, C., Svensson, B. and A. Henriksen (2009) Structure of Hordeum vulgare NADPH-dependent thioredoxin reductase 2. Unwinding the reaction mechanism. *Acta Crystallogr. D* **65:** 932—941. (Chapter 1 and Appendix E)

Kirkensgaard, K.G., Hägglund, P., Henriksen, A., Shahpiri, A., Finnie, C and B. Svensson. Probing molecular interactions between thioredoxin and NADPH-dependent thioredoxin reductase (NTR) through homology modelling and site-directed mutagenesis. *In preparation* (Chapter 4 and 5 and Appendix F)

Hägglund, P., **Kirkensgaard, K.**, Maeda, K., Finnie, C., Henriksen, A. and Svensson, B. (2009) Molecular Recognition in NADPH-Dependent Plant Thioredoxin Systems – Catalytic Mechanisms, Structural Snapshots and Target Identifications. Chapter 15 *in* Oxidative

stress and redox regulation in plants. Jacquot, J.-P. (Ed.) pp. 461—495. Advances in botanical research **52**, Burlington: Academic Press. (Appendix G).

During my PhD I have also made a number of oral and poster contributions in various settings. These are summarised in Appendix H.

Acknowledgments

I owe a huge thanks to all of my three supervisors, Associate Prof. Per Hägglund, Professor Birte Svensson and Professor Anette Henriksen. They have all shown great commitment and without their skilled guidance and fruitful discussions this thesis would not have been completed. A special thanks to Anette Henriksen for her help with crystallisation, data collection and solving the structure of HvNTR2 and help with writing the resulting manuscript. All three are also thanked for proof-reading of the thesis as well as the manuscripts.

I am very grateful for the DTU stipend which has financed most of the PhD as well as for the financial support received from the Oticon Foundation and Otto Mønsted Foundation during my stay in Australia. Furthermore, the PhD work is connected with the project 'A Quantitative Redox Proteomics and Protein Engineering Tool Box for Applications of Thioredoxin in Food Biotechnology' supported by Danish Council for Technology and Innovation (FTP) and also the network grants from the Centre for Advanced Food Studies (LMC) are thanked for supporting the thioredoxin project in general. Finally the access to synchrotron beam time was made possible by support from the Danish Centre for the use of Synchrotron X-ray and Neutron facilities (DANSCATT).

All the people at the department of Plant Industry, CSIRO, Canberra, Australia, are thanked for great help and a very pleasant work environment. Very special thanks to Dr. Frank Gubler for excellent guidance during my stay. Dr. John (Jake) V. Jacobsen is thanked for guidance concerning the experiments with aleurone layers, and Dr. Peter Chandler is thanked for delivery of mutant and wild-type barley grains as well as suggestions to the experiments. Post doc José Barrero is thanked for giving access to cDNA from barley embryo and to micro-array data on barley root and coleorhiza samples, as well as guidance concerning data-treatment and use of RT-PCR. Lab technicians Ingrid Venables and Trijntje Hughes are thanked for great help in the laboratory.

Former PhD student Azar Shahpiri is thanked for helpful discussions of the production of recombinant HvNTR2 and construction of pET15b-based plasmid encoding HvNTR2_R140A. Associate Prof. Christine Finnie is thanked for guidance concerning the

experiments with barley aleurone layers as well as proof-reading of the manuscript of the structure of HvNTR2.

Lab technician Aida Curovic is thanked for her great effort in expressing and purifying many of the proteins used throughout the thesis. Furthermore, she is thanked for having cloned plasmids encoding the used enzymes from *A. thaliana*. PhD student Petr Efler is thanked for his studies concerning expression of CBP-HvTrxh2 and complex formation, and former Master student Stig Johnson is acknowledged for constructing pET15b-based plasmids encoding the three Glycine-loop mutants.

I would like to thank post doc Olof Björnberg for guidance in the experiments of enzyme kinetics and calculations of second order reaction rates, and Post doc Nicolas Navrot for guidance using KaleidaGraph and for delivering data from the Gel Filtration Calibration kit. Furthermore, Olof, Nicolas, Petr and Per are thanked for being excellent room-mates and for creating a very nice atmosphere in the office as well as the laboratory. Former PhD student Kenji Maeda is thanked for fruitful discussions, guidance to using PyMOL as well as for being a great office-mate. Generally, I would like to thank former and present employees in Building 224 for creating a very kind and pleasant working environment.

The Anaerobic Flexible Vinyl Coy Chamber was kindly lent by Associate Professor, PhD Hans Erik Mølager Christensen. He and Post doc Ida Noemi Simon from DTU Chemistry are thanked for their guidance in the use of this instrument.

From Carlsberg Laboratory Post doc Joakim Lundqvist is thanked for his great help using the program DOT 2.0 for docking of whole proteins. Furthermore, lab technician Annette Kure, former PhD student Casper Elo Christensen, former Post doc Valerie Pye and Prof. Anette Henriksen are thanked for nice companionship and for being great room- and lab-mates.

From Aarhus University I would like to thank PhD, Associate Prof. Gregers Rom Andersen and lab technician Gitte K. Hartvigsen for advice and technical help using their crystallisation robot. I would also like to acknowledge beam line scientists Juan Weatherby at the ESRF ID14-2 beamline and Xavier Thibault at the ESRF ID23-2 beamline for their assistance during data collection in Grenoble. From Syddansk University Post doc Martin Zehl is thanked for having performed the electrospray mass spectroscopy measurements.

Professor Lise Arleth and my husband Post doc Jacob Kirkensgaard from the Life Science Faculty at the University of Copenhagen are thanked for help during preliminary SAXS measurements on MAX-lab, Lund.

Last but not least I owe a huge thanks to my family. My two wonderful daughters, Mikkeline and Nelli, have been able to put up with a very busy mom and are fantastic at cheering me up and making me laugh. My very special thanks go to my dear husband, Jacob, for many scientific discussions, proofreading, and his endless support.

Summary

In this thesis the crystal structure of one of the two isoforms of NADPH-dependent thioredoxin reductase (HvNTR2) from barley was determined. The overall structure of HvNTR2 resembled other low molecular weight (LMW) NTRs. However, the relative orientation of the NADPH and FAD domains of HvNTR2, is different from other LMW NTRs in the flavin oxidising (FO) and flavin reducing (FR) conformations. The difference can be described by a 38.2% closure, a 1.0 Å translation and a 24.7° rotational twist when compared to the only other plant NTR structure of AtNTR-B from *Arabidopsis thaliana* (which is in the FO conformation). It was thus suggested that the HvNTR2 structure represents an intermediate between the FO and the FR conformation indicating that the conformational change does not only involve domain rotation, but also bending of one domain relative to the other. Potentially there is room for binding HvTrxh2 to the FAD domain of HvNTR2 in the FO conformation, after which a conformational change of HvNTR2 could bring the active site cysteines of the NADPH domain in proximity to the active site of HvTrxh2. A reaction mechanism was proposed, which included binding of thioredoxin (Trx) in the FO conformation of HvNTR2.

A complex was produced of HvNTR2 bound covalently to one of the two isoforms of Trx from barley seeds, HvTrxh2. The complex is assumed to represent a reaction intermediate with NTR locked in the FR conformation through an intermolecular disulfide bond between active site cysteines of the two proteins. Attempts to crystallise the HvNTR2:HvTrxh2 complex were unfruitful, possibly due to sample heterogeneity as indicated by molecular weight and isoelectric point determinations.

Since no crystal structure of the HvNTR2:HvTrxh2 complex was obtained, a homology model based on the crystal structures of HvNTR2 and HvTrxh2 was built, using the structure of *Escherichia coli* NTR covalently bound to Trx (EcNTR:EcTrx) as a template (Lennon *et al*., 2000). The model provides new insight into how eukaryotic LMW NTRs in general bind Trx and suggests major differences in the NTR:Trx binding interface of HvNTR2:HvTrxh2 and EcNTR:EcTrx. Notably a large loop in HvNTR2 with the sequence EGWMANDIAAGG in the FAD domain (thus termed the FAD-loop), was predicted to have tight interactions with

HvTrxh2 through hydrophobic contacts. Sequence alignments suggest that this loop is present in LMW NTRs from other eukaryotes but appears to be absent in most prokaryotes.

The crystal structure of HvTrxh2 covalently bound to the barley α-amylase/subtilisin inhibitor (BASI, Maeda *et al*., 2006a), allowed comparison of the molecular features involved in the interactions between HvTrxh2 and its electron donor (NTR) and a protein disulfide substrate, respectively. This comparison suggested some overlapping interactions as amino acid residues from HvTrxh2 involved in the binding of BASI are also interacting with the FAD and NADPH domains of HvNTR2.

The model of HvNTR2:HvTrxh2 served as a guideline for a comprehensive mutational study of some of the residues and loops, which were indicated to be important for the binding between the two proteins. Enzyme kinetics analyses of these mutants suggest that the FAD-loop is critical for binding of HvTrxh2. Especially, $Trp42_{HvNTR2}$ and $Met43_{HvNTR2}$ appears to be important for the binding of HvTrxh2. $Met43_{HvNTR2}$ is the only HvNTR2 residue from the FAD-loop, which is not conserved in the HvNTR1 isoform, where it is replaced by a leucine. Surprisingly the FAD-loop appears to be less critical for binding of several Trx isoforms from *A. thaliana*. The residue $Arg73_{EcTrx}$ is essential for the binding of EcTrx to the NADPH domain of EcNTR2, and was predicted to be involved in the conformational change from FO to FR (Negri *et al*., 2009). However, a mutant of the corresponding residue Glu86 in HvTrxh2 showed retained activity with HvNTR2, indicating that this residue plays different roles in Trx from barley and *E. coli*

Finally, the expression levels of HvNTR1, HvNTR2, HvTrxh1, HvTrxh2 and α-amylase during imbibition was examined in different tissues of barley seeds by Q-PCR and micro-array data analysis. The effects of the plant hormone gibberellic acid, dormancy/after-ripening, light/darkness on these expression levels were examined as well as the role of the GA-receptor GID1. The expression of α-amylase in aleurone layers was significantly up-regulated by GA, and the response was dependent on GSE1. HvNTR1 seemed to be down-regulated by GA independently on the dose and GSE1. HvNTR2 seemed to be upregulated by GA leading to expression levels of HvNTR2 that were 10—40 times higher than of HvNTR1. Both HvTrxh1 and HvTrxh2 were expressed in higher amounts than the NTRs and seemed unaffected by GA.

Micro-array analysis was performed on available data from root and coleorhiza. Coleorhiza is a sheath-like structure that acts as a protective covering enclosing the plumule (growing point of embryo) and radicle (from which the root is developed). These were either dormant or after-ripened. It was observed that after-ripening leads to increased expression levels of both HvNTR1 (in coleorhiza) and HvNTR2 (in both roots and coleorhiza). HvNTR2 and HvTrxh1 were the most abundant isoforms in root and coleorhizae after imbibition and both showed increased expression levels in after-ripened seeds compared with dormant. For whole embryo the levels of Trxs was higher than of NTRs. While the expression of Trxs seemed unaffected by both after-ripening and light/darkness, the average levels of the NTRs increased in the after-ripened samples. Light had no effect on the expression levels.

All together the results presented in this thesis provide valuable new insights into the structure and function of the NTR/Trx system.

Dansk resumé

I dette ph.d. projekt blev krystalstrukturen bestemt af en af de to isoformer af den NADPH-afhængige thioredoxin reduktase (HvNTR2) fra byg. Overordnet lignede strukturen af HvNTR2 strukturen af andre lavmolekylære (LMW) NTR'er. Imidlertid er den relative orientering af NADPH of FAD domænerne forskellig fra andre LMW NTR'er i den flavin oxiderende (FO) og den flavin reducerende (FR) konformation. Forskellen kan beskrives ved en lukning på 38,2%, en translation på 1,0 Å og en rotation på 24,7°, når man sammenligner med den eneste anden struktur-bestemte plante-NTR AtNTR-B fra *A. thaliana* (som er i FO konformationen). Det blev derfor foreslået, at strukturen af HvNTR2 udgør et reaktions intermediat mellem FO og FR konformationen, hvilket indikerer at den konformationelle ændring ikke blot involverer domæne rotation, men også bøjning af ét domæne relativt til det andet. Potentielt er der plads til binding af HvTrxh2 til FAD domænet af HvNTR2 i FO konformationen, hvorefter et konformations-skifte bringer de aktive site cysteiner fra NADPH domænet i nærheden af HvTrxh2s aktive site. En reaktions-mekanisme blev foreslået, som omfatter binding af thioredoxin (Trx) i FO konformationen som et centralt reaktionstrin.

Et kompleks blev fremstillet, hvor HvNTR2 er bundet kovalent til en af de to isoformer af Trx fra byg frø, HvTrxh2. Dette kompleks menes at repræsentere et intermediat i reaktionen med NTR låst i FR konformationen gennem en intermolekylær disulfid-bro mellem aktive site cysteiner fra de to proteiner. Forsøg på at krystallisere dette HvNTR2:HvTrxh2 kompleks var ufrugtbare, hvilket kan skyldes prøve heterogenitet som indikeret af bestemmelse af molekylvægt samt isoelektrisk fokusering gelelektroforese.

Da der ikke blev opnået en krystalstruktur af HvNTR2:HvTrxh2 komplekset, blev en model lavet med homologi modellering baseret på eksisterende krystalstrukturer af HvNTR2 og HvTrxh2, hvor strukturen af *Escherichia coli* NTR kovalent bundet til Trx (EcNTR:EcTrx) blev brugt som skabelon for modelleringen (Lennon *et al.*, 2000). Den opnåede model giver ny indsigt i, hvordan eukaryote LMW NTR'er generelt binder Trx, og antyder store forskelle i NTR:Trx bindings-fladen i HvNTR2:HvTrxh2 og EcNTR:EcTrx. Navnlig et stort loop med

sekvensen EGWMANDIAAGG i FAD domænet (og derfor kaldet FAD-loopet) så ud til at have stor betydning for bindingen af HvTrxh2 *via* hydrofobe kontakter. Sekvens-sammenligninger viser at dette loop findes i LMW NTR'er fra andre eukaryoter, mens det tilsyneladende mangler i de fleste prokaryoter.

Krystalstrukturen af HvTrxh2 kovalent bundet til byg α-amylase/subtilisin hæmmer (BASI, Maeda *et al*., 2006a) gav mulighed for sammenligning af interaktionen mellem HvTrxh2 og henholdsvis dennes elektron-donor (NTR) og et protein disulfide substrat. Denne sammenligning viste et vist overlap i interaktionerne da aminosyrerester i HvTrxh2 der er involveret i bindingen af BASI også interagerer med FAD og NADPH domænet af HvNTR2.

Modellen for HvNTR2:HvTrxh2 har tjent som pejlemærke for et omfattende mutations-studium af nogle af de aminosyrerester og loops, der blev vurderet at være vigtige for bindingen mellem de to proteiner. Enzym-kinetik på disse mutanter afslørede, at FAD-loopet i HvNTR2 er afgørende for bindingen af HvTrxh2. Især $Trp42_{HvNTR2}$ og $Met43_{HvNTR2}$ var vigtige for bindingen af HvTrxh2 og det er interessant at $Met43_{HvNTR2}$ er den eneste af de rester i HvNTR2, der er involveret i kompleksdannelsen, som ikke er bevaret i HvNTR1 isoformen, hvori den er erstattet af en leucinrest. Overraskende nok forekom FAD-loopet mindre kritisk for binding af adskillige Trx'er fra *A. thaliana*. $Arg73_{EcTrx}$ er afgørende for bindingen af EcTrx til NADPH domænet af EcNTR2, og blev forudsagt at være involveret i det konformationelle skift fra FO til FR (Negri *et al*., 2009). I modsætning hertil førte mutation af den tilsvarende aminosyrerest $Glu86_{HvTrxh2}$ til en bevaret activitet med HvNTR2, hvilket tyder på, at denne aminosyrerest har forskellige roller i Trx fra byg og *E. coli*.

Endelig er niveauer af mRNA for HvNTR1, HvNTR2, HvTrxh1, HvTrxh2 og α-amylase under vandoptagelse blev undersøgt ved hjælp af Q-PCR og microarray-analyser fra forskelligt væv fra bygfrø. Effekterne af plante-hormonet gibberellinsyre (GA), vækstdvale/efter-modning samt lys/mørke på disse niveauer blev undersøgt samt rollen af GA-receptoren GID1. mRNA niveauet for α-amylase var betydeligt opreguleret i aleuronlagene som følge af GA, og responset afhang af GSE1. HvNTR1 syntes at være nedreguleret af GA uafhængigt af dosis og GSE1. HvNTR2 syntes at være opreguleret af GA, hvilket førte til mRNA niveauer af HvNTR2, der var 10—40 gange højere end for HvNTR1.

Både HvTrxh1 og HvTrxh2 var udtrykt i højere niveauer end NTR'erne og syntes upåvirket af GA.

Microarray-analyse blev udført på tilgængelige data fra rod og coleorhiza. Coleorhiza er en hylster-lignende struktur, der fungerer som et beskyttende dække, der omslutter plumule (voksende punkt af embryo) og radicle (hvorfra roden udvikles). Disse var enten i vækstdvale eller efter-modnet. Det blev observeret, at efter-modning fører til øget ekspression af såvel HvNTR1 (i coleorhiza) og HvNTR2 (i både rødder og coleorhiza). HvNTR2 og HvTrxh1 var de mest udbredte isoformer i roden og coleorhiza efter vandoptag og begge viste øget udtryks-niveau i efter-modnede frø sammenlignet med frø i vækst-dvale. For hele embryo var niveauet af Trx'erne højere end for NTR'erne. Mens mRNA niveauet for Trx'erne syntes upåvirket af både efter-modning og lys/mørke steg det gennemsnitlige niveau af mRNA for NTR'erne i efter-modnede frø. Lys havde heller ingen effekt på mRNA-niveauerne for NTR'erne.

Alt i alt giver resultaterne præsenteret i denne ph.d.-afhandling en ny værdifuld indsigt i struktur og funktion af NTR/Trx systemet.

Table of contents

Appendix B

LIGPLOT of possible interactions between HvNTR2 and HvTrxh2 in a complex model

Appendix C

Multiple alignment of selected NTRs

Appendix D

Primers used for site-directed mutagenesis

Appendix E

Kirkensgaard, K.G., Hägglund, P., Finnie, C., Svensson, B. and A. Henriksen (2009) Structure of Hordeum vulgare NADPH-dependent thioredoxin reductase 2. Unwinding the reaction mechanism. *Acta Crystallogr. D* **65:** 932—941.

Appendix F

Kirkensgaard, K.G., Hägglund, P., Henriksen, A., Shahpiri, A., Finnie, C and B. Svensson. Probing molecular interactions between thioredoxin and NADPH-dependent thioredoxin reductase (NTR) through homology modelling and site-directed mutagenesis. *In preparation.*

Appendix G

Hägglund, P., **Kirkensgaard, K.**, Maeda, K., Finnie, C., Henriksen, A. and Svensson, B. (2009) Molecular Recognition in NADPH-Dependent Plant Thioredoxin Systems – Catalytic Mechanisms, Structural Snapshots and Target Identifications. Chapter 15 *in* Oxidative stress and redox regulation in plants. Jacquot, J.-P. (Ed.) pp. 461—495. Advances in botanical research **52**, Burlington: Academic Press.

Appendix H

Oral and poster contributions

Abbreviations

$AADP^+$	3-amino-pyridine adenine dinucleotide phosphate
ABA	abscisic acid
ABS	Absorbance
ACN	Acetonitrile
ATP	Adenosine triphosphate
BASI	Barley α-amylase/subtilisin inhibitor
CBP	Calmodulin-binding peptide
cDNA	Complementary DNA
CSIRO	Commonwealth Scientific and Industrial Research Organisation
cv	Cultivar
CV	Column volumes
dNTP	Deoxyribonucleotide
Dsb	Disulfide bond protein
DTNB	5,5'-dithiobis-(2-nitrobenzoic acid), i.e. Ellman's reagent
DTT	Dithiothreitol
EGTA	Ethylene glycol tetraacetic acid
ER	Endoplamatic reticulum
EST	Expressed sequence tag
FAD	Flavin adenine dinucleotide (oxidised)
$FADH_2$	Flavin adenine dinucleotide (reduced)
FMN	Flavin mononucleotide
Fdx	Ferredoxin
FO	Flavin oxidising
FR	Flavin reducing
FTR	Ferredoxin-thioredoxin reductase
GA	Gibberellic Acid
GR	Glutahione reductase
Grx	Glutaredoxin
GSH	Reduced glutathione

GSSG	Oxidised glutathione
GST	Glutathione transferase
HMW	High molecular weight
IPTG	Isopropyl β-D-1-thiogalactopyranoside
k_{cat}	Turnover number
K_d	Dissociation constant
K_M	Michaelis constant
LMW	Low molecular weight
MALDI	Matrix-assisted laser desorption ionisation
MOPS	20 mM 3-[N-morpholine]propanesulfonic acid
mRNA	Messenger RNA (ribonucleic acid)
MSR	Methione sulfoxide reductase
MW	Molecular weight
$NADP^+$	Nicotinamide adenine dinucleotide phosphate (oxidised)
NADPH	Nicotinamide adenine dinucleotide phosphate (reduced)
NTR	NADPH-dependant thioredoxin reductase
PCR	Polymerase chain reaction
PDB	Protein Data Bank
PDI	Protein disulfide isomerase
pI	Isoelectric point
PMSF	Phenylmethylsulfonyl fluoride
PS I	Photosystem I
PS II	Photosystem II
Q-PCR	Quantitative real time polymerase chain reaction
RER	Rough endoplamatic reticulum
R.m.s.d.	Root mean scare deviation
RNR	Ribonucleotide reductase
RNS	Reactive nitrogen species
ROS	Reactive oxygen species
SAXS	small-angle X-ray scattering

SDS-PAGE	Sodium dodecyl sulfate-polyacrylamide gel electrophoresis
TFA	Trifluoroacetic acid
TLS	Translation Libration Screw-motion
TNB	2-nitro-5-thiobenzoate
Trx	Thioredoxin
V_{max}	Maximum rate
wt	Wild-type

Chapter 1

Introduction

1.1 Thiol redox control

1.1.1 Oxidative stress

Reactive oxygen species (ROS) are formed in aerobic environments and are detoxified by cellular antioxidant systems such as the NADPH-dependent glutathione/glutaredoxin system and thioredoxin system (both described below). If ROS are produced in an amount which exceeds the antioxidant capacity the cell is exposed to oxidative stress, which leads to increased oxidation of macromolecules such as lipids and proteins. ROS induce reversible and irreversible oxidative modifications of amino acids including formation of methionine sulfoxide and convertion of cysteine to sulfenic acid, sulfinic acid and sulfonic acid (also called cysteic acid, Figure 1.2). Such modifications can affect protein function, e.g. if the oxidised residue is important for the catalytic mechanism of an enzyme (Maeda *et al*., 2006b). Furthermore, carbonylation which is one of the most common protein oxidative modifications can occur in the residues His, Arg, Lys, Pro, Tyr and Trp (Sweetlove and Møller, 2009).

ROS can be produced from oxygen in different ways (Figure 1.1). A superoxide radical ($\cdot O_2^-$) is generated by a single-electron reduction of oxygen. ROS are formed in the mitochondria if oxygen is incompletely reduced during the mitochondrial electron transport chain (Møller, 2001). In plants a major source of superoxide is photosynthesis (Section 1.2.1). The antioxidant superoxide dismutase catalyses the dismutation of superoxide to oxygen and hydrogen peroxide (H_2O_2) (McCord and Fridovich, 1988). Another source of hydrogen peroxide is the *β*-oxidation of fatty acids. *β*-oxidation takes place in the mitochondria, where it is coupled to ATP-synthesis or in peroxisomes in which the high-potential electrons are transferred to oxygen instead of to ATP, yielding hydrogen peroxide (Wanders and Waterham, 2006, Figure 1.1).

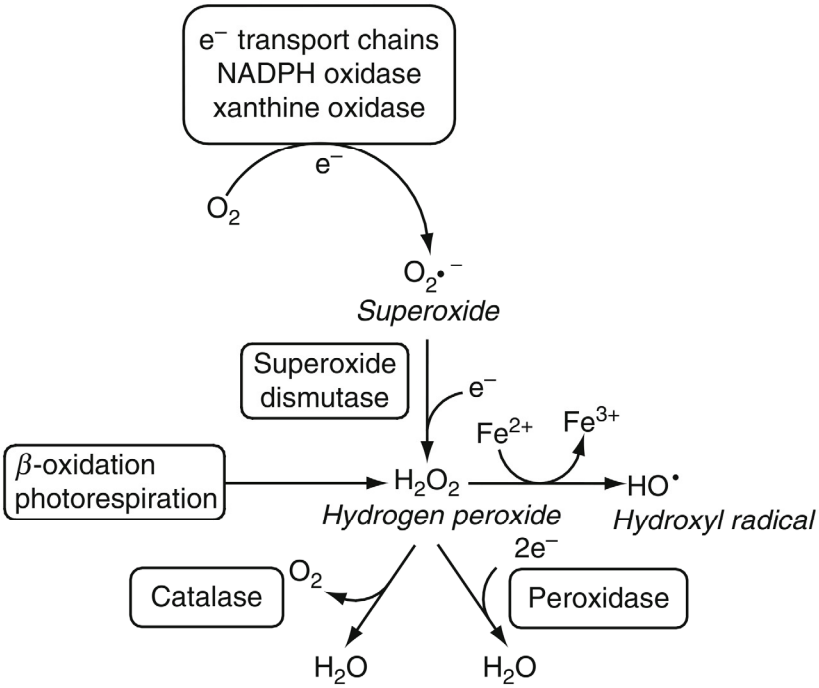

Figure 1.1. Mechanism of the formation of reactive oxygen species (ROS). Figure modified from Sweetlove and Møller, 2009.

Hydrogen peroxide can be converted to the very reactive hydroxyl radical (Figure 1.1) in the presence of a reduced transition ion such as Fe^{2+} (Jeong and Guerinot, 2009). Even though concentrations of free metal ions is maintained at low levels detoxification of H_2O_2 is critical for cell survival and is conducted by the enzymes catalase located in peroxisomes as well as thiol peroxidases, including thioredoxin peroxidase (Figure 1.1, Chelikani *et al*., 2004; Wood *et al*., 2003). Also methionine sulfoxide reductase (MSR) is involved under oxidative stress by enzymatically reducing methionine sulfoxide to methionine. Its proposed function is the repair of oxidative damage in proteins in order to restore biological activity (Moskovitz *et al*., 2001).

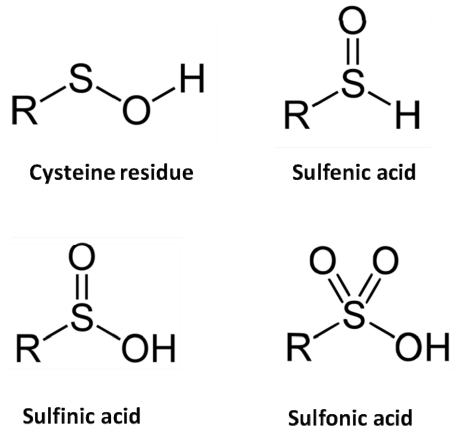

Figure 1.2. Structures of cysteine residues modified by ROS.

1.1.2 Thiol/disulfide exchange

In addition to the modifications displayed above (Figure 1.2), cysteine residues can be oxidized to form a covalent disulfide bond, also called an S-S bond or a disulfide bridge. Disulfide bonds are usually formed by the interaction of two thiol groups in an oxidation reaction which results in the release of two protons and two electrons (Figure 1.3). In proteins the thiol groups of two cysteines can form disulfide bonds within a polypeptide chain (intramolecular disulfide bond) or between two polypeptides (intermolecular disulfide bonds). A disulfide bond formed between a protein and a low molecular weight compound such as glutathione is referred to as a mixed disulfide bond. The reaction where a mixed disulfide is formed between a protein and glutathione is known as glutathionylation (Dalle-Donne *et al*., 2008).

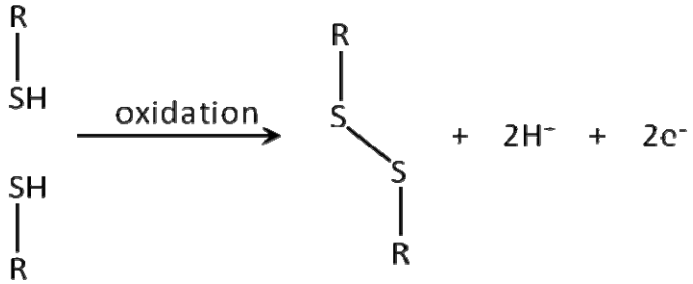

Figure 1.3. Formation of a disulfide bond. Two thiol groups are oxidised with formation of an S-S bond and release of two protons and two electrons to an electron acceptor.

Disulfide bond formation is reversible and a range of enzymes utilise catalytic cysteine residues in thiol/disulfide exchange reactions to transfer reducing equivalents in cellular

redox reactions, including glutaredoxin (Grx, Section 1.1.3) and thioredoxin (Trx, Section 1.1.4). Structural disulfide bonds contribute to stability of proteins (Raina and Missiakas, 1997), but is disfavoured in the reducing environment of the cytoplasm (redox potentiale of approximately -221 to -236 mV, Hwang *et al*., 1992) maintained by the low molecular weight tripeptide glutathione (GSH, see Section 1.1.3). Instead structural disulfides are therefore mainly found in areas isolated from the reducing environment of the cytosol; in secretory proteins, lysosomal proteins, and in the domains of membrane proteins facing the surroundings. In eukaryotes structural disulfide bonds are mainly formed in the more oxidative environment of the rough endoplasmic reticulum (RER) (redox potentiale of aproximately -170 to -185 in the secretory pathway, Hwang *et al*., 1992). A network of chaperones and folding catalysts ensure that the correct disulfides are formed as the protein matures prior to excretion from the endoplasmatic reticulum (ER). Furthermore, the disulfide bond formation and isomerisation is catalysed by protein disulfide isomerase (PDI) in eukaryotes, and by disulfide bond proteins (Dsb) in the periplamic space of *E. coli* (Gilbert, 1997; Kadokura *et al*., 2008).

1.1.3 Glutathione/glutaredoxin system

Grxs are small redox enzymes of approximately one hundred amino acid residues. They typically contain an active site monothiol (CXXS) or dithiol (CXXC) motif and are members of the thiol/disulfide oxidoreductase family (Holmgren, 1989). Some dimeric Grx bind [2Fe-2S] iron-sulfur clusters coordinated through active site cysteines (Lillig *et al.*, 2005). Grxs reduce disulfide bonds and are recycled non-enzymatically by reduced glutathione (GSH), which is a tripeptide with the sequence sequence γ-Glu-Cys-Gly (Figure 1.4). Oxidised glutathione (GSSG), composed of two glutathione tripeptides linked with a disulfide bond, is recycled by NADPH-dependent glutathione reductase (GR) belonging to the flavoprotein disulfide oxidoreductase family. Together Grx, GSH and GR constitute the glutathione/glutaredoxin system (Holmgren and Fernandes, 2004). GR is described further in Section 1.1.6.2.

Grx provides electrons to the enzyme ribonucleotide reductase (RNR), which catalyses the formation of deoxyribonucleotides (dNTPs) from ribonucleotides (Holmgren and Fernandes, 2004). dNTPs are the precursors to DNA synthesis, and thus ribonucleotide

reductase is essential for cell proliferation (Elledge *et al*., 1992). Grx acts in the antioxidant defence by reducing peroxiredoxins and MSR. As mentioned Grx is reduced by GSH, which is the most prevalent nonprotein thiol-based redox buffer in the cytosol of eukaryotic cells. Glutathione is almost exclusively found in its reduced form, since GR is constitutively active and inducible upon oxidative stress. The ratio of reduced to oxidised glutathione is the main control of cellular redox balance including the thiol-disulfide redox state (Pastore *et al*., 2003). The glutathione/glutaredoxin system of plants is described in Section 1.2.2.

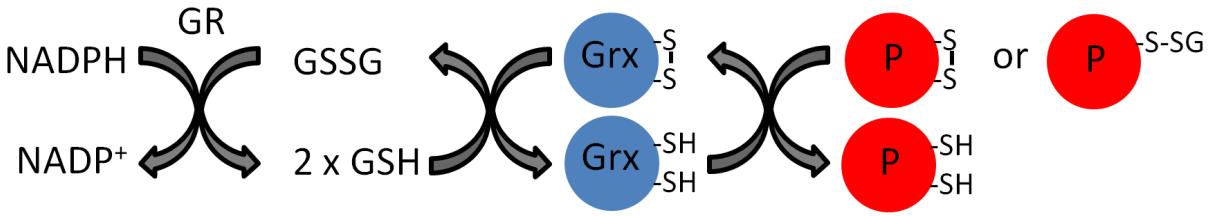

Figure 1.4. The glutathione/glutaredoxin system. Glutathione reductase (GR) reduces the oxidised form of glutathione (GSSG) in an NADPH-dependant manner. The reduced glutathione (GSH) acts as electron donor to the enzyme glutaredoxin (blue, Grx), which in turn reduces disulfide bonds in target proteins (red, P-S_2) or glutathionylated proteins (red, P-S-S-G).

1.1.4 NADPH-dependent thioredoxin system

Trxs are small redox enzymes with a molecular weight of 12—14 kDa found in nearly all known organisms. Like Grx they are members of the thiol/disulfide oxidoreductase family and catalyse disulfide reduction (Gelhaye *et al*., 2004). In non-chloroplastic environments, oxidised Trx is typically reduced and thus recycled enzymatically by the flavoenzyme NADPH-dependant thioredoxin reductase (NTR), which is a member of the family of pyridine nucleotide-disulfide oxidoreductases (Pai, 1991). NTR transfers reducing equivalents from NADPH to Trx *via* a bound FAD and a redox-active disulfide located in NTR (Williams, 1976, Figure 1.5). In turn, Trx reduces disulfide bonds in target proteins (Figure 1.5). Together, Trx, NTR and NADPH comprise the NADPH-dependent Trx system. Trx is the main substrate of NTR, but NTR has also been shown to activate 1-Cys peroxiredoxin in a Trx-independent manner (Pulido *et al*., 2009).

Similar to Grx, Trx provides electrons to RNR (Laurent *et al.*, 1964, Moore *et al.*, 1964), peroxiredoxins (Tripathi *et al.*, 2009) and MSR (Russel and Model, 1986). Generally Trx targets can be divided in three categories: (i) enzymes using Trx as suppliers of reducing

equivalents, including RNR and MSR (ii) redox-regulated transcription factors and enzymes that are activated/deactivated through disulfide reduction, and (iii) proteins that incorporate Trx as subunits of protein complexes, e.g. T7 DNA polymerase (Arnér and Holmgren, 2000). Trxs and NTR are further described in Section 1.1.6 and 1.2.3.

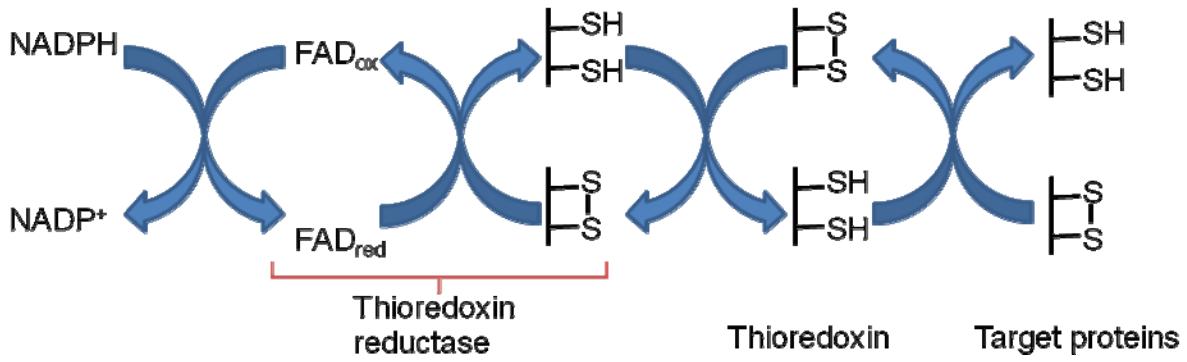

Figure 1.5. The NADPH-dependant thioredoxin system. Reducing equivalents are transferred from NADPH to an FAD molecule bound in NADPH-dependent thioredoxin reductase (NTR) and further to a disulfide, also located in NTR. NTR then reduces Trx, which in turn reduces disulfide bonds in target proteins.

1.1.5 Cross-talk between the Trx and Grx system

As described above several target proteins are shared between Trx and Grx. Besides sharing targets, examples of cross-talk between the two systems include Trxs which require Grx/GSH for their reduction (Gelhaye *et al.*, 2003, see Figure 1.19 below), Grx reduced by NTR (Johansson *et al*., 2004) as well as GSH reduced by the Trx system (Kanzok *et al*., 2001). Furthermore, a fusion protein of NTR with an N-terminal extension with homology to Grx has been found, which is able to reduce both Trx, GSSG as well as substrates specific for GR (see below, Sun *et al*., 2001). The significance of the overlapping interactions between the two systems is emphasised by the fact that mutants of *Escherichia coli* and *Saccharomyces cerevisiae* lacking either of the two systems are viable while double knock-out mutants are non-viable (Muller, 1996; Prinz *et al.*, 1997).

1.1.6 Structural aspects and reaction mechanism of the NTR/Trx system

1.1.6.1 Trx

Structurally Grx and Trx resemble each other and share the so-called Trx-fold (βαβαββα). The overall structure of Trx is highly conserved with a central five-stranded β-sheet surrounded by four α-helices in the topology (βαβαβαββα, Figure 1.6), which include the Trx-fold (Martin, 1995). The active-site C_NXXC_C motif is located at the N-terminus of α2 and the preceding loop (Figure 1.6). In most Trxs this motif is WC_NGPC_C (see Figure 1.6), but is in some h-type Trxs from subgroup I replaced by WC_NPPC_C. This substitution does not seem to change the disulfide reductase activity (Behm and Jacquot, 2000; Bréhélin *et al*., 2004), but appears to have an impact on some biological functions, such as sulphate assimilation (Bréhélin *et al*., 2000).

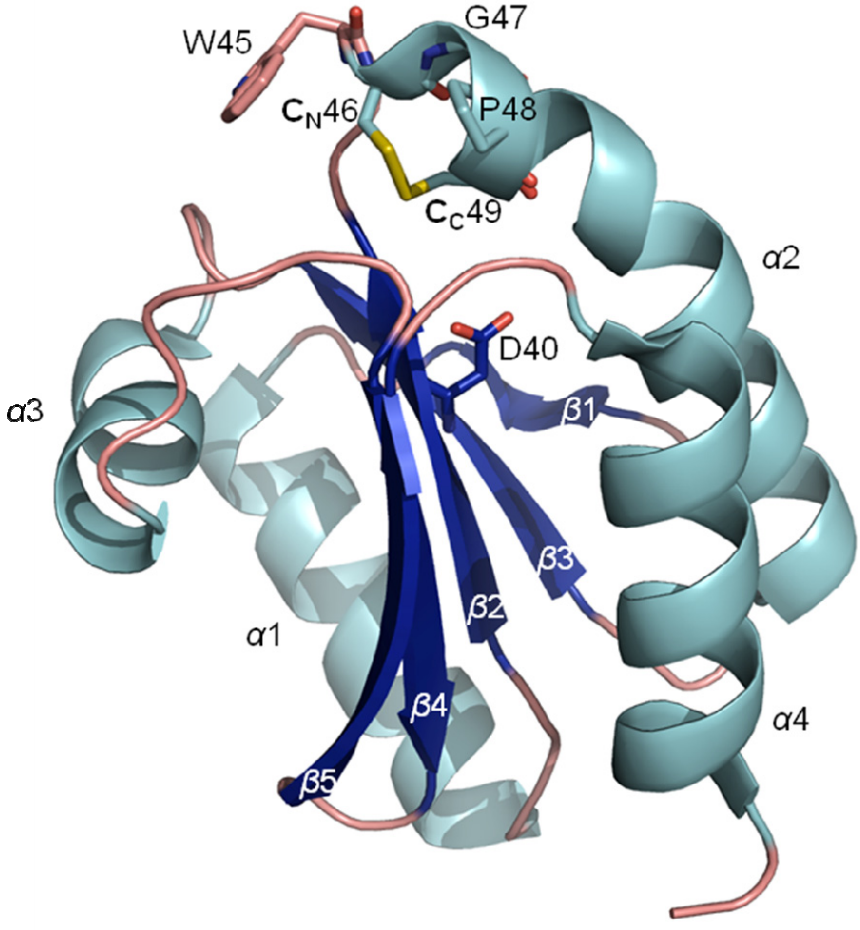

Figure 1.6. Structure of HvTrxh2 from barley in the oxidised form (pdb accession 2VLT, Maeda *et al*., 2008). The two redox-active cysteines in the $_{45}$WCGPC$_{49}$ motif are connected by a disulfide bond. C_N (C46) is exposed on the surface and initiates the reduction of protein substrates while C_C (C49) is buried. The aspartic acid residue D40 is proposed to act as a general acid/base during catalysis. β-strands and α-helices are labelled.

While C_C is buried, C_N is exposed to the surface (Figure 1.6). In the reduced state C_N initiates the reduction of protein substrates by attacking a target disulfide bond (Figure 1.7 I), resulting in the formation of an intermolecular disulfide intermediate (Figure 1.7 II). This disulfide is subsequently attacked by C_C, resulting in the release the reduced protein target and oxidised Trx (Figure 1.7 III) (Kallis and Holmgren, 1980). An aspartate residue (D26 in *E. coli* Trx and D40 in HvTrxh2 from barley, Figure 1.6) is proposed to act as a general acid/base for the protonation/deprotonation of the C_C thiol group during the catalysis (Chivers and Raines, 1997; Menchise *et al*., 2001). Furthermore, a conserved tryptophan residue at the immediate N-terminal side of the CXXC motif (W45 in HvTrxh2, Figure 1.6) was suggested to be important for efficient catalysis (Krause and Holmgren, 1991; Krimm *et al*., 1998). Insight into target recognition has been provided from structures of Trx in complex with substrates including MSR (Ma *et al*., 2011), 3'-Phosphoadenosine-5'-phosphosulfate reductase (Chartron *et al*., 2007) and arsenate reductase (Li *et al*., 2007).

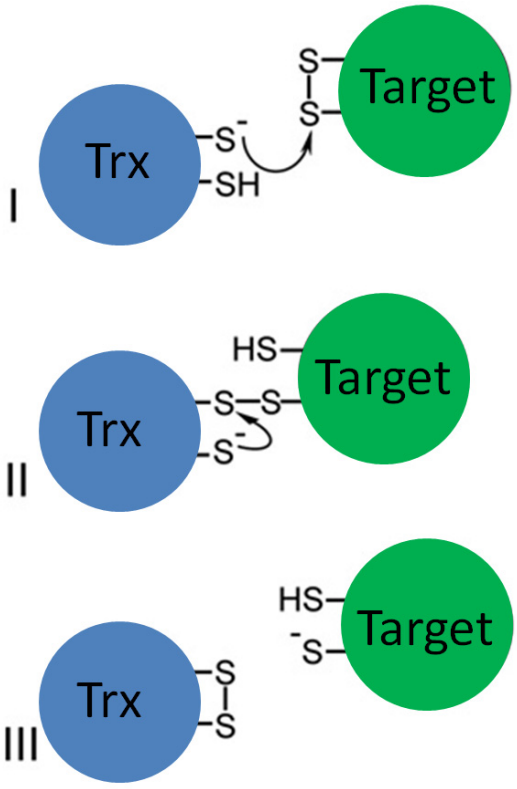

Figure 1.7. The reduction of protein disulfides by Trx. In the reduced dithiol state, the surface-exposed N-terminal cysteine (C_N) from the active site attacks the disulfide bond of a protein substrate (I) resulting in the formation of an intermolecular disulfide intermediate (II). This disulfide is subsequently attacked by the buried C-terminal cysteine (C_C), resulting in release of the reduced target protein and the oxidized Trx. Figure adapted from Maeda *et al*., 2006a.

1.1.6.2 NTR

As mentioned earlier, NTR transfers electrons from NADPH to Trx *via* a tightly bound FAD and a disulfide located in NTR (Figure 1.5) (Mustacich and Powis, 2000). In the process the isoalloxazine ring system of FAD is reduced to yield $FADH_2$ with the gain of two electrons (Figure 1.8). Simultaneously the nicotinamide ring of NADPH is oxidised to yield $NADP^+$ (Figure 1.9). FAD is synthesised from riboflavin (vitamin B_2) in an ATP-dependent reaction. First riboflavin is converted to flavin mononucleotide (FMN) by riboflavin kinase, and FMN is converted to FAD by FAD synthetase by adenylation (Bafunno *et al*., 2004; Figure 1.8). NADPH is mainly produced in the oxidative step of the pentose phosphate pathway (Kruger and von Schaewen, 2003). In chloroplasts of plants, NADPH is produced by the reduction of $NADP^+$ by ferredoxin-NADP reductase as a last step of the electron chain reaction (Shin, 2004).

FAD contributes with a characteristic absorbance spectrum which gives flavoprotein a yellow colour and additional absorbance maxima around 375 and 456 nm. FAD bound to NTR from *E. coli* had the same absorbance spectrum as free FAD: the extinction coefficient at 456 nm for bound FAD was determined to 11300 $M^{-1}cm^{-1}$, which equals that of free FAD at 450 nm (Williams *et al*., 1967). Upon reduction of FAD this absorbance decreases but is restored after re-oxidation (Williams *et al*., 1967; Figure 1.10).

Like GRs, NTRs belong to the flavoprotein disulfide oxidoreductase family (Pai, 1991). NTRs from mammals and other higher eukaryotes are closely related to GR (Figure 1.11) and are relatively rigid homodimeric proteins of >50 kDa (called high-molecular-weight NTRs, HMW NTRs in the following). Each subunit contains three domains; the NADPH domain, the FAD domain and the C-terminal domain. The latter forms the subunit interface (Manstein *et al*., 1988; Waksman *et al*., 1994; Williams *et al*., 2000).

In HMW NTRs from higher eukaryotes and GRs the active site disulfide is found in the FAD domain (Figure 1.11 and 1.16A and C). GR is very well studied and can serve as a model for describing the mechanism in these NTRs. The NADPH binding site in GR places the nicotinamide ring of NADPH in close proximity to one (*re*) side of the isoalloxazine ring system, which allows transfer of a hydride ion (H^-) to a disulfide bond of GR positioned on the other (*si*) side of the isoalloxazine ring system (Manstein *et al.*, 1988). Reducing equivalents are further transferred to oxidised glutathione (G-S-S-G) which binds GR at the

base of a deep crevice at the dimer interface. The whole reaction mechanism can take place without any major conformational changes (Waksman *et al.*, 1994). This is in contrast to NTRs from the low-molecular-weight (LMW) NTRs (described below).

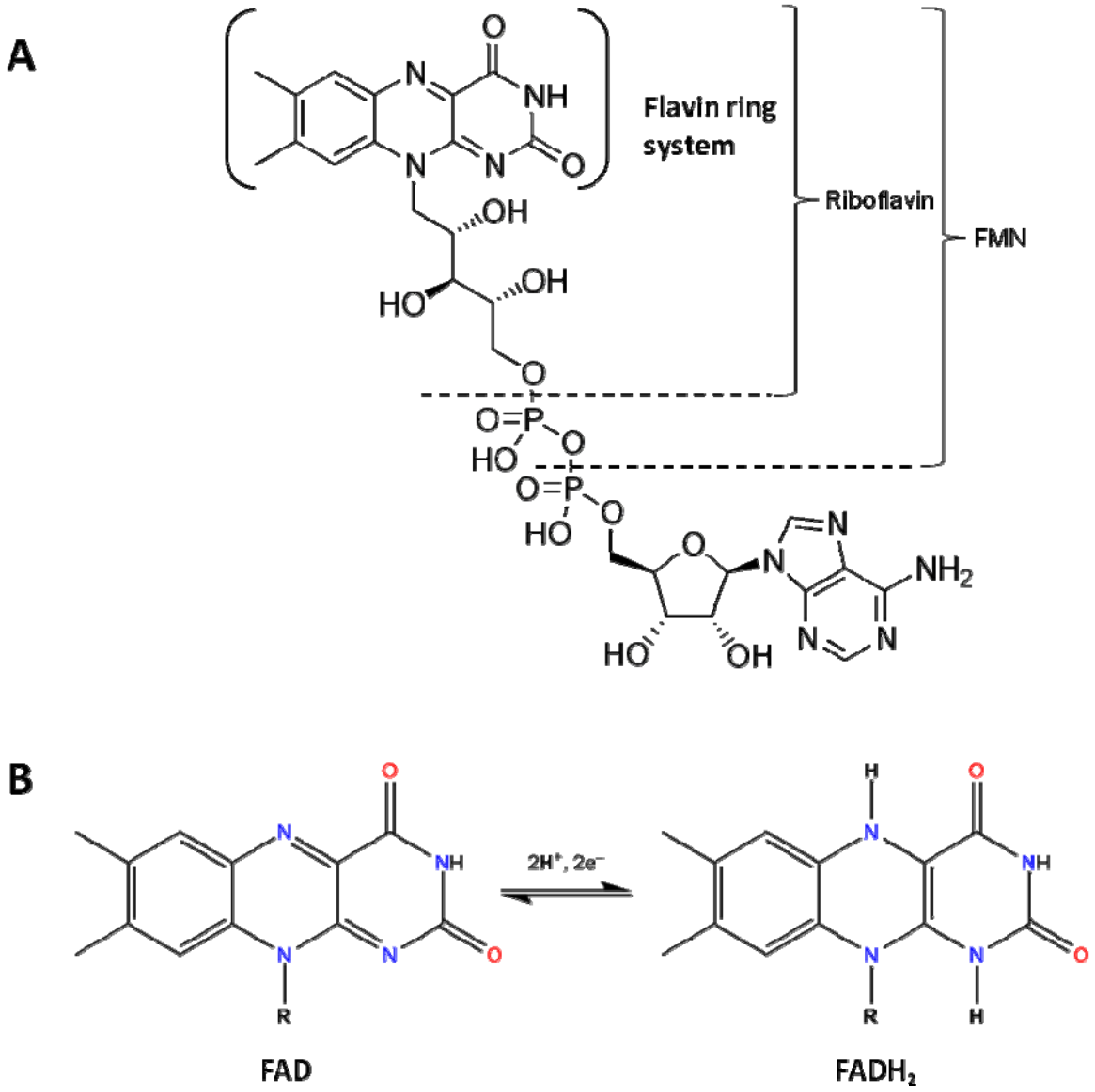

Figure 1.8. The structure of flavin adenine dinucleotide (FAD, whole structure), flavin mono nucleotide (FMN) and riboflavin (**A**). The reduction of the isoalloxazine ring system of FAD to yield $FADH_2$ (**B**). In the process two electrons and two protons are transferred to FAD. (Figure modified from Wikimedia).

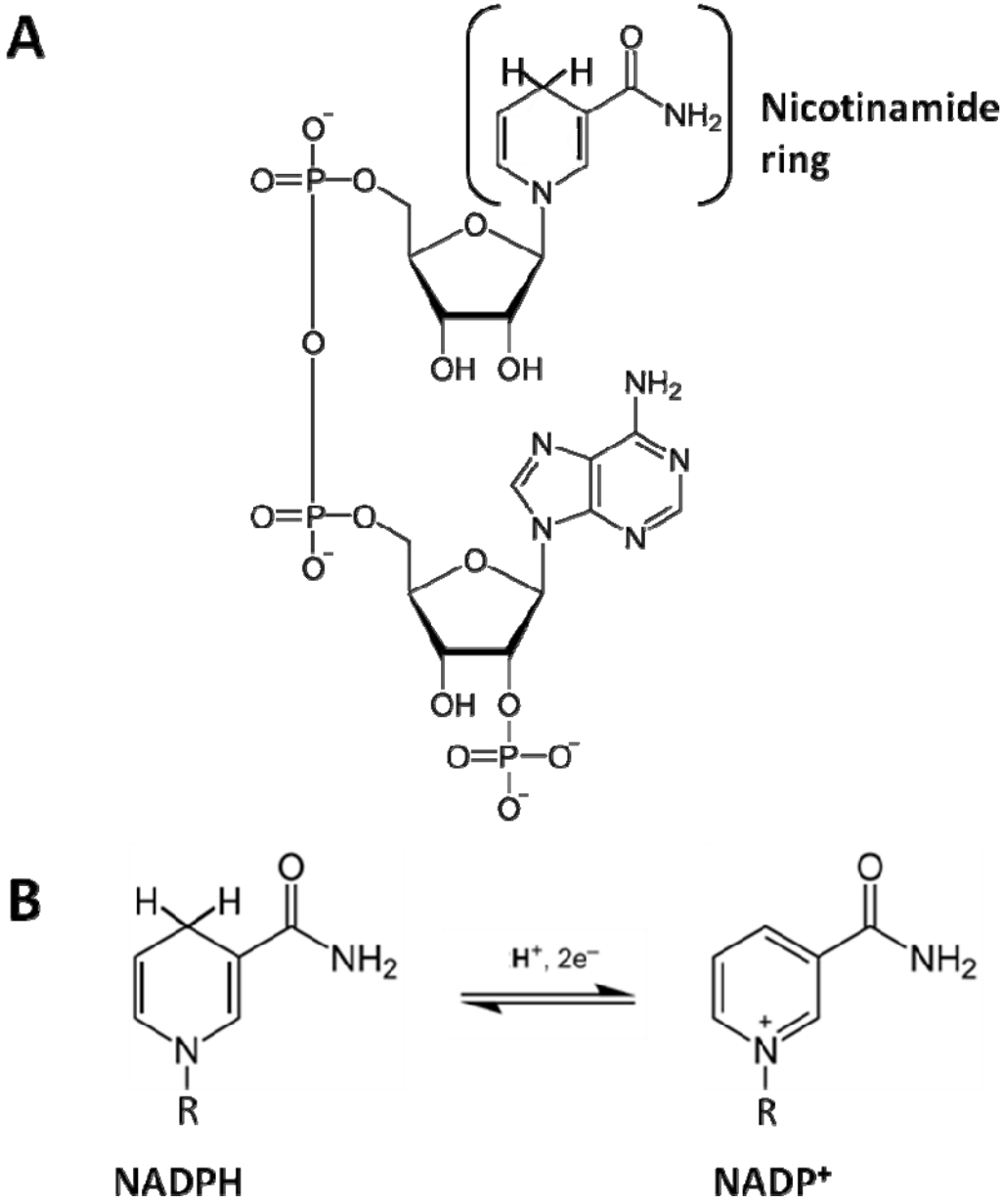

Figure 1.9. The structure of NADPH (**A**) and the oxidation of the nicotinamide ring to yield $NADP^+$ (**B**). (Figure modified from Wikimedia).

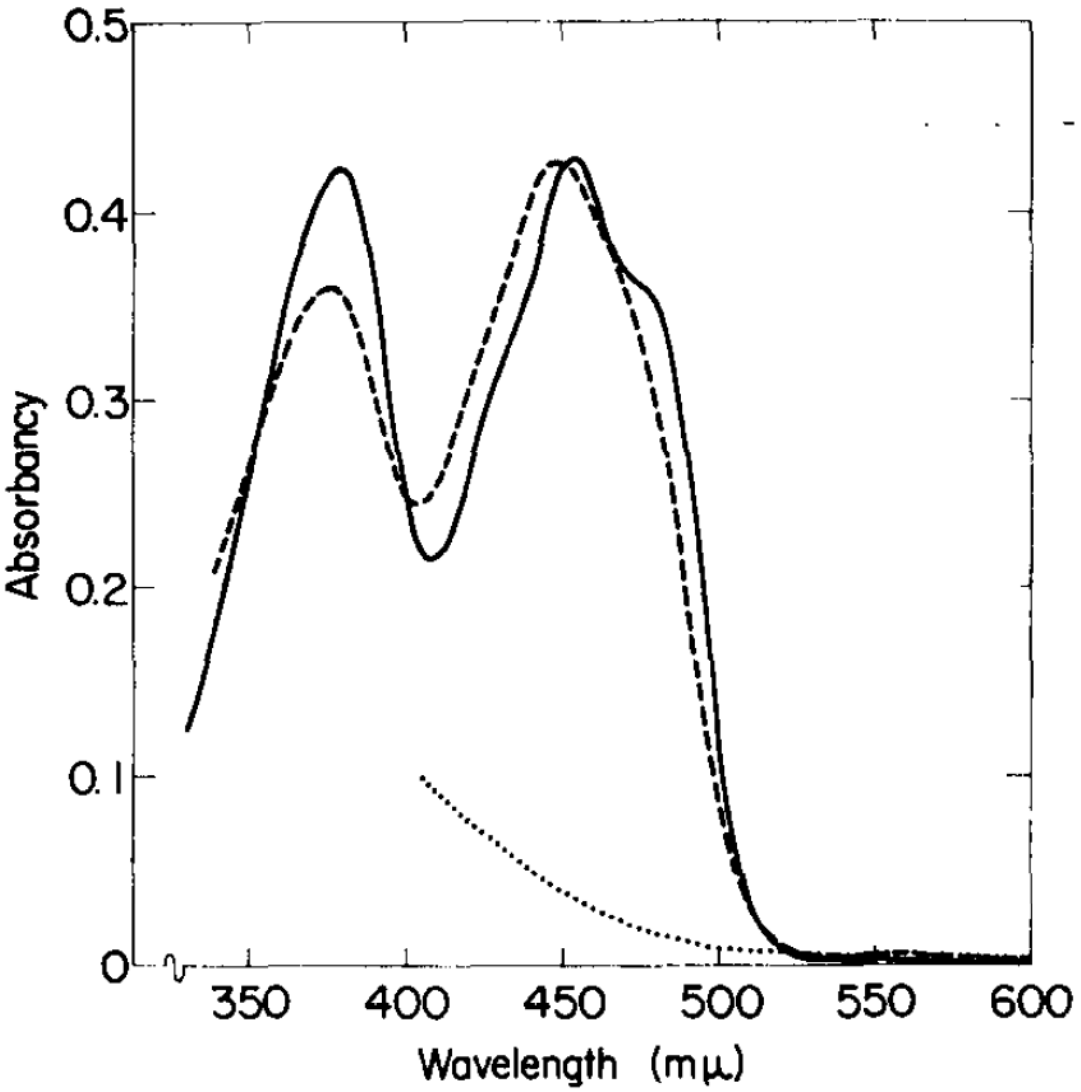

Figure 1.10. Absorbance spectrum of FAD. Absorbance of FAD bound in NTR from *E. coli* (EcNTR). Native protein (—) was reacted with the reducing agent sodium dithionite ($Na_2S_2O_4$) (·····). This decreased the absorbance, which was restored after mixing with air (- - -). Figure from Williams *et al.*, 1967.

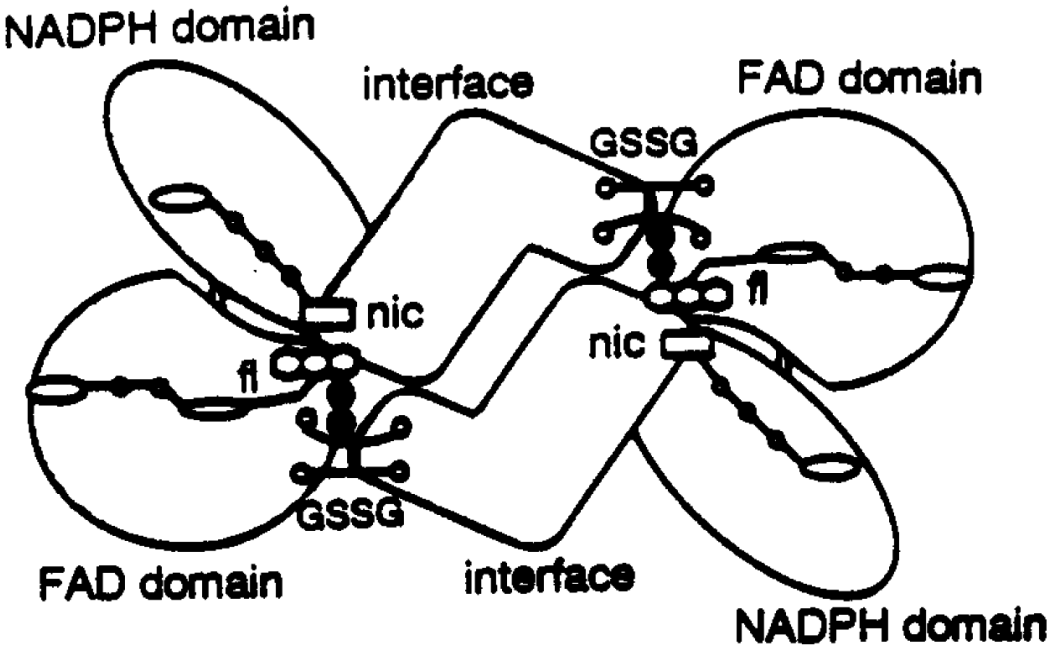

Figure 1.11. Schematic representation of the dimeric form of GR. FAD, NADPH and glutathione are indicated as fl, nic and GSSG, respectively. The disulfide bond of GR is indicated as two small black circles. Figure from Wang *et al*., 1996.

Another major difference between the two types of NTRs is that the HMW NTRs besides the active site (-Cys-X-X-X-Cys-) in the FAD-domain contain an additional C-terminal redox centre (not found in GR, Figure 1.16). This contains selenocysteine (SeCys) in some cases. Thus, NTRs from mammals and *C. elegans* contain the conserved sequence (-Gly-Cys-SeCys-Gly) while NTR from *P. falciparum* contains two cysteine residues in the sequence (-Cys-X-X-X-Cys-Gly) (Lee *et al.*, 2000). This additional active site has been found to be involved in catalysis (Wang *et al*., 1999), and structural studies of the mammalian HMW NTR suggest that the C-terminal is flexible and this redox active centre moves considerably during catalysis (Sandalova *et al*., 2001). Thus, the electrons are transferred from NADPH to FAD, then to the buried active site and further to the additional C-terminal active site of the other NTR subunit. From here they are transferred to Trx at the protein surface (Fritz-Wolf *et al*., 2011). Very recently a structure of mammalian NTR-Trx complex has been published (Fritz-Wolf *et al*., 2011). This shows how the flexible C-terminal end may adopt different conformations. After reduction of the C-terminal active site by the main active site and binding of Trx the C-terminal end most likely turns to the surface and reduces Trx (Fritz-Wolf *et al*., 2011).

Bacteria, yeast and plants contain LMW NTRs (approximately 35 kDa). They are homodimeric and each subunit contain two Rossman-type nucleotide binding domains, the FAD domain and the NADPH domain, similar to the high-molecular-weight NTRs but they lack the extra C-terminal domain (Figure 1.12, see Figure 1.16D below). The FAD domain is composted of the N-terminal and C-terminal end of the polypeptide chain, while the NADPH domain is formed by the middle part. The two domains are connected by a linker region consisting of two anti-parallel β-sheets (Figure 1.12) (Kuriyan *et al.*, 1991).

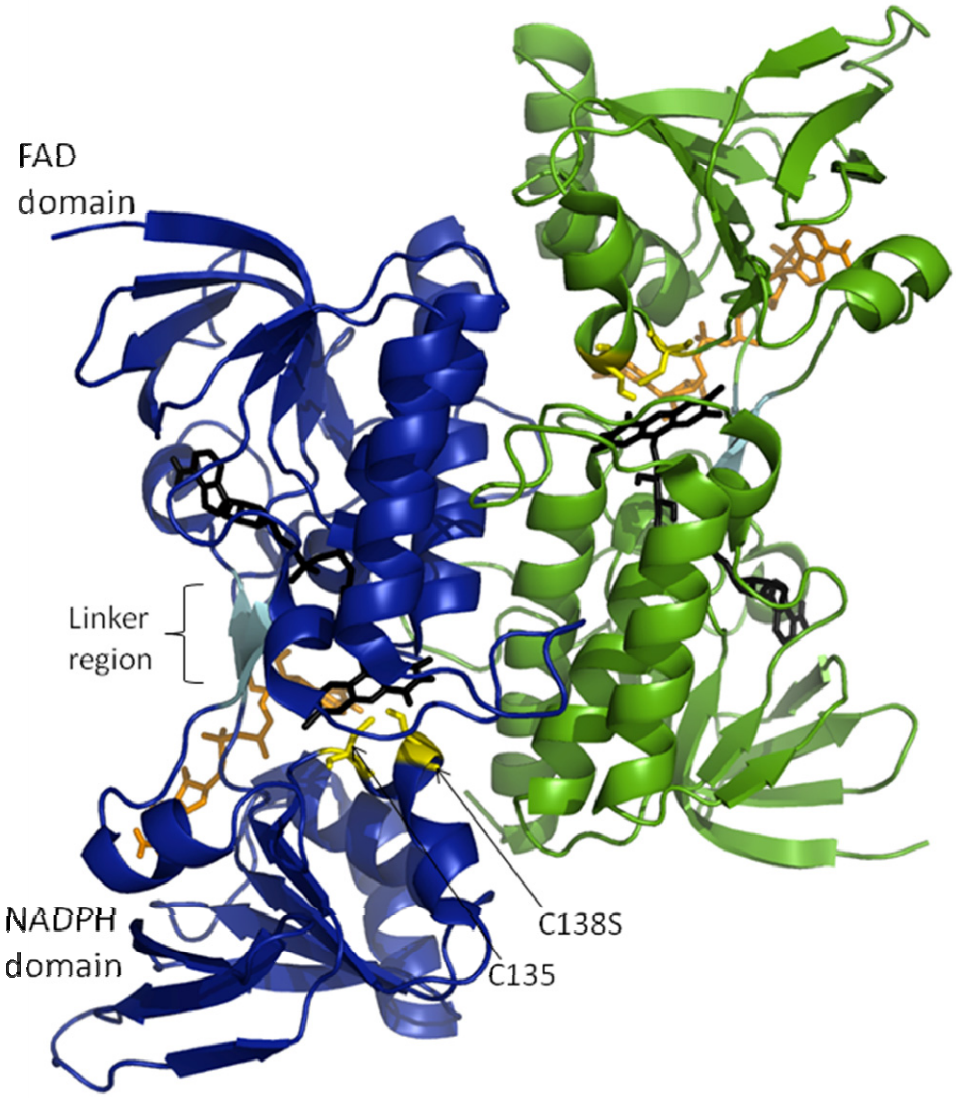

Figure 1.12. Structure of a C135S mutant of NTR from *E. coli* in the dimeric form, one monomer coloured blue and the other green (pdb accession 1TDF, Waksman *et al*., 1994). The two domains, FAD and NADPH domain, are separated by a linker region, consisting of a pair of anti-parallel β-sheets (cyan). C135 from the active site $_{135}$CATC$_{138}$ was mutated to serine, which improved crystallisation. C135S and C138 are shown in yellow positioned opposite the flavin ring system of FAD (black). $NADP^+$ (orange) is positioned far from FAD.

In contrast to HMW NTRs, the active site disulfide (-Cys-X-X-Cys-) of LMW NTRs is located in the NADPH domain (Figure 1.16D). In crystal structures of NTR this disulfide was observed to be inaccessible to Trx (Figure 1.12) (Kuriyan *et al.*, 1991; Waksman *et al.*, 1994). Therefore, a reaction mechanism was proposed by Waksman *et al.* (1994) in which the two domains rotate 66° about the β-strands of the linker region (Figure 1.13A). This rotation would expose the active site thiols in NTR enabling them to react with the active site disulfide of Trx (Figure 1.13B). Simultaneously the isoalloxazine ring system would be brought in contact with NADPH, which enables reduction of FAD. This conformation was named the FR (flavin reducing) conformation, in contrast to the FO (flavin oxidising) conformation in which the active site disulfide is inaccessible to Trx (Figure 1.13A).

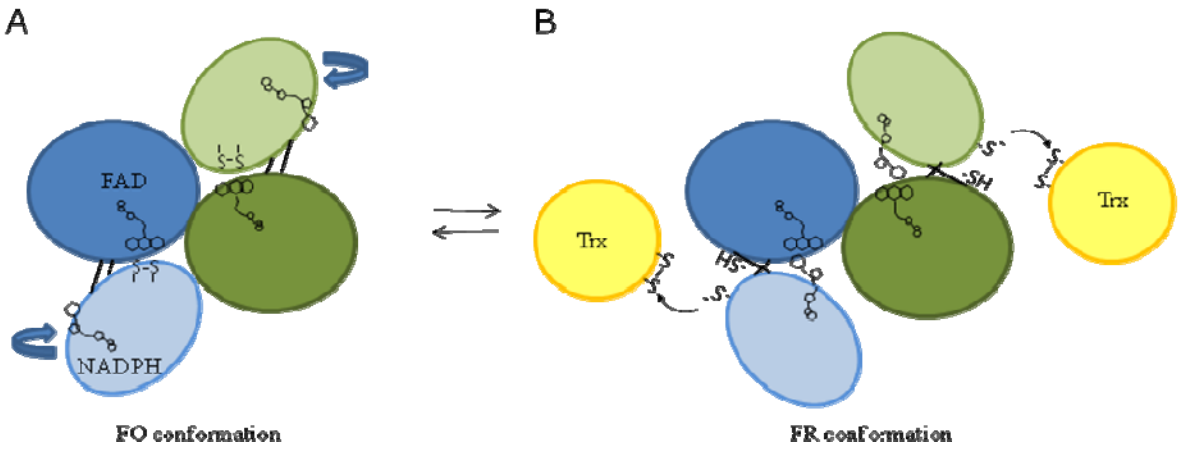

Figure 1.13. Proposed reaction mechanism of LMW NTRs (Waksman *et al.* (1994). In the flavin oxidising (FO) conformation (**A**) electrons are transferred from the isoalloxazine ring system of FAD to the active site disulfide. After a 66° rotation around the linker domain (shown as black lines) FAD is instead positioned to receive electrons from NADPH in the flavin reducing (FR) conformation. At the same time the active site dithiols are exposed on the surface enabling reduction of Trx. Figure from Kirkensgaard *et al.*, 2009 (modified from Waksman *et al*., 1994).

At least sixteen low molecular weight NTR structures are deposited in the Protein data bank (PDB). In addition to EcNTR (Kuriyan *et al.*, 1991; Lennon *et al*., 1999; Waksman *et al*., 1994) structures are available for NTRs from a range of prokaryotes including *Mycobacterium tuberculosis* (Akif *et al.*, 2005), *Helicobacter pylori* (Gustafsson *et al.*, 2007; Sanders *et al*., unpublished), *Thermoplasma acidophilum* (Hernandez *et al*., 2008), *Sulfolobus solfataricus* (Riggiero *et al*., 2009), *Deinococcus radiodurans* (Obiero *et al*., 2010),

and *Campylobacter jejuni* (Osipiuk *et al*., unpublished). Among eukaryotes, two structures of yeast NTR (Zhang *et al.*, 2009; Olivera *et al*., 2010) and two plant NTRs have been deposited; the NTR-B from *Arabidopsis thaliana* (Dai *et al.*, 1996) and HvNTR2 from barley (Kirkensgaard *et al*., 2009, see Chapter 2). A majority of the deposited structures shows NTR in the FO conformation, except the structures of NTR from *Campylobacter jejuni* (pdb 3R9U, Osipiuk *et al*., unpublished) and *Thermoplasma acidophilum,* the latter apparently not utilising NADPH as electron donor (pdb 3CTY, Hernandez *et al*., 2008). HvNTR2 is neither in the FO nor the FR conformation, but resembles the FO conformation most (see Chapter 2).

Lennon *et al.* (2000) succeeded in trapping NTR from *E. coli* (EcNTR) in the FR conformation by cross-linking it with EcTrx through an intermolecular disulfide bond between cysteine residues from the two active sites. The general mechanism of the redox reaction between the dithiols of NTR and the disulfide of Trx is similar to the reaction between Trx and its protein target and involves nucleophilic attack on the Trx disulfide by NTR (Figure 1.14A). The intermolecular disulfide thus formed is immediately attacked by the second active site cysteine residue in NTR. In order to obtain a stable NTR:Trx complex, the cysteines in the active site dithiol motif which are not part of the intermolecular disulfide are mutated to serines (Figure 1.14B) (Wang *et al.*, 1996). An activated mixed disulfide is initially formed by conjugation of TNB to the single-cysteine mutant of Trx, by a reaction with DTNB (5,5'-dithiobis-(2-nitrobenzoic acid), i.e. Ellman's reagent). The activated mixed disulfide is attacked by the free cysteine of NTR releasing TNB. TNB is a good leaving group and absorbs at 412 nm which allows the complex formation to be monitored spectrophotometrically (Lennon *et al.*, 2000; Wang *et al.*, 1996).

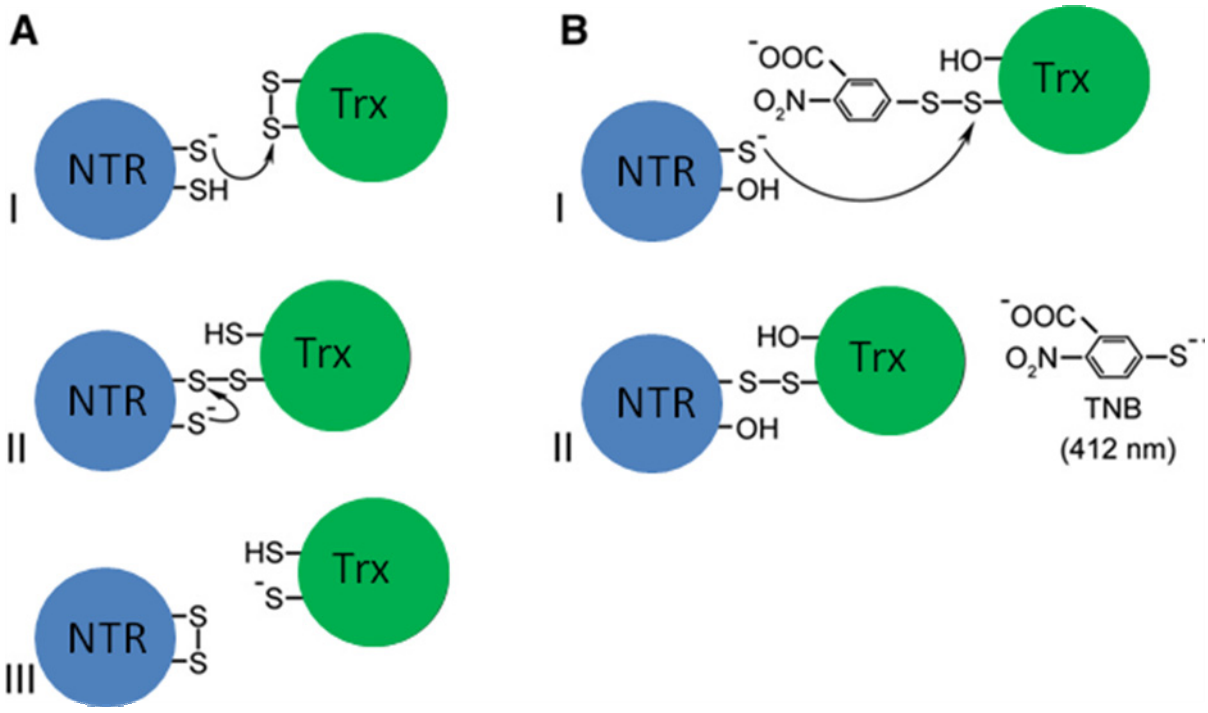

Figure 1.14. Mechanism of the redox reaction between NTR and Trx (**A**) and the strategy for formation of a stable mixed disulfide (**B**). (**A**) One of the cysteines from NTR makes a nucleophilic attack on the disulfide of Trx (I) and forms an intermolecular mixed disulfide intermediate (II). The mixed disulfide is attacked by the other cysteine of NTR to release the reduced Trx and oxidised NTR (III) (**B**) An activated disulfides is formed by conjugation of TNB to a single-cysteine mutant of Trx. The disulfide is attacked by the cysteine of a single-cysteine mutant of NTR (I) to form a stable mixed disulfide and the release of TNB, which can be followed spectrophomotetrically at 412 nm (II). Figure adapted from Maeda *et al*., 2006a.

The crystal structure of EcNTR cross-linked to EcTrx (Lennon *et al.*, 2000) supported the reaction mechanism proposed by Waksman *et al.* (1994). The complex illustrates how FAD is oriented for reduction by NADPH (Figure 1.15) and the reduced active site cysteines are exposed for Trx binding in the FR conformation. In a previous study, Lennon and Williams (1997) have studied the reductive half-reaction of NTR, which includes reduction of FAD by NADPH. It was shown that no single step in this reaction was solely rate-limiting in turnover. They proposed the FO to FR conformational change to be rate-limiting (Lennon and Williams, 1997).

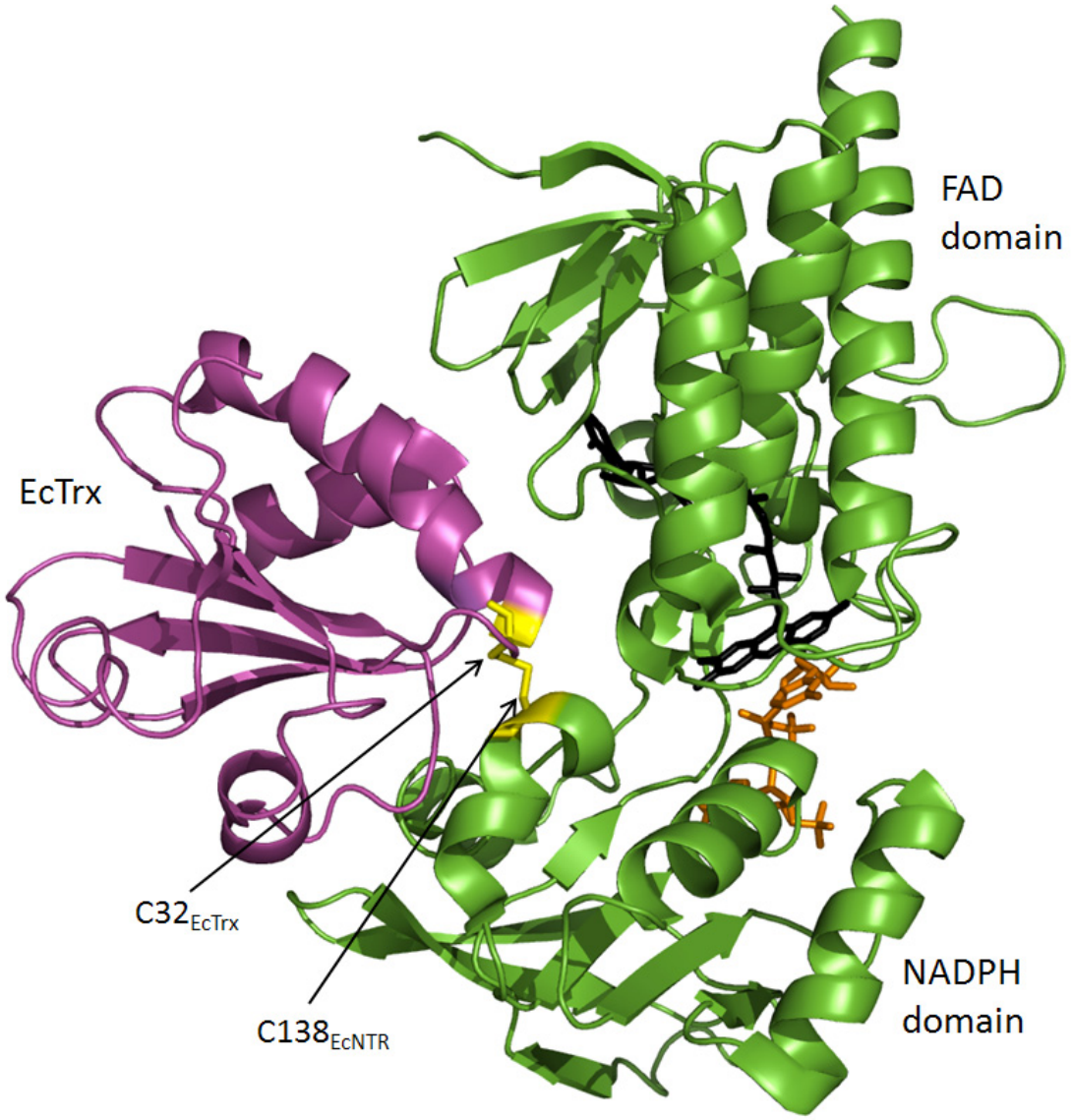

Figure 1.15. The structure of EcNTR in the FR conformation (green) bound by an intermolecular disulfide to EcTrx (magenta) (pdb 1F6M, Lennon *et al.,* 2000). The FAD molecule (black) is positioned opposite the NADPH analogue 3-aminopyridine-adenine dinucleotide phosphate (orange). The cysteines forming the intermolecular disulfide are shown in yellow.

Besides the protein architectures described above, NTRs are found in combination with other domains in various fusion proteins (Figure 1.16, Hirt *et al.*, 2002). These include the selenoenzyme thioredoxin-glutathione reductase, which is composed of HMW NTR with an N-terminal extension with homology to Grx (Figure 1.16B). This protein is able to reduce Trx and GSSG as well as substrates which are specific for GR (Sun *et al.*, 2001). Furthermore, the protein AhpF from bacteria resembles LMW NTRs but contains an N-terminal domain with a Trx fold and a CXXC motif which is involved in catalysis (Figure 1.16F). However, AhpF

reduce a substrate called alkyl hydroperoxidase AhpC (Martin 1995) instead of Trx. Finally, a subgroup of larger (51—58 kDa) NTRs, named NTR-C, located in chloroplasts have an extra C-terminal domain, which contains a Trx-like active site motif, CGPC (Alkhalfioui *et al*., 2007; Serrato *et al.*, 2004, Figure 1.16E). These are further described in Section 1.2.3.1. NTRs with this architecture are mainly found in plants but are also seen in the pathogenic bacterium *Mycobacterium leprae* (Wieles *et al*., 1995, see also Section 1.2.3.1).

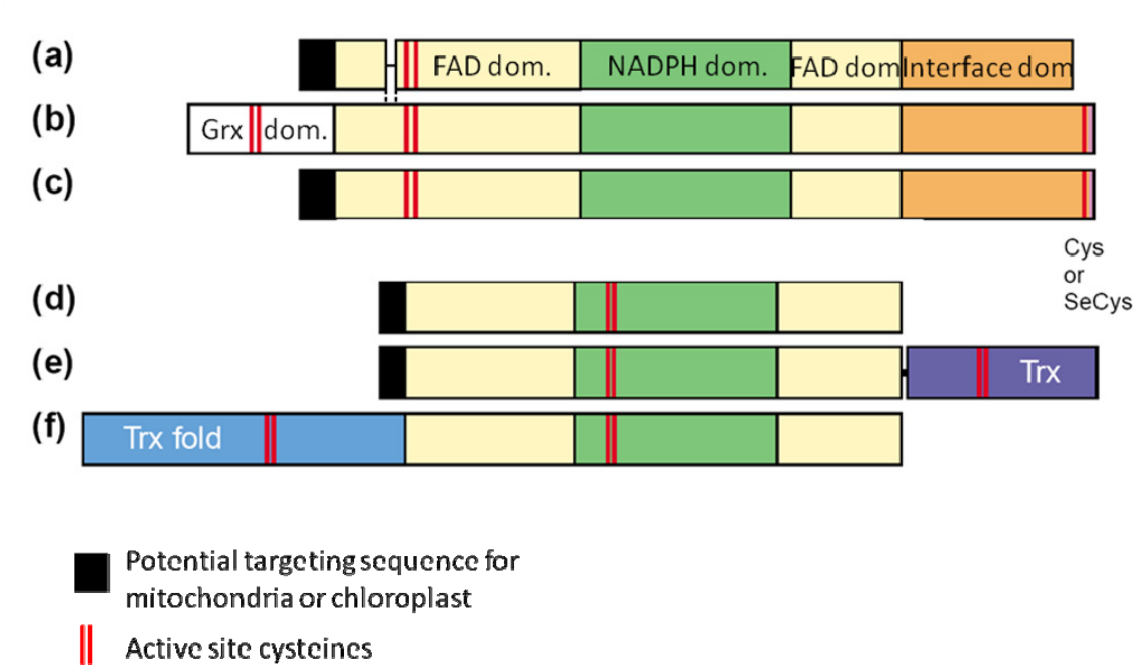

Figure 1.16. The diversity of NTR architecture. The sequences are from (**A**) GR, (**B**) thioredoxin-glutathione reductase, (**C**) HMW NTRs, (**D**) LMW NTRs, (**E**) NTR-C and NTR from *Mycobacterium leprae*, and (**F**) AhpF. Figure modified from Hirt *et al.*, 2002.

1.2 Plant redox control

1.2.1 Oxidative stress in plants

In addition to the sources of ROS mentioned in Section 1.1.1 the chloroplasts is an important site of ROS production in plants. Thus, superoxide is formed due to electron leakage from the photosynthetic electron transport chain and is converted to hydrogen peroxide by dismutation (Møller, 2001; Foyer and Noctor, 2003).

Another source of superoxide is found in the apoplast, which is the free diffusible space outside the plasma membrane. Here the membrane bound NADPH oxidase (Figure

1.1) release superoxide during transfer of electrons across the membrane from NADPH located inside the cell to oxygen in the apoplast. This superoxide is formed as a response to stresses and may inhibit growth of bacteria and fungi (Sagi and Fluhr, 2001).

1.2.2 Glutathione/glutaredoxin system in plants

GSH play important roles in plants, where it is found in many tissues and subcellular compartments. Hence, it is not only important in the maintenance of the redox balance but is also involved in detoxification of heavy metal and xenobiotic (foreign to the cell) compound as well as in cell signalling. GSH reacts both with hydrogen peroxide and with the reactive nitrogen species (RNS) nitric oxide forming the derivative GSNO (Rouhier *et al*., 2008).

Approximately 30 isoforms of Grx are described in the model plant *Arabidopsis thaliana*. Depending on their redox-active centre these are grouped in three classes of the CSY(C/S)-, CGSF-, and CC-type. Some plant Grx have been shown to bind iron-sulfur clusters and deliver them to enzymes on demand (Rouhier *et al*., 2008). Furthermore, Grxs are involved in glutathionylation/deglutationylation (Rouhier *et al*., 2008). Glutathionylation is favoured under high concentrations of ROS and can protect protein thiols from irreversible inactivation (Rouhier *et al*., 2008).

.

1.2.3 Trx systems in plants

1.2.3.1 NTRs in plants

Plants contain LMW NTRs (termed NTR-A/B) as described above. These are expressed in a short and a long version, where the longer version contains an N-terminal sequence targeting them for mitochondria or chloroplast (Figure 1.16D, Laloi *et al*., 2001). NTR-C is found in some cyanobacteria, green algae and plants including *A. thaliana*, rice (Serrato *et al*., 2004) and barley (Wulff *et al*., 2011), and acts as an electron donor to 2-Cys peroxiredoxin (Alkhalfioui *et al*., 2007). The discovery of NTR-Cs in chloroplasts suggests the presence of an NTR/Trx system in addition to the Fdx/Trx system (described below) in this compartment. This may enable reduction of Trxs in dark and independently from photosynthetic electron transport (Brehelin *et al*., 2004).

In contrast to mammals neither cytosolic nor mitochondrial NTRs of the A/B-type are essential, since double NTR knockout mutants of *A. thaliana* were both viable and fertile (Reichheld *et al*., 2007). However, they had a phenotype of slower plant growth, wrinkled seeds and reduced fitness. Trx was found to be not fully oxidised in the NTR mutant suggesting the existence of an alternative mechanism of Trx reduction. Interplay with the glutathione system is plausible since these mutants were hyper-sensitive to a specific inhibitor of glutathione biosynthesis (buthionine sulfoximine), and upon treatment with this inhibitor Trx was found to be fully oxidised (Reichheld *et al*., 2007).

1.2.3.2 Trxs in plants

In plants, Trxs are involved in a wide range of critical biological processes, ranging from photosynthesis to growth, flowering and the development and germination of seeds. A membrane-associated Trx has also been shown to be able to move from cell to cell, and was proposed to be involved in intercellular communication in plants (Meng *et al.*, 2010).

Higher plants have Trx systems that are unusually complex and diverse. This could be due to the increased generation of ROS caused by photosynthesis and/or to genome duplication (Meyer *et al*., 2008). For instance, 41 genes of Trx and Trx-like sequences have so far been identified in the genome of *A. thaliana* (Chibani *et al*., 2009). Plant Trxs are grouped into types (f, m, x, y, h, o, and s) based on sequence similarity. In general Trxs-m, -f, - x, and -y are localised in the chloroplasts whereas Trx-o is localised in mitochondria (Meyer *et al*., 2005). Trx-s seems to be unique to *M. truncatula* and is located in ER (Alkhalfioui *et al*., 2008). The h-type Trxs are mainly cytosolic but have also been located in other cell compartments including the nucleus and mitochondrion (Meyer *et al*., 2002; Meyer *et al*., 2005). Trx-h was also shown to be transported to the phloem sieve tubes in e.g. rice and maize (Ishiwatari *et al*., 1995, 1998; Santandrea *et al*., 2002).

Trx-f and -m are members of the ferredoxin (Fdx)/Trx in chloroplasts (Figure 1.17). This system is coupled to photosynthesis. In the photosynthesis reaction, electrons are excited due to light absorbed by photo system II (PS II) and I (PS I), and are transferred to Fdx. Fdx has an active site consisting of an iron-sulfur [Fe_2S_2] cluster (Figure 1.18), where the iron atoms are tetrahedrally coordinated by inorganic sulfur atoms and the sulfurs of four conserved cysteine residues. Fdx is able to initiate a dithiol disulfide exchange cascade,

where Fdx serves as electron donor for the enzyme ferredoxin-thioredoxin reductase (FTR, Figure 1.18). FTR contains an iron-sulfur [Fe_4S_4] centre but in addition it has a proximal dithiol motif which enables this enzyme to couple the photosystem to enzyme regulation through disulfide/thiol exchange (Droux *et al*., 1987).

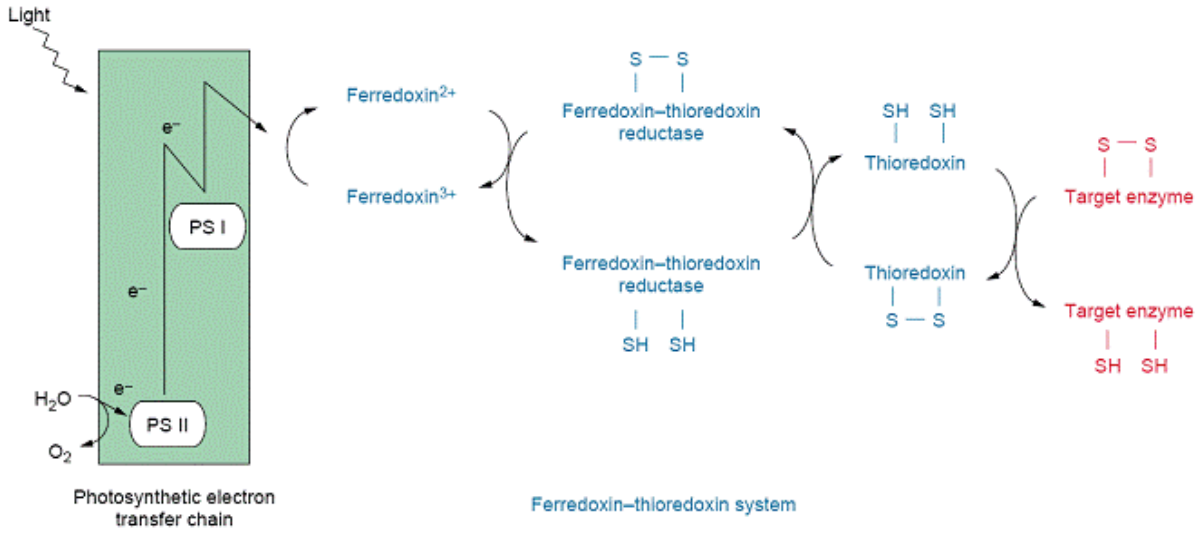

Figure 1.17. Ferredoxin (Fdx)/thioredoxin (Trx) system in chloroplasts. Light-driven excited electrons produced by photosystem II (PS II) and I (PS I) are transferred to an iron-sulfur cluster [Fe_2S_2] of ferredoxin (Fdx). Fdx and Trx-f or -m are both bound to ferredoxin-thioredoxin reductase (FTR), which contains both an iron sulfur centre [Fe_4S_4] and a disulfide bond. Electrons are transferred one at a time from Fdx via FTR to the active site disulfide of Trx (see text for details). Thus FTR is able to convert the light signal into a thiol signal (Dai *et al*., 2007). Figure from Ruelland and Miginiac-Maslow, 1999.

The crystal structures of four complexes in the pathway including a ternary complex of FTR bound to both Fdx and Trx-f shows that these can be bound simultaneously at different sites (Dai *et al*., 2007). After transfer of one electron from Fdx to FR, an intermediate is formed (Figure 1.18) where one of the cysteines from the FTR dithiol motif attacks the disulfide of Trx forming an intermolecular disulfide between FTR and Trx. Meanwhile, the other cysteine of the FTR disulfide is coordinated to the iron cluster. After transfer of another electron from the Fdx iron-sulfur cluster the intermolecular bond is cleaved, rendering Trx in the reduced form (Dai *et al*., 2007). In turn Trx-m or -f, reduces target proteins in the chloroplast (Ruelland and Miginiac-Maslow, 1999). These include key enzymes in the Calvin cycle and pentose phosphate pathway: Trx-f is specific for fructose-

1,6-bis-phosphatase and Trx-m for NADP-malate dehydrogenase (Buchanan and Balmer, 2005; Jacquot *et al*., 1997). FTR consists of two protein chains and its structure is very different from NTR (Figure 1.18, Dai *et al*., 2007).

The h- and o-type Trxs are members of the NTR/Trx system described in Section 1.1.4. Trx-h comprises the largest and most diverse group of Trxs. For instance *A. thaliana* encodes at least eight isoforms of Trx-h. The h-type Trxs can be further divided into three groups based on sequence similarity (Gelhaye *et al*., 2005). Subgroup I contains cytosolic Trxs, and some members containing a RKDD motif proposed to be involved in cell-to-cell transport through plasmodesmata (Ishiwatari *et al.*, 1998). Proteins from subgroup II have extensions in the N-terminal end and are translocated to mitochondria, the plasma membrane, or the extracellular matrix (Gelhaye *et al*., 2002, 2004; Juárez-Díaz *et al*., 2006; Shi and Bhattacharyya, 1996). Member from subgroup III are exceptional, since they are not reduces by NTR. Instead they depend on the GSH/Grx for their reduction (as mentioned in Section 1.1.5), by a proposed mechanism shown in Figure 1.19 (see the legend for details) (Gelhaye *et al*., 2003; Juttner *et al*., 2000; Koh *et al*., 2008).

Specific physiological roles have been assigned to individual Trx-h isoforms which exhibit differential time and tissue-specific expression patterns (Cazalis *et al*., 2006; Reichheld *et al*., 2002). For example AtTrxh1 and AtTrxh4 were shown to be correlated with the cell cycle, suggesting a role in redox control of cell proliferation (Menges *et al.*, 2002). AtTrxh1 reduce cytosolic malate dehydrogenase (Hara *et al*., 2006) and AtTrxh5 seems to be specifically involved in response to oxidative stresses and patogens (Laloi *et al.*, 2004). For example, HvTrxh5 was required for sensitivity toward the fungal pathogen *Cochliobolus Victoria,* which causes the disease victoria blight (Sweat *et al*., 2007). Insight into the specificity of Trx-h has also been provided from complementation studies using a yeast strain deprived of the two endogenous thioredoxin genes that was dramatically affected in viability and growth, and was sensitive towards oxidative stress (Verdoucq *et al*., 1999). Five h-type Trxs (AtTrxh1 to AtTrxh5) from *A. thaliana* were able to restore a normal cell cycle when expressed in this yeast mutant. Furthermore, the yeast gained the ability to grow on methionine sulfoxide as the sole sulfur source. Different roles were assigned to AtTrxh2 and AtTrxh3: AtTrxh2 restored sulfur assimilation but did not increase tolerance to hydrogen

peroxide, whereas AtTrxh3 increased tolerance to hydrogen peroxide but was unable to restore sulfur assimilation (Mouaheb *et al*., 1998).

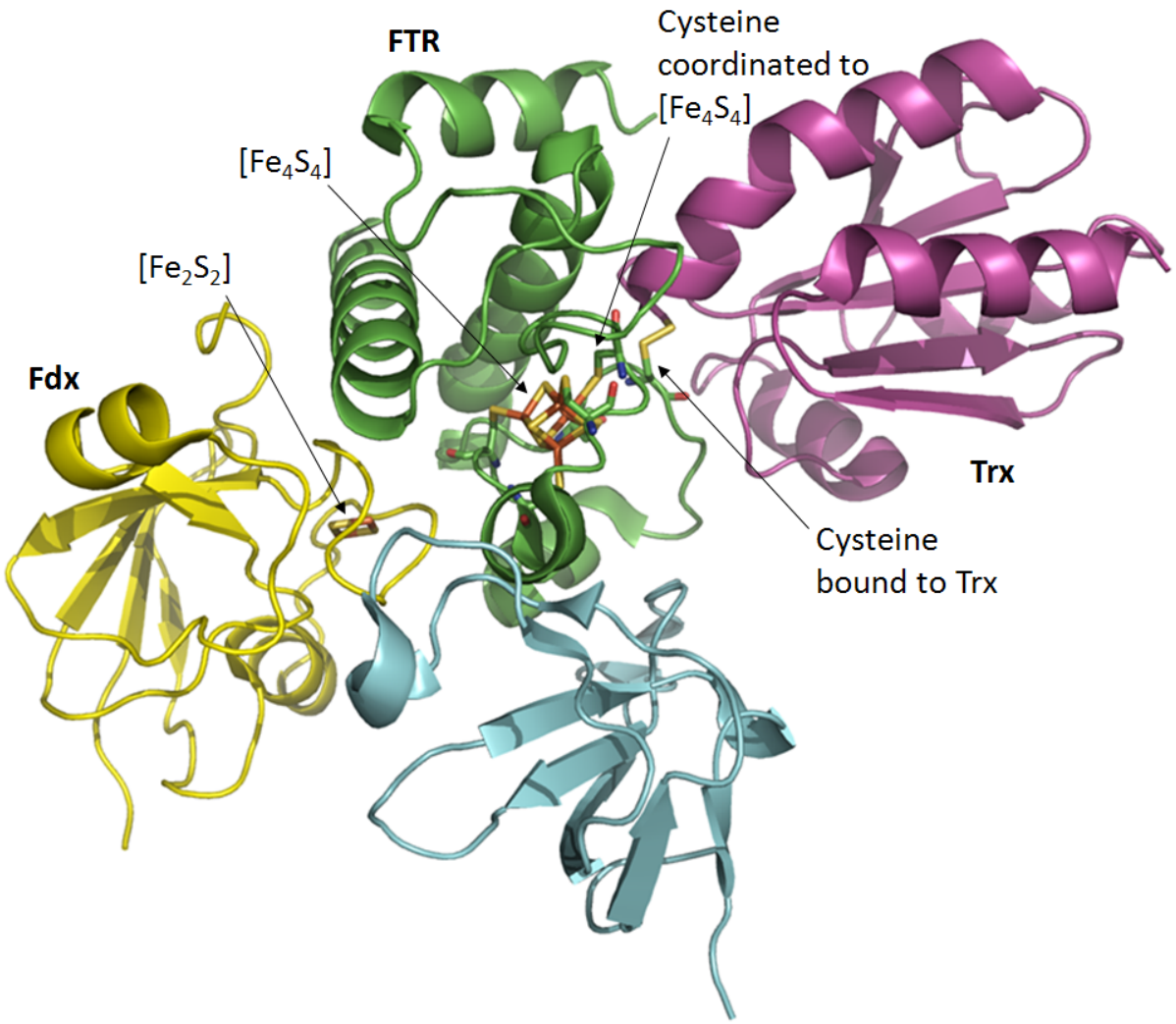

Figure 1.18. Complex of Fdx:FTR:Trx. Light-driven excited electrons produced by photosystem II (PS II) and I (PS I) are transferred to an iron-sulfur cluster [Fe_2S_2] of Fdx (yellow). Fdx and Trx-f (magenta) are both bound to FTR (consists of two chains; green and cyan), which contains both an iron sulfur centre [Fe_4S_4] and a disulfide bond. Electrons are transferred one at a time from Fdx via FTR to the active site disulfide of Trx. After transfer of the first electron an intermediate (shown) is formed in which one of the cysteines from the FTR disulfide attack the disulfide of Trx, forming an intermolecular disulfide. The other cysteine from the disulfide of FTR is coordinated to the [Fe_4S_4] centre (pdb accession 2pvo, Dai *et al*., 2007).

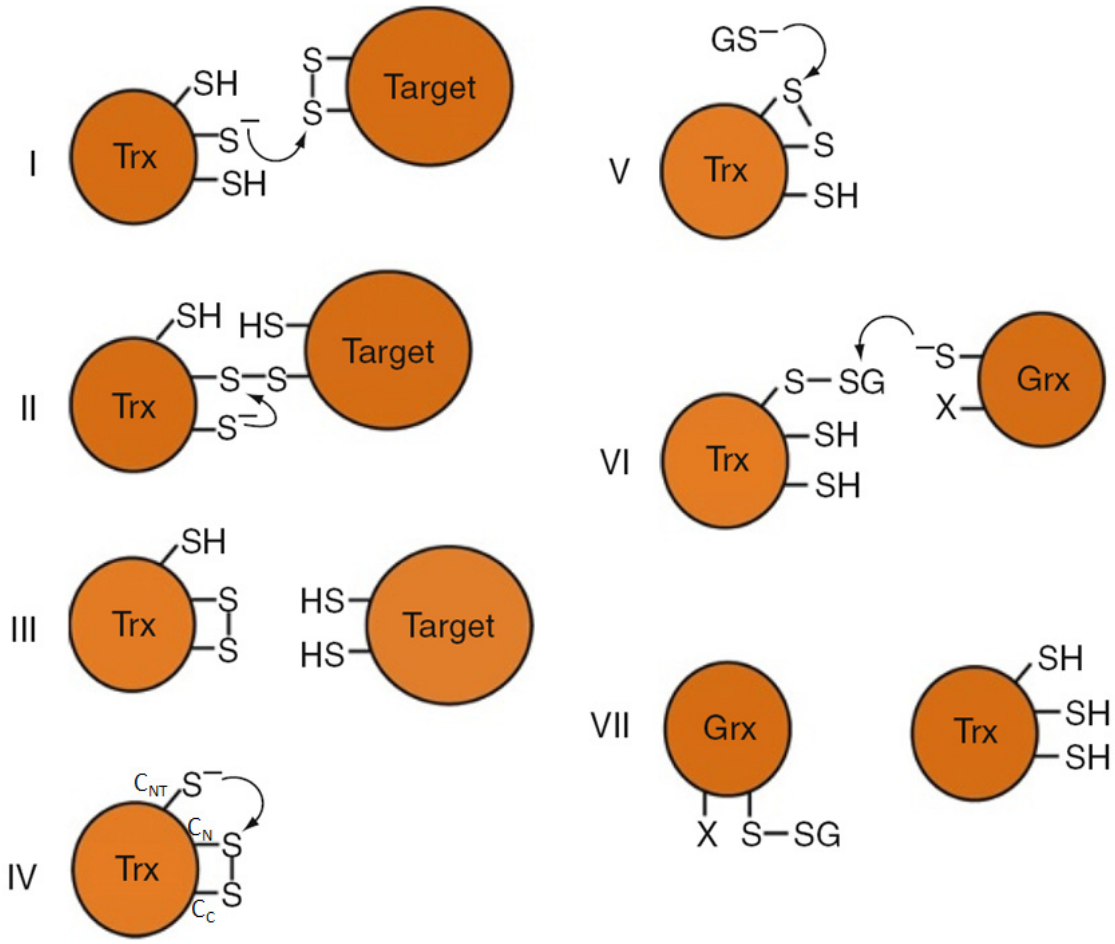

Figure 1.19. The catalytic mechanism proposed by Koh et al. (2008) of h-type Trxs from subgroup III. (**I-III**) These Trxs react with a protein target in the same way as other Trxs (compare with Figure 1.7). (**IV**) The C_N–C_C disulfide is then attacked by a third N-terminal cysteine (C_{NT}) leading to the formation of a C_{NT}–C_N disulfide. (**V**) C_{NT} is attacked by reduced glutathione (GS^-) and (**VI**) the glutathione is released from C_{NT} by Grx. Figure adapted from Hägglund *et al.*,2009.

As mentioned above the NTR/Trx system is involved in the regulation of many different systems in plants via thiol redox control. In mitochondria the role of the system has been linked to fundamental processes including the citric acid cycle and associated reactions as well as photorespiration, lipid metabolism, electron transport, ATP-synthesis/transformation, translation, protein assembly/folding, nitrogen and sulfur metabolism, hormone synthesis and stress-related reactions (Buchanan and Balmer, 2005).

The structures have been determined for several plant Trx-h, including HvTrxh1 and HvTrxh2 (Figure 1.6), AtTrxh1 from *A. thaliana*, PtTrxh1 and PtTrxh4 from poplar, and Trxh1 from the algae *Chlamydomonas reinhardtii* (Coudevylle *et al*., 2005; Koh *et al*., 2008; Maeda

et al., 2006a, 2008). With the exception of an elongated alpha helix (α1) (Figure 1.6) the structures of Trx-h are in general similar to other types of Trxs (Schürmann and Jacquot, 2000). The structure of HvTrxh2 linked covalently to BASI through an intermolecular disulfide was solved by using the method shown in Figure 1.14B (Maeda *et al*., 2006a). This complex is further described in Chapter 4.

1.3 Seed structure, germination and role of Trx-h

The barley seed consists of several tissues which plays various roles during seed germination and seedling growth. The seed is typical for monocots and contains a seed coat, a large endosperm, and an embryo (Figure 1.20). The embryo contains all necessary components to grow into a new plant with the endosperm providing supplementary nutrients to assist with seedling establishment. The endosperm consists of two parts: a starchy endosperm which contains dead cells and a surrounding aleurone layer which is a specialised secretory tissue (Figure 1.20). The starchy endosperm contains reserves made up mostly of starch and storage proteins, but also lipids and other nutrients (Bewley and Black, 1994; Ritchie *et al*., 2000). Disulfides are prominent in these storage proteins (and secretory proteins) and protect them against denaturation and decrease their susceptibility to proteolysis (Buchanan and Balmer, 2005).

The germination process is initiated with imbibition (water uptake) by the embryo at appropriate temperature. Upon imbibition the phytohormone gibberellic acid (GA), which is the germination signal, is newly synthesised in the embryo and diffuses to the aleurone layer. In the freshly imbibed seeds the aleurone cells are filled with vacuoles containing proteins and phytic acid (which is the principal storage form of phosphorus in many plant tissues). When the aleurone cells receive the GA signal from the embryo the content of the vacuoles are hydrolysed to provide amino acids and inorganic compounds. These are used by the aleurone cell to produce hydrolytic enzymes such as α-amylase, limit dextrinase, proteases and nucleases, which are released into the starchy endosperm (Bewley and Black, 1994; Ritchie *et al*., 2000). At least 40% of the newly synthesised protein in GA-treated aleurone cells is α-amylase, so this enzyme has been used as a marker for GA action in aleurone layers (Ho *et al*., 2003).

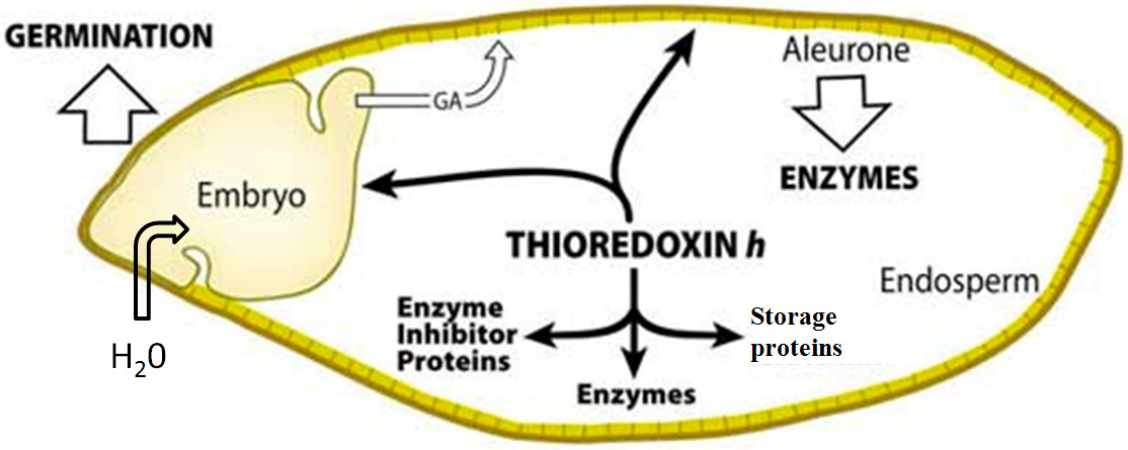

Figure 1.20. Structure of the barley seed and the role of Trx-h. The seed consists of an embryo, a starchy endosperm surrounded by the aleurone layer and the seed coat. Upon water uptake the plant hormone GA is transported from the embryo to the aleurone layer, which in turn secretes proteases and amylolytic enzymes into the starchy endosperm. The degraded components are supplied to the embryo. Trx-h converts storage proteins to the reduced state increasing their solubility and susceptibility to proteolysis. Furthermore, inhibitors of amylolytic enzymes are inactivated. Trx-h seems to function as a member of a communication network between the endosperm, the aleurone and embryo. Figure adapted from Wong *et al*., 2002.

Trx-h is proposed to play important roles during the germination process by reducing disulfide bonds in endosperm storage proteins (gliadins and glutenins) thereby increasing their solubility and susceptibility to proteolysis. Furthermore, BASI and other inhibitors of trypsin and amylolytic enzymes are inactivated by Trx-h *in vitro*, whereas the protease thiocalsin is activated (Besse *et al*., 1996; Kobrehel *et al*., 1992). Moreover, transgenic seeds overexpressing Trx-h in barley endosperm display increased amount and activity of α-amylase (Wong *et al*., 2002). Also an enhancement of GA synthesis was observed in these seeds, suggesting that Trx-h may communicate with the embryo (Figure 1.20). However, the increased amount and activity of α-amylase was also observed in deembryonated grains overexpressing Trx-h, indicating that Trx-h has a direct effect on the aleurone layer (Figure 1.20, Wong *et al*., 2002). In proteome analysis of seeds from barley, *Hordeum vulgare*, two isoforms of Trx-h with 51% identity were identified and termed HvTrxh1 and HvTrxh2 (Maeda *et al*., 2003). They were found to have overlapping spatiotemporal appearance and to be able to interact interchangeably with HvNTR1 and HvNTR2 (Maeda *et al*., 2003; Shahpiri *et al*., 2008a; Shahpiri *et al*., 2009).

1.3.1 GA response

There are two types of GA receptors in the aleurone layer, including soluble and membrane-bound forms (Ueguchi-Tanaka *et al.*, 2007). In the nucleus of the barley aleurone cell the transcription factor GAmyb (which mediate the GA response) is not present prior to the GA signal since the protein SLN1 represses the gene encoding GAmyb (Figure 1.21, Chandler *et al*., 2002). Upon imbibition GA interacts with a membrane-associated GA receptor of the aleurone cell and via second messengers a decrease of SLN1 concentration occurs, either by blocking its translation or modifying the active SLN1 in a way that promotes its degradation (Gubler *et al*., 2002). Decrease in SLN1 leads to enhanced expression of GAmyb, which leads to expression of GA-induced enzymes such as α-amylase (Figure 1.21, Gomez-Cadenas *et al*., 2001).

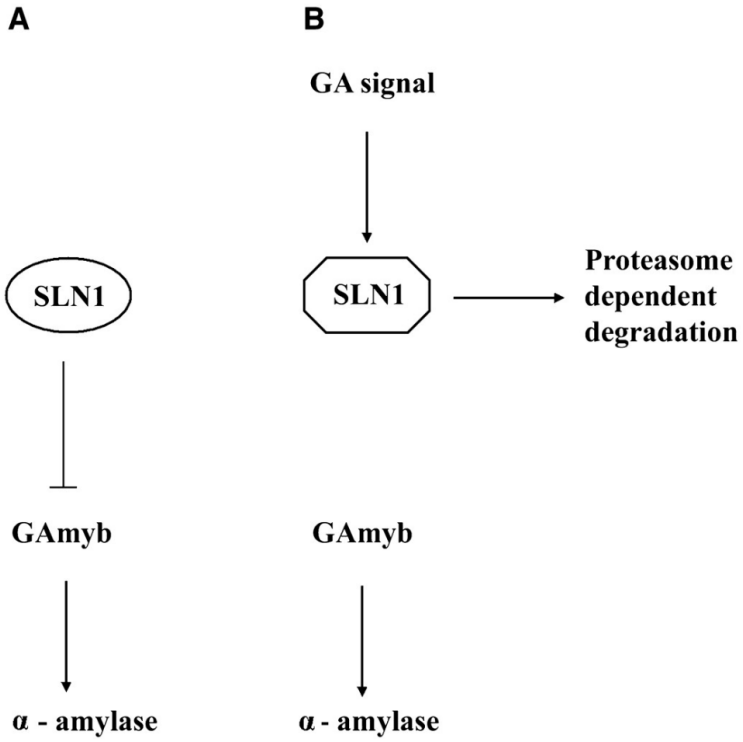

Figure 1.21. GA signalling pathway. **(A)** The active form of the protein SLN1 in the nucleus represses the gene encoding the transcription factor GAmyb **(B)** GA interacts with the membrane-associated GA receptor (*not shown*), thus activating signal transduction via second messengers. Upon GA signaling active SLN1 is modified of into a form that is degraded via a proteasome-dependent mechanism, resulting in the activation of GAmyb transcription and α-amylase production. Figure from Fu *et al.*, 2002.

Initiation of germination depends on both internal and external factors, of which the most important external ones are water, temperature, oxygen and sometimes light and darkness. However, the seeds of many plants are dormant at harvest and do not germinate even under favourable conditions. These seeds need more time, and/or specific environmental conditions before they germinate. Thus, dormancy disappears with time in a process called after-ripening. Factors affecting seed dormancy include the presence of phytohormones; abscisic acid (ABA) inhibits germination whereas GA is involved in breaking seed dormancy. Therefore, in the production of malt which is part of the brewing process, barley seeds are treated with GA to ensure a uniform seed germination (Raven *et al*., 2005).

1.4 Potential applications of the NTR/Trx system

The NTR/Trx system has several potential applications within the food industry. One example is the use of Trx in the baking industry to improve dough quality. The structure of the dough is dependent on disulfide bonds in the storage proteins glutelins and prolamins (Joudrier *et al*., 2005). Addition of the components of the NTR/Trx system to flour of poor quality has been shown to modulate viscoelasticity and increase loaf volume (Wong *et al*., 1993). Instead of adding the NTR/Trx components in vitro one could potentially use flour from transgenic wheat seeds overexpressing these proteins in the grain as done by Li *et al.* (2009).

As mentioned previously transgenic barley seeds overexpressing Trx-h display increased α-amylase and limit dextrinase activity and germinate earlier than wild-type seeds (Wong *et al.*, 2002; Cho *et al.*, 1999). These parameters are important for the malting process in beer production suggesting potential applications of transgenic Trx-h barley seeds in the brewing industry.

Other applications include meat packaging where addition of Trx potentially may suppress cross-linking of myosin heavy chains by disulfides, which reduces juiciness and tenderness of meat (Lund *et al*., 2007). Furthermore, the NTR/Trx system may potentially find applications in production of buttermilk and cheese where gram-positive bacteria such as *Lactococcus lactis* are used in starter cultures. These bacteria typically lack genes encoding for the glutathione synthesis machinery and the NTR/Trx system is therefore hypothesised to play particularly important roles in stability under stress conditions. Finally

Trx is able to increase the proteolytic digestibility of the allergen β-lactoglobulin, by reducing one or two of its disulfide bonds, and thus potentially decrease allergic reactions to milk products (de Val *et al*., 1999).

1.5 Objectives of the present study

Due to the importance of the NTR/Trx system it was desirable to gain insight into the structure/function of the involved proteins and investigate how NTR and Trx interact with one another. As mentioned, at the outset of this project structures had already been obtained for the two Trx isoforms from barley, HvTrxh1 and HvTrxh2, but no structure of barley NTR was available. A crystal structure of one of the NTR isoforms, HvNTR2, was obtained during this PhD (**Chapter 2, Appendix E**). It was further attempted to produce and crystallise a complex of HvNTR2 bound covalently through an intermolecular disulfide to HvTrxh2 (HvNTR2:HvTrxh2) similar to the complex of EcNTR:EcTrx described above (**Chapter 3**). This disulfide is established between cysteines from the active sites of HvNTR2 and HvTrxh2 and therefore such a complex is believed to resemble an intermediate of the catalytic cycle between the two proteins. The attempt to produce, purify and crystallise this complex is described (**Chapter 3**). Furthermore, the dependence of NADPH/$NADP^+$ in the complex formation was studied (**Chapter 3**). Since no crystal structure of the complex of HvNTR2:HvTrxh2 was obtained, a model of this complex was build based on existing crystal structures using homology modelling with EcNTR:EcTrx as template (**Chapter 4, Appendix F**). The model provides insight into which residues and loops could be involved in the binding between HvNTR2 and HvTrxh2. To further elucidate the role of these residues a comprehensive mutational study was combined with enzyme kinetics (**Chapter 5, Appendix F**). Furthermore, the thesis includes reflections concerning the catalytic mechanism of the interaction between HvNTR2 and HvTrxh2 (**Chapter 6**). As mentioned in the preface part of the PhD study was carried out at CSIRO, Australia. Here the expression levels of HvNTR1, HvNTR2, HvTrxh1, HvTrxh2 and α-amylase in different tissues of barley seeds were examined by Q-PCR and micro-array data analysis. The effects of the plant hormone gibberellic acid, dormancy/after-ripening and light/darkness on these expression levels were examined as well as the role of the GA-receptor GID1, an ortholog of GSE1 (**Appendix A**).

Chapter 2

Crystal structure of NADPH-dependent thioredoxin reductase HvNTR2

2.1 Introduction

This chapter describes crystallisation as well as structure determination of HvNTR2, one of the two isoforms of NTR from barley (Kirkensgaard *et al*., 2009; Appendix E). As described in Chapter 1 the structures of the two isoforms of Trx from barley had previously been determined (Maeda *et al*., 2006a, 2008), so the structure of HvNTR2 provided further knowledge concerning the NTR/Trx system in plants.

2.2 Results and discussion

2.2.1 Crystallisation of HvNTR2

His-tagged HvNTR2 was expressed, purified and dialysed in 10 mM Tris-HCl pH 8.0 (see Section 2.4.1). Initial crystallisation trials were performed using a PEG6000 grid-screen (Hampton Research) and the hanging drop vapour diffusion method (2 µL 2.5 mg mL^{-1} protein was mixed with 2 µL well solution). After 4 d at 22°C yellow needle clusters were detected in 5% (w/v) PEG6000, 0.1 M citric acid pH 4.0 (Figure 2.1A). A screen around this pH value showed better results at pH 3.5 and a screen around the PEG-size led to single thicker needles using 2% PEG400 (Section 2.4.2). The quality of the needles was lowered by decreasing the temperature to 4°C and the temperature was optimised to 25°C, which led to longer, thicker and more regular single needles with a maximum length of 0.7 mm (Figure 2.1B).

Further attempts to improve these needles did not lead to diffraction to more than ≈7 Å. However, hexagonal crystals (Figure 2.2) were discovered in one of the screens for PEG concentration, in 30% (w/v) PEG400. Optimisation revealed that 22% (w/v) PEG400 was the borderline for whether needles or hexagonal crystals were obtained. In some drops both

crystal forms were found. The concentration of PEG400 was further optimized to 24% (w/v) and the protein concentration to 5.7 mg mL^{-1}. Furthermore, it was found by using an additive screen (Hampton Research) that thicker sharper looking crystals could be obtained by adding 2% (w/v) of the polyetheramine Jeffamine® M-600 pH 7.0. These final conditions gave bright yellow crystals with hexagonal morphology within a week. The diameter of the crystals could reach 0.18 mm. The crystals were flash-frozen directly from the drop without using additional cryo-protectants. This was possible due to the high concentration of PEG400. One of the crystals diffracted to 2.6 Å. Data was collected as described in Section 2.4.2 and the structure determination and refinement performed as described in Section 2.4.3.

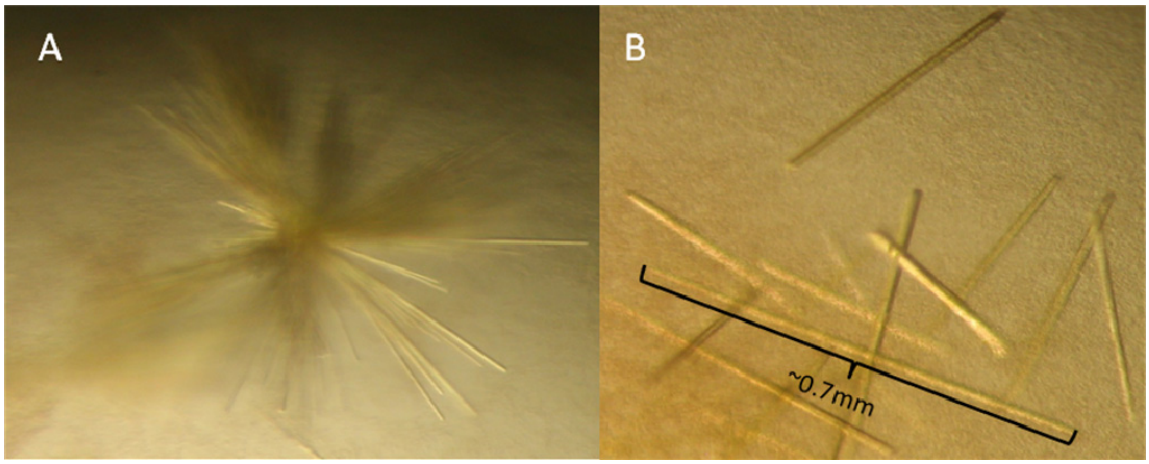

Figure 2.1. Yellow needle cluster and single needles of HvNTR2. (**A**) Crystals were grown in 5% (w/v) PEG6000 (Fluka) and 0.1 M citric acid-buffer pH 4.0 for four d at 22°C. (**B**) Crystal grown 12 d at 25°C in 2% (w/v) PEG400 and 0.1 M citric acid-buffer pH 3.5.

Attempts were made to soak NADPH into the crystals. However, this led to cracking of the crystals. The other isoform, HvNTR1, was also purified and attempts to crystallise this included seeding with crystals of HvNTR2. A wide variety of screens were used with no results.

Figure 2.2. Hexagonal crystals of HvNTR2. Crystals were grown in 30% (w/v) PEG400, 0.1 M citric acid buffer pH 3.5 and an incubation temperature of 22°C for > a week.

2.2.2 Quality of the crystal structure

Parameters for the refined model of HvNTR2 are summarised in Table 2.1. The final model contains two molecules in the asymmetric unit, covering residues 6—323 (chain A) and 5—323 (chain B), respectively. The numbering refers to the amino acid sequence of the wild-type HvNTR2. The obtained structure is a homodimer formed around the crystallographic two-fold axis. One FAD molecule with well-defined electron density and B-factors (~40 $Å^2$) comparable to the surrounding protein is present in each subunit. NADPH did not fit the excess electron density in the expected NADPH-binding pocket. Instead, the density fitted reasonably well with two citrate molecules accidentally present from the crystallisation conditions (real-space R-factor = 0.7—0.9). High B-factors but continuous main chain electron density is found in the N-terminal (residues 6—12), the loop between A1 and B3 (residues 33—35), B5 and surrounding loops (residues 96—105), the loop between B10 and B11 (residues 153—158), B12 and surrounding loops (residues 174—196) and B15 and surrounding loops (residues 220—245) (See Supplementary Figure 1 in Appendix E for numbering of the α-helices and β-sheets). The highest B-factors are found in the C-terminal part of the FAD domain. The two molecules in the asymmetric unit can be superimposed with a root-mean-square deviation (r.m.s.d.) of 0.1 Å for C_α-atoms. The

largest differences are found in the C-terminal part of the FAD domain and especially in the loop between β-strands B18 and B19 (Supplementary Figure 1 in Appendix E).

Table 2.1 Data collection and refinement statistics. Values in parenthesis are for the highest resolution bin. Table from Kirkensgaard *et al*., 2009.

	HvNTR2
Data collection	
Resolution (Å)	49.9—2.60 (2.74—2.60)
No. of unique reflections	27423 (3937)
Redundancy	7.1 (7.3)
Completeness (%)	99.6 (99.6)
R_{sym}† (%)	6.6 (35.0)
$\langle I \rangle / \sigma \langle I \rangle$	18.4 (4.4)
Wilson B-factor (Å^2)	59.8
Refinement	
No. of amino acid residues	635
No. of water molecules	48
R_{cryst}‡ (%)	19.0
R_{free}‡ (%)	23.8
Estimated coordinate error (Å)	0.33
R.m.s.d. from ideal geometry	
Bonds (Å)	0.011
Angles (°)	1.329
B-factors (Å^2)	
Protein (A chain/B chain)	59.2/60.9
FAD	39.3
Solvent	43.8
Ramachandran plot	
Most favoured (%)	82.8
Additionally allowed (%)	16.1
Generously allowed (%)	1.1
Disallowed (%)	0.0

† $R_{sym} = \sum_{hkl}\sum_i \left| I_i - \langle I \rangle \right| / \sum \langle I \rangle$, where ‹I› is the mean intensity of the N reflections with intensity I_i. ‡ $R_{cryst} = \sum_{hkl} \left| \left| F_{obs} \right| - k \left| F_{calc} \right| \right| / \sum_{hkl} \left| F_{obs} \right|$, where F_{obs} and F_{calc} are observed and calculated structure factors, respectively. For R_{free}, the sum is extended over a subset of reflections (5%) that were excluded from all stages of refinement.

2.2.3 Overall structure

As other low molecular weight (LMW) NTRs, HvNTR2 forms a homodimer with each subunit having two domains; the FAD and the NADPH domain (Figure 2.3). The two domains are quite similar to each other with 82 superimposable C_α-atoms giving a r.m.s.d. of 2.4 Å. The FAD-domain consists of residue 1—126 and 255—331 and has an α/β structure comprised of a central five-stranded parallel β-sheet flanked by a four-stranded β-sheet on one side and three α-helices on the other (Figure 2.3 and Appendix E: Supplementary Figure 1). The NADPH domain consists of amino acid residues 127—254 and here a five-stranded parallel β-sheet is flanked by a three-stranded β-sheet on one side and two α-helices, plus a third short α-helix containing the active site cysteines, on the other side of the sheet. The two domains are connected by two anti-parallel β-strands (amino acid residues 124—126 and 255—257), which per tradition are assigned to the FAD domain (Figure 2.3). Only few inter-domain interactions stabilise the relative orientation of the two domains (see Appendix E: Section 3.7 and Table 2).

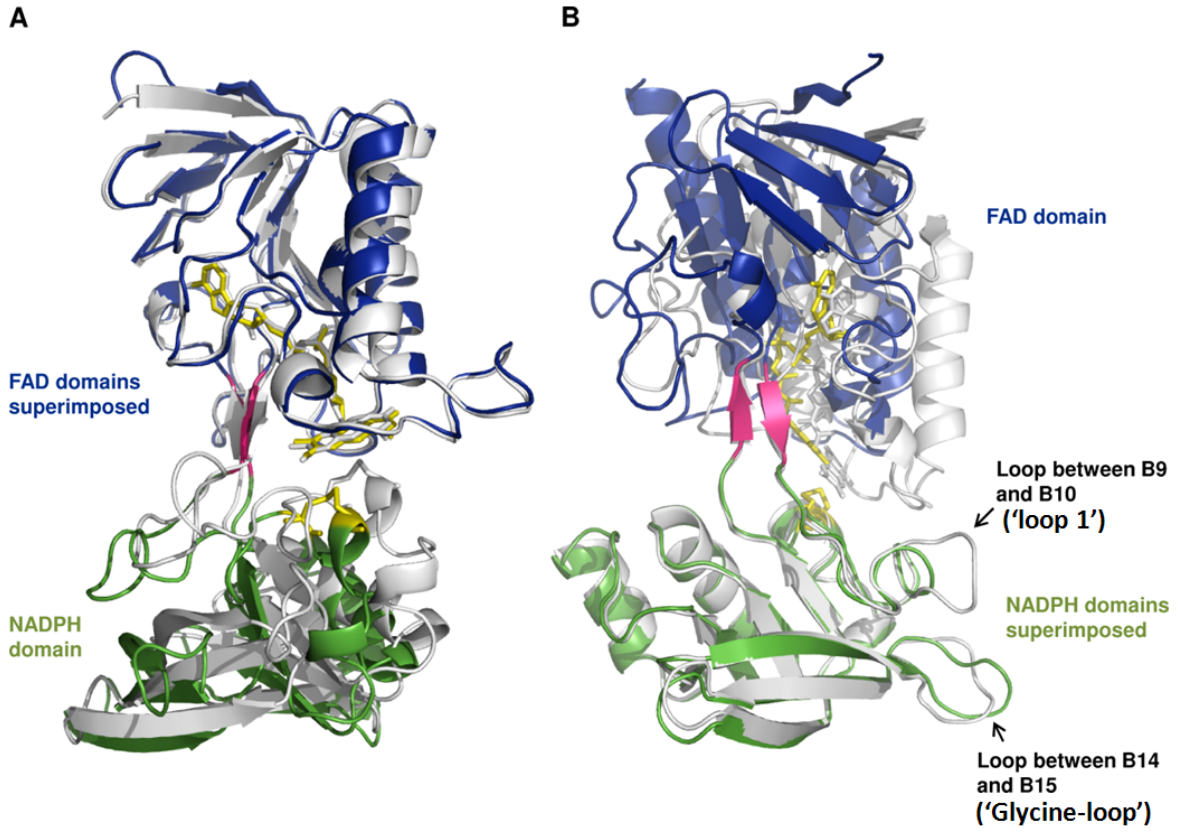

Figure 2.3. (**A**) Superposition of the FAD domain of HvNTR2 (blue, pdb accession: 2WHD) and AtNTR-B (white, pdb accession: 1VDC, Dai *et al.*, 2006). The NADPH domains (green) were not included in the superposition.

The HvNTR2 FAD and the disulfide bridge are shown in yellow and the β-strand linker in pink. (**B**) Superposition of the NADPH domain of HvNTR2 (green) and AtNTR-B. Figure modified from Kirkensgaard *et al*., 2009.

2.2.4 General NTR features

The overall structure of HvNTR2 is similar to other LMW NTRs (Dai *et al.*, 2006; Waksman *et al*., 1994; Zhang *et al*., 2009). Superposition of HvNTR2 C_α-atoms with the structure of AtNTR-B (pdb accession 1VDC, Dai *et al*., 2006) shows that they are quite comparable with r.m.s.d. of 0.7 Å and 1.0 Å for the FAD and NADPH domain, respectively (calculated as least-square-deviation using Coot, Emsley and Cowtan, 2004). However, the relative orientation of the two domains in HvNTR2 is quite different from their orientation in AtNTR-B and the other LMW NTRs in the FO conformation (Figure 2.3); the difference in orientation of the NADPH and FAD domains of HvNTR2 and AtNTR-B can be described by a 38.2% closure, a 1.0 Å translation and a 24.7° rotational twist, determined using the DynDom server (Hayward and Lee, 2002). The rotation is centred about amino acid residues 124—125 and 255—256, which are found in the short two-stranded β-sheet connecting the two domains, and it shifts the orientation of the FAD molecule with respect to the active site cysteines. The distance from $Cys148_{HvNTR2}$ to the nearest reducing nitrogen in the isoalloxazine rings is increased from the 3.4 Å observed in the structure of AtNTR-B to 5.9 Å, and the solvent accessibility of $Cys148_{HvNTR2}$ is increased by 66%. The solvent accessibility of the FAD molecule is increased by 450%. The dimer assembly is not affected by the changed subunit conformation, and FAD can still be reduced by NADPH as judged from the bleaching of the otherwise bright yellow colour of the crystals when they are subjected to a concentration of 10 mM NADPH for 30 min (the crystals crack upon this treatment).

If the structure of AtNTR-B is compared with that of EcNTR in the FR state (pdb accession 1F6M, Lennon *et al*., 2000) they differ by a minor translation of 1 Å and by a substantial 65.6° rotation about the two β-strands connecting the domains. However, comparing the structure of EcNTR in the FR conformation with the structure of HvNTR2 shows that they differ by a 6.7% closure, a translation of -1.4 Å and a rotation of 49.8°. The smaller rotation of 49.8° compared to 65.6° (for AtNTR) indicates that HvNTR2 is actually closer to the FR conformation than most other crystallised NTRs (see Chapter 1, Section 1.1.6.2). Yet, within the group of NTR structures determined in the FO conformation there

are minor variations in the relative orientation of the two domains. Superposition with EcNTR in the FO conformation requires an 8° inter-domain rotation for both AtNTR-B and ScNTR (Zhang *et al*., 2009) and an 11° rotation in the case of MtNTR (Akif *et al*., 2005) indicating that the relative position of the two domains in the absence of a target substrate is quite flexible. A room temperature structure of AtNTR-B is reported to be 2° off with respect to the relative orientation of the two domains compared to the deposited -175°C data (Dai *et al*., 1996). Unfortunately, the coordinates from this room temperature structure were not deposited in the Protein Data Bank (PDB), and it is not possible to relate it to the structural variation we observe in HvNTR2.

2.2.5 Plant specific NTR motifs

Besides HvNTR2, the structure of AtNTR-B is the only other available plant NTR structure. As mentioned, the two proteins have 75% sequence identity. A superposition of the FAD domains (Figure 2.3A) shows very similar orientation of loops, α-helices and β-sheets, and the aforementioned variation in relative domain orientation. Some major structural differences are observed in two loop regions, if the NADPH domains alone are superimposed (Figure 2.3B). The long loop region between strand B9 and B10 contains 4 additional protruding residues in AtNTR-B. The C-terminal end (called Loop 1 in the following, Figure 2.3B and 2.4) of this loop has the sequence G/E-E/K/T/D-G/A-N/P/S-G/N-G-F/Y-W-N-R-G in the dicot NTRs examined here (the four extra residues are missing in *Populus trichocarpa*), while monocot NTRs of the A/B type have the shorter sequence D-T/A-F/Y-W-N-R-G (Figure 2.4 and Appendix E: Supplementary Figure 1). The residues $Trp138_{HvNTR2}$ and $Asn139_{HvNTR2}$ from Loop 1 vary among species and were suggested by Oliveira *et al.* (2010) to contribute to the species-specificity. Notably, these residues are conserved in plant LMW NTRs (Figure 2.4).

A second loop (called the Glycine-loop in the following) is located between β-strand B14 and B15 (Figure 2.3B and 2.4). This loop is glycine-rich in HvNTR2 and other monocot NTRs, where a G-G-A/E/S-N/G/D-G-G-P motif is found. The loop is flexible as seen from a high B-factor in the crystal structure of HvNTR2. The corresponding loop in dicots appears variable in sequence and length. Both the Glycine-loop and the C-terminal part of Loop 1 are

expected to face the incoming Trx substrate molecule, based on comparison with the structure of EcNTR in complex with EcTrx (Lennon *et al*., 2000).

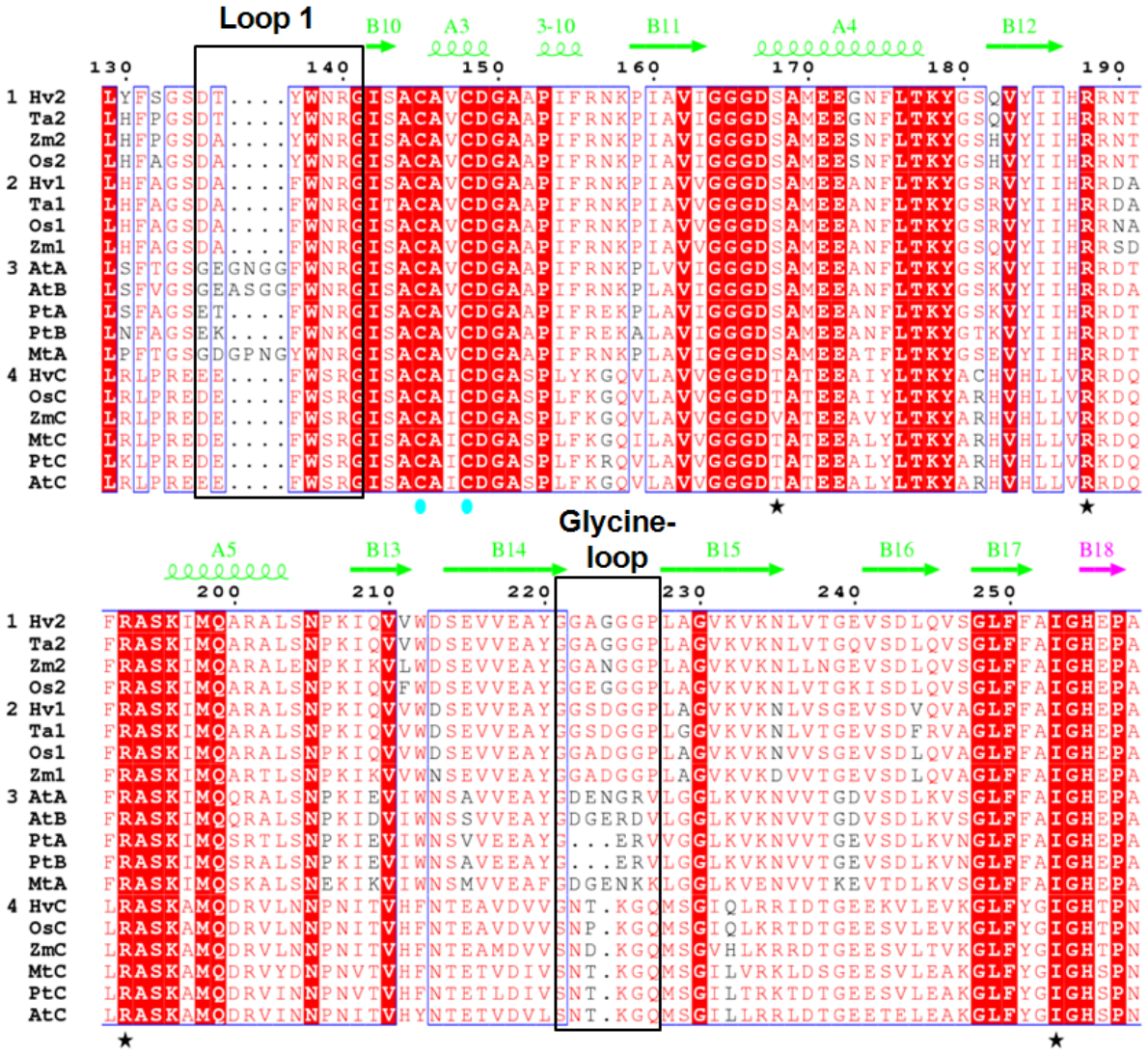

Figure 2.4. Segment of a sequence alignment of NTRs from different plants covering the two variable loop segments in plant NTRs. The complete alignment can be found in Appendix E: Supplementary material Figure 1. The NTRs and their accession numbers in parentheses are HvNTR1 (EU314717), HvNTR2 (EU250021) and HvNTRC from *Hordeum vulgare* (barley), TaNTR1 (Q8VX47) and TaNTR2 (TC297680) from *Triticum aestivum* (wheat), OsNTR1 (Q69PS6), OsNTR2 (Q6ZFU6) and OsNTRC (Q70G58) from *Oryza sativa* (rice), ZmNTR1 (EU966898), ZmNTR2 (BT054285) and ZmNTRC (BT037345) from *Zea mays* (maize), AtNTRA (Q39242), AtNTRB (Q39243) and AtNTRC (O22229) from *Arabidopsis thaliana* (Mouse-ear cress), PtNTRA (AC149479), PtNTRB (XM_002317595) and PtNTRC (XM_002308899) from *Populus trichocarpa* (western balsam poplar) and MtNTRA and MtNTRC from *Medicago truncatula* (Barrel Medic, legume). The sequences were aligned using CLUSTAL-W (Thomson *et al*., 1994) and divided into 4 groups based on the phylogenetic analysis. Group 1 and 2 are both monocotyledon subgroups of the A/B type, group 3 is the dicotyledons type A/B, and group 4 is the

subgroup of the C type NTRs, respectively. Strictly conserved residues have a red background and residues well conserved within a group according to the Risler matrix (Risler *et al*., 1988) are indicated by red letters. Residues conserved between groups are boxed. The secondary structure of HvNTR2 was added using ESPript (Gouet *et al*., 1999), and coloured according to domain; green is the NADPH domain and pink is the β-sheet linker between the two domains. Residues assumed to make hydrogen bonds to NADPH are marked by stars and the active site cysteines by cyan circles. The B9 – B10 and the B14 –B15 loops show the largest structural variation in a superposition of the HvNTR2 and the AtNTR-B structures. The primary structure of AtNTR-B in PDB entry 1VDC differs from the validated uniprot entry Q39243 at positions 120 (I→T), 135 (V→A), 136 (L→S) and 329 (E→Q). Figure modified from Kirkensgaard *et al*., 2009.

2.2.6 Inter-domain contacts and binding of FAD and NADPH

The binding sites for FAD and NADPH are described in Section 3.6—3.7 in Appendix E. The main inter-domain contacts in the FO conformation in EcNTR and AtNTR-B are centred in Loop 1 (Figure 2.5). This loop contains an arginine residue ($Arg130_{EcNTR}$ in EcNTR) conserved in plant NTR sequences ($Arg142_{AtNTR\text{-}B}$ in AtNTR-B and $Arg140_{HvNTR2}$ in HvNTR2) (Figure 2.4). It is also conserved in many NTR sequences from other species but is occasionally substituted with lysine or asparagine. $Arg130_{EcNTR}$ forms three out of seven hydrogen bonds to EcTrx upon binding of the substrate in the EcNTR FR conformation (pdb accession 1F6M, Figure 2.6). The neighbouring $Gly129_{EcNTR}$ and $Ala237_{EcNTR}$ within its spatial proximity are each involved in one hydrogen bond to EcTrx. The last two hydrogen bonds engage the active site amino acid residues, $Cys138_{EcNTR}$ and $Asp139_{EcNTR}$ (Figure 2.6).

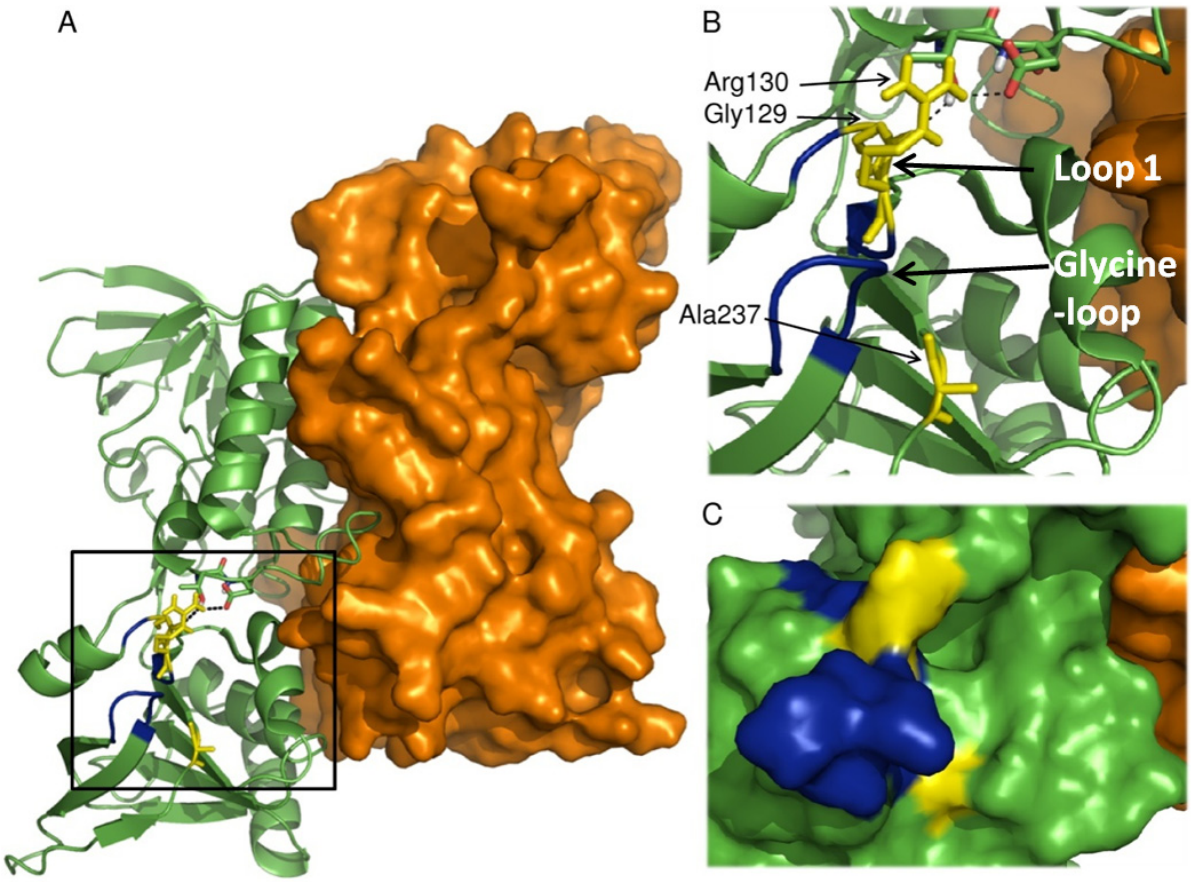

Figure 2.5. Thioredoxin binding patch defined by the covalent EcNTR-Trx complex. (**A**) The EcNTR dimer in the FO conformation (pdb accession: 1TDE, Waksman *et al*., 1994). One subunit is shown in green and the solvent accessible surface of the other in orange. Residue $Gly129_{HvNTR2}$ and $Arg130_{HvNTR2}$ in the NADPH domain form the only hydrogen bonds to the FAD domain in the FO conformation. These residues (yellow) together with Ala237 provides all (five) of the hydrogen bonds formed upon Trx binding to the FR conformation. The residues interacting in the dimer interface are adjacent to the two loops (blue) that possibly provide some selectivity towards Trx isoforms. Association of Trx to this area prior to the conformational shift would break the inter-domain hydrogen bonds and thereby facilitate the shift. (**B)** Close-up with hydrogen bonds indicated as dotted lines. (C) Solvent accessible surface of the same area. Figure modified from Kirkensgaard *et al*., 2009.

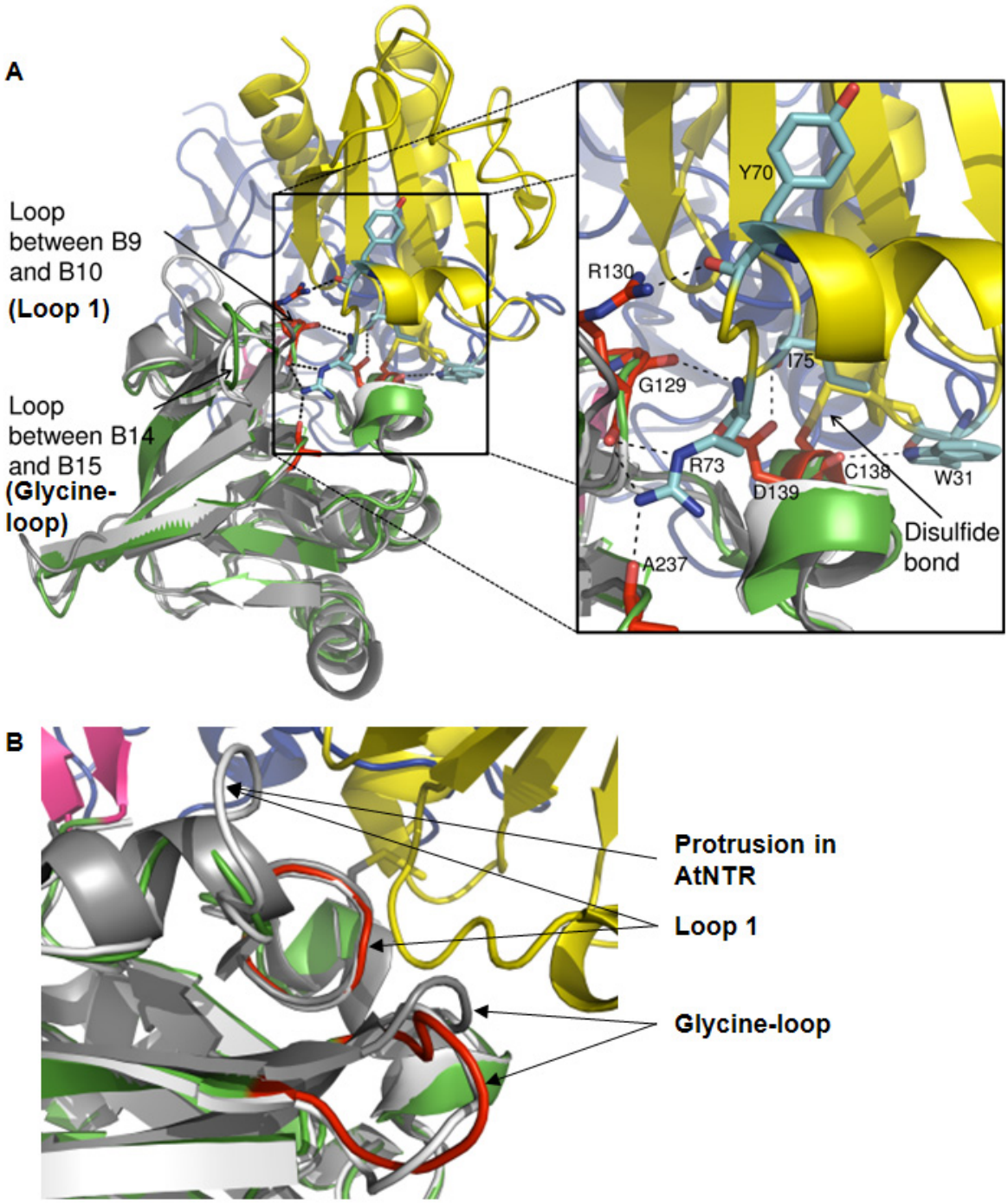

Figure 2.6. Superposition of the NADPH domains of HvNTR2, AtNTR-B (white, pdb: 1VDC) and EcNTR in the FR conformation (grey, pdb: 1F6M) covalently bound to Trx (yellow). HvNTR2 is coloured according to domain; blue is the FAD domain, green is the NADPH domain and pink is the β-sheet linker between the two domains. (**A**) The hydrogen bonds between residues in EcNTR (red) and Trx (cyan) are indicated by dotted lines. (**B**) Cartoon representation focused on the two loop areas with the largest structural variations. The loops of HvNTR2 are coloured red. Figure modified from Kirkensgaard *et al*., 2009.

2.2.7 Proposed reaction mechanism

A proposed reaction mechanism based on the structure of HvNTR2 (Kirkensgaard *et al.*, 2009; Appendix E) is described below and also discussed in Chapter 6.

The area providing the inter-domain contacts between the NADPH domain and the FAD domain in the FO state in both EcNTR and AtNTR-B supplies all hydrogen bonds specific for Trx binding besides the ones in the active site (Figure 2.5 and 2.6). If Trx is bound to this area already in the FO conformation the inter-domain contacts are lost and replaced with new ones: two hydrogen bonds are replaced by four to five new ones in the NTR-Trx interface plus van der Waals contacts. The binding of Trx could be guided by Loop 1 and the Glycine-loop (Figure 2.5B). These loops are free to interact with Trx in the FO conformation as seen from the structure of EcNTR (Figure 2.5).

A third loop (called the FAD-loop hereafter) found between strand B3 and a short 3_{10}-helix has been predicted to bind to Trx (Zhang *et al*., 2009). Dicot NTRs have a strictly conserved E-G-W-M-A-N-D-I-A-P-G-G sequence in this area, while monocot NTRs display more sequence variation and invariably have the proline exchanged with an alanine (see Chapter 4; Figure 4.5A). Simultaneous binding of Trx to the FAD-loop and active site cysteines would require the NTR domain twist to have occurred.

If the structure of HvNTR2 indeed is an intermediate between the FO and the FR conformation, it can be postulated that there is not room for bound NADPH during the domain rotation step (Figure 2.7B, clashes between $NADP^+$ and HvNTR2 are circled). The structure of EcNTR in the FR conformation (pdb accession 1F6M) shows that the NADPH binding site is relatively accessible (Figure 2.7C and D) suggesting that NADPH may bind to NTR after the conformation shift from FO to FR. If Trx is needed for efficient conformational shift from the FO to the FR conformation, it can be assumed that the NTR domain rotation primarily takes place when Trx is available.

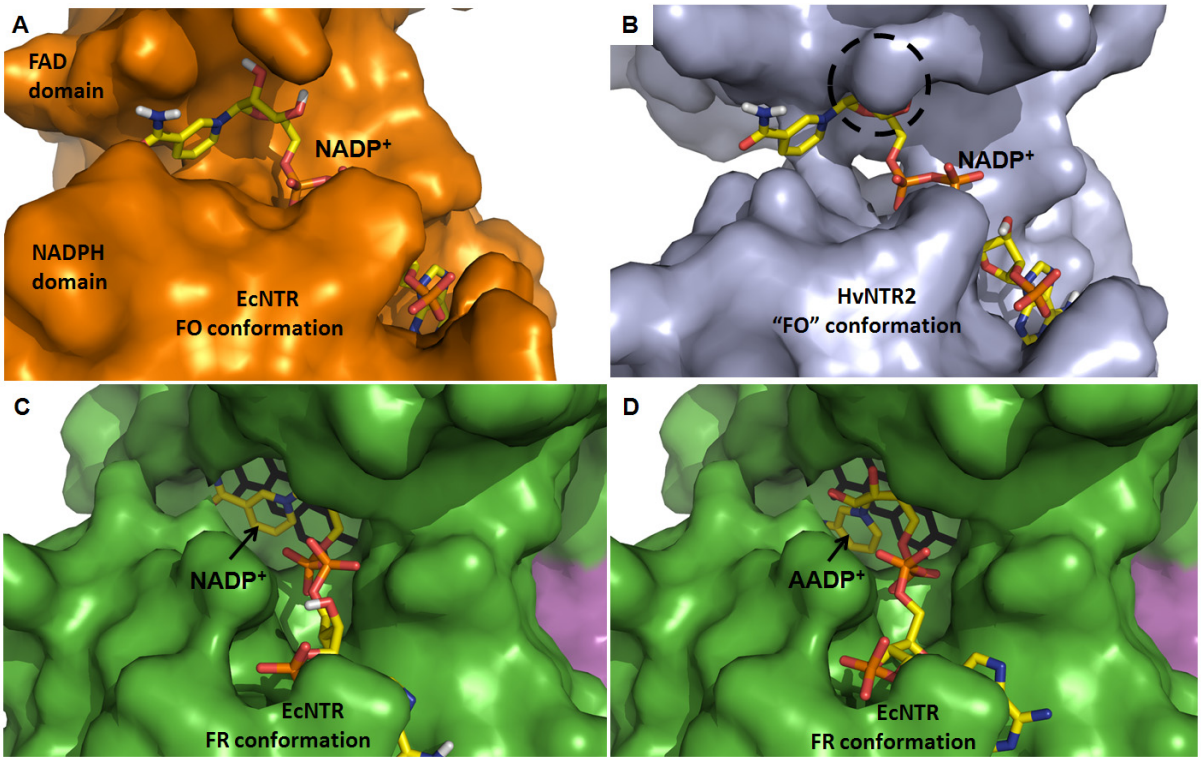

Figure 2.7. NADPH binding-sites in different NTRs. The NADPH binding domains of various NTRs were superposed enabling the NADP+ molecule from EcNTR (in the FO conformation) to be depicted in the other structures. (**A**) EcNTR in the FO conformation (pdc accession: 1tdf, Waksman *et al.*, 1994) shown with NADP+ bound. (**B**) HvNTR2 in a conformation nearest the FO conformation (pdb accession 2WHD, Kirkensgaard *et al.*, 2009) depicted with $NADP^+$ from pdb accession 1TDF. Clashes between the two are circled. (**C**) EcNTR (pdb accession 1F6M, Lennon *et al.*, 2000) in the FR conformation from a complex with Trx (purple in the background) depicted with $NADP^+$ from pdb accession 1TDF. (**D**) Same as (**C**) but depicted with 3-amino-pyridine adenine dinucleotide phosphate ($AADP^+$), the nonreducing $NADP^+$ analogue in whose presence the crystals were grown.

A new reaction mechanism is suggested based on the observations that i) the NADPH binding site is not accessible in the structure of HvNTR2 (Figure 2.7B), ii) the NADPH binding site seems accessible in the FR conformation (Figure 2.7C and D) allowing NADPH to bind after the FO to FR conformational change, and iii) loops (Loop 1 and the Glycine-loop) that may be involved in the binding of Trx are accessible in the FO conformation. The proposed reaction mechanism involves a partial binding of Trx to the NADPH domain already in the FO conformation (Figure 2.8). After a domain rotation Trx can be bound to the FAD domain as well. NADPH is proposed to bind in the FR conformation and directly reduce FAD.

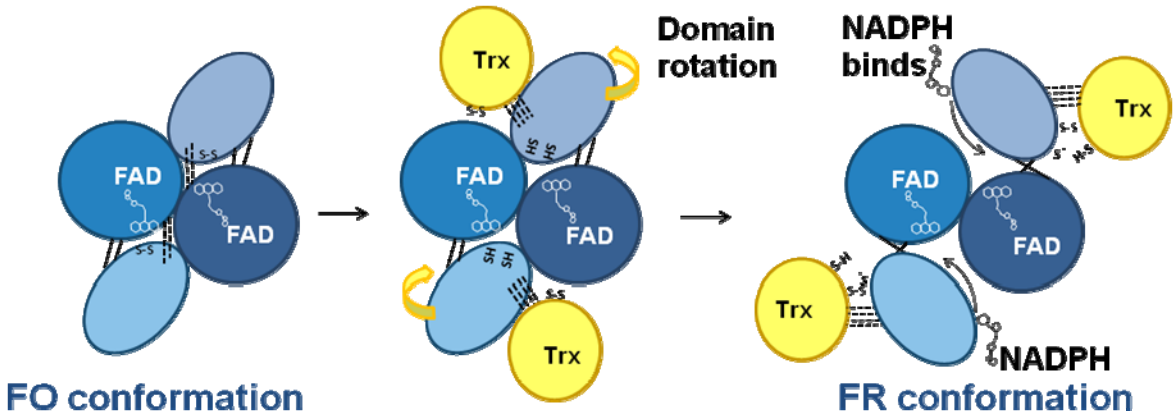

Figure 2.8. The NTR reaction scheme proposed in Kirkensgaard *et al*. (2009) modified to take the observation of differences in inter-domain interactions and lack of space for NADPH binding in the HvNTR2 crystal structure into account. Hydrogen bonds are shown by dotted lines. Trx is proposed to be partially bound in the FO conformation and initiate a conformational shift from FO to FR. NADPH is assumed to bind in the FR conformation. Figure modified from Kirkensgaard *et al*., 2009.

2.3 Conclusion

Hexagonal protein crystals of recombinant HvNTR2 which diffracted to 2.6 Å were obtained. The structure consists of the FAD binding domain and the NADPH binding domain, and is very similar to other LMW NTRs. However, the relative orientation of the two domains is quite different from those in AtNTR-B and other LMW NTRs in the FO conformation. The difference in orientation of the NADPH and FAD domains of HvNTR2 and AtNTR-B can be described by a 38.2% closure, a 1.0 Å translation and a 24.7° rotational twist. It is suggested that this structure represents an intermediate between the FO and the FR conformation indicating that the conformational change does not occur as a pure rotation, but could also involve bending of one domain relative to the other. The observed structure of HvNTR2 is not able to accommodate NADPH (Figure 2.7B). The NADPH binding site in the FR conformation of EcNTR (bound to ExTrx) is relatively open and may be accessible to NADPH (Figure 2.7C). Therefore it is suggested here that NADPH binds NTR after the shift to the FR conformation. The relative position of the domains in HvNTR2 increases the accessibility near the active site cysteines compared to other LMW NTRs in the FO conformation, which may enable partial binding of HvTrxh1/2 in the FO conformation possibly involving some of the loops in the NADPH domain. After the conformational change (to FR) HvTrxh1/2 may bind to the FAD domain which is predicted to involve the FAD-loop.

2.4 Materials and methods

2.4.1 Expression and purification of HvNTR2

Recombinant HvNTR2 was expressed in *E. coli* Rosetta (DE3) (Novagen) with the N-terminal His-tag MGSSHHHHHHSSGLVPRGSH as described previously (Shahpiri *et al*., 2008a). More specifically, His_6-HvNTR2 was purified on a HisTrap HP affinity column (GE Healthcare) pre-equilibrated with 10 mM imidazole, 0.5 M NaCl and 30 mM Tris-HCl pH 8.0 and eluted by a 0–100% gradient of 400 mM imidazole, 0.5 M NaCl and 30 mM Tris-HCl pH 8.0. Finally, the protein was dialyzed against 10 mM Tris-HCl pH 8.0, the purity checked by SDS-PAGE and the sample concentrated on an Amicon Ultra centrifugal filter unit (10 kDa MWCO, Millipore) to an OD_{280} of 3.96 corresponding to a concentration of approx. 2.5 mg mL^{-1}. The His_6-HvNTR2 solution was used for crystallisation experiments without further purification and was not subjected to thrombin cleavage.

2.4.2 Crystallisation and data collection

Initial crystal screening experiments were carried out using the PEG6000 grid-screen (Hampton Research) and the hanging drop vapour diffusion method. Drops of 2.0 µL protein solution were mixed with 2.0 µL reservoir solution and equilibrated over a reservoir of 500 µL. Yellow needles were detected in 5% (w/v) PEG6000 (Fluka) and 0.1 M citric acid-buffer pH 4.0 after four d of incubation at 22°C. Fine tuning of crystallisation conditions included screening of PEG concentration, the effect of the PEG molecular weight and the Hampton Research additive screen. Optimised results were obtained with 24% (w/v) PEG400, 2% (w/v) of the polyetheramine Jeffamine® M-600, 0.1 M citric acid-buffer pH 3.5, a protein concentration of 5.7 mg mL^{-1} and a temperature of 25°C. These conditions gave bright yellow crystals with hexagonal morphology within a week. The diameter of the crystals reached up to 0.18 mm. The crystals were flash-frozen directly from the drop without using additional cryo-protectants.

The final X-ray data set was collected at 100 K at the ID14-2 beamline at ESRF in Grenoble using a wavelength of 0.933 Å. A total of 120 frames were collected each covering an oscillation width of 0.5°. The data were indexed and integrated using MOSFLM (Leslie, 1992) and scaled using the program SCALA from the CCP4 suite (Collaborative Computing

Project, 1994). The best crystal diffracted to a resolution of 2.6 Å and belongs to the space group P6222 with unit cell parameters a = b = 133.7 Å and c = 166.1 Å. Assuming 2 molecules in the asymmetric unit gives a Mathews coefficient of 2.90 $Å^3$ Da^{-1} (Matthews, 1968). Final data collection and processing statistics are summarised in Table 2.1.

2.4.3 Structure determination and refinement

Molecular replacement was performed with the program MOLREP (Vagin and Teplyakov, 2000) from CCP4 using the structure of AtNTR-B as the initial search model. The HvNTR2 and AtNTR-B sequences are 75% identical. Significant molecular replacement solutions were only found when the FAD and the NADPH domains were used as independent search models. The model was first refined using REFMAC5 (Murshudov *et al*., 1997) and at later stages using Phenix (Adams *et al*. 2002). This including TLS (Translation Libration Screw-motion) refinement to describe anisotropic displacement interspaced with manual model rebuilding in Coot (Emsley and Cowtan, 2004) using the Coot validation procedures and MolProbity (Davis *et al*., 2007) to correct problematic areas of the model. The final model has an R_{cryst} of 19.0% and an R_{free} based on 5% of the reflections of 23.8%. The R_{free} reflections were picked by random selection of reflections.

The two molecules in the asymmetric unit, which do not represent the functional dimer, were divided in 5 TLS segments each using the TLSMD server (Painter and Merritt, 2006). The TLS segments in the A molecule in the asymmetric unit are residues 6—71, 72—127, 128—181, 182—258 and 259—323. In the B molecule, the TLS segments cover residues 5—60, 61—127, 128—168, 169—255 and 256—323. The two first TLS segments in each molecule belong to the FAD domain; the following two belong to the NADPH domain, while the last segment corresponds to the C-terminal of the FAD domain. Due to the limited resolution of the data, only 48 solvent molecules have been included and only where >3σ F_{obs}-F_{calc} electron density with optimal hydrogen bonding distances to hydrogen donor or acceptors were found. Four citrate molecules were included in excess electron density due to the appropriate size and geometry of this molecule and presence of citrate in the crystallisation conditions. Two citrate ions are bound in each NADPH domain. Some excess $2F_{obs}$-F_{calc} electron density in the active site adjacent to the FAD isoalloxazine could not be satisfactorily modelled by solvent or citrate. Parameters for the refined model are

summarised in Table 2.1. Solvent accessibility was calculated using Areaimol from the CCP4 suite with a 1.4 Å radius probe (Collaborative Computing Project, 1994). Differences in domain orientation were analysed using the DynDom server (Hayward and Lee, 2002). Superpositions were done in Coot (Emsley and Cowtan, 2004). Inter-domain and ligand interactions were plotted using the program LIGPLOT (Wallace *et al*., 1995). The molecular coordinates and structure factors have been deposited in the protein data bank with the accession code 2WHD and SFWHD, respectively.

Chapter 3

Formation of a complex between barley thioredoxin and NADPH-dependent thioredoxin reductase

3.1 Introduction

Most crystal structures of LMW NTRs determined so far are in the FO conformation, as described in Chapter 1, Section 1.1.6.2. As mentioned, Lennon *et al.* (2000) succeeded in solving the crystal structure of NTR from *E. coli* trapped in the FR conformation through an intermolecular disulfide bond to EcTrx. The disulfide was formed between the active site cysteines, and thus the crystal structure of this binary complex is suggested to represent a reaction intermediate (Chapter 1, Figure 1.15, Lennon *et al*., 2000). Comparison with structures of LMW NTRs of eukaryotic origin in the FO conformation from *A. thaliana* (Dai *et al*., 1996) barley (Kirkensgaard *et al*., 2009) and yeast (Zhang *et al.*, 2009; Oliveira *et al*., 2010) suggests major differences in the putative Trx-NTR interface area. To obtain insight into how NTRs from eukaryotic organisms bind Trx, it was attempted to produce and crystallise a complex of NTR and Trx from barley.

As mentioned in Chapter 1 a crystal structure has previously been reported of HvTrxh2 trapped in a reaction intermediate by an intermolecular disulfide bond (involving the active site) to the substrate protein BASI (Maeda *et al*., 2006a) (described in details in Chapter 4, Section 4.2.3). Hence, the HvTrxh2 isoform was used for NTR:Trx complex formation to enable comparison of features involved in Trx target recognition and the elements involved in binding to NTR. HvNTR2 was selected as partner for complex formation since the structure of this isoform has been determined (Kirkensgaard *et al*., 2009) and has previously been shown to react most efficiently with HvTrxh2. The k_{cat}/K_m ratios were thus determined to be $2.31x10^6$ $s^{-1}M^{-1}$ and $0.73x10^6$ $s^{-1}M^{-1}$ using HvTrxh2 as a substrate for HvNTR2 and HvNTR1, respectively (Shahpiri *et al*., 2008a).

The strategy for producing a stable disulfide linked complex of HvNTR2:HvTrxh2 was essentially the same as described previously (Chapter 1, Figure 1.14B, Veine *et al*., 1998a, Wang *et al*., 1996), which involved using single-cysteine mutants of HvNTR2 and HvTrxh2. Attempts to produce and purify the complex is described in the following.

3.2. Results and discussion

3.2.1 Formation of an intermolecular disulfide

In EcNTR $Cys138_{EcNTR}$ is proposed to initiate formation of the intermolecular disulfide bond through nucleophilic attack on EcTrx (Chapter 1, Figure 1.15; Lennon *et al*., 2000). This amino acid residue corresponds to $Cys148_{HvNTR2}$ in HvNTR2. The positions of the active site cysteines of HvNTR2 in the FR conformation were modelled by superposing the individual domains from the crystal structure of HvNTR2 described in Chapter 2 (pdb 2WHD, Kirkensgaard *et al*., 2009) to the corresponding domains of EcNTR from the EcNTR:EcTrx complex (Lennon *et al*., 2000) using Coot (Emsley and Cowtan, 2004). The resulting model is displayed in Figure 3.1 (a more comprehensive modelling of HvNTR2 in the FR conformation is presented in Chapter 4). $Cys145_{HvNTR2}$ appears more buried in this rough model, as assessed from the calculated solvent accessible surface areas for $Cys148_{HvNTR2}$ (89.10 $Å^2$) and $Cys145_{HvNTR2}$ (15.6 $Å^2$) using a 1.4 Å probe in the program AreaiMol from the CCP4 suite (Collaborative Computing Project, 1994).

These observations suggest that $Cys148_{HvNTR2}$ is likely to be involved in the initial nucleophilic attack on the disulfide bond in HvTrxh2. To investigate this further, the single cysteine mutants HvNTR2_C145S and HvNTR2_C148S were produced and purified (see Methods and Material, Section 3.4.1). These mutants were reacted with HvTrxh2_C49S-TNB, a single cysteine mutant of HvTrxh2 activated with 2-nitro-5-thiobenzoate (TNB) as described in Section 3.4.2, and the release of TNB was followed spectrophotometrically at 412 nm. The NTR mutants were first treated with 10 mM DTT for 30 min at room temperature, and excess DTT was removed using a NAP-5 column prior to the complex formation. Both HvNTR2_C145S and HvNTR2_C148S were able to react with HvTrxh2_C49S-TNB, but HvNTR2_C145S appears more reactive than HvNTR2_C148S (Figure 3.2), in good agreement with the accessible surface areas determined above.

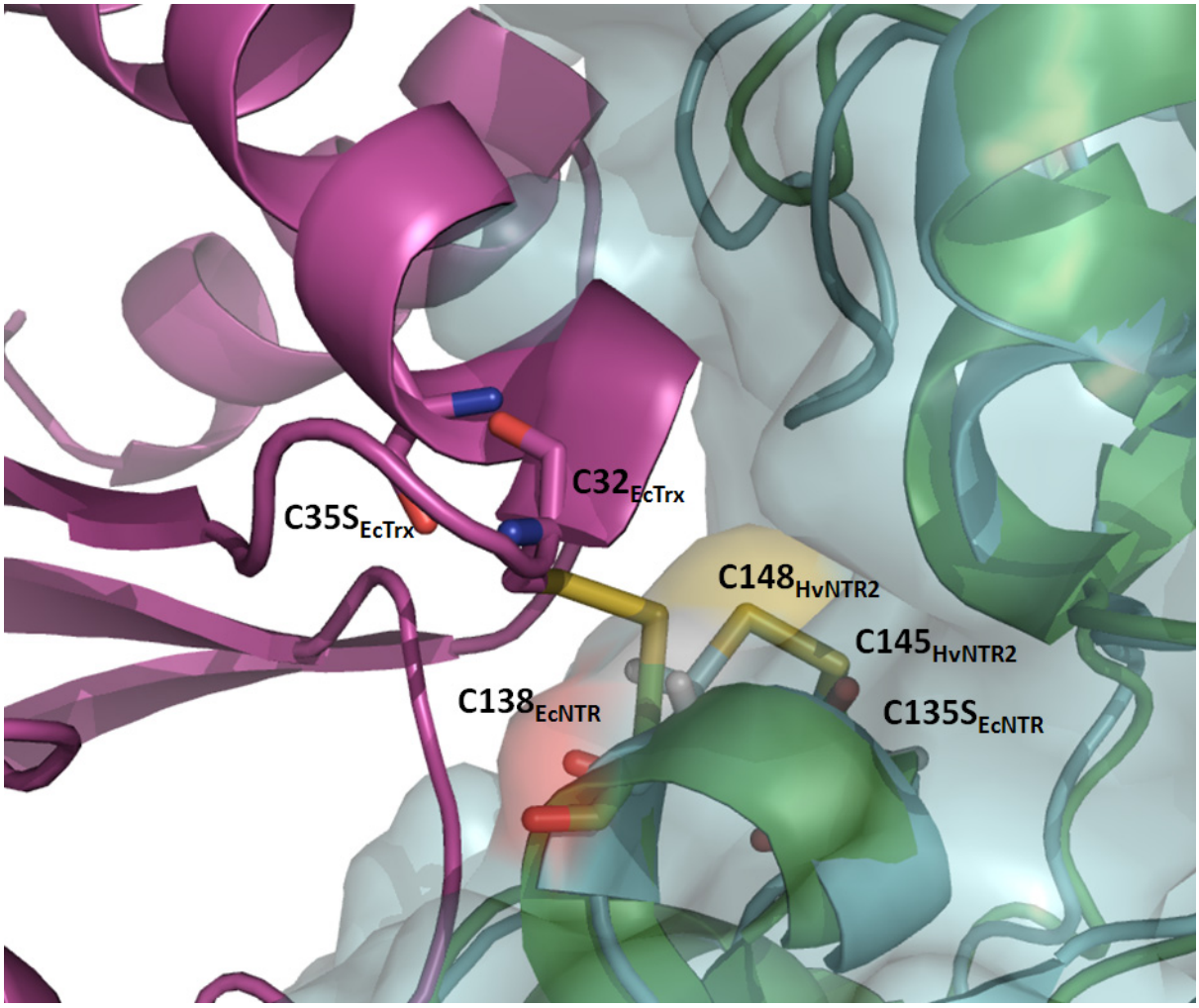

Figure 3.1. Predicted positions of active site cysteines in the FR conformation of HvNTR2. A rough model of the FR conformation of HvNTR2 (cyan) was produced by superposing the two individual domains of HvNTR2 (from crystal structure described in Chapter 2, pdb accession 2WHD, Kirkensgaard *et al.*, 2009) to the corresponding domains of EcNTR (green) in the FR conformation bound by an intermolecular disulfide to EcTrx (magenta) (pdb 1F6M, Lennon *et al.*, 2000). HvNTR2 is in the oxidised state with a disulfide between $C145_{HvNTR2}$ and $C148_{HvNTR2}$. The surface of HvNTR2 is shown, indicating that $C148_{HvNTR2}$ HvNTR2 is the most accessible active site cysteine in this model of HvNTR2.

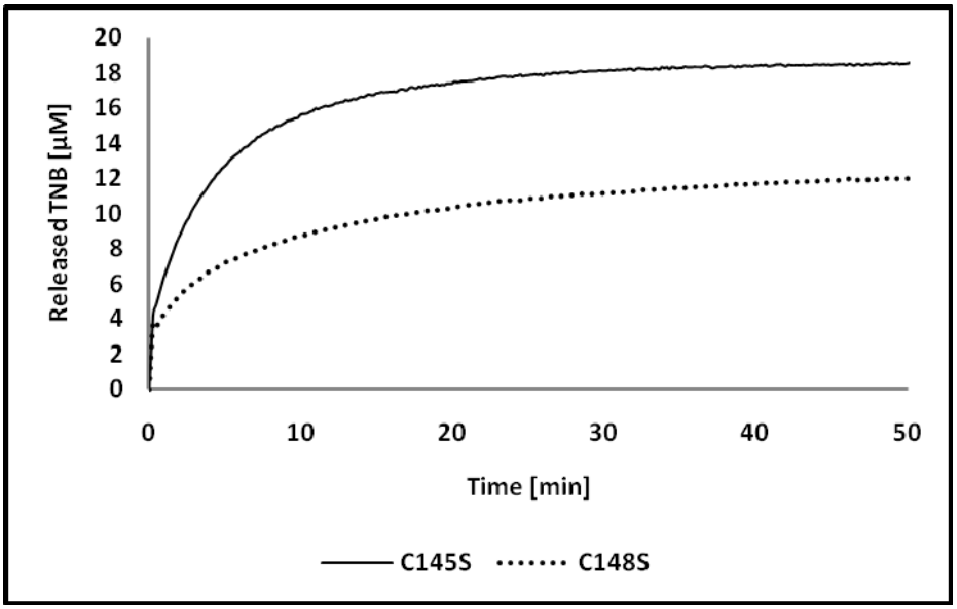

Figure 3.2. The time course of the reaction between 30 µM HvNTR2_C145S or HvNTR2_C148S with 20 µM TNB-conjugated HvTrxh2_C49S. The NTRs were first treated with 10 mM DTT for 30 min at room temperature, and excess DTT was removed using a NAP-5 column prior to the complex formation. Release of TNB monitored at 412 nm was calculated using an extinction coefficient of 13,600 M^{-1} cm^{-1} (Ellman, 1959).

It was previously shown that the complex formation was faster when EcNTR_C135S was conjugated to TNB instead of EcTrx_C35S. Hence, the half time ($t_{½}$) of the reaction between EcTrx_C35S and EcNTR_C135S-TNB was <5 s, whereas $t_{½}$ of the opposite reaction (EcNTR_C135S with EcTrx_C35S-TNB) was ≈1min (Veine *et al.*, 1998a). However, HvNTR2 has three additional cysteines in the FAD domain (Figure 3.3). $Cys14_{HvNTR2}$ is buried in the structure, while $Cys78_{HvNTR2}$ and $Cys310_{HvNTR2}$ are located at the NTR dimer interface. If part of the dimer interface area is exposed during the switch from the FO to FR conformation or if an equilibrium exist between dimeric and monomeric forms of NTR, there is a risk that TNB could react with these additional cysteines of the NTR monomer instead of the active site cysteine. Although this scenario is probably unlikely, since the dimer interface is large and no monomer was observed during size exclusion chromatography (see Chapter 5, Figure 5.4 and Table 5.1), it was decided to conjugate TNB with Trx, to prevent formation of unwanted intermolecular disulfides.

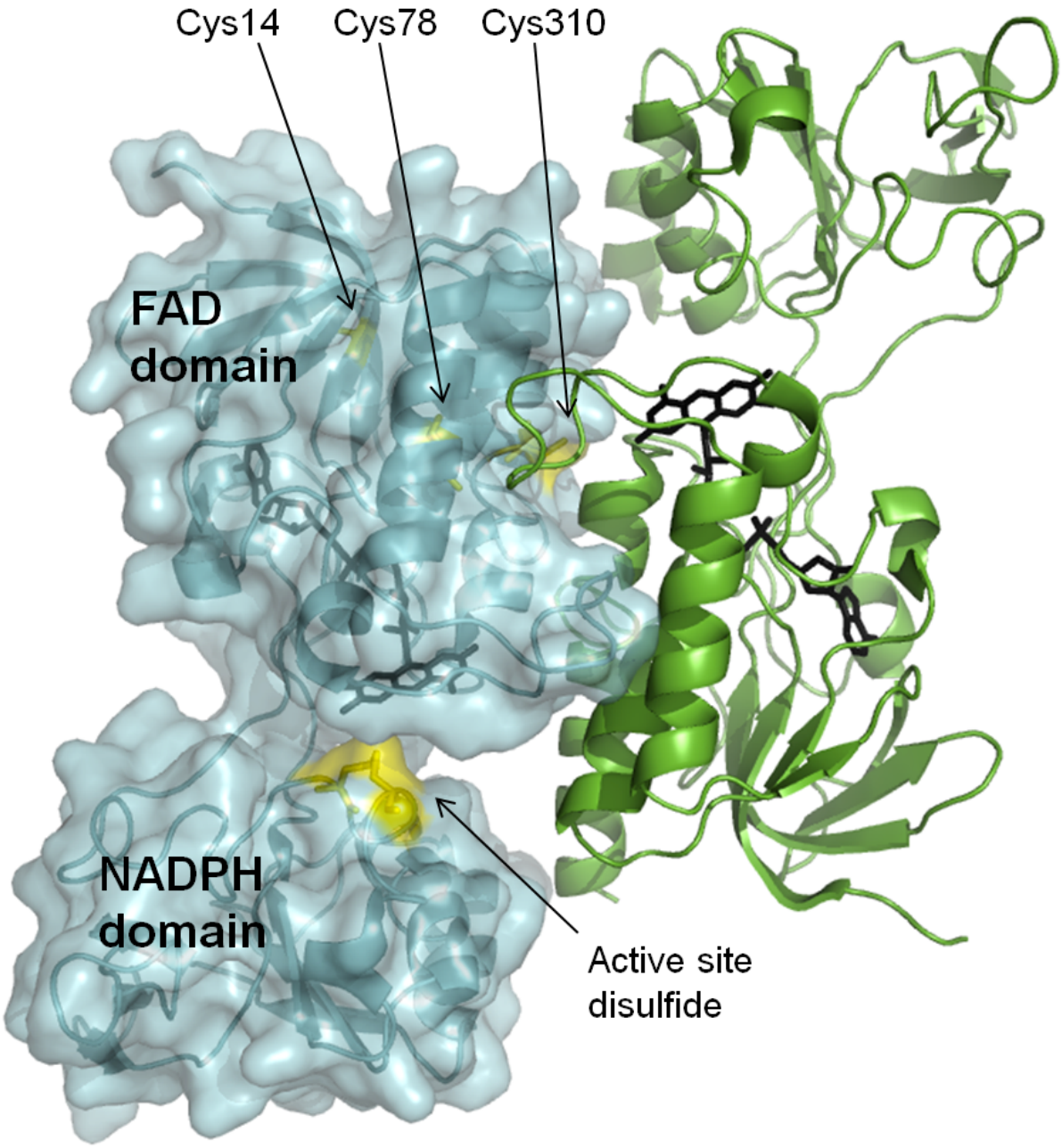

Figure 3.3. Position of cysteines in HvNTR2 (pdb 2WHD, Kirkensgaard *et al*., 2009). A dimer of HvNTR2 is shown coloured by chain (cyan and green). For one of the monomers the surface is shown (cyan) as well as the position of the cysteine residues (yellow). Three cysteines (which are not a part of the active site) are all positioned in the FAD domain; $Cys14_{HvNTR2}$ is buried in the structure, whereas $Cys78_{HvNTR2}$ and $Cys310_{HvNTR2}$ are located at the NTR dimer interface.

HvNTR2_C145S (45 µM) was reacted with 60 µM HvTrxh2_C49S-TNB and the release of TNB was measured at 412 nm (Figure 3.4). The reaction was slow if HvNTR2_C145S was not treated with DTT prior to the reaction (red curve, Figure 3.4). To attempt to increase the amount of product, HvNTR2_C145S was treated with DTT to fully reduce the free cysteine,

Cys148$_{HvNTR2}$ and DTT was removed before the reaction with HvTrxh2_C49S-TNB using a PD-10 desalting column (this was also done for the reactions in Figure 3.2). This resulted in a significant increase in the reaction rate with HvTrxh2_C49S-TNB (blue curve, Figure 3.4). A control with only buffer and 10 mM DTT was made to ensure that all DTT was removed on the PD-10 column (black curve Figure 3.4).

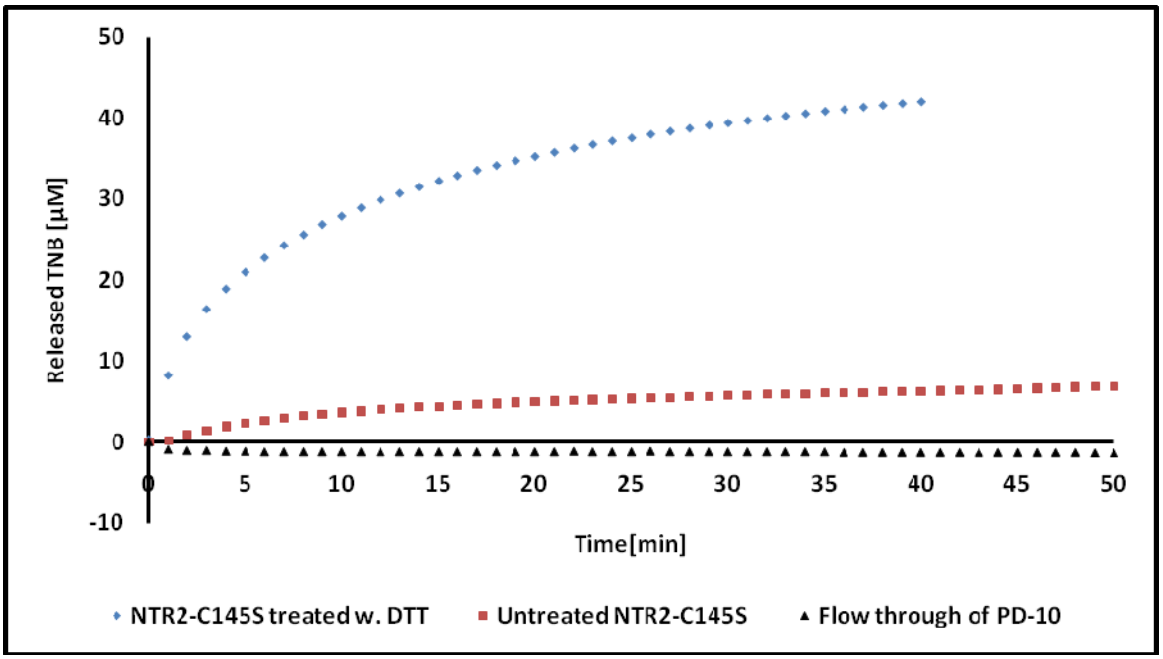

Figure 3.4. The time course of the reaction between HvNTR2_C145S and HvTrxh2_C49S-TNB. HvNTR2_C145S (45 µM) was reacted with 60 µM HvTrxh2_C49S-TNB and the release of TNB monitored at 412 nm. HvNTR2_C145S was either untreated or treated with 10 mM DTT for 1 h at room temperature. DTT was removed prior to the reaction using a PD-10 desalting column. As a control buffer containing 10 mM DTT was purified on the PD-10 column and reacted with HvTrxh2_C49S-TNB ('Flow through of PD-10').

3.2.2 Complex purification by using His-tagged proteins

The products of the reaction between HvNTR2_C145S and HvTrxh2_C49S-TNB (from Figure 3.4) were separated by size exclusion chromatography (Section 3.4.1.2). The chromatogram (blue curve, Figure 3.5) contains three main peaks of which peak 2 is asymmetric. Protein from individual fractions of the three peaks were analysed by SDS-PAGE (Figure 3.6 and Section 3.4.5).

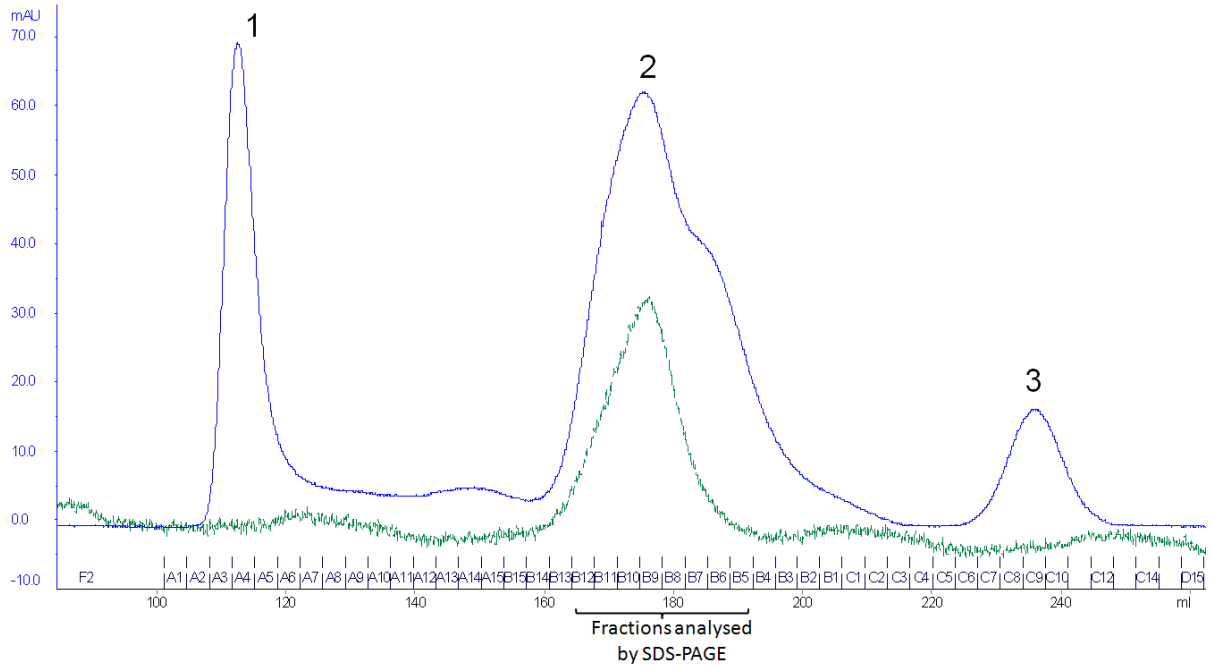

Figure 3.5. Products of the reaction between HvNTR2_C145S and HvTrxh2_C49S-TNB separated by size exclusion chromatography. After reacting 45 µM HvNTR2_C145S with 60 µM HvTrxh2_C49S-TNB (blue curve in Figure 3.4) for 1h, the resulting products were separated by gel filtration on a HiLoad™ 26/60 Superdex™ 200 column (blue curve). Protein from the individual fractions of the three peaks was analysed using SDS-PAGE (Figure 3.6). Fractions B12—B7 from peak 2 were later pooled and further purified on a MonoQ column (see below) and rerun on the gel filtration column (green curve).

The theoretical molecular weight (MW) of His-tagged HvNTR2_C145S and HvTrxh2_C49S is 35,941 Da and 15,313 Da respectively, resulting in a predicted MW of approximately 51.3 kDa and 102.6 kDa for a monomeric and a dimeric HvNTR2_C145S:HvTrxh2_C49S complex, respectively. The first peak in the chromatogram is located at the column void volume and most likely contains aggregated protein, as supported by SDS-PAGE in the absence of DTT, showing a major protein band at the top of the gel (left gel, fraction A4, Figure 3.6). Even the SDS-PAGE gel with DTT treated samples shows both NTR dimer and larger oligomers (right gel, fraction A4 and HvNTR2_C145S, Figure 3.6). Peak 1 also contains a band which match the predicted MW of the HvNTR2:HvTrxh2 complex (referred to as NTR:Trx), which disappears upon treatment with DTT. Peak 2 shows a shoulder towards the lower MWs, which contains mainly Trx dimer (expected MW 30.6 kDa) according to the SDS-PAGE gel (left gel, fractions B8—B5). A band matching the NTR:Trx complex is observed (most prominent in fractions B12 and B11 of

peak 2), as well as bands matching free NTR and Trx. It is plausible that free Trx derives from dissociated Trx:NTR complex since the observed monomeric form is expected to show a longer retention time (peak 3). Dissociation of the complex may potentially either occur during sample preparation or gel electrophoresis. High MW bands may correspond to Trx tetramer, NTR dimer and complex dimer. Peak 3 appears to contain mainly monomeric Trx.

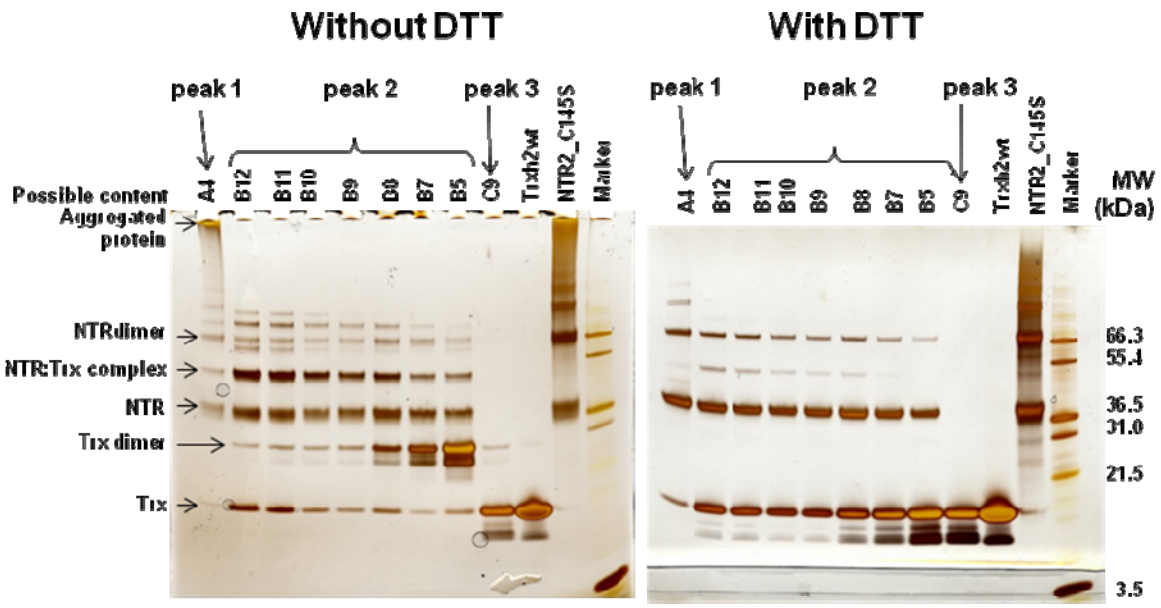

Figure 3.6. SDS-PAGE analysis of various fractions (indicated) from a mixture of HvNTR2_C145S reacted with HvTrxh2_C49S-TNB and separated by gel filtration on a HiLoad™ 26/60 Superdex™ 200 column (Figure 3.5, blue curve). Isolated Trxh2wt and NTR2_C145S were used as references. The 4—12% NuPage gels are silver-stained, and the samples in the right gel have been treated with 100 mM DTT.

Further purification of the pooled fractions B7—B12 from peak 2 (Figure 3.5) on a MonoQ anion exchange chromatography column (Section 3.4.1.3) resulted in two peaks (blue curve Figure 3.7). SDS-PAGE analysis suggests that the minor peak 1 contains mainly Trx dimer (lane 2, Figure 3.8) in agreement with the elution profile of HvTrxh2_C49S separated under the same conditions (brown curve Figure 3.7). Peak 2 contains bands corresponding to NTR:Trx but also free NTR and Trx (lane 3, Figure 3.8). The appearance of free NTR and Trx may partly be due to dissociation of the complex during SDS PAGE analysis, but may also represent co-eluting HvNTR2_C145S (peak a in Figure 3.7). Peak 2 (blue curve, Figure 3.7) was rechromatographed on a MonoQ column, with a less steep gradient, which again resulted in two peaks (*chromatogram not shown*).

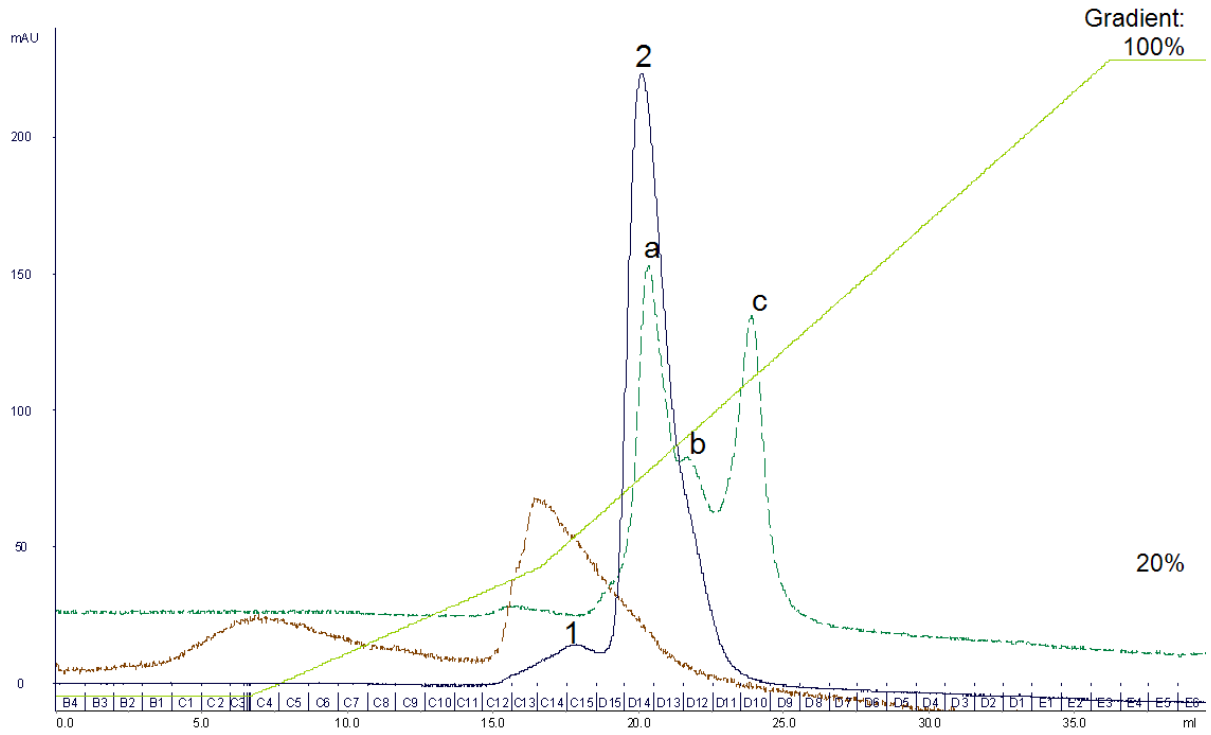

Figure 3.7. Anion exchange separation of peak 2 from the gel filtration chromatogram (Figure 3.5) on a MonoQ column (blue curve). The green and brown curves represent controls of isolated HvNTR2_C145S and HvTrxh2_C49S, respectively, separated under the same conditions. The gradient shown in light green indicates the percentage of buffer B (10 mM Tris-HCl pH 8.0 and 1 M NaCl). Buffer A contains 10 mM Tris-HCl pH 8.0.

Further separation by gel filtration on a HiLoad 26/60 Superdex 200 column demonstrated that the shoulder representing Trx dimer has been eliminated (green curve, Figure 3.5).

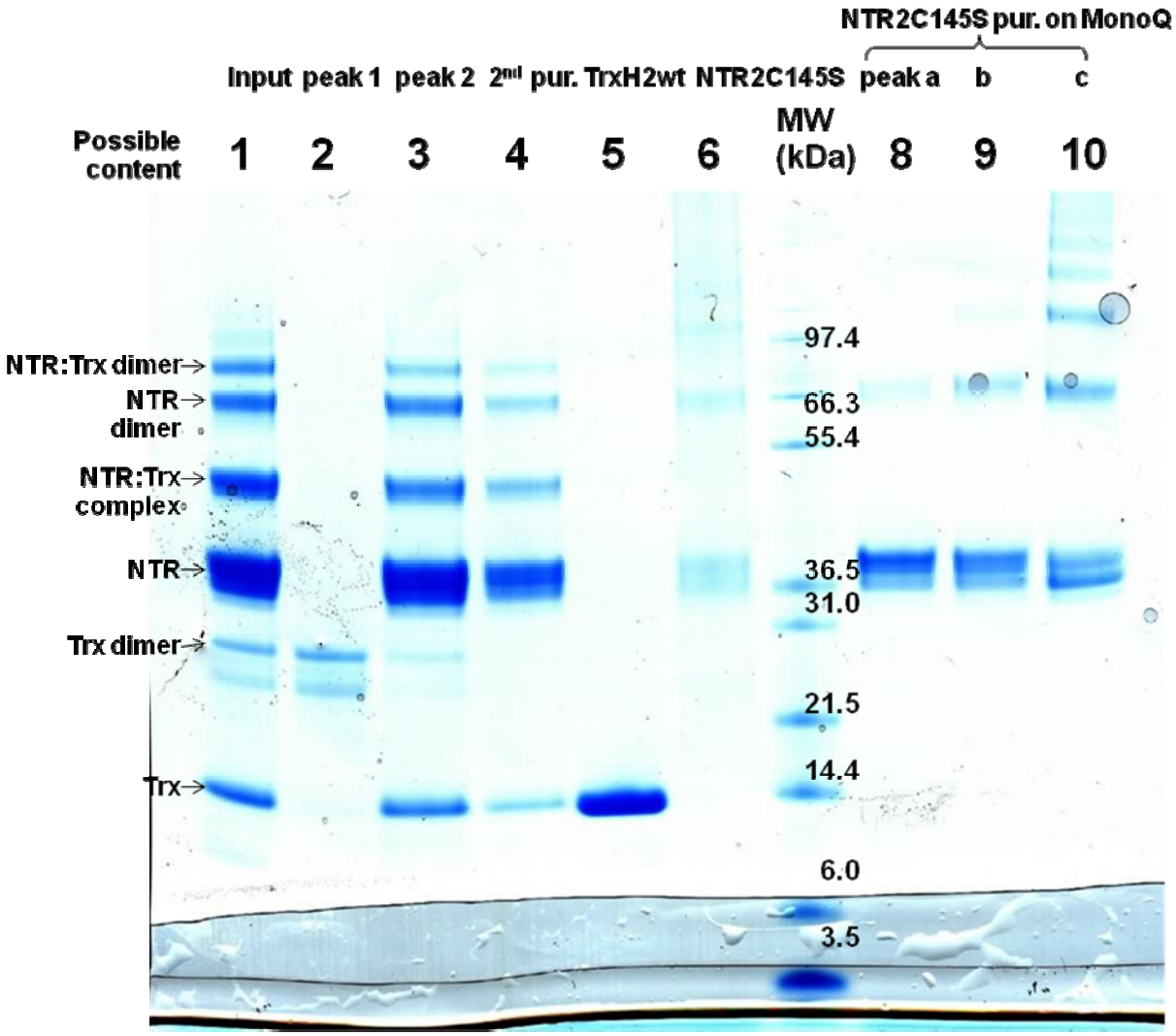

Figure 3.8. SDS-PAGE analysis of anion exchange separation of NTR:Trx on a MonoQ column (blue curve, Figure 3.7). **Lane 1:** input on the column (fraction B7—B12 from gelfiltration, Figure 3.5), **lane 2 and 3**: peak 1 and 2 respectively (blue curve, Figure 3.7), **lane 4** sample from rechromatographed peak 2 (lane 3), **lane 5**: HvTrxh2wt, **lane 6**: HvNTR2_C145S, **lane 8—10:** peak a-c from HVNTR2_C145S separated under the same conditions (green curve of Figure 3.7). The gel is a Coomassie stained 4—12% NuPage gel.

3.2.2.1 Attempts to separate free NTR from complex

Due to the co-elution of HvNTR2_C145S and the NTR:Trx complex (Figure 3.7) it was attempted to remove HvNTR2_C145S by other means. Wang *et al*. (1996) showed that unreacted EcNTR_C135S has a different solubility profile than the complex of EcNTR:EcTrx. By lowering the pH to 5.4 Wang *et al.* managed to precipitate unreacted EcNTR_C135S, which was removed by centrifugation. The same strategy was applied here in an attempt to remove free HvNTR2_C145S from NTR:Trx complex by varying the pH range from 4—7 (see Section 3.4.3). From SDS-PAGE analysis it is apparent that part of the unreacted

HvNTR2_C145S was removed by the treatment with lower pH-values (pH 4—7 Figure 3.9). However, the intensities of bands corresponding to the NTR:Trx complex are also reduced, possibly due to precipitation of the complex. Both HvNTR2_C145S and HvTrxh2_C49S tend to aggregate and form various oligomeric complexes (right side of Figure 3.9). Notably one of the bands in the sample of HvTrxh2_C49S appears at approximately the same position as the NTR:Trx complex, which complicates the interpretation further.

Crystallisation attempts using protein purified by the methods described above were unsuccessful. It was therefore decided to change the strategy for the complex purification (see below) in order to separate unreacted HvNTR2_C145S more efficiently from the complex of NTR:Trx.

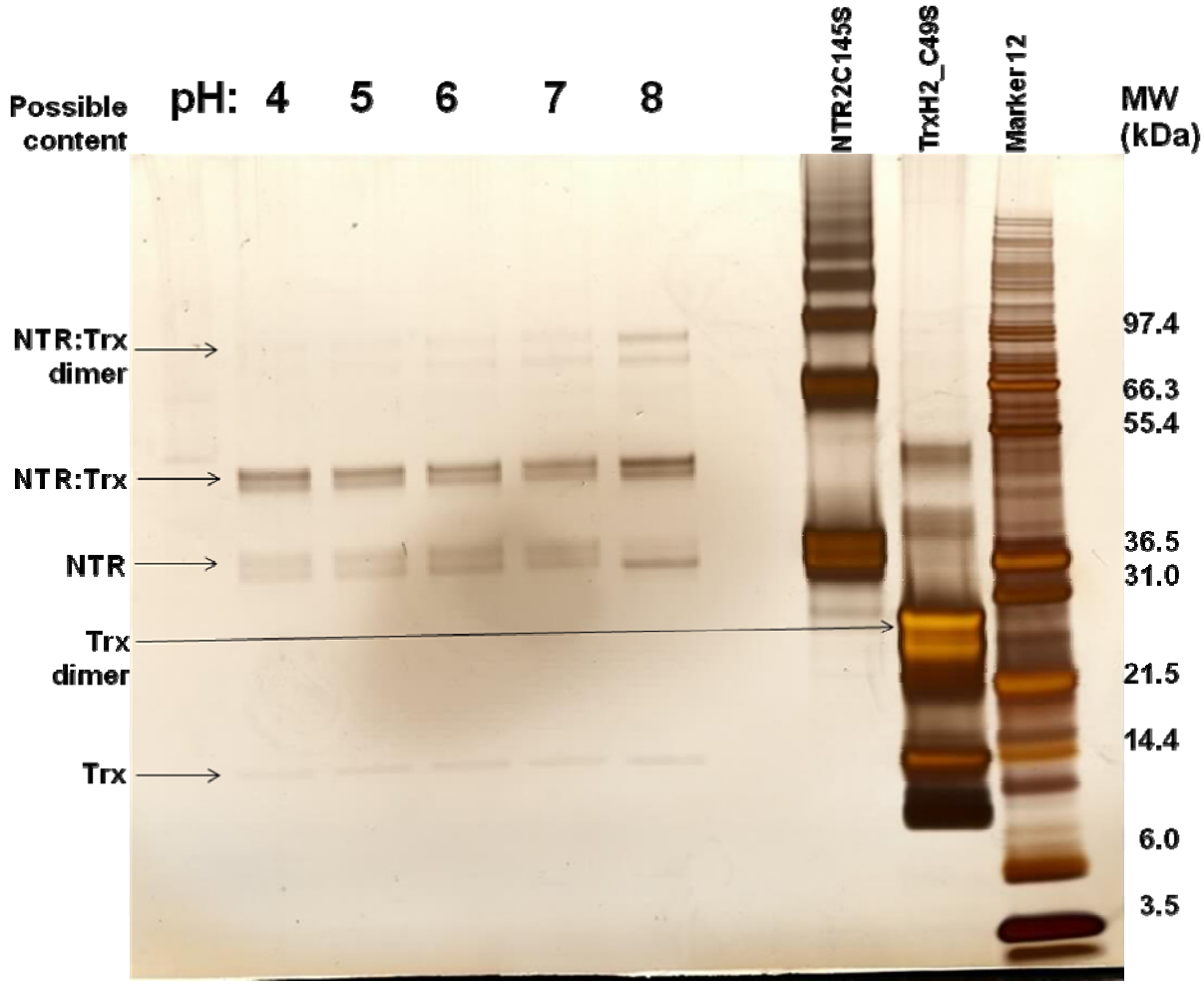

Figure 3.9. SDS-PAGE analysis of samples containing a reaction mixture of HvNTR2_C145S and HvTrxh2_C49S incubated at various pH-values. Aliquots were added 100 mM of various buffers (Na-acetate pH 4 or 5, NH_4-

acetate pH 6, K_2HPO4/KH_2PO4 pH 7) as described in Section 3.4.3. The untreated sample is in Tris-HCl pH 8.0. The same volume was loaded of each sample. The gel is a silver-stained 4—12% NuPage gel.

3.2.3 Complex purification by using NTR with removed His-tag

A new strategy involved removal of the His-tag from HvNTR2_C145S by aid of thrombin protease (Figure 3.10A). Uncleaved His-tagged HvNTR2_C145S is removed by affinity chromatography (3.10B) and cleaved HvNTR2_C145S from the flow-through is reacted with His-tagged HvTrxh2_C49S (3.10C). Unreacted HvNTR2_C145S is removed by affinity chromatography (3.10D) and dimer of HvTrxh2_C49S is subsequently separated from the NTR:Trx complex by anion exchange chromatography (3.10E) as shown previously (Figure 3.7 and 3.8).

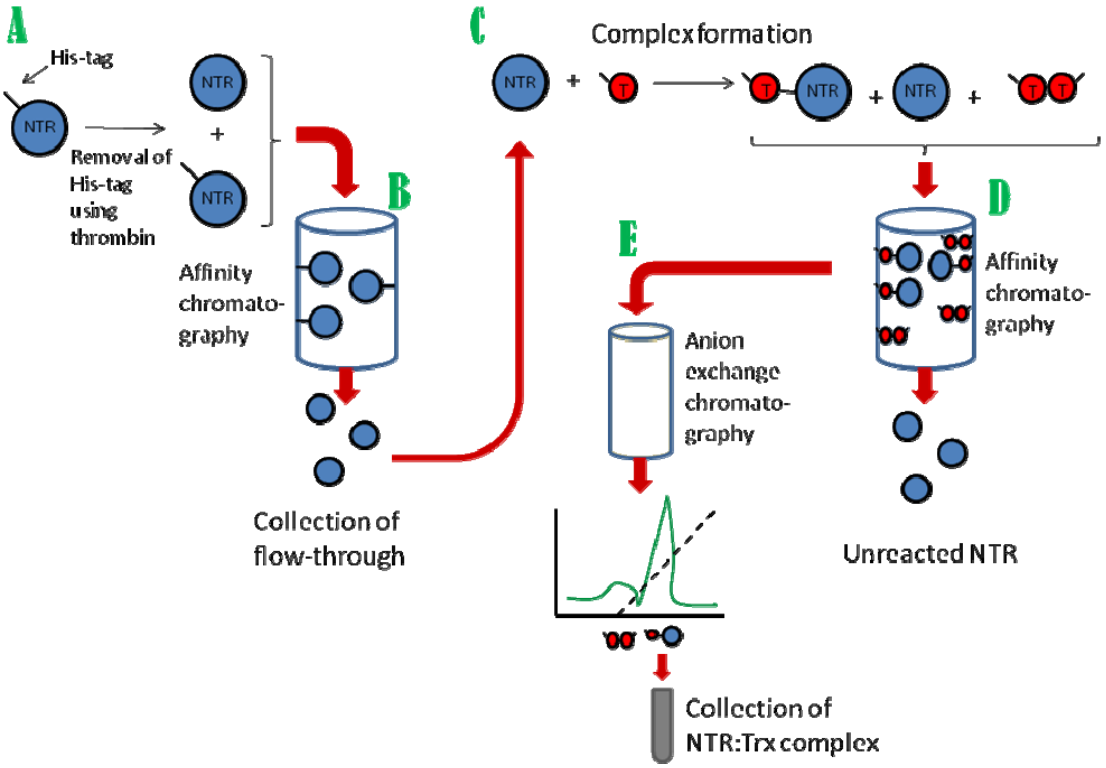

Figure 3.10. Strategy of complex formation and purification after removal of His-tag from HvNTR2_C145S. The His-tag of HvNTR2_C145S is removed using thrombin protease (**A**) and any uncleaved HvNTR2_C145S retained using affinity chromatography (**B**). Cleaved HvNTR2_C145S from the flow-through is reacted with His-tagged HvTrxh2_C49S-TNB (**C**) and any unreacted HvNTR2_C145S removed by affinity chromatography (**D**). Complex of NTR:Trx is separated from dimer of HvTrxh2_C49S using anion exchange chromatography (**E**).

3.2.3.1 Cleavage of the His-tag of NTR using thrombin

During initial attempts to remove the His-tag from HvNTR2_C145S by incubating with thrombin in 100 mM ammonium acetate, pH 6.0, precipitation was observed (seen as a large yellow precipitate in the Eppendorf tube) and almost all had precipitated after 48 h, as judged by SDS-PAGE (almost no visible bands left for the supernatant). Therefore, a range of pH values (6.0, 7.0 and 8.0), thrombin:substrate ratios (1:200 and 1:20), and incubation times (five and 18 h) were tested in an attempt to limit protein precipitation. There was precipitation in all samples which was removed by centrifugation and supernatants were analysed by SDS-PAGE (see Figure 3.11).

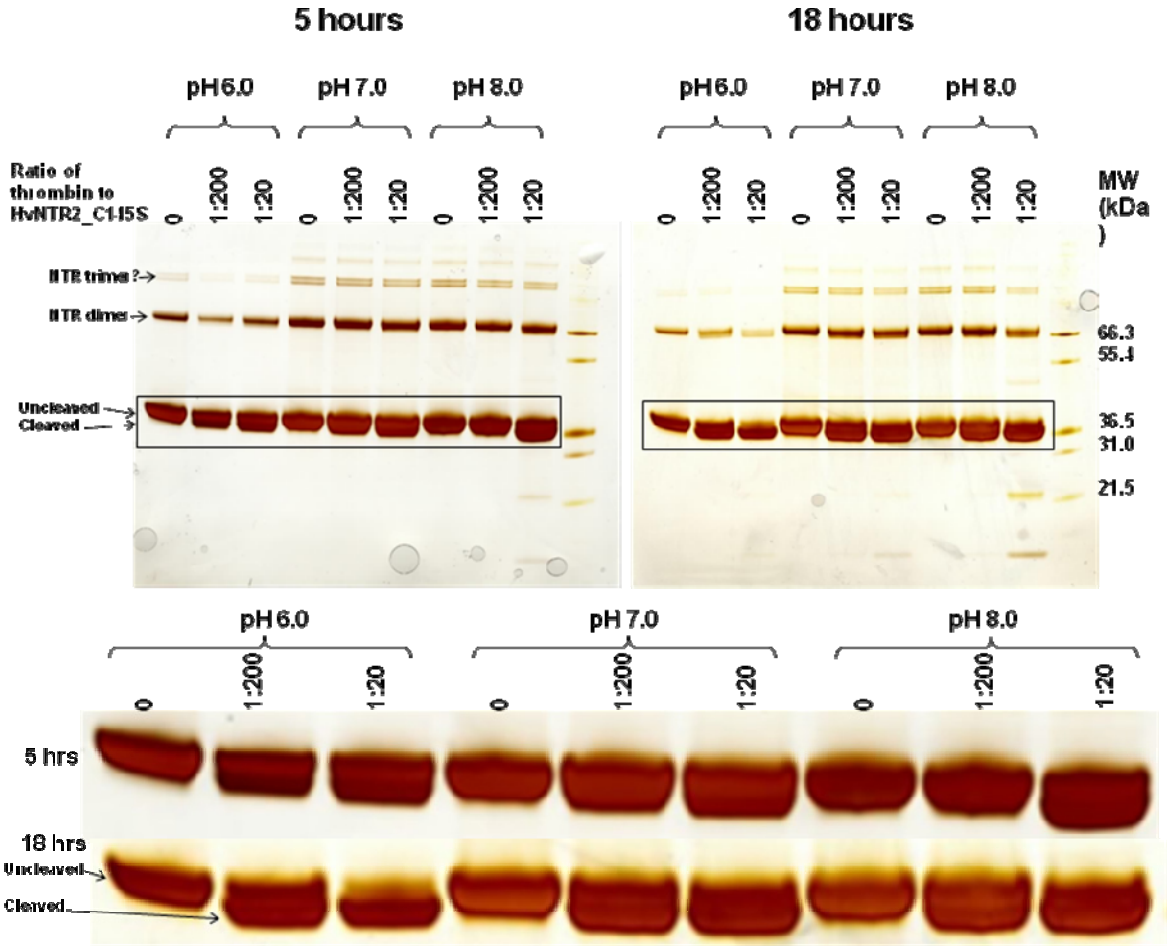

Figure 3.11. SDS-PAGE evaluation of cleavage of His-tag from HvNTR2_C145S using varying pH and thrombin:substrate ratios. The samples were incubated for 5 or 18 h in 150 mM NaCl containing buffer with various pH values (100 mM NH_4 acetate pH 6.0, K_2HPO_4/KH_2PO_4 pH 7.0 or Tris-HCl pH 8.0) and precipitates were removed by centrifugation. Below is a close-up of the bands boxed in the gels. The same volume was loaded of each sample. The gels are silver stained 4—12% NuPage gels.

The highest non his-tagged /his-tagged HvNTR2_C145S ratio appears at pH 6.0, 18 h with a 1:20 thrombin:substrate ratio. However, less soluble protein appears in samples incubated at pH 6.0 (most easily seen for the dimer and the more oligomerised bands, Figure 3.11), possibly due to precipitation of HvNTR2_C145S at lower pH values. It is also possible that the dimer to a greater extent dissociates to monomers at lower pH. With a 1:20 thrombin:substrate ratio at pH 8.0, some low MW bands were observed, possibly due to self-cleavage of thrombin or unspecific activity. Thus, pH 7.0 and 18 h incubation was used in subsequent reactions. Further trials with various thrombin concentrations lead to the conclusion that a thrombin:substrate ratio of 1:200 was almost as efficient as a 1:20 ratio (*data not shown*), and therefore a ratio of 1:200 was used in the following.

Attempts to cleave a larger amount (8.9 mg) of HvNTR2_C145S under these conditions (pH 7.0, 18 h and thrombin:NTR 1:200) still resulted in a large amount of precipitates (62%). The protein which was still in solution was purified using a PD-10 desalting column, and uncleaved HvNTR2_C145S was removed by affinity chromatography on a His-trap column. The final outcome was 1.6 mg (18%) cleaved HvNTR2_C145S.

Trials were made to decrease the amount of precipitates by adding 10 mM DTT during the thrombin cleavage and shake the tubes more vigorously (1100 rpm instead of 600 rpm). This resulted in 0.9 mg (39%) cleaved soluble protein out of 2.3 mg added. Further optimisation involved exclusion of NaCl from the cleavage buffer and rotation of the tubes (instead of shaking) during the cleavage. This led to a yield of 77% of cleaved and soluble HvNTR2_C145S. The removal of the His-tag was confirmed by mass spectrometric analysis (*data not shown*) of the full-length protein (see Section 3.4.7).

3.2.3.2 Complex formation and purification

Non his-tagged HvNTR2_C145S (30 µM) was reacted with 58 µM HvTrxh2_C49S-TNB and the reaction mixture was separated on a MonoQ column (Figure 3.12). Fractions B1—B4 (marked by bracket in Figure 3.12) were pooled and applied on a His-trap affinity column (Figure 3.13) to separate unreacted HvNTR2_C145S from the HvNTR2:HvTrxh2 complex. SDS-PAGE analysis revealed that the main peak (fractions A2—A8, Figure 3.13) apparently contained HvTrxh2_C49S with removed His-tag (lane 3—4 Figure 3.14). The presence of non his-tagged HvTrxh2_C49S may be due to residual thrombin, possibly detached from the

agarose beads. Alternatively the His-tag was lost even in the absence of thrombin as observed previously (lane 2, Figure 3.8 and lane 7 Figure 3.14). Some of the HvNTR2_C145S was apparently not cleaved properly, explaining how the NTR:Trx complex was retained on the His-Trap column. Fractions B10—B5 which was retained more sufficiently using affinity chromatography contained uncleaved HvTrxh2_C49S and mainly cleaved HvNTR2_C145S as attended (lane 5—6 Figure 3.14). However much of the NTR:Trx complex may have been lost in the wash fractions (lane 2, too dilute to be observed), since the His-tag was lost from a large portion of HvTrxh2_C49S.

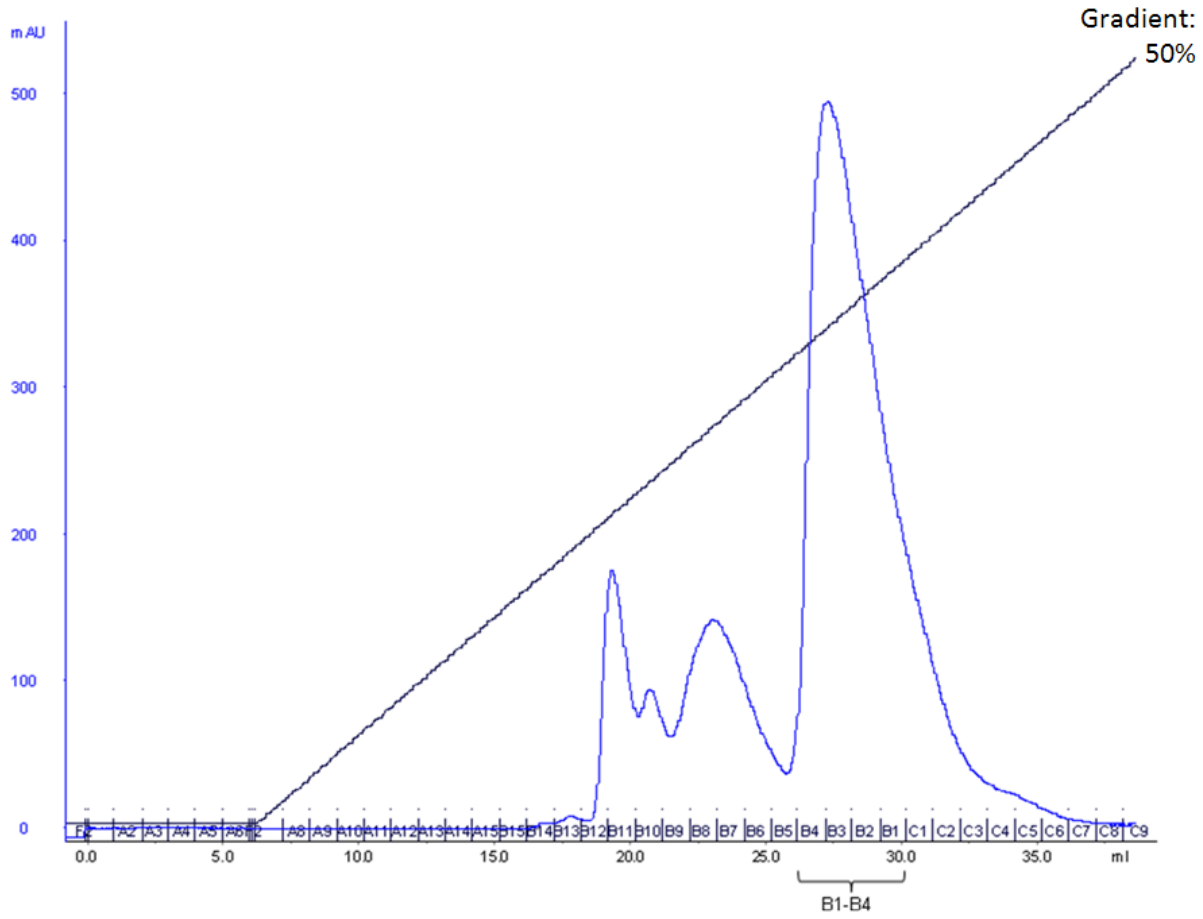

Figure 3.12. Reaction mixture of thrombin-cleaved HvNTR2_C145S (30 µM) and 58 µM HvTrxh2_C49S-TNB separated on a MonoQ anion exchange column.

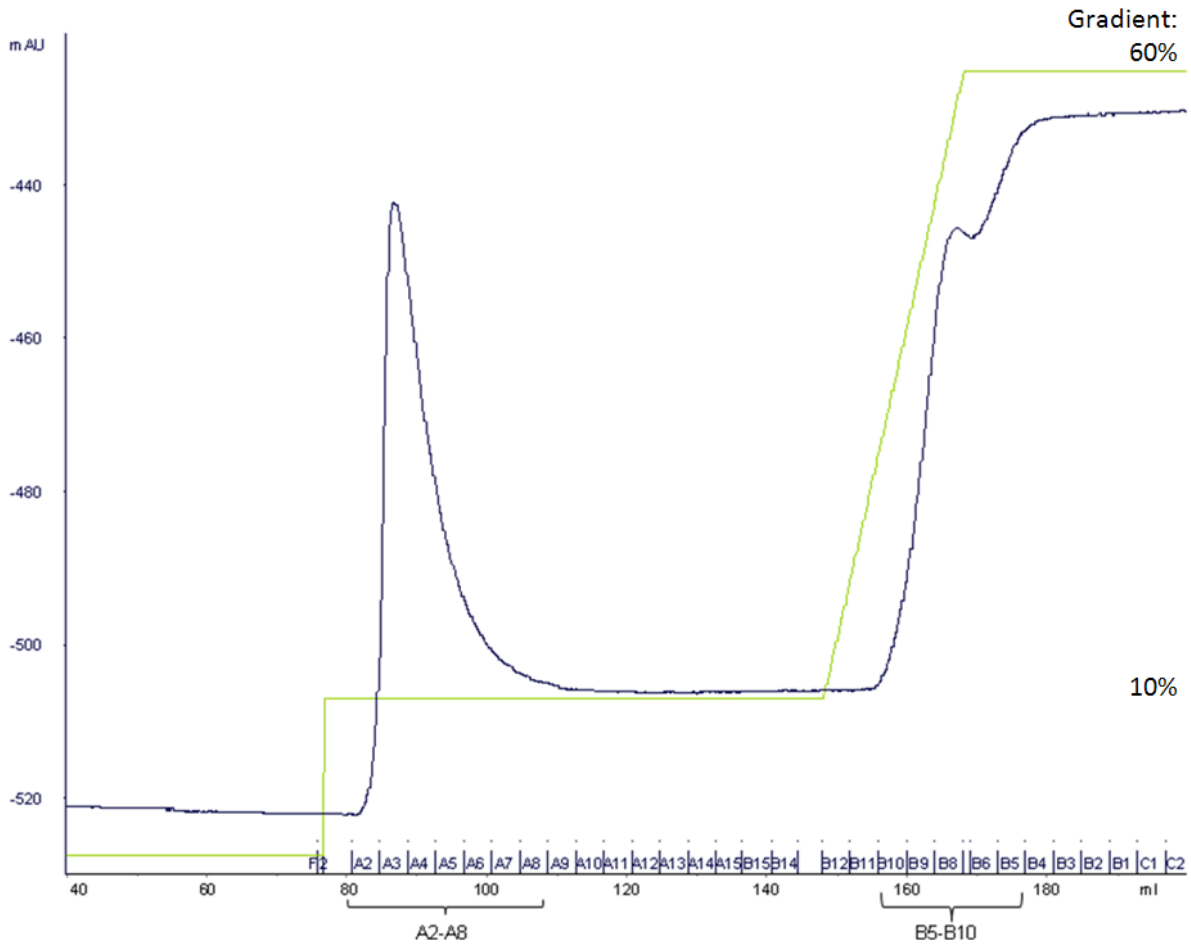

Figure 3.13. Separation of fractions B1—B4 from the MonoQ anion exchange chromatogram (Figure 3.12) on a His-trap affinity chromatography column. The gradient shown in light green indicates the percentage of buffer B (400 mM imidazole, 30 mM Tris-HCl pH 8.0, 500 mM NaCl). Buffer A contains 10 mM imidazole, 30 mM Tris-HCl pH 8.0, 500 mM NaCl.

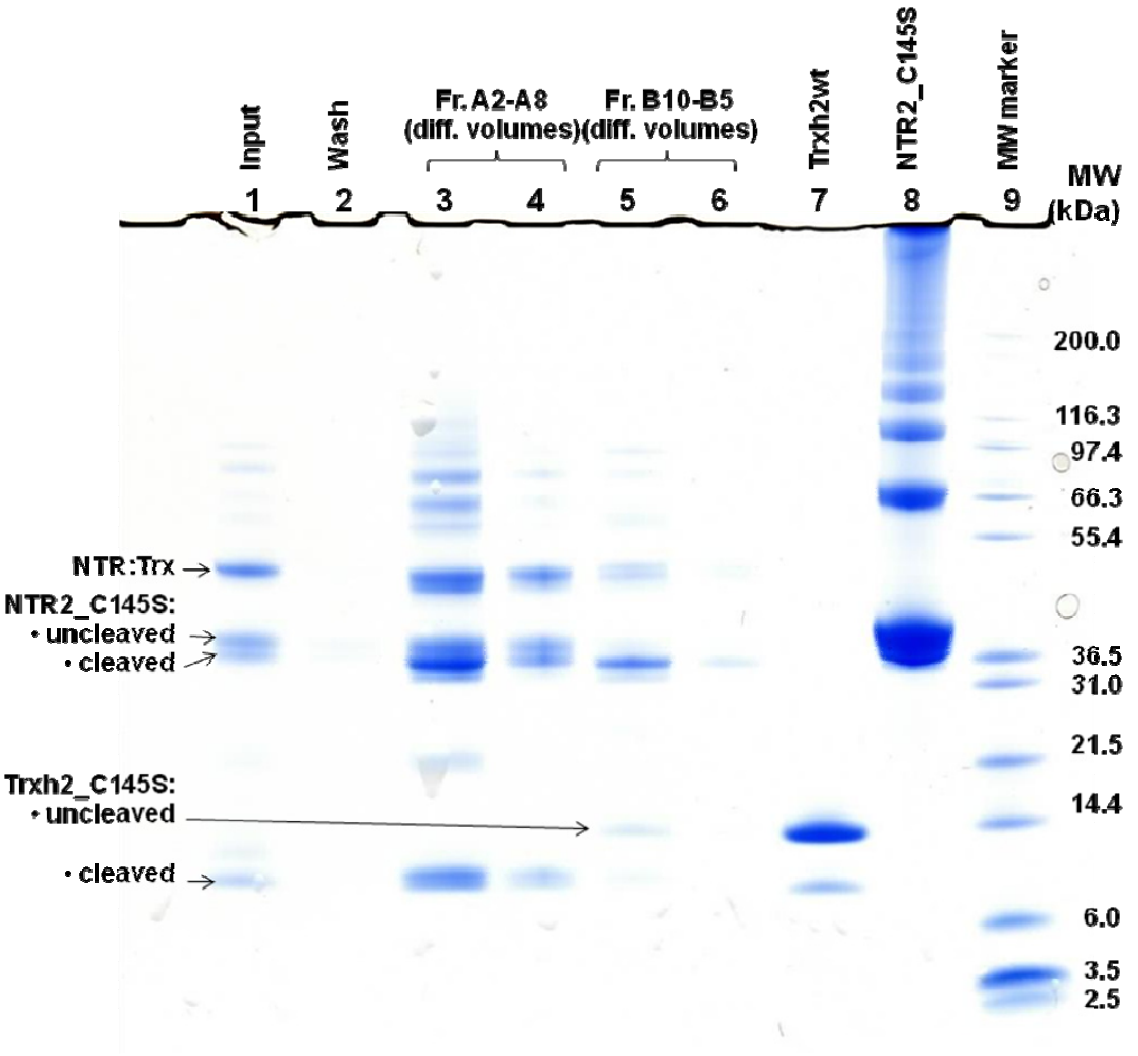

Figure 3.14. SDS-PAGE of fractions from affinity chromatography (Figure 3.13). A complex of HvNTR2_C145S (His-tagged cleaved) and HvTrxh2_C49S (NTR:Trx) was purified. The gel is a Coomassie stained 4—12% NuPage gel.

Due to these complications a different procedure was pursued in which the His-tag of HvTrxh2_C49S was exchanged with a calmodulin-binding-peptide-tag (see below).

3.2.4 Complex purification using a calmodulin-binding-peptide-tag.

The gene encoding HvTrxh2 was inserted in the vector pCAL-n. The resulting plasmid expresses HvTrxh2_C49S with an N-terminal calmodulin-binding peptide (CBP) with the sequence (M)KRRWKKNFIAVSAANRFKKISSSGAL followed by a thrombin cleavage site (CBP-HvTrxh2_C49S). The use of CBP as an affinity tag is based on the relatively high affinity (K_d = $1x10^{-9}$ M) for calmodulin exhibited by this 26-amino-acid fragment from muscle myosin

light-chain kinase at physiological pH in the presence of calcium (Figure 3.15A). Upon removal of calcium by the chelating agent ethylene glycol tetraacetic acid (EGTA), calmodulin undergoes a conformational change that results in the release of its ligand (Figure 3.15B).

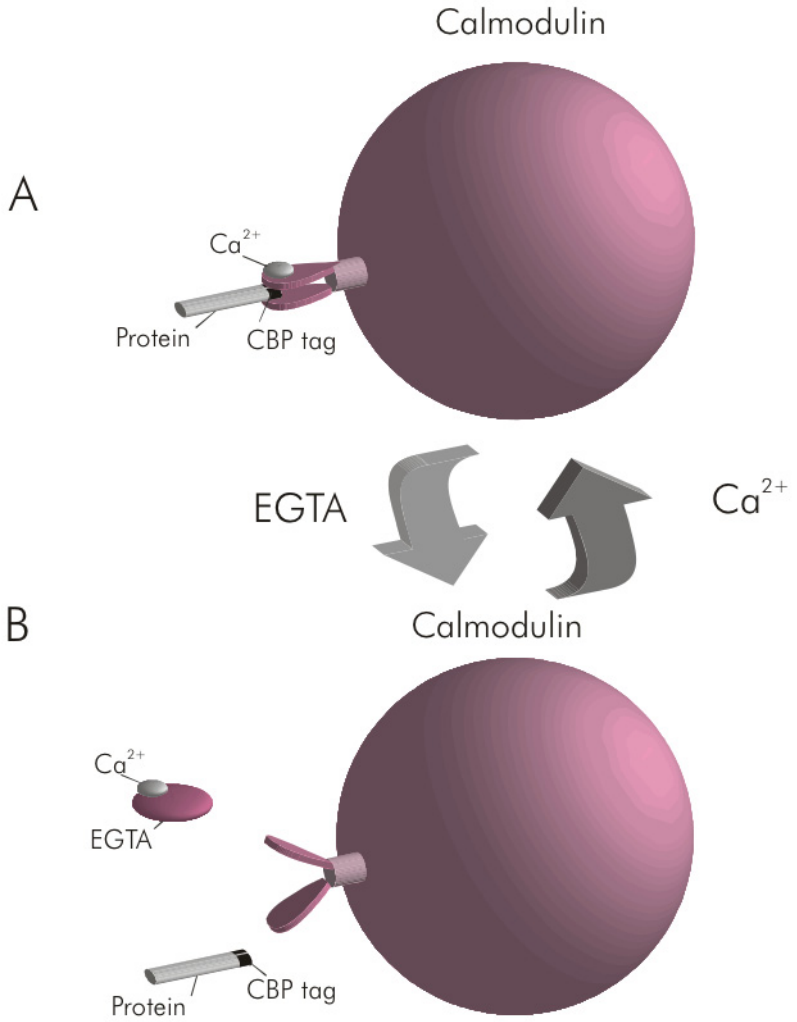

Figure 3.15. Calmodulin binding peptide (CBP) purification system. (**A**) Calmodulin from a resin binds to the CBP-tagged fusion protein in the presence of low concentrations of calcium. (**B**) Calmodulin changes conformation upon removal of calcium with 2 mM of the chelator EGTA and the fusion protein is released from the resin. Figure from Agilent Technologies, Instruction manual #204300 (see references).

CBP-HvTrxh2_C49S was expressed in *E. coli* Rosetta cells at 20°C overnight after induction by IPTG. SDS-PAGE analysis indicated that most of the expressed protein was

insoluble after extraction with Bugbuster (Figure 3.16 left gel and Section 3.4.5) so it was not attempted to purify this further.

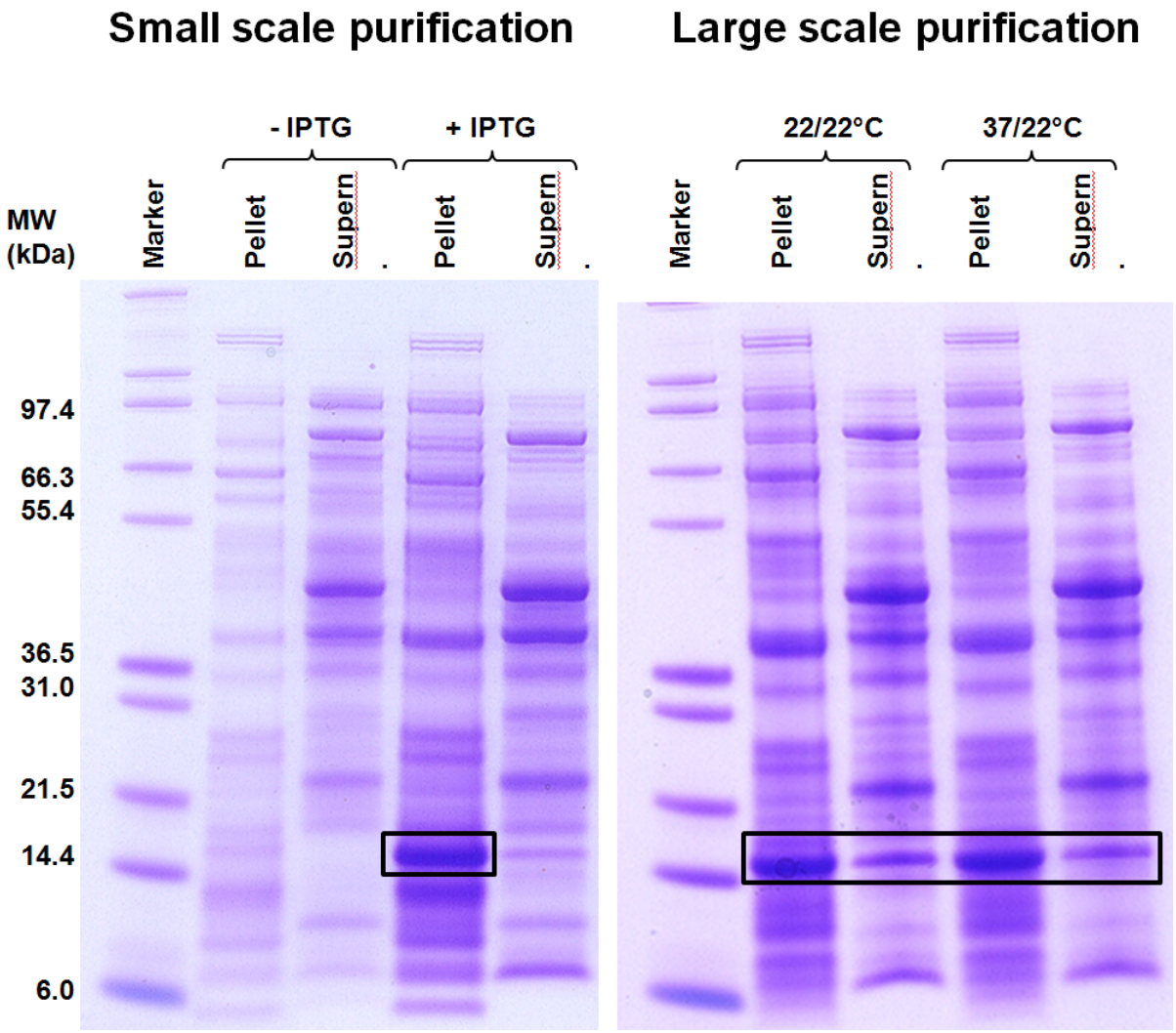

Figure 3.16. SDS-PAGE analysis of expression of CBP-HvTrxh2_C49S. **Left gel:** Small scale purification from 1 mL culture. The culture was grown at 37°C, and samples were taken prior to addition of IPTG (-IPTG) and after induction at 20°C overnight (+IPTG). **Right gel:** Purification from 2 x 500 mL culture. The temperature prior to addition of IPTG was either 22 or 37°C and was lowered to 22°C after the addition. Insoluble pellets were dissolved by 8 M urea (see Section 3.4.5). The boxed areas highlight a band matching the expected molecular weight of CBP-HvTrxh2_C49S (expected MW: 16837 Da). The gels are Coomassie stained 4—12% NuPage gels.

The temperature prior to induction was changed from 37 to 22°C, but this did not increase the amount of soluble protein (*data not shown*). However, by scaling up the protein extraction from 1 to 500 mL culture a larger percentage of soluble protein was obtained (Figure 3.16 right gel). A total of 5 mg CBP-HvTrxh2_C49S obtained from 1 L

culture was purified on a Calmodulin affinity column (Section 3.4.1.4), conjugated to TNB (Section 3.4.2) and dialysed against 30 mM Tris-HCl pH 8.0. CBP-HvTrxh2_C49S-TNB was reacted with His-tagged HvNTR2_C145S (Section 3.4.2) and the resulting complex of His-HvNTR2:CBP-HvTrxh2 was purified by tandem affinity chromatography on a Calmodulin column (Section 3.4.1.4) and a His-tag column (Section 3.4.1.1) in order to remove access His-HvNTR2_C145S (with intact His-Tag) and CBP-HvTrxh2_C49S, respectively.

The low solubility of CBP-HvTrxh2_C49S was still a problem and precipitation occurred, which resulted in only a very small amount of purified complex. Attempts to increase the solubility by varying pH and including NaCl in all steps did not improve the yield substantially (*data not shown*).

3.2.5 Characterisation of the HvNTR2:HvTrxh2 complex

3.2.5.1 Determination of MW using Mass spectrometry

MALDI-TOF analysis of full-length his-tagged HvNTR2:HvTrxh2 complex in fractions A2—A8 (from Figure 3.13), resulted in a signal at approximately 49300 m/z (Figure 3.17A). The theoretical MWs of the HvNTR2:HvTrxh2 complex with no and one His-tag are 48.47 and 50.37 kDa, respectively.

Signals at m/z 48460 and 50480 (Figure 3.17B) were detected in a MALDI-TOF mass spectrum of fractions B5—B10 (from Figure 3.13) possibly corresponding to complex with no and one His-tag, respectively. No peaks for unreacted HvNTR2_C145S or HvTrxh2_C49S were detected.

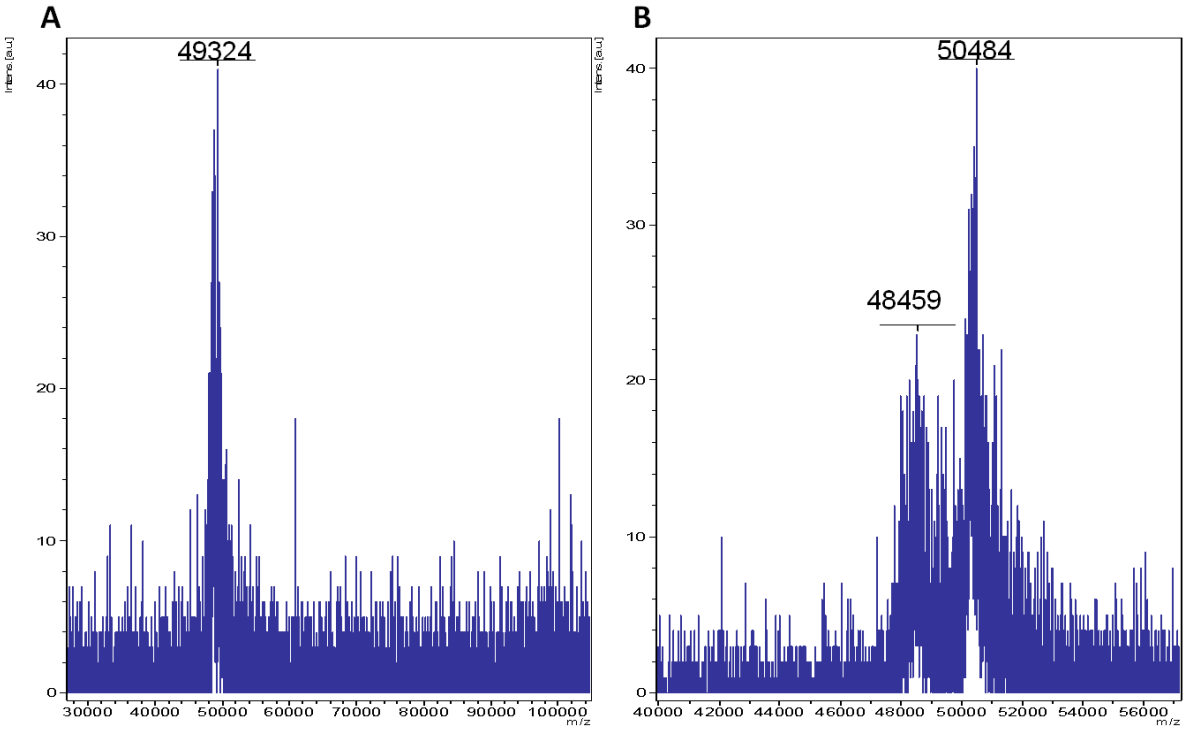

Figure 3.17. Mass spectrometric analysis of full length HvNTR2:HvTrxh2 complex by MALDI-TOF. HvNTR2_C145S was bound through an intermolecular disulfide to HvTrxh2_C49S and subjected to anion exchange and affinity chromatography. Content of (**A**) fractions A2—A8 (from His-trap Figure 3.13), and (**B**) fractions B10—B5 from the same purification were analysed. The His-tag of HvNTR2 was subjected to thrombin cleavage prior to complex formation, and apparently the His-tag of HvTrh2_C49S was also lost. Expected MW of complex is 48.459 and 50.351 kDa with no or one intact His-tags, respectively.

The MWs of the HvNTR2:HvTrxh2 complex from a subsequent purification (performed the same way) was also determined by ESI-QTOF mass spectrometry (Figure 3.18). The average MW of the transformed m/z signal (Figure 3.18) was around 50.3 kDa, which fits with the expected MW for a complex with one intact His-tag. However, the peak is quite broad ranging from approximately 50.0 to 51.0 kDa, which indicates that the NTR:Trx complex is not homogenous.

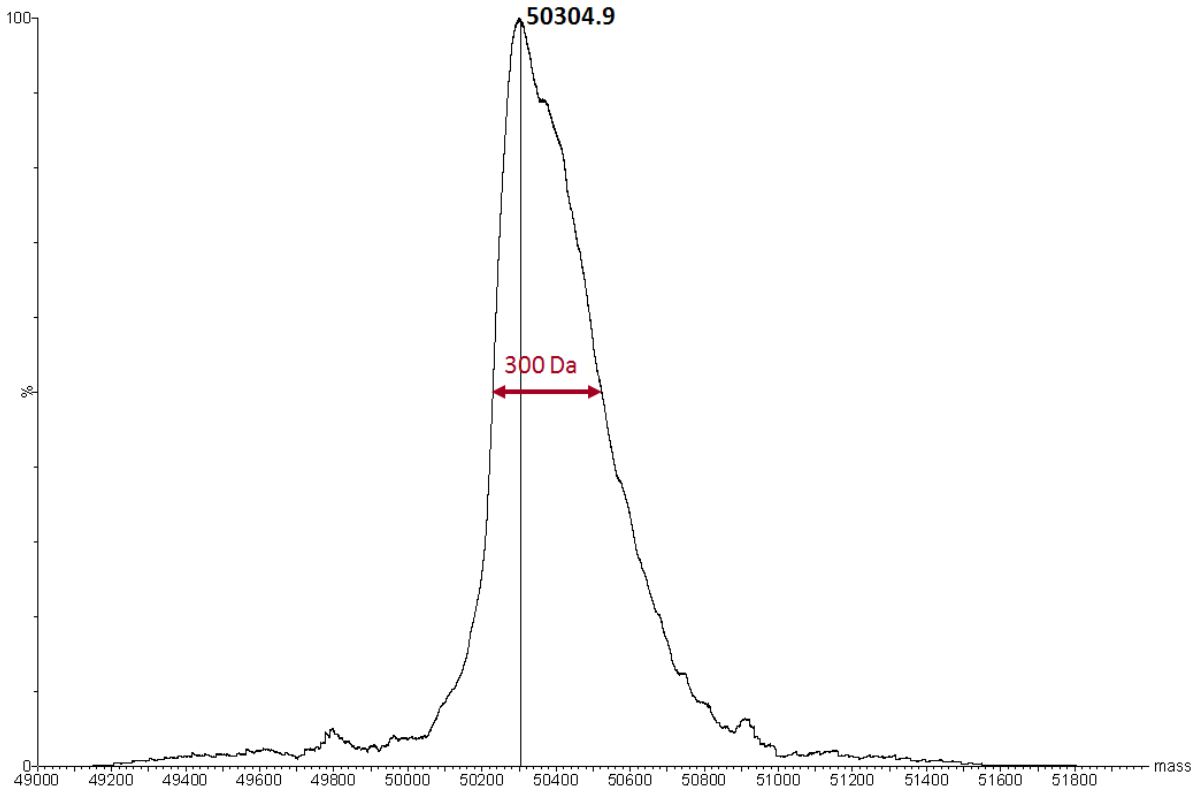

Figure 3.18. Transformed ESI-QTOF mass spectrum of the complex of HvNTR2_C49S:HvTrxh2_C49S. The His-tag of HvNTR2_C145S has been removed by thrombin prior to complex formation.

3.2.5.2 Determination of isoelectric point using IEF

Complex of HvNTR2:HvTrxh2 was analysed by isoelectric focusing (IEF) (Section 3.4.6) using a pI range from 3—9 (see lane 4—5 Figure 3.19). Also His-tagged HvNTR2_C145S (lane 1—2) and his-tagged HvTrxh2_C49S (lane 3) were analysed. Experimental pI values were estimated from migration distances of marker standard proteins plotted against log pI values (right side of Figure 3.19). The sample of HvNTR2:HvTrxh2 analysed is fractions A2—A8 from Figure 3.13, which seemed to contain complex with both His-tagged removed (one peak of 49.3 kDa detected by mass spectrometry, Figure 3.17A). The theoretical pI of non-his tagged HvNTR2_C145S plus non-his tagged HvTrxh2_C49S was calculated to 5.8 using ProtParam (Gasteiger *et al*., 2005) without taking the intermolecular disulfide into account. Lane 5 shows four bands for NTR:Trx in the range between 4.7 and 4.9. This heterogeneity may be due to various modifications of the complex.

The theoretical pI value of His-tagged HvNTR2_C145S is 6.35 and the broad band in lane 2 is determined to be between 5.7 and 6.1. For His-tagged HvTrxh2_C49S the

theoretical pI value is 6.28. The sample in lane 3 shows a main broad band between 5.9 and 6.7 as well as three additional bands at 5.1, 5.3 and 5.4. This sample may contain both aggregated protein, Trx dimer, Trx monomer, and Trx which had lost the His-tag. The latter has a theoretical pI of 5.31, which corresponds well with one of these bands.

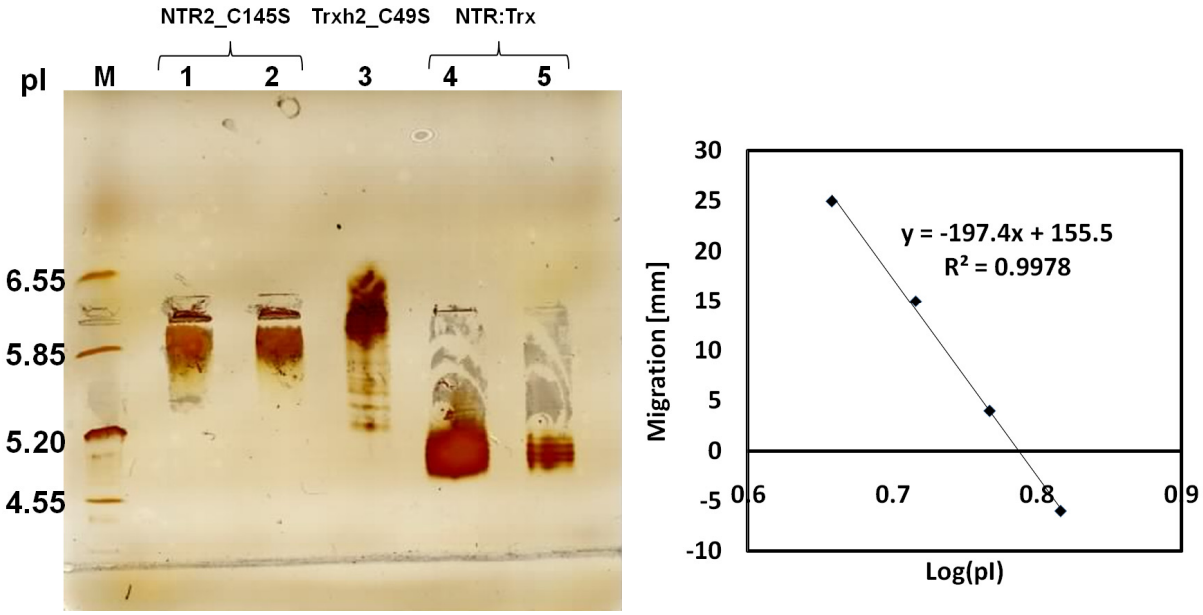

Figure 3.19. Isoelectric focusing analysis. Lane 1—2 is His-tagged HvNTR2_C145S (10 and 5 µg, respectively), lane 3 is His-tagged HvTrxh2_C49S and lane 4—5 is a complex of HvNTR2_C145S:HvTrxh2_C49S from which both His-tagged apparently has been cleaved. Silver stained PhastGel™ pI 3—9.

3.2.6 Crystallisation trials

A wide range of screens were used in order to attempt crystallisation of the HvNTR2:HvTrxh2 complex. Different batches from the various purifications were tested and screens included the available standard screens in Carlsberg Laboratory, various screens at Århus University as well as at a PhD course in protein crystallography at University of Copenhagen. No protein crystals were obtained in these screens. This may be due to impurities and/or heterogeneity of the HvNTR2:HvTrxh2 complex preparation. Since HvNTR2 forms a dimer it is possible that only one of the monomers is bound to HvTrxh2. It is possible that analytical gel filtration or small-angle X-ray scattering (SAXS) could clarify whether this is the case. However, preliminary SAXS measurements on the HvNTR2:HvTrxh2 complex failed due to sample aggregation. This line of work has not been pursued any

further. The instability of the His-tags in HvNTR2_C145S and HvTrxh2_C49S is another potential source of heterogeneity. It was not attempted to remove his-tags from complex after purification since only small amounts of complex were obtained and thrombin cleavage of HvNTR2_C145S had previously resulted in precipitation. It has also been observed that the FAD incorporation in HvNTR2 is incomplete (see Chapter 5, Section 5.2.2), which again may lead to a non-uniform sample.

3.2.7 Influence of NADPH and $NADP^+$ on complex formation

It was tested whether NADPH would influence the reaction rate of complex formation by measuring the release of TNB from HvTrxh2_C49S-TNB at 412 nm (Section 3.4.2). When NADPH was added to 30 µM HvNTR2_C145S 20 minutes prior to mixing with 20 µM HvTrxh2_C49S-TNB, an increase in the rate of initial absorbance change was observed when compared to an equivalent reaction in the absence of NADPH (Figure 3.20A). However, the data is not entirely conclusive as the endpoint absorbance of the samples incubated in the presence of NADPH was lower compared to the control without NADPH (Figure 3.20A). This may be due to changes in absorbance from reduced FAD, which overlaps with TNB absorbance at 412 nm (Figure 3.21) and contributes substantially to the background in the used concentration of 30 µM (Figure 3.21, note only 7.2 µM is used here). Thus A_{412} of 30 µM HvNTR2_C145S (reduced with DTT) was approximately 0.156 compared to buffer.

This hypothesis was tested by performing the complex formation in the presence of $NADP^+$ instead of NADPH. In this case the background absorbance from FAD is expected to be constant since $NADP^+$ is unable to reduce FAD and the experiment is performed under anaerobic conditions. Indeed no drop in absorbance was detected during the reaction with $NADP^+$ (Figure 3.20B, yellow and green curves). Furthermore, an increase in the initial absorbance change at 412 nm is observed relative to the control without $NADP^+$. The second order reaction rates were calculated to 139 $M^{-1}s^{-1}$ without $NADP^+$ and about 3 times higher (408 $M^{-1}s^{-1}$) with 40 µM $NADP^+$ and about 4.8 times higher (635 $M^{-1}s^{-1}$) using 300 µM $NADP^+$. The results thus indicate that the complex formation reaction rate is increased in the presence of $NADP^+$ possibly by influencing the equilibrium between the FO and FR conformations.

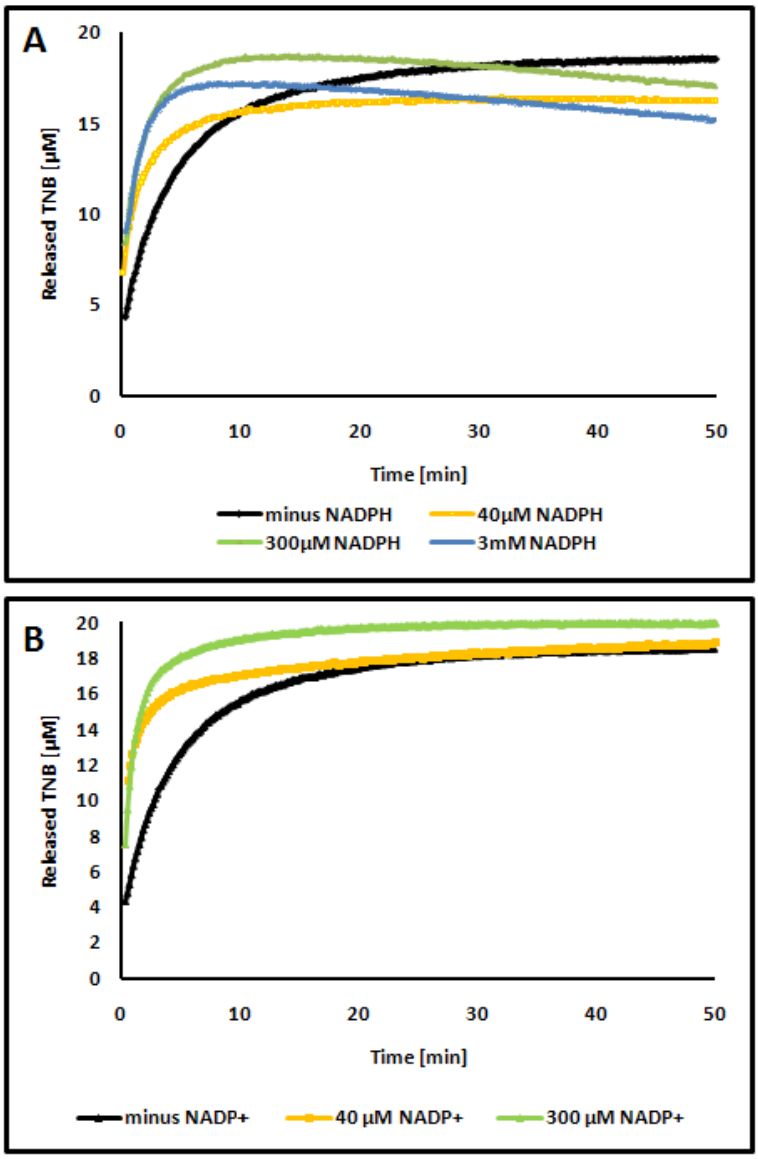

Figure 3.20. Influence of NADPH on complex formation. Release of TNB followed at A_{412} upon reaction of 30 µM HvNTR2_C145S with 20 µM HvTrxh2_C49S-TNB (black lines). (**A**) Addition of NADPH initially increased the rate of the complex formation but ended at lower absorbance than without NADPH (**B**) Addition of $NADP^+$ increases the reaction rate.

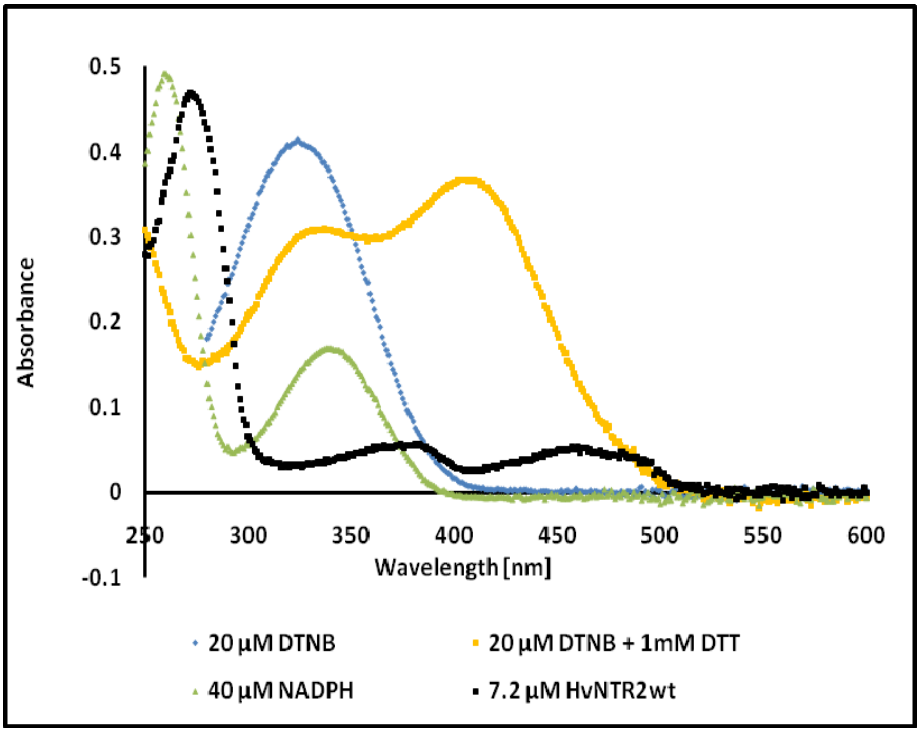

Figure 3.21. Absorbance spectra of NADPH, DTNB and TNB. The samples are (blue curve) 20 µM of DTNB dissolved in in 50 mM Na-acetate and diluted in 30 mM Tris-HCl pH 8.0 measured from 280 nm, (yellow curve) the same sample but preincubated with DTT five min at room temperature prior to the measurement, (green curve) 40 µM NADPH prepared in argon-purged ddH_20 and (black curve) 7.2 µM non-reduced HvNTR2wt in 30 mM Tris-HCl pH 8.0.

3.3 Conclusion

A complex was produced of HvNTR2_C145S bound through an intermolecular disulfide to HvTrxh2_C49S. The complex purification was hampered due to difficulties separating unreacted HvNTR2_C145S from the complex, precipitation of HvNTR2_C145S during thrombin cleavage as well as accidental loss of the His-tag of HvTrxh2_C49S. Attempts to shift the His-tag of HvTrxh2_C49S with a calmodulin-binding-peptide tag led to small amounts of soluble protein and problems with insolubility of the complex. Crystallisation of the complex failed potentially due to sample heterogeneity as determined by mass spectrometry and isoelectric focusing. SAXS may be useful for determining whether there is a 1:1 stoichiometry of HvNTR2 and HvTrxh2 in the sample, but preliminary SAXS measurements did not give usable data due to aggregation.

Results where NADPH/$NADP^+$ was added prior to complex formation indicate that HvNTR2_C145S is able to react with HvTrxh2_C49S-TNB independently of either NADPH/$NADP^+$, but binding of the ligand apparently facilitates complex formation.

3.4 Materials and methods

3.4.1 Protein expression and purification

Rosetta cells were used containing a pCAL-n based plasmid expressing CBP_HvTrxh2_C49S or pET15b based plasmids encoding various proteins (e.g. HisHvNTR2_C145S, HisHvNTR2_C148S or HisHvTrxh2_C49S). Overnight cultures of these cells were added to a total of 1—3 L fresh LB media supplemented with ampicillin (100 µg/mL) and chloramphenicol (5 µg/mL) for a starting OD_{600} ≈ 0.1 and grown at 37°C with vigorous shaking until OD_{600} ≈ 0.6 when IPTG (isopropyl β-D-1-thiogalactopyranoside) was added to a final concentration of 100 µM. Either the temperature was kept at 37°C for 3 h, or the temperature was lowered to 20°C or 22°C for expression overnight. Harvested cultures were incubated on ice for 15—30 min prior to centrifugation (4000 rpm, 4°C, 20 min) after which pellet was either frozen at -20°C or purified directly.

The pellet from a 1 L culture was dissolved in 10 mL BugBuster® Protein Extraction reagent (Novagen®) and 2 µL Benzonase® Nuclease (stock ≥250 units/µL, Sigma-Aldrich) and shaken for 30 min at room temperature. After centrifugation (10,000 rpm, 4°C for 15 min) the supernatant was filtered (0.45 µm syringe filter, Frisenette ApS).

3.4.1.1 Affinity chromatography - HisTrap

Protein was applied on a 1 or 5 mL HisTrap™ HP column (GE Healthcare) pre-equilibrated with five column volumes (CV) buffer A (10 mM imidazole, 30 mM Tris-HCl pH 8.0, 500 mM NaCl). An ÄKTAprime™ plus (GE Healthcare) was used for purifying the protein. The columns were washed with 10 CV buffer A followed by 15 CV buffer A mixed with 10% buffer B (400 mM imidazole, 30 mM Tris-HCl pH 8.0, 500 mM NaCl), before elution of the protein by a gradient of buffer B increasing to 100%. Protein containing fractions were pooled and dialysed overnight (Spectra/Por® Membrane of 6—8.000 MWCO, Spectrum Laboratories Inc.) against 30 mM Tris-HCl pH 8.0.

3.4.1.2 Size exclusion chromatography

The volume of pooled samples from the HisTrap column was decreased to 1—5 mL by concentrating the protein on an Amicon® Ultra-15 centrifugal filter device of 10,000 MWCO (Millipore). The sample was filtered and applied to HiLoad™ 26/60 (or 16/60) Superdex™ 200 (or 75) prep grade columns (Amersham Biosciences) equilibrated in 200 mM NaCl, 30 mM Tris-HCl pH 8.0. An Äkta TM explorer Air (Amersham Biosciences) system was used for the gel filtration. Fractions were dialysis against 30 mM Tris-HCl pH 8.0, concentrated to 100—500 µM protein concentration and stored at -80°C. The purity of the proteins was checked by SDS-PAGE.

3.4.1.3 Anion exchange chromatography

After complex formation (Section 3.4.2) the reaction mixture was in some cases subjected to anion exchange chromatography, using a MonoQ 5/50GL 1 mL column pre-equilibrated with 10 mM Tris-HCl pH 8.0. An Äkta TM explorer Air (Amersham Biosciences) was used for the purification. After sample application the column was washed with 10 mM Tris-HCl pH 8.0, and protein was eluted using a two-step gradient of buffer B (10 mM Tris-HCl pH 8.0 and 1 M NaCl) from 0—20% over 10 mL and from 20%—100% over 20 mL. Later a shallower one step gradient from 0—50% buffer B over 50 mL was used.

3.4.1.4 Affinity chromatography - calmodulin column

The purification of CBP-HvTrxh2_C49S was performed according to the manual of the Affinity® protein expression and purification system (Agilent Technologies, Instruction manual #204300, see references) with slight modifications. A column containing Calmodulin Affinity Resin (Stratagene) was pre-equilibrated with five column CV calmodulin binding buffer (50 mM Tris-HCl pH 8.0, 150 mM NaCl, 1 mM MgAc, 1 mM imidazole, 2 mM $CaCl_2$, and 5 mM DTT). CBP-HvTrxh2_C49S was dialysed in calmodulin binding buffer and circulated through the calmodulin column for typically 1½ h. The column was washed with 2 CV calmodulin binding buffer and ≥ 4 CV calmodulin binding buffer without DTT (buffer A). Protein was eluted with an increasing gradient of buffer B (50 mM Tris-HCl pH 8.0, 2 mM EGTA, and 1 M NaCl). The gradient was typically from 0—50% buffer B over 40 mL. In the

cases where complex of His-HvNTR2:CBP-HvTrxh2 was purified DTT was completely omitted from the procedure.

3.4.2 Complex formation

The single-cysteine mutants HvNTR2_C145S and HvTrxh2_C49S (Maeda *et al*., 2006a) were expressed and purified by affinity chromatography (His-Trap Section 3.4.1.1 or calmodulin column Section 3.4.1.4). HvTrxh2_C49S was reacted with a 10 times excess of DTNB for 1 h at room temperature, prior to further purification using size-exclusion chromatography (see Section 3.4.1.2). HvNTR2_C145S and HvTrxh2_C49S-TNB were dialysed against 30 mM Tris-HCl pH 8.0, and in some cases the His-tag of HvNTR2_C145S was subjected to cleavage by thrombin. HvNTR2_C145S was reduced with 10 mM DTT for 30 min to 1 h at room temperature, and DTT was removed using a PD-10 or NAP-5 column (GE Healthcare) using argon-purged 30 mM Tris-HCl pH 8.0 to prevent reoxidation of $Cys148_{HvNTR2}$. Varying concentrations of HvNTR2_C145S was reacted with HvTrxh2_C49S-TNB in 30 mM Tris-HCl pH 8.0 for 1 h at room temperature. The release of TNB was monitored spectrophotometrically (Ultrospec 2100 *pro*, Amersham Biosciences) at 412 nm in a sample volume of 100 µL.

3.4.3. Precipitation of NTR in various pH-buffers

HvNTR2_C145S and HvTrxh2_C49S-TNB were reacted in a 1:1 ratio and the resulting mixture was separated on a gel filtration column (data not shown). A fraction containing complex of NTR:Trx but also some unreacted HvNTR2_C145S as well as a smaller amount of HvTrxh2_C49S was dialysed against 10 mM Tris-HCl pH 8.0 and aliquoted into Eppendorf tubes. The following pH-buffers were added to a final concentration of 100mM: Na-acetate pH 4.0 and 5.0, NH_4-acetate pH 6.0, or K_2HPO_4/KH_2PO_4 pH 7.0. The samples were incubated at room temperature for 30 min and centrifuged (30 min, 14,000 rpm, 4°C). The supernatant was transferred to new tubes and analysed by SDS-PAGE.

3.4.4 Removal of His-tag using thrombin protease

For cleavage of His-tags immobilised thrombin conjugated to agarose beads (thrombin from human plasma, stock conc. 0.37 mg/mL, Calbiochem®) was used in ratios ranging from

1:20 to 1:1000 ($\mu g_{thrombin}$: μg_{HvNTR2_C145S}). The following pH-buffers were used in a final concentration of 100 mM: NH_4-acetate pH 6.0, K_2HPO_4/KH_2PO_4 pH 7.0, or Tris-HCl pH 8.0. In some cases 150 mM NaCl or 10 mM DTT was included. The samples were incubated at 25°C between 5 and 48 h either shaking at 600 or 1100 rpm (using a Thermomixer Comfort, Eppendorf) or rotating. After the cleavage immobilised thrombin and precipitated protein was removed by centrifugation (20 min, 14,000 rpm, 4°C), and in the cases DTT was used the buffer was changed using a PD-10 desalting column (GE Healthcare). Uncleaved HvNTR2_C145S was retained by affinity chromatography using a His-Trap column (see Section 3.4.1.1).

3.4.5 SDS-PAGE gel electrophoresis

Pellets from centrifuged 1 mL protein expression samples were dissolved in 50 µL BugBuster® Protein Extraction reagent (Novagen®) and 0.2 µL Benzonase® Nuclease (stock concentration ≥250 units/µL, Sigma-Aldrich) and shaken at 900 rpm for 30 min at room temperature. The samples were centrifuged (14,000 rpm, 4°C, 15 min) and supernatants transferred to new tubes. Insoluble protein was dissolved in 50 µL 8 M urea in 0.5 M Tris-HCl pH 8.3. Samples were mixed with 1 µL 1 M DTT, 2.5 µL NuPAGE® LDS (Lithium Dodecyl Sulfate) sample buffer (Invitrogen) and milliQ water to a total volume of 10 µL and heated at 99°C for 20 min. Following centrifugation (14,000 rpm for 3 min), samples were analysed on NuPAGE® 4—12% Bis-Tris gels (Invitrogen) using 1 X NuPAGE® SDS Running Buffer at 200 V, 120 mA for 35 min. Gels were stained by silver or Coomassie Brilliant Blue R-250. Mark12™ (Invitrogen) was used as molecular weight marker.

3.4.6 Isoelectric focusing

Varying volumes of protein as well as 2 µL Marker (pI 4—6.5, GE Healthcare) was resolved on a PhastGel™ pI 3—9 (GE Healthcare) by the Phast system (GE Healthcare). The gel was stained by silver using according to the protocol of the Phast staining system (GE Healtcare) and dried.

3.4.7 Mass spectrometry

A 20 µL GELoader tip (Eppendorf) was bent in the end. A slurry of Selfpack POROS® 20 R1 (for NTR and NTR:Trx) or POROS® 20 R2 (for Trx) (both from Applied Biosystems) in methanol was applied, and a 2—5 mm column was packet at the constricted tip. This small column was equilibrated with 10 µL of 0.1% trifluoroacetic acid (TFA). An appropriate amount of full-length protein was diluted in 0.1% TFA and 10 µL of this sample was loaded. The column was washed with 2 x 10 µL of 0.1% TFA, and proteins were eluted directly on a MTP 384 target plate ground steel TF (Bruker Daltonics®) in small droplets using 20 mg/mL sinapinic acid in 70% acetonitrile (ACN)/0.033% TFA. Following crystallisation samples were analysed by MALDI-TOF using an Ultraflex II mass spectrometer (Bruker Daltonics®). Protein Standard I (range 5—17.5 kDa) or II (range 20—70 kDa) (Bruker Daltonics®) diluted in 0.1% TFA was used for calibration.

Electrospray mass spectrometry was performed at Syddansk University by Post doc Martin Zehl.

3.4.8 Complex formation using NADPH and $NADP^+$

The experiment was carried out under anaerobic conditions using a glove-box (Anaerobic Flexible Vinyl Coy Chamber, Coy Laboratories) with nitrogen/hydrogen atmosphere, 2—4 % hydrogen, kindly made available by Associate Professor, PhD Hans Erik Mølager Christensen and supervised by Post doc Ida Noemi Simon. Following treatment of HvNTR2_C145S with 1 mM DTT for 30 min at room temperature, excess DTT was removed using a NAP-5 desalting column (GE Healthcare). HvNTR2_C145S was pre-incubated with NADPH or $NADP^+$ in varying concentrations for 20 min. A spectrophotometer (Hewlett Packard 8453 UV/visible spectrophotometer) was reset using a reaction mixture in which HvTrxh2_C49S-TNB was omitted. The final reaction mixture in a 100 µL cuvette contained 30 µM HvNTR2_C145S, 20 µM HvTrxh2_C49S-TNB, varying concentrations of NADPH/$NADP^+$, 2 mM EDTA, 30 mM Tris-HCl pH 8.0. The reaction was started by addition of HvTrxh2_C49S-TNB, and the release of TNB was followed at 412 nm every 10 s for 50 min.

Chapter 4

Homology model of a complex between thioredoxin and NADPH-dependent thioredoxin reductase

4.1 Introduction

This chapter describes a model of HvNTR2 covalently bound to HvTrxh2 through an intermolecular disulfide bond between the two active sites, thus mimicking a catalytic intermediate. The model is based on the crystal structures of HvTrxh2 (Maeda *et al*., 2006a) and HvNTR2 (Chapter 2; Kirkensgaard *et al*., 2009), and was constructed using computational tools, since all attempts to obtain a crystal structure of the complex were unsuccessful. The crystal structure of a corresponding complex from *E. coli*, EcNTR covalently linked to EcTrx (Lennon *et al.*, 2000), served as a template for the homology modelling. The hypothesis was that the HvNTR2:HvTrxh2 model could provide new insight concerning the interactions between Trxs and LMW NTRs in a eukaryotic Trx system.

4.2 Results and discussion

4.2.1 Building and evaluating a complex model between HvNTR2 and HvTrxh2

A model was constructed of HvNTR2 in the FR conformation covalently bound to HvTrxh2 *via* an intermolecular disulfide between the two active sites (described in detail in Section 4.4.1). Briefly the two domains of HvNTR2 were separated and independently superposed with the corresponding domains of EcNTR from the crystal structure of EcNTR:EcTrx (pdb 1F6M, Lennon *et al.*, 2000). Likewise a crystal structure of HvTrxh2 was superposed to EcTrx. The model was build by homology modelling using MOE (Chemical Computing Group Inc.) and the modelling involved building the linker region between the

FAD domain and NADPH domain, since the rotation of one domain relative to the other positions these differently. Furthermore, a disulfide was build between $Cys148_{HvNTR2}$ and $Cys46_{HvTrxh2}$ followed by several rounds of energy minimisation coupled with parallel analysis of angles and bond lengths.

Superposition of the final model with the crystal structure of the EcNTR:EcTrx complex (Figure 4.1) gives an overall r.m.s.d. of 1.12 Å of C^{α}-atoms. The individual r.m.s.d. are 0.94 Å for the FAD domain, 1.04 Å for the NADPH domain, and 1.60 Å for the Trxs, calculated as least-square deviations using Coot (Emsley & Cowtan, 2004).

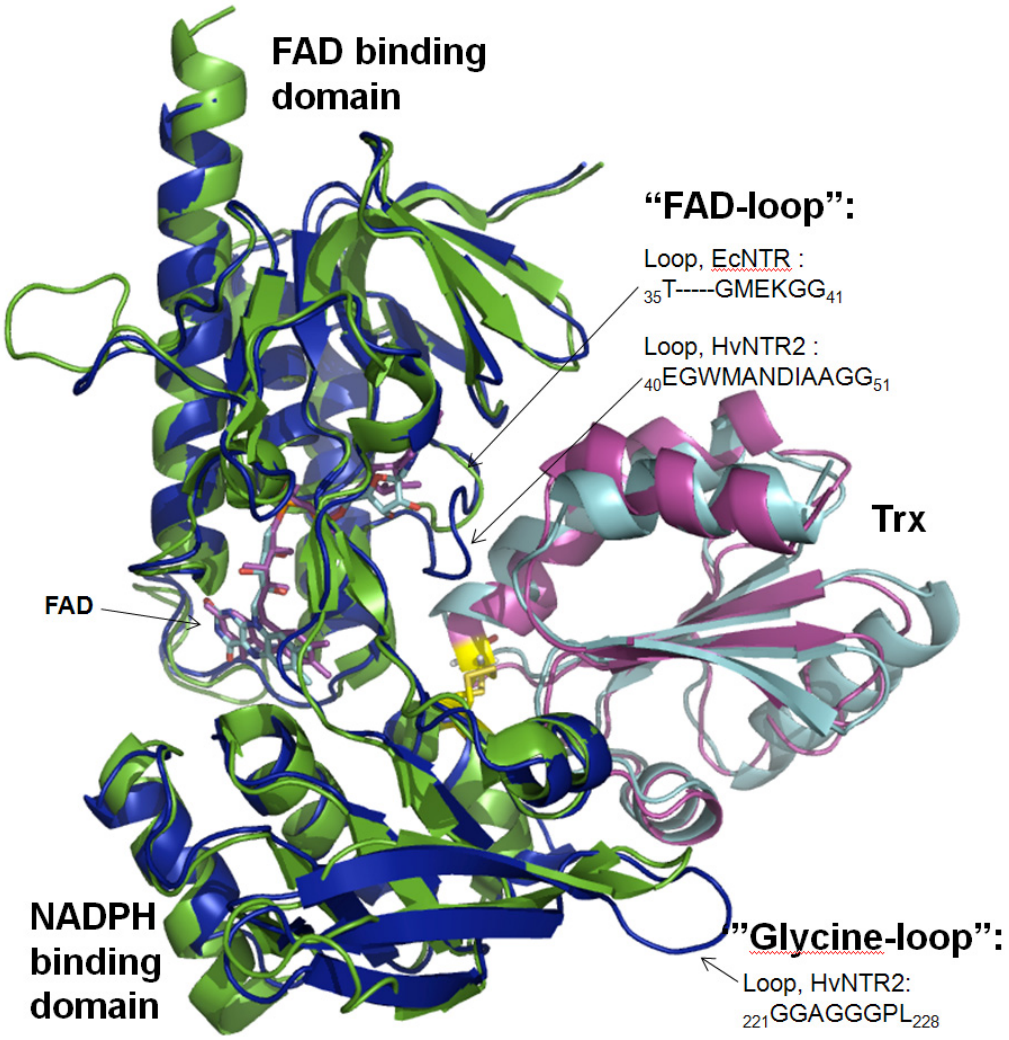

Figure 4.1. A model of the complex of HvNTR2 (dark blue) bound covalently through an intermolecular disulfide bond (yellow) to HvTrxh2 (cyan). The model is superposed with the crystal structure of EcNTR in the FR conformation (green) bound to EcTrx (magenta) (pdb 1F6M, Lennon *et al.,* 2000). The FAD molecules in HvNTR2 and EcNTR are shown in cyan and magenta respectively, and the positions of two examined loops, called the 'FAD-loop' and the 'Glycine-loop' in the following, are marked with arrows. Image generated in PyMOL (DeLano, 2002).

The quality of the model was evaluated by inspecting bond angles and lengths of the protein backbone. The lengths of all examined bonds deviate less than four standard deviations (4σ) from standard bond lengths (Figure 4.2).

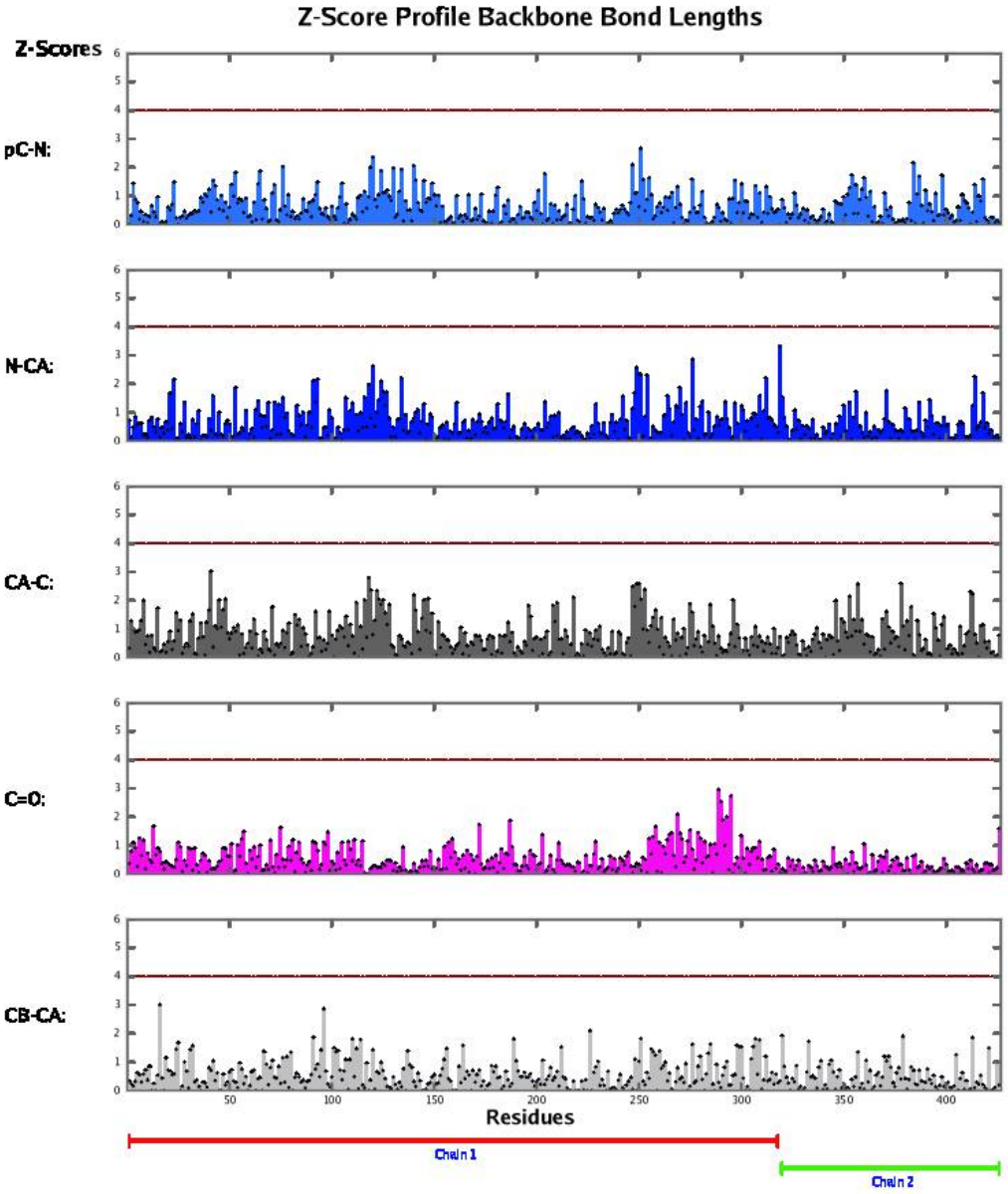

Figure 4.2. Evaluation of covalent backbone bond lengths in the final complex model. Z-scores (deviation from standard bond lengths) for the different bonds of the backbone are shown for the complex of HvNTR2 (Chain 1, red line) and HvTrxh2 (Chain2, green line). Values <4σ (marked with brown lines) are allowed. The image was generated using MOE.

Furthermore, backbone dihedral bond angles from Ramachandran plots (calculated using MOE) of the final model showed no outliers (residues with disallowed combinations of psi and phi angles, Figure 4.3). Of the 426 residues in total, 398 (93%) are in the most

favourable area, whereas 28 residues are within the allowed area (open circles in the figure).

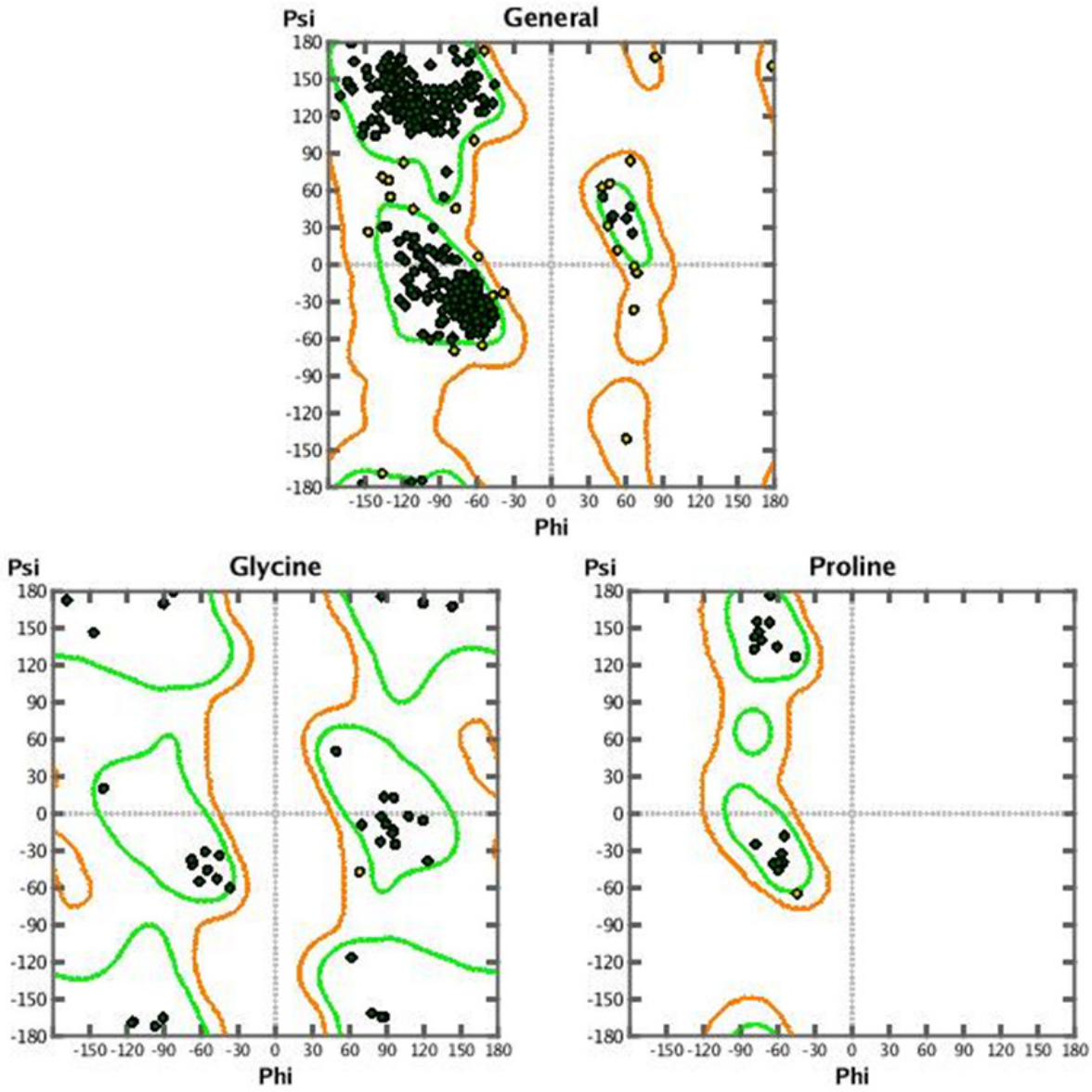

Figure 4.3. Ramachandran plots generated by the program MOE of the final model of a HvNTR2:HvTrxh2 complex. The three plots show the combination of psi and phi angles of all residues (except glycine and proline), glycine and proline, respectively. Green areas and filled circles are the most favourable whereas brown areas and open circles are allowed areas.

For HvNTR2 most of the residues in the allowed area are also found in the allowed area for the original crystal structure. However, some of the residues were in the favoured region in the crystal structure. These are found in the linker regions between the NADPH and FAD domain as well as in the loop $_{40}$EGWMANDIAAGG$_{51}$ found in the FAD domain of

HvNTR2 (called FAD-loop in the following, position shown in Figure 4.1). Underlined residues have shifted from being in the most favoured region in the crystal structure to being in the allowed region (not shown) in the model of HvNTR2:HvTrxh2. For HvTrxh2 most of the residues which were in the allowed region of the model were also in the allowed region in the original crystal structure (*not shown*). One residue, $Lys108_{HvTrxh2}$, which is bound to the FAD domain of HvNTR2 (see below), has improved from allowed to favoured, while the residue next to is, $Ala109_{HvTrxh2}$, has changed from favoured to allowed. $Pro48_{HvTrxh2}$ from the active site was before in the favoured but is now located at the border to the allowed area. It is possible that more rounds of energy minimisation could increase the number of residues in the most favourable area in the model. However, there is a risk of over-fitting the structure.

The original crystal structure of HvNTR2 (resembling the FO conformation most) and the final model in the FR conformation were used as templates for docking HvTrxh2 using the program DOT 2.0 (Baker *et al*., 2001; Word *et al*., 1999; Sanner *et al*., 1996). In both cases, HvTrxh2 was positioned outside the active site on HvNTR2 in the docked model, and mainly in the NADPH binding site. Several positively charged arginines from this site were mutated to alanine *in silico* since these may cause the attraction to the NADPH binding site. However, this did not improve the docking experiments. It was further attempted to dock EcTrx into EcNTR (both from the complex crystal structure). However, this was also unsuccessful.

4.2.2 Intermolecular HvNTR2:HvTrxh2 interactions

Identified interactions between HvNTR2 and HvTrxh2 in the complex model were listed using the program LIGPLOT (Wallace *et al*., 1995) (see Section 4.4.1.7 for a description of LIGPLOT). The identified intermolecular interactions in the complex (listed in Appendix B) are shown schematically (Figure 4.4). The number of atoms involved in the hydrophobic contact between pairs of residues is indicated in Figure 4.4 by the width of the connecting blue lines.

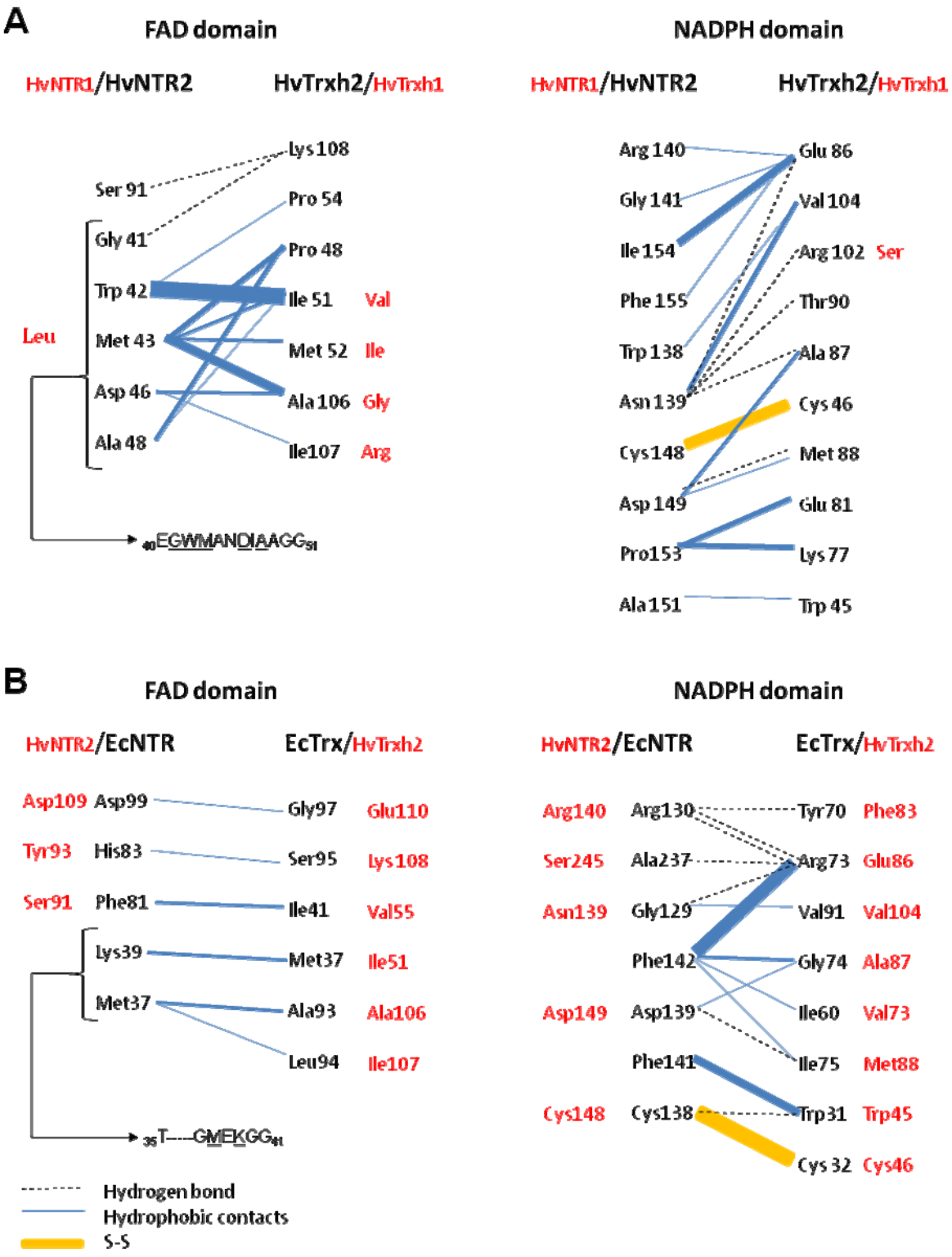

Figure 4.4. Trx-NTR interactions identified by LIGPLOT (Wallace *et al.*, 1995) on (**A**) the model of a complex between HvNTR2 and HvTrxh2 and (**B**) on the crystal structure of a complex of EcNTR:EcTrx (pdb 1F6M, Lennon *et al.,* 2000). In (A), HvNTR1 or HvTrxh1 residues corresponding to the HvNTR2 and HvTrxh2 residues in the model are included and shown in red in case they are not identical to the residues in the HvNTR2 and

HvTrx2 isoforms. The interactions are shown for the FAD domain (left panel) and for the NADPH domain (right panel) of HvNTR2. The residues marked with a left bracket are all positioned in the FAD-loop with the sequence $_{40}$EGWMANDIAAGG$_{51}$ found in the FAD domain of HvNTR2. Its position is shown in Figure 4.1. In B), the corresponding residues in HvNTR2 or HvTrxh2 are shown in red (for a few of the residues they could not be assigned since the sequences and structures vary too much). The residues marked with a left bracket are positioned in a loop (corresponding to the FAD-loop of HvNTR2) with the sequence $_{35}$T-----GMEKGG$_{41}$. The width of the connecting blue lines is scaled to indicate the number of hydrophobic contacts between atoms in the residues.

4.2.2.1 Interactions between HvTrx2 and the FAD domain of HvNTR2

For the FAD domain of HvNTR2 all but one of the residues predicted to interact with HvTrxh2 are positioned in the FAD-loop (Figure 4.4A). An alignment of various NTRs (Figure 4.5A, full alignment in Appendix C) shows that with the exception of the residues Trp42$_{HvNTR2}$ and Met43$_{HvNTR2}$, this sequence is conserved among NTRs from monocot plants. Between NTR isoforms 1 and 2, only two very conservative substitutions are observed at Trp42 (Trp/Phe) and Met43 (Met/Leu). Among dicot plants Ala49 is replaced by a proline, which could have some consequences for the flexibility and adaptability to different Trx isoforms. However the position of the backbone of the loop is not changed due to this proline (Figure 4.5B). For NTR-Cs, which are described in Chapter 1, the corresponding sequence, EG(Y/C)Q(M/V)GG-VPGG, is one residue shorter than in the other plant NTRs. The FAD-loop is positioned the same way (Figure 4.5B) in the available structures of eukaryotic LMW NTRs (HvNTR2 from Kirkensgaard *et al*., 2009; AtNTR-B from Dai *et al*., 2006; and the two structures of NTR from yeast from Zhang *et al*., 2009 and Oliveira *et al*., 2010), and the proline of the dicot AtNTR-B does not change the position of the loop (Figure 4.5B).

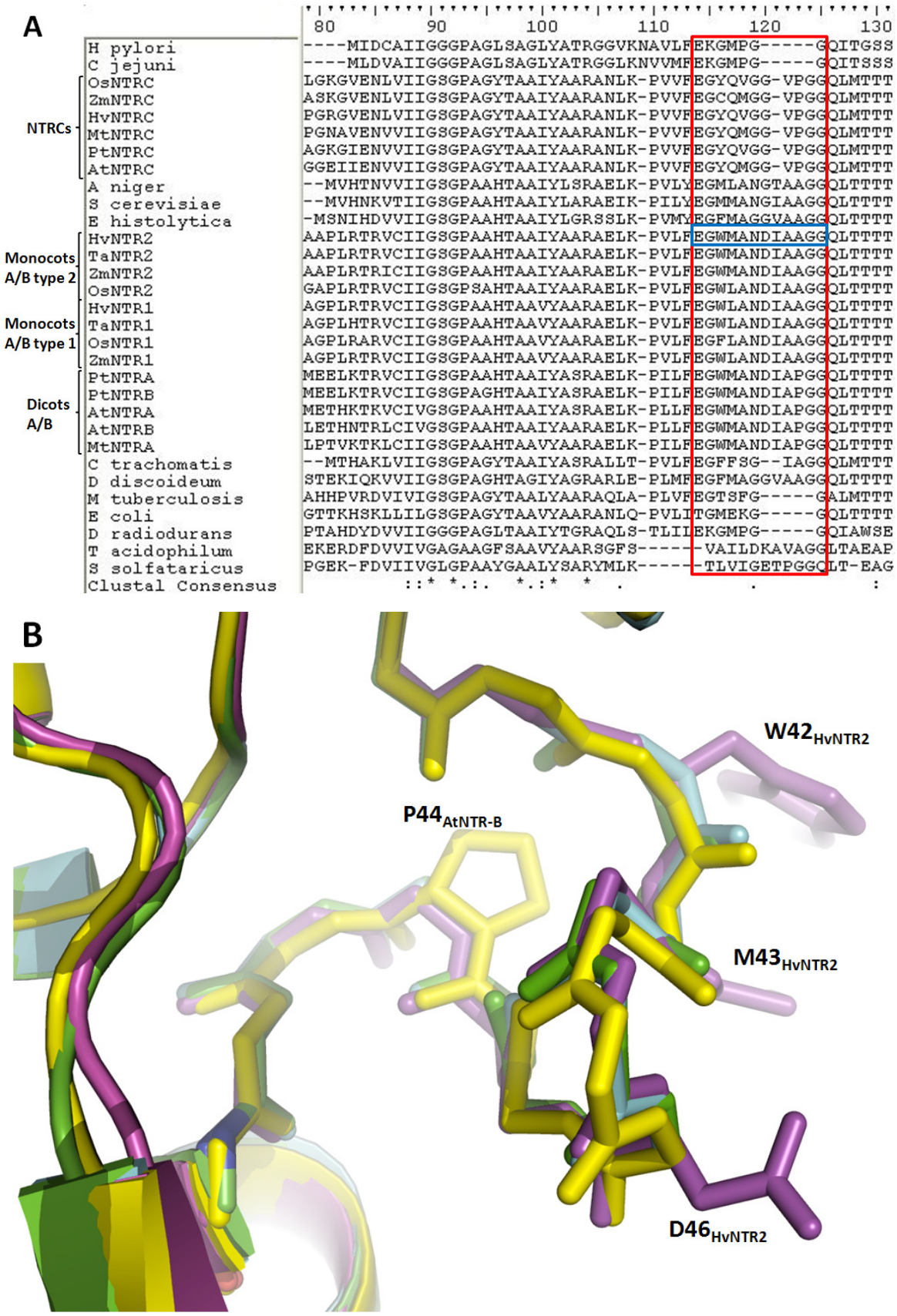

Figure 4.5. Partial alignment of selected NTRs (see below) and structural comparison of the FAD-loop. (**A**) The FAD-loop is conserved in plants and yeast (boxed in red). The same loop is boxed in blue for HvNTR2. (**B**)

Comparison of the FAD-loop in the available structures of eukaryotic LMW NTRs: HvNTR2 (magenta, pdb 2WHD, Kirkensgaard *et al*., 2009), AtNTR-B (yellow, pdb 1VDC, Dai *et al*., 2006), and two structures of NTR from yeast (cyan, pdb 3D8X, Zhang *et al*., 2009 and green, pdb 3ITJ, Oliveira *et al*., 2010). Only the backbones of the loops are shown for clarity, except the proline from AtNTR-B and three of the residues from HvNTR2 predicted to interact with HvTrxh2. (**A)** The NTRs, with their accession numbers given in parentheses, are HvNTR1 (A9YZV9), HvNTR2 (A9LN30) and HvNTRC (B0FXK2) from *Hordeum vulgare* (barley); TaNTR1 (Q8VX47) and TaNTR2 (TC297680) from *Triticum aestivum* (wheat); OsNTR1 (Q69PS6), OsNTR2 (Q6ZFU6) and OsNTRC (Q70G58) from *Oryza sativa* (rice); ZmNTR1 (B6TPI3), ZmNTR2 (B7ZY93) and ZmNTRC (B4FJQ7) from *Zea mays* (maize); AtNTRA (Q39242), AtNTRB (Q39243) and AtNTRC (O22229) from *Arabidopsis thaliana* (mouse-ear cress); PtNTRA (AC149479), PtNTRB (B9I0K8) and PtNTRC (B9H9S9) from *Populus trichocarpa* (western balsam poplar); MtNTRA (A6XJ26) and MtNTRC (A6XJ27) from *Medicago truncatula* (barrel medic, a legume); S_cerevisiae (P29509) from *Saccharomyces cerevisiae* (yeast); D_discoideum (Q54UU8) from *Dictyostelium discoideum* (amoeba "slime mold"); E_histolytica (C4LW95) from *Entamoeba histolytica* (anaerobic parasitic protozoan); A_niger (XP_001389279) from *Aspergillus niger* (fungus); T_acidophilum (Q9HJI4) from *Thermoplasma acidophilum* (facultative anaerobe archaea); S_solfataricus (Q97W27) NTRB from *Sulfolobus solfataricus* (archaea); E_coli (P0A9P4) from *Escherichia coli* (Gram-negative bacteria); C_trachomatis (O84101) from *Chlamydia trachomatis* (Gram-negative bacteria); M_tuberculosis (P52214) from *Mycobacterium tuberculosis* (bacteria); H_pylori (P56431) from *Helicobacter pylori* (Gram-negative bacteria); D_radiodurans (Q9RSY7) from *Deinococcus radiodurans* (extremophilic bacteria, Gram-positive), and C_jejuni (Q0PBZ1) from *Campylobacter jejuni* (Gram-negative bacteria). The alignment is made in ClustalW2 (Thompson *et al*., 1994) and edited using BioEdit (Hall, 1999). A full alignment is given in Appendix C.

In *Saccharomyces cerevisiae* (yeast), the FAD-loop has the sequence EGMMANGIAA, and was predicted to be involved in the binding of Trx by hydrophobic contacts (Zhang *et al*., 2009). A corresponding sequence is found in LMW NTRs from other eukaryotes as well, e.g. *Aspergillus Niger* (fungus), *Entamoeba histolytica* (anaerobic parasitic protozoan) and *Dictyostelium discoideum* (amoeba), all have varieties of this sequence (Figure 4.5). Examples of bacteria containing a similar hydrophobic sequence are also found; the Gram-negative bacteria *Chlamydia trachomatis* has the two residue shorter FAD-loop sequence EGFFSG--IAGG. The corresponding loop of EcNTR is five residues shorter ($_{35}$T-----G<u>M</u>E<u>K</u>GG$_{41}$). It has very little resemblance to the loop of HvNTR2 and it interacts with EcTrx through few hydrophobic contacts (Figure 4.4B). By contrast, the FAD-loop in HvNTR2 was predicted by the model to interact with HvTrxh2 through multiple hydrophobic contacts, primarily mediated by Trp42$_{HvNTR2}$ and Met43$_{HvNTR2}$ (Figure 4.4A).

The modelled position of the FAD-loop in HvNTR2:HvTrxh2 is not comparable to the position of the loop in the EcNTR:EcTrx structure (Figure 4.6). Central in the FAD-loop of HvNTR2 is $Met43_{HvNTR2}$ which fits into a cavity on the surface of HvTrxh2 (Figure 4.6A and C). $Met43_{HvNTR2}$ is predicted to interact with four nearby residues; $Ile51_{HvTrxh2}$, $Met52_{HvTrxh2}$, $Ala106_{HvTrxh2}$ and $Ile107_{HvTrxh2}$ (Figure 4.4A). $Met43_{HvNTR2}$ forms one of three 'fingers', together with $Trp42_{HvNTR2}$ and $Asp46_{HvNTR2}$, protruding on the surface (Figure 4.7). $Ile51_{HvTrxh2}$ is wedged in between $Met43_{HvNTR2}$ and $Trp42_{HvNTR2}$ and positioned for multiple hydrophobic interactions with $Trp42_{HvNTR2}$ (Figure 4.4A, 4.6C and 4.7). $Ala106_{HvTrxh2}$ is placed between $Met43_{HvNTR2}$ and $Asp46_{HvNTR2}$. $Ile51_{HvTrxh2}$ is found only two residues after the active site motif of HvTrxh2. It is not conserved in plants and is in HvTrxh1 replaced by a valine (see alignment Chapter 5, Figure 5.16). Together with the other residues interacting with $Trp42_{HvNTR2}$ and $Met43_{HvNTR2}$ it may have some effect for the minor preference of NTR for specific Trx isoforms.

The FAD-loop of EcNTR, $_{35}$T-----G<u>M</u>E<u>K</u>GG_{41}, also has a central methionine ($Met37_{EcNTR}$), which, however, has a different role in the intermolecular interaction than $Met43_{HvNTR2}$ (compare Figure 4.6C and D). $Met37_{EcNTR}$ has hydrophobic contacts to $Ala93_{EcTrx}$ and $Leu94_{EcTrx}$. The only other contact involving the FAD-loop of EcNTR is between $Lys39_{EcNTR}$ and $Met37_{EcTrx}$. Thus, EcNTR only has two residues from the FAD-loop involved in the binding of Trx (Figure 4.6B and D).

The central $Ile51_{HvTrxh2}$ is in EcTrx replaced by $Met37_{EcTrx}$, while $Ala106_{HvTrxh2}$ corresponds to $Ala93_{EcTrx}$ (Figure 4.4B). These residues protrude from the surfaces of both HvTrxh2 and EcTrx, and are placed in fairly similar positions in the two Trxs. The charge distribution and shape of the surface surrounding these residues are also very similar in the two Trxs (Figure 4.6C and D). It is thus plausible that EcTrx can accommodate the longer FAD-loop from HvNTR2, as described in Chapter 5 and that the longer FAD-loop plays a more central role in complex formation in the barley complex by providing a relatively large part of the interaction surface area.

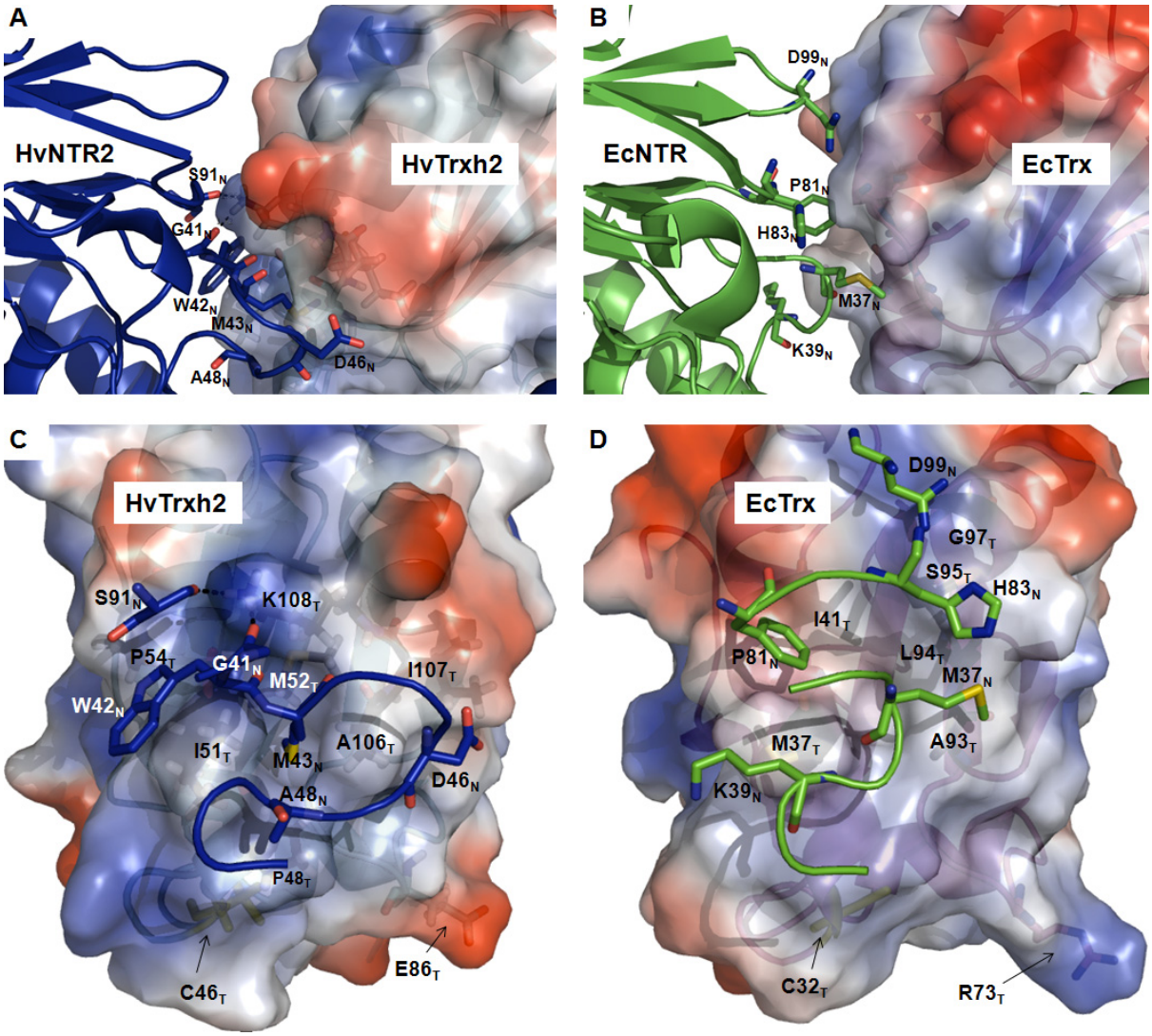

Figure 4.6. Residues involved in interactions between Trx and the FAD domain of NTR in complexes of HvNTR2 (dark blue):HvTrxh2 ((**A**) and (**C**)) and EcNTR (green):EcTrx ((**B**) and (**D**), pdb 1F6M, Lennon *et al.,* 2000). Residues from NTR and Trx are marked with 'N' and 'T', respectively. The surfaces of the Trxs are shown as electrostatic surface potential plots, where blue is positive and red negative. In (**C**) and (**D**) the active site cysteine (C32 in HvTrxh2 and C46 in EcTrx) and a residue involved in binding to the NADPH domain (R73 in EcTrx and E86 in HvTrxh2) are marked with arrows. The images were generated using the software PyMOL (Delano, 2002).

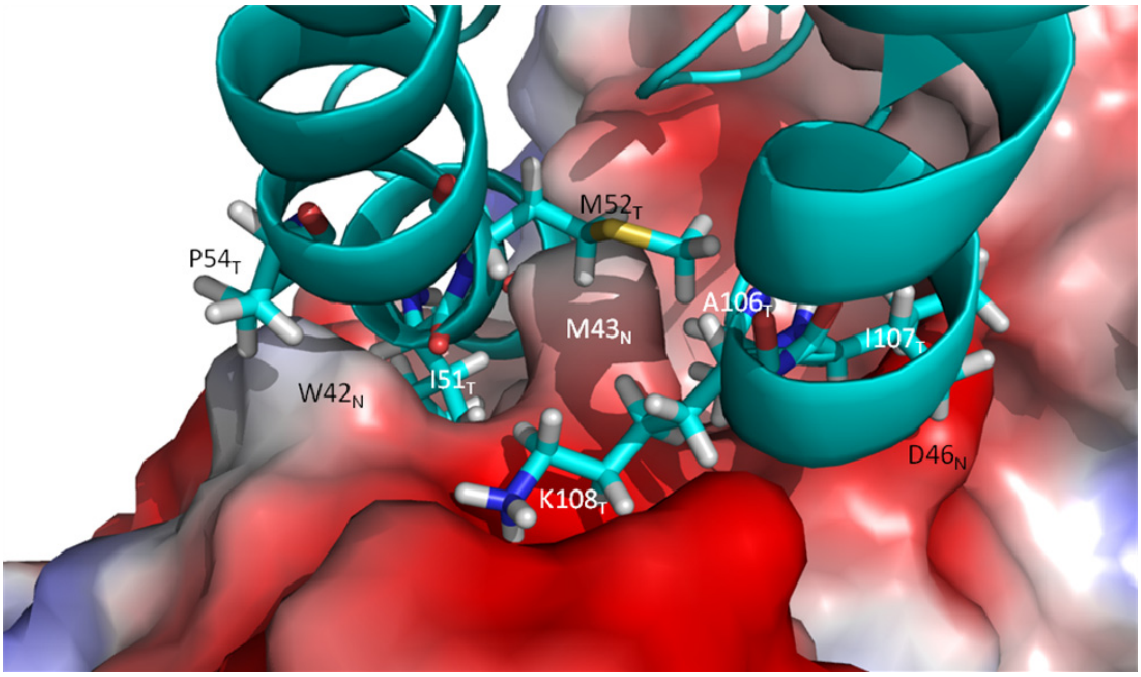

Figure 4.7. Close-up of the surface of HvNTR2 from the complex model showing interactions between HvTrxh2 (cyan) and the FAD-loop in the FAD domain of HvNTR2 (shown as electrostatic surface potential plot, where red is negative and blue positive). The residues Met43$_{HvNTR2}$, Trp42$_{HvNTR2}$ and Asp46$_{HvNTR2}$ form three 'fingers' protruding on the surface of HvNTR2. All the residues of HvTrxh2 interacting with the FAD domain are shown except Pro48$_{HvTrxh2}$ which is located behind Met43$_{HvNTR2}$.

Other contacts to the FAD domain of HvNTR2 include Lys108$_{HvTrxh2}$ forming hydrogen bonds both to Gly41$_{HvNTR2}$ from the FAD-loop and to Ser91$_{HvNTR2}$, belonging to another loop (Figure 4.4A, 4.6A and C). The positively charged Lys108$_{HvTrxh2}$ is embedded in a negatively charged area (Figure 4.7). It is conserved in most h-type plant Trxs and may be important for the binding to the FAD domain (see alignment Chapter 5, Figure 5.16). However, since the side chains of lysines are relatively flexible, a prediction of the exact conformation of the side chain of Lys108$_{HvTrxh2}$ is not appropriate. In the case of EcNTR, EcTrx exclusively binds via hydrophobic contacts to the FAD domain. Contacts, besides the ones involving the FAD-loop include Phe81$_{EcNTR}$ (corresponds to Ser91$_{HvNTR2}$) and His83$_{EcNTR}$ from a second loop in EcNTR (Figure 4.6B) interacting with Ile41$_{EcTrx}$ and Ser95$_{EcTrx}$, respectively. A third loop (Figure 4.6B) in EcNTR contains Asp99$_{EcNTR}$, which binds to the backbone of Gly97$_{EcTrx}$. This aspartate is conserved in HvNTR2, as well as in most other plant NTRs. However, the model of HvNTR2:HvTrxh2 does not bring the aspartate within intermolecular interaction distance of HvTrxh2.

To summarise, HvTrxh2 appears bound by the FAD domain of HvNTR2 through multiple hydrophobic interactions involving the FAD-loop according to the model of HvNTR2:HvTrxh2. Especially, $Trp42_{HvNTR2}$ is likely to have significant interactions with $Ile51_{HvTrxh2}$, which is situated between $Trp42_{HvNTR2}$ and $Met43_{HvNTR2}$. $Met43_{HvNTR2}$ fits into a cavity on the surface of HvTrxh2. Besides the hydrophobic contacts, $Gly41_{HvNTR2}$ from the FAD-loop as well as $Ser91_{HvNTR2}$, from another loop, are predicted to form hydrogen bonds with $Lys108_{HvTrxh2}$ (Figure 4.4A, 4.6A and C). All contacts between EcTrx and the FAD domain of EcNTR are hydrophobic, but distributed very differently from the contacts in the HvNTR2:HvTrxh2 model. There are very few contacts to the FAD-loop of EcNTR, but several to other sites in the FAD domain. Overall there seems to be a much tighter binding of HvTrxh2 to the FAD domain of HvNTR2 than of EcTrx to the FAD domain of EcNTR, which might be enabled by the longer FAD-loop offering a larger exposed surface for complex formation.

4.2.2.2 Interactions between HvTrxh2 and the NADPH domain of HvNTR2

The most significant contact between HVTrxh2 and the NADPH domain of HvNTR2 is the intermolecular disulfide bond formed by the two cysteines, $Cys148_{HvNTR2}$ and $Cys46_{HvTrxh2}$ (Figure 4.4A and 4.8A). Nearby, a hydrogen bond is formed between one of the oxygens of the side chain of $Asp149_{HvNTR2}$ and the backbone amide nitrogen of $Met88_{HvTrxh2}$ (Figure 4.8A). The corresponding $Asp139_{EcNTR}$ from EcNTR forms a similar hydrogen bond to the backbone nitrogen of $Ile75_{EcTrx}$ (Figure 4.4B and 4.8B). $Asp139_{EcNTR}$ has been proposed to be the acid/base catalyst of the dithiol-disulfide interchange in the catalytic cycle of NTR (Chapter 1, Mulrooney and Williams, 1994). In the EcNTR:EcTrx complex there is an additional hydrogen bond between the carbonyl group of $Cys138_{EcNTR}$ and the indole ring NH of $Trp41_{EcTrx}$ (Figure 4.8B). In the HvNTR:HvTrxh2 model, the corresponding tryptophan adopted a different conformation and was not predicted to interact with $C148_{HvNTR}$ (Figure 4.8A). There is however no obvious steric rationale for a different conformation of $Trp45_{HvTrxh2}$ and the result might be an artefact from the energy minimisation.

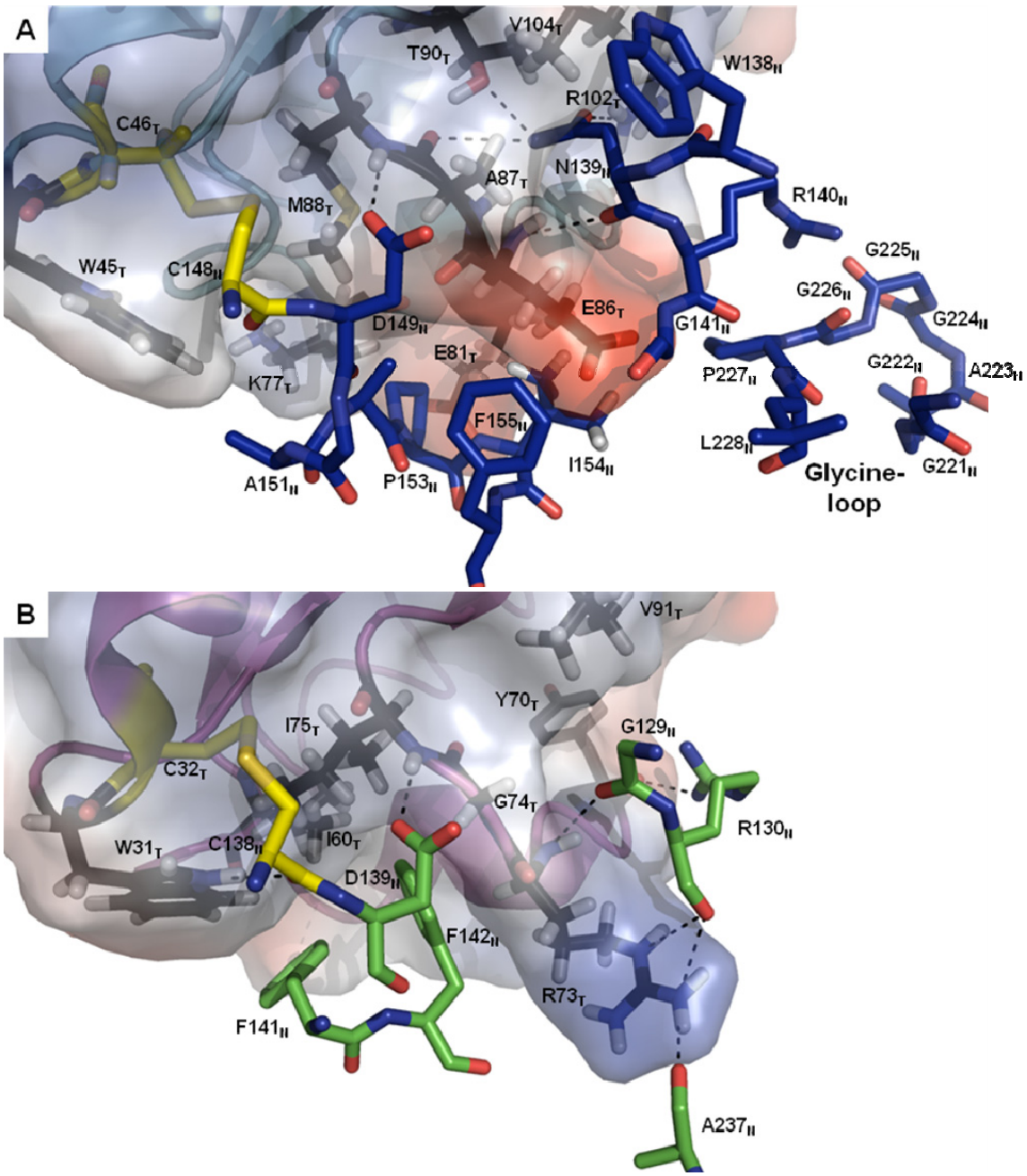

Figure 4.8. Comparison of residues involved in the interactions between of Trx and the NADPH domain of NTR in (**A**) the modelled complex of HvNTR2 (dark blue):HvTrxh2 and (**B**) EcNTR (green):EcTrx (pdb 1F6M, Lennon *et al.,* 2000). The Trxs are shown as electrostatic surface potential plots, where red is negative and blue positive. The active site cysteines are in yellow. In (**A**) the position of the Glycine-loop, $_{221}$GGAGGGPL$_{228}$, is shown (see also Figure 4.1 for its position in the structure).

As noted by Stehr *et al.* (2001) the interaction between EcTrx and EcNTR is characterized by two major features besides the interaction of the redox active cysteines; i) the docking of two phenylalanine residues from the NTR into a hydrophobic pocket of Trx next to the active site, and ii) the binding of a loop (residues 71—76 in EcTrx) into a groove

on the surface of NTR. This loop is called the *cis*-proline-loop in the following, since residue 76 is a *cis*-proline. The mentioned phenylalanines ($Phe141_{EcNTR}$ and $Phe142_{EcNTR}$) in EcNTR (see Figure 4.8B), are conserved in many bacterial NTRs (see alignment in Appendix C), and contribute multiple hydrophobic contacts to EcTrx. Thus $Phe141_{EcNTR}$ interacts with $Trp31_{EcTrx}$ from the active site motif WCGPC (Figure 4.4B and 4.8B), while $Phe142_{EcNTR}$ interacts with four different residues of which the most interactions are to $Arg73_{EcTrx}$, which protrudes from the surface of EcTrx (Figure 4.4B, 4.6D and 4.8B). In the eukaryotic LMW NTRs examined here, $Phe141_{EcNTR}$ and $Phe142_{EcNTR}$ are replaced by a proline and isoleucine (leucine in NTR-Cs), respectively. Furthermore, there is an insertion of two residues prior to these, so the sequence for plant NTRs is AAPI ($_{151}AAPI_{154}$ in HvNTR2). In the model of HvNTR2:HvTrxh2, these residues and the following $Phe155_{HvNTR2}$ are bound in a complementary pocket on HvTrxh2 by hydrophobic contacts (Figure 4.8A). The AAPIF sequence motif is also found in the other eukaryotic NTRs examined here (see alignment in Supplementary data 2) with the more general sequence A(A/L/V/S)P(I/L)(F/Y).

$Arg73_{EcTrx}$ is accommodated in a large open negatively charged groove of EcNTR (Figure 4.9B). Besides $Arg73_{EcTrx}$ forming hydrophobic contacts to $Phe142_{EcNTR}$, its guanidinium group makes two hydrogen bonds to the backbone carbonyl of $Arg130_{EcNTR}$ and one to the backbone carbonyl of $Ala237_{EcNTR}$ (Figure 4.8B and 4.9B). Furthermore the backbone nitrogen of $Arg73_{EcTrx}$ forms a forth hydrogen bond with the backbone carbonyl of $Gly129_{EcTrx}$ (Figure 4.8B and 4.9B).

The corresponding *cis*-proline-loop in HvTrxh2 (residues 84—89) is bound in a similar fashion in the current model of HvNTR2:HvTrxh2, but the groove is blocked midway by $Ile154_{HvNTR2}$ and $Pro227_{HvNTR2}$ (Figure 4.8A and 4.9A). $Pro227_{HvNTR2}$ belongs to the Glycine-loop (Figure 4.1 and 4.8A). According to the model of HvNTR2:HvTrxh2, $Glu86_{HvTrxh2}$ (corresponding to $Arg73_{EcTrx}$) is accommodated in this groove and binds through a single backbone-backbone hydrogen bond to $Asn139_{HvNTR2}$, and has several hydrophobic contacts involving $Arg140_{HvNTR2}$, $Gly141_{HvNTR2}$, $Ile154_{HvNTR2}$ and $Phe155_{HvNTR2}$ (Figure 4.4A, 4.8A and 4.9A). $Asn139_{HvNTR2}$ binds in a pocket of HvTrxh2 *via* hydrophobic contacts and four hydrogen bonds (Figure 4.4A and 4.8A). As noted by Oliveira *et al.* (2010) this residue as well as the preceding $Trp138_{HvNTR2}$ vary among species and have been suggested to contribute to

the species-specificity. Notably, Trp138$_{HvNTR2}$ and Asn139$_{HvNTR2}$ are conserved in plant LMW NTRs, but Asn139$_{HvNTR2}$ is replaced by a serine in NTR-Cs (see alignment in Appendix C).

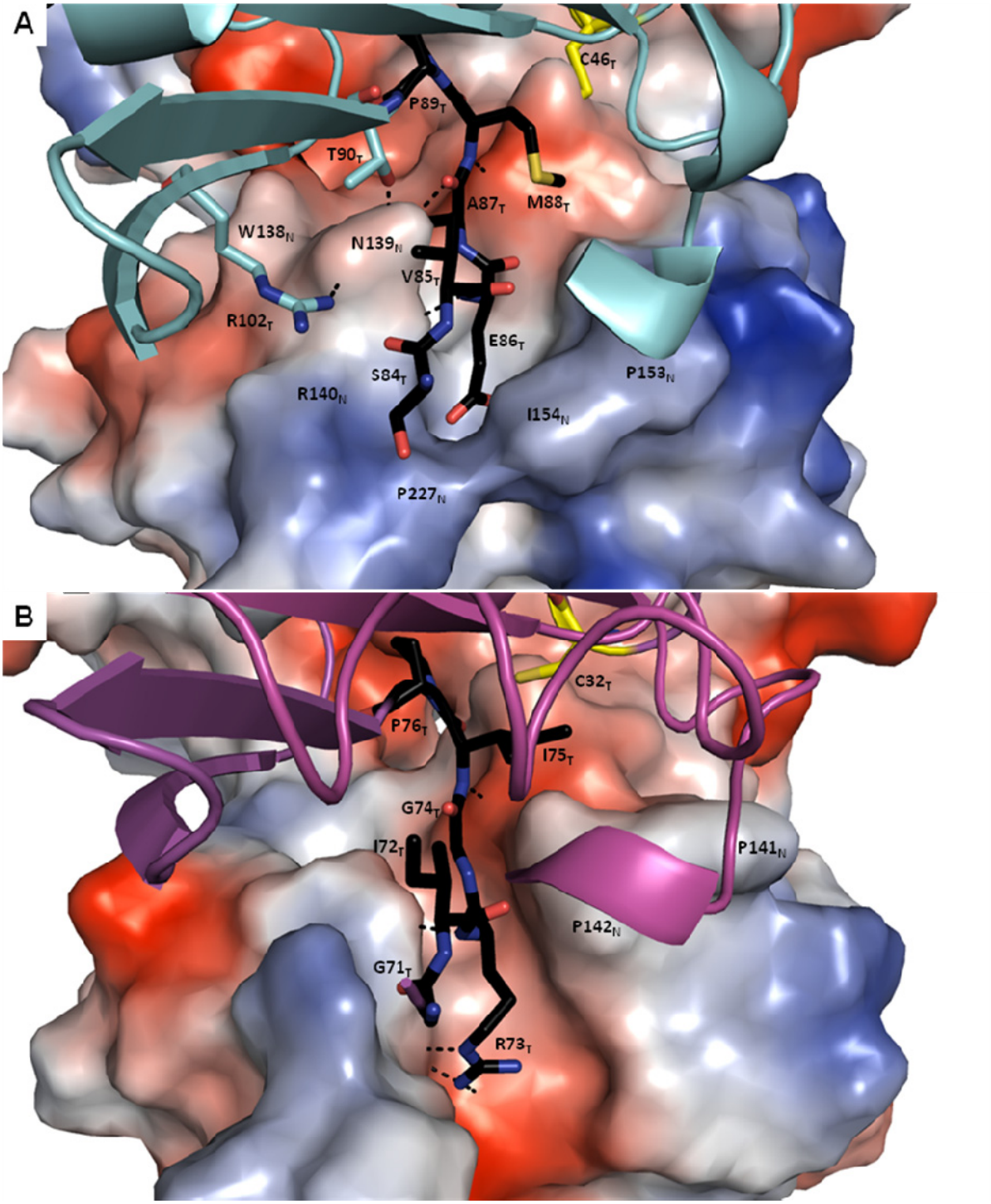

Figure 4.9. Comparison of the Trx binding surfaces in the NADPH domain of NTR in (**A**) the modelled complex of HvNTR2:HvTrxh2 (cyan) and (**B**) EcNTR:EcTrx (magenta, pdb 1F6M, Lennon *et al.,* 2000). The surfaces of the NTRs are shown as electrostatic surface potential plots, where red is negative and blue positive. Residues 23—29 and 80-83 of HvTrxh2 as well as 68—70 of EcTrx are omitted for clarity. Residues from the bound *cis*-proline-loop in Trx are shown in black. The active site cysteines in Trxs are in yellow.

4.2.3 HvNTR2:HvTrxh2 interactions and Trx substrate binding

The intermolecular interactions predicted from the model of HvTrxh2 in complex with its electron donor (HvNTR2) were compared to those present in the crystal structure of HvTrxh2 in complex with the substrate barley α-amylase/subtilisin inhibitor (BASI) (Figure 4.10A). In general, the interactions in Trxh2:BASI are fewer and quite different from those predicted in the HvNTR2:HvTrxh2 model (Figure 4.10B).

Similar to HvTrxh2:HvNTR2, HvTrxh2 is stabilised through an intermolecular disulphide bond involving the active site ($C46_{HvTrxh2}$ and $C148_{BASI}$) in the crystal structure of HvTrxh2:BASI (pdb 2IWT, Maeda *et al.*, 2006a). This was formed by allowing the single-cysteine mutant HvTrxh2_C49S to react with the single-cysteine mutant BASI_C144S conjugated to TNB (Maeda *et al.*, 2006a). Backbone atoms from BASI are found in a hydrophobic groove (Figure 4.10B) that also accommodates the active site of HvNTR2. The groove of HvTrxh2 is formed by of the active site ($_{45}$WCGP$_{48}$) as well as $_{87}$AMP$_{89}$ and $_{104}$VGA$_{106}$, and constitutes the so-called target recognition motif (Maeda *et al.*, 2006a). Underlined residues are also directly involved in binding HvNTR2 in the HvNTR2:HvTrxh2 model (Figure 4.4A). $_{87}$AMP$_{89}$ is a part of the *cis*-proline-loop, mentioned above, that is bound in a groove in the NADPH domain of HvNTR2 (Figure 4.9A). Interestingly, $Pro48_{HvTrxh2}$ and $Ala106_{HvTrxh2}$ are both involved in binding the central $Met42_{HvNTR2}$ from the FAD-loop of HvNTR2 (Figure 4.4A and 4.6C). Besides van der Waals interactions, the HvTrxh2:BASI complex has three backbone-backbone hydrogen bonds (Figure 4.10B) (Maeda *et al.*, 2006a): $Ala106_{HvTrxh2}$ to $Asp146_{BASI}$, and $Met88_{HvTrxh2}$ to the backbone oxygen and nitrogen of the cysteine, $Cys148_{BASI}$. In the model of HvNTR2:HvTrxH2 the carbonyl group of $Met88_{HvTrxh2}$ also forms a hydrogen bond, but to $Asp149_{HvNTR2}$ next to the active-site cysteine. $Glu86_{HvTrxh2}$, which seems central in the binding to the NADPH domain of HvNTR2 (Figure 4.4.A) also contributes to the binding of BASI by van der Waals interactions with $Glu168_{BASI}$ and $Glu149_{BASI}$ (Maeda *et al.*, 2006a, Figure 4.10B).

All together, there is an overlap in the residues of HvTrxh2 that are involved in the binding of HvNTR2 and BASI. Furthermore, both residues that are predicted to be involved in binding of the FAD-loop and the NADPH domain of HvNTR2 participate in the binding of BASI. One main difference is that the contact with BASI only involves few residues from both

proteins whereas the binding to HvNTR2 is much more complex. Therefore the binding to BASI does not seem very specific, and can explain why Trx can react with multiple targets.

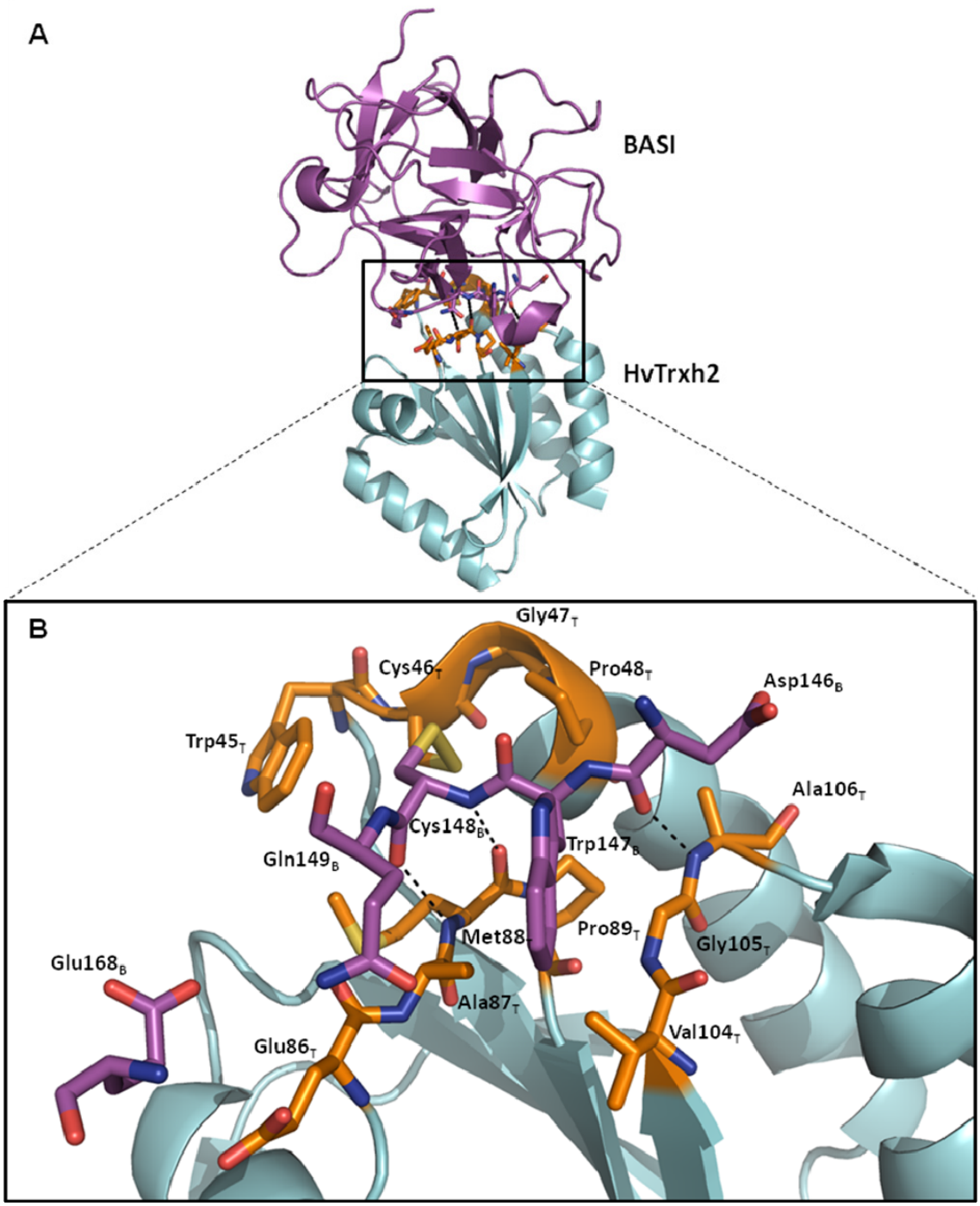

Figure 4.10. Residues in HvTrxh2 involved in binding of the protein substrate BASI. (**A**) The crystal structure of HvTrxh2 (cyan) bound covalently to BASI (purple) (pdb 2IWT, Maeda *et al.*, 2006a). The residues of HvTrxh2 interacting with BASI are in orange. (**B**) Close-up of the binding site.

4.3 Conclusion

The model suggests that the FAD domain of HvNTR2 binds HvTrxh2 by multiple hydrophobic interactions through the FAD-loop, $_{40}$EGWMANDIAAGG$_{51}$ (interacting residues underlined). Especially the residues Trp42$_{HvNTR2}$ and Met43$_{HvNTR2}$ seem to be of central importance. Interestingly, Met43$_{HvNTR2}$ is the only residue in the predicted binding interface that is not conserved in the other isoform of barley (Leu43$_{HvNTR1}$). These two residues vary between type 1 and 2 of monocot plants and could therefore provide some selectivity towards certain isoforms of Trxs. The FAD-loop is also found in other eukaryotes, but the corresponding loop of EcNTR is five residues shorter, has no resemblance to the loop of HvNTR2, and binds EcTrx with only a few hydrophobic contacts.

Concerning contacts involving the NADPH domain of NTR there are also many differences between the two complexes. In EcNTR two phenylalanines conserved in many bacteria are accommodated in a pocket of EcTrx and provide some of the main contacts. In eukaryotes these phenylalanines are not conserved and the complementary pocket of HvTrxh2 accommodated the less hydrophobic residues AAPIF. This motif is also found in other eukaryotes. EcNTR contains a large open negatively charged groove that accommodates residues 71—76 from the *cis*-proline-loop of EcTrx. The Arg73$_{EcTrx}$ protrudes on the surface of EcTrx, and is bound tightly herein. The complementary groove of HvNTR2 also accommodates a loop (residues 84—89) from HvTrxH2. However, in HvNTR2 the groove is shortened by the residues Pro227$_{HvNTR2}$ and Ile154$_{HvNTR2}$, and the residue Glu86$_{HvTrxh2}$ (corresponding to Arg73$_{EcTrx}$) does not seem to be as tightly bound.

A comparison of the binding of HvTrxh2 to the substrate BASI, revealed that many of the same residues from HvTrxh2 are involved in binding both NTR and a protein substrate (BASI). Both residues predicted to bind to the NADPH and the FAD domains of NTR are seen to interact with BASI (Maeda *et al*., 2006a). The binding of HvNTR2 is much more complex than the binding of BASI, which can explain why Trx can react with multiple targets, whereas the NTRs mainly react with Trx.

All together, the interface between HvNTR2 and HvTrxh2 in the model is very different from that of EcNTR:EcTrx. Many of the motifs found to be involved in the binding of HvTrxh2 are also found in other eukaryotes. Therefore, the modelled complex of HvNTR2:HvTrxh2 provides new insight into how eukaryote LMW NTRs in general may

interact with Trx. For example a sequence corresponding to the FAD-loop in HvNTR2 is found in NTRs from plants, yeast, fungi and amoebae. Since NTRs from these organisms have little resemblance to the human NTRs (Chapter 1, Section 1.1.6.2) inhibitors specific for these LMW NTRs may be designed for medical applications.

4.4 Material and methods

4.4.1 Homology modelling and refining

4.4.1.1 Superpositioning with FR conformation from *E. coli* using Coot

A model was made of HvNTR2 bound via an intermolecular disulfide to HvTrxh2 based on crystal structures of the two proteins. The crystal structure of NTR from *E. coli* bound by an intermolecular disulfide to EcTrx (pdb 1F6M, Lennon *et al*., 2000) was used as a template for positioning the two domains of HvNTR2 as well as HvTrxh2. From pdb 1F6M chain A (EcNTR) and chain C (EcTrx) were chosen. The pdb file of HvNTR2 (2WHD, Kirkensgaard *et al.*, 2009) contains two chains of HvNTR2 of which chain A was chosen. The domains of HvNTR2 were superposed individually to the corresponding domains of EcNTR using the SSM Superpose function in the software Coot (Emsley & Cowtan, 2004; Krissinel & Henrick 2004). The FAD domain consists of residues 6—126 and 255—323 (residues 1—5 and 324—331 missing in the crystal structure of HvNTR2) and the NADPH domain consists of residue 127—254. HvTrxh2 was taken from a complex of HvTrxh2 covalently bound via an intermolecular disulfide bond to the protein substrate barley alpha-amylase/subtilisin inhibitor (BASI) (pdb 2IWT, Maeda *et al.*, 2006a), and superposed with that of EcTrx.

4.4.1.2 Modelling the linker region

The two oriented domains of HvNTR2 were combined in a single pdb file and the linker regions connecting the FAD and NADPH domains were modelled using the program MOE (Chemical Computing Group Inc.) enabling the two domains to be connected. The FAD molecule was omitted since it was not recognised by MOE.

The linker regions from EcNTR (pdb 1F6M) served as a template for homology modelling. First the sequence of the HvNTR2 FAD domain was copied. The residues containing one of the β-sheet linkers plus some additional residues, $_{113}$TG**ASA**R$_{117}$ (β-sheet linker in bold), in EcNTR were selected. Homology modelling was performed using the

original HvNTR2 sequence as a general template but choosing 'use selected residues to override template' to keep all residues except the selected once fixed. The forcefield Amber94 was used in MOE. The process was repeated for the other linker selecting residues $_{245}$**HSP**$_{247}$ in EcNTR to override the template.

4.4.1.3 Energy minimisation of interface between HvNTR2 and HvTrxh2

Clashes between HvTrxh2 and Trp42$_{HvNTR2}$/Met43$_{HvNTR2}$ from the FAD-loop of HvNTR2 were observed. These were identified by choosing:

MOE|Compute|Ligand Interactions

and selecting NTR as the receptor and residues within 4.5 Å from NTR in Trx as the ligand. Residues from the interface between HvTrxh2 and HvNTR2 (within 4.5 Å from one another) were selected and energy minimised in two steps:

1. First everything was fixed, and only the side chains of the selected residues were unrestrained. Energy minimisation was performed choosing "Adjust H and LP" and "Tether Atoms: Selected" to fix backbone atoms, while allowing the side chains to move slightly (tethered) away from poor contacts.
2. Backbone and side chain atoms were unrestrained and the energy minimisation was repeated choosing "Tether Atoms: Backbone" to allow the side chains to move more freely whereas the backbone atoms are only able to move slightly.

The two steps were repeated to further optimise energy minimisation. However, there were still clashes between Met43$_{HvNTR2}$ and Trx. After a third round of energy minimisation these clashes were eliminated.

4.4.1.4 Checking the model and doing a 2nd refinement

By selecting

SEQ|Measure|Protein Geometry

the Ramachandran plots were calculated of the complex of HvNTR2:HvTrxh2. These showed outliers in the following residues belonging to the linker regions; Ala126$_{HvNTR2}$, Arg128$_{HvNTR2}$, Gly254$_{HvNTR2}$ and His255$_{HvNTR2}$. Furthermore, there were outliers in the FAD-loop, that clashed with Trx earlier in the modelling process; Trp42$_{HvNTR2}$, Met43$_{HvNTR2}$ and Ala49$_{HvNTR2}$.

In Trx Pro48$_{HvTrxh2}$ from the active site $_{45}$WCGPS$_{49}$ was an outlier (the second cysteine residues is changed to serine in the structure of Trxh2:BASI and thus also in the modelled structure of HvNTR2:HvTrxh2). This proline is not an outlier in the original structure in pdb (2IWT).

Areas around the outliers of the linker regions were chosen; $_{123}$G**AVA**RRL$_{129}$ and $_{254}$G**HEP**AT$_{259}$ (β-sheet linkers in bold, outliers underlined) and energy minimisations performed twice without tethering the atoms. This removed the outliers from the second linker but not for the first. From inspecting the model superposed with the EcTrx:EcNTR structure it was clear that an area involving the linker as well as some residues downstream, $_{125}$VARRLYFSGS$_{134}$, were positioned differently than in EcNTR (Figure 4.11, orange loop). For instance the last residues form part of an α-helix in EcNTR which was not found in HvNTR2.

Homology modelling of the residues $_{125}$VARRLYFSGS$_{134}$ in HvNTR2 with the *E. coli* complex as the template resulted in removal of the initial outliers, but positioned Tyr130$_{HvNTR2}$ outside the allowed regions of the ramachandran plots. However, this residue was transferred to the allowed region after one round of energy minimisation of the same residues.

Three outliers were found in the FAD-loop in the following residues; $_{34}$EGWMANDIAAGG$_{46}$. After a single round of energy minimisation of this loop and residues in HvTrxH2 within 4.5 Å, Trp37$_{HvNTR2}$ and Ala106$_{HvTrxh2}$ still appeared as outliers in the ramachandran plots. Further energy minimisation with the same residues, but only tethering the backbone of Trx removed Trp37$_{HvNTR2}$ from the disallowed area. Remaining outliers were removed when Ala106$_{HvTrxh2}$ along with two residues on each side were also untethered and the minimisation performed yet another time.

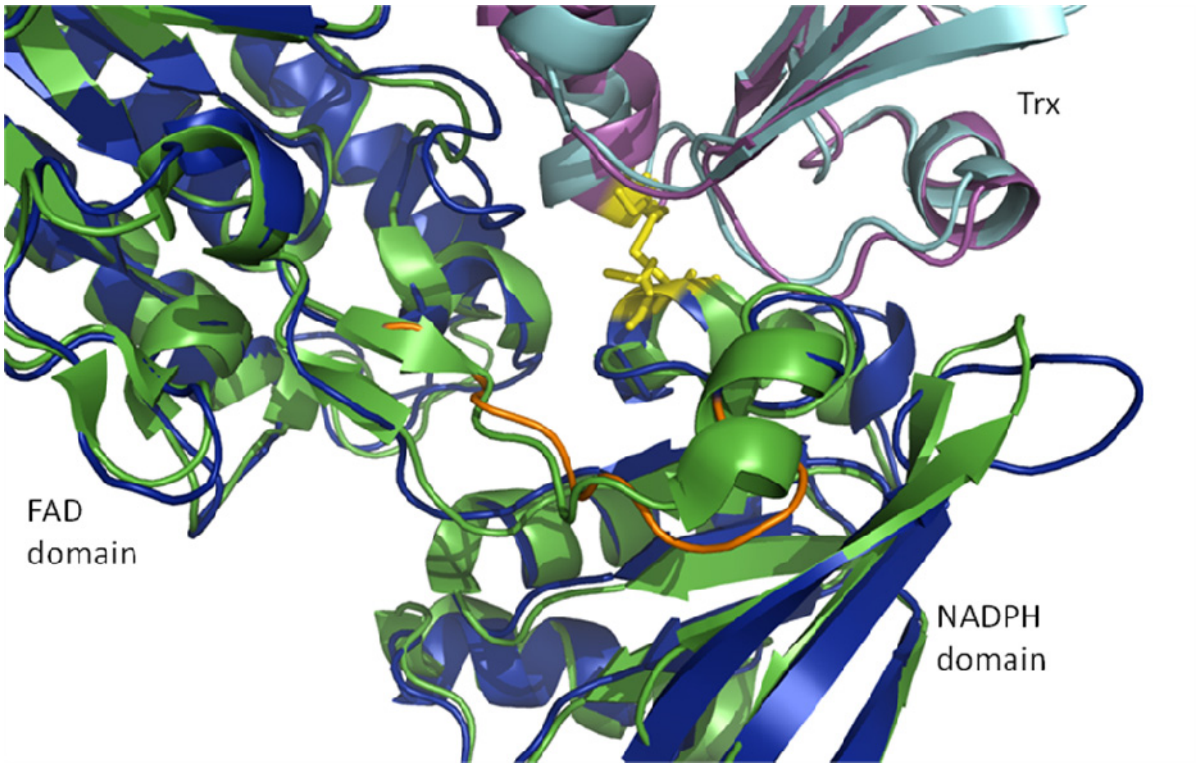

Figure 4.11. Superposition of an unrefined complex model between HvNTR2 (dark blue) and HvTrxh2 (cyan). The model is superposed with the crystal structure of EcNTR (green) bound to EcTrx (magenta) (pdb 1F6M, Lennon *et al.,* 2000). Part of the linker region in HvNTR2, residues $_{125}$VARRLYFSGS$_{134}$ (outliers underlined), are in orange. The cysteines involved in the intermolecular disulfide bond formation are in yellow.

4.4.1.5 Optimising bond lengths in the model

The bond lengths of the residues were checked and revealed the presence of too long bonds for the following residues; Ile253$_{HvNTR2}$, Gly254$_{HvNTR2}$, Asn139$_{HvNTR2}$ and Arg140$_{HvNTR2}$. These had bond lengths above the allowed threshold of 4σ (4 standard deviations) from the mean bond length. Energy minimisation was performed without tethering the backbone on these residues as well as two residues on each side. This gave acceptable bond lengths and angles.

4.4.1.6 Building the disulfide bond and final energy minimisation

The only remaining outlier, Pro48$_{HvTrxh2}$ in the active site of HvTrxh2, was left untouched while the disulfide between HvTrxh2 and HvNTR2 was formed. First different rotamers of Cys148$_{HvNTR2}$ and Cys46$_{HvTrxh2}$ were investigated but the closest were still 3.37 Å apart (see Figure 4.12), whereas a Cys-Cys bond has a length of 1.8 to 2.4 Å (Veine, 1998b).

By comparing with the complex of EcNTR:EcTrx it was found that the residues from $Phe41_{HvTrxh2}$ to $Phe56_{HvTrxh2}$ (orange in Figure 4.12) were not positioned in the same angle relative to HvNTR2 as EcTrx, which prevented the bond formation. Therefore, these residues as well as residues $_{145}CAVCD_{149}$ in NTR were energy minimised without tethering the backbone to allow disulfide bond formation using MOE and further energy minimisation. Finally energy minimisation was performed for the entire interface by selecting residues in Trx within 4.5 Å from NTR and *vice versa*.

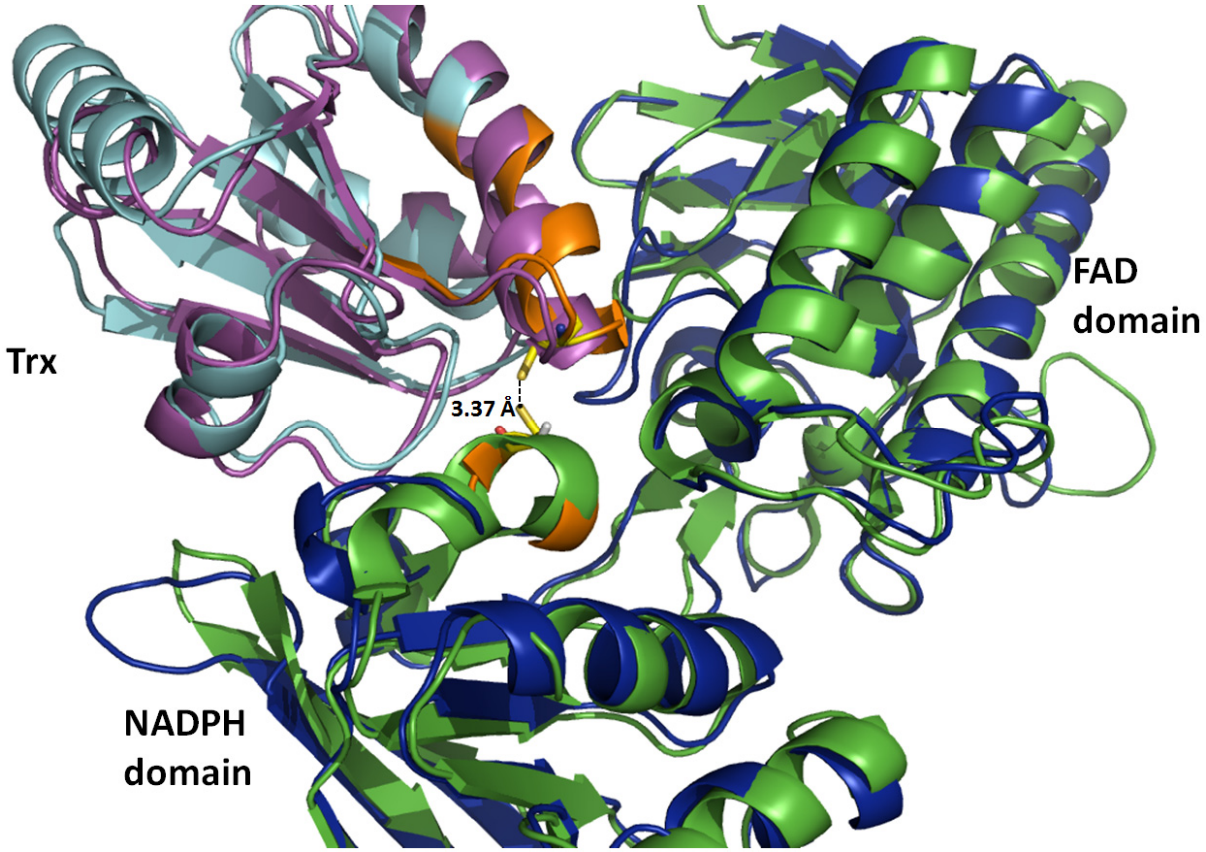

Figure 4.12. Regions that were energy minimised to build the disulfide bond. The unrefined complex model between HvNTR2 (dark blue) and HvTrxh2 (cyan) is shown superposed onto the crystal structure of EcNTR (green) bound to EcTrx (magenta) (pdb 1F6M, Lennon *et al.,* 2000). The cysteine residues involved in the disulfide bond formation are coloured yellow. The regions (orange) including residues $Phe41_{HvTrxh2}$ to $Phe56_{HvTrxh2}$ in HvTrxh2 as well as $_{145}CAVCD_{149}$ in HvNTR2 were minimised in order to form the disulfide bond between $Cys148_{HvNTR2}$ and $Cys46_{HvTrxh2}$.

4.4.1.7 Determining possible interactions between HvNTR2 and HvTrxh2 using LIGPLOT

Interactions between HvTrxh2 and HvNTR2 in the complex model were identified by the program LIGPLOT (Wallace *et al.* 1995). LIGPLOT relies on yet another program named HBPLUS (McDonald and Thornton, 1994), which calculates the hydrogen bonds and non-bonded contacts. One example of how HBPLUS calculates hydrogen bonds is shown in Figure 4.13. The criteria are that the donor atom (D) is attached to two atoms (DD) other than hydrogen, and the donor is trigonal planar (one atom at the center and three atoms at the corners of a triangle, see Figure 4.13). The NH group of the side chains of arginine, tryptophan and histidine falls into this category. In this case the program computes all possible positions of hydrogen (H) atoms attached to donor atom which satisfies the following geometric criteria relative to the acceptor (A) atom: The H-A distance should be <2.5 Å and the D-D distance <3.9 Å. Furthermore the three angles D-H-A, D-A-AA and H-A-AA should be >90°, where AA is the atom attached to A (McDonald and Thornton, 1994). HBPLUS also lists all non-bonded contacts that are less than a specified distance apart. The cut-off used for LIGPLOT is 3.9 Å (Wallace *et al*., 1995).

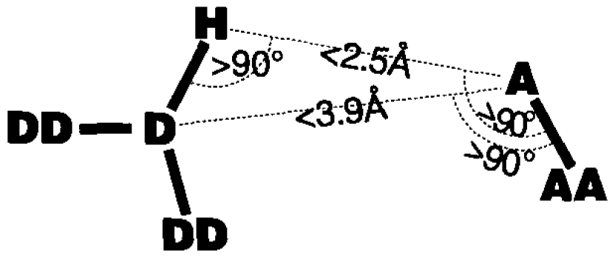

Figure 4.13. Example of geometric criteria for hydrogen bonds in the program HBPLUS. Satisfying angles and bonds are shown between the donor (D) and acceptor (A) atoms. DD are the atoms (besides hydrogen) attached to the donor, and AA is the atom attached to the acceptor. These criteria are used when the donor is trigonal planar and attached to two atoms other than hydrogen. The NH group of the side chains of arginine, tryptophan and histidine falls into this category (McDonald and Thornton, 1994). Figure from McDonald and Thornton,1994.

In the program a single or multiple residues can be chosen as well as a whole chain by writing

ligplot [name of pdb].pdb [start residue] [end residue] [chain]

and the interactions to the selected are listed. E.g. HvTrxh2 is chain B and contains the residues 13—120 and can hence be selected by typing

ligplot complex.pdb 13 120 B

resulting in a list of interactions between Trx and NTR divided in hydrogen bonds and non-bonded contacts.

Chapter 5

Study of the binding site of NTR through mutagenesis and enzyme kinetics

5.1 Introduction

The presented model of HvNTR2:HvTrxh2 (described in Chapter 4) indicated residues that could be involved in the complex formation between the two proteins. To further validate the model and assess the importance of selected amino acid residues, a number of mutants were designed and kinetically characterised. In this chapter their production and their enzyme kinetic properties in the reaction between NTR and Trx are described.

5.2 Results and discussion

5.2.1 Production and purification of mutants of HvNTR2 and HvTrxh2

HvNTR2 was mutated by site-directed mutagenesis (see Section 5.4.1) in the FAD-loop (HvNTR2_W42A, HvNTR2_M43A, HvNTR2_W42A_M43A, HvNTR2_N45A_D46A and HvNTR2_Δ42-47), as well as of some selected residues of the NADPH-domain (HvNTR2_N139A and HvNTR2_R140A). Especially $Asn139_{HvNTR2}$ was predicted to be central in the binding of HvTrxh2 because of its involvement in many intermolecular interactions (Figure 4.4A). Also mutations in the Glycine-loop were produced (HvNTR2_G225R_G226D_P227V, HvNTR2_G225R_G226D and HvNTR2_G222D_A223G _G224E), since this loop was previously suggested to be involved in the binding of Trx (Kirkensgaard *et al*., 2009, Chapter 2). For HvTrxh2 the residue $Ile51_{HvTrxh2}$ predicted to be involved in the binding to the FAD-loop (HvTrxh2_I51G) and $Glu86_{HvTrxh2}$ (HvTrxh2_E86A), predicted to be important for the binding to the NADPH domain of HvNTR2 were mutated. Finally, an active site mutant (HvTrxh2_G47P) was produced (see below). All proteins were purified using metal affinity chromatography (HisTrap) and size exclusion chromatography (gel filtration). For expression and purification see Chapter 3, Section 3.4.1.

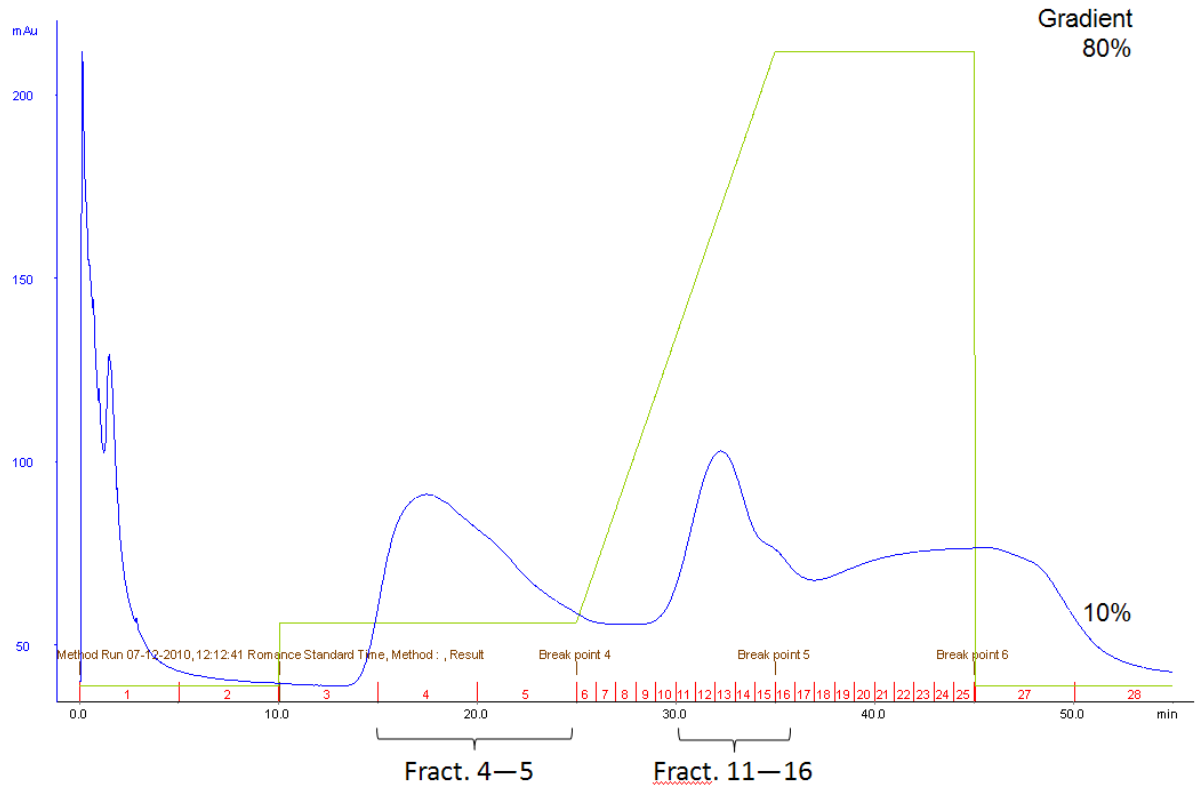

Figure 5.1. Chromatogram (blue line) from the purification of HvTrxh2_I51G from 1 L media on a 1 mL HisTrap™ HP column. The light green line shows the gradient between buffer A (10 mM imidazole, 30 mM Tris-HCl pH 8.0 and 500 mM NaCl) and B (400 mM imidazole, 30 mM Tris-HCl pH 8.0 and 500 mM NaCl) with the maximum corresponding to 80% buffer B.

A chromatogram from HisTrap purification of HvTrxh2_I51G displays peaks during the gradient from 10—80% buffer B (≈fractions 11—16) and in isocratic elution at 10% of buffer B (Figure 5.1) Both peaks appear to contain relatively pure HvTrxh2_I51G as judged from SDS-PAGE analysis (lane 4—5 in Figure 5.3) and were pooled. Further purification by size exclusion chromatography resulted in two peaks (Figure 5.2). A small peak (fraction A1) appears near the void volumn of the column, and may correspond to aggregated protein as discussed later. The major peak (fractions A6—A8) contained about 23 mg of protein and these fractions were pooled, dialysed and the protein used for kinetic studies. The purity of the sample was judged using SDS-PAGE (Figure 5.3).

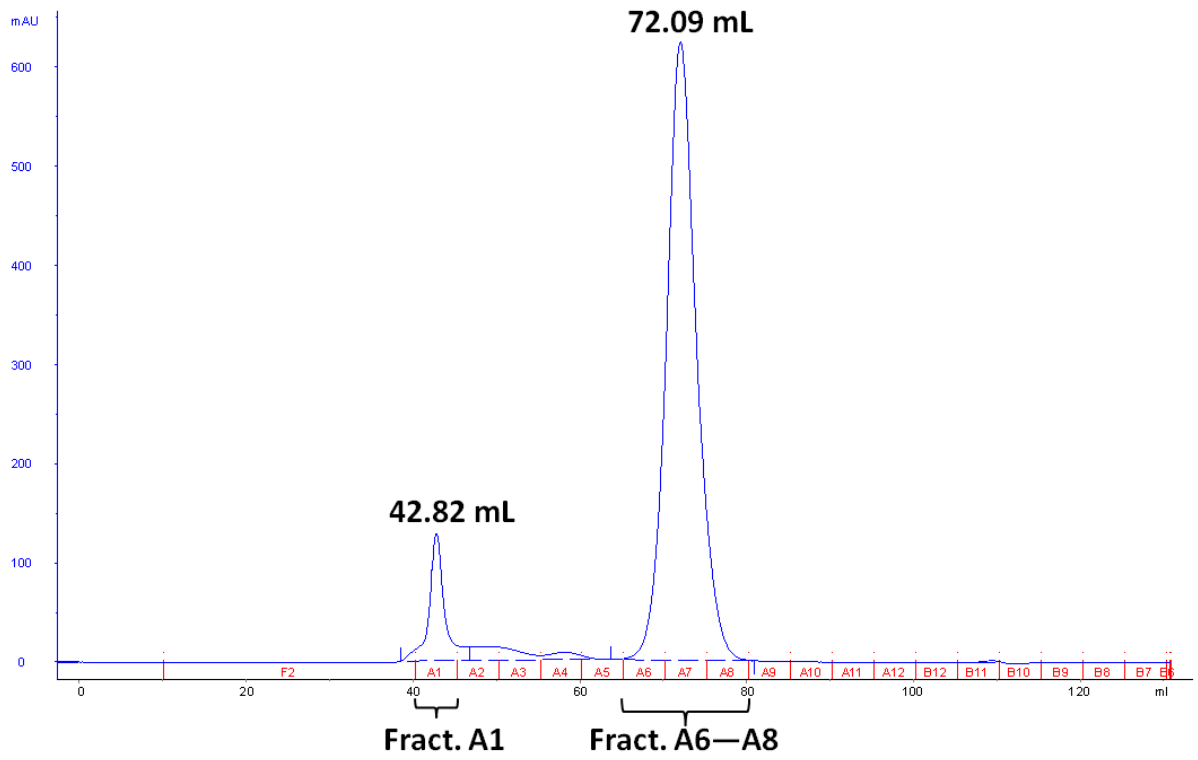

Figure 5.2. Chromatogram from gel filtration on a HiLoad™ 16/60 Superdex™ 75 column of HvTrxh2_I51G from 1 L culture. Prior to gel filtration the protein was purified on a 1 mL HisTrap™ HP column.

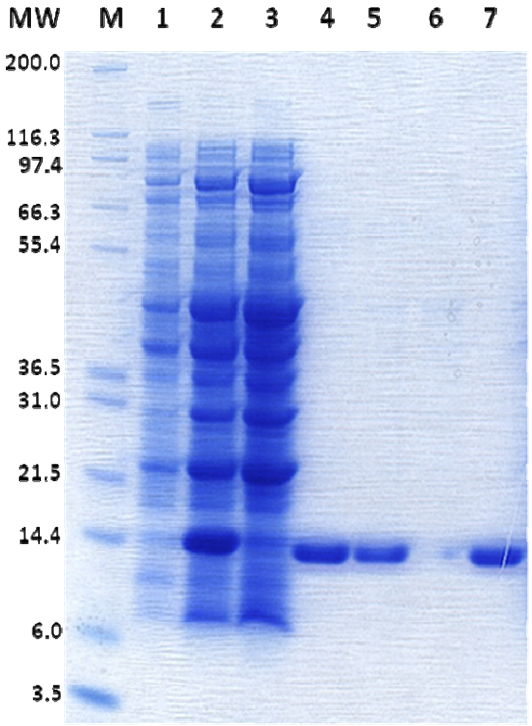

Figure 5.3. SDS-PAGE of the various purification steps of HvTrxh2_I51G. 'M' is the molecular marker Mark12™ (the molecule weights (MW) are shown in kDa). Samples were treated as described in Section 3.4.5. The lanes contain protein from (**1**) culture before induction with IPTG, (**2**) culture incubated overnight after induction

with IPTG, (**3**) flow through from the HisTrap™ HP column, (**4**) first eluting peak from the HisTrap column (fractions 4—5 in Figure 5.1), (**5**) second eluting peak from the HisTrap column (fractions 11—16 in Figure 5.1), (**6**) the first eluting peak from gel filtration on a HiLoad™ 16/60 Superdex™ 75 column (fraction A1 in Figure 5.2), and (**7**) the second peak from gel filtration (fractions A6—A8 in Figure 5.2).

HisTrap purification of HvNTR2wt and mutants resulted in chromatograms similar to the one in Figure 5.1. A typical chromatogram from gel filtration of HvNTR2wt or mutant is shown in Figure 5.4 (for HvNTR2_M42A). A front peak near the void volume (fraction A5) was followed by a peak containing yellow coloured protein (fractions A6—A7). The ratio between the areas of these two peaks varied from mutant to mutant, and was in some cases 1:1, but the first peak was always colourless and apparently contained NTR with no FAD bound (see below). Both peaks contained pure HvNTR2wt or mutant protein as judged from SDS-PAGE (Figure 5.5). The migration in the SDS-PAGE corresponded to the molecular mass of the NTR monomer.

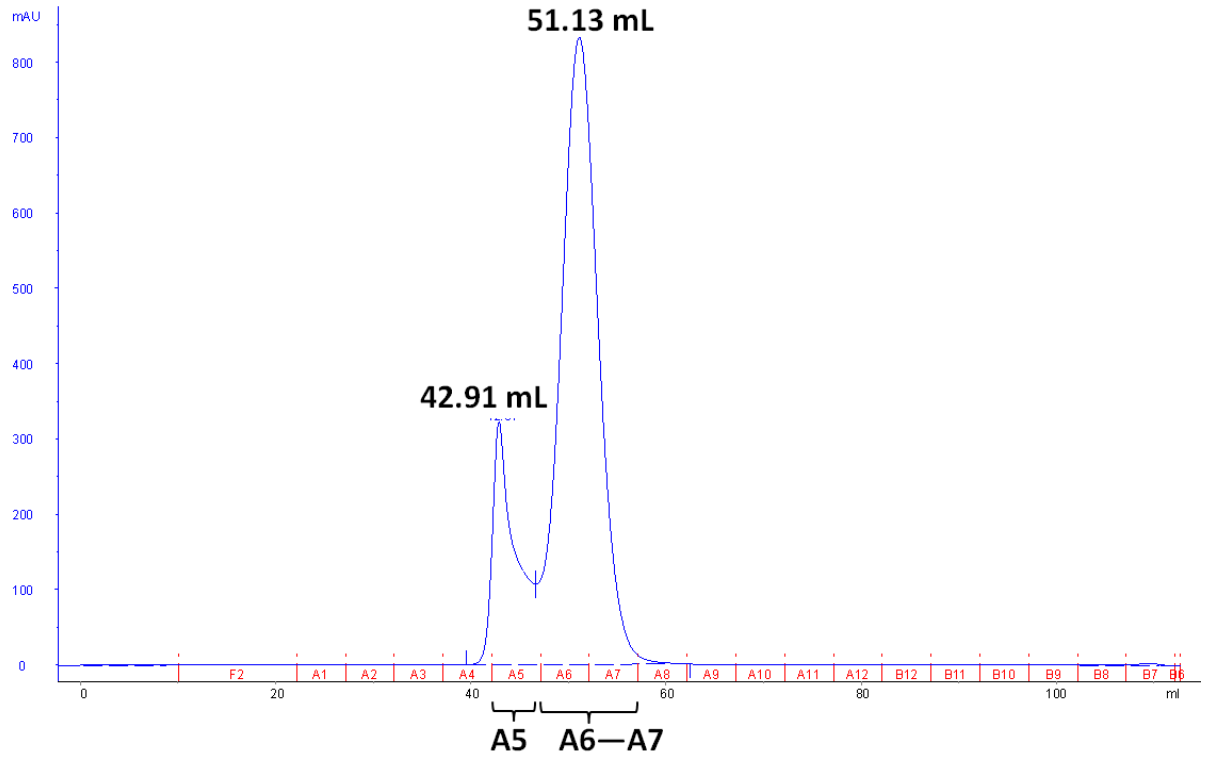

Figure 5.4. Chromatogram from gel filtration on a HiLoad™ 16/60 Superdex™ 75 column of HvNTR2_M43A from 1 L culture. Prior to gel filtration the protein was purified by nickel affinity chromatography on a 1 mL HisTrap™ HP column.

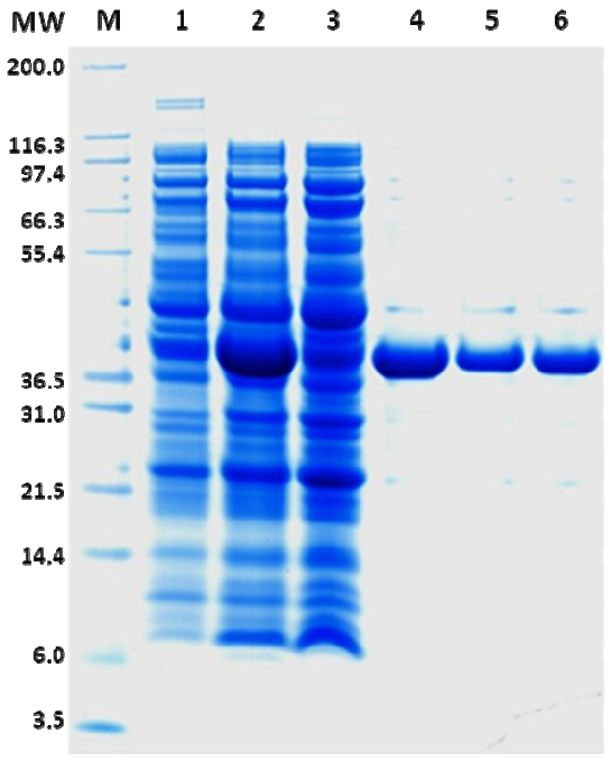

Figure 5.5. SDS-PAGE of the various purification steps of HvNTR2_M43A. 'M' is the molecular marker Mark12™; the molecule weights (MW) are shown in kDa. The lanes contain protein from (**1**) culture before induction with IPTG, (**2**) culture after overnight incubation with IPTG, (**3**) flow-through from the HisTrap™ HP column, (**4**) elution peak from the HisTrap column (**5**) first peak from the gel filtration on the HiLoad™ 16/60 Superdex™ 75 column (fraction A5 in Figure 5.4) and (**6**) second peak from the gel filtration (fractions A6—A7).

Comparison was made with the standards (blue curve in Figure 5.6) from a Gel Filtration Calibration Kit (GE Healthcare) to estimate the molecular weight of the proteins in the two peaks. From the elution volumes, V_e, of the standards the partition coefficient, K_{av}, was calculated using the equation

$$K_{av} = (V_e - V_0)/(V_c - V_0)$$

where V_0 = column void volume, V_e = elution volume, and V_c = geometric column volume. V_c for this column equals 120 mL. V_0 equals the elution volume for Blue Dextran 2000 (red curve in Figure 5.6) and was found to be 42.54 mL. A calibration curve is plotted in Figure 5.7 as K_{av} versus log(molecular weight). The molecular weights of the proteins of the standard are listed in the legend of Figure 5.6. K_{av} and the apparent MW (Table 5.1) were calculated using the elution volumes in Figure 5.2 and 5.4. The first peak from both the gel filtration of HvNTR2_M43A and HvTrxh2_I51G has an elution volume very close to the

column void volume and probably contains aggregated protein. The second peak of HvNTR2_M43A corresponds to 2.0 times the size of the monomer in agreement with the observed dimeric structure of NTR. For HvTrxh2_I51G the second peak corresponds to 1.3 times the size of the monomer. The same elution volumes were obtained for the wild-type proteins (*data not shown*).

To summarise, a fraction of both HvTrxh2 and HvNTR2 wild-type as well as mutants seemed to aggregate and was eluted with the column void volume. The protein that was not aggregated was estimated to be a dimer for HvNTR2 and a monomer for HvTrxh2.

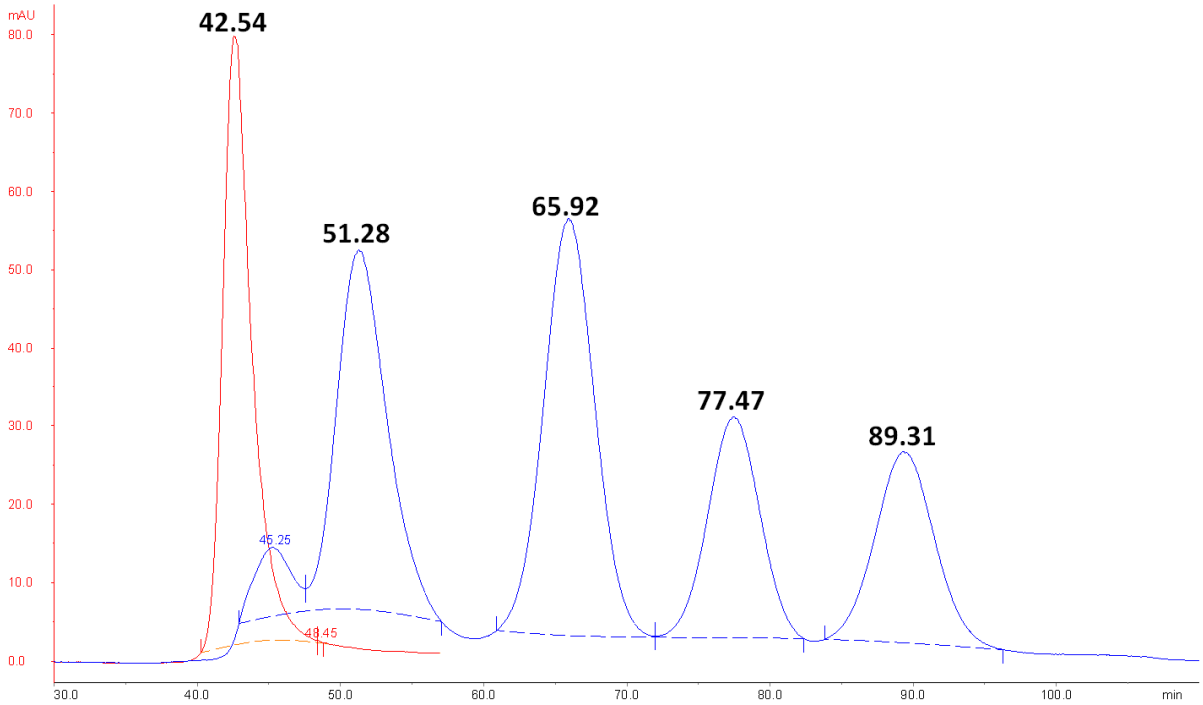

Figure 5.6. Chromatogram from the run of a Gel Filtration Calibration kit (blue curve, GE Healthcare) on a HiLoad™ 16/60 Superdex™ 75 column. Peaks for the following proteins are seen (elution volume, V_e, in brackets); Conalbumin (MW = 75 kDa, V_e = 51.28), Carbonic anhydrase (MW = 29 kDa, V_e = 65.93), Ribonuclease A (MW = 13.7 kDa, V_e = 77.48) and Aprotinin (MW = 6.5 kDa, V_e = 89.32). 3 mg/mL of each protein was used. To determine the void volume (V_0) a solution of 1 mg/mL Blue Dextran 2000 was run (red curve); V_0 = 42.54.

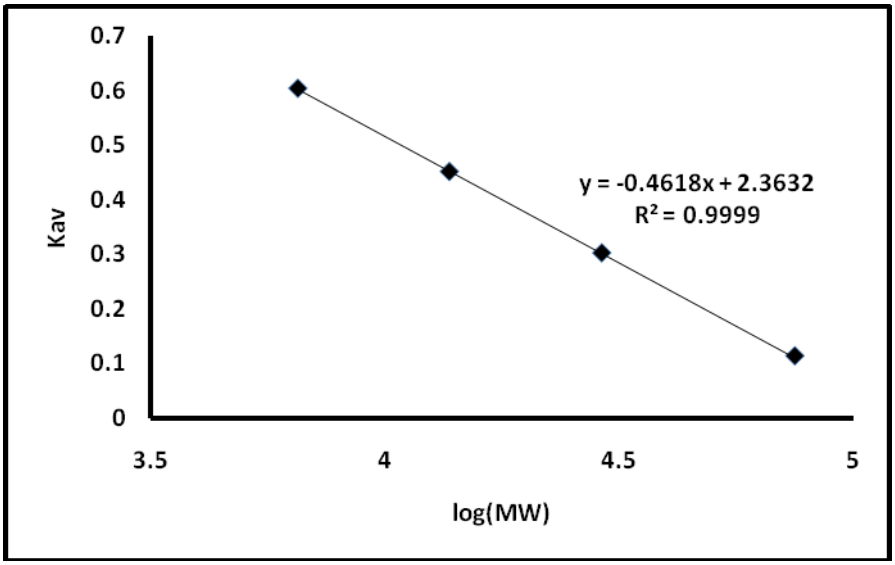

Figure 5.7. Standard curve of the partition coefficient (K_{av}) *versus* log(MW) of proteins from a gel filtration calibration kit (see Figure 5.6).

Table 5.1. Estimation of the molecular weight of the protein from peaks in Figure 5.2 and 5.4. The partition coefficient, K_{av}, is calculated from the elution volume, V_e, using the equation $K_{av} = (V_e - V_0)/(V_c - V_0)$. From K_{av} log(apparent MW) is calculated using the equation in Figure 5.7. The theoretical MW of HvNTR2_M43A and HvTrxh2_I51G is 36897 and 15272 Da, respectively.

Protein	Peak	V_e	K_{av}	log(app. MW)	App. MW	Calc. numb. of monomers	Integer numb. Of monomers
HvNTR2_M43A	1st	42.9	0.005	5.11	127945	3.5	4 (aggregate?)
	2nd	51.1	0.111	4.88	75375	2.0	2
HvTrxh2_I51G	1st	42.8	0.004	5.11	128688	8.4	8 (aggregate?)
	2nd	72.1	0.381	4.29	19556	1.3	1

5.2.2 FAD content and activity of HvNTR2

Gel filtration of HvNTR2wt resulted as shown above in two peaks. Absorbance spectra of the protein from the two elution peaks are shown in Figure 5.8. The protein from elution peak 1 was colourless and the absorbance spectrum resulted in a maximum around 273 nm, corresponding to absorbance from aromatic amino acids (mainly tyrosine and tryptophan) in protein. The broad shoulder towards higher wavelengths is likely due to aggregation. Protein from elution peak 2 was yellow and the absorbance spectrum showed two additional maxima around 375 and 456 nm. These stem from FAD, which contributes with this characteristic absorbance (Figure 1.10, Williams *et al*., 1967). Williams *et al*. (1967) have

shown that FAD bound to EcNTR has the same absorbance spectrum as free FAD: the extinction coefficient at 456 nm for bound FAD was determined to 11,300 $M^{-1}cm^{-1}$, which equals that of free FAD at 450 nm. The colourless protein from peak 1 show no detectable maxima 375 and 456 nm and thus appears to contain no FAD.

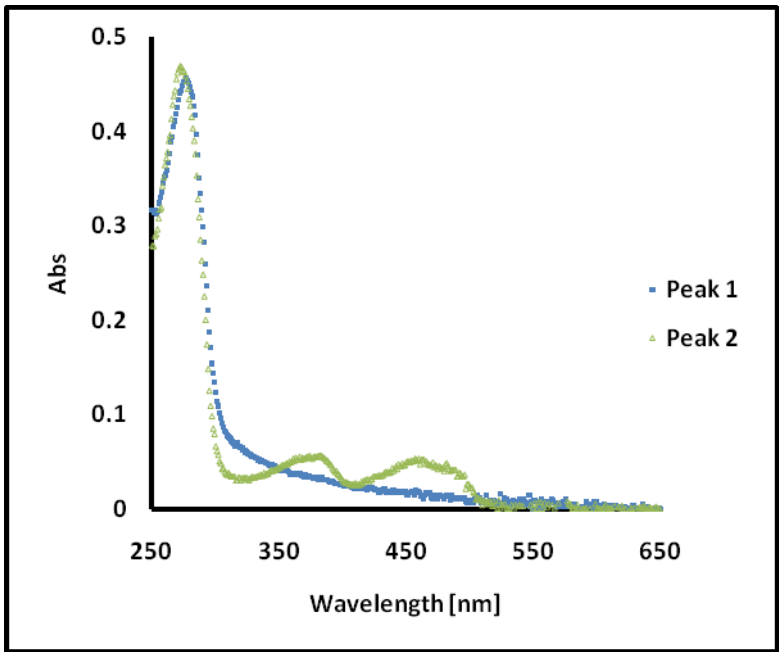

Figure 5.8. Wavelength scan of the protein from the two elution peaks obtained upon gel filtration of HvNTR2wt. The sample in peak 2 was bright yellow, whereas peak 1 was colourless and was eluted near the column void volume.

The enzymatic activity of the protein from the two elution peaks from the gel filtration was tested. Furthermore, it was examined whether reintroduction of FAD could result in reinsertion of FAD into the folded protein by carrying out an assay with and without exogenous FAD added (Section 5.4.3 and Figure 5.9). In the assay DTNB is used for quantifying the free thiols in Trx and therefore indirectly the transfer of reducing equivalents from NADPH *via* NTR to Trx. In the reaction two TNB ions are released per Trx molecule as measured at 412 nm (Section 5.4.2 and Figure 5.9). The addition of FAD after purification had insignificant effects on the enzyme activity of HvNTR2 from either of the elution peaks (Figure 5.9). NTR from elution peak 1 had almost no activity. Possibly aggregation of the protein could have led to partial unfolding and loss of FAD. Alternatively FAD was never incorporated in the protein during folding making it less stable.

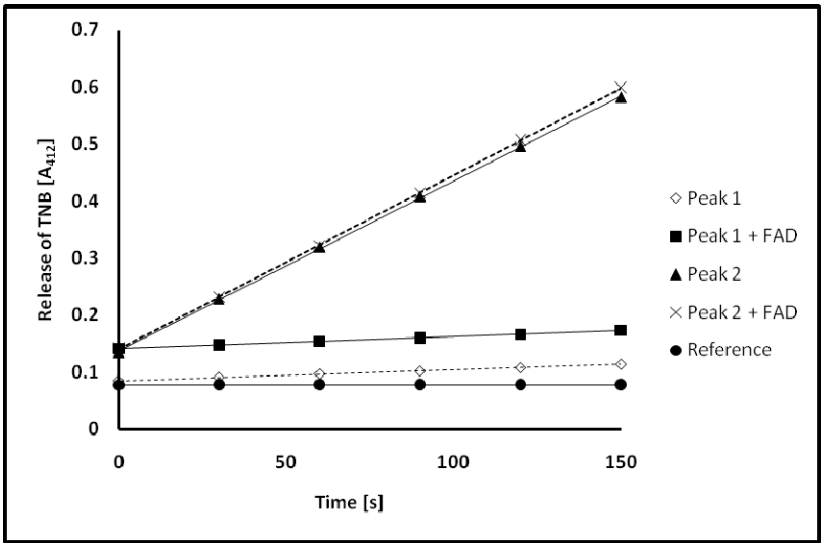

Sample	Activity [$\Delta A_{412} \cdot s^{-1}$]
Peak 1	0.72
Peak 1 + FAD	0.78
Peak 2	10.74
Peak 2 + FAD	10.98
Reference	0.00

Figure 5.9. Enzymatic activity (ΔA_{412} s^{-1}) of the protein from peak 1 and the yellow peak 2 from gel filtration of HvNTR2wt. HvNTR2 (1.6 µM, peak 1 or 2) was mixed with 16 µM FAD and pre-incubated 30 min at room temperature. The reaction was tested at the following conditions: 80 nM HvNTR2, 5 µM HvTrxh1, 0.1 M Tris-HCl pH 8.0, 1.0 mM EDTA, 0.2 mM DTNB, 0.3 mM NADPH and 0.1 mg/mL BSA. The reference buffer contains the same components but is devoid of HvNTR2.

Unsuccessful attempts to reintroduce FAD to protein from either of the peaks could be due to misfolded or partially unfolded protein. Alternatively the accessibility of FAD is limited once the protein is folded. If the latter is true HvNTR2 has to be folded in the presence of FAD and once folded, FAD can neither enter nor leave the protein unless changes in the protein folding occurs. Thus, the low FAD content could be due to a limited concentration of FAD in the Rosetta strain. Mulrooney (1997) also observed that up to as much as 68% of the recombinant EcNTR produced was expressed as apoprotein, i.e. lacking FAD. It was further observed that the amount of apoprotein increased with increasing amounts of IPTG, indicating that the protein was produced too fast and/or in too large quantities for the bacteria to keep up with the production of the FAD cofactor. Addition of 100 µM riboflavin to the growth medium did not increase the amount of active enzyme, but by adding FAD to the cell extract the apoprotein was rapidly activated (Mulrooney, 1997). As stated above, all attempts to reintroduce FAD after purification of HvNTR2 were unsuccessful, but as shown by Mulrooney (1997) it may be possible by adding the FAD earlier in the purification process or to the cell extract.

It was speculated whether HvNTR2 could lose the bound FAD and thereby have unstable activity. From the absorbance spectrum of the protein from peak 2 (Figure 5.8) is seen that the protein does not have full occupancy of FAD: A_{280} is 0.427 corresponding to 7.2 µM protein (using an extinction coefficient of 58,906 $M^{-1}cm^{-1}$ determined by amino acid analysis). Concerning the FAD content A_{456} of 0.051 corresponds to 4.5 µM (using an extinction coefficient of 11,300 $M^{-1}cm^{-1}$, Williams *et al*., 1967). Hence, only approximately 63% of the protein from peak 2 contains FAD.

The stability of the protein from peak 2 was estimated by keeping an aliquot of the HvNTR2 on ice for a prolonged period of time and quantifying the enzyme activity at a series of time points (the assay used is described in Section 5.4.2). In this measurement only one concentration of HvTrxh2 (6 µM) was used. The activity of HvNTR2wt from peak 2 was stable for around 10 d on ice and only decreased slightly after 14 d (Figure 5.10). Therefore, the FAD content was estimated to be a stable measure of the amount of active protein, and will henceforth be used to determine the concentration of active HvNTR2wt or mutant.

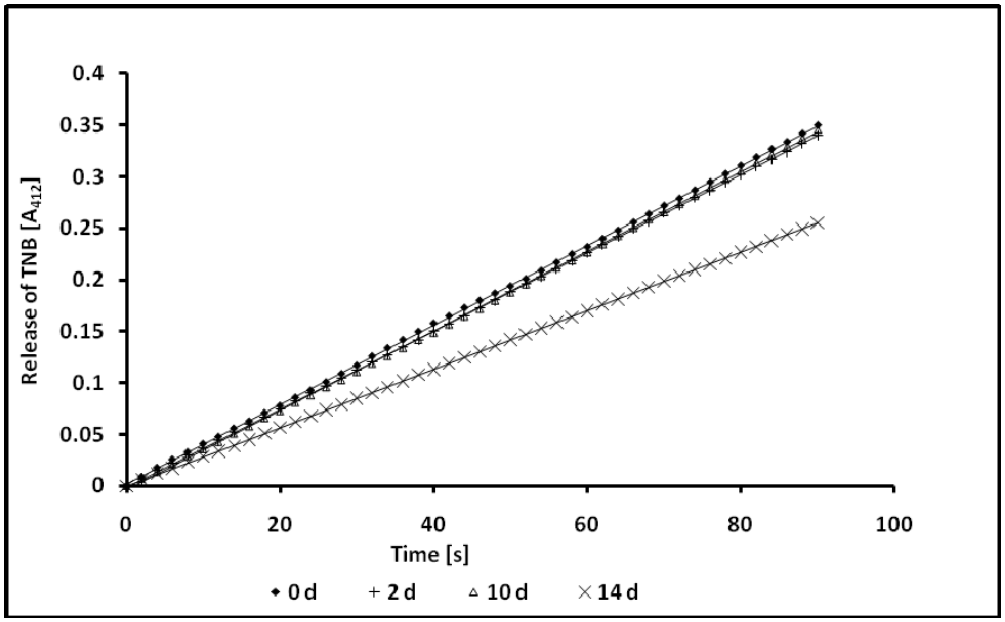

Figure 5.10. Stability of HvNTR2wt. The protein was kept on ice for 14 days and the activity was measured at different time point. The concentration of active HvNTR2wt was estimated from the A_{456} (absorbance of FAD). The assay conditions were 20 nM HvNTR2, 6 µM HvTrxh2, 0.1 M KH_2PO_4 pH 7.5, 2.0 mM EDTA, 0.2 mM DTNB, 0.2 mM NADPH and 0.1 mg/mL BSA. The proteins were diluted in enzyme dilution buffer (0.1 M KH_2PO_4 pH 7.5, 2.0 mM EDTA and 0.1 mg/mL BSA).

5.2.3 Kinetics of wild-type and mutants of NTR2 and Trx

The activity of various wild-type and mutant NTR and Trx was measured using an assay which utilises DTNB (5,5'-dithiobis-(2-nitrobenzoic acid), i.e. Ellman's reagent) to quantify the concentration of free thiols in Trx. The assay includes NADPH, NTR, Trx and DTNB (see Section 5.4.2). The reaction was carried out in either 1 mL or 100 µL cuvettes and followed for about 90 s (with measurements every 2 s) in a spectrophotometer (Ultrospec 2100 *pro*, Amersham Biosciences). This produced data with a good linear correlation between A_{412} and time [s] (Figure 5.11). K_m and V_{max} were determined from the slopes using KaleidaGraph (Synergy Software) (Figure 5.12). The unit for the obtained values of V_{max} was $A_{412nm} \cdot s^{-1}$. These were converted to nM Trx s^{-1} by dividing with the absorbance of the TNB ion (13,600 $M^{-1}cm^{-1}$, Ellman, 1959) and dividing by 2 since there are two cysteines per Trx molecule. Further, V_{max} was converted to k_{cat} by dividing with the concentration of NTR (20 nM).

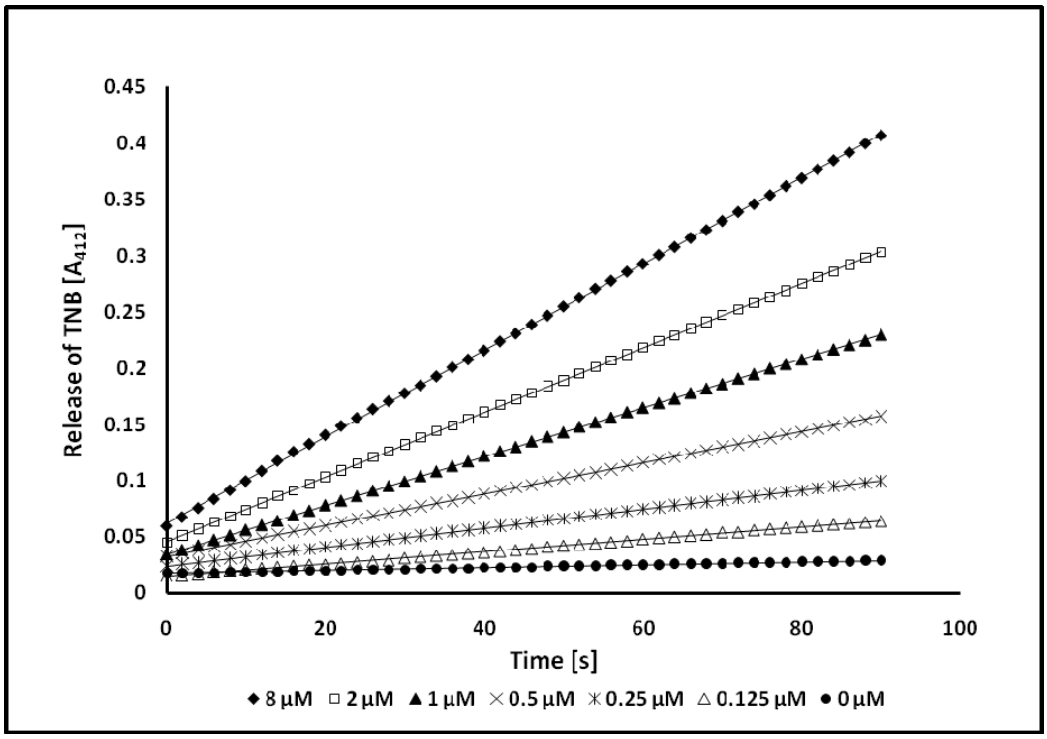

Figure 5.11. Data from assay with 20 nM HvNTR2 and varying concentrations of HvTrxh2. The assay was performed in a total volume of 1 mL or 200 µL and A_{412} was monitored in a spectrophotometer (Ultrospec 2100 *pro*, Amersham Biosciences). The reaction mix contains 0.1 M KH_2PO_4 pH 7.5, 2.0 mM EDTA, 0.2 mM DTNB, 0.2 mM NADPH and 0.1 mg/mL BSA. Proteins were diluted in enzyme dilution buffer (0.1 M KH_2PO_4 pH 7.5, 2.0 mM EDTA and 0.1 mg/mL BSA).

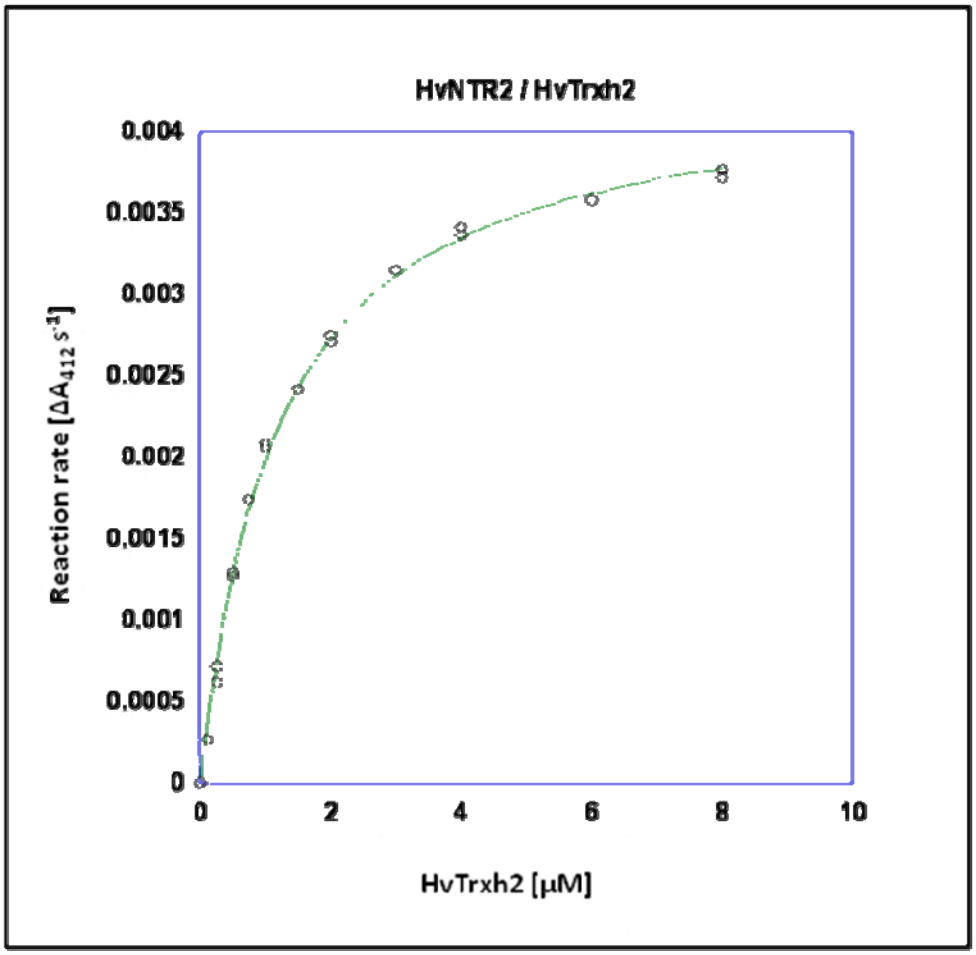

Figure 5.12. Reaction rates ($\Delta A_{412}\, s^{-1}$) plotted against the concentration of HvTrxh2. In the assay 20 nM HvNTR2 and varying concentrations of HvTrxh2 was used in a buffer of 0.1 M KH_2PO_4 pH 7.5, 2.0 mM EDTA, 0.2 mM DTNB, 0.2 mM NADPH and 0.1 mg/mL BSA. Proteins were diluted in enzyme dilution buffer (0.1 M KH_2PO_4 pH 7.5, 2.0 mM EDTA and 0.1 mg/mL BSA). V_{max} = 0.0043 $A_{412nm} \cdot s^{-1}$, K_m = 1.17 µM HvTrxH2.

The reactions for the slowest mutants were carried out in microtiter plates and followed for 30 min, with measurements every 30 s (ELISA plate reader, Power Wave XS, BIO-TEK®, Holm & Halby). This resulted in data exemplified by Figure 5.13, which did not lead to saturation (Figure 5.14).

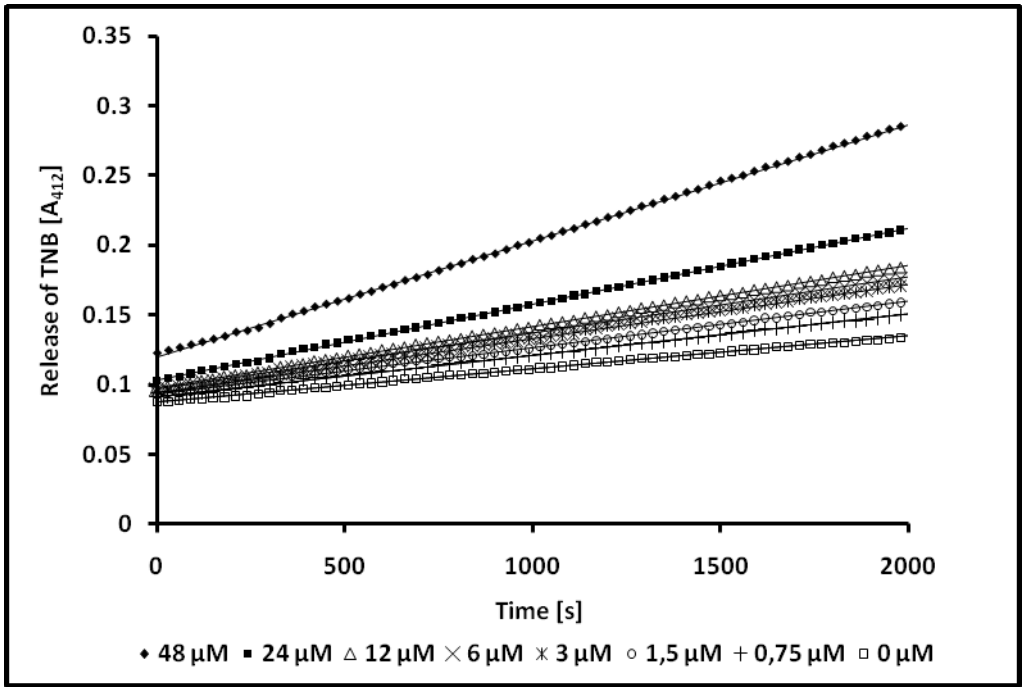

Figure 5.13. Data from assay with 20 nM HvNTR2_Δ42-47 and varying concentrations of HvTrxh2. The assay was performed in a total volume of 250 µL in microtiterplates and measured using an ELISA plate reader of the model Power Wave XS, BIO-TEK® (Holm & Halby) set to measure A_{412} every 30 s for 30 min. The reaction mixture contains 0.1 M KH_2PO_4 pH 7.5, 2.0 mM EDTA, 0.2 mM DTNB, 0.2 mM NADPH and 0.1 mg/mL BSA. Proteins were diluted in 0.1 M KH_2PO_4 pH 7.5, 2.0 mM EDTA and 0.1 mg/mL BSA.

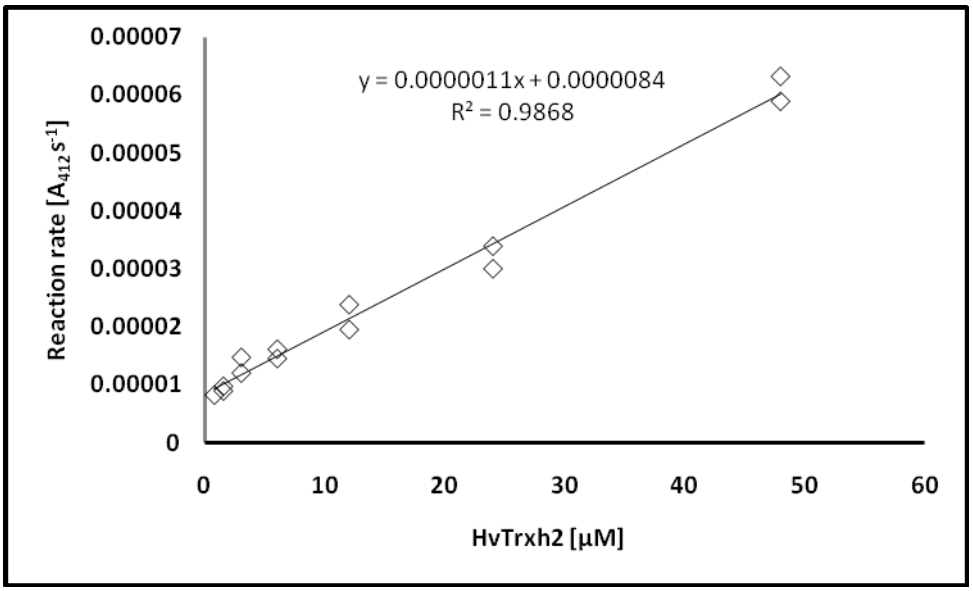

Figure 5.14. Reaction rates for HvNTR2_Δ42-47 fitted against the concentration of HvTrxh2. The background where HvTrxh2 was omitted was subtracted from the reaction rates determined in Figure 5.13 (given as $A_{412} \cdot s^{-1}$) prior to plotting.

The kinetic parameters obtained for the various wild-type and mutated enzymes are listed (Table 5.2). As stated above, some of the mutants of NTR displayed ≥1000 times less activity than the HvNTR2wt, and V_{max} was not reached even with 50 µM Trx. In these cases K_m and k_{cat} could not be determined. Instead, the slope of the reaction [A_{412} s^{-1} μM^{-1}] (Figure 5.14) is listed as a relative percentage of the initial slope (slope for the very lowest substrate concentrations) of HvNTR2wt/HvTrxh2wt. There is a relatively good correlation between k_{cat}/K_m and this initial slope (last two columns of Table 5.2).

Table 5.2. Kinetic parameters for the activity of wild-type and mutants of HvNTR2 in reactions with wild-type (wt) and mutant HvTrxh2 and AtTrxH3. Some reactions were too slow to be used to determine K_m and V_{max} marked by n.d. (not detectable). Instead the slope of the reaction [A_{412} s^{-1} μM^{-1}] is given as a relative percentage (last column) of the initial slope (slope for the very lowest substrate concentrations) of HvNTR2wt/HvTrxh2wt.

Wild-type

HvNTR2	HvTrxh2	K_m [µM]	k_{cat} [s^{-1}]	k_{cat}/K_m [M^{-1} s^{-1}]	k_{cat}/K_m [%]	initial slope [%]
wt	wt	1.17 ± 0.04	8.0 ± 0.10	(6.80 ± 0.25) · 10^6	100 ± 4	100
wt	HvTrxh1	1.23 ± 0.08	12.1 ± 0.20	(9.84 ± 0.66) · 10^6	145 ± 10	151
wt	AtTrxh3	0.80 ± 0.05	4.8 ± 0.09	(6.00 ± 0.39) · 10^6	88 ± 6	91
wt	EcTrx	149 ± 13	9.4 ± 0.38	(6.31 ± 0.61) · 10^4	0.9 ±0.1	1.0
AtNTR-B	AtTrxh3	0.48 ± 0.03	5.9 ± 0.10	(1.23 ± 0.08) · 10^7	181 ± 11	177
AtNTR-B	wt	60 ± 7	8.5 ± 0.48	(1.40 ± 0.18) · 10^5	2.1 ± 0.3	2.0

FAD-domain mutants

HvNTR2	HvTrxh2	K_m [µM]	k_{cat} [s^{-1}]	k_{cat}/K_m [M^{-1} s^{-1}]	k_{cat}/K_m [%]	initial slope [%]
Wt	I51G	15.5 ± 0.7	15.9 ± 0.3	(1.03 ± 0.05) · 10^6	15 ± 1	23
M43A	wt	16.0 ± 0.8	11.4 ± 0.2	(7.13 ± 0.39) · 10^5	11 ± 1	15
M43A	I51G	n.d.	n.d.	n.d.	-	0.4
M43A	AtTrxh3	14.1 ± 1.2	14.8 ± 0.6	(1.05 ± 0.10) · 10^6	16 ± 1	15
M43A	EcTrx	n.d.	n.d.	n.d.	-	0.03
W42A	Wt	45.7 ± 4.0	10.4 ± 0.4	(2.28 ± 0.22) · 10^5	3.3 ± 0.3	3.8
W42A	I51G	n.d.	n.d.	n.d.	-	0.5
W42A	AtTrxh3	2.4 ± 0.2	10.4 ± 0.4	(4.24 ± 0.41) · 10^6	62 ± 6	61
W42A	EcTrx	n.d.	n.d.	n.d.	-	0.016
W42A/M43A	wt	n.d.	n.d.	n.d.	-	0.09
W42A/M43A	I51G	n.d.	n.d.	n.d.	-	0.3
W42A/M43A	AtTrxh3	30.5 ± 3.4	11.0 ± 0.6	(3.61 ± 0.44) · 10^5	5.3 ± 0.6	5.5
W42A/M43A	EcTrx	n.d.	n.d.	n.d.	-	0.002
Δ42-47	wt	n.d.	n.d.	n.d.	-	0.06

Δ42-47	AtTrxh3	54.3 ± 5.2	15.3 ± 1.0	(2.82 ± 0.32) · 10^5	4.1 ± 0.5	4.9
Δ42-47	EcTrx	n.d.	n.d.	n.d.	-	0.0
wt	G47P	1.4 ± 0.1	7.9 ± 0.3	(5.49 ± 0.56) · 10^6	73 ± 8	77
Δ42-47	G47P	n.d.	n.d.	n.d.	-	0.0
W42A/M43A	G47P	n.d.	n.d.	n.d.	-	0.0
N45A_D46A	wt	2.2 ± 0.2	7.3 ± 0.2	(3.30 ± 0.27) · 10^6	49 ± 4	47
N45A_D46A	AtTrxh3	4.2 ± 0.6	10.7 ± 0.7	(2.55 ± 0.38) · 10^6	38 ± 6	37
N45A_D46A	EcTrx	n.d.	n.d.	n.d.	-	0.2
AtNTR-B	I51G	n.d.	n.d.	n.d.	-	0.1
AtNTR-B	G47P	n.d.	n.d.	n.d.	-	1.3

NADPH-domain mutants

HvNTR2	HvTrxh2	K_m [μM]	k_{cat} [s^{-1}]	k_{cat}/K_m [M^{-1} s^{-1}]	k_{cat}/K_m [%]	Initial slope [%]
wt	E86A	0.57 ± 0.03	5.3 ± 0.1	(9.23 ± 0.50) · 10^6	137 ± 7	131
N139A	wt	0.68 ± 0.04	4.2 ± 0.1	(6.18 ± 0.37) · 10^6	91 ± 5	89
N139A	E86A	0.41 ± 0.01	4.2 ± 0.04	(1.02 ± 0.26) · 10^7	151 ± 4	128
R140A	wt	3.43 ± 0.27	5.1 ± 0.1	(1.49 ± 0.25) · 10^6	22 ± 2	22
R140A	E86A	1.60 ± 0.20	2.6 ± 0.1	(1.63 ± 0.21) · 10^6	24 ± 3	27
G225R_G226D_P227V	AtTrxh3	0.73 ± 0.07	3.9 ± 0.1	(5.34 ± 0.53) · 10^6	79 ± 8	79
G225R_G226D_P227V	wt	1.05 ± 0.06	1.8 ± 0.03	(1.71 ± 0.25) · 10^6	25 ± 1	32
G225R_G226D	AtTrxh3	0.67 ± 0.03	5.0 ± 0.1	(7.46 ± 0.35) · 10^6	110 ± 5	116
G225R_G226D	wt	1.28 ± 0.06	8.1 ± 0.1	(6.33 ± 0.31) · 10^6	93 ± 5	98
G222D_A223G_G224E	AtTrxh3	0.52 ± 0.04	5.0 ± 0.1	(9.62 ± 0.76) · 10^6	141 ± 11	133
G222D_A223G_G224E	wt	1.46 ± 0.06	7.9 ± 0.1	(5.41 ± 0.23) · 10^6	80 ± 3	82

5.2.3.1 Activity of wild-type NTRs and Trxs

HvNTR2 has K_m of 1.2 μM for both HvTrxh1 and HvTrxh2 but a higher k_{cat} for HvTrxh1; 12.1 s^{-1} compared to 8.0 s^{-1} for HvTrxh2 (Table 5.2). k_{cat}/K_m of HvTrxh1 is thus 145% relative to HvTrxh2, in agreement with previous findings (Shahpiri *et al.*, 2008a). With AtTrxh3 as a substrate for HvNTR2 k_{cat} and K_m were found to decrease (K_m of 0.8 μM) and k_{cat}/K_m was 88% relative to HvTrxh2. HvNTR2 and AtNTR-B have 75% sequence identity, which may explain why AtTrxh3 works as an excellent substrate. HvNTR2 has 45% sequence identity with EcNTR, and EcTrx is a poorer substrate for HvNTR2 (Table 5.2); k_{cat} is slightly higher than for HvTrxh2, but K_m increased to 149 μM. This possibly reflects the very different Trx binding site in the NADPH domain, where the groove has a different charge distribution and might be too short to accommodate $Arg73_{EcTrx}$ (Figure 4.9A).

AtNTR-B was revealed to transfer electrons well to its own substrate, AtTrxh3 (181% compared to HvNTR2 on HvTrxh2) but surprisingly poorly to HvTrxh2 (2%) with a K_m of 60 µM. Thus, HvNTR2 can accept AtTrxh3 almost as well as its own substrate, whereas AtNTR-B does not work well using HvTrxh2. This could indicate that HvTrxhs binds to HvNTR2 *via* specific patterns not conserved among the h-type isoforms, while HvNTR2 has the ability to transfer electrons *via* both specific and generic interactions.

5.2.3.2 Interactions involving the FAD domain of HvNTR2

The role of the FAD-loop ($_{40}$EGWMANDIAAGG$_{51}$) was examined. Underlined residues were predicted to bind to HvTrxh2 based on the model of HvNTR2:HvTrxh2 (Chapter 4, Figure 4.4A). This motivated deletion of part of the loop (HvNTR2_Δ42-47, lacking residues $_{42}$WMANDI$_{47}$). These residues were chosen because that part of the loop contained the most bulky residues and was predicted by the model to be in closest proximity to HvTrxH2. Furthermore, three of these residues (Trp42$_{HvNTR2}$, Met43$_{HvNTR2}$ and Asp46$_{HvNTR2}$) were predicted to bind directly to HvTrxh2. HvNTR2_Δ42-47 showed a very low activity with HvTrxh2 so values of k_{cat} and K_m could not be determined. However, a linear correlation between the activity and the concentration of HvTrxh2 was obtained. It could thus be estimated that HvNTR2_Δ42-47 has 0.06% activity towards HvTrxh2 (last column in Table 5.2), showing that binding to this loop is essential.

The following mutants HvNTR2_M43A, HvNTR2_W42A, HvNTR2_W42A_M43A, HvNTR2_N45A_D46A and HvTrxh2_I51G were made to elucidate, which residues of this loop are most important for the binding. The reason for mutating Ile51$_{HvTrxh2}$ to glycine was to shorten the amino acid side chain sufficiently to avoid side chain interactions with the loop. HvTrxh2_I51G showed 15.1% activity. Combined with the mutants HvNTR2_W42A or HvNTR2_M43A the HvTrxh2_I51G mutation gave activities of 0.5 and 0.4% respectively, which makes it plausible that the model of HvNTR2:HvTrxh2 is correct in placing Ile51$_{HvTrxh2}$ with significant interactions with Trp42$_{HvNTR2}$ and Met43$_{HvNTR2}$. Hydrophobic interactions could be a major driving force for complex formation.

As mentioned a sequence corresponding to the FAD-loop is also present in NTRs from dicot plants (Chapter 4, Figure 4.5A). The importance of this sequence in dicots was examined by assaying the HvNTR2 mutants with Trx from *Arabidopsis thaliana.* This plant

encodes at least eight isoforms of Trx-h, of which AtTrxh3, AtTrxh4 and AtTrxh5 were tested for activity, as they are of the same sub-type (type I), as HvTrxh1 and HvTrxh2 (Gelhaye *et al*., 2005). Furthermore, the mutants were assayed on EcTrx, to test if the loop can bind this substrate in the same way as HvTrxh2, as postulated because the charge distribution and surface of the two Trxs are very similar in the region binding the FAD-loop.

The kinetic parameters are given in Table 5.2, but the activity for EcTrx is very low compared to the other substrates. Therefore the activity of HvNTR2wt with HvTrxh2, AtTrxh3 and EcTrx were all normalised to 100%, and the activity of the mutants are illustrated relative to these (Figure 5.15). For HvNTR2_W42A most activity was lost for HvTrxh2 and EcTrx being only 3.3 and 1.7%, respectively. Surprisingly, 71% activity was maintained for AtTrxh3, rendering this a much better substrate for that mutant. Changing $Met43_{HvNTR2}$ to alanine affected binding of all three substrates, but again the effect on the binding of AtTrxh3 was less affected than for the other substrates. Combining these two mutations in HvNTR2_W42A_M43A reduced activity for HvTrxh2 and EcTrx to 0.09 and 0.2% of wild-type, whereas there was 5.5% activity for AtTrxh3 (Figure 5.15). Only the mutant HvNTR2_N45A_D46A lost slightly more activity towards AtTrxh3 than displayed by HvTrxh2. Deleting five residues of the loop in HvNTR2_Δ42-47 destroyed activity towards EcTrx and very little activity was found towards HvTrxh2 as mentioned (0.06%). However, there was still 4.9% activity towards AtTrxh3 (Figure 5.15). Essentially, the same activity was obtained for this mutant towards AtTrxh4 and AtTrxh5 (*data not shown*), and activity towards HvTrxh1 was in the same range as of HvTrxh2 (*data not shown*). The results presented indicate that the *A. thaliana* Trxs assayed depend less on the FAD-loop. They may instead have a stronger interaction with other parts of the FAD domain or with the NADPH domain. This may explain why AtNTR-B does not react well with HvTrxh2, which may not have strong interactions to other parts of AtNTR-B.

The central $Met43_{HvNTR2}$ is the only interacting residue that is not conserved in HvNTR1, where it is replaced by a leucine residue (see Figure 4.4A). This may explain a higher preference of HvNTR2 for HvTrxh1. Even though $Ile51_{HvTrxh2}$ is important for the binding, this residue is not conserved either and is in HvTrxh1 replaced by a valine (see alignment Figure 5.16). These conservative substitutions may when added to the varieties in the other residues interacting with $Trp42_{HvNTR2}$ and $Met43_{HvNTR2}$ (Figure 4.4A), be responsible

for the difference between the activities with the two substrates. In AtTrxh3 and AtTrxh5, $Ile51_{HvTrxh2}$ is substituted with phenylalanine, whereas it is methionine in AtTrxh4. In EcTrx the corresponding residue is $Met37_{EcTrx}$.

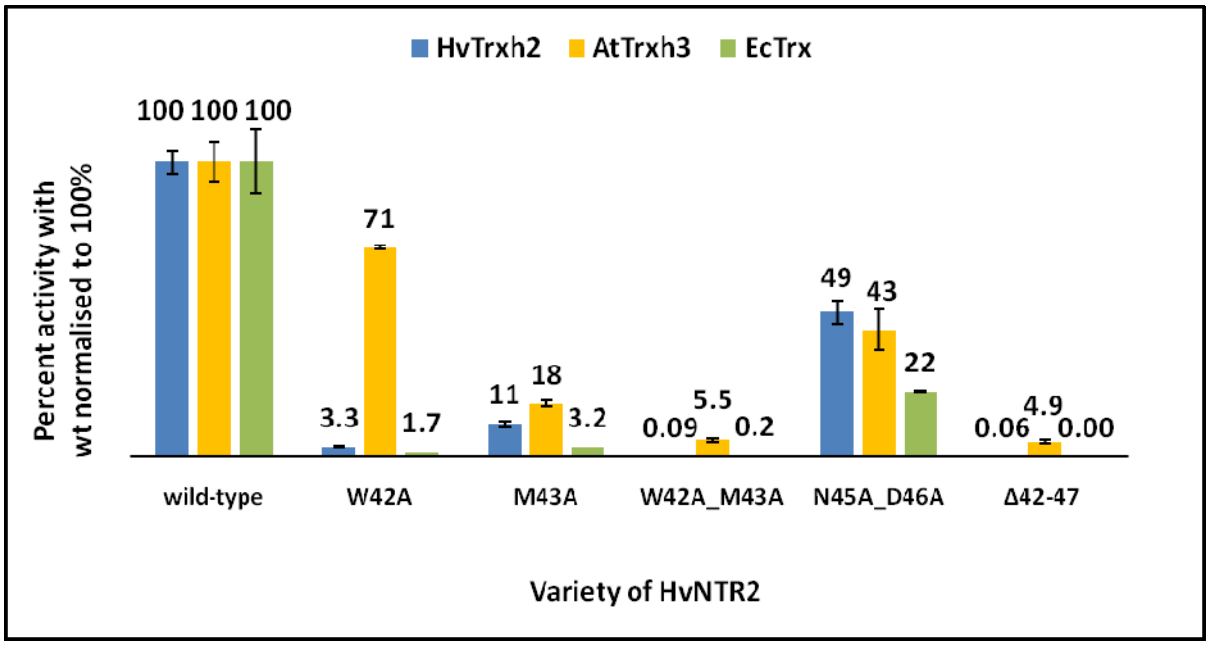

Figure 5.15. Relative k_{cat}/K_m. The values for the activity of HvNTR2wt with the three different substrates HvTrxh2, AtTrxh3 and EcTrx were all set to 100%. The activities of different mutants of HvNTR2 are shown relative to these.

Both the model of HvNTR2:HvTrxh2 and the data in Figure 5.15 suggest that the loop of HvNTR2 is able to bind EcTrx in the same manner as HvTrxh2. AtTrxh3 is not bound in the same way and is much less dependant on $Trp42_{HvNTR2}$, which is essential for binding the other substrates. This is notable since AtNTR-B has the same FAD-loop sequence. Unfortunately, there are no crystal structures available of neither AtTrxh3, AtTrxh4 nor AtTrxh5 to enlighten what could cause this difference.

The data of Table 5.2 and Figure 5.15 may indicate that AtTrxh3 (and h4 and h5) has a stronger binding to the NADPH domain (or another area of the FAD domain), and therefore is less dependent on the FAD-loop. In order to find an explanation for this, the sequences of the three *A. thaliana* Trxs and the two barley Trxs were aligned and examined (Figure 5.16). Here all the residues of HvTrxh2 predicted by the complex model to interact with HvNTR2 are marked. Since all three Trxs from *A. thaliana* had similar activity with HvNTR2_Δ42-47,

and HvTrxh1 and HvTrxh2 both had extremely low activity, the explanation must be a difference between the Trxs from the two plants; i.e. the three Trxs from *A. thaliana* must have something in common, which is lacking in HvTrxh1 and HvTrxh2 or *vice versa*. One possible explanation found among the interacting residues was that the positively charged lysine in HvTrxh2/h1 (residue 77 in h2, yellow in Figure 5.16) is changed in the three Trxs from *A. thaliana* to glutamine or asparagine. $Lys77_{HvTrxh2}$ was predicted to interact with $Pro153_{HvNTR2}$ through hydrophobic contacts between the C^{γ} and C^{δ} atoms of both residues. It is a part of the binding pocket corresponding to the hydrophobic pocket of EcTrx (see Chapter 4, Figure 4.8). This minor difference in hydrophobic interaction pattern is however not likely to fully account for the differences in the interaction of HvNTR2 with Trxs from barley and *A. thaliana*.

Another important difference was the three AtTrxs having the active site of CPPC instead of CGPC (boxed in Figure 5.16). The only available crystal structure of an h-type Trx from *A. thaliana* is of AtTrxh1 (pdb 1XFL, Peterson *et al*., 2005), which has the classical CGPC active site. A search for structures with the WCPPC motif in the *Protein Data Bank* revealed a structure of Trxh1 from *Populus tremula* (poplar) (pdb 1TI3, Coudevylle *et al.* 2005) in a reduced state. Superpositioning this structure with that of HvTrxh2 in the HvNTR2:HvTrxh2 model showed only little difference in the surface complementary of the two Trxhs in this region (Figure 5.17). The mutant HvTrxh2_G47P (which has the active site motif CPPC) was made to examine the role of the different active site. HvNTR2wt showed slightly increased K_m (1.6 µM) with this mutant (Table 5.2) and neither HvNTR2_Δ42-47 nor the double mutant HvNTR2_W42A_M43 had any activity above background with HvTrxh2_G47P. This indicates that the different active site of the three Trxs from *A. thaliana* is not responsible for the much higher activity with the loop mutants. It seems more plausible that the answer is an overall different distribution of contacts or electrostatic potential complementarity. This means that it is not likely that any single residue is responsible for the difference, which is more likely to be a result of an additive effect integrating several differences.

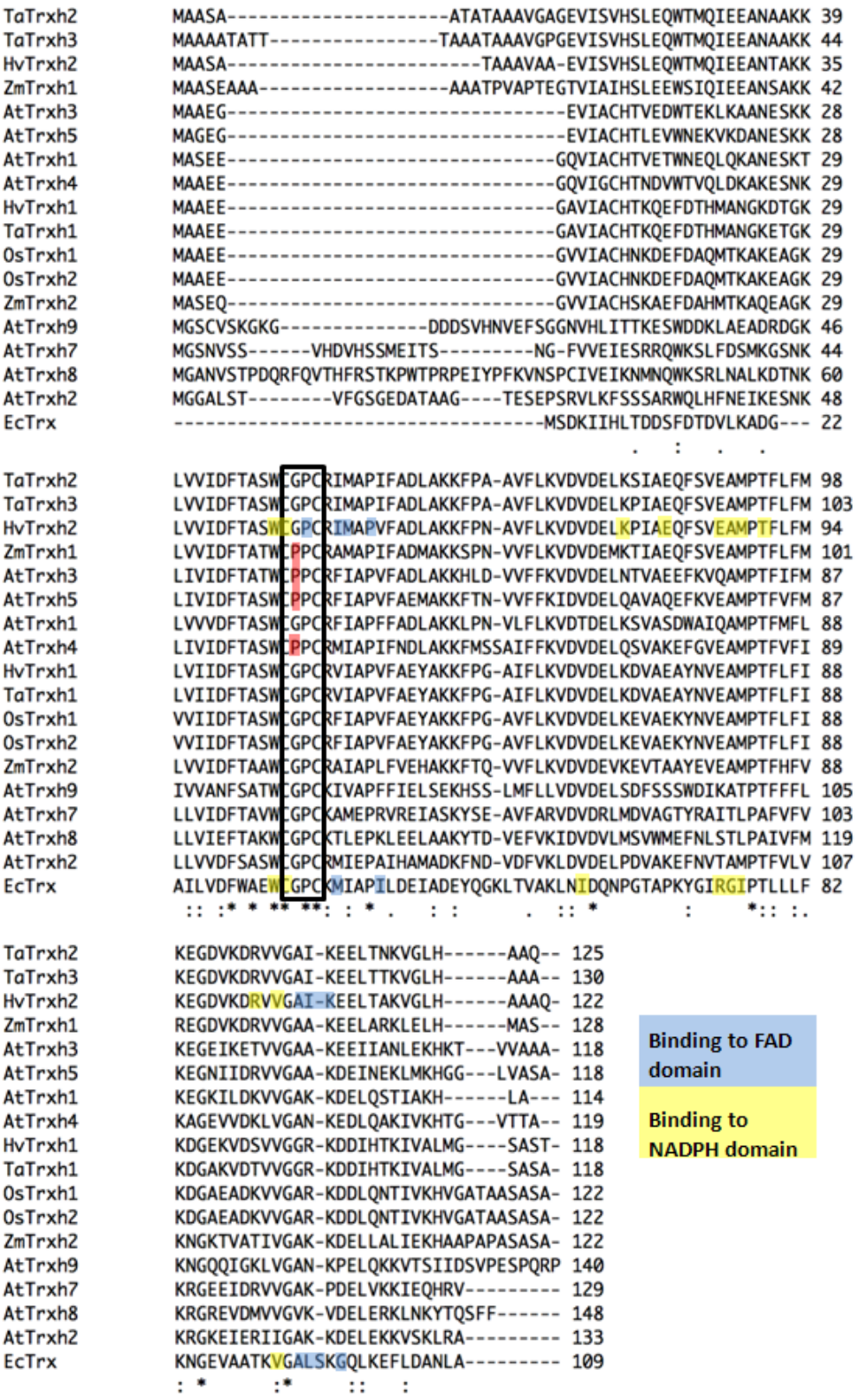

Figure 5.16. Multiple sequence alignment of selected thioredoxins from plants and from *E. coli*. The residues in HvTrxh2 which were predicted to bind to the FAD domain and the NADPH domain in the modelled complex of HvNTR2:HvTrxh2 are marked in blue and yellow, respectively. For EcTrx the residues interacting with EcNTR in the complex of EcNTR:EcTrx (pdb accession number 1F6M) were determined using LIGPLOT (Lennon *et al.*,

2000). The active site is boxed. In some of the sequences, the classical active site CGPC is replaced by the sequence CPPC (first proline marked in red). The sequences were aligned using Clustal-W2 (Thompson *et al*., 1994). The Trxs and their accession numbers in parentheses are TaTrxh1 (Q8GVD3), TaTrxh2 (Q9LDX4) and TaTrxh3 (Q7FT21) from *Triticum aestivum* (wheat), HvTrxh1 (Q7XZK3) and HvTrxh2 (Q7XZK2) from *Hordeum vulgare* (barley), ZmTrxh1 (Q4W1F7) and ZmTrxh2 (Q4W1F6) from *Zea mays* (maize), OsTrxh1 (Q0D840) and OsTrxh2 (A2YIW7) from *Oryza sativa* (rice) and AtTrxh1 (P29448), AtTrxh2 (Q38879), AtTrxh3 (Q42403), AtTrxh4 (Q39239), AtTrxh5 (Q39241), AtTrxh7 (NP_176182), AtTrxh8 (NP_177146) and AtTrxh9 (Q9C9Y6) from *Arabidopsis thaliana* (mouse-ear cress), and EcTrx (P0AA25) from *E. coli*.

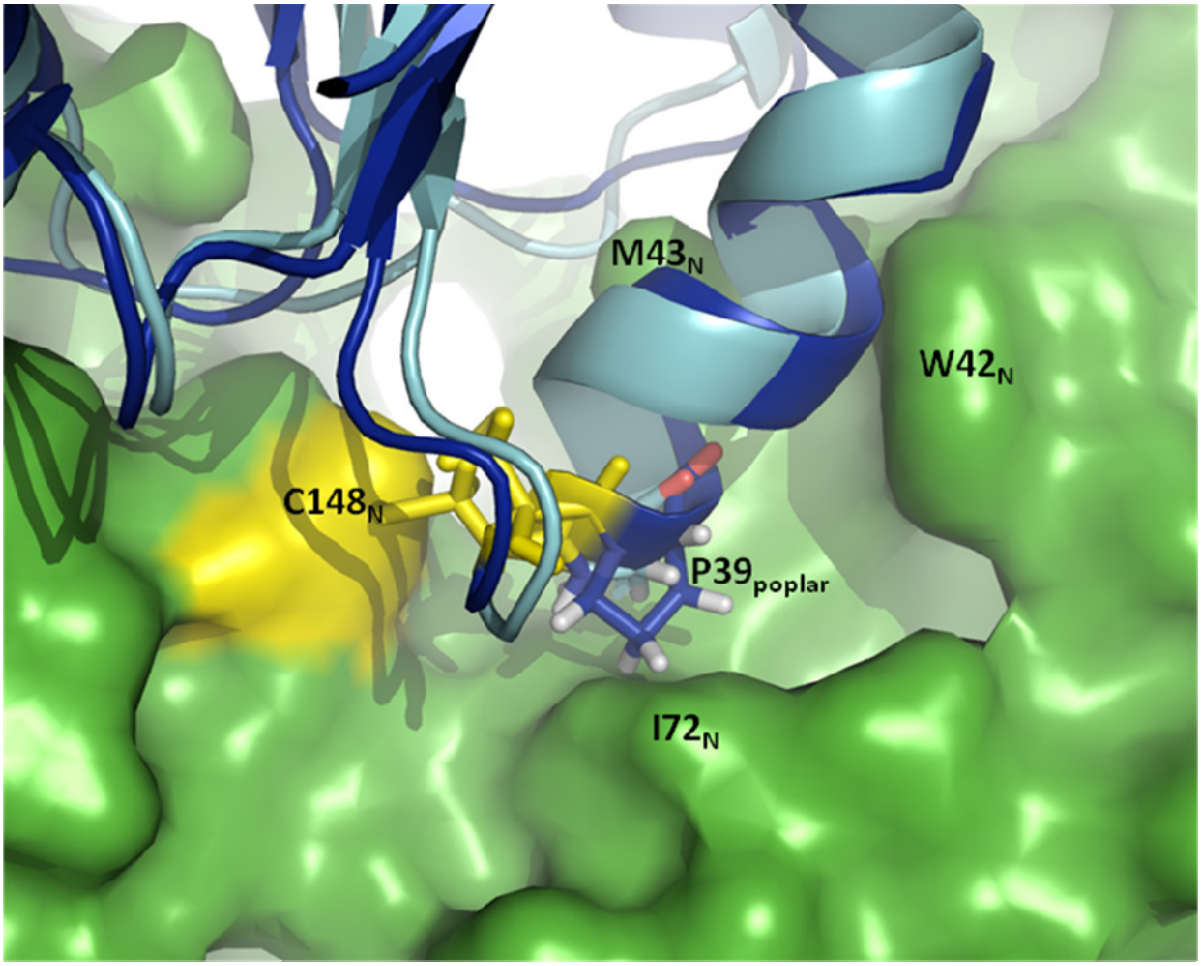

Figure 5.17. Superposition of PtTrxh1 from *Populus tremula* (poplar, pdb 1TI3, Coudevylle *et al.* 2005, shown in dark blue) and HvTrxh2 (cyan) in a modelled complex with HvNTR2 (green). The cysteines forming the disulfide between the two are shown in yellow. PtTrxh1 has an extra proline (Pro39) in the active site (WCPPC) compared to HvTrxh2 (WCGPC). The important residues $Trp42_{HvNTR2}$ and $Met43_{HvNTR2}$ from the FAD-loop of HvNTR2 are marked to show their proximity to the active site.

5.2.3.3 Interactions involving the NADPH domain of HvNTR2

The role of some of the contacts involving the NADPH domain was examined by mutational studies. The model of HvNTR2:HvTrxh2 predicts that the residues forming most interactions between HvTrxh2 and the NADPH domain of HvNTR2 are $Asn139_{HvNTR2}$ and $Glu86_{HvTrxh2}$ (see Figure 4.4A). The corresponding mutants HvNTR2_N139A and HvTrxh2_E86A were assayed as well as HvNTR2_R140A towards HvTrxhwt (HvNTR2wt for HvTrxh2_E86A) as well as in combinations with each other. HvTrxh2_E86A showed a decrease of both k_{cat} (from 8.0 to 5.3 s^{-1}) and K_m (from 1.2 to 0.6 µM), resulting in an overall increase of k_{cat} /K_m to 137% of the wild-type combination (Table 1). HvNTR2_N139A also showed a decreased k_{cat} (4.2 s^{-1}) and K_m (0.7 µM), resulting in k_{cat} /K_m of 91% of the wild-types. When combining the two mutants (assaying HvNTR2_N139A towards HvTrxh2_E86A) k_{cat} was the same as for HvNTR2_N139A with HvTrxh2wt but K_m decreased even further to 0.4 µM, resulting in k_{cat}/K_m of 151% of the wild-type combination. Furthermore, the positively charged mutant, HvTrxh2_E86R, was shown (Björnberg *et al.;* manuscript in preparation) to have only minor effect on the activity with HvNTR2. These findings suggest that $Asn139_{HvNTR2}$ and $Glu86_{HvTrxh2}$ are not critical for the binding between HvNTR2 and HvTrxh2. It is possible that water molecules are able to fill out the voids and contribute by hydrogen bonding instead of the missing side chains. By contrast, the residue $Arg73_{EcTrx}$ in EcTrx, which corresponds to $Glu86_{HvTrxh2}$, is essential for activity. Thus, a mutant of EcTrx_R73G showed substantially decreased activity (to 0.6%) with EcNTR compared to EcTrxwt (Negri *et al*., 2009).

HvNTR2_R140A decreased k_{cat} to 5.1 s^{-1} and increased K_m almost 3 fold to 3.4 µM, resulting in k_{cat}/K_m of 22% of the HvNTR2wt (Table 1). Combined with HvTrxh2_E86A, k_{cat} decreased further to 2.6 s^{-1}, but K_m (1.6 µM Trx s^{-1}) was almost at the value of the combined wild-types, resulting in k_{cat} /K_m of 24% of the wild-type combination. It is not possible from these results to conclude whether the model of HvNTR2:HvTrxh2 has predicted the position of the examined residues correctly. As mentioned, introduction of shorter side chains can make room for water molecules that may provide hydrogen bond contacts.

It was further examined whether the Glycine-loop with the sequence $_{221}GGAGGGPL_{228}$ (Figure 4.1 and 4.8A, Chapter 4) is involved in binding HvTrxh2. This loop is flexible as reflected by a high B-factor in the crystal structure of HvNTR2 (Kirkensgaard *et al*., 2009).

The proline of the loop, $Pro227_{HvNTR2}$, was predicted by the model of HvNTR2:HvTrxh2 to shorten the length of the groove in which $Glu86_{HvTrxh2}$ is accommodated (Figure 4.8A). Mutants were constructed at some of the residues and changed to the corresponding residues of AtNTR-B ($_{223}$GDGERDVL$_{230}$) to examine whether this increased the preference for AtTrxs. The mutants HvNTR2_G222D_A223G_G224E, HvNTR2_G225R_G226D and HvNTR2_G225R_G226D_P227V were assayed on both HvTrxh2 and AtTrxh3.

HvNTR2_G222D_A223G_G224E showed a slight increase of K_m towards HvTrxh2 (to 1.46 µM) resulting in k_{cat}/K_m of 80% of the wild-type (Table 5.2 and Figure 5.18). K_m towards AtTrxh3 was decreased from 0.52 µM, leading to k_{cat}/K_m of 141% (compared to 88% for HvNTR2wt). For HvNTR2_G225R_G226D there was a smaller decrease of K_m to 0.67 µM for AtTrxh3 and k_{cat}/K_m increased from 88 to 110%. For HvTrxh2 a minor increase of K_m was observed (from 1.17 to 1.28; 93% activity). For HvNTR2_G225R_G226D_P227V k_{cat} was lowered for HvTrxh2 resulting in 25% activity compared to the wild-type. For AtTrxh3 the activity was lowered to 79%. To summarise there is a slight negative effect on activity for HvTrxh2 when substituting residues in the loop to mimic AtNTR-B. Only when changing $Pro227_{HvNTR2}$ to a valine the effect was more pronounced, leading to 25% activity. This may be due to valine being positioned in the groove, which accommodate $Glu86_{HvTrxh2}$ (Chapter 4, Figure 4.9A), and thus interfering with binding of this residues. For AtTrxh3 this mutant showed slightly decreased activity, which again may be due to blockage of the groove. Both HvNTR2_G222D_A223G_G224E and HvNTR2_G225R_G226D showed increased activity towards AtTrxh3, which may indicate that the Glycine-loop is involved in the binding of Trx.

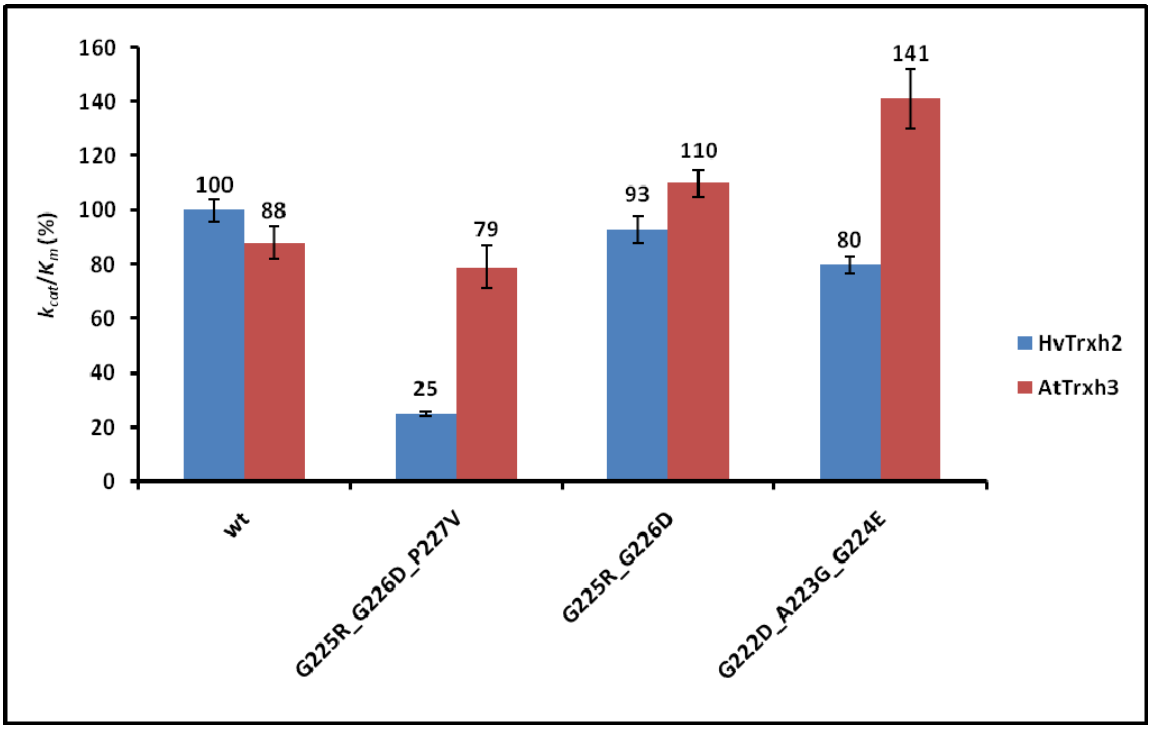

Figure 5.18. Relative values for k_{cat}/K_m. The value for the activity of HvNTR2wt with the HvTrxh2 was set to 100%. The activities of different mutants of HvNTR2 with either HvTrxh2 or AtTrxh3 are shown relative to these.

5.2.3.4 Assays without Trx

To verify that the most inactive mutants still have functional active sites an assay was used where HvTrxh2 was omitted, as described by Holmgren (1977). In this assay DTNB is used directly as a substrate for HvNTR2. HvNTR2wt was assayed as well as HvNTR2_W42A, HvNTR2_M43A, HvNTR2_W42A_M43A, HvNTR2_N45A_D46A and HvNTR2_Δ42-47. The same assay is used as described in Section 5.4.2 except HvTrxh2 is omitted, 100 nM HvNTR2 (wt or mutant) was used and varying concentrations of DTNB (from 1 to 8 mM). The reaction was followed spectrophotometrically with measurements every 2 s as described above. The reaction was only linear for a short period (about 1 min) so the measurements from 4—50 s were used. Holmgren (1977) also observed that the reaction is linear only for a very limited period, and noted that this could be explained most simply by a secondary chemical modification of thiol groups which inactivate the protein. As shown previously (Chapter 3, Figure 3.3), there are additional cysteine residues in the dimer interface of HvNTR2. It is possible that DTNB at high concentrations is able to bind these if equilibrium exists between dimer and monomer. This could interfere with the dimer formation and

lower the activity if the monomer is less active than the dimer. Another explanation could be that not only $Cys148_{HvNTR2}$ but also $Cys145_{HvNTR2}$ reacts with DTNB at high DTNB concentrations. This would lead to both cysteines being bound to TNB and therefore an inactive protein.

The results obtained are shown in Figure 5.19. Values of k_{cat} and K_m are connected to a great deal of uncertainty (and therefore not shown) due to the assay only being linear for about 1 min. However to compare to the assay with HvTrxh2 k_{cat} for HvNTR2wt was estimated to 0.5 s^{-1}. This is 16 times lower than for HvTrxh2. K_m was determined to 4.0 mM which is ~3400 times higher than for HvTrxh2. k_{cat}/K_m is 125 $M^{-1}s^{-1}$, and therefore ~54,000 times lower than for HvTrxh2.

The curves (Figure 5.19) are compared by the activity at the highest concentrations of DTNB. The curve of HvNTR2_W42A is very similar to that of the wild-type, whereas the activity is increased slightly for the mutants HvNTR2_M43A, HvNTR2_W42A_M43A and HvNTR2_N45A_D46A. The mutant with a part of the FAD-loop deleted, HvNTR2_Δ42-47, shows a significant increase of activity. This increase could be due to the loop being near the active site as shown by a roughly modelled FR conformation of HvNTR2 (Figure 5.20, see legend for details, the model is the same as in Figure 3.1) and therefore a removal of the loop or some the residues lead to increased accessibility for DTNB. The closest distance between the loop and the active site cysteines is 5.60 Å (between $Cys145_{HvNTR2}$ and $Asp46_{HvNTR2}$ in the model of the FR conformation (Figure 5.20). This distance may not limit the accessibility of DTNB, but the distance could be shorter if one domain is bent relative to the other. This is possible as seen in the crystal structure of HvNTR2 (Kirkensgaard *et al*., 2009; Chapter 2). Another explanation for the differences in activity towards DTNB could be that some mutants are slightly more unfolded leading to more accessible active site cysteines. However, this would influence the functionality of the protein, which should not be able to transfer reducing equivalents from NADPH to the cysteines. Furthermore, it was observed above that HvNTR2_Δ42-47 had activity with AtTrxh3 and thus it seems not to be folded incorrectly.

The activity with DTNB alone is significantly lower than when Trx is included. This may indicate that HvNTR2 is mainly found in the FO conformation in solution which would bury the cysteines, rendering them inaccessible. In the presence of Trx HvNTR2 may shift to the

FR conformation and the cysteines can react. Negri *et al.* (2009) modelled the shift from the FO to the FR conformation for EcNTR. They found that most likely both NADPH and EcTrx are bound to EcNTR in the FO conformation before the shift to the FR confirmation occurs (see Chapter 6).

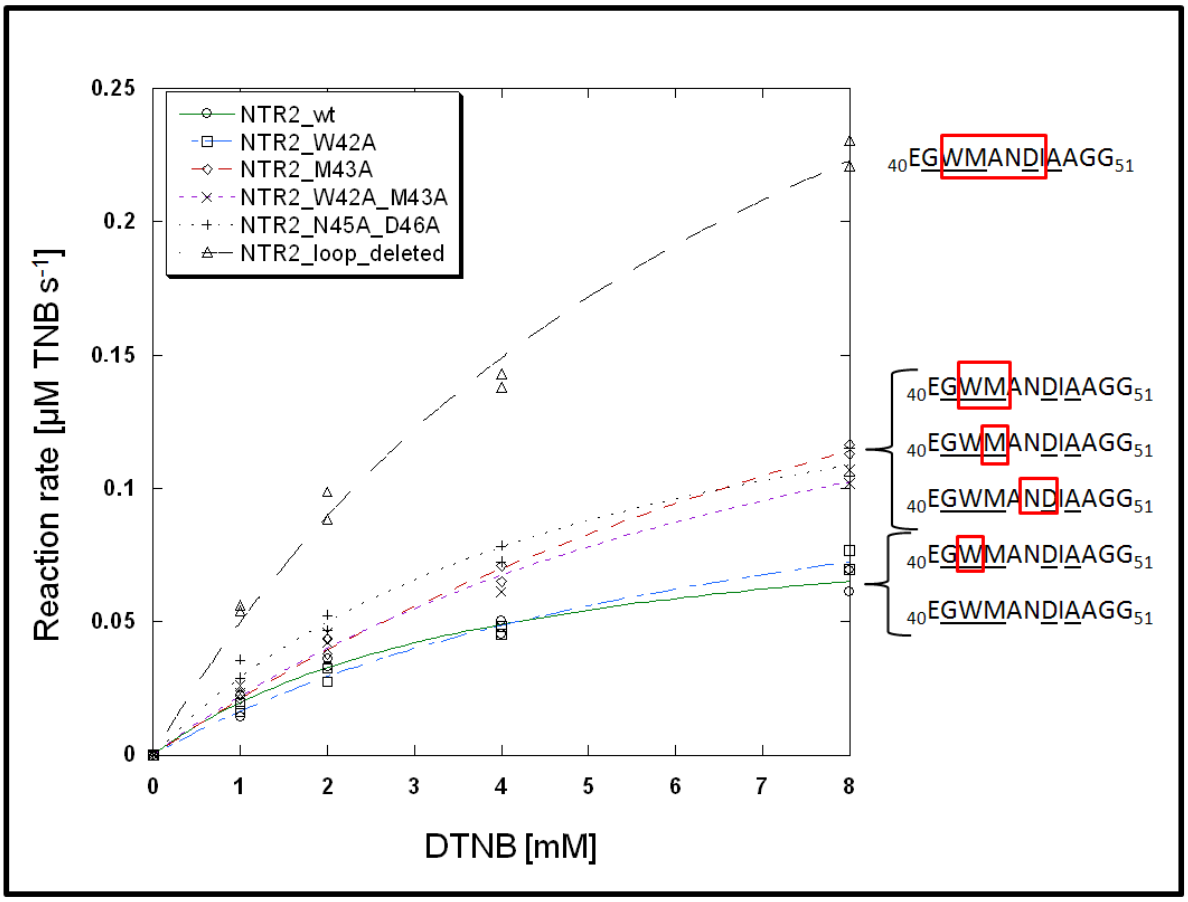

Figure 5.19. Reaction rates (µM TNB released s^{-1}) plotted against the concentration of DTNB. In the assay 100 nM HvNTR2 (wt or mutant) and varying concentrations of DTNB was used in 0.1 M KH_2PO_4 pH 7.5, 2.0 mM EDTA, 0.2 mM NADPH and 0.1 mg/mL BSA. Proteins were diluted in 0.1 M KH_2PO_4 pH 7.5, 2.0 mM EDTA and 0.1 mg/mL BSA. The residues mutated are boxed in red in the sequences to the right.

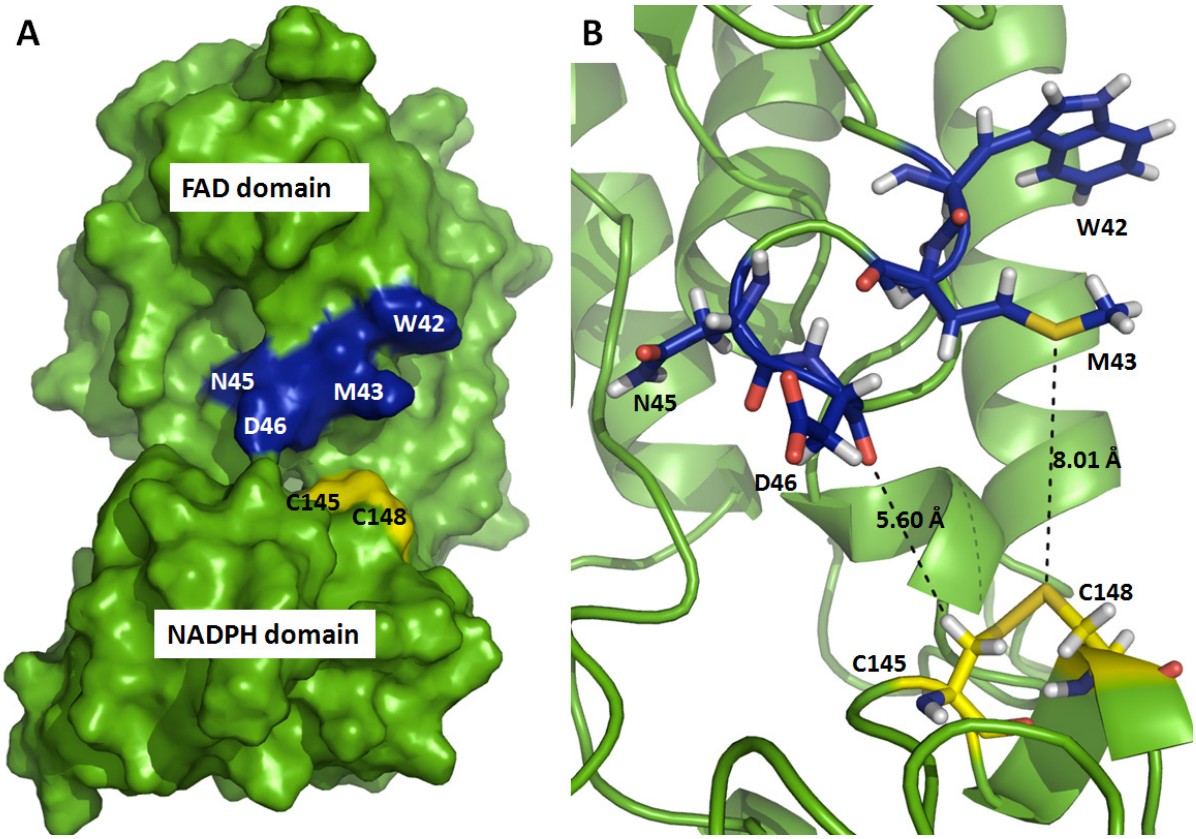

Figure 5.20. Position of the residues from the FAD-loop relative to the active site cysteines in the FR conformation. (**A**) HvNTR2 from an unrefined model of the FR conformation of HvNTR2. The two domains of HvNTR2 were individually superposed to the corresponding domains of EcNTR from the complex of EcNTR:EcTrx (pdb 1F6M, Lennon *et al*., 2000). Some mutants of HvNTR2 led to an increased activity with DTNB. The residues involved are shown in blue, and the active site cysteines are shown in yellow. (**B**) Close-up of the active site. $Met43_{HvNTR2}$ and $Asp46_{HvNTR2}$ are positioned closest to the active site cysteines. Measured distances shown in Ångströms.

5.3 Conclusion

The kinetic data above confirmed that the FAD-loop, $_{40}$EGWMANDIAAGG$_{51}$, in HvNTR2 is critical for binding HvTrxh2. Deletion of a part of the loop, $_{42}$WMANDI$_{47}$, lowered activity for HvTrxh2 about 1700 fold. According to the structural model of HvNTR2:HvTrxh2 (Chapter 4, Figure 4.4A) the FAD-loop binds HvTrxh2 through multiple hydrophobic contacts, primarily involving $Trp42_{HvNTR2}$ and $Met43_{HvNTR2}$. In the model $Ile51_{HvTrxh2}$ is positioned between these two residues. Mutating either $Trp42_{HvNTR2}$ or $Met43_{HvNTR2}$ to alanine decreased activity toward HvTrxh2 to about 4 and 15%, respectively. Mutating $Ile51_{HvTrxh2}$ to glycine led to 23% activity with HvNTR2. Combining each of these NTR mutants with

HvTrxh2_I51G lowered the activity further to 0.4-0.5%, which makes it plausible that $Ile51_{HvTrxh2}$ is placed between $Trp42_{HvNTR2}$ and $Met43_{HvNTR2}$. For the mutant HvNTR2_W42A_M43A the activity was reduced about 1100 times to 0.09%. This confirms that these residues are critical for the binding of HvTrxh2. Interestingly binding AtTrxh3 did not seem to depend as much on this loop. Especially $Trp42_{HvNTR2}$ was dispensable, so the activity of HvNTR2_W42A was only slightly lowered to 71% towards AtTrxh3, compared to HvNTR2wt/AtTrxh3. Thus HvNTR2_W42A has 20 times higher activity with AtTrxh3 than with its own substrate, HvTrxh2. Also HvNTR2_Δ42-47 had much higher activity (80 times), with AtTrxh3 than with HvTrxh2. These differences could not be attributed the different active site of AtTrxh3 (WCPPC instead of the classical WCGPC), as concluded by assaying with the active-site mutant HvTrxh2_G47P. Thus, the relative contribution of the FAD-loop to the binding energy of the NTR:Trxh complex seem to vary considerably among species. Even though the FAD-loop is not conserved in EcNTR, the loop of HvNTR2 seems able to bind EcTrx in a similar way than HvTrxh2.

For the mutations in the NADPH domain of HvNTR2 the results were less clear. For both HvNTR2_N139A and HvTrxh2_E86A k_{cat} and K_m decreased, leading to an almost unchanged k_{cat}/K_m. This indicate that these residues are not critical for the binding between HvNTR2 and HvTrxh2. Substituting residues in the Glycine-loop $_{221}GGAGGGPL_{228}$ of HvNTR2 to mimic the loop of AtNTR-B had slightly negative effect on the binding of HvTrxh2 and a positive effect on the binding of AtTrx3. Changing $P227_{HvNTR2}$ to valine decreased activity to 25% for HvTrxh2 which may be due to a shortening of a groove accommodating $Glu86_{HvTrxh2}$.

An assay without Trx showed that k_{cat}/K_m is ~54,000 times lower for DTNB than for HvTrxh2. This may indicate that Trx should be present for the conformational change from FO to FR (see Chapter 6).

5.4 Methods and materials

5.4.1 Cloning and site-directed mutagenesis

Mutants of HvNTR2 and HvTrxh2 were made by site-directed mutagenesis using the QuikChange® II Site-Directed Mutagenesis Kit (Agilent Technologies) with the recommended concentrations. Primers were designed using the Primer design guidelines for the kit and delivered HPLC-purified since high purity is important for optimal cloning (Eurofins MWG

Operon, Germany). A list of all primers used is given in Appendix D. The template plasmids encoding HvNTR2 or HvTrxh2 with an N-terminal His_6-tag were constructed in pEt15b (Shahpiri *et al.*, 2008a).

For the synthesis reaction of the mutant strand the following was used: 5 µL of 10x reaction buffer, 20 ng of DNA template (purified by GeneJet™ Plasmid Miniprep kit, Fermentas), 125 ng of each primer (5'- and 3'-), 1 µL of dNTPs, 1 µL *PfuUltra* HF DNA polymerase (2.5 U/1 µL) and ddH20 to a total volume of 50 µL. The cycling parameters used were as recommended for the kit.

After the reaction, the parental strand was digested for 1—2 h using *Dpn*I (final concentration 0.2 units/µL) provided in the kit. Either XL-Blue from the kit or chemical competent *E. coli* strain DH5α were transformed with 1—4 µL of the resulting mixture, using the procedure recommended by the manufacturer. However, for DH5α incubation at 42°C was prolonged from 45 to 90 s, and 800 µL instead of 500 µL SOC media (20 g/L tryptone, 5 g/L yeast extract, 0.5 g/L NaCl, 2.5 mM KCl, 20 mM glucose, adjusted to pH 7.0 with NaOH) was added. Plasmid was purified from 5—10 mL overnight culture of selected colonies using GeneJet™ Plasmid Miniprep kit (Fermentas) and sequenced in both directions by Eurofins MWG Operon using T7 and T7 term primers (provided by the company). Once the correct sequence was confirmed, heat-chock competent Rosetta cells were transformed with the plasmid as described above for DH5α and plated/restreaked on LB/agar plates containing ampicillin (100 µg/mL) and chloramphenicol (20 µg/mL). A Rosetta strain expressing HvNTR2_R140A was kindly provided by Azar Shahpiri (Shahpiri, 2008b).

Plasmids containing the genes encoding the following three h-type Trxs and NTR from *Arabidopsis thaliana* were obtained from BRC Experimental Plant Division, RIKEN Tsukuba Institute; AtTrxh3 (pda04909-RAFL08-16-J17), AtTrxh4 (pda11571-RAFL19-77-A10), AtTrxh5 (pda01954-RAFL09-16-K07) and AtNTR-B (pda13160-RAFL16-02-L06). The genes were amplified by PCR using primers, which contained restriction sites for *BamHI* and *NdeI*, and the genes were inserted into pET15b vectors. A pET14b based plasmid encoding EcTrx was obtained from MWG. Rosetta was transformed with these plasmids as described above.

For protein expression and purification see Chapter 3, Section 3.4.1. For SDS-PAGE see Section 3.4.5.

5.4.2 Kinetics

An assay using DTNB (5,5'-dithiobis-(2-nitrobenzoic acid) as the final disulfide substrate as described (Miranda-Vizuete *et al*., 1997) was used with slight modifications. In the assay reducing equivalents are transferred from NADPH over NTR to Trx which reacts with DTNB (Figure 5.21). One TNB ion is released and has a strong absorbance at 412 nm (extinction coefficient of 13,600 M^{-1} cm^{-1}, Ellman, 1959). The other thiol in the active site of Trx restores the disulfide releasing yet another TNB ion.

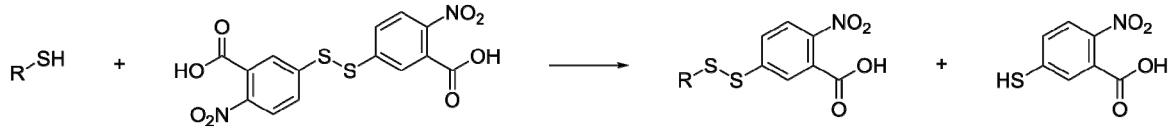

Figure 5.21. Reaction of a thiol with DTNB (5,5'-dithiobis-(2-nitrobenzoic acid) or Ellman's reagent. The thiol from e.g. a cysteine residue reacts with DTNB and releases a TNB ion which absorbs at 412 nm with an extinction coefficient of 13,600 M^{-1} cm^{-1} (Ellman, 1959).

The final reaction mixture contained 20 nM NTR wt or mutant as determined from the FAD content (extinction coefficient 11.300 M^{-1} cm^{-1} at 456 nm, Williams *et al*., 1967), varying concentrations of Trx wt or mutant (typically between 0.125 and 8 µM) in 0.1 M KH_2PO_4 pH 7.5, 2.0 mM EDTA, 0.2 mM DTNB, 0.2 mM NADPH and 0.1 mg/mL BSA. Protein dilutions were performed in 0.1 M KH_2PO_4 pH 7.5, 2.0 mM EDTA and 0.1 mg/mL BSA. The reaction was initiated by addition of NTR, and for the slowest reactions performed in 96-well microtiter plates containing 250 µL per well, and A_{412} monitored for 30 min with measurements every 30 s (ELISA plate reader, Power Wave XS, BIO-TEK®, Holm & Halby). A standard curve for the absorbance of free TNB was made using known concentrations of N-acetyl cysteine in 0.1 M KH_2PO_4 pH 7.5, 2.0 mM EDTA, 0.2 mM DTNB, 0.2 mM NADPH and 0.1 mg/mL BSA measuring (Figure 5.22). The mixture was incubated 5 min at room temperature before measuring A_{412}. The obtained extinction coefficient of 9,600 M^{-1} $(path\ length)^{-1}$ is lower than the generally used 13,600 M^{-1} cm^{-1} (Ellman, 1959) due to a path length of less than 1 cm.

Most reactions were performed in a quartz cuvette in a spectrophotometer (Ultrospec 2100 *pro*, Amersham Biosciences), using the standard extinction coefficient of TNB of 13,600 M^{-1} cm^{-1} (Ellman, 1959). The reaction was followed for typically 90 s with measurements of

A_{412} every 2 s. Independent duplicates of each measurement were made, and K_m and V_{max} were determined using the program KaleidaGraph (Synergy Software).

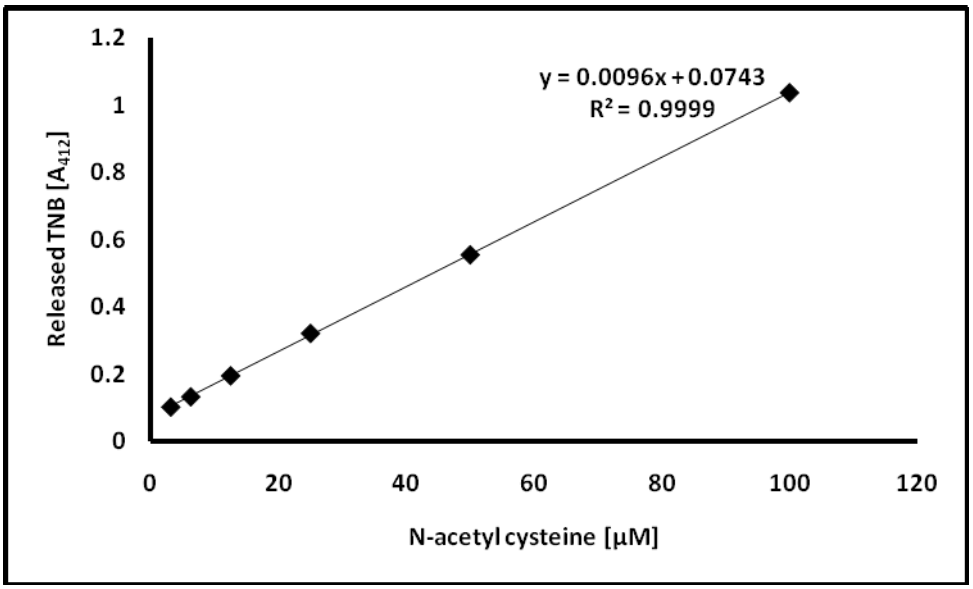

Figure 5.22. Standard curve for N-acetyl cysteine reacted with DTNB. Known concentrations of N-acetyl cysteine in 0.1 M KH_2PO_4 pH 7.5 was mixed with 2.0 mM EDTA, 0.2 mM DTNB, 0.2 mM NADPH and 0.1 mg/mL BSA in a 96-well microtiter plate containing 250 µL per well. After 5 min of incubation at room temperature A_{412} was measured (ELISA plate reader, Power Wave XS, BIO-TEK®, Holm & Halby). The datapoints are averages of two independant replica.

5.4.3 Attempted reintroduction of FAD to HvNTR2

The protein concentration was estimated using Bradford reagent (Bradford, 1976) and 1.6 µM HvNTR2 from either of two peaks in the chromatogram obtained from size exclusion chromatography (*data not shown*) was mixed with 16 µM FAD and preincubated 30 min at room temperature. The enzyme activity was tested under the following conditions: 80 nM HvNTR2, 5 µM HvTrxh1, 0.1 M Tris-HCl pH 8.0, 1.0 mM EDTA, 0.2 mM DTNB, 0.3 mM NADPH and 0.1 mg/mL BSA. HvNTR2 was excluded from the reference. The release of TNB was measured at 412 nm with measurements every 30 s in a spectrophotometer (Ultrospec 2100 *pro*, Amersham Biosciences). See Section 5.4.2 for more details concerning DTNB.

Chapter 6

Reaction mechanism of NTR

6.1 Introduction

This chapter is a brief summary of the various aspects concerning the reaction mechanism of NTR discussed throughout the other chapters of this thesis.

6.2 Results and discussion

The reaction mechanism for NTR proposed in Chapter 2, Section 2.2.7 is based on the following observations: i) Visual inspection indicated the NADPH binding site of EcNTR in the FR conformation to be accessible, suggesting that binding of NADPH can occur after the conformational change from FO to FR conformation. ii) In the structure of HvNTR2 (which most resembles the FO conformation) the two domains are tilted relative to each other in such a way that the binding site of NADPH is in part occluded and thus not able to accommodate NADPH, whereas the accessibility to the active site cysteines has increased when comparing to other structures in the FO conformation. This could be an artefact due to a bound citrate molecule in the NADPH binding site, but it could also demonstrate that the transition from FO to FR does not necessarily go through a pure rotation. Indeed the transition may involve tilting of one domain relative to the other. iii) Further comparison of the FR and FO conformation of EcNTR showed that some of the areas that may be important for the binding of Trx are accessible in the FO conformation and made us suggest that the reaction is initiated with binding of Trx to the NADPH domain already in the FO conformation (Chapter 2, Figure 2.8). Subsequent rotation from the FO to the FR conformation will allow NADPH to bind and reduce FAD in a direct contact.

HvNTR2_C145S is able to react with HvTrxh2_C49S-TNB in the absence of NADPH (Chapter 3, Section 3.2.1 and 3.2.7) indicating that NADPH is not, as earlier suggested (Waksman *et al.*, 1994), required to bind to NTR prior to the binding of Trx. Furthermore, in the absence of HvTrxh2 the reactivity of HvNTR2 with DTNB is low (Chapter 5, Section

5.2.3.4) in agreement with previous observations (Holmgren *et al*., 1977; Shahpiri *et al*., 2008b). This behaviour indicates that the active site cysteines in NTR are very poorly accessible for DTNB and suggests that NTR is mostly found in the FO conformation in the absence of Trx.

Even though the reaction between HvNTR2_C145S and HvTrxh2_C49S-TNB occurs without NADPH (if the active site cysteine $Cys148_{HvNTR2}$ is reduced by DTT), the reaction rate is substantially increased by addition of NADPH (Chapter 3, Section 3.2.7). In this assay performed under anaerobic conditions NADPH was reacted with HvNTR2_C145S (20 min) prior to the addition of HvTrxH2_C49S-TNB. After rapid reaction with HvTrxH2_C49S-TNB (monitored at 412 nm) a drop is seen in the absorbance. The drop could be due to reduction of FAD, since the FAD contributes substantially to the background absorbance at 412nm, due to a fair amount of HvNTR2_C145S (30 µM) being used in the assay. Since the drop is seen after addition of Trx it could indicate that the FAD is more accessible for reduction in the presence of Trx, meaning that Trx may facilitate the change from FO to FR conformation.

It is further seen (Chapter 3, Section 3.2.7) that even addition of $NADP^+$ increases the reaction rate between HvNTR2_C145S and HvTrxh2_C49S-TNB, but without an accompanying drop in absorbance, probably since $NADP^+$ is unable to reduce FAD. Apparently it is not the reduction of FAD itself, but the binding of $NADP^+$ or NADPH that increases the reaction rate.

All together the observations indicate that both NADPH (or $NADP^+$) and Trx are involved in the conformational change of NTR from FO to FR. Negri *et al.* (2009) simulated a full catalytic cycle of EcNTR using molecular dynamics and docking: From visual inspection of the structures of EcNTR in the FO and FR conformation it was concluded that NADPH can only bind EcNTR in the FO conformation (Negri *et al.*, 2009). This is in contrast to the observations reported here (Chapter 2, Figure 2.7C). However, the results in Chapter 3 Section 3.2.7, suggest that NADPH (or $NADP^+$) increased the reaction rate of the complex formation, and could indicate that NADPH entry takes place in the FO conformation.

When $EcTrx_{ox}$ was docked into EcNTR in the FO conformation the top scoring solutions placed EcTrx in the NADPH domain with the disulfide in an orientation suitable for catalysis (left side of Figure 6.1, Negri *et al*., 2009). Based on these docking studies, it was found plausible that the FO conformation is the target for $EcTrx_{ox}$ binding (Negri *et al*., 2009). This

is in agreement with the suggested mechanism in Chapter 2, Figure 2.8 and the finding that HvNTR2 reacts poorly with DTNB alone. In the reaction mechanism suggested by Negri *et al*., NADPH entry immediately precedes or is coupled to $EcTrx_{ox}$ binding to NTR in the FO conformation. This corresponds well with the present findings that the reaction rate of complex formation is increased by NADPH, and that a reaction with DTNB alone is much slower than with HvTrxh2 present.

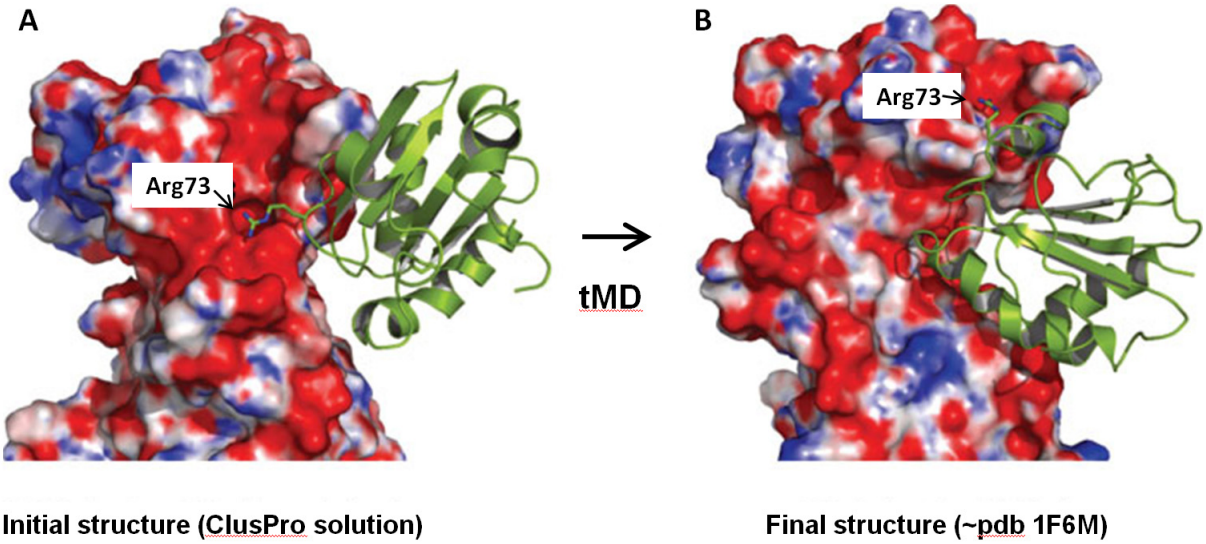

Figure 6.1. Close-up view of the NADP-binding domain of EcNTR enveloped in a van der Waals surface that has been coloured according to the molecular electrostatic potential calculated by the APBS program (positive and negative regions in blue and red, respectively). The green ribbon represents oxidized EcTrx, which is shown docked as suggested by the ClusPro program (**A**) and at the end of the tMD procedure (**B**) that brought EcNTR from the initial FO state to the FR conformation. The guanidinium of $Arg73_{EcTrx}$ is lodged in a negatively charged pocket in EcNTR in the starting structure and slides in a groove (which is also negatively charged) during the conformational transition. Results and figure from Negri *et al*., 2009.

In the docking studies by Negri *et al*. the guanidinium of $Arg73_{EcTrx}$ is lodged in a negatively charged pocket in EcNTR in the starting structure (Figure 6.1A) and slides in a groove during the conformational transition from FO to FR (Figure 6.1B). This groove is the same as the one accommodating $Arg73_{EcTrx}$ in Figure 4.9B, Chapter 4. That it is accessible in the FO conformation is seen from Figure 2.5C. The MD simulations strongly suggested that $Arg73_{EcTrx}$ is crucial both with regard to the electrostatic interaction between the two proteins and for the twisting motion of the NTR domains. Futhermore, the mutant EcTrx_R73G showed a reduction of activity to 0.6% with EcNTR (Negri *et al*., 2009). This

residue is not conserved in plants and is a glutamate in HvTrxh2, $Glu86_{HvTrxh2}$. In the HvTrxh2:HvNTR2 complex model $Glu86_{HvTrxh2}$ is positioned in a complementary groove of HvNTR2 (Chapter 4, Figure 4.9A). However, the HvNTR2 groove is shorter and less contacts are formed with the side-chain of $Glu86_{HvTrxh2}$ than found for $Arg73_{EcTrx}$ (Chapter 4, Figure 4.9B). The mutational analysis described in Chapter 5 included a mutant with this residue substituted by alanine. The HvTrxh2_E86A mutant had K_m for HvNTR2 decreased by 50%, and k_{cat} /K_m increased to 137% of the wild-type values. When combining with the HvNTR2_N139A mutant, K_m was decreased even further by a total of 65%, and as a consequence k_{cat} /K_m increased to 150% of the wild-type HvTrxh2 value. These results indicate that $Glu86_{HvTrxh2}$ does not play the same role as $Arg73_{EcTrx}$ and seems less critical in the complex formation with NTR than that residue. The mutations of $Trp42_{HvNTR2}$ and $Met43_{HvNTR2}$ in the FAD-loop (Figure 4.6C and Table 5.2) were more severe (1000 times reduction in k_{cat} /K_m for the double mutant) than the mutations of selected residues in the NADPH domain examined in Chapter 5 (Section 5.2.3.3 and Table 5.2). $Met43_{HvNTR2}$ appears to be central for the binding of HvTrxh2, both based on this large reduction in k_{cat} /K_m and its position in a pocket on HvTrxh2. Noticeably this is the only interacting residue which is not identical in the other barley NTR isoform, HvNTR1.

The FAD domains of the crystal structure of HvNTR2 and the modelled complex of HvNTR:HvTrxh2 were superposed (Figure 6.2). This shows that there is room for binding of HvTrxh2 to the FAD domain in the FO conformation. The orange arrow in Figure 6.2 indicates how the conformational change from FO to FR would bring the active site cysteines from HvNTR2 in proximity to the active site cysteines of HvTrxh2.

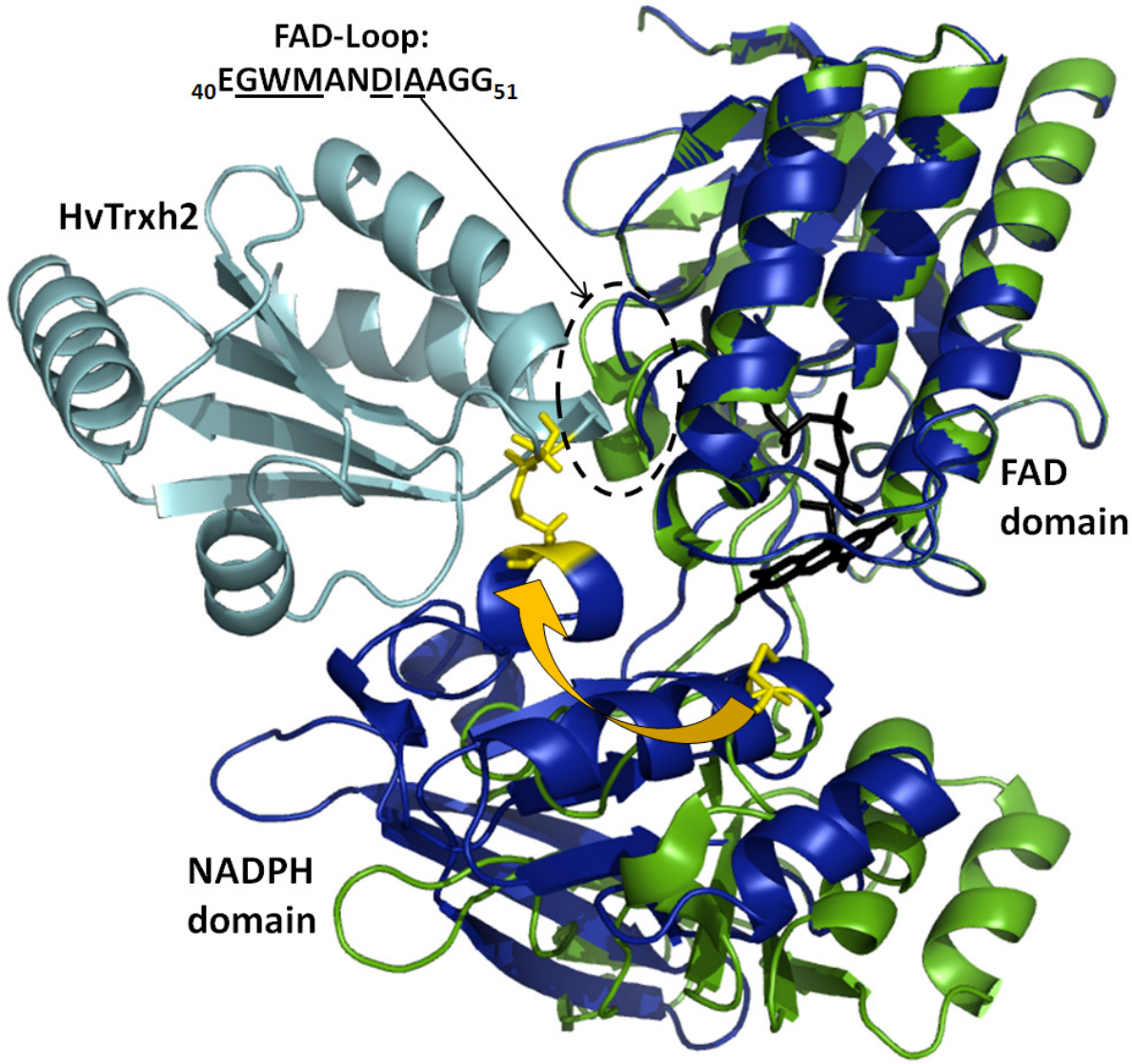

Figure 6.2. Superposition of the FAD domains of the modelled complex of HvNTR2 (dark blue):HvTrxh2 (cyan) and of the crystal structure of HvNTR2 (green, pdb accession 2WHD). The FAD-loop is circled and the active site cysteines are in yellow. The orange arrow indicates how the active site cysteines of HvNTR2 are brought in proximity to the active site cysteines of HvTrxh2, when HvNTR2 changes from FO to FR conformation.

6.3 Conclusion

Even though HvNTR2_C145S reacts with HvTrxh2_C49S-TNB in the absence of NADPH, the reaction rate is increased in the presence of NADPH as well as of $NADP^+$. This indicates that it is not the reduction of FAD bound in HvNTR2 ass such, but the binding of NADPH/$NADP^+$ to HvNTR2 that influences the rate of the reaction with HvTrxh2. Furthermore, the activity of HvNTR2 with DTNB is much lower than with HvTrxh2. These findings support the reaction mechanism suggested by Negri *et al*. (2009) in which both

$EcTrx_{ox}$ and NADPH are bound to EcNTR in the FO conformation and induce a shift to the FR conformation. Negri *et al*. (2009), however, found $Arg73_{EcTrx}$ essential for the binding as well as for the twisting motion of EcNTR. Mutating the corresponding residue $Glu86_{HvTrxh2}$ to alanine led to an increase in k_{cat}/K_m, which shows the structural events critical for the reaction mechanism are not identical for the NTRs of the two organisms. The structural studies here (Figure 6.2) implicate that HvTrxh2 may be able to bind the FAD domain instead of the NADPH domain in the FO conformation and a subsequent conformational shift can bring the active site cysteines of HvNTR2 in the proximity of the active site of HvTrxh2.

Outlook

As a final comment this outlook includes a few thoughts concerning possible future investigations of the NTR/Trx system in continuation of this PhD study.

The obtained structure of HvNTR2 as well as the produced model of HvNTR2:HvTrxh2 and the mutational studies provide knowledge which leads to a deeper understanding of the NTR/Trx system of barley and especially the structural requirements for the recognition between the two proteins. The model may be used as a guideline for an optimisation of the system by producing even more efficient enzymes by protein engineering which can be used in the various applications presented in Chapter 1.

To further investigate thermodynamics and kinetics of interactions between NTR and Trx from barley several bioanalytical tools could potentially be applied including analytical gel filtration, isothermal titration calorimetry and surface plasmon resonance (Biacore). For these types of analyses it may be preferable to apply mutants lacking both the cysteines of the active sites (HvNTR2_C145S_C148A and HvTrxh2_C49S_C46A) to avoid disulfide bond formation which most likely interfers with data interpretation. If it is possible to measure the binding between the two proteins, experiments could be designed with/without NADPH to further elucidate the role of this ligand in the binding between NTR and Trx. Furthermore, various mutations of selected residues could be added to verify how much these residues contribute to the binding. The mutant HvNTR2_C145S_C148A could also be used as a reference for the labelling with DTNB to investigate whether the cysteines located in the dimer interface of HvNTR2 are labelled with TNB.

The determined crystal structure of HvNTR2 did not resemble other NTRs in the FO conformation, due to a different relative orientation of the two domains. Whether this is an artefact from the crystallisation or this structure exists in solution is an interesting question since the structure may represent a reaction intermediate. In principle the overall solution structure can be determined by SAXS. Especially when a crystal structure is available, SAXS is a very strong tool for determining whether this structure corresponds to what is present in

solution. However, preliminary SAXS-measurements did not provide a usable dataset due to sample aggregation, so optimisation is required.

Concerning the reaction mechanism of NTR it was suggested (Chapter 6) that HvTrxh2 may bind the FAD domain of HvNTR2 in the FO conformation. To verify this HvNTR2 could be locked in the FO conformation by using a crosslinking reagent and the binding of HvTrxh2 could be investigated further by the methods mentioned above. It has previously been shown possible to restrict EcNTR to the FO conformation by using the bifunctional reagent N,N,1,2 phenylenedimaleimide and a mutant of EcNTR with two residues ($Glu48_{EcNTR}$ located in the FAD domain and $Arg130_{EcNTR}$ located in the NADPH domain) mutated to cysteines (Veine *et al*., 1998b).

As discussed (Chapter 4) the structural requirements of NTR for recognition of Trx may very well be the same for other eukaryotic LMW NTRs as the sequence of the FAD-loop is similar in NTRs from plants, yeast, fungi and amoebae. Therefore, the detailed structural studies of HvNTR2 provide new insight into how these NTRs may interact with Trx. Further, since NTR from humans does not resemble the LMW NTRs, future perspectives could include design of specific inhibitors for medical applications, tailored towards NTRs from pathogenic organisms.

References

Adams, P.D., Grosse-Kunstleve, R.W., Hung, L.W., Ioerger, T.R., McCoy, A.J., Moriarty, N.W., Read, R.J., Sacchettini, J.C., Sauter, N.K. and Terwilliger, T.C. (2002). PHENIX: building new software for automated crystallographic structure determination. *Acta Crystallogr D* **58**: 1948—1954.

Agilent Technologies, Instruction manual #204300: Affinity Protein Expression and Purification System and Affinity Protein Expression Vectors. http://www.genomics.agilent.com/files/Manual/204300_A.pdf

Akif, M., Suhre, K., Verma, C. and Mande, S.C. (2005). Conformational flexibility of *Mycobacterium tuberculosis* thioredoxin reductase: crystal structure and normal-mode analysis. *Acta Crystallogr D* **61**: 1603—1611.

Alkhalfioui, F., Renard, M. and Montrichard, F. (2007). Unique properties of NADP-thioredoxin reductase C in legumes. *J Exp Bot* **58**: 969—978.

Alkhalfioui, F., Renard, M., Frendo, P., Keichinger, C., Meyer, Y., Gelhaye, E., Hirasawa, M., Knaff, D. B., Ritzenthaler, C. and Montrichard, F. (2008). A novel type of thioredoxin dedicated to symbiosis in legumes. *Plant Physiol* **148:** 424—435.

Arnér, E.S.J. and Holmgren, A. (2000). Physiological functions of thioredoxin and thioredoxin reductase. *European Journal of Biochemistry* **267:** 6102—6109.

Baker, N.A., Sept, D., Joseph, S., Holst, M.J. and McCammon, J.A. (2001). Electrostatics of nanosystems: application to microtubules and the ribosome. *P Natl Acad Sci USA* **98**: 10037—10041.

Bafunno, V., Giancaspero, T.A., Brizio, C., Bufano, D., Passarella, S., Boles, E. and Barile, M. (2004). Riboflavin Uptake and FAD Synthesis in *Saccharomyces cerevisiae* Mitochondria. Involvement of the Flx1p carrier in FAD export. *J Biol Chem* **279** (1): 95—102.

Barrero, J.M., Talbot, M.J., White, R.G., Jacobsen, J.V. and Gubler, F. (2009). Anatomical and Transcriptomic Studies of the Coleorhiza Reveal the Importance of This Tissue in Regulating Dormancy in Barley. *Plant Physiol* **150:** 1006—1021.

Behm, M. and Jacquot, J.P. (2000). Isolation and characterization of thioredoxin h from poplar xylem. *Plant Physiol Bioch* **38:** 363—369.

Besse, I., Wong, J.H., Kobrehel, K. and Buchanan, B.B. (1996). Thiocalsin: A thioredoxin-linked, substrate-specific protease dependent on calcium. *P Natl Acad Sci USA* **93:** 3169—3175.

Bewley, JD and Black, M (1994). Seeds: Physiology of Development and Germination. New York, Plenum. pp. 1—33.

Bradford, M.M. (1976). A rapid and sensitive method for the quantitation of microgram quantities of protein utilizing the principle of protein-dye binding. *Anal Biochem* **72:** 248—254.

Bréhélin, C., Mouaheb, N., Verdoucq, L., Lancelin, J.M. and Meyer, Y. (2000). Characterization of determinants for the specificity of Arabidopsis thioredoxins h in yeast complementation. *J Biol Chem* **275:** 31641—31647.

Bréhélin, C., Laloi, C., Setterdahl, A.T., Knaff, D.B. and Meyer, Y. (2004). Cytosolic, mitochondrial thioredoxins and thioredoxin reductases in *Arabidopsis thaliana*. *Photosynth Res* **79:** 295—304.

Buchanan, B.B. and Balmer, Y. (2005). Redox regulation: A broading horizon. *Annu Rev Plant Biol* **56:** 187—220.

Cazalis, R., Pulido, P., Aussenac, T., Pérez-Ruiz, J.M. and Cejudo, F.J. (2006). Cloning and characterization of three thioredoxin h isoforms from wheat showing differential expression in seeds. *J Exp Bot* **257:** 2165—2172.

Chandler, P.M., Marion-Poll, A., Ellis, M. and Bubler, F. (2002). Mutants at the *Slender1* locus of barley cv himalaya. Molecular and physiological characterization. *Plant Physiol* **129**: 181—190.

Chandler, P.M., Harding, C.A., Ashton, A.R., Mulcair, M.D., Dixon, N.E. and Mander L.N. (2008). Characterization of Gibberellin Receptor Mutants of Barley (Hordeum vulgare L.). *Mol Plant* **1**(2): 285—294.

Chartron, J., Shiau, C., Stout, C.D., and Carroll, K.S. (2007). 3'-Phosphoadenosine-5'-phosphosulfate reductase in complex with thioredoxin: a structural snapshot in the catalytic cycle. *Biochemistry* **46:** 3942—3951.

Chelikani, P., Fita, I. and Loewen, P.C. (2004). Diversity of structures and properties among catalases. *Cell. Mol Life Sci* **61** (2): 192—208.

Chibani, K., Wingsleb, G., Jacquot, J.P., Gelhayea, E. and Rouhiera, N. (2009). Comparative genomic study of the thioredoxin family in photosynthetic organisms with emphasis on *Populus trichocarpa*. *Mol Plant* **2:** 308—322.

Chivers, P.T. and Raines, R.T. (1997). General acid/base catalysis in the active site of *Escherichia coli* thioredoxin. *Biochemistry* **36:** 15810—15816.

Collaborative Computing Project, n. 4. (1994). The CCP4 suite: programs for protein crystallography. *Acta Crystallogr D* **50:** 760—763.

Cho, M.J., Wong, J.H., Marx, C., Jiang, W., Lemaux, P.G. and Buchanan, B.B. (1999). Overexpression of thioredoxin h leads to enhanced activity of starch debranching enzyme (pullulanase) in barley grain. *P Natl Acad Sci USA* **96:** 14641—14646.

Coudevylle, N., Thureau, A., Hemmerlin, C., Gelhaye, E., Jacquot, J.P. and Cung, M.T (2005). Solution structure of a natural CPPC active site variant, the reduced form of thioredoxin h1 from poplar. *Biochemistry* **44:** 2001—2008.

Coudevylle, N., Thureau, A., Hemmerlin, C., Gelhaye, E., Jacquot, J. P. and Cung, M.T. (2005). Solution structure of a natural CPPC active site variant, the reduced form of thioredoxin h1 from poplar. *Biochemistry* **44:** 2001–2008.

Dai, S., Saarinen, M., Ramaswamy, S., Meyer, Y., Jacquot, J. P. and Eklund, H. (1996). Crystal structure of *Arabidopsis thaliana* NADPH dependent thioredoxin reductase at 2.5 Å resolution. *J Mol Biol* **264:** 1044—1057.

Dalle-Donne, I., Rossi, R., Giustarini, D., Colombo, R. and Milzani, A. (2008). Molecular mechanisms and potential clinical significance of S-Glutathionylation. *Antioxid Redox Sign* **10:** 445—474.

Davis, I.W., Leaver-Fay, A., Chen, V.B., Block, J.N., Kapral, G.J., Wang, X., Murray, L.W., Arendall, W.B., III, Snoeyink, J., Richardson, J.S. and Richardson, D.C. (2007). MolProbity: all-atom contacts and structure validation for proteins and nucleic acids. *Nucleic Acids Res.* **35:** W375—W383.

DeLano, W.L. (2002). The PyMOL Molecular Graphics System, DeLano Scientific, San Carlos, CA, USA. http://www.pymol.org.

del Val, G., Yee, B.C., Lozano, R.M., Buchanan, B.B., Ermel, R.W., Lee, Y.M. and Frick, O.L. (1999). Thioredoxin treatment increases digestibility and lowers allergenicity of milk. *J Allergy Clin Immun* **103**: 690—697.

Droux, M., Jacquot, J.P., Miginac-Maslow, M., Gadal, P., Huet, J.C., Crawford, N.A., Yee, B.C. and BUCHANAN, B.B. (1987). Ferredoxin-Thioredoxin Reductase, an Iron-Sulfur Enzyme Linking Light to Enzyme Regulation in Oxygenic Photosynthesis: Purification and Properties of the Enzyme from Cs, C4, and Cyanobacterial Species. *Arch Biochem Biophys* **252** (2): 426—439.

Elledge, S.J., Zhou, Z. and Allen, J.B. (1992). Ribonucleotide reductase: regulation, regulation, regulation. *Trends Biochem Sci* **17** (3): 119—23.

Ellman, G. L. (1959). Tissue sulfhydryl groups. *Arch Biochem Biophys* **82:** 70–77.

Emsley, P. and Cowtan, K. (2004). Coot: model-building tools for molecular graphics. *Acta Crystallogr D* **60:** 2126—2132.

Fritz-Wolf, K., Kehr, S., Stumpf, M., Rahlfs, S. and Becker, K. (2001). Crystal structure of the human thioredoxin reductase-thioredoxin complex. *Nat Commun* **2:** 383.

Foyer, C.H. and Noctor, G. (2003). Redox sensing and signalling associated with reactive oxygen in chloroplasts, peroxisomes and mitochondria. *Physiol Plantarum* **119:** 355—364.

Gas, E., Flores-Perez, U., Sauret-Gueto, S. and Rodriguez-Concepcion, M. (2009). Hunting for plant nitric oxide synthase provides new evidence of a central role for plastids in nitric oxide metabolism. *Plant Cell* **21:** 18—23.

Gasteiger, E., Hoogland, C., Gattiker, A., Duvaud, S., Wilkins, M.R., Appel, R.D. and Bairoch, A.; Protein Identification and Analysis Tools on the ExPASy Server; (In) John M. Walker (ed): The Proteomics Protocols Handbook, Humana Press (2005) pp. 571-607.

Gelhaye, E., Rouhier, N., Laurent, P., Sautière, P.E., Martin, F. and Jacquot, J.P. (2002). Isolation and characterization of an extended thioredoxin h from poplar. *Physiol Plantarum* **114:** 165—171.

Gelhaye, E., Rouhier, N. and Jacquot, J.P. (2003). Evidence for a subgroup of thioredoxin h that requires GSH/Grx for its reduction. *FEBS Lett* **555**: 443—448.

Gelhaye, E., Rouhier, N. and Jacquot, J.P. (2004). The thioredoxin h system of higher plants. *Plant Physiol Biochem* **42:** 265—271.

Gelhaye, E., Rouhier, N., Navrot, N. and Jacquot, J. P. (2005). The plant thioredoxin system. *Cell Mol Life Sci* **62**: 24–35.

Gilbert, H.F. (1997). Protein disulfide isomerase and assisted protein folding. *J Biol Chem* **272:** 29399—29402.

Gomez-Cadenas, A., Zentella, R., Walker-Simmons, M.K. and Ho, T.H. (2001). Gibberellin/abscisic acid antagonism in barley aleurone cells: site of action of the protein kinase PKABA1 in relation to gibberellin signaling molecules. *Plant Cell* **13:** 667—679.

Gouet, P., Courcelle, E., Stuart, D. I. and Metoz, F. (1999). ESPript: analysis of multiple sequence alignments in PostScript. *Bioinformatics* **15:** 305—308.

Gubler, F., Chandler, P.M., White, R.G., Llewellyn, D.J. and Jacobsen J.V. (2002). Gibberellin signaling in barley aleurone cells. Control of SLN1 and GAMYB expression. *Plant Physiol* **129:** 191—200.

Guo, F.Q. and Crawford, N.M. (2005). *Arabidopsis* nitric oxide synthase1 is targeted to mitochondria and protects against oxidative damage and dark-induced senescence. *Plant Cell* **17:** 3436—3450.

Gustafsson, T.N., Sandalova, T., Lu, J., Holmgren, A. and Schneider, G. (2007). High-resolution structures of oxidized and reduced thioredoxin reductase from *Helicobacter pylori*. *Acta Crystallogr D* **63:** 833—843.

Hägglund, P., Kirkensgaard, K., Maeda, K., Finnie, C., Henriksen, A. and Svensson, B. (2009) Molecular Recognition in NADPH-Dependent Plant Thioredoxin Systems – Catalytic Mechanisms, Structural Snapshots and Target Identifications. Chapter 15 *in* Oxidative stress and redox regulation in plants. Jacquot, J.P. (Ed.) pp. 461—495. Advances in botanical research **52**, Burlington: Academic Press.

Hall, T.A. (1999). BioEdit: a user-friendly biological sequence alignment editor and analysis program for Windows 95/98/NT. *Nucl Acids S* **41:** 95—98.

Hara, S., Motohashi, K., Arisaka, F., Romano, P.G.N., Hosoya-Matsuda, N., Kikuchi, N., Fusada, N. and Hisabori, T. (2006). Thioredoxin-h1 reduces and reactivates the

oxidized cytosolic malate dehydrogenase dimer in higher plants. *J Biol Chem* **281:** 32065—32071.

Hatahet, F., Nguyen, V.D., Salo, K.E.H. and Ruddock, L.W. (2010). Disruption of reducing pathways is not essential for efficient disulfide bond formation in the cytoplasm of *E. coli*. *Microb Cell Fact* **9** (67): 67—75.

Hayward, S. and Lee, R.A. (2002). Improvements in the analysis of domain motions in proteins from conformational change: DynDom version 1.50. *J Mol Graph Model* **21:** 181—183.

Hernandez, H.H., Jaquez, O.A., Hamill, M.J., Elliott, S.J. and Drennan, C.L. (2008). Thioredoxin reductase from *Thermoplasma acidophilum*: a new twist on redox regulation. *Biochemistry* **47:** 9728—9737.

Ho, T.H.D., Gomez-Cadenas, A., Zentella, R. and Casaretto, J. (2003). Crosstalk between gibberellin and abscisic acid in cereal aleurone layer. *Plant Growth Regul* **22:** 185—194.

Holmgen, A. (1977). Bovine Thioredoxin System. Purification of Thioredoxin Reductase from calf liver and thymus and studies of its function in disulfide reduction. *J Biol Chem* **252** (13): 4600—4606.

Holmgren, A. (1989) Thioredoxin and glutaredoxin system. *J Biol Chem* **264:** 13963—-13966.

Holmgren, A. and Fernandes, A.P. (2004). Glutaredoxins: glutathione-dependent redox enzymes with functions far beyond a simple thioredoxin backup system. *Antioxid Redox Sign* **6** (1): 63—74.

Hwang, C., Sinskey, A.J. and Lodish, H.F. (1992). Oxidized redox state of glutathione in the endoplasmatic reticulum. *Science* **257** (5076): 1496—1502.

Ishiwatari, Y., Honda, C., Kawashima, I., Nakamura, S., Hirano, H., Mori, S., Fujiwara, T., Hayashi, H. and Chino, M. (1995). Thioredoxin h is one of the major proteins in rice phloem sap. *Planta* **195:** 456—463.

Ishiwatari, Y., Fujiwara, T., McFarland,K.C., Nemoto,K., Hayashi,H., Chino,M. and Lucas, W. J. (1998). Rice phloem thioredoxin h has the capacity to mediate its own cell-to-cell transport through plasmodesmata. *Planta* **205:** 12—22.

Jacquot, J.P., Rivera-Madrid, R., Marinho, P., Kollarova, M., Le Maréchal, P., Miginiac-Maslow, M. and Meyer Y. (1994) *Arabidopsis thaliana* NADPH thioredoxin reductase.

cDNA characterization and expression of the recombinant protein in *Escherichia coli*. *J Mol Biol* **235**: 1357—1363.

Jacquot, J.P., Lancelin, J.M. and Meyer, Y. (1997). Thioredoxins: structure and function in plant cells. *New phytol* **136:** 543—570.

Jeong, J. and Guerinot, M.L. (2009). Homing in on iron homeostasis in plants. *Trends Plant Sci* **14:** 280—285.

Jiao, J.A., Yee, B.C., Wong, J.H., Kobrehel, K. and Buchanan, B.B. (1993). Thioredoxin-linked changes in regulatory properties of barley alpha-amylase/subtilisin inhibitor protein. *Plant Physiol Bioch* **31**: 799—804.

Johansson, C., Lillig, C.H. and Holmgren, A. (2004). Human mitochondrial glutaredoxin reduces S-glutathionylated proteins with high affinity accepting electrons from either glutathione or thioredoxin reductase. *J Biol Chem* **279:** 7537—7543.

Joudrier, P., Gautier, M.F., de Lamotte, F. and Kobrehel, K. (2005). The thioredoxin h system: potential applications. *Biotechnol Adv* **23:** 81—85.

Juárez-Díaz, J.A., McClure, B., Vázquez-Santana, S., Guevara-García, A., León-Mejía, P., Márquez-Guzmán, J. and Cruz-García, F. (2006). A novel thioredoxin h is secreted in Nicotiana alata and reduces S-RNase in vitro. *J Biol Chem* **281:** 3418—3424.

Kadokura, H., Beckwith, J. and Gilbert, H.F. (2008). Oxidative Folding. In: Banerjee R, Becker D, Dickman M, Gladyshev V, Ragsdale S (Eds.) Redox Biochemistry. New Jersey, Wiley-Interscience, pp. 113—120

Kallis, G.B. and Holmgren, A. (1980). Differential reactivity of the functional sulfhydryl groups of cysteine-32 and cysteine-35 present Substrate Recognition Mechanism of Thioredoxin in the reduced form of thioredoxin from *Escherichia coli. J Biol Chem* **255:** 10261—10265.

Kanzok, S.M., Fechner, A., Bauer, H., Ulschmid, J.K., Muller, H.M., Botella-Munoz, J., Schneuwly, S., Schirmer, R. and Becker, K. (2001). Substitution of the thioredoxin system for glutathione reductase in Drosophila melanogaster. *Science* **291:** 643—646.

Kirkensgaard, K.G., Hägglund, P., Finnie, C., Svensson, B. and A. Henriksen (2009) Structure of Hordeum vulgare NADPH-dependent thioredoxin reductase 2. Unwinding the reaction mechanism. *Acta Crystallogr D* **65:** 932—941.

Knowles, R.G. and Moncada, S. (1994). Nitric oxide synthases in mammals. *Biochem J* **298**: 249—258.

Kobrehel, K., Yee, B.C. and Buchanan, B.B. (1991). Role of the NADP/thioredoxin system in the reduction of alpha-amylase and trypsin inhibitor proteins. *J Biol Chem* **266:** 16135—16140.

Kobrehel, K., Wong, J.H., Balogh, A., Kiss, F., Yee, B.C. and Buchanan, B.B. (1992). Specific reduction of wheat storage proteins by thioredoxin h. *Plant Physiol* **99:** 919—924.

Koh, C. S., Navrot, N., Didierjean, C., Rouhier, N., Hirasawa, M., Knaff, D. B., Wingsle, G., Samian, R., Jacquot, J.P., Corbier, C. and Gelhaye, E. (2008). An atypical catalytic mechanism involving three cysteines of thioredoxin. *J Biol Chem* **283:** 23062—23072.

Krause, G. and Holmgren, A. (1991). Substitution of the conserved tryptophan 31 in Escherichia coli thioredoxin by site-directed mutagenesis and structure–function analysis. *J Biol Chem* **266:** 4056—4066.

Krimm, I., Lemaire, S., Ruelland, E., Miginiac-Maslow, M., Jacquot, J.P., Hirasawa, M., Knaff, D. B. and Lancelin, J. M. (1998). The single mutation Trp35–>Ala in the 35–40 redox site of Chlamydomonas reinhardtii thioredoxin h affects its biochemical activity and the pH dependence of C36–C39 1H–13C NMR. *Eur J Biochem* **255:** 185—195.

Krissinel, E. and Henrick, K. (2004). Secondary-structure matching (SSM), a new tool for fast protein structure alignment in three dimensions *Acta Crystallogr D* **60:** 2256—2268.

Kruger, N.J. and von Schaewen, A. (2003). The oxidative pentose phosphate pathway: structure and organisation. *Curr Opin Plant Biol* **6** (3): 236—46

Kuriyan, J., Krishna, T. S., Wong, L., Guenther, B., Pahler, A., Williams, C. H.Jr. and Model, P. (1991). Convergent evolution of similar function in two structurally divergent enzymes. *Nature* **352:** 172—174.

Laloi, C., Rayapuram, N., Chartier, Y., Grienenberger, J.M., Bonnard, G. and Meyer, Y. (2001). Identification and characterization of a mitochondrial thioredoxin system in plants. *P Natl Acad Sci USA* **98:** 14144—14149.

Laloi, C., Mestres-Ortega, D., Marco, Y., Meyer, Y. and Reichheld J.P. (2004). The *Arabidopsis* cytosolic thioredoxin *h*5 gene induction by oxidative stress and its W-box-mediated response to pathogen elicitor. *Plant Physiol* **134:** 1006—1016.

Laurent, T.C., Moore, E.C. and Reichard, P. (1964). Enzymatic synthesis of deoxyribonucleotides. IV. Isolation and characterization of thioredoxin, the hydrogen donor from *Escherichia coli* B. *J Biol Chem* **239:** 3436—3444.

Lee, S.R., Bar-Noy, S., Kwon, J., Levine, R.L., Stadtman, T.C. and Rhee, S.G. (2000). Mammalian thioredoxin reductase: Oxidation of the C-terminal cysteineyselenocysteine active site forms a thioselenide, and replacement of selenium with sulfur markedly reduces catalytic activity. *P Natl Acad Sci USA* **97** (6): 2521—2526.

Lennon, B. W. and Williams, C.H.Jr. (1997). Reductive half-reaction of thioredoxin reductase from *Escherichia coli*. *Biochemistry* **36**: 9464—9477.

Lennon, B.W., Williams, C.H.Jr. and Ludwig, M.L. (1999). Crystal structure of reduced thioredoxin reductase from *Escherichia coli*: structural flexibility in the isoalloxazine ring of the flavin adenine dinucleotide cofactor. *Protein Sci* **8:** 2366—2379.

Lennon, B.W., Williams Jr., C.H. and Ludwig, M.L. (2000) Twists in catalysis: alternating conformations of Escherichia coli thioredoxin reductase. *Science* **289:** 1190—1194.

Leslie, A. G. W. (1992). Jnt CCP4/ESF–EACBM. *Newsl Protein Crystallogr* **26**.

Li Y, Hu Y, Zhang X, Xu H, Lescop E, Xia B, and Jin C. (2007). Conformational fluctuations coupled to the thiol-disulfide transfer between thioredoxin and arsenate reductase in *Bacillus subtilis*. *J Biol Chem* **282** (15): 11078—11083.

Li, Y.C., Ren, J.P., Cho, M.J., Zhou, S.M., Kim, Y.B., Guo, H.X., Wong, J.H., Niu, H.B., Kim, H.K., Morigasaki, S., Lemaux, P.G., Frick, O.L., Yin, J. and Buchanan, B.B. (2009). The level of expression of thioredoxin is linked to fundamental properties and applications of wheat seeds. *Mol Plant* **2** (3): 430—441.

Lillig, C.H., Berndt, C., Vergnolle, O., Lönn, M.E., Hudemann, C., Bill, E. and Holmgren, A. (2005). Characterization of human glutaredoxin 2 as iron-sulfur protein: A possible role as redox sensor. *P Natl Acad Sci USA* **102** (23): 8168—8173.

Lund, M.N., Lametsch, R., Hviid, M.S., Jensen, O.N. and Skibsted L.H. (2007). High-oxygen packaging atmosphere influences protein oxidation and tenderness of porcine longissimus dorsi during chill storage. *Meat Sci* **77**: 295—303.

Ma, X.X., Guo, P.C., Shi, W.W., Luo, M., Tan, X.F., Chen, Y. and Zhou, C.Z. (2011). Structural plasticity of the thioredoxin recognition site of yeast methionine-S-sulfoxide reductase Mxr1, *J Biol Chem.* In press.

Maeda, K., Finnie, C., Østergaard, O. and Svensson, B. (2003). Identification, cloning and characterization of two thioredoxin h isoforms, HvTrxh1 and HvTrxh2, from the barley seed proteome. *Eur J Biochem* **270:** 2633—2643.

Maeda, K., Hagglund, P., Finnie, C., Svensson, B. and Henriksen, A. (2006a). Structural basis for target protein recognition by the protein disulfide reductase thioredoxin. *Structure* **14:** 1701—1710.

Maeda, K., Hagglund, P., Finnie, C. and Svensson, B. (2006b). Proteomics of disulfide and cysteine oxidoreduction. In: Finnie C (Ed.) Plant Proteomics, Annu Plant Rev, vol. 28.Oxford, Blackwell. pp. 71—97.

Maeda, K., Hagglund, P., Finnie, C., Svensson, B. and Henriksen, A. (2008). Crystal Structures of Barley Thioredoxin H Isoforms Hvtrxh1 and Hvtrxh2 Reveal Features Involved in Protein Recognition and Possibly in Discriminating the Isoform Specificity. *Protein Sci* **17:** 1015—1024.

Manstein, D. J., Massey, V., Ghisla, S. and Pai, E.F. (1988). Stereochemistry and accessibility of prosthetic groups in flavoproteins. *Biochemistry* **27:** 2300—2305.

Martin, J.L. (1995). Thioredoxin—a fold for all reasons. *Structure* **3:** 245—250.

Matthews, B. W. (1968). Solvent content of protein crystals. *J Mol Biol* **33:** 491—497.

Menchise, V., Corbier, C., Didierjean, C., Saviano, M., Benedetti, E., Jacquot, J.P. and Aubry, A. (2001). Crystal structure of the wild-type and D30A mutant thioredoxin h of Chlamydomonas reinhardtii and implications for the catalytic mechanism. *Biochem J* **359:** 65—75.

Meng, L., Wong, J., Feldman, L., Lemaux, P. and Buchanan, B. (2010). A membrane-associated thioredoxin required for plant growth moves from cell to cell, suggestive of a role in intercellular communication. *P Natl Acad Sci USA* **107** (8): 3900—3905.

Menges M., Hennig L., Gruissem W. and Murray J.A. (2002). Cell cycle-regulated gene expression in *Arabidopsis*. *J Biol Chem* **277:** 41987—42002.

McCord, J.M. and Fridovich, I. (1988). Superoxide dismutase: the first twenty years (1968-1988). *Free Radical Biol Med* **5** (5-6)**:** 363—369.

McDonald, I.K. and Thornton, J.M. (1994). Satisfying hydrogen bonding potential in proteins. *J Mol Biol* **238:** 777—793.

Meyer, Y., Vignols, F. and Reichheld, J.P. (2002). Classification of plant thioredoxins by sequence similarity and intron position. *Method Enzymol* **347:** 394—402.

Meyer, Y., Reichheld, J.P. and Vignols, F. (2005). Thioredoxins in *Arabidopsis* and other plants. *Photosynth Res* **86**: 419—433.

Meyer, Y., Siala, W., Bashandy, T., Riondet, C., Vignols, F. and Reichheld, J.P (2008). Glutaredoxins and thioredoxins in plants. *Biochim Biophys Acta* **1783:** 589—600.

Miranda-Vizuete, A., Damdimopoulos, A.E., Gustafsson, J. and Spyrou, G. (1997). Cloning, expression, and characterization of a novel *Escherichia coli* thioredoxin. *J Biol Chem* **272**: 30841–30847.

Moore, E.C., Reichard, P. and Thelander, L. (1964). Enzymatic synthesis of deoxyribonucleotides. V. Purification and properties of thioredoxin reductase from *Escherichia coli* B. *J Biol Chem* **239:** 3445—3452.

Moskovitz, J., Bar-Noy, S., Williams, W.M., Requena, J., Berlett, B.S. and Stadtman, E.R. (2001). Methionine sulfoxide reductase (MsrA) is a regulator of antioxidant defense and lifespan in mammals. *P Natl Acad Sci USA* **98** (23): 12920–12925.

Mouaheb, N., Thomas, D., Verdoucq, L., Monfort, P. and Meyer, Y. (1998). In vivo functional discrimination between plant thioredoxins by heterologous expression in the yeast Saccharomyces cerevisiae. *P Natl Acad Sci USA* **95:** 3312—3317.

Muller, E.G.D. (1996). A glutathione reductase mutant of yeast accumulates high levels of oxidized glutathione and requires thioredoxin for growth. *Mol Biol Cell* **7:** 1805—1813.

Mulrooney, S.B. and Williams, C.H. (1994). Potential Active-Site Base of Thioredoxin reductase from Escherichia coli: Examination of Histidine245 and Aspartate139 by Site-Directed Mutagenesis. *Biochemistry* **33** (11): 3148—3154.

Murshudov, G.N., Vagin, A.A. and Dodson, E.J. (1997). Refinement of macromolecular structures by the maximum-likelihood method. *Acta Crystallogr D* **53:** 240—255.

Mustacich, D. and Powis, G. (2000). Thioredoxin reductase. *Biochem J* **346:** 1—8.

Møller, I.M. (2001). Plant mitochondria and oxidative stress: electron transport, NADPH turnover, and metabolism of reactive oxygen species. *Annu Rev Plant Phys* **52:** 561—591.

Nakajima, M., Shimada, A., Takashi, Y., Kim, Y.C., Park, S.H., Ueguchi-Tanaka, M., Suzuki, H., Katoh, E., Iuchi, S., Kobayashi, M., Maeda, T., Matsuoka, M. and Yamaguchi, I. (2006). Identification and characterization of Arabidopsis gibberellin receptors. *Plant J* **46:** 880—889.

Negri, A., Rodríguez-Larrea, D., Marco, E., Jiménez-Ruiz, A., Sánchez-Ruiz, J.M. and Gago, F. (2010), Protein–protein interactions at an enzyme–substrate interface: Characterization of transient reaction intermediates throughout a full catalytic cycle of *Escherichia coli* thioredoxin reductase. *Proteins* **78:** 36—51.

Nordberg, J. and Arnér, E. (2001). Reactive oxygen species, antioxidants, and the mammalian thioredoxin system. *Free Radical Bio Med* **31** (11): 1287—1312.

Obiero, J., Pittet, V., Bonderoff, S.A., and Sanders, D.A. (2010). Thioredoxin system from *Deinococcus radiodurans*. *J Bacteriol* **192**: 494—501.

Oliveira, M. A., Discola, K.F., Alves, S.V., Medrano, F.J., Guimarães, B.G. and Netto, L.E.S. (2010). Insights into the Specificity of Thioredoxin Reductase-Thioredoxin Interactions. A Structural and Functional Investigation of the Yeast Thioredoxin System, *Biochemistry* **49:** 3317—3326.

Osipiuk, J., Zhou, M., Kwon, K., Anderson, W.F. and Joachimiak, A. Thioredoxin-disulfide reductase from *Campylobacter jejuni*. Pdb accession 3r9u, unpublished.

Pai, E.F. (1991). Variations on a theme: the family of FAD-dependent NAD(P)H-(disulfide)-oxidoreductases. *Curr Opin Struc Biol* **1:** 796—803.

Painter, J. and Merritt, E.A. (2006). Optimal description of a protein structure in terms of multiple groups undergoing TLS motion. *Acta Crystallogr D* **62:** 439—450.

Pastore, A. Piemonte, F., Locatelli, M., Russo, A.L., Gaeta, L. M., Tozzi, G. and Federici, G. (2003). Determination of blood total, reduced, and oxidized glutathione in pediatric subjects. *Clin Chem* **47** (8): 1467—1469.

Peterson, F.C., Lytle, B.L., Sampath, S., Vinarov, D., Tyler, E., Shahan, M., Markley, J.L. and Volkman, B.F. (2005). Solution structure of thioredoxin h1 from *Arabidopsis thaliana*. *Protein Sci* **14**: 2195—2200.

Prinz, W.A., Åslund, F., Holmgren, A. and Beckwith, J. (1997). The role of the thioredoxin and glutaredoxin pathways in reducing protein disulfide bonds in the *Escherichia coli* cytoplasm. *J Biol Chem* **272:** 15661—15667.

Pulido, P., Cazalis, R. and Cejudo, F.J. (2009). An antioxidant redox system in the nucleus of wheat seed cells suffering oxidative stress. *Plant J* **57:** 132—145.

Raina, S. and Missiakas, D. (1997). Making and breaking disulfide bonds. *Annu Rev Microbiol* **51:** 179—202.

Raven, P.H., Evert, R.F., and Eichhorn, S.E. (2005). Biology of Plants, 7th Edition. New York: W.H. Freeman and Company Publishers. pp. 504—508.

Reichheld, J.P., Mestres-Ortega, D., Laloi, C. and Meyer, Y. (2002). The multigenic family of thioredoxin h in *Arabidopsis thaliana*: Specific expression and stress response. *Plant Physiol Bioch* **40:** 685—690.

Reichheld, J. P., Meyer, E., Khafif, M., Bonnard, G. and Meyer, Y. (2005). AtNTRB is the major mitochondrial thioredoxin reductase in *Arabidopsis thaliana*. *FEBS Lett* **579:** 337—342.

Reichheld, J.P., Khafif, M., Riondet, C., Droux, M., Bonnard, G. and Meyer, Y. (2007). Inactivation of thioredoxin reductases reveals a complex interplay between thioredoxin and glutathione pathways in *Arabidopsis* development. *Plant Cell* **19:** 1851—1865.

Ritchie, S., Swanson, S.J. and Gilory, S. (2000). Physiology of the aleurone layer and starchy endosperm during grain development and early seedling growth: new insights from cell and molecular biology. *Seed Sci Res* **10:** 193—212.

Ruggiero, A., Masullo, M., Ruocco, M.R., Grimaldi, P., Lanzotti, M.A., Arcari, P., Zagari, A. and Vitagliano, L. (2009). Structure and stability of a thioredoxin reductase from *Sulfolobus solfataricus*: A thermostable protein with two functions. *Biochim Biophys Acta* **1794:** 554—562.

Risler, J.L., Delorme, M.O., Delacroix, H. and Henaut, A. (1988). Amino acid substitutions in structurally related proteins. A pattern recognition approach. Determination of a new and efficient scoring matrix. *J Mol Biol* **204:** 1019—1029.

Rivera-Madrid, R., Mestres, D., Marinho, P., Jacquot, J.P., Decottignies, P., Miginiac-Maslow, M. and Meyer, Y. (1995). Evidences for five divergent thioredoxin h sequences in *Arabidopsis thaliana*. *P Natl Acad Sci USA* **92:** 5620—5624.

Rouhier, N., Lemaire, S.D. and Jacquot, J.P. (2008). The role of glutathione in photosynthetic organisms: emerging functions for glutaredoxins and glutathionylation. *Annu Rev Plant Biol* **59:** 143—66.

Ruelland, E. and Miginiac-Maslow, M. (1999). Regulation of chloroplast enzyme activities by thioredoxins: activation or relief from inhibition? *Trends Plant Sci* **4:** 136—141.

Russel, M. and Model, P. (1986). The role of thioredoxin in filamentous phage assembly. Construction, isolation, and characterization of mutant thioredoxins. *J Biol Chem* **261:** 14997—15005.

Sagi, M. and Fluhr, R. (2001). Superoxide production by plant homologues of the gp91(phox) NADPH oxidase. Modulation of activity by calcium and by tobacco mosaic virus infection. *Plant Physiol* **126:** 1281—1290.

Sandalova, T., Zhong, L., Lindqvist, Y., Holmgren, A. and Schneider, G. (2001). Three-dimensional structure of a mammalian thioredoxin reductase: implications for mechanism and evolution of a selenocysteine-dependent enzyme. *P Natl Acad Sci USA* **98:** 9533—9538.

Sanders, D., Obiero, J. and van Straaten, K. Crystal structure of *Helicobacter pylori* thioredoxin reductase. Pdb accession 3ish, unpublished.

Sanner, M., Olson, A.J. and Spehner, J.C. (1996). Reduced Surface: an efficient way to compute molecular surfaces. *Biopolymers* **38:** 305—320.

Santandrea, G., Guo, Y., O'Connell, T. and Thompson, R. D. (2002). Post-phloem protein trafficking in the maize caryopsis: zmTRXh1, a thioredoxin specifically expressed in the pedicel parenchyma of Zea mays L., is found predominantly in the placentochalaza. *Plant Mol Biol* **50:** 743—756.

Schürmann, P. and Jacquot, J.P. (2000). Plant thioredoxin system revisted. *Annu Rev Plant Phys* **51:** 371—400.

Serrato, A. J., Pérez-Ruiz, J.M. and Cejudo, F.J. (2002). Cloning of thioredoxin h reductase and characterization of the thioredoxin reductase-thioredoxin h system from wheat. *Biochem J* **367:** 491—497.

Serrato, A.J., Perez-Ruiz, J.M., Spinola, M.C. and Cejudo, F.J. (2004). A novel NADPH thioredoxin reductase, localized in the chloroplast, which deficiency causes hypersensitivity to abiotic stress in *Arabidopsis thaliana*. *J Biol Chem* **279:** 43821—43827.

Shahpiri, A., Svensson, B. and C. Finnie (2008a). The NADPH-Dependent Thioredoxin Reductase/Thioredoxin System in Germinating Barley Seeds: Gene Expression, Protein

Profiles, and Interactions between Isoforms of Thioredoxin h and Thioredoxin Reductase. *Plant Physiol* **146:** 789—799.

Shahpiri, A. (2008b). Hormone-dependence of gene and protein expression in barley aleurone layer & Characterization of NADPH-dependent thioredoxin reductase/thioredoxin system in barley seeds, PhD thesis, Enzyme and Protein Chemistry, Department of Systems Biology-DTU, Technical University of Denmark.

Shahpiri, A., Svensson, B., and Finnie, C. (2009). From Proteomics to Structural Studies of Cytosolic/Mitochondrial-Type Thioredoxin Systems in Barley Seeds. *Mor Plant* **2**(3): 378—389.

Shi, J. and Bhattacharyya, M. K. (1996). A novel plasma membrane-bound thioredoxin from soybean. *Plant Mol Biol* **32:** 653—662.

Shin, M. (2004). How is ferredoxin-NADP reductase involved in the NADP photoreduction of chloroplasts? *Photosynth Res* **80:** 307—313.

Stehr, M., Schneider, G., Aslund, F., Holmgren, A. and Lindqvist, Y. (2001). Structural Basis for the Thioredoxin-like Activity Profile of the Glutaredoxin-like NrdH-redoxin from *Escherichia coli. J Biol Chem* **276** (38): 35836–35841.

Sun, Q.A., Kirnarsky, L., Sherman, S. and Gladyshev, V.N. (2001). Selenoprotein oxidoreductase with specificity for thioredoxin and glutathione systems. *P Natl Acad Sci USA* **98:** 3673—3678.

Sweat, T.A. and Wolpert, T.J. (2007). Thioredoxin H5 is required for victorin sensitivity mediated by CCNBS-LRR gene in *Arabidopsis*. *Plant Cell* **19:** 673—687.

Sweetlove, L.J. and Møller, I.M. (2009). Oxidation of proteins in plants – mechanisms and consequences. Chapter 1 *in* Oxidative stress and redox regulation in plants. Jacquot, J.P. (Ed.) pp. 1—23. Advances in botanical research **52**, Burlington: Academic Press.

Szabó, C., Ischiropoulos, H. and Radi, R. (2007). Peroxynitrite: biochemistry, pathophysiology and development of therapeutics. *Nat Rev Drug Discov* **6:** 662—680.

Thompson, J.D., Higgins, D.G. and Gibson, T.J. (1994). CLUSTAL W: improving the sensitivity of progressive multiple sequence alignment through sequence weighting, position-specific gap penalties and weight matrix choice. *Nucleic Acids Res* **22:** 4673—4680.

Timbo, B., Koehler, K.M., Wolyniak, C. and Klontz, K.C. (2004). Sulfites - a food and drug administration review of recalls and reported adverse events. *J Food Protect* **67**, 1806—1811.

Trevaskis, B., Hemming, M.N., Peacock, W.J. and Dennis, E.S. (2006). HvVRN2 responds to daylength, whereas HvVRN1 is regulated by vernalization and developmental status. *Plant Physiol* **140:** 1397—1405.

Tripathi, B.N., Bhatt, I. and Dietz, K.J. (2009). Peroxiredoxins: a less studied component of hydrogen peroxide detoxification in photosynthetic organisms. *Protoplasma* **235:** 3—15.

Ueguchi-Tanaka, M., Ashikari, M., Nakajima, M., Itoh, H., Katoh, E., Kobayashi, M., Chow, T.Y., Hsing, Y.I., Kitano, H., Yamaguchi, I. and Matsuoka, M. (2005). GIBBERELLININ SENSITIVE DWARF1 encodes a soluble receptor for gibberellin. *Nature* **437:** 693—698.

Ueguchi-Tanaka, M., Nakajima, M., Motoyuki, A. and Matsuoka, M. (2007) Gibberellin receptor and its role in gibberellin signaling in plants. *Annu Rev Plant Biol* **58:** 183-198.

Vagin, A. and Teplyakov, A. (2000). An approach to multi-copy search in molecular replacement. *Acta Crystallogr D* **56:** 1622—1624.

Veine, D.M., Mulrooney, S.B., Wang, P.F. and Williams, C.H.Jr. (1998a). Formation and properties of mixed disulfides between thioredoxin reductase from *Escherichia coli* and thioredoxin: Evidence that cysteine-138 functions to initiate dithiol-disulfide interchange and to accept the reducing equivalent from reduced flavin. *Protein Sci* **7** (44): 71441—71450.

Veine, D.M., Ohnishi, K. and Williams, C.H.Jr. (1998b). Thioredoxin reductase from *Escherichia coli*: Evidence of restriction to a single conformation upon formation of a crosslink between engineered cysteines. *Protein Sci* **7** (2): 369—375.

Verdoucq, L., Vignols, F., Jacquot, J.P., Chartier, Y. and Meyer, Y. (1999). In vivo characterization of a thioredoxin h target protein defines a new peroxiredoxin family. *J Biol Chem* **274:** 19714—19722.

Waksman, G., Krishna, T.S., Williams, C.H.Jr. and Kuriyan, J. (1994). Crystal structure of *Escherichia coli* thioredoxin reductase refined at 2 Å resolution. Implications for a large conformational change during catalysis. *J Mol Biol* **236:** 800—816.

Wallace, A.C., Laskowski, R.A. and Thornton, J.M. (1995). LIGPLOT: A program to generate schematic diagrams of protein-ligand interactions. *Protein Eng* **8:** 127—134.

Wanders, R.J.A. and Waterham, H.R. (2006). Peroxisomal disorders: The single peroxisomal enzyme deficiencies. *Biochim Biophys Acta* **1763**: 1707—1720.

Wang, P.F., Veine, D.M., Ahn, S.H. and Williams, C.H.Jr. (1996). A Stable Mixed Disulfide between Thioredoxin Reductase and Its Substrate, Thioredoxin: Preparation and Characterization. *Biochemistry* **35:** 4812—4819.

Wang, P.F., Arscott, L.D., Gilberger, T.W., Müller, S. and Williams, C.H.Jr. (1999). Thioredoxin reductase from *Plasmodium falciparum*: evidence for interaction between the C-terminal cysteine residues and the active site disulfide-dithiol. *Biochemistry* **38:** 3187—3196.

Wieles, B., van Noort, J., Drijfhout, J.W., Offringa, R., Holmgren, A. and Ottenhoff, T.H. (1995). Purification and functional analysis of the *Mycobacterium leprae* thioredoxin/thioredoxin reductase hybrid protein. *J Biol Chem* **270:** 25604—25606.

Williams, C.H.Jr, Zanetti, G., Arscott, L.D. and McAllister, J.K. (1967). Lipoamide dehydrogenase, glutathione reductase, thioredoxin reductase, and thioredoxin. *J Biol Chem* **242**(22): 5226—5231.

Williams, C.H.Jr. (1976). Flavin containing dehydrogenases, Vol. 13, The Enzymes, edited by P. D. Boyer, pp. 89–173. New York: Academic Press.

Williams, C.H., Arscott, L.D., Muller, S., Lennon, B.W., Ludwig, M.L., Wang, P.F., Veine, D.M., Becker, K. and Schirmer, R.H. (2000). Thioredoxin reductase two modes of catalysis have evolved. *Eur J Biochem* **267:** 6110—6117.

Wong, J.H., Kobrehel, K., Nimbona, C., Yee, B.C., Balogh, A., Kiss, F. and Buchanan, B.B. (1993). Thioredoxin and bread wheat. *Cereal Chem* **70:** 113—114.

Wong, J.H., Kim, Y.B., Ren, P.H., Cai, N., Cho, M.J., Hedden, P., Lemaux, P.G. and Buchanan, B.B. (2002). Transgenic barley grain overexpressing thioredoxin shows evidence that the starchy endosperm communicates with the embryo and the aleurone. *P Natl Acad Sci USA* **99:** 16325—16330.

Wong, J.H., Cai, N., Tanaka, C.K., Vensel, W.H., Hurkman, W.J. and Buchanan, B.B. (2004). Thioredoxin reduction alters the solubility of proteins of wheat starchy endosperm: an early event in cereal germination. *Plant Cell Physiol* **45**: 407–415.

Wood, Z.A., Poole, L.B. and Karplus, P.A. (2003). Peroxiredoxin Evolution and the Regulation of Hydrogen Peroxide Signaling. *Science* **25:** 650—653.

Word, J.M., Lovell, S.C., Richardson, J.S. and Richardson, D.C. (1999). Asparagine and Glutamine: Using hydrogen atom contacts in the choice of side-chain amide orientation. *J Mol Biol* **285:** 1735—1747.

Wulff, R.P., Lundqvist, J., Rutsdottir, G., Hansson, A., Stenbaek, A., Elmlund, D., Elmlund, H., Jensen, P.E. and Hansson M. (2011). The activity of barley NADPH-dependent thioredoxin reductase C is independent of the oligomeric state of the protein: tetrameric structure determined by cryo-electron microscopy. *Biochemistry* **50** (18): 3713—3723.

Zhang, Z., Bao, R., Zhang, Y., Yu, J., Zhou, C. Z. and Chen, Y. (2009). Crystal structure of *Saccharomyces cerevisiae* cytoplasmic thioredoxin reductase Trr1 reveals the structural basis for species-specific recognition of thioredoxin. *Biochim Biophys Acta* **1794**: 124—128.

Ziegler, D.M. (1985). Role of reversible oxidation-reduction of enzyme thiols-disulfides in metabolic regulation. *Annu Rev Biochem* **54:** 305—329.

Appendix A

Expression of Trx and NTR in barley seeds

A.1 Introduction

The results of this appendix are obtained during a five month period of the PhD spend at Commonwealth Scientific and Industrial Research Organisation (CSIRO) in the department of Plant Industry in Canberra, Australia. Part of this period was not financed by the PhD scholarship from DTU but instead supported by scholarships from the Oticon Foundation and Otto Mønsted Foundation. Furthermore, the objectives of this part of the thesis falls into another area than the rest of the thesis, which is why it was chosen to place the results in this appendix.

Dr. Peter Chandler from CSIRO has a selection of mutant barley seeds, mutated in the gene *gse1* which is thought to encode a GA-receptor (Chandler *et al*., 2008). Notably, it has been observed that GID1, the ortholog of GSE1 (see Chapter 1, Section 1.3.1), in rice predominantly occurred in the nucleus which suggests that intracellular GA may be responsible for initiating GA signalling. Rice *gid1* mutants were dwarfs and had phenotypes indicating that the GID1 GA receptor was essential for two well characterised GA responses; leaf sheath growth, and α-amylase production by aleurone tissue (Ueguchi-Tanaka *et al.*, 2005). Furthermore, yeast two-hybrid experiments indicated a GA-dependent interaction between GID1 and SLR1, which is an ortholog of SLN1 (Nakajima *et al.*, 2006). Chandler *et al.* (2008) had shown that *gse1* mutant barley half-grains (seeds without embryo) had a lower production of α-amylase upon addition of exogenous GA (Figure A1).

To examine whether the expression of NTR and Trx from barley aleurone layers is also controlled through this GA-receptor, experiments were planned in which aleurone layers of both wild-type (*Hordeum vulgare* cv. Himalaya) and mutants were to be compared. The mutant *gse1l* was chosen since it exhibits the lowest response to GA (Figure A1). All the other mutants have amino acid substitutions in the putative GA receptor, whereas this

mutant has a substitution (G to A) in the 5' untranslated region, which was predicted to destabilise a hairpin structure. This may impair translation initiation at the AUG codon, resulting in a decrease in the amounts of the synthesised protein (Chandler *et al*., 2008).

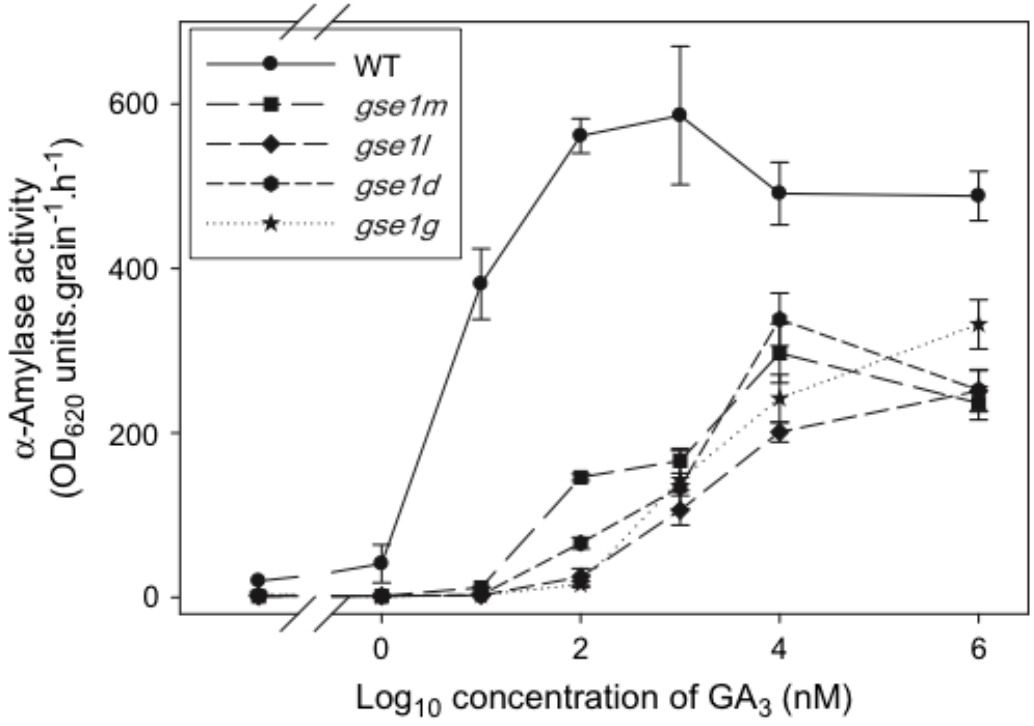

Figure A1. Production of α-amylase in half-grains of barley (Himalaya) wild-type and four mutants of *gse1* after 3 d incubation in various concentrations of exogenous GA (GA_3). Figure from Chandler *et al*., 2008.

Dr. Frank Gublers group at CSIRO studies the molecular mechanisms that control dormancy as well as the onset, maintenance, and release from dormancy during after-ripening in barley seeds. They had obtained micro-array data from root and coleorhiza from both dormant and after-ripened barley wild-type seeds (cv. Betzes). Coleorhiza is a sheat-like structure that acts as a protective covering enclosing the plumule (growing point of embryo) and radicle (from which the root is developed). These data were also examined for the expression of NTR and Trx, to determine whether dormancy has an effect on their expression in root and coleorhiza. Furthermore, cDNA was available for whole barley embryos (cv. Betzes), which were either dormant or after-ripened and grown in either light or darkness. These were also subjected to examinations of mRNA levels of NTR and Trx.

A.2 Results and discussion

A.2.1. Expression levels of NTR and Trx-h in aleurone layers of wild-type and mutant barley seeds

The mutant seed (*gse1l*, see above) appeared smaller than the wild-type Himalaya seeds (Figure A2). Thus the average weight was 51 mg/grain for the wt and 31 mg/grain for the mutant grain, corresponding to 61% of the wt weight.

Figure A2. Barley half-grains. Grains of the mutant *gse1l* had an average weight of 61% of the weight of wild-type (Himalaya) grains. The half-grains have been imbibed for 3 d. Both sides of the half-grains are shown.

For each experiment half-grains were produced of both the mutant and wild-type (Section A.4.1), which were imbibed for three d. Hereafter, the aleurone layers were stripped from the starchy endosperm and incubated in various concentrations of GA_3 with three biological replica of each condition. From extracted mRNA (Section A.4.2 and A.4.3) cDNA was produced (Section A.4.4). Expression levels of HvNTR1, HvNTR2, HvTrxh1 and HvTrxh2 was estimated by quantitative real-time PCR (Q-PCR) using designed primers. The

expression levels of the high pI α-amylase AMY 6-4 was used as a positive control for GA induced expression, and primers against HvActin was used as an internal control to normalise gene expression (see Section A.4.5 and A.4.6).

For the control α-amylase, there is a very clear response to GA in the wild-type aleurone layers (Figure A3). Thus, for the lowest concentration of GA (10 nM) the relative expression increases from 3 to about 500 over 24 h, while the number increases from 3 to 6 in samples without GA. The response is dose-dependent so the levels after 24 h are around 900 for 100 nM GA and around 1200 for 5 µM GA. The mutant (*gse1l*) clearly exhibits a significantly lower response to GA, especially at the lower concentrations, and the relative expression levels after 24 h increase from 0.2 to around 40 (10 nM GA), 90 (100 nM GA) and 660 (5 µM GA).

For HvNTR1 (Figure A4) there seems to be a slight down-regulation of the expression level without GA treatment, and this decrease is more obvious upon addition of GA. However, this response does not seem to be dose-dependant and is apparently not dependent on this GA-receptor (GSE1), since the response was also observed for the mutant. For HvNTR2 (Figure A5) the response is less unclear. For the untreated wild-type aleurone layers there is a slight increase after 6 h followed by a decrease. Upon GA treatment the level stays fairly constant but is significantly higher than for untreated samples after 24 h. This is especially observed for the highest GA concentrations. For the mutant a slightly higher expression is also observed after 24 h upon GA treatment, but this is not as significant as for the wild-type. From these results is seems like there is a slight dose-dependence in the expression of HvNTR2 and it also seems as the mutant has lower responses than the wild-type but the results are not significant enough to conclude whether the GSE1 receptor is involved. However, it can be concluded that there is a clear difference in the expression levels of HvNTR1, which is down-regulated by GA, and HvNTR2, which is apparently up-regulated by GA. Thus, after 24 h the levels of HvNTR2 in the GA treated wild-type aleurone layers are 38, 19 and 13 times higher than for HvNTR1 for the three concentrations of GA, respectively.

HvTrxh1 (Figure A6) has very similar expression levels as HvTrxh2 (Figure A7), which are significantly higher than for the NTRs (note the difference in values on the y-axis for the NTRs and Trxs). The levels for HvTrxh1 and HTrxh2 are fairly constant and seem unaffected

by both GA treatment and the mutation. Thus, the levels of the Trxs are constant, whereas the NTRs seem to be regulated by GA.

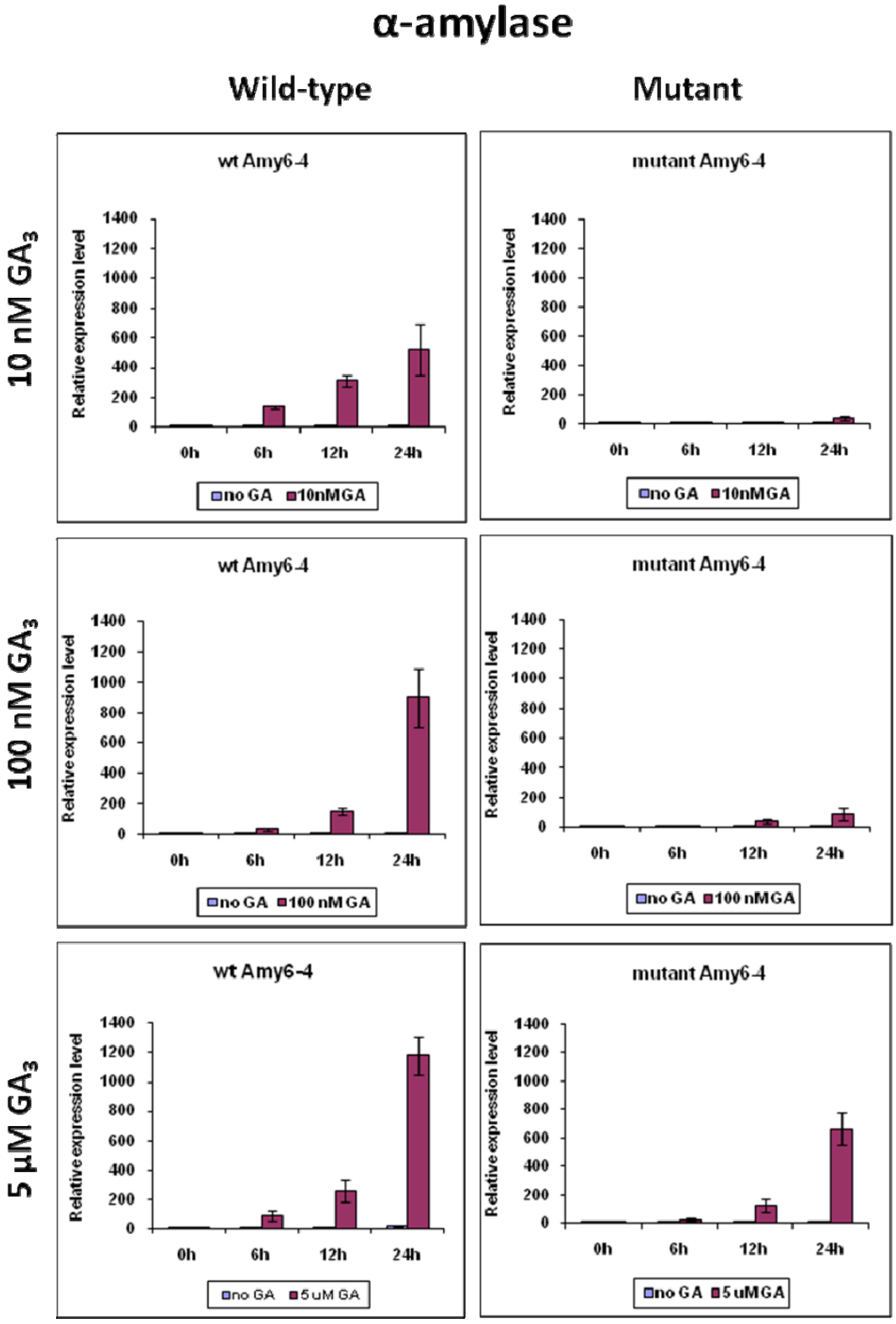

Figure A3. Relative expression of **α-amylase (AMY6-4)** in wild-type and mutant (*gse1l*) barley aleurone layers in varying concentrations of gibberellic acid (GA_3).

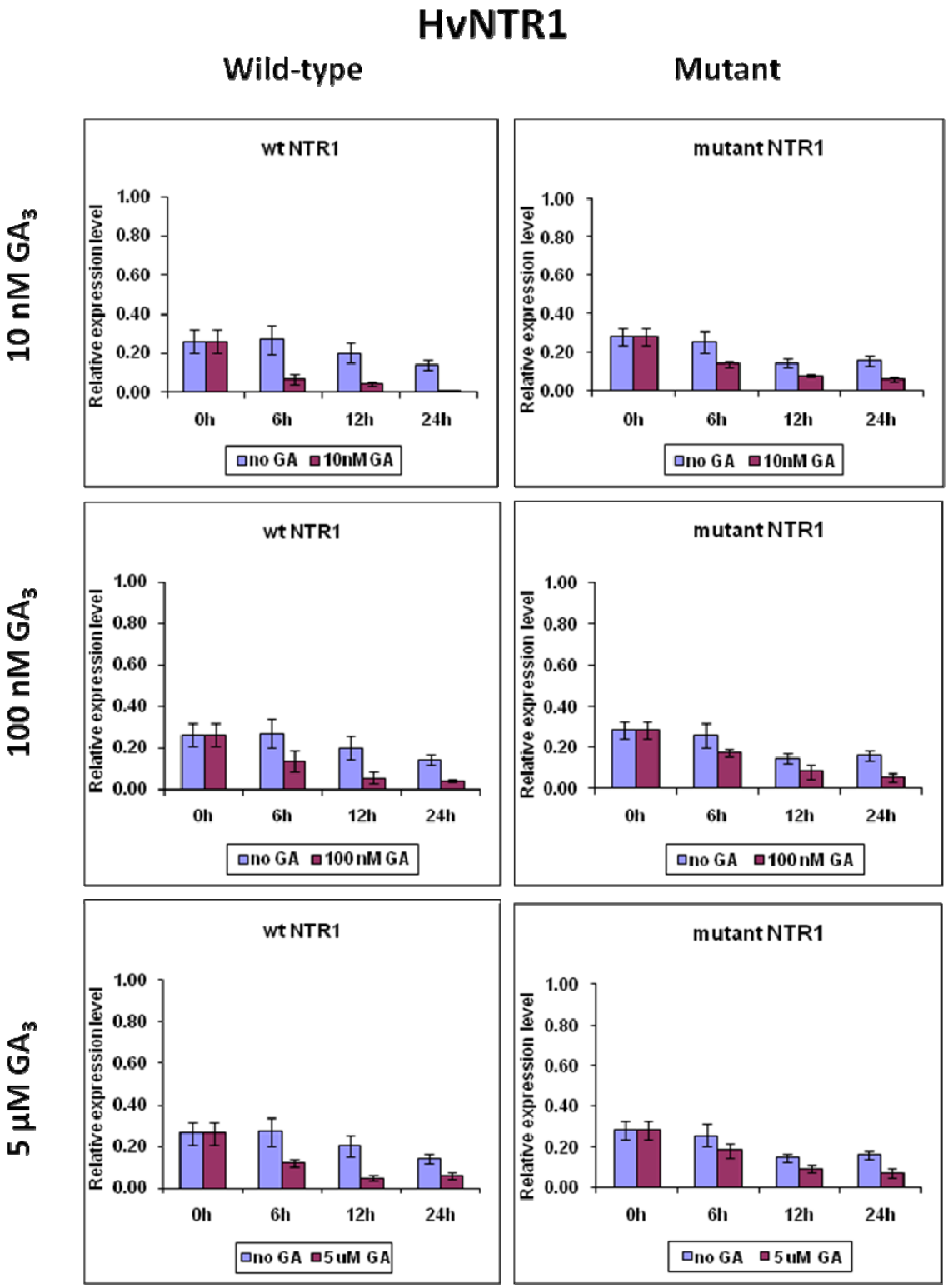

Figure A4. Relative expression of **HvNTR1** in wild-type and mutant (*gse1l*) barley aleurone layers in varying concentrations of gibberellic acid (GA_3).

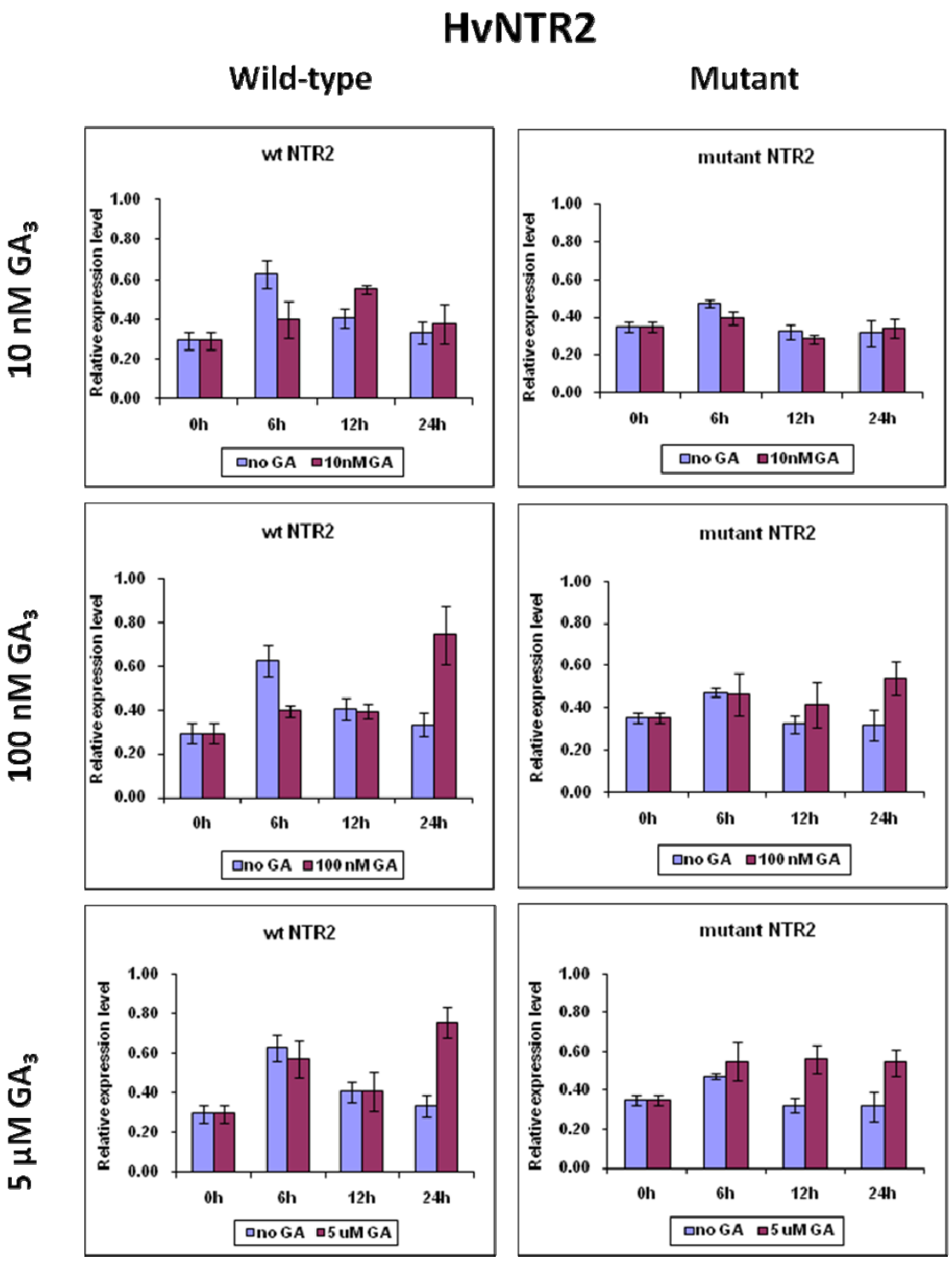

Figure A5. Relative expression of **HvNTR2** in wild-type and mutant (*gse1l*) barley aleurone layers in varying concentrations of gibberellic acid (GA_3).

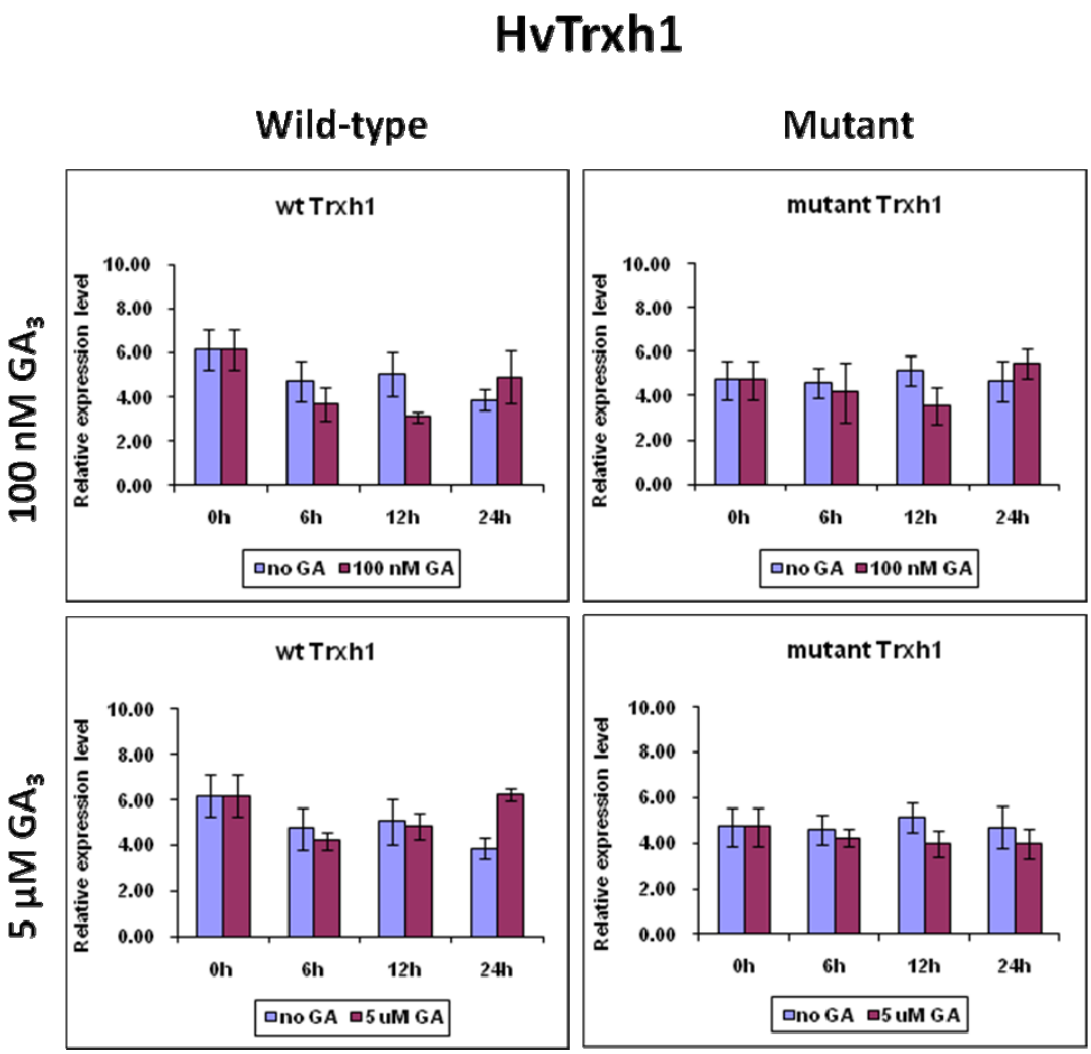

Figure A6. Relative expression of **HvTrxh1** in wild-type and mutant (*gse1l*) barley aleurone layers in varying concentrations of gibberellic acid (GA_3).

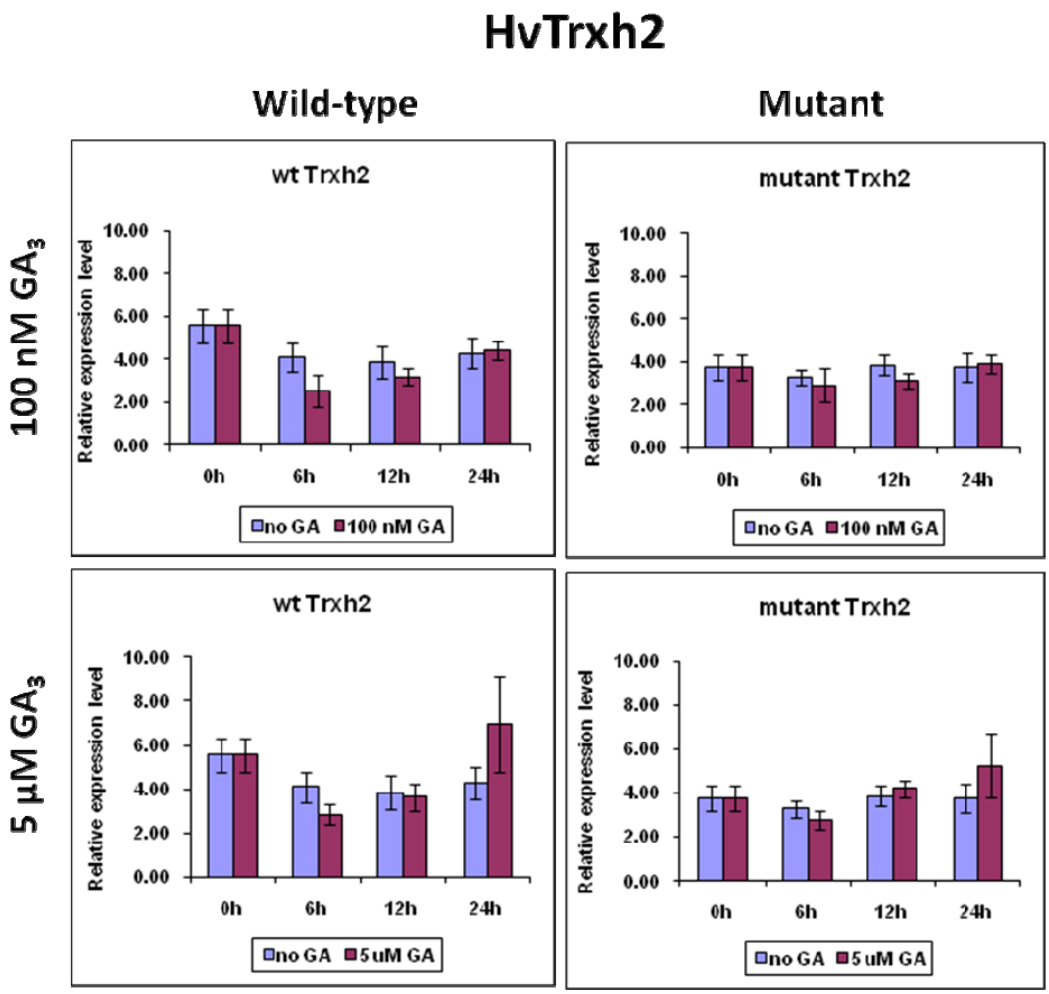

Figure A7. Relative expression of **HvTrxh2** in wild-type and mutant (*gse1l*) barley aleurone layers in varying concentrations of gibberellic acid (GA_3).

A.2.2. Expression levels of NTR and Trx-h in coleorhiza and root of dormant and after-ripened barley seeds

Micro-array data was available from barley grains, which were either dormant or after-ripened (Barrero *et al*., 2009). Tissue had been collected from either the root or coleorhiza at 8 or 18 h after imbibition, and mRNA levels had been measured by micro-array (Section A.4.7).

The dataset was analysed for the content of HvTrxh1, HvTrxh2, HvNTR1 and HvNTR2 (Figure A8). After-ripening has the largest effect of the levels of HvNTR2, especially in the root. Here the normalised expression levels increase 3.4 times from 336 ± 9 to 1127 ± 3 from 8 to 18 h of imbibition. Even in the dormant root the level of HvNTR2 almost doubles from 327 ± 32 to 652 ± 15. In the dormant coleorhiza HvNTR2 expression is stable on 582 ±

30 after 8 h and 546 ± 5 after 18 h whereas for the after-ripened coleorhiza the levels almost double from 690 ± 10 to 1212 ± 42.

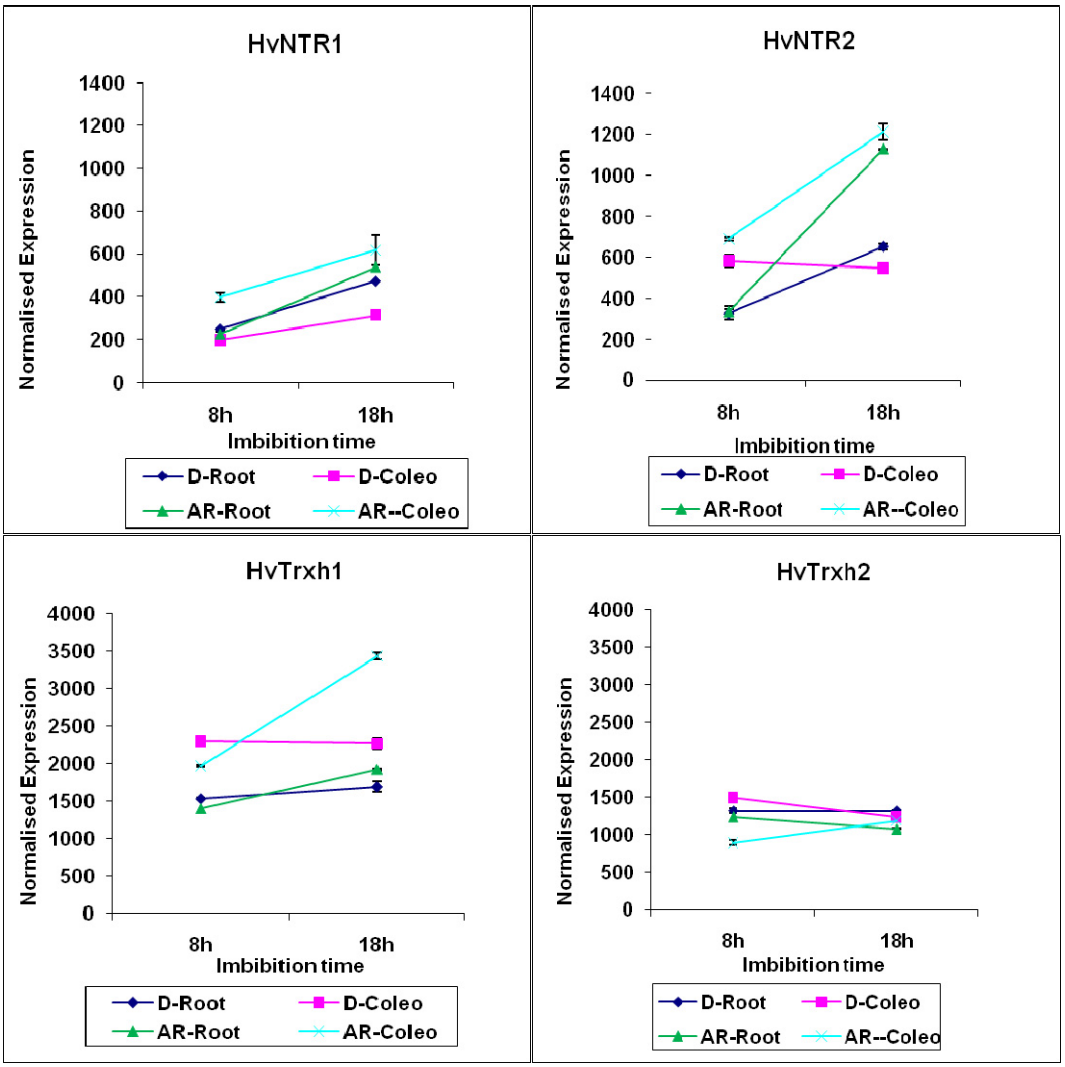

Figure A8. Relative expression levels of HvNTR1, HvNTR2, HvTrxh1 and HvTrxh2 from barley grains, which were either dormant (D) or after-ripened (AR). Tissue has been collected from either root or coleorhiza (Coleo) at 8 or 18 h after imbibition, and mRNA levels were examined by micro-array. Note the different scales on the y-axis.

Also for NTR1 there is an increase in the expression in the dormant roots from 248 ± 1 to 474 ± 1. This increase is slightly higher in the after-ripened roots from 224 ± 11 to 537 ± 12 but is not as profound as for HvNTR2. For HvNTR1 the levels increase less than two times in the coleorhiza for both dormant and after-ripened tissue. However, both at 8 and 18 h the levels for the after-ripened coleorhiza are about twice as high as for the dormant.

It can thereby be concluded that after-ripening leads to increased expression of both HvNTR1 (in coleorhiza) and HvNTR2 (in both roots and coleorhiza). The levels of HvNTR2 are also twice as high as the levels for HvNTR1 in the after-ripened tissues after 18 h, indicating that HvNTR2 may be the most important isoform in both root and coleorhiza at this stage.

For the thioredoxins (Figure A8) the level of HvTrxh2 is stable in both tissues independent of after-ripening and imbibition. Also the expression of HvTrxh1 seems stable in the roots. However, in the coleorhizae the expression increases from 1973 ± 18 to 3432 ± 40 in the after-ripened seeds whereas it is constant around 2300 for the dormant seeds. For all samples the expression of HvTrxh1 is higher than HvTrxh2, and since only HvTrxh1 seems effected by the after-ripening it could indicate that HvTrxh1 plays a more important role right after imbibition in these tissues, and especially in coleorhiza.

A.2.3. Effects of dormancy and light on expression levels of NTR and Trx-h in whole embryo

Time samples had been taken of barley whole embryos at the following time points after imbibition: 0, 6, 12, 18, 24 and 32 h (by Post Doc José Barrero, and lab technicians Ingrid Venables and Trijntje Hughes). The seeds were either dormant or afterripened and had been subjected to either darkness or light. Three biological replicas had been produced, mRNA had been substracted and cDNA produced as described (Barrero *et al*., 2009).

The expression of HvTrxh1, HvTrxh2, HvNTR1 and HvNTR2 was measured (with HvActin as the internal standard) using Q-PCR on this cDNA.

The after-ripened seeds are compared with the dormant (Figure A9). For both HvNTR1 and HvNTR2 the average expression levels are higher for the after-ripened seeds than for the dormant; 2.2 times higher for HvNTR1 and 1.9 times for HvNTR2. For the Trxs there seem to be no effect of after-ripening. As for the aleurone layers a higher expression is observed for the Trxs than for the NTRs (approximately 10 times higher for the dormant embryos, note the different values on the y-axis in Figure A9).

The effect of light versus darkness is shown in Figure A10. The dataset is the same as the one shown in Figure A9 but rearranged to clarify the effect of light. Neither the NTRs nor the Trxs exhibit any difference in expression as an effect of light.

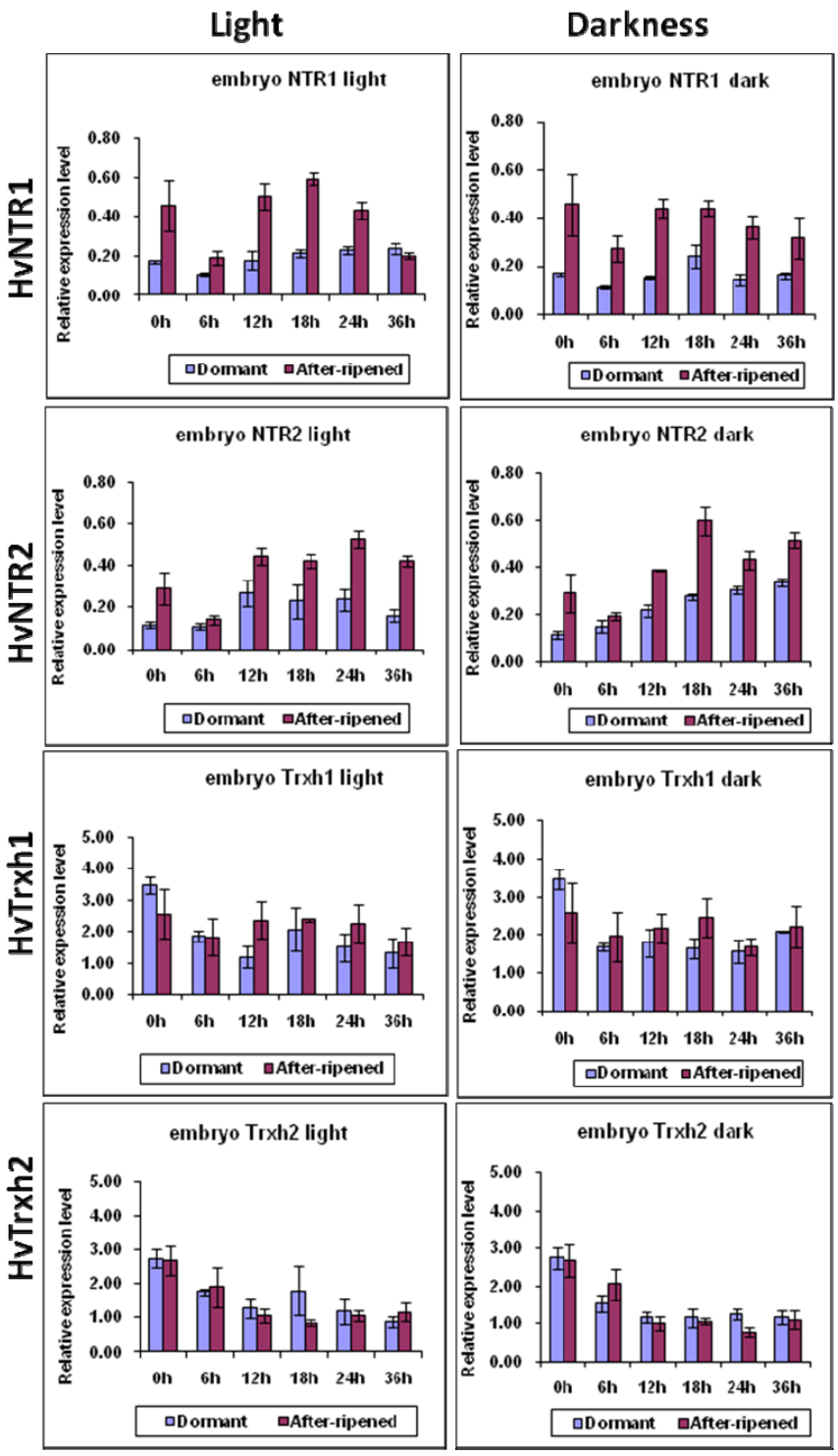

Figure A9. Expression levels of HvNTR1, HvNTR2, HvTrxh1 and HvTrxh2 in barley embryos. The seeds were either dormant or after-ripened and imbibed in either light or darkness. The x-axis are time points after imbibition, whereas the y-axis are normalised expression measured using Q-PCR on cDNA from the samples. Note the different scales for NTR and Trx on the y-axis.

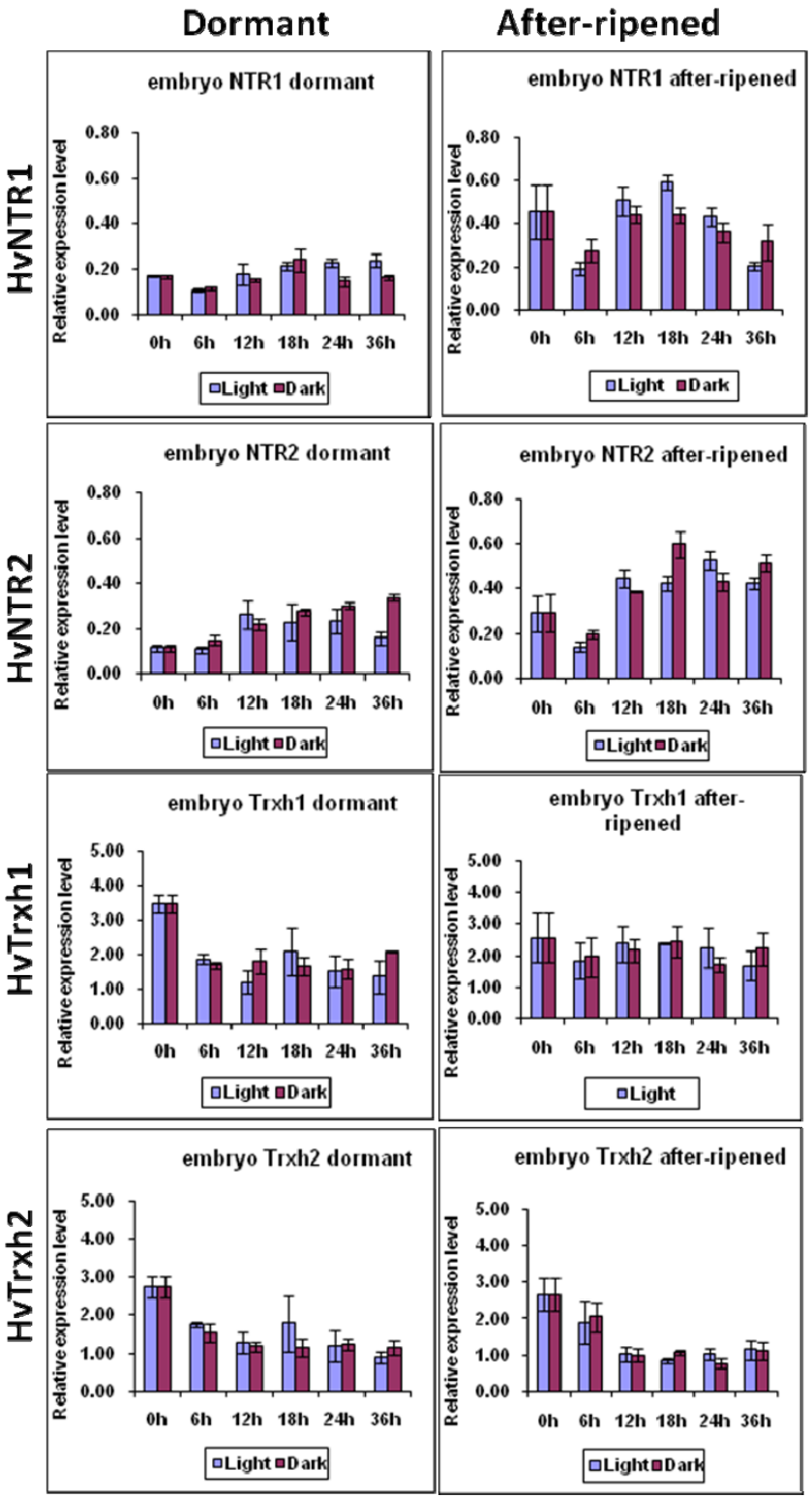

Figure A10. Expression levels of HvNTR1, HvNTR2, HvTrxh1 and HvTrxh2 in barley embryos (the results are the same as in Figure A9 but rearranged to show the difference between dormant and after-ripened seeds). The seeds were either dormant or after-ripened and imbibed in either light or darkness. The x-axis are time points after imbibition, whereas the y-axis are normalised expression measured using Q-PCR on cDNA from the samples. Note the different scales for NTR and Trx on the y-axis.

A.3 Conclusion

The expression of α-amylase in aleurone layers was significantly up-regulated by GA, and the response was dependent on GSE1. HvNTR1 seemed to be down-regulated by GA independently on the dose and GSE1. HvNTR2 may be up-regulated especially at the highest GA concentrations after 24 h. Thus, the expression level of HvNTR2 is 10—40 times higher than of HvNTR1 in these samples. Both HvTrxh1 and HvTrxh2 are expressed in higher amounts than the NTRs and seem unaffected by GA.

For the micro-array data on coleorhiza and root it be concluded that after-ripening leads to increased expression of both HvNTR1 (in coleorhiza) and HvNTR2 (in both roots and coleorhiza). The levels of HvNTR2 are twice as high as the levels for HvNTR1 in the after-ripened tissues after 18 h, indicating that HvNTR2 may be the most important isoform in both root and coleorhiza at this stage. For the Trxs the levels were higher than for the NTRs. While HvTrxh2 levels were stable and independent of after-ripening, the level of HvTrxh1 increased in after-ripened coleorhiza and for all samples the expression of HvTrxh1 was higher than for HvTrxh2, which could indicate that HvTrxh1 plays a more important role right after imbibition in these tissues, and especially in coleorhiza. The overall conclusion is that HvNTR2 and HvTrxh1 are the most abundant isoforms in root and coleorhizae after imbibition and both have increased expression levels in afterripened seeds compared with dormant.

For whole embryo the levels of Trxs was also higher than of NTRs. While the expression of Trxs seemed unaffected by both after-ripening and light the average levels of the NTRs increased in the after-ripened samples. The light had no effect on these expression levels.

A.4 Materials and methods

A.4.1. Incubation of aleurone layers in gibberellic acid

Barley seeds were kindly provided by Dr. Peter Chandler. For each experiment half-grains were produced from 80 wt and 80 mutant (*gse1l*) grains by removing the embryo and a small part of the opposite end of the grain using a scalpel. The half-grains were sterilised with 1% bleach for 30 min and washed thoroughly with sterile milliQ-water. A total of 80

half-grains were spread on two layers of filter paper in a glass petri dish and were imbibed by addition of 4 mL of sterile water. The dish was wrapped in aluminium foil and incubated at 21°C for 3 d. The aleurone layers were stripped from the starchy endosperm by using two spatulas. 10 layers of each strain were flash frozen in liquid N_2 and stored at -80°C whereas the other layers were placed in small Erlenmeyer flasks (10 layers pr flask). In each flask 2 mL solution was added containing 150 µg/mL cefotaxime, 50 units/mL nystatin and 20 mM $CaCl_2$. Furthermore, some flasks contained a selected concentration of gibberillic acid (GA_3). Concentrations of GA_3 used were; 10 nM, 100 nM and 5 µM. The flasks were gently shaken and incubated at 24°C. Time samples were taken after 6, 12 and 24 h by thoroughly washing the layers with sterile milliQ-water, removing excess water by spreading on paper towels and flash freezing in liquid N_2 and store at -80°C. Three biological replicas were made of each condition.

A.4.2. Extraction of mRNA

RNA was extracted from aleurone layers by the following procedure. A mortar was cooled with liquid N_2 and the layers from one sample (10 layers) were kept in liquid N_2 while finely grinded. Each sample was poured into a centrifuge tube containing 5 mL Pine Tree extraction buffer (2% CTAB, 2%PVP K30), 100 mM Tris-HCl pH 8.0, 25 mM EDTA, 20 M NaCl, 2% β-mercatoethanol (added right before heating)), that had been preheated to 65°C. The tube was vortexed and immediately 5 mL of chloroform/IAA was added and the sample mixed well. The sample was kept at room temperature till all samples were ready and centrifuged (4°C, 4 min, 14,000 rpm). The upper phase was transferred to another tube containing 5 mL of chloroform/IAA, mixed and centrifuged again. The upper phase was transferred to a falcon tube, 1/4 volume of 10 M LiCl was added and the sample stored overnight at 4°C.

Samples were centrifuged (20 min at 10,000 rpm and 4°C), and the supernatant was discarded. Pellet was dissolved by vortexing well in 500 µL SSTE (1 M NaCL, 0.5% SDS, 10 mM Tris-HCL pH 8.0 and 1 mM EDTA pH 8.0). The SSTE had been heated to 65°C and brought back to room temperature right before use. An equal volume chloroform/IAA was added and the sample vortexed well. The pellet was removed by centrifugation (2 min,

10,000 rpm and 4°C) and the supernatant carefully transferred to a fresh tube. Two volumes of 100% ethanol were added and RNA precipitated for 30 min at -80°C.

The samples were centrifuged (20 min at 14,000 rpm and 4°C), and the supernatant was removed. Pellet was washed with 500 µL 70 % ethanol, centrifuged (2 min, 14,000 rpm and 4°C) and the supernatant was carefully removed. After air drying the pellet was re-suspended in 50 µL sterile milliQ-water, and the concentration of RNA+DNA determined in a nanodrop spectrophotometer.

A.4.3. Clean-up of mRNA, DNase treatment and mRNA quality

A total of 20 µg RNA/DNA was used and the volume adjusted to 100 µL with sterile milliQ-water. This was purified using the RNeasy Mini kit (Qiagen), from which 350 µL buffer RLT was added and the samples mixed well. A volume of 250 µL 96% ethanol was added, the samples mixed well by pipetting and immediately transferred to an RNeasy Mini spin column. This was centrifuged (15 s, 14,000 rpm), and flow through discarded. Buffer RW1 (300 µL) was added, the samples centrifuged and flow through discarded. Buffer RDD (70 µL) was mixed with 10 µL DNaseI stock solution and added to the RNeasy column membrane. This was incubated at room temperature for 15 min. Buffer RW1 (350 µL) was added, and the column was centrifuged (15 s, 14,000 rpm). Two times 500 µL RPE buffer was run through the column in the same way and the column emptied completely by centrifugation (1 min, 14,000 rpm). RNA was extracted with 40 µL RNase free water and the concentration was determined again. To secure that the RNA was not degraded a sample was analysed by agarose gel electrophoresis. Agarose (1.2 g) was added to 100 mL FA gel buffer (20 mM 3-[N-morpholine]propanesulfonic acid (MOPS), 5 mM sodium acetate, 1 mM EDTA, pH 7.0) and heated in a microwave. The solution was cooled to 65°C and 1.8 mL 37% formaldehyde and 1 µL 10 mg/mL ethidium bromide was added prior to pouring and cooling the gel. It was equilibrated in FA gel running buffer (FA gel buffer plus 0.07% formaldehyde) for at least 30 min. RNA (1 µg) was mixed with 3 µL 5xRNA loading buffer and RNase free water to 15 µL. The samples were heated 3—5 min at 65°C, chilled on ice and loaded on the gel. The gel was run at 80 V for 1 h in FA running buffer.

A.4.4 Production of cDNA

A total of 2 µg of mRNA was mixed with 1 µL oligo dT, 2 µL 5mM dNTPs and sterile milliQ-water to a total volume of 13 µL. This was incubated 5 min at 65°C and 1 min on ice. After a short spin the following was added; 4 µL 5x first strand buffer, 1 µL 100 mM DTT, 1 µL sterile milliQ, 1 µL SS III RT. The solutions were mixed by pipetting and incubated at 50°C for 1 h and 70°C for 15 min (the latter to inactivate). RNaseH (0.5 µL) was added and incubated 30 min at 37°C. 79.5 µL TE was added to a total of 100 µL and the sample stored at -20°C until use.

A.4.5 Primer design

As an internal standard primers for HvActin (see Section A.4.6) were used (provided by CSIRO). As a positive control for GA induced expression, primers against the high pI α-amylase AMY 6-4 were designed. Primers were designed from ESTs of the various proteins, and it was insured that they could only bind to a specific isoform. The melting temperature (Tm) of the primers should be 64°C (calculated as 2x[A+T] + 4x[G+C]) and they should not contain too many Gs and Cs at the 3' end; maximum 3 out of the last 5 residues. Furthermore, the product lengths should be fairly similar in order to compare the expression of mRNA for different proteins. The following primers were designed and used: HvTrxh1 (5'-GGAAGAGTGATTGCCCGGTTA-3' and 5'-CAGAACAACC GGTGCATATCTT'-3), HvTrxh2 (5'-CTATTGGTGTAGTATTCGCCTAA-3' and 5'- CACACTAGCTTGGATCAAGCAT-3'), HvNTR1 (5'-GCGGCTGGTAATTCTACGAGA-3' and 5'-CAACAGCGTATCATATACTTGTG-3'), HvNTR2 (5'-CTGGTCAAGCGACGGTCATC-3' and 5'-GGACAACCAACCTCATCAAGC-3'), AMY6-4 (5'-GCAAAATTGCGAGAGCAGCTC-3' and 5'-CAATGCATGTCCCTCATCCTC-3').

A.4.6 Quantitative real-time PCR

For each reaction 10 µL cDNA was used in 20 µL PCR samples with Platinum Taq (Invitrogen Life Sciences) and SYBR Green (Invitrogen). Reactions were run on a Rotor-gene 3000A real-time PCR machine (Corbett Research), and data were analysed with Rotor-gene software using the comparative quantitation tool. The expression of HvActin (AY145451; 5'-GCCGTGCTTTCCCTCTATG-3' and 5'-GCTTCTCCTTGATGTCCCTTA-3'; Trevaskis *et al*., 2006) was

used as an internal control to normalise gene expression. Three biological replicates were performed for each experiment.

A.4.7 Micro-array analysis

The micro-array data used was already available, produced by Post Doc José Barrero. Samples used in the microarray experiment (coleorhiza and roots) had been dissected from dormant and after-ripened grains (cv. Betzes) imbibed for 8 and 18 h under blue light as described (Barrero *et al*., 2009). RNA had been extracted as described above. Probe synthesis, labelling, and hybridisation to a Barley1 gene chip (Affymetrix) had been carried out at the Australian Genome Research Facilities following the manufacturer's recommendations (Affymetrix). Microarray analyses had been performed on three biological replicates of RNA, and data treated as described (Barrero *et al*., 2009).

Appendix B

LIGPLOT of possible interactions between HvNTR2 and HvTrxh2 in a complex model

ligplot.hhb output:

Donor			Acceptor			Distance
MET B	88	N	ASP A	149	OD1	2.95
ASN A	139	ND2	THR B	90	OG1	2.73
ASN A	139	ND2	ALA B	87	O	3.28
ARG B	102	NH1	ASN A	139	OD1	2.71
GLU B	86	N	ASN A	139	O	3.31
LYS B	108	NZ	SER A	91	O	2.70
LYS B	108	NZ	GLY A	41	O	2.74

ligplot.nnb output:

Atom 1			Atom 2			Distance
GLU B	86	CB	PHE A	155	CZ	3.77
GLU B	86	CD	ILE A	154	CG2	3.31
GLU B	86	CD	ILE A	154	CG1	3.84
GLU B	86	CG	ILE A	154	CG1	3.57
GLU B	86	CD	ILE A	154	CB	3.47
GLU B	86	CG	ILE A	154	CB	3.66
LYS B	77	CD	PRO A	153	CD	3.31
LYS B	77	CG	PRO A	153	CD	3.50
GLU B	81	CD	PRO A	153	CG	3.75
GLU B	81	CG	PRO A	153	CG	3.33
LYS B	77	CD	PRO A	153	CG	3.84
LYS B	77	CG	PRO A	153	CG	3.45
GLU B	81	CD	PRO A	153	CB	3.43
GLU B	81	CG	PRO A	153	CB	3.64
TRP B	45	CH2	ALA A	151	CB	3.72
ALA B	87	CB	ASP A	149	CG	3.62
ALA B	87	CA	ASP A	149	CG	3.51
MET B	88	CE	ASP A	149	CA	3.79
CYS B	46	SG	CYS A	148	C	3.81
CYS B	46	SG	CYS A	148	CA	3.44
GLU B	86	CD	GLY A	141	CA	3.62
GLU B	86	CD	ARG A	140	C	3.73
VAL B	104	CG2	ASN A	139	CG	3.67
VAL B	104	CG2	ASN A	139	CB	3.25
VAL B	104	CG1	ASN A	139	CB	3.61
VAL B	104	CB	TRP A	138	CD1	3.74
ILE B	51	CD1	ALA A	48	CB	3.83
PRO B	48	CD	ALA A	48	CB	3.81
PRO B	48	CG	ALA A	48	CB	3.74
PRO B	48	CA	ALA A	48	CB	3.82
ILE B	107	CG1	ASP A	46	CG	3.76
ALA B	106	CB	ASP A	46	C	3.40
ALA B	106	CB	ASP A	46	CA	3.49
ALA B	106	CA	MET A	43	CE	3.72
MET B	52	CG	MET A	43	CE	3.22

MET	B	52	CB	MET	A	43	CE	3.72
PRO	B	48	C	MET	A	43	CE	3.49
ALA	B	106	CB	MET	A	43	SD	3.42
ALA	B	106	CA	MET	A	43	SD	3.72
PRO	B	48	CB	MET	A	43	SD	3.88
PRO	B	48	C	MET	A	43	SD	3.75
PRO	B	48	CA	MET	A	43	SD	3.58
ALA	B	106	CB	MET	A	43	CG	3.56
ALA	B	106	CA	MET	A	43	CG	3.78
ILE	B	51	CG2	MET	A	43	CG	3.62
ALA	B	106	CB	MET	A	43	CB	3.85
ILE	B	51	CG2	MET	A	43	CB	3.85
ILE	B	51	CG1	TRP	A	42	CZ3	3.88
ILE	B	51	CG2	TRP	A	42	CE3	3.69
ILE	B	51	CG1	TRP	A	42	CE3	3.89
ILE	B	51	CA	TRP	A	42	CE2	3.67
ILE	B	51	CG2	TRP	A	42	CD2	3.41
PRO	B	54	CG	TRP	A	42	CD1	3.88
ILE	B	51	C	TRP	A	42	CD1	3.64
ILE	B	51	CA	TRP	A	42	CD1	3.78
ILE	B	51	CG2	TRP	A	42	CG	3.37
ILE	B	51	CG2	TRP	A	42	CB	3.64
ILE	B	51	CG2	TRP	A	42	C	3.03
ILE	B	51	CG2	TRP	A	42	CA	3.27

Appendix C

Multiple alignment of selected NTRs

```
H_pylori          ------------------------------------------------------------
C_jejuni          ------------------------------------------------------------
OsNTRC            -MAVTRLAVAAALSAKALR-----------------------------------------A 19
ZmNTRC            -MAVTRVAVAAALSAAPLSSRRHRVALPSACRLLPASATCCNSRAPMSL-----QAAAAA 54
HvNTRC            --------RAAA------------------------------------------------A 5
MtNTRC            -MATAKIGL-FGVATLPPTHNHRITTASSHHRFIFINSRRSL------------RTRSSS 46
PtNTRC            ---------------MP---------------WLLIWC---------------------- 8
AtNTRC            MAASPKIGIGIASVSSPHRVSAASSALSPPPHLFFLTTTTTTRHGGSYLLRQPTRTRSSD 60
A_niger           ------------------------------------------------------------
S_cerevisiae      ------------------------------------------------------------
E_histolytica     ------------------------------------------------------------
HvNTR2            ------------------------------------------------------------M 1
TaNTR2            ------------------------------------------------------------M 1
ZmNTR2            ------------------------------------------------------------M 1
OsNTR2            ------------------------------------------------------------M 1
HvNTR1            ------------------------------------------------------------M 1
TaNTR1            ------------------------------------------------------------M 1
OsNTR1            ------------------------------------------------------------M 1
ZmNTR1            ------------------------------------------------------------M 1
PtNTRA            ------------------------------------------------------------
PtNTRB            ------------------------------------------------------------
AtNTRA            ------------------------MCWISMSQSRFIIKSLFSTAGGFLLGSALSNPPSL 35
AtNTRB            ------------------------MNCVSRLKCLISKARSFARLGG---ESTLSQPPSL 32
MtNTRA            ----------------------------MKFRFCPNNNWITLFNKARNLISTQRASV 29
C_trachomatis     ------------------------------------------------------------
D_discoideum      ------------------------------------------------------------
M_tuberculosis    ------------------------------------------------------------
E_coli            ------------------------------------------------------------
D_radiodurans     ------------------------------------------------------------
T_acidophilum     ------------------------------------------------------------
S_solfataricus    ------------------------------------------------------------
```

FAD-loop

```
H_pylori          ----------------------MIDCAIIGGGPAGLSAGLYATRGGVKNAVLFEKGMPG- 37
C_jejuni          ----------------------MLDVAIIGGGPAGLSAGLYATRGGLKNVVMFEKGMPG- 37
OsNTRC            SAAPAVDEEAPASPPPSDLGKGVENLVIIGSGPAGYTAAIYAARANLK-PVVFEGYQVGG 78
ZmNTRC            PAAGAVDEETPASSPPSDASKGVENLVIIGSGPAGYTAAIYAARANLK-PVVFEGCQMGG 113
HvNTRC            PAADAVDEDAPASPPPSDPGRGVENLVIIGSGPAGYTAAIYAARANLK-PVVFEGYQVGG 64
MtNTRC            SLTLRASSDTSS-SSVASPGNAVENVVIIGSGPAGYTAAIYAARANLK-PVVFEGYQMGG 104
PtNTRC            ---------------LFPAGKGIENVVIIGSGPAGYTAAIYAARANLK-PVVFEGYQVGG 52
AtNTRC            SLRLRVSATANSPSSSSSGGGEIIENVVIIGSGPAGYTAAIYAARANLK-PVVFEGYQMGG 119
A_niger           ---------------------MVHTNVVIIGSGPAAHTAAIYLSRAELK-PVLYEGMLANG 39
S_cerevisiae      ---------------------MVHNKVTIIGSGPAAHTAAIYLARAEIK-PILYEGMMANG 39
E_histolytica     -------------------MSNIHDVVIIGSGPAAHTAAIYLGRSSLK-PVMYEGFMAGG 40
HvNTR2            EG--------------SAAAPLRTRVCIIGSGPAAHTAAIYAARAELK-PVLFEGWMAND 46
TaNTR2            EGS-------------AAAAPLRTRVCIIGSGPAAHTAAIYAARAELK-PVLFEGWMAND 47
ZmNTR2            EG--------------SAAAPLRTRICIIGSGPAAHTAAIYAARAELK-PVLFEGWMAND 46
OsNTR2            EG--------------SAGAPLRTRVCIIGSGPSAHTAAIYAARAELK-PVLFEGWLAND 46
HvNTR1            EEA-------------AAGPLRTRVCIIGSGPAAHTAAVYAARAELK-PVLFEGWLAND 46
TaNTR1            EEA-------------AAGPLHTRVCIIGSGPAAHTAAVYAARAELK-PVLFEGWLAND 46
OsNTR1            EEA-------------AAGPLRARVCIIGSGPAAHTAAVYAARAELK-PVLFEGFLAND 46
ZmNTR1            EEAV------------AAAGPLRTRVCIIGSGPAAHTAAVYAARAELK-PVLFEGWLAND 48
PtNTRA            ------------------MEELKTRVCIIGSGPAAHTAAIYASRAELK-PILFEGWMAND 41
PtNTRB            ------------------MEELKTRVCIIGSGPAGHTAAIYASRAELK-PILFEGWMAND 41
AtNTRA            ATAFSSSSSSSSAAAAVDMETHKTKVCIVGSGPAAHTAAIYASRAELK-PLLFEGWMAND 94
AtNTRB            ASAAFSSSAVMNG-----LETHNTRLCIVGSGPAAHTAAIYAARAELK-PLLFEGWMAND 86
MtNTRA            SSAASATAMTDT----TTLPTVKTKLCIIGSGPAAHTAAVYAARAELK-PILFEGWMAND 84
C_trachomatis     --------------------MTHAKLVIIGSGPAGYTAAIYASRALLT-PVLFEGFFSG- 38
D_discoideum      -----------------MSTEKIQKVVIIGSGPAGHTAGIYAGRARLE-PLMFEGFMAGG 42
M_tuberculosis    -PESVPDBAMTAPPVHDRAHHPVRDVIVIGSGPAGYTAALYAARAQLA-PLVFEGTSFG- 57
E_coli            -----------------MGTTKHSKLLILGSGPAGYTAAVYAARANLQ-PVLITGMEKG- 41
D_radiodurans     ---------------MTAPTAHDYDVVIIGGGPAGLTAAIYTGRAQLS-TLILEKGMPG- 43
T_acidophilum     -------MEFNLHAVSSEEKERDFDVVIVGAGAAGFSAAVYAARSGFS-----VAILDK 47
S_solfataricus    -------MSLLPRTTSVKPGEK-FDVIIVGLGPAAYGAALYSARYMLK-----TLVIGE 46
                                        ::* *.:.  *.:*  *  .          .
```

FAD-loop (continued)

```
H_pylori          ----GQITGSSEIENYPGVKEVVSGLDFMQPWQEQCFRFGLKHEMTAVQRVSKK-DS--- 89
C_jejuni          ----GQITSSSEIENYPGVAQVMDGISFMAPWSEQCMRFGLKHEMVGVEQILKNSDG--- 90
OsNTRC            -VPGGQLMTTTEVENFPGFPDGVTGPDLMDKMRKQAERWGAELHQEDVEFVNVKSR---- 133
ZmNTRC            -VPGGQLMTTTEVENFPGFPDGITGPDLMDRMRKQAERWGAELYQEDVEFVNVKSS---- 168
HvNTRC            -VPGGQLMTTTEVENFPGFPDGITGPDLMDKMRKQAERWGAELHQEDVEFVDVKSR---- 119
MtNTRC            -VPGGQLMTTTEVENFPGFPDGITGPDLMDRMRRQAERWGAELHHEDVEAIDVKTS---- 159
PtNTRC            -VPGGQLMTTTEVENFPGFPDGITGPDLMDRMRRQAERWGAELFQEDVESLDVKSS---- 107
AtNTRC            -VPGGQLMTTTEVENFPGFPDGITGPDLMEKMRKQAERWGAELYPEDVESLSVTTA---- 174
A_niger           TAAGGQLTTTTDIENFPGFPDGIGGGELMENMRKQSVRFGTEVITETITKVDFSQR---- 95
S_cerevisiae      IAAGGQLTTTTEIENFPGFPDGLTGSELMDRMREQSTKFGTEIITETVSKVDLSSK---- 95
E_histolytica     VAAGGQLTTTTIIENFPGFPNGIDGNELMMNMRTQSEKYGTTIITETIDHVDFSTQ---- 96
HvNTR2            IAAGGQLTTTTDVENFPGFPTGIMGIDLMDNCRAQSVRFGTNILSETVTEVDFSAR---- 102
TaNTR2            IAAGGQLTTTTDVENFPGFPTGIMGIDLMDNCRAQSARFGTNILSETVTEVDFSAR---- 103
ZmNTR2            IAAGGQLTTTTDVENFPGFPNGIMGADLMDNCRAQSLRFGTNILSETVTAVDFSAC---- 102
OsNTR2            IAAGGQLTTTTDVENFPGFPEGILGGELMDRCRAQSLRFGTSIISETVTAVDFSAR---- 102
HvNTR1            IAAGGQLTTTTDVENFPGFPDGILGIDLMDRCRAQSVRFGTKIFSETVTSVDFSSR---- 102
TaNTR1            IAAGGQLTTTTDVENFPGFPDGILGIDLMDRCRAQSVRFGTKIFSETVTSVDFSSR---- 102
OsNTR1            IAAGGQLTTTTDVENFPGFPDGILGADLMDRCRAQSVRFGTRILTETVTAVDLSSR---- 102
ZmNTR1            IAAGGQLTTTTDVENFPGFPDGILGADLMDRCRAQSLRFGTKILTETVTTVDFSAR---- 104
PtNTRA            IAPGGQLTTTTDVENFPGFPEGIMGGDLTEKFRAQSARFGTQIFTETVTKVNFSKT---- 97
PtNTRB            IAPGGQLTTTTDVENFPGFPEGIMGVELTEKFRAQSARFGTQILTETVTKVDFSRT---- 97
AtNTRA            IAPGGQLTTTTDVENFPGFPEGILGIDIVEKFRKQSERFGTTIFTETVNKVDFSSK---- 150
AtNTRB            IAPGGQLTTTTDVENFPGFPEGILGVELTDKFRKQSERFGTTIFTETVTKVDFSSK---- 142
MtNTRA            IAPGGQLTTTTDVENFPGFPDGILGGELMERCRQQSAKFGTEIFTETVSKVDFSAR---- 140
C_trachomatis     -IAGGQLMTTTEVENFPGFPEGVLGHQLMDLMKTQAQRFGTQVLSKDITAVDFSVR---- 93
D_discoideum      VAAGGQLTTTTEIENFPGFPIDISGSELMDKMREQNIKCGTTIETKTISKVDLKQR---- 98
M_tuberculosis    ----GALMTTTDVENYPGFRNGITGPELMDEMREQALRFGADLRMEDVESVSLHGP---- 109
E_coli            ----GQLTTTTEVENWPGDPNDLTGPLLMERMHEHATKFETEIIFDHINKVDLQNR---- 93
D_radiodurans     ----GQIAWSEEVENFPGFPEPIAGMELAQRMHQQAEKFGAKVEMDEVQGVQHDATSHPY 99
T_acidophilum     AVAGGLTAEAPLVENYLGFKS-IVGSELAKLFADHAANYAKIREGVEVRSIKKTQG---- 102
S_solfataricus    TPGGQLT-EAGIVDDYLGLIE-IQASDMIKVFNKHIEKYEVPVLLDIVEKIENRGD---- 100
                        :  :::: *    : .  :      :  .          :  :
```

Active site

```
H_pylori          HFVILAEDG------KTFEAKSVIIATGGSPKRTGIKGESE----YWGKGVSTCATCDG- 138
C_jejuni          SFTIKLEGG------KTELAKAVIVCTGSAPKKAGFKGEDE----FFGKGVSTCATCDG- 139
OsNTRC            PFVIRSSDR-------EVKCHSVIIATGAAAKRLRLPREDE----FWSRGISACAICDGA 182
ZmNTRC            PFVIRSSDR-------EVKCHSLIIATGATAKRLRLPREDE----FWSRGISACAICDGA 217
HvNTRC            PFVIRSSDR-------EVKCHSVIIATGATAKRLRLPREEE----FWSRGISACAICDGA 168
MtNTRC            PFTVQSSER-------KVKSHTVIIATGATAKRLRLPREDE----FWSRGISACAICDGA 208
PtNTRC            PFTVKSSER-------KVKCHSIIYATGATARRLKLPREDE----FWSRGISACAICDGA 156
AtNTRC            PFTVQTSER-------KVKCHSIIYATGATARRLRLPREEE----FWSRGISACAICDGA 223
A_niger           PFKLWTEWSDGPTDEPAHTADAVIIATGANARRLNLPGEEK----YWQNGISACAVCDGA 151
S_cerevisiae      PFKLWTEFN---EDAEPVTTDAIILATGASAKRMHLPGEET----YWQKGISACAVCDGA 148
E_histolytica     PFKLFTEEG------KEVLTKSVIIATGATAKRMHVPGEDK----YWQNGVSACAICDGA 146
HvNTR2            PFRVTSDST-------TVLADTVVVATGAVARRLYFSGSDT----YWNRGISACAVCDGA 151
TaNTR2            PFRVTSDST-------TVLADTVVVATGAVARRLHFPGSDT----YWNRGISACAVCDGA 152
ZmNTR2            PFRVSADST-------TVLADAVIVATGAVARRLHFPGSDA----YWNRGISACAVCDGA 151
OsNTR2            PFRVASDST-------TVLADAVVVATGAVARRLHFAGSDA----YWNRGISACAVCDGA 151
HvNTR1            PFRVASDDT-------VVHADSVVVATGAVARRLHFAGSDA----FWNRGISACAVCDGA 151
TaNTR1            PFRVSSDDT-------VVHADSVVVATGAVARRLHFAGSDA----FWNRGITACAVCDGA 151
OsNTR1            PFRVASGDT-------VVHADAVVVATGAVARRLHFAGSDA----FWNRGISACAVCDGA 151
ZmNTR1            PFRVASDDT-------VVHADSVVVATGAVARRLHFAGSDA----FWNRGISACAVCDGA 153
PtNTRA            PFEVFTDSK-------RVVADSVIVSTGAVAKKLSFAGSET----FWNRGISACAVCDGA 146
PtNTRB            PFEVFTDSK-------RVVADSVIVATGAAAKKLNFAGSEK----FWNKGISACAVCDGA 146
AtNTRA            PFKLFTDSR-------TVLADSVIISTGAVAKRLSFTGSGEGNGGFWNRGISACAVCDGA 203
AtNTRB            PFKLFTDSK-------AILADAVILATGAVAKRLSFVGSGEASGGFWNRGISACAVCDGA 195
MtNTRA            PFRVFTDSR-------TVEADSVIVATGAVAKRLPFTGSGDGPNGYWNRGISACAVCDGA 193
C_trachomatis     PFVLKSGKE-------TFTCDACIIATGASAKRLSIPGAGD--NEFWQKGVTACAVCDGA 144
D_discoideum      PFTIYVEDE----EDKPIKAQSIIIATGATAKRMGVPGETE----FWSKGVSACAVCDGA 150
M_tuberculosis    LKSVVTADG------QTHRARAVILAMGAAARYLQVPGEQE----LLGRGVSSCATCDG- 158
E_coli            PFRLNGDNG-------EYTCDALIIATGASARYLGLPSEEA----FKGRGVSACATCDG- 141
D_radiodurans     PFTVRGYNG-------EYRAKAVILATGADPRKLGIPGEDN----FWGKGVSTCATCDG- 147
T_acidophilum     GFDIETN-DD------TYHAKYVIITTGTTHKHLGVKGESE----YFGKGTSYCSTCDG- 150
S_solfataricus    EFVVKTKRKG------EFKADSVILGIGVKRRKLGVPGEQE----FAGRGISYCSVCDA- 149
                     :                  :   *   :   .           .* : *: **.
```

```
H_pylori            -FFYKNKEVAVLGGGDTAVEEAIYLANICKKVYLIHRRDGFRCAPITLEHAKN---NDKI 194
C_jejuni            -FFYKNKEVAVLGGGDTALEEALYLANICSKIYLIHRRDEFRAAPSTVEKVKK---NEKI 195
OsNTRC              SPLFKGQVLAVVGGGDTATEEAIYLTKYARHVHLLVRKDQLRASKAMQDRVLN---NPNI 239
ZmNTRC              SPLFKGQVLAVVGGGDVATEEAVYLTKYARHVHLLVRKDQLRASKAMQDRVLN---NPNI 274
HvNTRC              SPLYKGQVLAVVGGGDTATEEAIYLTKYACHVHLLVRRDQLRASKAMQDRVLN---NPNI 225
MtNTRC              SPLFKGQILAVVGGGDTATEEALYLTKYARHVHLLVRRDQLRASKAMQDRVYD---NPNV 265
PtNTRC              SPLFKRQVLAVVGGGDTATEEALYLTKYARHVHLLVRKDQLRASKAMQDRVIN---NPNV 213
AtNTRC              SPLFKGQVLAVVGGGDTATEEALYLTKYARHVHLLVRRDQLRASKAMQDRVIN---NPNI 280
A_niger             VPIFRNKPLFVIGGGDSAAEEAMFLAKYGSSVTVLVRRDKLRASKAMANRLLS---HPKV 208
S_cerevisiae        VPIFRNKPLAVIGGGDSACEEAQFLTKYGSKVFMLVRKDHLRASTIMQKRAEK---NEKI 205
E_histolytica       VPIFRNKVLMVVGGGDAAMEEALHLTKYGSKVIILHRRDAFRASKTMQERVLN---HPKI 203
HvNTR2              APIFRNKPIAVIGGGDSAMEEGNFLTKYGSQVYIIHRRNTFRASKIMQARALS---NPKI 208
TaNTR2              APIFRNKPIAVIGGGDSAMEEGNFLTKYGSQVYIIHRRNTFRASKIMQARALS---NPKI 209
ZmNTR2              APIFRNKPIAVIGGGDSAMEESNFLTKYGSHVYIIHRRNTFRASKIMQARALE---NPKI 208
OsNTR2              APIFRNKPIAVIGGGDSAMEESNFLTKYGSHVYIIHRRNTFRASKIMQARALS---NPKI 208
HvNTR1              APIFRNKPIAVVGGGDSAMEEANFLTKYGSRVYIIHRRDAFRASKIMQARALS---NPKI 208
TaNTR1              APIFRNKPIAVVGGGDSAMEEANFLTKYGSRVYIIHRRDAFRASKIMQARALS---NPKI 208
OsNTR1              APIFRNKPIAVVGGGDSAMEEANFLTKYGSRVYIIHRRNAFRASKIMQARALS---NPKI 208
ZmNTR1              APIFRNKPIAVVGGGDSAMEEANFLTKYGSQVYIIHRRSDFRASKIMQARTLS---NPKI 210
PtNTRA              APIFREKPLAVIGGGDSAMEEANFLTKYGSKVYIIHRRDTFRASKIMQSRTLS---NPKI 203
PtNTRB              APIFREKALAVIGGGDSAMEEANFLTKYGTKVYIIHRRDTFRASKIMQSRALS---NPKI 203
AtNTRA              APIFRNKPLVVIGGGDSAMEEANFLTKYGSKVYIIHRRDTFRASKIMQQRALS---NPKI 260
AtNTRB              APIFRNKPLAVIGGGDSAMEEANFLTKYGSKVYIIHRRDAFRASKIMQQRALS---NPKI 252
MtNTRA              APIFRNKPLAVIGGGDSAMEEATFLTKYGSEVYIIHRRDTFRASKIMQSKALS---NEKI 250
C_trachomatis       SPIFRDKDLFVVGGGDSALEEAMFLTRYGKRVFVVHRRDTLRASKVMVNKAQA---NEKI 201
D_discoideum        LPIYRNKHLVVVGGGDTAAEEATFLTHFASKVTLLVRRNVMRASKAMQQKVFS---NPKI 207
M_tuberculosis      -FFFRDQDIAVIGGGDSAMEEATFLTRFARSVTLVHRRDEFRASKIMLDRARN---NDKI 214
E_coli              -FFYRNQKVAVIGGGNTAVEEALYLSNIASEVHLIHRRDGFRAEKILIKRLMDKVENGNI 200
D_radiodurans       -FFYKGKKVVVIGGGDAAVEEGMFLTKFADEVTVIHRRDTLRANKVAQARAFA---NPKM 203
T_acidophilum       -YLFKGKRVVTIGGGNSGAIAAISMSEYVKNVTIIEYMPKYMCENAYVQEIKKR----NI 205
S_solfataricus      -PLFKNRVVAVIGGGDSALEGAEILSSYSTKVYLIHRRDTFKAQPIYVETVKKKP---NV 205
                      ::: : : .:***: .   .  ::     : ::       .              ::
```

Glycine-loop

```
H_pylori            EFLTPYVVEEIKGDAS---GVSSLSIKNTATNE-KRELVVPGFFIFVGYDVNNAVLKQED 250
C_jejuni            ELITSASVDEVYGDKM---GVAGVKVK-LKDGS-IRDLNVPGIFTFVGLNVRNEILKQDD 250
OsNTRC              TVHFNTEAVDVVSNPK--GQMSGIQLKRTDTGE-ESVLEVKGLFYGIGHTPNSQLLQG-- 294
ZmNTRC              TVHFNTEAMDVVSNDK--GQMSGVHLKRRDTGE-ESVLTVKGLFYGIGHTPNSQLLQG-- 329
HvNTRC              TVHFNTEAVDVVGNTK--GQMSGIQLRRIDTGE-EKVLEVKGLFYGIGHTPNSQLLEG-- 280
MtNTRC              TVHFNTETVDIVSNTK--GQMSGILVRKLDSGE-ESVLEAKGLFYGIGHSPNTQLLKG-- 320
PtNTRC              TVHFNTETLDIVSNTK--GQMSGILTRKTDTGE-ESVLEAKGLFYGIGHSPNSQLLEG-- 268
AtNTRC              TVHYNTETVDVLSNTK--GQMSGILLRRLDTGE-ETELEAKGLFYGIGHSPNSQLLEG-- 335
A_niger             TVRFNSVATEVLGEEKPNGLMTHLKVKNVVSGE-EEVVDANGLFYAVGHDPATTLVKG-- 265
S_cerevisiae        EILYNTVALEAKGDGK---LLNALRIKNTKKNE-ETDLPVSGLFYAIGHTPATKIVAG-- 259
E_histolytica       EVIWNSELVELEGDGD---LLNGAKIHNLVSGE-YKVVPVAGLFYAIGHSPNSKFLGG-- 257
HvNTR2              QVVWDSEVVEAYGGAG-GGPLAGVKVKNLVTGE-VSDLQVSGLFFAIGHEPATKFLNG-- 264
TaNTR2              QVVWDSEVVEAYGGAG-GGPLAGVKVKNLVTGQ-VSDLQVSGLFFAIGHEPATKFLNG-- 265
ZmNTR2              KVLWDSEVVEAYGGAN-GGPLAGVKVKNLLNGE-VSDLQVSGLFFAIGHEPATKFLGG-- 264
OsNTR2              QVFWDSEVVEAYGGEG-GGPLAGVKVKNLVTGK-ISDLQVSGLFFAIGHEPATKFLGG-- 264
HvNTR1              QVVWDSEVVEAYGGSD-GGPLAGVKVKNLVSGE-VSDVQVAGLFFAIGHEPATKFLAG-- 264
TaNTR1              QVVWDSEVVEAYGGSD-GGPLGGVKVKNLVTGE-VSDFRVAGLFFAIGHEPATKFLAG-- 264
OsNTR1              QVVWDSEVVEAYGGAD-GGPLAGVKVKNVVSGE-VSDLQVAGLFFAIGHEPATKFLGG-- 264
ZmNTR1              KVVWNSEVVEAYGGAD-GGPLAGVKVKDVVTGE-VSDLQVAGLFFAIGHEPATKFLGG-- 266
PtNTRA              EVIWNSVVEEAYG----ERVVGGLKVKNVVTGE-VSDLKVNGLFFAIGHEPATRFLDG-- 256
PtNTRB              EVIWNSAVEEAYG----ERVLGGLKVKNVVTGE-VSDLKVNGLFFAIGHEPATRFMDG-- 256
AtNTRA              EVIWNSAVVEAYGDEN-GRVLGGLKVKNVVTGD-VSDLKVSGLFFAIGHEPATKFLDG-- 316
AtNTRB              DVIWNSSVVEAYGDGE-RDVLGGLKVKNVVTGD-VSDLKVSGLFFAIGHEPATKFLDG-- 308
MtNTRA              KVIWNSMVVEAEGDGE-NKKLGGLKVENVVTKE-VTDLKVSGLFFAIGHEPATKFLDG-- 306
C_trachomatis       FFLWNSEIVKISGDT----LVRSIDIYNNVDET-TTTMEAAGVFFAIGHQPNTAFLGG-- 254
D_discoideum        EVLWDTTLVEIKGEKS----VTSVGIYNSETKV-SSNLDAQGLFYAIGHTPNSAFLNG-- 260
M_tuberculosis      RFLTNHTVVAVDGDTT----VTGLRVRDTNTGA-ETTLPVTGVFVAIGHEPRSGLVRE-- 267
E_coli              ILHTNRTLEEVTGDQM---GVTGVRLRDTQNSDNIESLDVAGLFVAIGHSPNTAIFEG-- 255
D_radiodurans       KFIWDTAVEEIQGADS----VSGVKLRNLKTGE-VSELATDGVFIFIGHVPNTAFVKD-- 256
T_acidophilum       PYIMNAQVTEIVGDG---KKVTGVKYKDRTTGE-EKLIETDGVFIYVGLIPQTSFLKDS- 260
S_solfataricus      EFVLNSVVKEIKGD----KVVKQVVVENLKTGE-IKELNVNGVFIEIGFDPPTDFAKSN- 259
                              .       :                . . *.*  :*    . .
```

```
H_pylori            NSMLCKCDEYGSIVVDF-----SMKTNVQGLFAAGDIRIF--APKQVVCAASDGATAALS 303
C_jejuni            SKFLCNMEEGGQVSVDL-----KMQTSVAGLFAAGDLRKD--APKQVICAAGDGAVAALS 303
OsNTRC              ---QIDLDDAGYILVEE----GTAKTSVDGVFAAGDVQDH--EWRQAVTAAGSGCVAALS 345
ZmNTRC              ---QIELDSAGYILVKE----GSAKTSVDGVLAAGDVQDH--EWRQAITAAGSGCIAALS 380
HvNTRC              ---QIELDSSGYILVEE----GTAKTSVDGVFAAGDVQDH--EWRQAVTAAGSGCIAALS 331
MtNTRC              ---QVELDQSGYLLVKE----GTAKTSVEGVFAAGDVQDH--EWRQAVTAAGSGCIAALS 371
PtNTRC              ---QVELDSAGYVLVQD----GSGKTSVEGVFAAGDVQDH--EWRQAITAAGSGCIAALS 319
AtNTRC              ---QVELDSSGYVLVRE----GTSNTSVEGVFAAGDVQDH--EWRQAVTAAGSGCIAALS 386
A_niger             ---QIKLDEDGYIVTQP----GTSYTSVEGVFACGDVQDK--RYRQAITSAGSGCIAALE 316
S_cerevisiae        ---QVDTDEAGYIKTVP----GSSLTSVPGFFAAGDVQDS--KYRQAITSAGSGCMAALD 310
E_histolytica       ---QVKTADDGYILTE------GPKTSVDGVFACGDVCDR--VYRQAIVAAGSGCMAALS 306
HvNTR2              ---QLELHADGYVATKP----GSTHTSVEGVFAAGDVQDK--KYRQAITAAGSGCMAALD 315
TaNTR2              ---QLELHADGYVATKP----GSTHTSVEGVFAAGDVQDK--KYRQAITAAGSGCMAALD 316
ZmNTR2              ---QLELDSDGYVETKP----GSTHTSVKGVFAAGDVQDK--KYRQAITAAGSGCMAALD 315
OsNTR2              ---QLELDADGYVATKP----GSTHTSVKGVFAAGDVQDK--KYRQAITAAGSGCMAALD 315
HvNTR1              ---QLELDSEGYVATKP----GSTHTSVKGVFAAGDVQDK--KYRQAITAAGSGCMAALD 315
TaNTR1              ---QLELDSEGYVATKP----GSTHTSVKGVFAAGDVQDK--KYRQAITAAGSGCMAALD 315
OsNTR1              ---QLELDSDGYVVTKP----GSTHTSVKGVFAAGDVQDK--KYRQAITAAGSGCMAALD 315
ZmNTR1              ---QLELDSDGYVVTKP----GSTHTSVQGVFAAGDVQDK--KYRQAITAAGSGCMAALD 317
PtNTRA              ---QLELDSDGYVATKP----GTTKTSVRGVFAAGDVQDK--KYRQAITAAGTGCMAALD 307
PtNTRB              ---QLELDSDGYVVTKP----GTTKTSVRGVFAAGDVQDK--KYRQAITAAGTGCMAALD 307
AtNTRA              ---QLELDEDGYVVTKP----GTTKTSVVGVFAAGDVQDK--KYRQAITAAGTGCMAALD 367
AtNTRB              ---GVELDSDGYVVTKP----GTTQTSVPGVFAAGDVQDK--KYRQAITAAGTGCMAALD 359
MtNTRA              ---QLELDSDGYVVTKP----GTTKTSVEGVFAAGDVQDK--KYRQAITAAGSGCMAALD 357
C_trachomatis       ---QVALDENGYIITEK----GSSRTSVPGVFAAGDVQDK--YYRQAITSAGSGCMAALD 305
D_discoideum        ---QLNTDETGYIITQP----GSTKTNVEGVFACGDVQDK--VYRQAITAAGNGCMAALD 311
M_tuberculosis      ---AIDVDPDGYVLVQG----RTTSTSLPGVFAAGDLVDR--TYRQAVTAAGSGCAAAID 318
E_coli              ---QLELEN-GYIKVQSGIHGNATQTSIPGVFAAGDVMDH--IYRQAITSAGTGCMAALD 309
D_radiodurans       ---TVSLRDDGYVDVRD-----EIYTNIPMLFAAGDVSDY--IYRQLATSVGAGTRAAMM 306
T_acidophilum       ---GVKLDERGYIVVDS-----RQRTSVPGVYAAGDVTSG--NFAQIASAVGDGCKAALS 310
S_solfataricus      ---GIETDTNGYIKVDE-----WMRTSVPGVFAAGDCTSAWLGFRQVITAVAQGAVAATS 311
                           * : .          *.:  . *.**         *   :.. *  **

H_pylori            VISYLEHH---------------------------------------------------- 311
C_jejuni            AMAYIESLH--------------------------------------------------- 312
OsNTRC              VERYLVANDLLVEFHQPVREEKEKEITDRDVEMGFDISHTKHRGQYALRKVYHESPRLVC 405
ZmNTRC              VERYLVANDLLVEFHQPVQEETKKDITDKDVQMGFDISHRKHKGQYALRKLYHESPRLIC 440
HvNTRC              VERYLVSSDLLIEFHQPVREEKKKEIEGKDVEMGFDITHTKHKGQYALRKLYHGSPRLIL 391
MtNTRC              VERYLVSSGLLIEFHQPKHEEVKKELTDRDVQAGFDITLTKHKGQYALRKLYHDSPRLIC 431
PtNTRC              VERYLVSNNLLIEFHQRQTEEVKKELTDRDVHEGFDITITKHKGQYSLRKLYHESPRLIC 379
AtNTRC              AERYLTSNNLLVEFHQPQTEEAKKEFTQRDVQEKFDITLTKHKGQYALRKLYHESPRVIL 446
A_niger             AEKYIAE----RESGEEPATSTEKAAIKPATQEVNGEVKQDAQGAAAEYKSNPLL----- 367
S_cerevisiae        AEKYLTS----LE---------------------------------------------- 319
E_histolytica       CEKWLQT----H----------------------------------------------- 314
HvNTR2              AEHYLQE----VGAQVGKSD--------------------------------------- 331
TaNTR2              AEHYLQE----VGAQEGKSD--------------------------------------- 332
ZmNTR2              AEHYLQE----IGAQEGKSD--------------------------------------- 331
OsNTR2              AEHYLQE----VGAQEGKAD--------------------------------------- 331
HvNTR1              AEHYLQE----VGAQEGKTD--------------------------------------- 331
TaNTR1              AEHYLQE----VGAQEGKTD--------------------------------------- 331
OsNTR1              AEHYLQE----IGAQEDKTD--------------------------------------- 331
ZmNTR1              AEHYLQE----VGAQEGKTD--------------------------------------- 333
PtNTRA              AEHYLQE----IGSQEGKSD--------------------------------------- 323
PtNTRB              AEHYLQE----IGAEDGKTD--------------------------------------- 323
AtNTRA              AEHYLQE----IGSQEGKSD--------------------------------------- 383
AtNTRB              AEHYLQE----IGSQQGKSD--------------------------------------- 375
MtNTRA              AEHFLQG----VGLQQDKSD--------------------------------------- 373
C_trachomatis       AERFLEN---------------------------------------------------- 312
D_discoideum        CERFLSS----L----------------------------------------------- 319
M_tuberculosis      AERWLAEH---AATGEADSTDALIGAQR------------------------------- 343
E_coli              AERYLDG------LADAK----------------------------------------- 321
D_radiodurans       TERQLAA----LEVEGEEVTAAD------------------------------------ 325
T_acidophilum       LYSDSISKK-------------------------------------------------- 319
S_solfataricus      AYRYVTEKKGKK----------------------------------------------- 323
```

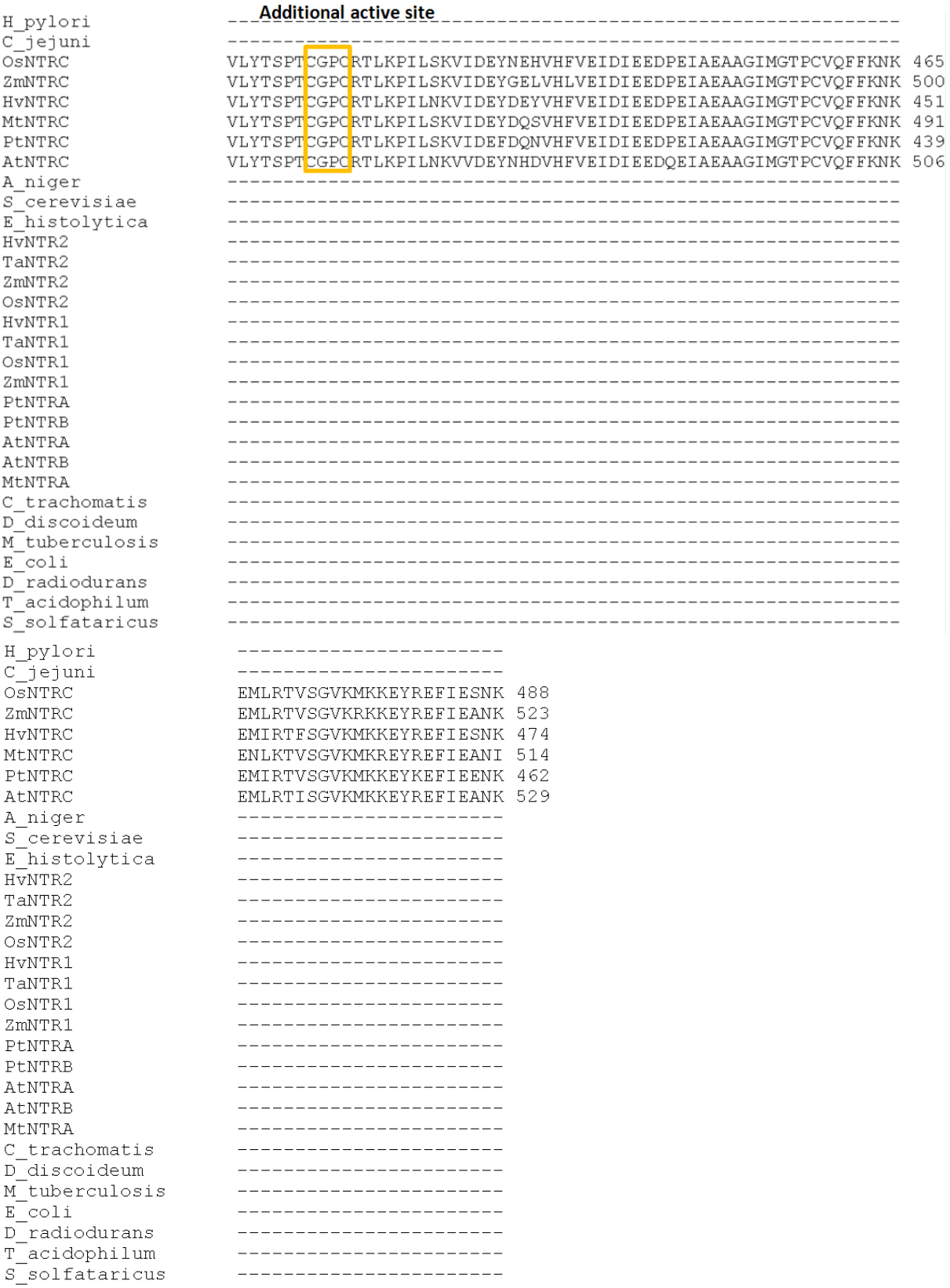

Multiple alignment of selected NTRs The NTRs, with their accession numbers given in parentheses, are HvNTR1 (A9YZV9), HvNTR2 (A9LN30) and HvNTRC (B0FXK2) from *Hordeum vulgare* (barley); TaNTR1 (Q8VX47) and TaNTR2 (TC297680) from *Triticum aestivum* (wheat); OsNTR1 (Q69PS6), OsNTR2 (Q6ZFU6) and OsNTRC

(Q70G58) from *Oryza sativa* (rice); ZmNTR1 (B6TPI3), ZmNTR2 (B7ZY93) and ZmNTRC (B4FJQ7) from *Zea mays* (maize); AtNTRA (Q39242), AtNTRB (Q39243) and AtNTRC (O22229) from *Arabidopsis thaliana* (mouse-ear cress); PtNTRA (AC149479), PtNTRB (B9I0K8) and PtNTRC (B9H9S9) from *Populus trichocarpa* (western balsam poplar); MtNTRA (A6XJ26) and MtNTRC (A6XJ27) from *Medicago truncatula* (barrel medic, a legume); S_cerevisiae (P29509) from *Saccharomyces cerevisiae* (yeast); D_discoideum (Q54UU8) from *Dictyostelium discoideum* (amoeba "slime mold"); E_histolytica (C4LW95) from *Entamoeba histolytica* (anaerobic parasitic protozoan); A_niger (XP_001389279) from *Aspergillus niger* (fungus); T_acidophilum (Q9HJI4) from *Thermoplasma acidophilum* (facultative anaerobe archaea); S_solfataricus (Q97W27) NTRB from *Sulfolobus solfataricus* (archaea); E_coli (P0A9P4) from *Escherichia coli* (Gram-negative bacteria); C_trachomatis (O84101) from *Chlamydia trachomatis* (Gram-negative bacteria); M_tuberculosis (P52214) from *Mycobacterium tuberculosis* (bacteria); H_pylori (P56431) from *Helicobacter pylori* (Gram-negative bacteria); D_radiodurans (Q9RSY7) from *Deinococcus radiodurans* (extremophilic bacteria, Gram-positive), and C_jejuni (Q0PBZ1) from *Campylobacter jejuni* (Gram-negative bacteria). The alignment is made in ClustalW2 (Thompson *et al*., 1994).

Appendix D:

Primers used for site-directed mutagenesis

Mutated codons are marked in red and mismatches underlined.

Mutant/primer	Sequence
HvNTR2_G222D_A223G_G224E	
NTR2_1F	5'-CGAGGCTTACGGCGACGGAGAAGGCGGCCCATTAGCTG -3’
NTR2_1R	5’- CAGCTAATGGGCCGCCTTCTCCGTCGCCGTAAGCCTCG -3’
HvNTR2_G225R_G226D_P227V	
NTR2_2F	5’-GCTTACGGCGGTGCAGGCAGGGACGTATTAGCTGGGGTCAAG -3’
NTR2_2R	5’- CTTGACCCCAGCTAATACGTCCCTGCCTGCACCGCCGTAAGC -3’
HvNTR2_Δ42-47	
NTR2_3F	5’-CTTCGAGGGCGCCGCGGGGG -3’
NTR2_3R	5’-CCCCCGCGGCGCCCTCGAAG-3’
HvNTR2_ G225R_G226D (the mutant HvNTR2_G225R_G226D_P227V used as template)	
Name: NTR2_8F	5’- GTGCAGGCAGGGACCCATTAGCTGGGGTCAAG -3’
Name: NTR2_8R	5’- CTTGACCCCAGCTAATGGGTCCCTGCCTGCAC-3’
HvNTR2_ M43A	
HvNTR2_9_fw	**5'-**ACTTCGAGGGCTGGGCGGCCAACGACATCG-3’
HvNTR2_9_rv	**5’-**CGATGTCGTTGGCCGCCCAGCCCTCGAAG-3’
HvNTR2_M43A_W42A	
HvNTR2_10_fw	5’-GTGCTCTTCGAGGGCGCGGCGGCCAACGACATCG-3’
HvNTR2_10_rv	5’-CGATGTCGTTGGCCGCCGCGCCCTCGAAGAGCAC-3’
HvNTR2_N139A	
HvNTR2_11_fw	5’-CGACACCTACTGGGCCCGCGGCATCTCC-3’
HvNTR2_11_rv	5’-GGAGATGCCGCGGGCCCAGTAGGTGTCG-3’
HvNTR2_W42A	
HvNTR2_13_fw	5’-GCTCTTCGAGGGCGCGATGGCCAACGAC-3’
HvNTR2_13_rv	5’-GTCGTTGGCCATCGCGCCCTCGAAGAGC-3’
HvNTR2_N45A_D46A	
HvNTR2_14_fw	5’-GCTGGATGGCCGCCGCCATCGCCGCGG-3’
HvNTR2_14_rv	5’-CCGCGGCGATGGCGGCGGCCATCCAGC-3’

HvTrxh2_I51G

HvTrxH2_1_fw	5′-GCGGACCATGCCGCGGGATGGCTCCAGTTTTCG-3′
HvTrxH2_1_rv	5′-CGAAAACTGGAGCCATCCCGCGGCATGGTCCGC-3′

HvTrxh2_E86A

HvTrxH2_2_fw	5′-GCAATTCAGTGTCGCGGCCATGCCAACG-3′
HvTrxH2_2_rv	5′-CGTTGGCATGGCCGCGACACTGAATTGC-3′

HvTrxh2_G47P

HvtrxH2_3_fw	5′-CACTGCATCATGGTGCCCACCATGCCGCATC-3′
HvtrxH2_3_rv	5′-GATGCGGCATGGTGGGCACCATGATGCAGTG-3′

Appendix E

Acta Crystallographica Section D
Biological Crystallography
ISSN 0907-4449

Structure of *Hordeum vulgare* NADPH-dependent thioredoxin reductase 2. Unwinding the reaction mechanism

Kristine G. Kirkensgaard,[a,b] Per Hägglund,[b] Christine Finnie,[b] Birte Svensson[b] and Anette Henriksen[a]*

[a]Carlsberg Laboratory, Denmark, and [b]Enzyme and Protein Chemistry, Department of Systems Biology, Technical University of Denmark, Denmark

Correspondence e-mail: anette@crc.dk

Received 4 May 2009
Accepted 9 June 2009

PDB Reference: *Hv*NTR2, 2whd, r2whdsf.

Thioredoxins (Trxs) are protein disulfide reductases that regulate the intracellular redox environment and are important for seed germination in plants. Trxs are in turn regulated by NADPH-dependent thioredoxin reductases (NTRs), which provide reducing equivalents to Trx using NADPH to recycle Trxs to the active form. Here, the first crystal structure of a cereal NTR, *Hv*NTR2 from *Hordeum vulgare* (barley), is presented, which is also the first structure of a monocot plant NTR. The structure was determined at 2.6 Å resolution and refined to an $R_{\rm cryst}$ of 19.0% and an $R_{\rm free}$ of 23.8%. The dimeric protein is structurally similar to the structures of *At*NTR-B from *Arabidopsis thaliana* and other known low-molecular-weight NTRs. However, the relative position of the two NTR cofactor-binding domains, the FAD and the NADPH domains, is not the same. The NADPH domain is rotated by 25° and bent by a 38% closure relative to the FAD domain in comparison with *At*NTR-B. The structure may represent an intermediate between the two conformations described previously: the flavin-oxidizing (FO) and the flavin-reducing (FR) conformations. Here, analysis of interdomain contacts as well as phylogenetic studies lead to the proposal of a new reaction scheme in which NTR–Trx interactions mediate the FO to FR transformation.

1. Introduction

Thioredoxin (Trx) systems are ubiquitous redox regulators that facilitate the reduction of other proteins *via* disulfide-exchange reactions (Fig. 1*a*). In most organisms, Trx is reduced enzymatically by NADPH *via* NADPH-dependent thioredoxin reductase (NTR; Williams, 1976). The tripartite system of Trx, NTR and NADPH is known to be involved in DNA synthesis, oxidative-stress response and apoptosis (Arnér & Holmgren, 2000). Thus, reduced thioredoxin can activate ribonucleotide reductase (Laurent *et al.*, 1964; Moore *et al.*, 1964), methionine sulfoxide reductase (Russel & Model, 1986) and peroxiredoxins (Tripathi *et al.*, 2009).

Plants exhibit a unique thioredoxin system with a complex time-, tissue- and organelle-specific expression pattern of a diverse selection of Trx isozymes that are not found in other organisms (Gelhaye *et al.*, 2004; Ishiwatari *et al.*, 1998). Furthermore, some plant Trxs are reduced by ferredoxin and ferredoxin reductase (FTR; de la Torre *et al.*, 1979) or by the glutaredoxin system: glutaredoxin (Grx), glutathione and glutathione reductase (GR; Gelhaye *et al.*, 2003). The NTR/Trx system in plants has a variety of functions and a wide range of target proteins have been identified by proteomics

approaches (Hägglund *et al.*, 2008). Cytosolic Trx h plays important roles during seed germination by reducing disulfides in storage proteins and inhibitors of proteases and α-amylases (Jiao *et al.*, 1993; Serrato & Cejudo, 2003; Wong *et al.*, 2004). Barley seeds contain two forms each of Trx h and NTR that have an overlapping spatio-temporal appearance and can interact interchangeably (Maeda *et al.*, 2003; Shahpiri *et al.*, 2008, 2009).

NTRs are members of the family of pyridine nucleotide-disulfide oxidoreductases (Pai, 1991) and contain two Ross-

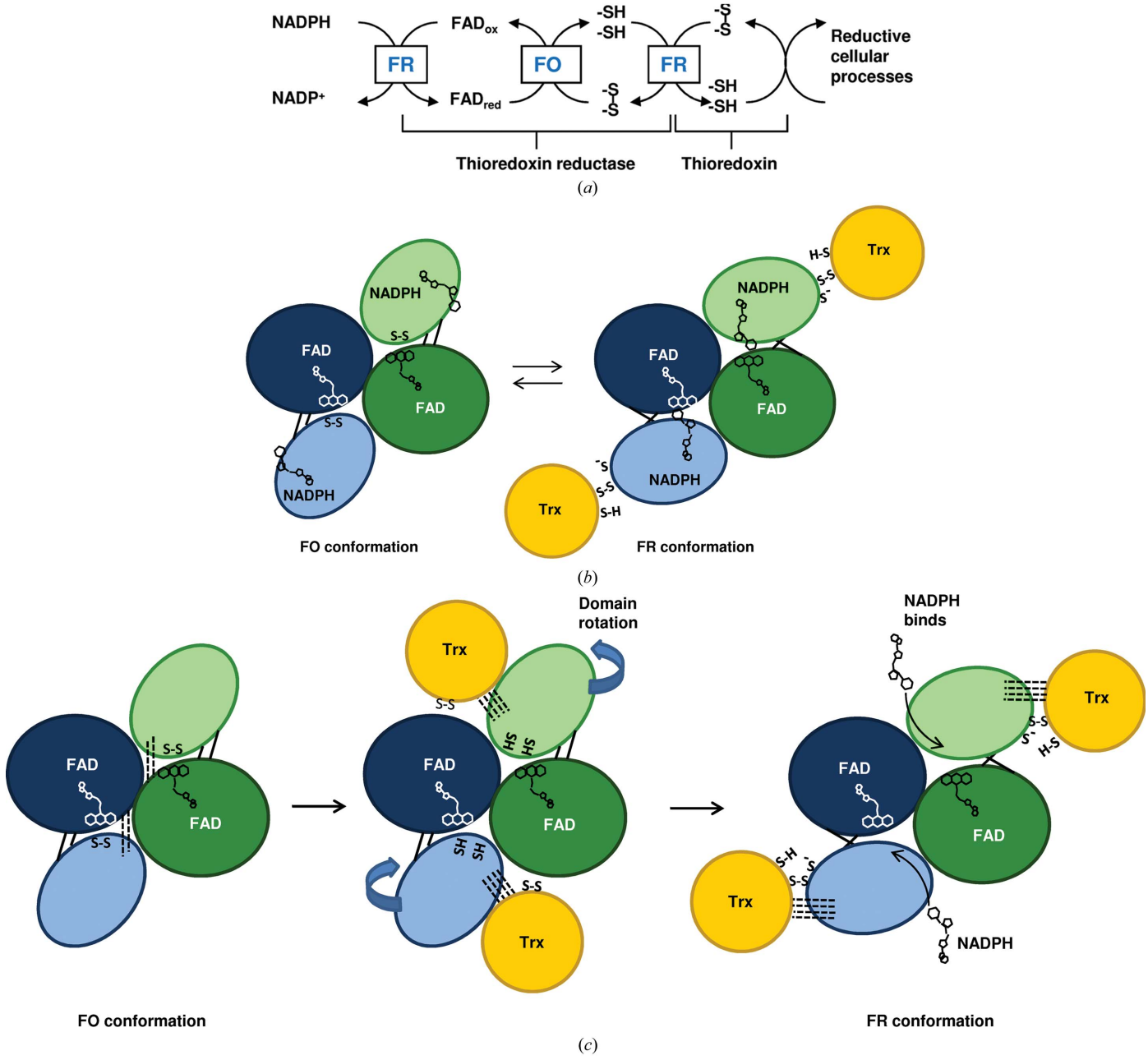

Figure 1
(*a*) Reaction catalyzed by NTR. Reducing equivalents are transferred from NADPH to FAD bound to NTR. From FAD they are transferred to a disulfide bond in the NADPH domain of NTR and further to a disulfide in the Trx substrate. In order to catalyze the entire reaction, NTR needs to swap between two conformations: the flavin-oxidizing (FO) and flavin-reducing (FR) conformations. The electron transfer linked to each conformation is framed. (*b*) A schematic view of the FO and FR conformations as proposed by Waksman *et al.* (1994). The two subunits in each NTR dimer are shown in blue and green, respectively. The darker coloured ovals symbolize the FAD domains, while the lighter coloured ovals show the NADPH domains. Disulfide and thiols are indicated as S-S and S-H, respectively. The black lines connecting the two domains symbolize the antiparallel β-sheets around which a 66° rotation occurs to bring NTR from the FO to the FR conformation. Thereby, the nicotine amide ring is positioned in proximity to the flavin isoalloxazine-ring system and the dithiols are brought to the surface of the protein where they can reduce Trx (shown in yellow). (*c*) The NTR reaction scheme modified to take the observation of differences in inter-domain interactions and lack of space for NADPH binding in the *Hv*NTR2 crystal structure into account. Hydrogen bonds are shown by dotted lines. Trx interaction is required for breakage of inter-domain contacts in the FO conformation and domain reorientation, and NADPH/NADP$^+$ is assumed not to bind during domain reorientation.

mann-type domains that bind FAD and NADPH, respectively. NTRs from mammals and other higher eukaryotes are closely related to GR and are relatively rigid homodimeric proteins of >50 kDa. Each subunit contains three domains, of which the C-terminal domain forms the subunit interface (Manstein *et al.*, 1988; Waksman *et al.*, 1994; Williams *et al.*, 2000). Bacteria, yeast and plant NTRs (~35 kDa) also contain two Rossmann-type nucleotide-binding domains, but they lack the extra C-terminal domain. A subgroup of larger (51–58 kDa) chloroplastidial NTRs contain an extra C-terminal domain with a Trx-like active-site motif CGPC (Alkhalfioui *et al.*, 2007; Serrato *et al.*, 2004). This domain is not related to the C-terminal domain found in NTRs from higher eukaryotes and its presence defines the plant NTR-C subtype.

In the NTR-mediated reactivation of Trx, electrons are transferred from NADPH to Trx *via* a tightly bound FAD and a disulfide bridge (Mustacich & Powis, 2000). The active-site disulfide is found in the FAD domain in NTRs from higher eukaryotes and GRs and electron transfer occurs without any major structural changes. However, in the low-molecular-weight NTRs the disulfide is located in the NADPH domain and in the first crystal structure of the enzyme it is inaccessible to Trx in the so-called flavin-oxidizing conformation (FO), in which FAD is oriented for transfer of electrons to the NTR disulfide (Kuriyan *et al.*, 1991).

It was proposed that a 66° rotation about two β-strands connecting the FAD and the NADPH domains could expose the active-site cysteines and bring them into contact with the Trx active site and at the same time bring the FAD isoalloxazine into contact with NADPH for reduction (Waksman *et al.*, 1994; Fig. 1*b*). The crystal structure of *Escherichia coli* NTR (*Ec*NTR) cross-linked to Trx demonstrated that the proposed reaction mechanism was indeed plausible (Lennon *et al.*, 2000). The complex illustrates how FAD is oriented for reduction by NADPH and the reduced active-site cysteines exposed for Trx binding in the so-called flavin-reducing (FR) conformation. In a previous study, Lennon and Williams showed that no single step in the reductive half-reaction of NTR was solely rate-limiting in turnover and reported a slight decrease in the observed rate constant for the rate-limiting step as a function of NADPH concentration. They proposed the FO to FR conformational change to be rate-limiting (Lennon & Williams, 1997).

Fifteen low-molecular-weight NTR structures have been deposited in the PDB; five of these are structures of *Ec*NTR (Kuriyan *et al.*, 1991; Lennon *et al.*, 1999, 2000; Waksman *et al.*, 1994). Eight other bacterial NTRs have had their structures determined (Akif *et al.*, 2005; Gustafsson *et al.*, 2007; Hernandez *et al.*, 2008; Ruggiero *et al.*, 2009 and the unpublished deposition 2q7v; D. A. R. Sanders, J. Obiero, S. A. Bonderoff & M. M. Goertzen), while only one yeast (Zhang *et al.*, 2009) and one plant NTR, the *Arabidopsis thaliana* NTR-B (*At*NTR-B; Dai *et al.*, 1996), have been deposited. All deposited structures, except for the *Ec*NTR–Trx complex and the structure of *Thermoplasma acidophilum* NTR, which apparently does not need NADPH as an electron donor, show an NTR in the FO conformation.

The present analysis of the structural and functional properties of plant NTRs reports the structure of barley (*Hordeum vulgare*) NTR2 (*Hv*NTR2), the first structure of a monocot NTR, which moreover falls into a distinct phylogenetic class of NTRs (Shahpiri *et al.*, 2008). The overall structure of *Hv*NTR2 is found to be the same as previously reported for *Ec*NTR and *At*NTR-B, but has a different relative orientation of the FAD and NADPH domains which would interfere with NADPH binding as defined by the structure of *Ec*NTR with bound $NADP^+$ or $AADP^+$ (Lennon *et al.*, 2000; Waksman *et al.*, 1994). The results lead to the proposal that domain reorientation facilitated by binding of Trx to the NTR FO state precedes the binding of NADPH.

2. Experimental procedures

2.1. Protein expression and purification

Recombinant *Hv*NTR2 was expressed in *E. coli* Rosetta (DE3) (Novagen) with an N-terminal His tag MGSSHHHHHHSSGLVPRGSH as described previously (Shahpiri *et al.*, 2008). More specifically, His_6-*Hv*NTR2 was purified on a HisTrap HP affinity column (GE Healthcare) pre-equilibrated with 10 m*M* imidazole, 0.5 *M* NaCl and 30 m*M* Tris–HCl pH 8.0 and eluted with a 0–100% gradient of 400 m*M* imidazole, 0.5 *M* NaCl and 30 m*M* Tris–HCl pH 8.0. Finally, the protein was dialyzed against 10 m*M* Tris–HCl pH 8.0, the purity was checked by SDS–PAGE and the sample was concentrated on an Amicon Ultra centrifugal filter unit (10 kDa molecular-weight cutoff; Millipore) to an OD_{280} of 3.96, which corresponds to a concentration of approximately 2.5 mg ml^{-1}. The His_6-*Hv*NTR2 solution was used for crystallization experiments without further purification and was not subjected to thrombin cleavage.

2.2. Crystallization and data collection

Initial crystallization screening experiments were carried out using the PEG 6000 Grid Screen (Hampton Research) and the hanging-drop vapour-diffusion method. Drops of 2.0 µl protein solution were mixed with 2.0 µl reservoir solution and equilibrated over a 500 µl reservoir. Yellow needles were detected in 5%(*w*/*v*) PEG 6000 (Fluka) and 0.1 *M* citrate buffer pH 4.0 after 4 d of incubation at 295 K. Fine-tuning of crystallization conditions included screening of the PEG concentration, the effect of the PEG molecular weight and use of the Hampton Research Additive Screen. The optimized conditions consisted of 24%(*w*/*v*) PEG 400, 2% Jeffamine M-600, 0.1 *M* citrate buffer pH 3.5, a protein concentration of 5.7 mg ml^{-1} and an incubation temperature of 298 K. These conditions gave bright yellow crystals with hexagonal morphology within a week. The diameter of the crystals could reach 0.18 mm. The crystals were flash-frozen directly from the drop without using additional cryoprotectants.

The final X-ray data set was collected at 100 K on the ID14-2 beamline at ESRF in Grenoble using a wavelength of 0.933 Å. A total of 120 frames were collected, each covering an oscillation width of 0.5°. The data were indexed and inte-

grated using *MOSFLM* (Leslie, 1992) and scaled using the program *SCALA* from the *CCP*4 suite (Collaborative Computational Project, Number 4, 1994). The best crystal diffracted to a resolution of 2.6 Å and belonged to space group $P6_222$, with unit-cell parameters $a = b = 133.7$, $c = 166.1$ Å. Assuming the presence of two molecules in the asymmetric unit gave a Matthews coefficient of 2.90 Å^3 Da^{-1} (Matthews, 1968). Final data-collection and processing statistics are summarized in Table 1.

2.3. Structure determination and refinement

Molecular replacement was performed with the program *MOLREP* (Vagin & Teplyakov, 2000) from *CCP*4 using the structure of *At*NTR-B as the initial search model. The *Hv*NTR2 and *At*NTR-B sequences are 75% identical. Significant molecular-replacement solutions were only found when the FAD and the NADPH domains were used as independent search models. The model was first refined using *REFMAC*5 (Murshudov *et al.*, 1997) and at later stages using *Phenix* (Adams *et al.*, 2002) and including TLS refinement interspaced with manual model rebuilding in *Coot* (Emsley & Cowtan, 2004) using the *Coot* validation procedures and *MolProbity* (Davis *et al.*, 2007) to correct problematic areas of the model. The final model had an $R_{\rm cryst}$ of 19.0% and an $R_{\rm free}$ of 23.8% based on 5% of the reflections. The $R_{\rm free}$ reflections were picked by random selection of reflections. The two molecules in the asymmetric unit, which do not represent the functional dimer, were divided into five TLS segments each using the *TLSMD* server (Painter & Merritt, 2006). The TLS segments in molecule *A* in the asymmetric unit are residues 6–71, 72–127, 128–181, 182–258 and 259–323. In molecule *B* the TLS segments cover residues 5–60, 61–127, 128–168, 169–255 and 256–323. The two first TLS segments in each molecule belong to the FAD domain, the following two belong to the NADPH domain and the last segment corresponds to the C-terminus of the FAD domain. Owing to the limited resolution of the data, only 48 solvent molecules were included and only where $F_{\rm obs} - F_{\rm calc}$ electron density of $>3\sigma$ with optimal hydrogen-bonding distances to hydrogen donors or acceptors was found. Four citrate molecules were included in excess electron density owing to the appropriate size and geometry of this molecule and the presence of citrate in the crystallization conditions. Two citrate ions are bound in each NADPH domain. Some excess $2F_{\rm obs} - F_{\rm calc}$ electron density in the active site adjacent to the FAD isoalloxazine could not be satisfactorily modelled by solvent or citrate. Parameters for the refined model are summarized in Table 1. Solvent accessibility was calculated using *AREAIMOL* from the *CCP*4 suite with a 1.4 Å radius probe (Collaborative Computational Project, Number 4, 1994). Differences in domain orientation were analyzed using the *DynDom* server (Hayward & Lee, 2002). Superpositions were performed in *Coot* (Emsley & Cowtan, 2004). Inter-domain and ligand interactions were plotted using the program *LIGPLOT* (Wallace *et al.*, 1995). The molecular coordinates and structure factors have been deposited in the Protein Data Bank under the accession code 2whd.

Table 1
Data-collection and refinement statistics.

Values in parentheses are for the highest resolution bin.

Data collection	
Resolution (Å)	49.9–2.60 (2.74–2.60)
No. of unique reflections	27423 (3937)
Redundancy	7.1 (7.3)
Completeness (%)	99.6 (99.6)
$R_{\rm merge}$† (%)	6.6 (35.0)
$\langle I/\sigma(I)\rangle$	18.4 (4.4)
Wilson *B* factor (Å^2)	59.8
Refinement	
No. of amino-acid residues	635
No. of water molecules	48
$R_{\rm cryst}$‡ (%)	19.0
$R_{\rm free}$‡ (%)	23.8
Estimated coordinate error (Å)	0.33
R.m.s.d. from ideal geometry	
Bonds (Å)	0.011
Angles (°)	1.329
B factors (Å^2)	
Protein (chain *A*/chain *B*)	59.2/60.9
FAD	39.3
Solvent	43.8
Ramachandran plot	
Most favoured (%)	82.8
Additionally allowed (%)	16.1
Generously allowed (%)	1.1
Disallowed (%)	0.0

† $R_{\rm merge} = \sum_{hkl}\sum_i |I_i(hkl) - \langle I(hkl)\rangle| / \sum_{hkl}\sum_i I_i(hkl)$, where $\langle I(hkl)\rangle$ is the mean intensity of i reflections with intensity $I_i(hkl)$. ‡ $R_{\rm cryst} = \sum_{hkl} ||F_{\rm obs}| - |F_{\rm calc}|| / \sum_{hkl} |F_{\rm obs}|$, where $F_{\rm obs}$ and $F_{\rm calc}$ are observed and calculated structure factors, respectively. For $R_{\rm free}$, the sum is extended over a subset of reflections (5%) that were excluded from all stages of refinement.

3. Results and discussion

3.1. Structure quality

The final model of *Hv*NTR2 contains two molecules in the asymmetric unit, covering residues 6–323 (chain *A*) and 5–323 (chain *B*). The numbering refers to the amino-acid sequence of wild-type *Hv*NTR2. The biologically relevant dimer, inferred by analogy to the *E. coli* NTR system, is formed around the crystallographic twofold axis. The structure was determined at 2.6 Å resolution and refined to an $R_{\rm cryst}$ of 19.0% and an $R_{\rm free}$ of 23.8%. One FAD molecule with well defined electron density and *B* factors (∼40 Å^2) comparable to the surrounding protein is present in each subunit. NADPH did not fit the excess electron density in the expected NADPH-binding pocket. Instead, the density fitted reasonably well to a citrate molecule accidentally present from the crystallization conditions (real-space *R* factor = 0.7–0.9). High *B* factors but continuous main-chain electron density is found in the N-terminus (residues 6–12), the loop between A1 and B3 (residues 33–35), B5 and surrounding loops (residues 96–105), the loop between B10 and B11 (residues 153–158), B12 and surrounding loops (residues 174–196) and B15 and surrounding loops (residues 220–245) (Supplementary Fig. 1[1]).

[1] Supplementary material has been deposited in the IUCr electronic archive (Reference: BE5129). Services for accessing this material are described at the back of the journal.

Table 2
Inter-domain contacts in the FO states of *Ec*NTR (PDB code 1tde, no NADPH bound), *At*NTR-B and *Hv*NTR2.

	NADPH domain	FAD domain	Hinge region	Distance (Å)	Interaction type
*Ec*NTR	Gly129	Thr47		3.1	Hydrogen bond
	Arg130	Glu48		3.0	Hydrogen bond
		Gln42	Ala116	3.1	Hydrogen bond
	Gly129	Thr47		3.9	van der Waals
	Phe142	Glu50		3.3/3.9/3.8	van der Waals
*At*NTR-B	Trp140	Thr53		2.7	Hydrogen bond
	Asn141	Thr53		3.1	Hydrogen bond
		Gln50	Ala124	2.9	Hydrogen bond
	Lys125		Glu258	3.4	van der Waals
*Hv*NTR2		Tyr273	His255	3.1	Hydrogen bond
	Arg127		Glu256	3.3	Hydrogen bond
	Arg127		Glu256	3.8	van der Waals
		Arg300	His255	3.7/3.7	van der Waals
		Asn45	Val125	3.8	van der Waals
		Ile47	Val125	3.8	van der Waals

The highest *B* factors were found in the C-terminal part of the FAD domain. The two molecules in the asymmetric unit can be superimposed with an r.m.s.d. of 0.1 Å for C^{α} atoms. The largest differences are found in the C-terminal part of the FAD domain and especially in the loop between β-strands B18 and B19. Structure-quality parameters are summarized in Table 1.

3.2. Overall structure

As in other low-molecular-weight NTRs, *Hv*NTR2 forms a homodimer with each subunit having two domains: the FAD and the NADPH domain. The two domains are quite similar, with 82 superimposable C^{α} atoms giving a root-mean-square deviation of 2.4 Å. The FAD domain consists of residues 1–126 and 255–331 and has an α/β structure comprised of a central five-stranded parallel β-sheet flanked by a four-stranded β-sheet on one side and three α-helices on the other (Fig. 2 and Supplementary Fig. 2). The NADPH domain consists of amino-acid residues 127–254; here, a similar five-stranded parallel β-sheet is flanked by a three-stranded β-sheet on one side and two α-helices plus a third short α-helix containing the active-site cysteines on the other side of the sheet. The two domains are connected by two antiparallel β-strands (amino-acid residues 124–126 and 255–257), which as per tradition are assigned to the FAD domain (Fig. 2). Only a few inter-domain interactions stabilize the relative orientation of the two domains (see §3.7 and Table 2).

3.3. General NTR features

The overall structure of *Hv*NTR2 is the same as the structure of other low-molecular-weight NTRs. Superposition of *Hv*NTR2 C^{α} atoms with the structure of *At*NTR-B shows that that they are quite comparable, with root-mean-square deviations of 0.7 and 1.0 Å for the FAD and NADPH domains, respectively (calculated as least-square deviations using *Coot*). However, the relative orientation of the two domains in *Hv*NTR2 is quite different from their orientation in *At*NTR-B and other low-molecular-weight NTRs in the FO conformation (Fig. 2); the difference in orientation of the NADPH and FAD domains can be described by a 38.2% closure, a 1.0 Å translation and a 24.7° rotational twist. The rotation is centred about amino-acid residues 124–125 and 255–256, which are found in the short two-stranded β-sheet connecting the two domains, and shifts the orientation of the FAD molecule with respect to the active-site cysteines. The distance from Cys148 to the nearest reducing nitrogen in the isoalloxazine rings is increased from the 3.4 Å observed in the structure of *At*NTR-B to 5.9 Å, the solvent accessibility of the FAD molecule is increased by 450% and that of the active-site disulfide is increased by 66%. The dimer assembly is not affected by the changed subunit conformation and FAD can still be reduced by NADPH as judged from the bleaching of the otherwise bright yellow colour of the crystals when they are subjected to a concentration of 10 m*M* NADPH for 30 min.

When the structure of *At*NTR-B is compared with that of the *Ec*NTR in the FR state (PDB code 1f6m), they differ by a minor translation of 1 Å and by a

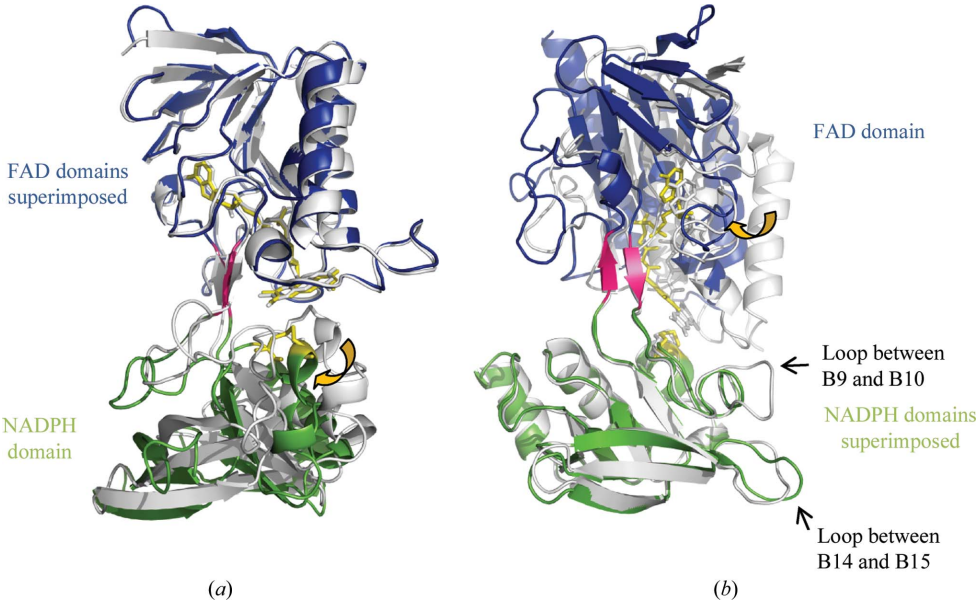

Figure 2
(*a*) Superposition of the FAD domains of *Hv*NTR2 (blue) and *At*NTR-B (white; PDB code 1vdc). The NADPH domains (green) were not included in the superposition. The *Hv*NTR2 FAD and the disulfide bridge are shown in yellow and the β-strand linker is shown in pink. (*b*) Superposition of the NADPH domains of *Hv*NTR2 (green) and *At*NTR-B (white; PDB code 1vdc). Yellow arrows indicate the relative change in domain arrangement between the two structures.

substantial 65.6° rotation about the two β-strands connecting the domains. However, comparing the structure of *Ec*NTR in the FR conformation with the structure of *Hv*NTR2 shows that they differ by a 6.7% closure, a translation of −1.4 Å and a rotation of 49.8°. The smaller rotation of 49.8° compared with 65.6° indicates that *Hv*NTR2 is actually closer to the FR conformation than other crystallized NTRs, which have all been in the FO conformation. Yet, within the group of NTR structures determined in the FO conformation there are minor variations in the relative orientation of the two domains. Superposition with *Ec*NTR requires an 8° inter-domain rotation for both *At*NTR-B and *Saccharomyces cerevisiae* NTR (*Sc*NTR; Zhang *et al.*, 2009) and an 11° rotation in the case of *Mycobacterium tuberculosis* NTR (*Mt*NTR; Akif *et al.*, 2005),

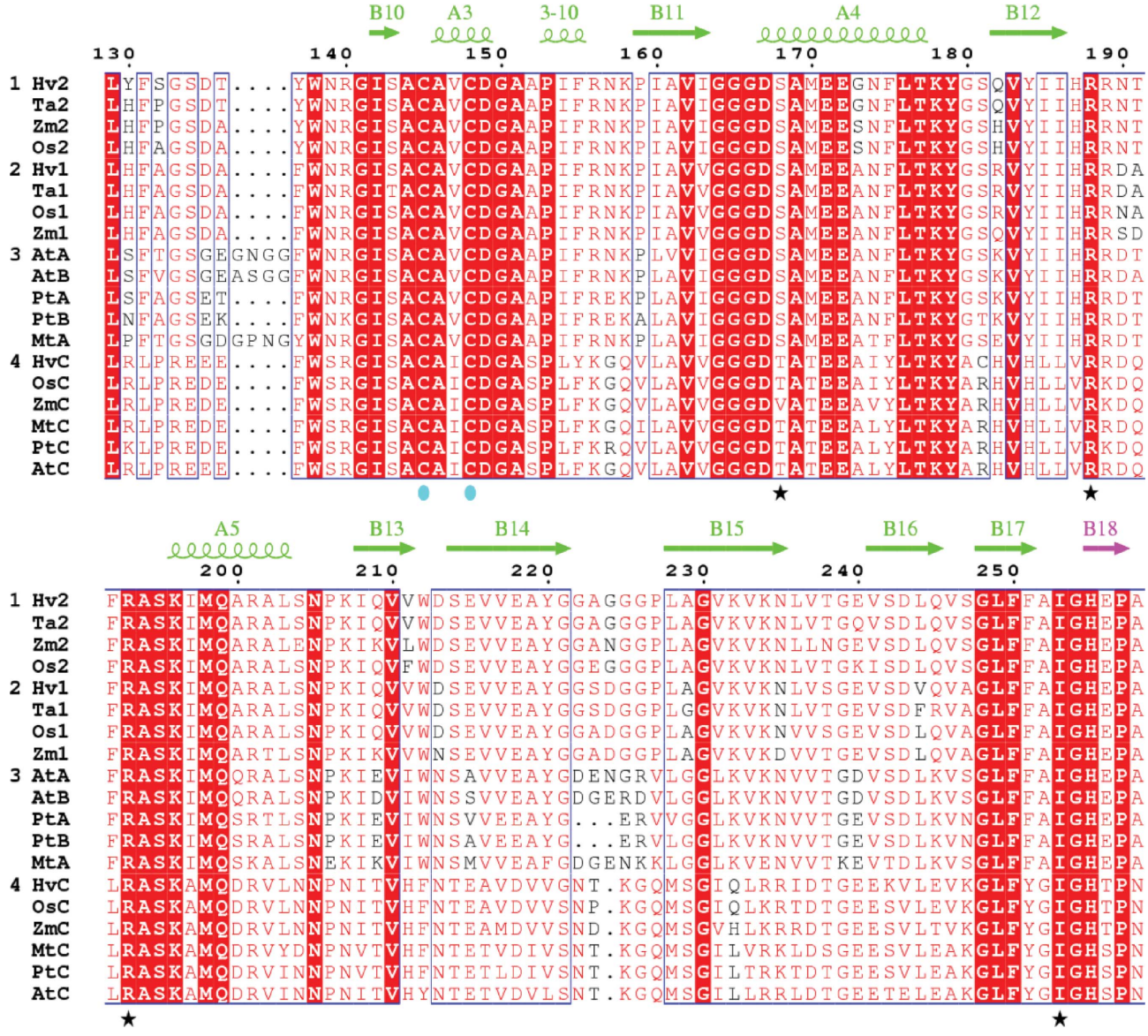

Figure 3
Segment of a sequence alignment of NTRs from different plants covering the two variable-loop segments in plant NTRs. The complete alignment can be found in Supplementary Fig. 1. The NTRs, with their accession numbers given in parentheses, are *Hv*NTR1 (EU314717), *Hv*NTR2 (EU250021) and *Hv*NTRC from *Hordeum vulgare* (barley); *Ta*NTR1 (Q8VX47) and *Ta*NTR2 (TC297680) from *Triticum aestivum* (wheat); *Os*NTR1 (Q69PS6), *Os*NTR2 (Q6ZFU6) and *Os*NTRC (Q70G58) from *Oryza sativa* (rice); *Zm*NTR1 (EU966898), *Zm*NTR2 (BT054285) and *Zm*NTRC (BT037345) from *Zea mays* (maize); *At*NTRA (Q39242), *At*NTRB (Q39243) and *At*NTRC (O22229) from *Arabidopsis thaliana* (mouse-ear cress); *Pt*NTRA (AC149479), *Pt*NTRB (XM_002317595) and *Pt*NTRC (XM_002308899) from *Populus trichocarpa* (western balsam poplar); and *Mt*NTRA and *Mt*NTRC from *Medicago truncatula* (barrel medic, a legume). The sequences were aligned using *ClustalW* (Thompson *et al.*, 1994) and divided into four groups based on the phylogenetic analysis. Groups 1 and 2 are both monocotyledon subgroups of the A/B type, group 3 is the dicotyledon type A/B and group 4 is the subgroup of the C-type NTRs. Strictly conserved residues have a red background and residues that are well conserved within a group according to the Risler matrix (Risler *et al.*, 1988) are indicated by red letters. Residues conserved between groups are boxed. The secondary structure of *Hv*NTR2 was added using *ESPript* (Gouet *et al.*, 1999) and coloured according to domain: the NADPH domain is in green and the β-sheet linker between the two domains is in pink. Residues assumed to make hydrogen bonds to NADPH are marked by stars and the active-site cysteines are marked by cyan circles. The B9–B10 and the B14–B15 loops show the largest structural variation in a superposition of the *Hv*NTR2 and the *At*NTR-B structures. The primary structure of *At*NTR-B differs from the validated Q39243 sequence at positions 120 (I→T), 135 (V→A), 136 (L→S) and 329 (E→Q).

indicating that the relative position of the two domains in the absence of a target substrate is quite flexible. A room-temperature structure of *At*NTR-B has been reported to be 2° off with respect to the relative orientation of the two domains compared with the deposited 98 K data (Dai *et al.*, 1996). Unfortunately, the coordinates from the room-temperature study have not been deposited in the PDB and it is not possible to relate this to the structural variation that we observe in *Hv*NTR2.

3.4. Plant-specific NTR motifs

The structure of *At*NTR-B is the only other plant NTR structure reported to date. As mentioned previously, the two proteins have 75% sequence identity. A superposition of the FAD domains (Fig. 2*a*) shows a very similar orientation of loops, α-helices and β-sheets and the aforementioned variation in relative domain orientation. Some major structural differences are observed in two loop regions when the NADPH domains alone are superimposed (Fig. 2*b*). The long loop region between strand B9 and B10 contains four additional residues in *At*NTR and therefore has a protrusion. This loop has the sequence S/N/P-F-T/V/A-G-S-G/E-E/K/T/D-G/A-N/P/S-G/N-G in dicot NTRs (the four extra residues are missing in *Populus trichocarpa*), while monocot NTRs of the A/B type have a H/Y-F-S/P/A-G-S-D-T/A sequence (Fig. 3 and Supplementary Fig. 2). The second variable loop is located between β-strands B14 and B15. This loop is glycine-rich in *Hv*NTR2 and other monocot NTRs, in which a G-G-A/E/S-N/G/D-G-G-P-L-A/G motif is found. The corresponding loop in dicots appears to be variable in sequence and length. Both loops are expected to face the incoming Trx substrate molecule (Fig. 4).

The sequence combination in the two loops appears to vary between isoforms from the same species and the combined effect of the variation in the loops might result in the observed species-dependent interaction between NTR and Trx (Jacquot *et al.*, 1994; Rivera-Madrid *et al.*, 1995; Shahpiri *et al.*, 2008) and could indicate that Trx substrate specificity could be somewhat differentiated *via* these loops. All monocots included in the phylogenetic analysis of the plant NTRs have two low-molecular-weight NTRs of the A/B-type clustering in different subgroups (Fig. 3 and Supplementary Fig. 2). In contrast, dicot NTRs of the A/B type appear to be more similar and are not subdivided. Both monocots and dicots express a single NTR of the C type, which has been characterized as chloroplast-specific (Alkhalfioui *et al.*, 2007; Serrato *et al.*, 2004).

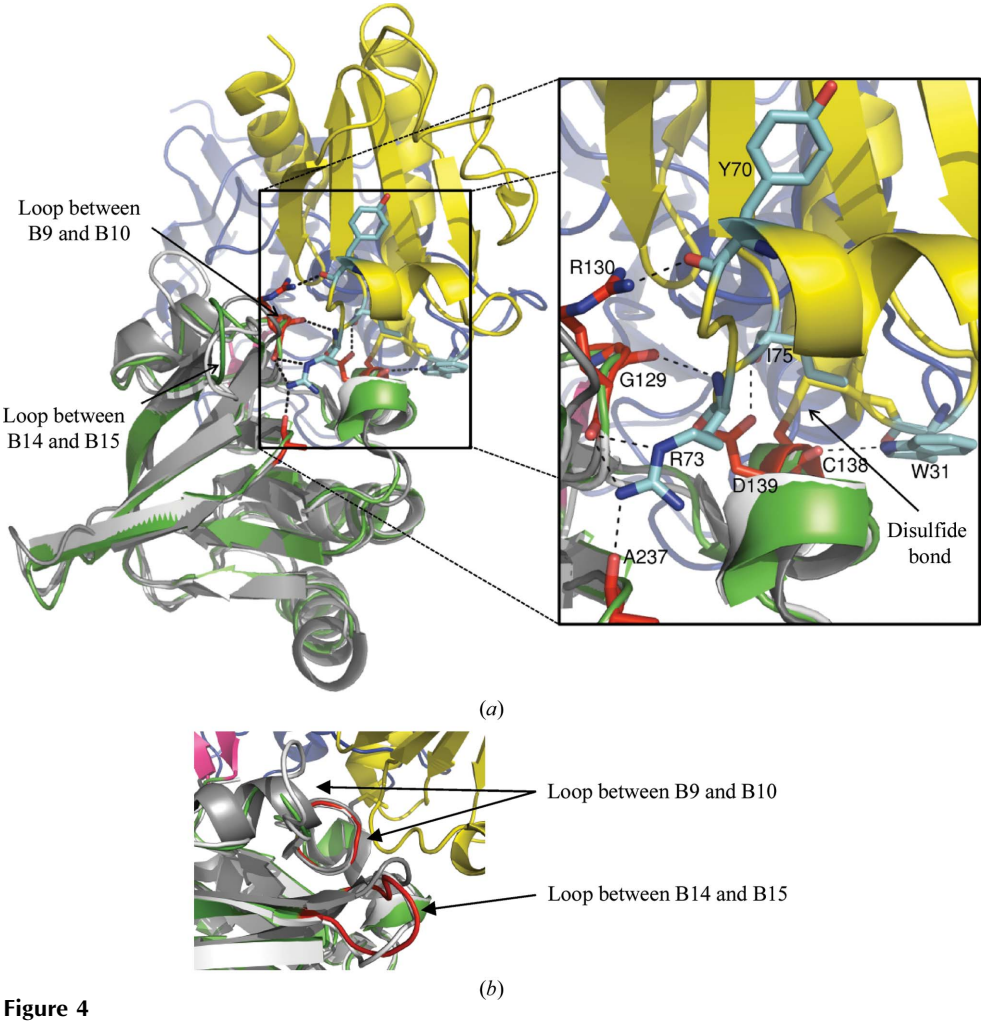

Figure 4
Superposition of the NADPH domains of *Hv*NTR2, *At*NTR-B (white; PDB code 1vdc) and *Ec*NTR in the FR conformation (grey; PDB code 1f6m) covalently bound to Trx (yellow). *Hv*NTR2 is coloured according to domain, with the FAD domain in blue, the NADPH domain in green and the β-sheet linker between the two domains in pink. (*a*) The hydrogen bonds between residues in *Ec*NTR (red) and Trx (cyan) are indicated by dotted lines. (*b*) Cartoon representation focused on the two loop areas with the largest structural variations. The loops of *Hv*NTR2 are coloured red.

3.5. FAD binding

The FAD-binding domain encloses the FAD between its two nonsequential halves, with the FMN part buried in the first half of the domain. Both hydrogen bonds (eight amino-acid residues contributing ten hydrogen bonds; Ser18, Ala21, Ile27, Gln52, Asn61, Val94, Asp293 and Ala302) and van der Waals interactions (involving 25 amino-acid residues) contribute to FAD binding. The hydrogen-bonding residues are conserved among the plant NTRs but are not conserved among all NTRs (Supplementary Fig. 2). Only a

few conservative substitutions are found among the van der Waals interacting residues, *e.g.* *At*NTR-B residues Val14 and Ile120 are substituted by *Hv*NTR2 residues Ile16 and Thr122, respectively.

3.6. NADPH binding

The binding of $NADP^+$ to *Ec*NTR in the FO conformation (PDB code 1tdf) was used for comparison with the potential NADPH-binding pockets of *At*NTR-B and *Hv*NTR2. The residues involved in the binding of $NADP^+$ in *Ec*NTR and potentially in *Hv*NTR2 and *At*NTR-B are listed in Supplementary Table 1. All of the likely NADPH-binding residues are identical in *Hv*NTR2 and *At*NTR-B and only a few conservative substitutions are found when compared with the actual binding pocket of *Ec*NTR.

A sulfate ion was found in the NADPH-binding pocket in the *At*NTR-B crystal structure and the partly occupied NADPH molecule also found in the pocket was in a distorted NADPH-binding mode. The likely binding of a citrate ion in the *Hv*NTR2 NADPH-binding pocket not only occludes NADPH binding but could also be the cause of the observed change in the relative domain orientation, which obstructs any possibility of NADPH binding owing to spatial limitations. Also, the unassigned electron density below the isoalloxazine-ring system in the *Hv*NTR2 structure might influence the twist and closure in the domain structure.

The overall charge distributions and shapes of the *Ec*NTR and *Hv*NTR2 NADPH-binding pockets were examined and showed very similar charge distributions, with a large number of positive charges matching the negative charges of the NADPH phosphates. However, the superposition also showed that there is not enough space in the *Hv*NTR2 NADPH pocket to accommodate the ribose moiety of $NADP^+$ owing to the changed orientation of the FAD domain. Thus, if *Hv*NTR2 represents an intermediate between the FO and the FR states, NADPH would have to undergo a considerable conformational change during catalysis. It appears likely that NADPH binds following the conformational change, which would also be in agreement with the previously observed slight decrease in the observed rate constant for the domain reorientation event with increasing NADPH concentration (Lennon & Williams, 1997). The NADPH-binding pocket is fully solvent-accessible in the FR conformation (PDB code 1f6m). However, it is also possible that the observed domain orientation only reflects the binding of citrate in the active site and therefore is of no relevance to the reaction mechanism.

3.7. Inter-domain contacts

The inter-domain contacts in the FO conformation were mapped for *Ec*NTR (PDB code 1tde), *At*NTR-B and *Hv*NTR2 (Table 2). The hydrogen bonds between the two domains in *Ec*NTR originate from the loop between strands B9 and B10. Here, Gly129 and Arg130 form bonds to Thr47 and Glu48, respectively, in the FAD domain (Table 2 and Fig. 5). A third hydrogen bond connects Gln42 from the FAD domain to Ala116 in the hinge region. The inter-domain contacts are dislocated by two residues in *At*NTR-B, but involve the same loop. Here, Trp140 and Asn141 from the NADPH domain form hydrogen bonds to Thr53 in the FAD domain. As in *Ec*NTR, a third hydrogen bond between Gln50 and Ala124 connects the FAD domain to the hinge region. The residues involved in hydrogen bonds between domains are conserved in the *Hv*NTR2 and *At*NTR-B primary

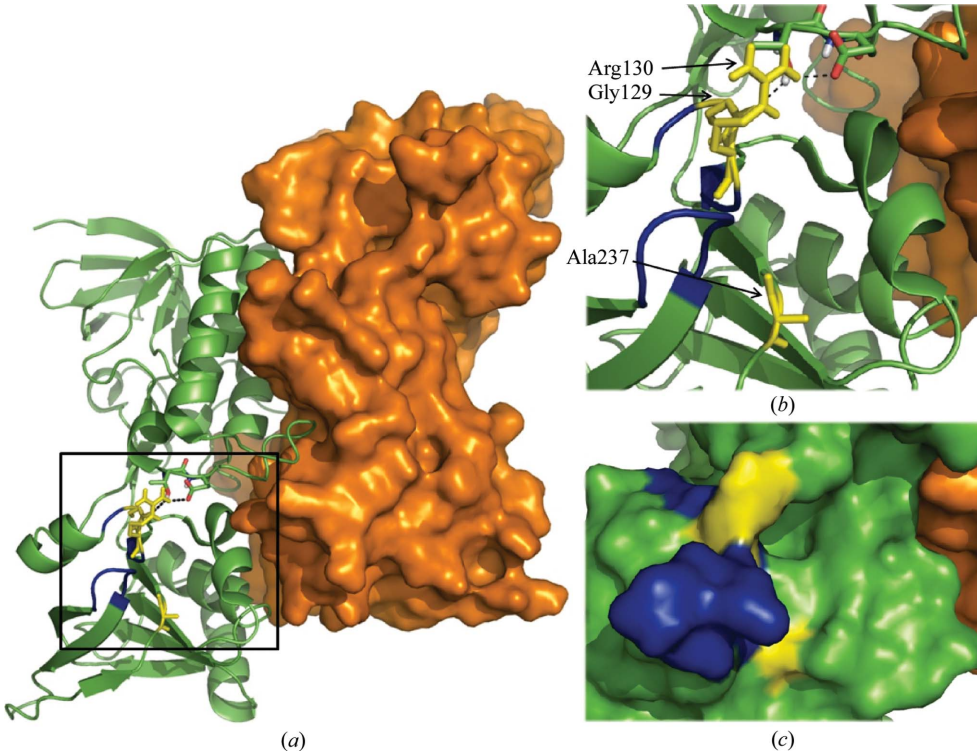

Figure 5
Thioredoxin-binding patch defined by the covalent *Ec*NTR–Trx complex. (*a*) The *Ec*NTR dimer in the FO conformation (PDB code 1tde). One subunit is shown in green and the solvent-accessible surface of the other is shown in orange. Residues Gly129 and Arg130 in the NADPH domain form the only hydrogen bonds to the FAD domain in the FO conformation. These residues (yellow) together with Ala237 provide all five of the hydrogen bonds formed upon Trx binding to the FR conformation. The residues interacting in the dimer interface are adjacent to the two loops (blue) that possibly provide some selectivity towards Trx isoforms. The association of Trx with this area prior to the conformational shift would break the inter-domain hydrogen bonds and thereby facilitate the shift. (*b*) A close-up view with hydrogen bonds indicated as dotted lines. (*c*) Solvent-accessible surface of the same area.

sequences, but since the domains are in different relative orientations the same hydrogen bonds cannot be formed. Only two inter-domain hydrogen bonds are found in *Hv*NTR2, both of which are mediated through the hinge region.

Nonbonded (van der Waals) interactions are located in the Gly129 and Thr47 area in *Ec*NTR and there are additional interactions between residue Phe142 in α-helix A3 carrying the active cysteines and Glu50 in the FAD domain. In *At*NTR-B the only inter-domain van der Waals interaction is between Glu258 in the hinge region and Lys125 located very nearby in the NADPH domain; similarly, in *Hv*NTR2 the van der Waals interactions are mediated through the hinge region only. These are from Glu256 to Arg127 of the NADPH domain, from His255 to Arg300 of the FAD-binding domain and from Val125 to Asn45 and Ile47 of the FAD-binding domain.

3.8. The reaction mechanism

The main inter-domain contacts in the FO conformation in *Ec*NTR and *At*NTR-B are centred on the loop between β-strands B9 and B10. This loop contains an arginine residue (Arg130 in *Ec*NTR) that is conserved in plant NTR sequences (Arg142 in *At*NTR-B and Arg140 in *Hv*NTR2; Fig. 3). It is also found in most NTR sequences from other species, but can be substituted by lysine or asparagine. Arg130 forms three of the seven hydrogen bonds to Trx upon binding of the substrate in the *Ec*NTR FR conformation (PDB code 1f6m). The neighbouring Gly129 and Ala237 within its spatial proximity are each involved in one hydrogen bond to Trx. The last two hydrogen bonds engage the active-site amino-acid residues Cys138 and Asp139 (Fig. 4).

This patch, which adjoins the variable loops in the NADPH domain, supplies all hydrogen bonds specific for Trx binding besides those in the active site. The same area provides the interactions for anchoring of the NADPH domain to the FAD domain in the FO state in both *Ec*NTR and *At*NTR-B. If Trx binds to this patch in the FO conformation, the main anchoring between the domains will be broken and thereby two hydrogen bonds are replaced by four to five new ones in the NTR–Trx interface (Fig. 1*c*). The binding of Trx could be guided by the two variable loops, ensuring binding to the optimal Trx isoform. The loop area is free to interact with Trx as observed for the FO conformation of *Ec*NTR (Fig. 5).

A third loop found between strand B3 and a short 3_{10}-helix has been predicted to bind to Trx (Zhang *et al.*, 2009). Dicot NTRs have a strictly conserved E-G-W-M-A-N-D-I-A-P-G-G sequence in this area, while monocot NTRs display a greater sequence variation and invariably have the proline exchanged for an alanine. The C-type plant NTRs have a loop which is one amino-acid residue shorter in this region and has the consensus motif E-G-Y/C-Q-M/V-G-G-V-P-G-G. Simultaneous binding of Trx to this loop and active-site cysteines would require the NTR domain twist to have occurred.

Association of Trx with the FO conformation prior to NADPH binding might help in defining the NADPH-binding site. Our postulation that Trx breaks the inter-domain contacts as the first part of the reaction mechanism implies that the NTR domain rotation only happens, or only happens sufficiently, when Trx is available and would explain why almost all NTRs crystallized to date have been in the FO conformation. If the structure of *Hv*NTR2 is an intermediate between the FO and the FR conformations, it shows that there is not room for bound NADPH during the domain-rotation step. The conformational change from the FO to the FR state could be part of the mechanism that secures the release of $NADP^+$ from FR.

The authors are grateful to Dr Azar Shahpiri for helpful discussion of the production of recombinant NTR2. The access to synchrotron beam time was made possible by support from DANSCATT. We would like to acknowledge the beamline scientists Juan Weatherby at the ESRF ID14-2 beamline and Xavier Thibault at the ESRF ID23-2 beamline for their assistance during data collection. This project was supported by a DTU PhD stipend to KGK and by the Center for Advanced Food Studies (LMC). PH was supported in part by a grant from the Carlsberg Foundation.

References

Adams, P. D., Grosse-Kunstleve, R. W., Hung, L.-W., Ioerger, T. R., McCoy, A. J., Moriarty, N. W., Read, R. J., Sacchettini, J. C., Sauter, N. K. & Terwilliger, T. C. (2002). *Acta Cryst.* D**58**, 1948–1954.

Akif, M., Suhre, K., Verma, C. & Mande, S. C. (2005). *Acta Cryst.* D**61**, 1603–1611.

Alkhalfioui, F., Renard, M. & Montrichard, F. (2007). *J. Exp. Bot.* **58**, 969–978.

Arnér, E. S. J. & Holmgren, A. (2000). *Eur. J. Biochem.* **267**, 6102–6109.

Collaborative Computational Project, Number 4 (1994). *Acta Cryst.* D**50**, 760–763.

Dai, S., Saarinen, M., Ramaswamy, S., Meyer, Y., Jacquot, J. P. & Eklund, H. (1996). *J. Mol. Biol.* **264**, 1044–1057.

Davis, I. W., Leaver-Fay, A., Chen, V. B., Block, J. N., Kapral, G. J., Wang, X., Murray, L. W., Arendall, W. B. III, Snoeyink, J., Richardson, J. S. & Richardson, D. C. (2007). *Nucleic Acids Res.* **35**, W375–W383.

Emsley, P. & Cowtan, K. (2004). *Acta Cryst.* D**60**, 2126–2132.

Gelhaye, E., Rouhier, N. & Jacquot, J. P. (2003). *FEBS Lett.* **555**, 443–448.

Gelhaye, E., Rouhier, N. & Jacquot, J. P. (2004). *Plant Physiol. Biochem.* **42**, 265–271.

Gouet, P., Courcelle, E., Stuart, D. I. & Métoz, F. (1999). *Bioinformatics*, **15**, 305–308.

Gustafsson, T. N., Sandalova, T., Lu, J., Holmgren, A. & Schneider, G. (2007). *Acta Cryst.* D**63**, 833–843.

Hägglund, P., Bunkenborg, J., Maeda, K. & Svensson, B. (2008). *J. Proteome Res.* **7**, 5270–5276.

Hayward, S. & Lee, R. A. (2002). *J. Mol. Graph. Model.* **21**, 181–183.

Hernandez, H. H., Jaquez, O. A., Hamill, M. J., Elliott, S. J. & Drennan, C. L. (2008). *Biochemistry*, **47**, 9728–9737.

Ishiwatari, Y., Fujiwara, T., McFarland, K. C., Nemoto, K., Hayashi, H., Chino, M. & Lucas, W. J. (1998). *Planta*, **205**, 12–22.

Jacquot, J. P., Rivera-Madrid, R., Marinho, P., Kollarova, M., Le, M. P., Miginiac-Maslow, M. & Meyer, Y. (1994). *J. Mol. Biol.* **235**, 1357–1363.

Jiao, J. A., Yee, B. C., Wong, J. H., Kobrehel, K. & Buchanan, B. B. (1993). *Plant Physiol. Biochem.* **31**, 799–804.

Kuriyan, J., Krishna, T. S., Wong, L., Guenther, B., Pahler, A., Williams, C. H. Jr & Model, P. (1991). *Nature (London)*, **352**, 172–174.
Laurent, T. C., Moore, E. C. & Reichard, P. (1964). *J. Biol. Chem.* **239**, 3436–3444.
Lennon, B. W. & Williams, C. H. Jr (1997). *Biochemistry*, **36**, 9464–9477.
Lennon, B. W., Williams, C. H. J. & Ludwig, M. L. (1999). *Protein Sci.* **8**, 2366–2379.
Lennon, B. W., Williams, C. H. Jr & Ludwig, M. L. (2000). *Science*, **289**, 1190–1194.
Leslie, A. G. W. (1992). *Jnt CCP4/ESF–EACBM Newsl. Protein Crystallogr.* **26**.
Maeda, K., Finnie, C., Østergaard, O. & Svensson, B. (2003). *Eur. J. Biochem.* **270**, 2633–2643.
Manstein, D. J., Massey, V., Ghisla, S. & Pai, E. F. (1988). *Biochemistry*, **27**, 2300–2305.
Matthews, B. W. (1968). *J. Mol. Biol.* **33**, 491–497.
Moore, E. C., Reichard, P. & Thelander, L. (1964). *J. Biol. Chem.* **239**, 3445–3452.
Murshudov, G. N., Vagin, A. A. & Dodson, E. J. (1997). *Acta Cryst.* D**53**, 240–255.
Mustacich, D. & Powis, G. (2000). *Biochem. J.* **346**, 1–8.
Pai, E. F. (1991). *Curr. Opin. Struct. Biol.* **1**, 796–803.
Painter, J. & Merritt, E. A. (2006). *Acta Cryst.* D**62**, 439–450.
Risler, J. L., Delorme, M. O., Delacroix, H. & Henaut, A. (1988). *J. Mol. Biol.* **204**, 1019–1029.
Rivera-Madrid, R., Mestres, D., Marinho, P., Jacquot, J. P., Decottignies, P., Miginiac-Maslow, M. & Meyer, Y. (1995). *Proc. Natl Acad. Sci. USA*, **92**, 5620–5624.
Ruggiero, A., Masullo, M., Ruocco, M. R., Grimaldi, P., Lanzotti, M. A., Arcari, P., Zagari, A. & Vitagliano, L. (2009). *Biochim. Biophys. Acta*, **1794**, 554–562.
Russel, M. & Model, P. (1986). *J. Biol. Chem.* **261**, 14997–15005.
Serrato, A. J. & Cejudo, F. J. (2003). *Planta*, **217**, 392–399.
Serrato, A. J., Perez-Ruiz, J. M., Spinola, M. C. & Cejudo, F. J. (2004). *J. Biol. Chem.* **279**, 43821–43827.
Shahpiri, A., Svensson, B. & Finnie, C. (2008). *Plant Physiol.* **146**, 789–799.
Shahpiri, A., Svensson, B. & Finnie, C. (2009). In the press.
Thompson, J. D., Higgins, D. G. & Gibson, T. J. (1994). *Nucleic Acids Res.* **22**, 4673–4680.
Torre, A. de la, Lara, C., Wolosiuk, R. A. & Buchanan, B. B. (1979). *FEBS Lett.* **107**, 141–145.
Tripathi, B. N., Bhatt, I. & Dietz, K. J. (2009). *Protoplasma*, **235**, 3–15.
Vagin, A. & Teplyakov, A. (2000). *Acta Cryst.* D**56**, 1622–1624.
Waksman, G., Krishna, T. S., Williams, C. H. Jr & Kuriyan, J. (1994). *J. Mol. Biol.* **236**, 800–816.
Wallace, A. C., Laskowski, R. A. & Thornton, J. M. (1995). *Protein Eng.* **8**, 127–134.
Williams, C. H. Jr (1976). *The Enzymes*, edited by P. D. Boyer, Vol. 13, pp. 89–173. New York: Academic Press.
Williams, C. H., Arscott, L. D., Muller, S., Lennon, B. W., Ludwig, M. L., Wang, P. F., Veine, D. M., Becker, K. & Schirmer, R. H. (2000). *Eur. J. Biochem.* **267**, 6110–6117.
Wong, J. H., Cai, N., Tanaka, C. K., Vensel, W. H., Hurkman, W. J. & Buchanan, B. B. (2004). *Plant Cell Physiol.* **45**, 407–415.
Zhang, Z., Bao, R., Zhang, Y., Yu, J., Zhou, C.-Z. & Chen, Y. (2009). *Biochim. Biophys. Acta*, **1794**, 124–128.

Appendix F

Probing molecular interactions between thioredoxin and NADPH-dependent thioredoxin reductase (NTR) through homology modelling and site-directed mutagenesis

Manuscript in preparation

Kristine G. Kirkensgaard[a,b], Per Hägglund[a*], Anette Henriksen[b], Azar Shahpiri[c], Christine Finnie[a] and Birte Svensson[a]

*[a]Enzyme and Protein Chemistry, Department of Systems Biology, Technical University of Denmark, Denmark, [b]Department of Agriculture Biotechnology, College of Agriculture, Isfahan University of Technology, Isfahan, Iran, and [c]Carlsberg Laboratory, Denmark. *E-mail: ph@bio.dtu.dk*

Abstract

Thioredoxins (Trxs) are protein disulfide reductases involved in regulation of a number of important biological processes including seed germination in plants. Trxs, are themselves regulated by the flavoproteins NADPH-dependent thioredoxin reductases (NTRs), which in a multi-step electron transfer process eventually transfer reducing equivalents from NADPH to Trx and return Trx to its active form. NTR needs to shift between two conformations in order to go through a full catalytic cycle: The flavin oxidicing (FO) and the flavin reducing (FR) conformations, respectively. Almost all crystal structures of NTRs are found to be in the FO conformation. We have previously determined the structure of barley NTR2, HvNTR2 in an intermediate conformation. Here we present a complex model between NTR in the FR

conformation and Trx from *Hordeum vulgare*, barley. In this model, the two proteins are covalently bound by an intermolecular disulfide bond between the active site cysteines mimicking a catalytic intermediate. The model has implications for the regulation of Trx activity by low-molecular-weight NTRs and thereby the regulation of the multitude of cellular processes in which Trxs are involved in plants but also in eukaryotes in general.

Introduction

Thioredoxins (Trxs) are small ubiquitous redox proteins involved in essential biological processes such as DNA synthesis, oxidative stress response and apoptosis (Arnér & Holmgren, 2000). Trx are disulfide reductases and activate enzymes like ribonucleotide reductase (Laurent *et al*., 1964; Moore *et al*., 1964), methionine sulfoxide reductase (Russel and Model, 1986) and peroxiredoxins (Tripathi *et al*., 2009) by reduction of disulphide bonds of these enzymes. In non-chloroplastic environments, oxidised Trx is typically recycled enzymatically by NADPH-dependant thioredoxin reductase (NTR), which transfers reducing equivalents from NADPH to Trx *via* a bound FAD and a redox-active disulfide (Williams, 1976). NTRs are members of the family of pyridine nucleotide-disulfide oxidoreductases (Pai, 1991). In plants, Trxs are involved in a wide range of physiological processes including photosynthesis, flowering, seed development, and cell-to-cell communication (Buchanan and Balmer, 2005; Wong *et al*., 2002; Meng *et al*. 2010).

Plants exhibit a unique multigene family thioredoxin system with complex time, tissue and organelle specific expression pattern of a diverse selection of Trx isozymes. (Gelhaye *et al*., 2004; Ishiwatari *et al*., 1998). The occurrence of multigene families in plants is not unique to the Trx-NTR redox couple but is a well-known phenomenon for a large selection of plant proteins and enzymes. The implications of the presence of multigene families in plants are not clear (Gelhaye *et al.*, 2005). At least six different sub-types of Trxs exists in plants, f, m, x, y, h, and o. The cytosolic h-type Trxs play roles during seed germination by reducing disulfides in storage proteins and inhibitors of proteases and α-amylases (Jiao *et al*., 1993; Serrato and Cejudo, 2003; Wong *et al*., 2004), activating the stored proteins and enzymes for mobilisation of metabolites for plant growth. Barley seeds contain two isoforms of both Trx-h and NTR that have overlapping spatiotemporal appearance and can interact

interchangeably *in-vitro* with each other (Maeda *et al*., 2003; Shahpiri *et al*., 2008; Shahpiri *et al*., 2009).

Bacteria, yeast and plants all have low-molecular-weight (LWM) NTRs (~35 kDa) that contain two domains; the FAD domain that has a bound FAD molecule, and the NADPH domain with a NADPH binding site and the active site disulfide. NTR can exist in at least two well-documented conformations i.e. the flavin oxidizing (FO) and the flavin reducing conformation (Figure 1). In the FO conformation, the active site disulfide is buried and positioned in front of the FAD to allow transfer of electrons from the FAD to the disulfide, reducing it to dithiols. When NTR shifts to the flavin reducing (FR) conformation, the dithiols get exposed on the molecular surface and available for reaction with Trx. Furthermore, the FR conformation allows transfer of reducing equivalents from the nicotinamide ring of NADPH (yielding $NADP^+$) to the flavin ring system of FAD reducing it to $FADH_2$ with the gain of two electrons. A 67° rotation about the two β-strands connecting the FAD and the NADPH domains brings the protein from one conformation to the other (Waksman *et al*., 1994; Lennon *et al*., 2000).

The low molecular weight NTR structures deposited in the Protein Data Bank are in the FO conformation with few exceptions; The structure of the two NTRs found to be in the FR conformation are from the Gram-negative bacteria *Campylobacter jejuni* (pdb 3R9U, Osipiuk *et al*., unpublished) and the facultative anaerobe archaea *Thermoplasma acidophilum* (pdb 3CTY, Hernandez *et al*., 2008), the latter is special by apparently not needing NADPH as electron donor. We previously found the HvNTR2 isoform from barley to adopt neither of the FO nor the FR conformation, but have the NADPH domain rotated by 25° and bent by a 38% closure relative to the FAD domain when comparing with NTRs in the FO conformation (Kirkensgaard *et al*., 2009).

A structure of EcNTR covalently bound to EcTrx (Lennon *et al*., 2000), is the only available structure in which the interactions with Trx can be observed. In the present study, a similar complex was modelled between HvNTR2 and one of the two isoforms of the h-type thioredoxins (HvTrxh2) from barley. The model was based on crystal structures of HvTrxh2 (Maeda *et al*., 2006) and HvNTR2 and used the complex of EcNTR and EcTrx as a template for homology modelling. Based on this model, a wide series of mutants of key amino acid residues were produced to assess their roles in Trx recognition and recycling. The model

elucidates how eukaryotic LMW NTRs in general bind Trx, since many of the residues involved are conserved in eukaryotes.

Results and discussion

Building and evaluating a complex model between HvNTR2 and HvTrxh2

A model was constructed of HvNTR2 in the FR conformation covalently bound to HvTrxh2 *via* an intermolecular disulfide between the two active sites, thus mimicking a catalytic intermediate based on the EcNTR:EcTrx complex (pdb 1F6M, Lennon *et al.*, 2000).

Superposition of the final model with the crystal structure of the EcNTR:EcTrx complex (Figure 2) gives an overall r.m.s.d. of 1.12 Å of C^{α}-atoms. The individual r.m.s.d. are 0.94 Å for the FAD domain, 1.04 Å for the NADPH domain, and 1.60 Å for the Trxs, calculated as least-square deviations using Coot (Emsley & Cowtan, 2004). The quality of the model was evaluated by inspecting bond angles and lengths of the protein backbone. The lengths of all examined bonds deviate less than four standard deviations (4σ) from standard bond lengths. Furthermore, backbone dihedral bond angles from Ramachandran plots of the final model showed no outliers (residues with disallowed combinations of psi and phi angles (Ramachandran plots calculated using MOE). Of the 426 residues in total, 398 (93%) are in the most favourable area, whereas 28 residues are within the allowed area

Intermolecular HvNTR2:HvTrxh2 interactions

Identified intermolecular interactions in the complex are shown schematically (Figure 3). The number of atoms involved in the hydrophobic contact between pairs of residues is indicated in Figure 3 by the width of the connecting blue lines.

.

Interactions between HvTrxh2 and the FAD domain of HvNTR2

For the FAD domain of HvNTR2 all but one of the interacting residues are positioned in the FAD-loop (Figure 3A). An alignment of various NTRs (Figure 4A, full alignment in Supplementary data 1) shows that with the exception of the residues $Trp42_{HvNTR2}$ and $Met43_{HvNTR2}$, this sequence is conserved among NTRs from monocot plants. Between NTR

isoforms 1 and 2, only two very conservative substitutions are observed at Trp42 (Trp/Phe) and Met43 (Met/Leu). Among dicot plants Ala49 is replaced by a proline, which could have some consequences for the flexibility and adaptability to different Trx isoforms. However the position of the backbone of the loop is not changed due to this proline (Figure 4B). For NTR-Cs, which are plant NTRs with an integrated Trx located in chloroplasts (Alkhalfioui *et al*., 2007; Serrato *et al.*, 2004), the corresponding sequence, EG(Y/C)Q(M/V)GG-VPGG, is one residue shorter than in the other plant NTRs. The FAD-loop is positioned the same way (Figure 4B) in the available structure of eukaryotic LMW NTRs (HvNTR2 from Kirkensgaard *et al*., 2009; AtNTR-B from Dai *et al*., 2006; and the two structures of NTR from yeast from Zhang *et al*., 2009 and Oliveira *et al*., 2010), and the proline of the dicot AtNTR-B does not change the position of the loop (Figure 4B).

In *Saccharomyces cerevisiae* (yeast), the FAD-loop has the sequence EGMMANGIAA, and was predicted to be involved in the binding of Trx by hydrophobic contacts (Zhang *et al*., 2009). A corresponding sequence is found in LMW NTRs from other eukaryotes as well, e.g. *Aspergillus Niger* (fungus), *Entamoeba histolytica* (anaerobic parasitic protozoan) and *Dictyostelium discoideum* (amoeba), all have varieties of this sequence (Figure 4A). Examples of bacteria containing a similar hydrophobic sequence are also found; the Gram-negative bacteria *Chlamydia trachomatis* has the two residue shorter FAD-loop sequence EGFFSG--IAGG. The corresponding loop of EcNTR is five residues shorter ($_{35}$T-----G<u>M</u>E<u>K</u>GG$_{41}$). It has very little resemblance to the loop of HvNTR2 and it interacts with EcTrx through few hydrophobic contacts (Figure 3B). By contrast, the FAD-loop in HvNTR2 was predicted by the model to interact with HvTrxh2 through multiple hydrophobic contacts, primarily mediated by Trp42$_{HvNTR2}$ and Met43$_{HvNTR2}$ (Figure 3A).

The modelled position of the FAD-loop in HvNTR2:HvTrxh2 is not comparable to the position of the loop in the EcNTR:EcTrx structure (Figure 5). Central in the FAD-loop of HvNTR2 is Met43$_{HvNTR2}$, which fits into a cavity on the surface of HvTrxh2 (Figure 5A and C). Met43$_{HvNTR2}$ interacts with four nearby residues; Ile51$_{HvTrxh2}$, Met52$_{HvTrxh2}$, Ala106$_{HvTrxh2}$ and Ile107$_{HvTrxh2}$ (Figure 3A). Met43$_{HvNTR2}$ forms one of three 'fingers', together with Trp42$_{HvNTR2}$ and Asp46$_{HvNTR2}$, protruding on the surface. Ile51$_{HvTrxh2}$ is wedged in between Met43$_{HvNTR2}$ and Trp42$_{HvNTR2}$ and has multiple hydrophobic interactions with Trp42$_{HvNTR2}$ (Figure 3A and 5C). Ala106$_{HvTrxh2}$ is positioned between Met43$_{HvNTR2}$ and Asp46$_{HvNTR2}$. Ile51$_{HvTrxh2}$ is found only two residues after the active site motif of HvTrxh2. It is not conserved in plants and is in

HvTrxh1 replaced by a valine. Together with the other residues interacting with $Trp42_{HvNTR2}$ and $Met43_{HvNTR2}$ it may have some effect for the minor preference of NTR for specific Trx isoforms.

The FAD-loop of EcNTR, $_{35}$T-----G<u>M</u>E<u>K</u>GG$_{41}$, also has a central methionine ($Met37_{EcNTR}$), which, however, has a different role in the intermolecular interaction than $Met43_{HvNTR2}$ (compare Figure 5C and D). $Met37_{EcNTR}$ has hydrophobic contacts to $Ala93_{EcTrx}$ and $Leu94_{EcTrx}$. The only other contact involving the FAD-loop of EcNTR is between $Lys39_{EcNTR}$ and $Met37_{EcTrx}$. Thus, EcNTR only has two residues from the FAD-loop involved in the binding of EcTrx (Figure 5B and D).

The central $Ile51_{HvTrxh2}$ is in EcTrx replaced by $Met37_{EcTrx}$, while $Ala106_{HvTrxh2}$ corresponds to $Ala93_{EcTrx}$ (Figure 3B). These residues protrude from the surfaces of both HvTrxh2 and EcTrx, and are placed in fairly similar positions in the two Trxs. The charge distribution and shape of the surface surrounding these residues are also very similar in the two Trxs (Figure 5C and D). It is thus plausible that EcTrx can accommodate the longer FAD-loop from HvNTR2, as described below and that the longer FAD-loop plays a more central role in complex formation in the barley complex by providing a relatively large part of the interaction surface area.

Other contacts to the FAD domain of HvNTR2 include $Lys108_{HvTrxh2}$ forming hydrogen bonds both to $Gly41_{HvNTR2}$ from the FAD-loop and to $Ser91_{HvNTR2}$, belonging to another loop (Figure 3A, 5A and C). The positively charged $Lys108_{HvTrxh2}$ is embedded in a negatively charged area. It is conserved in most h-type plant Trxs (see alignment Figure 9) and may be important for the binding to the FAD domain. However, since the side chains of lysines are relatively flexible, a prediction of the exact conformation of the side chain of $Lys108_{HvTrxh2}$ is not appropriate. Contacts, besides the ones involving the FAD-loop include $Phe81_{EcNTR}$ (corresponds to $Ser91_{HvNTR2}$) and $His83_{EcNTR}$ from the same loop (Figure 5B) interacting with $Ile41_{EcTrx}$ and $Ser95_{EcTrx}$, respectively. A third loop (Figure 5B) in EcNTR contains $Asp99_{EcNTR}$, which binds to the backbone of $Gly97_{EcTrx}$. This aspartate is conserved in HvNTR2, as well as in most other plant NTRs. However, the model of HvNTR2:HvTrxh2 does not bring the aspartate within intermolecular interaction distance of HvTrxh2.

To summarise, HvTrxh2 appears bound by the FAD domain of HvNTR2 through multiple hydrophobic interactions involving the FAD-loop according to the model of HvNTR2:HvTrxh2. Especially, $Trp42_{HvNTR2}$ is likely to have significant interactions with

Ile51$_{HvTrxh2}$, which is situated between Trp42$_{HvNTR2}$ and Met43$_{HvNTR2}$. Met43$_{HvNTR2}$ fits into a cavity on the surface of HvTrxh2. Besides the hydrophobic contacts, Gly41$_{HvNTR2}$ from the FAD-loop as well as Ser91$_{HvNTR2}$, from another loop, form hydrogen bonds with Lys108$_{HvTrxh2}$ (Figure 3A, 5A and C). All contacts between EcTrx and the FAD domain of EcNTR are hydrophobic, but distributed very differently from the contacts in the HvNTR2:HvTrxh2 model. There are very few contacts to the FAD-loop of EcNTR, but several to other sites in the FAD domain. Overall there seems to be a much tighter binding of HvTrxh2 to the FAD domain of HvNTR2 than of EcTrx to the FAD domain of EcNTR, which might be enabled by the longer FAD-loop offering a larger exposed surface for complex formation.

Interactions between HvTrxh2 and the NADPH domain of HvNTR2

The most significant contact between HvTrxh2 and the NADPH domain of HvNTR2 is the intermolecular disulfide bond formed by the two cysteines, Cys148$_{HvNTR2}$ and Cys46$_{HvTrxh2}$ (Figure 3A and 6A). Nearby, a hydrogen bond is formed between one of the oxygens of the side chain of Asp149$_{HvNTR2}$ and the backbone amide nitrogen of Met88$_{HvTrxh2}$ (Figure 6A). The corresponding Asp139$_{EcNTR}$ from EcNTR forms a similar hydrogen bond to the backbone nitrogen of Ile75$_{EcTrx}$ (Figure 6B). Asp139$_{EcNTR}$ has been proposed to be the acid catalyst of the dithiol-disulfide interchange in the catalytic cycle of NTR (Mulrooney and Williams, 1994). In the EcNTR:EcTrx complex there is an additional hydrogen bond between the carbonyl group of Cys138$_{EcNTR}$ and the indole ring NH of Trp41$_{EcTrx}$ (Figure 6B). In the HvNTR:HvTrxh2 model, the corresponding tryptophan adopted a different conformation and was not predicted to interact with C148$_{HvNTR}$ (Figure 6A). There is however no obvious steric rationale for a different conformation of Trp45$_{HvTrxh2}$ and the result might be an artefact from the energy minimisation.

As noted by Stehr *et al.* (2001) the interaction between EcTrx and EcNTR is characterized by two major features besides the interaction of the redox active cysteines; i) the docking of two phenylalanine residues from the NTR into a hydrophobic pocket of Trx next to the active site, and ii) the binding of a loop (residues 71—76 in EcTrx) into a groove on the surface of NTR. This loop is called the *cis*-proline-loop in the following, since residue 76 is a *cis*-proline. The mentioned phenylalanines (Phe141$_{EcNTR}$ and Phe142$_{EcNTR}$) in EcNTR (see Figure 6B), are conserved in many bacterial NTRs (see alignment in Supplementary data

1). Thus Phe141$_{EcNTR}$ interacts with Trp31$_{EcTrx}$ from the active site motif WCGPC (Figure 3B and 6B), while Phe142$_{EcNTR}$ interacts with four different residues of which the most interactions are to Arg73$_{EcTrx}$, which protrudes from the surface of EcTrx (Figure 3B, 5D and 6B). Arg73$_{EcTrx}$ is accommodated in a large open negatively charged groove of EcNTR (Figure 7B). Besides Arg73$_{EcTrx}$ forming hydrophobic contacts to Phe142$_{EcNTR}$, its guanidinium group makes two hydrogen bonds to the backbone carbonyl of Arg130$_{EcNTR}$ and one to the backbone carbonyl of Ala237$_{EcNTR}$ (Figure 6B and 7B). Furthermore the backbone nitrogen of Arg73$_{EcTrx}$ forms a forth hydrogen bond with the backbone carbonyl of Gly129$_{EcTrx}$ (Figure 6B and 7B).

The corresponding *cis*-proline-loop in HvTrxh2 (residues 84—89) is bound in a similar fashion in the current model of HvNTR2:HvTrxh2, but the groove is blocked midway by Ile154$_{HvNTR2}$ and Pro227$_{HvNTR2}$ (Figure 6A and 7A). Pro227$_{HvNTR2}$ belongs to the Glycine-loop (Figure 2 and 6A). According to the model of HvNTR2:HvTrxh2, Glu86$_{HvTrxh2}$ (corresponding to Arg73$_{EcTrx}$) is accommodated in this groove and binds through a single backbone-backbone hydrogen bond to Asn139$_{HvNTR2}$, and has several hydrophobic contacts involving Arg140$_{HvNTR2}$, Gly141$_{HvNTR2}$, Ile154$_{HvNTR2}$ and Phe155$_{HvNTR2}$ (Figure 3A, 6A and 7A). Asn139$_{HvNTR2}$ binds in a pocket of HvTrxh2 *via* hydrophobic contacts and four hydrogen bonds (Figure 3A and 6A). As noted by Oliveira *et al.* (2010) this residue as well as the preceding Trp138$_{HvNTR2}$ vary among species and have been suggested to contribute to the species-specificity. Notably, Trp138$_{HvNTR2}$ and Asn139$_{HvNTR2}$ are conserved in plant LMW NTRs, but Asn139$_{HvNTR2}$ is replaced by a serine in NTR-Cs (see alignment in Supplementary data 1).

HvNTR:HvTrxh2 interactions and Trx substrate binding

The intermolecular interactions predicted from the model of HvTrxh2 in complex with its electron donor (HvNTR2) were compared to those present in the crystal structure of HvTrxh2 in complex with the substrate barley α-amylase/subtilisin inhibitor (BASI). In general, the interactions in Trxh2:BASI are fewer and quite different from those predicted in the HvNTR2:HvTrxh2 model.

Similar to HvTrxh2:HvNTR2, HvTrxh2 is stabilised through an intermolecular disulphide bond involving the active site (C46$_{HvTrxh2}$ and C148$_{BASI}$) in the crystal structure of

HvTrxh2:BASI (pdb 2IWT, Maeda *et al.*, 2006). This was formed by allowing the single-cysteine mutant HvTrxh2_C49S to react with the single-cysteine mutant BASI_C144S conjugated to TNB (Maeda *et al.*, 2006). Backbone atoms from BASI are found in a hydrophobic groove that also accommodates the active site ($_{45}$WCGP$_{48}$) as well as $_{87}$AMP$_{89}$ and $_{104}$VGA$_{106}$, and constitutes the so-called target recognition motif (Maeda *et al.*, 2006). Underlined residues are also directly involved in binding HvNTR2 in the HvNTR2:HvTrxh2 model (Figure 3A). $_{87}$AMP$_{89}$ is a part of the *cis*-proline-loop, mentioned above, that is bound in a groove in the NADPH domain of HvNTR2 (Figure 7A). Interestingly, Pro48$_{HvTrxh2}$ and Ala106$_{HvTrxh2}$ are both involved in binding the central Met42$_{HvNTR2}$ from the FAD-loop of HvNTR2 (Figure 3A and 5C). Besides van der Waals interactions, the HvTrxh2:BASI complex has three backbone-backbone hydrogen bonds (Maeda *et al.*, 2006): Ala106$_{HvTrxh2}$ to Asp146$_{BASI}$, and Met88$_{HvTrxh2}$ to the backbone oxygen and nitrogen of the cysteine, Cys148$_{BASI}$. In the model of HvNTR2:HvTrxH2 the carbonyl group of Met88$_{HvTrxh2}$ also forms a hydrogen bond, but to Asp149$_{HvNTR2}$ next to the active-site cysteine. Glu86$_{HvTrxh2}$, which seems central in the binding to the NADPH domain of HvNTR2 (Figure 3.A) also contributes to the binding of BASI by van der Waals interactions with Glu168$_{BASI}$ and Glu149$_{BASI}$ (Maeda *et al.*, 2006).

All together, there is an overlay in the residues of HvTrxh2 that are involved in the binding of HvNTR2 and BASI. Furthermore, both residues that are predicted to be involved in binding of the FAD-loop and the NADPH domain of HvNTR2 participate in the binding of BASI. One main difference is that the contact with BASI only involves few residues from both proteins whereas the binding to HvNTR2 is much more complex. Therefore the binding to BASI does not seem very specific, and can explain why Trx can react with multiple targets.

Kinetic studies

The presented model of HvNTR2:HvTrxh2 indicated residues that could be involved in the complex formation between the two proteins. To further validate the model and assess the importance of selected amino acid residues, a number of mutants were designed and kinetically characterised

HvNTR2 was mutated by site-directed mutagenesis (see Methods) in the FAD-loop (HvNTR2_W42A, HvNTR2_M43A, HvNTR2_W42A_M43A, HvNTR2_N45A_D46A and

HvNTR2_Δ42-47), as well as of some other selected residues of the NADPH-domain (HvNTR2_N139A and HvNTR2_R140A). Especially $Asn139_{HvNTR2}$ was predicted to be central in the binding of HvTrxh2 because of its involvement in many intermolecular interactions (Figure 3A). Also mutations in the Glycine-loop were produced (HvNTR2_G225R_G226D_P227V, HvNTR2_G225R_G226D and HvNTR2_G222D_A223G _G224E), since this loop was previously suggested to be involved in the binding of Trx (Kirkensgaard *et al*., 2009). For HvTrxh2 the residue $Ile51_{HvTrxh2}$ predicted to be involved in the binding to the FAD-loop (HvTrxh2_I51G) and $Glu86_{HvTrxh2}$ (HvTrxh2_E86A), predicted to be important for the binding to the NADPH domain of HvNTR2 were mutated. Finally, an active site mutant, (HvTrxh2_G47P) was produced (see below).

Some of the mutants of NTR displayed ≥1000 times less activity than the HvNTR2wt (Table 1), and V_{max} was not reached even with 50 µM Trx. In these cases K_m and k_{cat} could not be determined. Instead, the slope of the reaction [A_{412} s^{-1} μM^{-1}] is listed as a relative percentage of the initial slope (slope for the very lowest substrate concentrations) of HvNTR2wt/HvTrxh2wt. There is a relatively good correlation between k_{cat}/K_m and this initial slope (last two columns of Table 1).

Activity of wild-type NTRs and Trxs

HvNTR2 has K_m of 1.2 µM for both HvTrxh1 and HvTrxh2 but a higher k_{cat} for HvTrxh1; 12.1 s^{-1} compared to 8.0 s^{-1} for HvTrxh2 (Table 1). k_{cat}/K_m of HvTrxh1 is thus 145% relative to HvTrxh2, in agreement with previous findings (Shahpiri *et al.*, 2008). With AtTrxh3 as a substrate for HvNTR2 k_{cat} and K_m were found to decrease (K_m of 0.8 µM) and k_{cat}/K_m was 88% relative to HvTrxh2. HvNTR2 and AtNTR-B have 75% sequence identity, which may explain why AtTrxh3 works as an excellent substrate. HvNTR2 has 45% sequence identity with EcNTR, and EcTrx is a poorer substrate for HvNTR2 (Table 1); k_{cat} is slightly higher than for HvTrxh2, but K_m increased to 149 µM. This possibly reflects the very different Trx binding site in the NADPH domain, where the groove has a different charge distribution and might be too short to accommodate $Arg73_{EcTrx}$ (Figure 7A).

AtNTR-B was revealed to transfer electrons well to its own substrate, AtTrxh3 (181% compared to HvNTR2 on HvTrxh2) but surprisingly poor to HvTrxh2 (2%) with a K_m of 60 µM. Thus, HvNTR2 can accept AtTrxh3 almost as well as its own substrate, whereas AtNTR-B

does not work well using HvTrxh2. This could indicate that HvTrxhs binds to HvNTR2 *via* specific patterns not conserved among the h-type isoforms, while HvNTR2 has the ability to transfer electrons *via* both specific and generic interactions.

Interactions involving the FAD domain of HvNTR2

The role of the FAD-loop ($_{40}$E<u>GWM</u>AN<u>D</u>I<u>A</u>AGG$_{51}$) was examined. Underlined residues were predicted to bind to HvTrxh2 based on the model of HvNTR2:HvTrxh2 (Figure 3A). This motivated deletion of part of the loop (HvNTR2_Δ42-47, lacking residues $_{42}$WMANDI$_{47}$). These residues were chosen because that part of the loop contained the most bulky residues and was predicted by the model to be in closest proximity to HvTrxH2. Furthermore, three of these residues (Trp42$_{HvNTR2}$, Met43$_{HvNTR2}$ and Asp46$_{HvNTR2}$) were predicted to bind directly to HvTrxh2. HvNTR2_Δ42-47 showed a very low activity with HvTrxh2 so values of k_{cat} and K_m could not be determined. However, a linear correlation between the activity and the concentration of HvTrxh2 was obtained. It could thus be estimate that HvNTR2_Δ42-47 has 0.06% activity towards HvTrxh2 (last column in Table 1), showing that binding to this loop is essential.

The following mutants HvNTR2_M43A, HvNTR2_W42A, HvNTR2_W42A_M43A, HvNTR2_N45A_D46A and HvTrxh2_I51G were made to elucidate, which residues of this loop are most important for the binding. The reason for mutating Ile51$_{HvTrxh2}$ to glycine was to shorten the amino acid side chain sufficiently to avoid side chain interactions with the loop. HvTrxh2_I51G showed 15.1% activity. Combined with the mutants HvNTR2_W42A or HvNTR2_M43A the HvTrxh2_I51G mutation gave activities of 0.5 and 0.4% respectively, which makes it plausible that the model of HvNTR2:HvTrxh2 is correct in placing Ile51$_{HvTrxh2}$ with significant interactions with Trp42$_{HvNTR2}$ and Met43$_{HvNTR2}$. Hydrophobic interactions could be a major driving force for complex formation.

A sequence corresponding to the FAD-loop is also present in NTRs from dicot plants (Figure 4). The importance of this sequence in dicots was examined by assaying the HvNTR2 mutants with Trx from *Arabidopsis thaliana.* This plant encodes at least eight isoforms of Trx-h, of which AtTrxh3, AtTrxh4 and AtTrxh5 were tested for activity, as they are of the same sub-type (type I), as HvTrxh1 and HvTrxh2 (Gelhaye *et al*., 2005). Furthermore, the mutants were assayed on EcTrx, to test if the loop can bind this substrate in the same way

as HvTrxh2, as postulated because the charge distribution and surface of the two Trxs are very similar in the region binding the FAD-loop.

The kinetic parameters are given in Table 1, but the activity for EcTrx is very low compared to the other substrates. Therefore the activity of HvNTR2wt with HvTrxh2, AtTrxh3 and EcTrx were all normalised to 100%, and the activity of the mutants are illustrated relative to these (Figure 8). For HvNTR2_W42A most activity was lost for HvTrxh2 and EcTrx being only 3.3 and 1.7%, respectively. Surprisingly, 71% activity was maintained for AtTrxh3, rendering this a much better substrate for that mutant. Changing $Met43_{HvNTR2}$ to alanine affected binding of all three substrates, but again the effect on the binding of AtTrxh3 was less affected than for the other substrates. Combining these two mutations in HvNTR2_W42A_M43A reduced activity for HvTrxh2 and EcTrx to 0.09 and 0.2% of wild-type, whereas there was 5.5% activity for AtTrxh3 (Figure 8). Only the mutant HvNTR2_N45A_D46A lost slightly more activity towards AtTrxh3 than displayed by HvTrxh2. Deleting five residues of the loop in HvNTR2_Δ42-47 destroyed activity towards EcTrx and very little activity was found towards HvTrxh2 as mentioned (0.06%). However, there was still 4.9% activity towards AtTrxh3 (Figure 8). Essentially, the same activity was obtained for this mutant towards AtTrxh4 and AtTrxh5 (*data not shown*), and activity towards HvTrxh1 was in the same range as of HvTrxh2 (*data not shown*). The results presented indicate that the *A. thaliana* Trxs assayed depend less on the FAD-loop. They may instead have a stronger interaction with other parts of the FAD domain or with the NADPH domain. This may explain why AtNTR-B does not react well with HvTrxh2, which may not have strong interactions to other parts of AtNTR-B.

The central $Met43_{HvNTR2}$ is the only interacting residue that is not conserved in HvNTR1, where it is replaced by a leucine residue (see Figure 3A). This may explain a higher preference of HvNTR2 for HvTrxh1. Even though $Ile51_{HvTrxh2}$ is important for the binding, this residue is not conserved either and is in HvTrxh1 replaced by a valine (see alignment Figure 9). These conservative substitutions may when added to the varieties in the other residues interacting with $Trp42_{HvNTR2}$ and $Met43_{HvNTR2}$ (Figure 3A), be responsible for the difference between the activities with the two substrates. In AtTrxh3 and AtTrxh5, $Ile51_{HvTrxh2}$ is substituted with phenylalanine, whereas it is methionine in AtTrxh4. In EcTrx the corresponding residue is $Met37_{EcTrx}$.

Both the model of HvNTR2:HvTrxh2 and the data in Figure 8 suggest that the loop of HvNTR2 is able to bind EcTrx in the same manner as HvTrxh2. AtTrxh3 is not bound in the same way and is much less dependant on $Trp42_{HvNTR2}$, which is essential for binding the other substrates. This is notable since AtNTR-B has the same FAD-loop sequence. Unfortunately, there are no crystal structures available of neither AtTrxh3, AtTrxh4 nor AtTrxh5 to enlighten what could cause this difference.

The data of Table 1 and Figure 8 may indicate that AtTrxh3 (and h4 and h5) has a stronger binding to the NADPH domain (or another area of the FAD domain), and therefore is less dependent on the FAD-loop. In order to find an explanation for this, the sequences of the three *A. thaliana* Trxs and the two barley Trxs were aligned and examined (Figure 9). Here all the residues of HvTrxh2 predicted by the complex model to interact with HvNTR2 are marked. Since all three Trxs from *A. thaliana* had similar activity with HvNTR2_Δ42-47, and HvTrxh1 and HvTrxh2 both had extremely low activity, the explanation must be a difference between the Trxs from the two plants; i.e. the three Trxs from *A. thaliana* must have something in common, which is lacking in HvTrxh1 and HvTrxh2 or *vice versa*. One possible explanation found among the interacting residues was that the positively charged lysine in HvTrxh2/h1 (residue 77 in h2, yellow in Figure 9) is changed in the three Trxs from *A. thaliana* to glutamine or asparagine. $Lys77_{HvTrxh2}$ was predicted to interact with $Pro153_{HvNTR2}$ through hydrophobic contacts between the C^{γ} and C^{δ} atoms of both residues. It is a part of the binding pocket corresponding to the hydrophobic pocket of EcTrx (see Figure 6A). This minor difference in hydrophobic interaction pattern is however not likely to fully account for the differences in the interaction of HvNTR2 with Trxs from barley and *A. thaliana*.

Another important difference was the three AtTrxs having the active site of CPPC instead of CGPC (boxed in Figure 9). The only available crystal structure of an h-type Trx from *A. thaliana* is of AtTrxh1 (pdb 1XFL, Peterson *et al*., 2005), which has the classical CGPC active site. A search for structures with the WCPPC motif in the *Protein Data Bank* revealed a structure of Trxh1 from *Populus tremula* (poplar) (pdb 1TI3, Coudevylle *et al.* 2005) in a reduced state. Superpositioning this structure with that of HvTrxh2 in the HvNTR2:HvTrxh2 model showed only little difference in the surface complementarity of the two Trxhs in this region. The mutant HvTrxh2_G47P (which has the active site motif CPPC) was made to examine the role of the different active site. HvNTR2wt showed slightly increased K_m (1.6

μM) with this mutant (Table 1) and neither HvNTR2_Δ42-47 nor the double mutant HvNTR2_W42A_M43 had any activity above background with HvTrxh2_G47P. This indicates that the different active site of the three Trxs from *A. thaliana* is not responsible for the much higher activity with the loop mutants. It seems more plausible that the answer is an overall different distribution of contacts or electrostatic potential complementarity. This means that it is not likely that any single residue is responsible for the difference, which is more likely to be a result of an additive effect integrating several differences.

Interactions involving the NADPH domain of HvNTR2

The role of some of the contacts involving the NADPH domain was examined by mutational studies. The model of HvNTR2:HvTrxh2 predicts that the residues forming most interactions between HvTrxh2 and the NADPH domain of HvNTR2 are $Asn139_{HvNTR2}$ and $Glu86_{HvTrxh2}$ (see Figure 3A). The corresponding mutants HvNTR2_N139A and HvTrxh2_E86A were assayed as well as HvNTR2_R140A towards HvTrxhwt (HvNTR2wt for HvTrxh2_E86A) as well as in combinations with each other. HvTrxh2_E86A showed a decrease of both k_{cat} (from 8.0 to 5.3 s^{-1}) and K_m (from 1.2 to 0.6 μM), resulting in an overall increase of k_{cat}/K_m to 137% of the wild-type combination (Table 1). HvNTR2_N139A also showed a decreased k_{cat} (4.2 s^{-1}) and K_m (0.7 μM), resulting in k_{cat}/K_m of 91% of the wild-types. When combining the two mutants (assaying HvNTR2_N139A towards HvTrxh2_E86A) k_{cat} was the same as for HvNTR2_N139A with HvTrxh2wt but K_m decreased even further to 0.4 μM, resulting in k_{cat}/K_m of 151% of the wild-type combination. Furthermore, the positively charged mutant, HvTrxh2_E86R, was shown (Björnberg *et al.*; manuscript in preparation) to have only minor effect on the activity with HvNTR2. These findings suggest that $Asn139_{HvNTR2}$ and $Glu86_{HvTrxh2}$ are not critical for the binding between HvNTR2 and HvTrxh2. It is possible that water molecules are able to fill out the voids and contribute by hydrogen bonding instead of the missing side chains. By contrast, the residue $Arg73_{EcTrx}$ in EcTrx, which corresponds to $Glu86_{HvTrxh2}$, is essential for activity. Thus, a mutant of EcTrx_R73G showed substantially decreased activity (to 0.6%) with EcNTR compared to EcTrxwt (Negri *et al*., 2009).

HvNTR2_R140A decreased k_{cact} to 5.1 s^{-1} and increased K_m almost 3 fold to 3.4 μM, resulting in k_{cat}/K_m of 22% of the HvNTR2wt (Table 1). Combined with HvTrxh2_E86A, k_{cat} decreased further to 2.6 s^{-1}, but K_m (1.6 μM Trx s^{-1}) was almost at the value of the combined

wild-types, resulting in k_{cat} /K_m of 24% of the wild-type combination. It is not possible from these assays to conclude whether the model of HvNTR2:HvTrxh2 has predicted the position of the examined residues correctly. As mentioned, introduction of shorter side chains can make room for water molecules that may provide hydrogen bond contacts.

It was further examined whether the Glycine-loop with the sequence $_{221}$GGAGGGPL$_{228}$ (see Figure 2 and 6A) is involved in binding HvTrxh2. This loop is flexible as reflected by a high B-factor in the crystal structure of HvNTR2 (Kirkensgaard *et al*., 2009). The proline of the loop, Pro227$_{HvNTR2}$, was predicted by the model of HvNTR2:HvTrxh2 to shorten the length of the groove in which Glu86$_{HvTrxh2}$ is accommodated (Figure 6A). Mutants were constructed at some of the residues and changed to the corresponding residues of AtNTR-B ($_{223}$GDGERDVL$_{230}$) to examine whether this increased the preference for AtTrxs. The mutants HvNTR2_G222D_A223G_G224E, HvNTR2_G225R_G226D and HvNTR2_G225R_G226D _P227V were assayed on both HvTrxh2 and AtTrxh3.

HvNTR2_G222D_A223G_G224E showed a slight increase of K_m towards HvTrxh2 (to 1.46 µM) resulting in k_{cat} /K_m of 80% of the wild-type (Table 1 and Figure 10). K_m towards AtTrxh3 was decreased from 0.52 µM, leading to k_{cat}/K_m of 141% (compared to 88% for HvNTR2wt). For HvNTR2_G225R_G226D there was a smaller decrease of K_m to 0.67 µM for AtTrxh3 and k_{cat}/K_m increased from 88 to 110%. For HvTrxh2 a minor increase of K_m was observed (from 1.17 to 1.28; 93% activity). For HvNTR2_G225R_G226D_P227V k_{cat} was lowered for HvTrxh2 resulting in 25% activity compared to the wild-type. For AtTrxh3 the activity was lowered to 79%. To summarise there is a slight negative effect on activity for HvTrxh2 when substituting residues in the loop to mimic AtNTR-B. Only when changing Pro227$_{HvNTR2}$ to a valine the effect was more pronounced, leading to 25% activity. This may be due to valine being positioned in the groove, which accommodate Glu86$_{HvTrxh2}$ (Figure 7A), and thus interfering with binding of this residues. For AtTrxh3 this mutant showed slightly decreased activity, which again may be due to blockage of the groove. Both HvNTR2_G222D_A223G_G224E and HvNTR2_G225R_G226D showed increased activity towards AtTrxh3, which may indicate that the Glycine-loop is involved in the binding of Trx.

Reaction mechanism

The complex formation involved production of single cysteine mutants of both HvNTR2 and HvTrxh2 (HvNTR2_C145S and HvTrxh2_C49S) producing a stable mixed disulfide between $Cys148_{HvNTR2}$ and $Cys46_{HvTrxh2}$ Since $Cys148_{HvNTR2}$ is reduced by DTT the complex formation should be independent of NADPH and FAD. If, however, NADPH could increase the reaction rate during complex formation, it would indicate that NADPH is involved in the conformational change from FO to FR. Reaction of 30 µM HvNTR2_C145S with 20 µM HvTrxh2_C49S-TNB resulted in the black curves of Figure 11, which shows that HvNTR2_C145S is able to react with HvTrxh2_C49S-TNB independently of NADPH. When NADPH was added to HvNTR2_C145S 20 minutes prior to the reaction, the initial rate increased. However, the absorbance either ended at a lower level than without NADPH (yellow curve Figure 11A) or, for the highest concentrations of NADPH, started decreasing after a maximum absorbance was reached after approximately five min (Figure 11A, blue and green line). This could be due to a reduction of FAD, since the absorbance of FAD contributes substantially to the background at this NTR concentration (30 µM). A reduction of FAD results in a decrease in the absorbance (Williams *et al*., 1967). This could indicate that HvNTR2_C145S changes conformation upon addition of HvTrxh2_C49S-TNB: Changing to the FR conformation would bring FAD in the proximity of NADPH and enable reduction.

Upon addition of $NADP^+$ instead of NADPH, the reaction rate of the complex formation is also increased (Figure 11B, yellow and green curves). The second order reaction rates were calculated to 139 $M^{-1}s^{-1}$ without $NADP^+$ and about 3 times higher (408 $M^{-1}s^{-1}$) with 40 µM $NADP^+$ and about 4.8 times higher (635 $M^{-1}s^{-1}$) using 300 µM $NADP^+$. In this case no drop in absorbance was observed. During this assay the reduction state of FAD should be constant since $NADP^+$ is unable to reduce FAD, and the experiment is performed under anaerobic conditions. Apparently, it is not the reduction of FAD itself but the binding of $NADP^+$/ NADPH that increases the reaction rate. The results indicate that HvNTR2_C145S is able to react with HvTrxh2_C49S-TNB independently of either NADPH/$NADP^+$, but binding of the ligand apparently facilitates the conformational shift from FO to FR.

We have previously suggested (Kirkensgaard *et al*., 2009) that Trx is partially bound to the NADPH domain in the FO conformation, which facilitates the conformational shift to FR. This was based on the findings that the structure of HvNTR2 had adopted a conformation

which had a more accessible active site due to other NTRs in the FO conformation. Furthermore, this structure could not accommodate NADPH so therefore it was suggested that NADPH is bound in the FR conformation. However, the findings here support the reaction mechanism suggested by Negri *et al*. (2009), who simulated the conformational change from FO to FR for EcNTR. The studies showed that both $EcTrx_{ox}$ and NADPH are possibly both bound in the FO conformation and induce the conformational change (Negri *et al*., 2009). These MD simulations strongly suggested that $Arg73_{EcTrx}$ is a crucial residue both for the electrostatic interaction between the two proteins and for the following twisting motion. Furthermore, a mutant of EcTrx_R73G showed substantially decreased activity (to 0.6%) with EcNTR compared to EcTrxwt (Negri *et al*., 2009) showing that this arginine is essential for activity.

By contrast, mutation of the corresponding residue in HvTrxh2, $Glu86_{HvTrxh2}$, resulted in an increase in k_{cat} /K_m to 137%. These results indicate that $Glu86_{HvTrxh2}$ does not play the same essential role as $Arg73_{EcTrx}$, and the binding mechanism for the two organisms are not necessarily identical. The mutations in the FAD-loop were more severe than the mutations in the NADPH domain examined here. Furthermore, $Met43_{HvNTR2}$, which is central for the binding, is the only interacting residue, which is not identical in the two barley NTR isoforms.

The FAD domains were superposed of the crystal structure of HvNTR2 and the model of HvNTR2:HvTrxh2 (Figure 12). This shows that there is room for binding of HvTrxh2 to the FAD domain in the FO conformation (or the conformation of this crystal structure). The orange arrow in Figure 12 indicates how the conformational change from FO to FR would bring the active site cysteines in proximity to the cysteines of HvTrxh2.

Conclusion

The model of HvNTR2:HvTrxh2 shows that the FAD domain of HvNTR2 binds HvTrxh2 by multiple hydrophobic interactions through the FAD-loop, $_{40}$E<u>GWM</u>AN<u>D</u>I<u>A</u>AGG$_{51}$ (interacting residues underlined). Especially the residues $Trp42_{HvNTR2}$ and $Met43_{HvNTR2}$ were shown both by the model and mutational studies to be central in the binding. Interestingly, $Met43_{HvNTR2}$ is the only residue in the predicted binding interface that is not conserved in the other isoform of barley, HvNTR1 having a leucine. These two residues vary between

type 1 and 2 of monocot plants and could therefore provide some selectivity towards certain isoforms of Trxs. The FAD-loop is also found in other eukaryotes, but the corresponding loop of EcNTR is five residues shorter, has no resemblance to the loop of HvNTR2, and binds EcTrx with only a few hydrophobic contacts. Surprisingly some of the FAD-loop mutants had much higher activity with AtTrxh3 than with HvTrxh2 (around 60 times higher for HvNTR2_W42A_M43A and 80 times higher for HvNTR2_Δ42-47). Therefore, the relative contribution of the FAD-loop to the binding energy of the NTR:Trxh complex seem to vary considerably among species.

Concerning contacts involving the NADPH domain of NTR it has previously been shown that $Arg73_{EcTrx}$ is central in the binding (Lennon *et al*., 2000; Negri *et al*., 2009) and may induce the conformational shift of EcNTR from FO to FR. Notably, mutating $Glu86_{HvTrxh2}$, which corresponds to $Arg73_{EcTrx}$, increased k_{cat}/K_m of with HvNTR2 to 130% compared to HvTrxh2wt, indicating that the binding mechanisms are not identical for the two organisms.

Complex formation using HvNTR2_C145S and HvTrxh2_C49S-TNB was independent of NADPH. However both NADPH and $NADP^+$ increased the reaction rate of the complex formation. The findings support the reaction mechanism suggested by Negri *et al*. (2009) in which both $EcTrx_{ox}$ and NADPH are bound to EcNTR in the FO conformation and induce a shift to the FR conformation. However, the mutational studies here indicate that the reaction mechanism is not necessarily identical for the two organisms. Alternatively, HvTrxh2 may bind the FAD domain instead of the NADPH domain in the FO conformation and a conformational shift brings the active site cysteines of HvNTR2 in the proximity of the active site of HvTrxh2.

The model presented here gives an insight into how eukaryotic NTRs in general may bind Trx since many of the involved residues are conserved. Such knowledge may have great applications in future design of NTR inhibitors tailored against various pathogens.

Materials and method

Homology modelling and refining

A model was made of HvNTR2 bound *via* an intermolecular disulfide to HvTrxh2 based on crystal structures of the two proteins. The crystal structure of NTR from *E. coli* bound by an intermolecular disulfide to EcTrx (pdb 1F6M, Lennon *et al*., 2000) was used as a template

for positioning the two domains of HvNTR2 as well as HvTrxh2. From pdb 1F6M chain A (EcNTR) and chain C (EcTrx) were chosen. The pdb file of HvNTR2 (2WHD, Kirkensgaard *et al.*, 2009) contains two chains of HvNTR2 of which chain A was chosen. The domains of HvNTR2 were superposed individually to the corresponding domains of EcNTR using the SSM Superpose function in the software Coot (Emsley & Cowtan, 2004; Krissinel & Henrick 2004). The FAD domain consists of residues 6—126 and 255—323 (residues 1—5 and 324—331 missing in the crystal structure of HvNTR2) and the NADPH domain consists of residue 127—254. HvTrxh2 was taken from a complex of HvTrxh2 covalently bound via an intermolecular disulfide bond to the protein substrate barley alpha-amylase/subtilisin inhibitor (BASI) (pdb 2IWT, Maeda *et al.*, 2006), and superposed with that of EcTrx.

The position of the linker region between the two domains of HvNTR2 was modelled using MOE (Chemical Computing Group Inc) with EcNTR as the template (pdb accession 1F6M). Several rounds of energy minimisation were performed for this linker region and for residues within 4.5 Å from the interface between HvNTR2 and HvTrxh2. A disulfide bond between Cys148 of HvNTR2 and Cys46 of HvTrxh2 was built in MOE, and further energy minimisation was performed again only including the residues within 4.5 Å of the intermolecular interface using the Amber94 forcefield.

Cloning and site-directed mutagenesis

Mutants of HvNTR2 and HvTrxh2 were made by site-directed mutagenesis using the QuikChange® II Site-Directed Mutagenesis Kit (Agilent Technologies) with the recommended concentrations. Primers were designed using the Primer design guidelines for the kit and delivered HPLC-purified since high purity is important for optimal cloning (Eurofins MWG Operon, Germany). A list of all primers used is given in Supplementary data 2. The template plasmids encoding HvNTR2 or HvTrxh2 with an N-terminal His_6-tag were constructed in pET15b (Shahpiri *et al.*, 2008).

After the reaction, the parental strand was digested for 1—2 h using *Dpn*I (final concentration 0.2 units/µL) provided in the kit. Either XL-Blue from the kit or chemical competent *E. coli* strain DH5α were transformed with 1—4 µL of the resulting mixture, using the procedure recommended by the manufacturer. However, for DH5α incubation at 42°C was prolonged from 45 to 90 s, and 800 µL instead of 500 µL SOC media (20 g/L tryptone, 5

g/L yeast extract, 0.5 g/L NaCl, 2.5 mM KCl, 20 mM glucose, adjusted to pH 7.0 with NaOH) was added. Plasmid was purified from 5—10 mL overnight culture of selected colonies using GeneJet™ Plasmid Miniprep kit (Fermentas) and sequenced in both directions by Eurofins MWG Operon using T7 and T7 term primers (provided by the company).

Plasmids containing the genes encoding the following three h-type Trxs and NTR from *Arabidopsis thaliana* were obtained from BRC Experimental Plant Division, RIKEN Tsukuba Institute; AtTrxh3 (pda04909-RAFL08-16-J17), AtTrxh4 (pda11571-RAFL19-77-A10), AtTrxh5 (pda01954-RAFL09-16-K07) and AtNTR-B (pda13160-RAFL16-02-L06). The genes were amplified by PCR using primers, which contained restriction sites for *BamHI* and *NdeI*, and the genes were inserted into pET15b vectors. A pET-14b based plasmid encoding EcTrx was obtained from MWG. Rosetta was transformed with these plasmids as described above.

Protein expression and purification

Overnight cultures were inoculated with Rosetta transformants of the various wild-type and mutant plasmids encoding NTR and Trx in 50 mL LB media supplemented with ampicillin (100 µg/mL) and chloramphenicol (5 µg/mL). Overnight culture was added to a total of 1 L fresh media for a starting OD_{600} ≈ 0.1 and grown at 37°C with vigorous shaking until OD_{600} ≈ 0.6. 100 µg/mL IPTG (Isopropyl β-D-1-thiogalactopyranoside) was added and the culture was incubated at 20°C overnight. The cell culture were incubated on ice for 15—30 min prior to centrifugation (4000 rpm, 4°C for 20 min), after which pellet was either frozen at -20°C or purified directly.

The pellet was dissolved in 10 mL BugBuster® Protein Extraction reagent (Novagen®) and 2 µL Benzonase® Nuclease (≥250 units/µL, Sigma-Aldrich) and shaken for 30 min at room temperature. After centrifugation (10,000 rpm, 4°C for 15 min), the supernatant was filtered (0.45 µm syringe filter, Frisenette ApS) and the filtrate was applied to a 1 mL HisTrap™ HP column (GE Healthcare) preequilibrated with 5 mL buffer A (10 mM imidazole, 30 mM Tris-HCl pH 8.0, 500 mM NaCl). An ÄKTAprime™ plus (GE Healthcare) was used for purifying the protein using affinity chromatography as described (Maeda *et al*., 2006). The column was washed with 10 column volumes (CV, 10x1 mL in this case) of buffer A followed by 15 CV buffer A mixed with 10% buffer B (400 mM imidazole, 30 mM Tris-HCl pH 8.0, 500 mM NaCl), before elution of the protein by a gradient of buffer B increasing to 100%. The

fractions containing protein (identified by the obtained chromatogram) were pooled and dialysed overnight (Spectra/Por® Membrane of 6-8.000 MWCO, Spectrum Laboratories Inc.) against 30 mM Tris-HCl pH 8.0. The volume was reduces to 1 mL by concentrating the protein (Amicon® Ultra-15 Centrifugal Filter Divice of 10,000 MWCO, Millipore), and the sample filtered and gelfiltrated on a HiLoad™ 16/60 Superdex™ 75 prep grade column (Amersham Biosciences) in 200 mM NaCl, 30 mM Tris-HCl pH 8.0. An Äkta TM explorer Air (Amersham Biosciences) system was used for the gel filtration. This was followed by dialysis against 30 mM Tris-HCl pH 8.0, concentrating to 100—500 µM and storage at -80°C. The purity of the protein was checked by SDS-PAGE.

Kinetics

An assay using DTNB (5,5'-dithiobis-(2-nitrobenzoic acid) as the final disulfide substrate as described (Miranda-Vizuete *et al*., 1997) was used with slight modifications. The final reaction mixture contained 20 nM NTR wt or mutant as determined from the FAD content (extinction coefficient 11.300 M^{-1} cm^{-1} at 456 nm, Williams *et al*., 1967), varying concentrations of Trx wt or mutant (typically between 0.125 and 8 µM) in 0.1 M KH_2PO_4 pH 7.5, 2.0 mM EDTA, 0.2 mM DTNB, 0.2 mM NADPH and 0.1 mg/mL BSA. Protein dilutions were performed in 0.1 M KH_2PO_4 pH 7.5, 2.0 mM EDTA and 0.1 mg/mL BSA. The reaction was initiated by addition of NTR, and for the slowest reactions performed in 96-well microtiter plates containing 250 µL per well, and A_{412} monitored for 30 min with measurements every 30 s (ELISA plate reader, Power Wave XS, BIO-TEK®, Holm & Halby). A standard curve for the absorbance of free TNB was made using known concentrations of N-acetyl cysteine in 0.1 M KH_2PO_4 pH 7.5, 2.0 mM EDTA, 0.2 mM DTNB, 0.2 mM NADPH and 0.1 mg/mL BSA measuring. The mixture was incubated 5 min at room temperature before measuring A_{412}.

Most reactions were performed in a quartz cuvette in a spectrophotometer (Ultrospec 2100 *pro*, Amersham Biosciences), using the standard extinction coefficient of TNB of 13,600 M^{-1} cm^{-1} (Ellman, 1959). The reaction was followed for typically 90 s with measurements of A_{412} every 2 s. Duplicates of each measurement were made, and K_m and V_{max} were determined using the program KaleidaGraph (Synergy Software).

Complex formation using single-cysteine mutants of HvNTR2 and HvTrxh2

The single-cysteine mutants HvNTR2_C145S and HvTrxh2_C49S were expressed and purified as described for the other mutants and wild-type protein. Before the purification step of size-exclusion chromatography HvTrxh2_C49S was reacted with a 10 times excess of DTNB for 30 min at room temperature.

The rest of the experiment was kept under anaerobic conditions using a glove-box (Anaerobic Flexible Vinyl Coy Chamber, Coy Laboratories) with nitrogen/hydrogen atmosphere, 2-4 % hydrogen. This was done in order to prevent oxidation of $Cys148_{HvNTR2}$ or the FAD molecule. HvNTR2_C145S was treated with 1mM DTT for 30 min at room temperature, which was removed using a NAP-5 desalting column (GE Healthcare). HvNTR2_C145S was in some of the reaction pre-incubated with NADPH or $NADP^+$ in varying concentrations (see Figure 11) for 20 min. A spectrophotometer was reset on a reaction mixture containing everything but HvTrxh2_C49S-TNB. The reaction was started in a 100 µL cuvette by the addition of HvTrxh2_C49S-TNB and the release of TNB followed at 412 nm every 10 s for 50 min. The final reaction mixture contained: 30 µM HvNTR2_C145S, 20 µM HvTrxh2_C49S-TNB, varying concentrations of NADPH/$NADP^+$, 2 mM EDTA, 30 mM Tris-HCl pH 8.0.

Acknowledgements

Lab technician Aida Curovic is thanked for expression and purification of protein as well as construction of plasmid encoding various proteins from *A. thaliana* and *E. coli*. Associate Professor, PhD Hans Erik Mølager Christensen and Post doc Ida Noemi Simon are thanked for providing access to and help using the Anaerobic Flexible Vinyl Coy Chamber (Coy Laboratories). Former master student Stig Johnsen is thanked for constructing pET15b-based plasmids encoding the three Glycine-loop mutants. This project was supported by a DTU PhD stipend to KGK and supported by the Centre for Advanced Food Studies (LMC) and by a grant from The Danish Council for Technology and Innovation (FTP, grant number 274-08-0413).

References

Alkhalfioui, F., Renard, M. and Montrichard, F. (2007). Unique properties of NADP-thioredoxin reductase C in legumes. *J. Exp. Bot.* **58**: 969–978.

Arnér, E.S.J. and Holmgren, A. (2000). Physiological functions of thioredoxin and thioredoxin reductase. *Eur. J. Biochem.* **267**: 6102–6109.

Bradford, M.M. (1976). A rapid and sensitive method for the quantification of microgram quantities of protein utilizing the principle of protein-dye binding. *Anal. Biochem.* **72**: 248–254.

Buchanan, B.B., and Balmer, Y. (2005). Redox regulation: a broadening horizon. *Annu. Rev. Plant Biol*. **56**: 187–220.

Coudevylle, N., Thureau, A., Hemmerlin, C., Gelhaye, E., Jacquot, J.P. and Cung, M.T (2005). Solution structure of a natural CPPC active site variant, the reduced form of thioredoxin h1 from poplar. *Biochemistry* **44:** 2001–2008.

Ellman, G. L. (1959). Tissue sulfhydryl groups. *Arch. Biochem. Biophys.* **82:** 70–77.

Emsley, P. and Cowtan, K. (2004). Coot: model-building tools for molecular graphics. *Acta Crystallogr. D* **60**: 2126–2132.

Gelhaye, E., Rouhier, N. and Jacquot, J. P. (2004). The thioredoxin h system of higher plants. *Plant Physiol. Biochem.* **42**: 265–271.

Gelhaye, E., Rouhier, N., Navrot, N. and Jacquot, J. P. (2005). The plant thioredoxin system. *Cell Mol Life Sci* **62**: 24–35.

Hall, T.A. (1999). BioEdit: a user-friendly biological sequence alignment editor and analysis program for Windows 95/98/NT. *Nucl Acid S* **41:** 95—98.

Hernandez, H.H., Jaquez, O.A., Hamill, M.J., Elliott, S.J. and Drennan, C.L. (2008). Thioredoxin reductase from *Thermoplasma acidophilum*: a new twist on redox regulation. *Biochemistry* **47**: 9728–9737.

Ishiwatari, Y., Fujiwara, T., McFarland, K.C., Nemoto, K., Hayashi, H., Chino, M. and Lucas, W.J. (1998). Rice phloem thioredoxin h has the capacity to mediate its own cell-to-cell transport through plasmodesmata. *Planta* **205**: 12–22.

Kirkensgaard, K.G, Hägglund, P., Finnie, C., Svensson, B. and Henriksen, A. (2009). Structure of *Hordeum vulgare* NADPH-dependent thioredoxin reductase 2. Unwinding the reaction mechanism. *Acta Crystallogr. D* **65**: 932–941.

Laurent, T.C., Moore, E.C. and Reichard, P. (1964). Enzymatic synthesis of deoxyribonucleotides. IV. Isolation and characterization of thioredoxin, the hydrogen donor from *Escherichia coli* B. *J. Biol. Chem.* **239**: 3436–3444.

Lennon, B.W., Williams, C.H.Jr. and Ludwig, M.L. (2000). Twists in catalysis: alternating conformations of *Escherichia coli* thioredoxin reductase. *Science* **289**: 1190–1194.

Maeda, K., Finnie, C., Østergaard, O., and Svensson, B. (2003). Identification, cloning and characterization of two thioredoxin h isoforms, HvTrxh1 and HvTrxh2, from the barley seed proteome. *Eur. J. Biochem.* **270**: 2633–2643.

Maeda, K., Hagglund, P., Finnie, C., Svensson, B. and Henriksen, A. (2006). Structural basis for target protein recognition by the protein disulfide reductase thioredoxin. *Structure* **14**: 1701–1710.

Meng, L., Wong, J., Feldman, L., Lemaux, P. and Buchanan, B. (2010). A membrane-associated thioredoxin required for plant growth moves from cell to cell, suggestive of a role in intercellular communication. *P. Natl. Acad. Sci. USA* **107** (8): 3900–3905.

Miranda-Vizuete, A., Damdimopoulos, A.E., Gustafsson, J. and Spyrou, G. (1997). Cloning, expression, and characterization of a novel *Escherichia coli* thioredoxin. *J. Biol. Chem.* **272**: 30841–30847.

Moore, E.C., Reichard, P. and Thelander, L. (1964). Enzymatic synthesis of deoxyribonucleotides. V. Purification and properties of thioredoxin reductase from *Escherichia coli* B. *J. Biol. Chem.* **239**: 3445–3452.

Mulrooney, S.B. and Williams, C.H.Jr. (1994). Potential Active-Site Base of Thioredoxin Reductase from *Escherichia coli:* Examination of Histidine^{245} and Aspartate^{139} by Site-Directed Mutagenesis, *Biochemistry* **33**: 3148–3154.

Negri, A., Rodríguez-Larrea, D., Marco, E., Jiménez-Ruiz, A., Sánchez-Ruiz, J.M. and Gago, F. (2010). Protein–protein interactions at an enzyme–substrate interface: Characterization of transient reaction intermediates throughout a full catalytic cycle of *Escherichia coli* thioredoxin reductase. *Proteins* **78**: 36–51.

Oliveira, M.A., Discola, K.F., Alves, S.V., Medrano, F.J., Guimarães, B.G. and Netto, L.E.S. (2010). Insights into the Specificity of Thioredoxin Reductase-Thioredoxin Interactions. A Structural and Functional Investigation of the Yeast Thioredoxin System, *Biochemistry* **49**: 3317–3326.

Osipiuk, J., Zhou, M., Kwon, K., Anderson, W.F. and Joachimiak, A. Thioredoxin-disulfide reductase from *Campylobacter jejuni*. Pdb accession 3r9u, unpublished.

Pai, E.F. (1991). Variations on a theme: the family of FAD-dependent NAD(P)H-(disulfide)-oxidoreductases. *Curr. Opin. Struct Biol.* **1**: 796–803.

Peterson, F.C., Lytle, B.L., Sampath, S., Vinarov, D., Tyler, E., Shahan, M., Markley, J.L. and Volkman, B.F. (2005). Solution structure of thioredoxin h1 from *Arabidopsis thaliana*. *Protein Sci*. **14:** 2195–2200.

Russel, M. and Model, P. (1986). The role of thioredoxin in filamentous phage assembly. Construction, isolation, and characterization of mutant thioredoxins. *J. Biol. Chem.* **261**: 14997–15005.

Serrato, A.J. and Cejudo, F.J. (2003). Type-h thioredoxins accumulate in the nucleus of developing wheat seed tissues suffering oxidative stress. *Planta* **217**: 392–399.

Serrato, A.J., Perez-Ruiz, J.M., Spinola, M.C. and Cejudo, F.J. (2004). A novel NADPH thioredoxin reductase, localized in the chloroplast, which deficiency causes hypersensitivity to abiotic stress in *Arabidopsis thaliana*. *J. Biol. Chem.* **279**: 43821–43827.

Shahpiri, A., Svensson, B. and C. Finnie (2008). The NADPH-Dependent Thioredoxin Reductase/Thioredoxin System in Germinating Barley Seeds: Gene Expression, Protein Profiles, and Interactions between Isoforms of Thioredoxin h and Thioredoxin Reductase *Plant Physiol* **146**: 789–799.

Shahpiri, A., Svensson, B., and Finnie, C. (2009). From proteomics to structural studies of cytosolic/mitochondrial type thioredoxin systems in barley seeds. *Mol. Plant* **2**(3): 378–389.

Tripathi, B.N., Bhatt, I. and Dietz, K.J. (2009). Peroxiredoxins: a less studied component of hydrogen peroxide detoxification in photosynthetic organisms. *Protoplasma* **235**: 3–15.

Waksman, G., Krishna, T.S., Williams, C.H.Jr. and Kuriyan, J. (1994). Crystal structure of *Escherichia coli* thioredoxin reductase refined at 2 Å resolution. Implications for a large conformational change during catalysis. *J. Mol. Biol.* **236**: 800–816.

Wallace, A.C., Laskowski, R.A. ánd Thornton, J.M. (1995). LIGPLOT: a program to generate schematic diagrams of protein-ligand interactions, *Protein Eng.* **8**: 127**–**134.

Williams, C.H.Jr., Zanetti, G., Arscott, L.D. and McAllister, J.K. (1967). Lipoamide dehydrogenase, glutathione reductase, thioredoxin reductase, and thioredoxin, *J. Biol. Chem.* **242**(22): 5226–5231.

Williams, C.H.Jr. (1976). Flavin containing dehydrogenases, Vol. 13, The Enzymes, edited by P. D. Boyer, pp. 89–173. New York: Academic Press.

Wong, J.H., Kim, Y.B., Ren, P.H., Cai, N., Cho, M.J., Hedden, P., Lemaux, P.G. and Buchanan, B.B. (2002). Transgenic barley grain overexpressing thioredoxin shows evidence that the starchy endosperm communicates with the embryo and the aleurone. *P. Natl. Acad. Sci. USA* **99**: 16325–16330.

Zhang, Z., Bao, R., Zhang, Y., Yu, J., Zhou, C.-Z. and Chen, Y. (2009). Crystal structure of Saccharomyces cerevisiae cytoplasmic thioredoxin reductase Trr1 reveals the structural basis for species-specific recognition of thioredoxin. *Biochim. Biophys. Acta* **1794**: 124–128.

Figures and tables

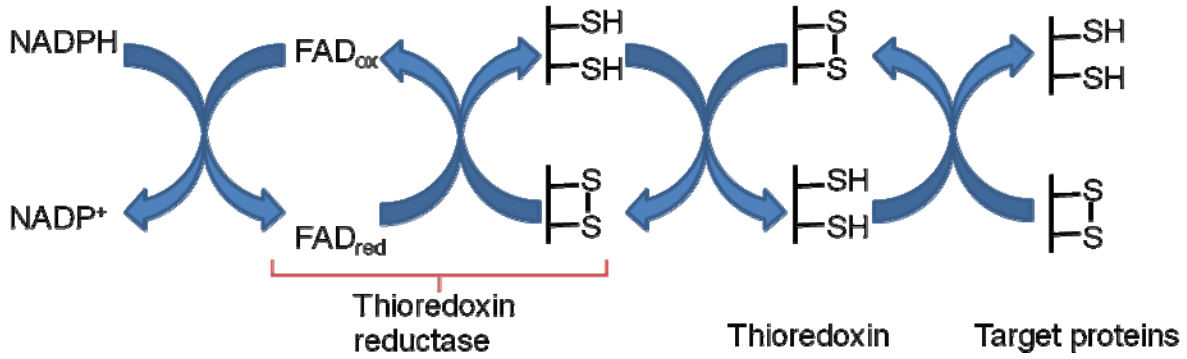

Figure 1. The NADPH-dependant thioredoxin system. Reducing equivalents are transferred from NADPH to an FAD molecule bound in NADPH-dependent thioredoxin reductase (NTR) and further to a disulfide, also located in NTR. NTR then reduces Trx, which in turn reduces disulfide bonds in target proteins.

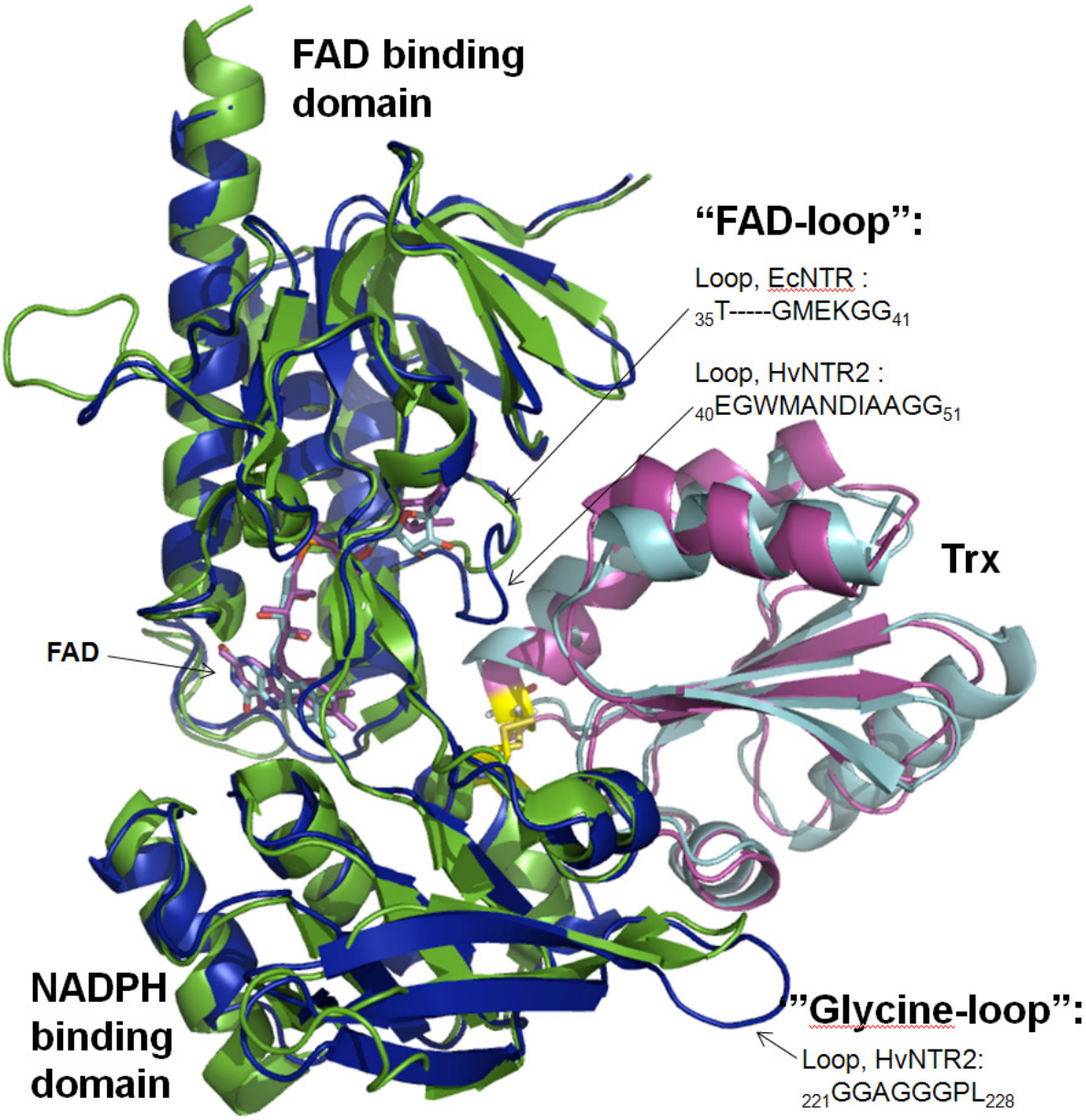

Figure 2. A model of the complex of HvNTR2 (dark blue) bound covalently through an intermolecular disulfide bond (yellow) to HvTrxh2 (cyan). The model is superposed with the crystal structure of EcNTR in the FR conformation (green) bound to EcTrx (magenta) (pdb 1F6M, Lennon *et al.,* 2000). The FAD molecules in HvNTR2 and EcNTR are shown in cyan and magenta respectively, and the positions of two examined loops, called the 'FAD-loop' and the 'Glycine-loop' in the following, are marked with arrows. Image generated in PyMOL (DeLano, 2002).

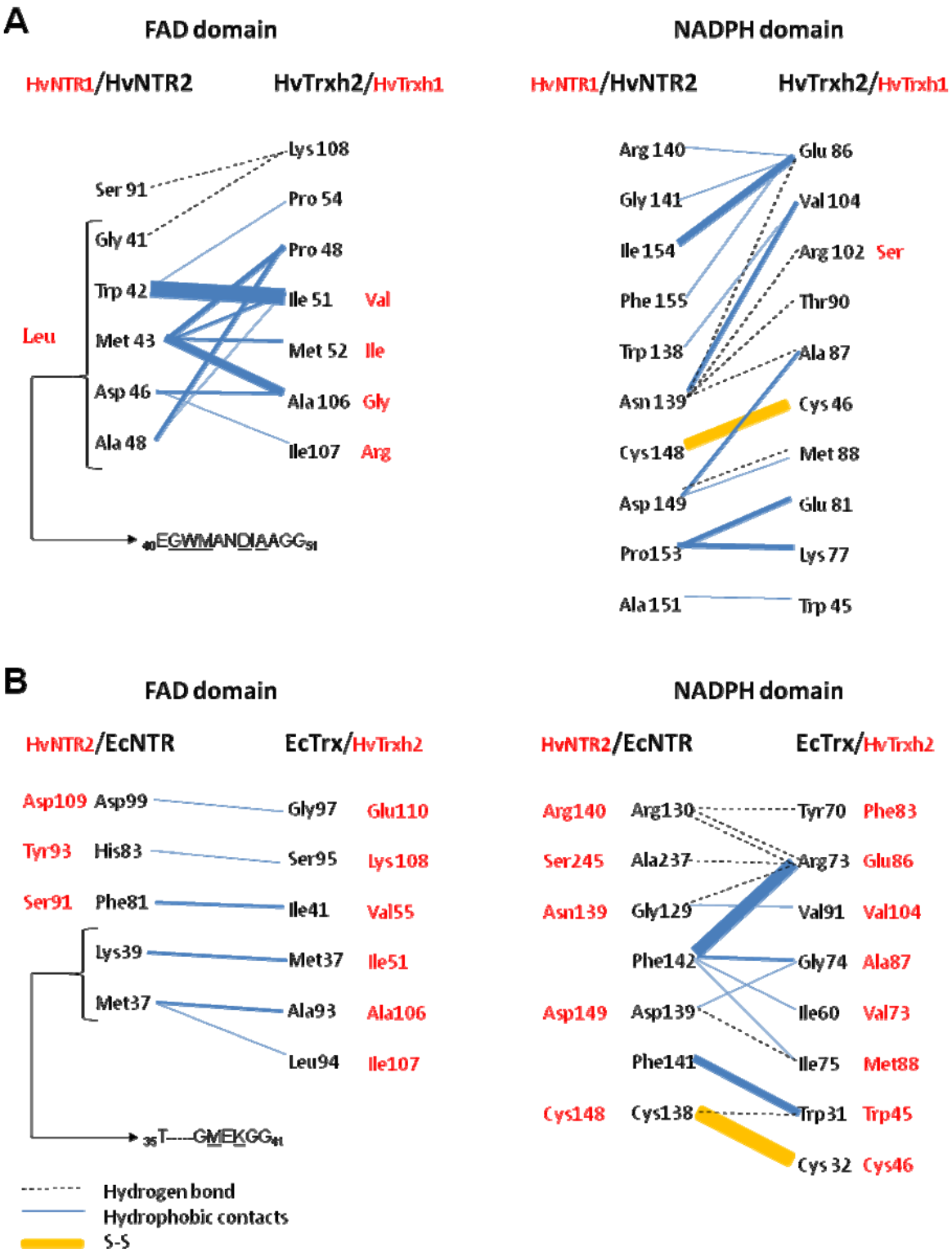

Figure 3. Interactions identified by LIGPLOT (Wallace *et al*., 1995) on (**A**) the model of a complex between HvNTR2 and HvTrxh2 and (**B**) on the crystal structure of a complex of EcNTR:EcTrx (pdb 1F6M, Lennon *et al.,* 2000). In (A), HvNTR1 or HvTrxh1 residues corresponding to the HvNTR2 and HvTrxh2 residues in the model are included and shown in red in case they are not identical to the residues in the HvNTR2 and HvTrx2

isoforms. The interactions are shown for the FAD domain (left panel) and for the NADPH domain (right panel) of HvNTR2. The residues marked with a left bracket are all positioned in the FAD-loop with the sequence $_{40}$EGWMANDIAAGG$_{51}$ found in the FAD domain of HvNTR2. Its position is shown in Figure 2. In B), the corresponding residues in HvNTR2 or HvTrxh2 are shown in red (for a few of the residues they could not be assigned since the sequences and structures vary too much). The residues marked with a left bracket are positioned in a loop (corresponding to the FAD-loop of HvNTR2) with the sequence $_{35}$T-----GMEKGG$_{41}$. The width of the blue connecting lines is scaled to indicate the number of hydrophobic contacts between atoms in the residues.

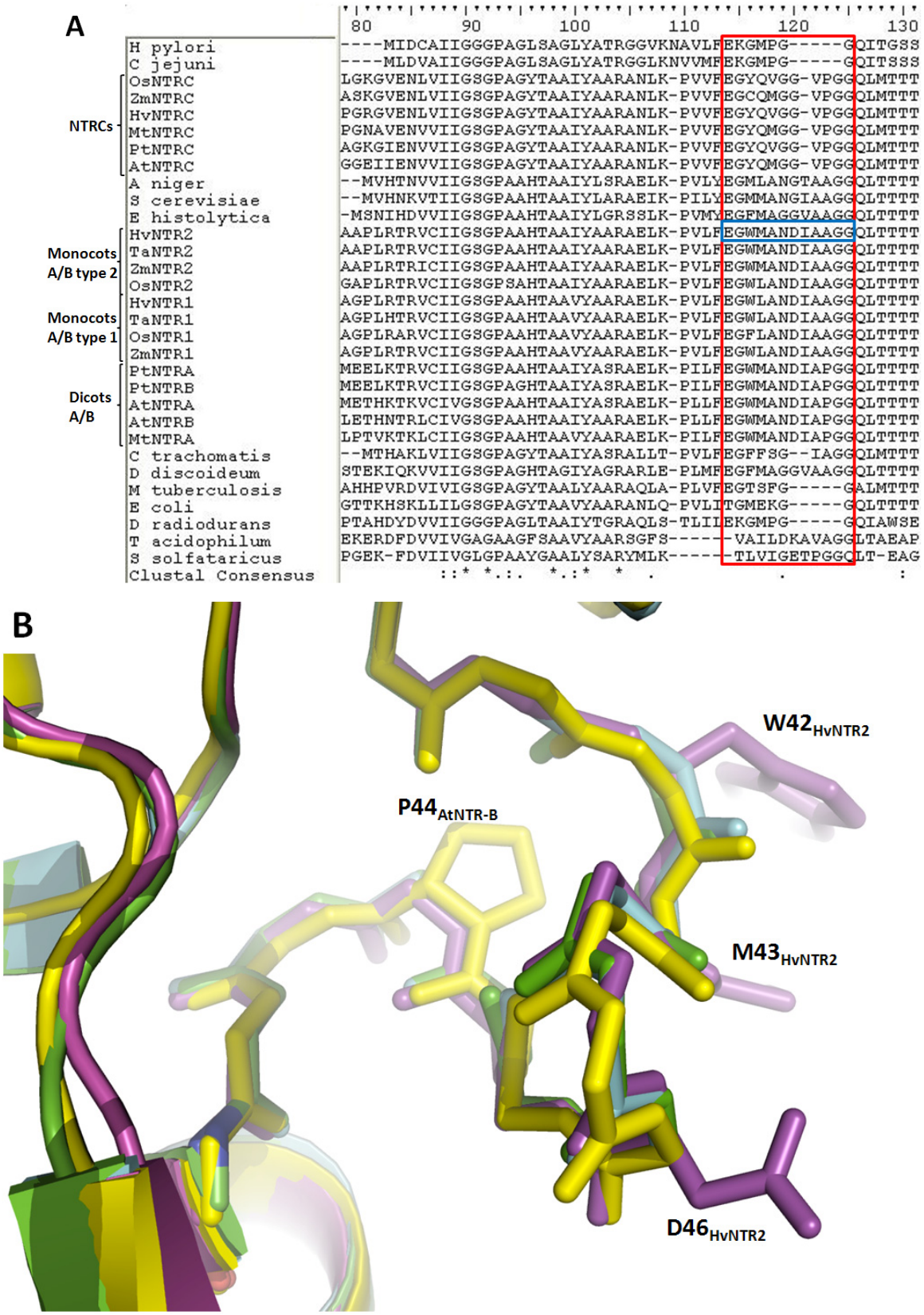

Figure 4. Partial alignment of selected NTRs (see below) and structural comparison of the FAD-loop. (**A**) The boxed FAD-loop is conserved in plants and yeast (red). The same loop is boxed in blue for HvNTR2. (**B**) Comparison of the FAD-loop in the available structures of eukaryotic LMW NTRs: HvNTR2 (magenta, pdb 2WHD, Kirkensgaard *et al.*, 2009), AtNTR-B (yellow, pdb 1VDC, Dai *et al.*, 2006), and two structures of NTR

from yeast (cyan, pdb 3D8X, Zhang *et al*., 2009 and green, pdb 3ITJ, Oliveira *et al*., 2010). Only the backbones of the loops are shown for clarity, except the proline from AtNTR-B and three of the residues from HvNTR2 predicted to interact with HvTrxh2. (**A)** The NTRs, with their accession numbers given in parentheses, are HvNTR1 (A9YZV9), HvNTR2 (A9LN30) and HvNTRC (B0FXK2) from *Hordeum vulgare* (barley); TaNTR1 (Q8VX47) and TaNTR2 (TC297680) from *Triticum aestivum* (wheat); OsNTR1 (Q69PS6), OsNTR2 (Q6ZFU6) and OsNTRC (Q70G58) from *Oryza sativa* (rice); ZmNTR1 (B6TPI3), ZmNTR2 (B7ZY93) and ZmNTRC (B4FJQ7) from *Zea mays* (maize); AtNTRA (Q39242), AtNTRB (Q39243) and AtNTRC (O22229) from *Arabidopsis thaliana* (mouse-ear cress); PtNTRA (AC149479), PtNTRB (B9I0K8) and PtNTRC (B9H9S9) from *Populus trichocarpa* (western balsam poplar); MtNTRA (A6XJ26) and MtNTRC (A6XJ27) from *Medicago truncatula* (barrel medic, a legume); S_cerevisiae (P29509) from *Saccharomyces cerevisiae* (yeast); D_discoideum (Q54UU8) from *Dictyostelium discoideum* (amoeba "slime mold"); E_histolytica (C4LW95) from *Entamoeba histolytica* (anaerobic parasitic protozoan); A_niger (XP_001389279) from *Aspergillus niger* (fungus); T_acidophilum (Q9HJI4) from *Thermoplasma acidophilum* (facultative anaerobe archaea); S_solfataricus (Q97W27) NTRB from *Sulfolobus solfataricus* (archaea); E_coli (P0A9P4) from *Escherichia coli* (Gram-negative bacteria); C_trachomatis (O84101) from *Chlamydia trachomatis* (Gram-negative bacteria); M_tuberculosis (P52214) from *Mycobacterium tuberculosis* (bacteria); H_pylori (P56431) from *Helicobacter pylori* (Gram-negative bacteria); D_radiodurans (Q9RSY7) from *Deinococcus radiodurans* (extremophilic bacteria, Gram-positive), and C_jejuni (Q0PBZ1) from *Campylobacter jejuni* (Gram-negative bacteria). The alignment is made in ClustalW2 (Thompson *et al*., 1994) and edited using BioEdit (Hall, 1999). A full alignment is given in Supplementary data 1.

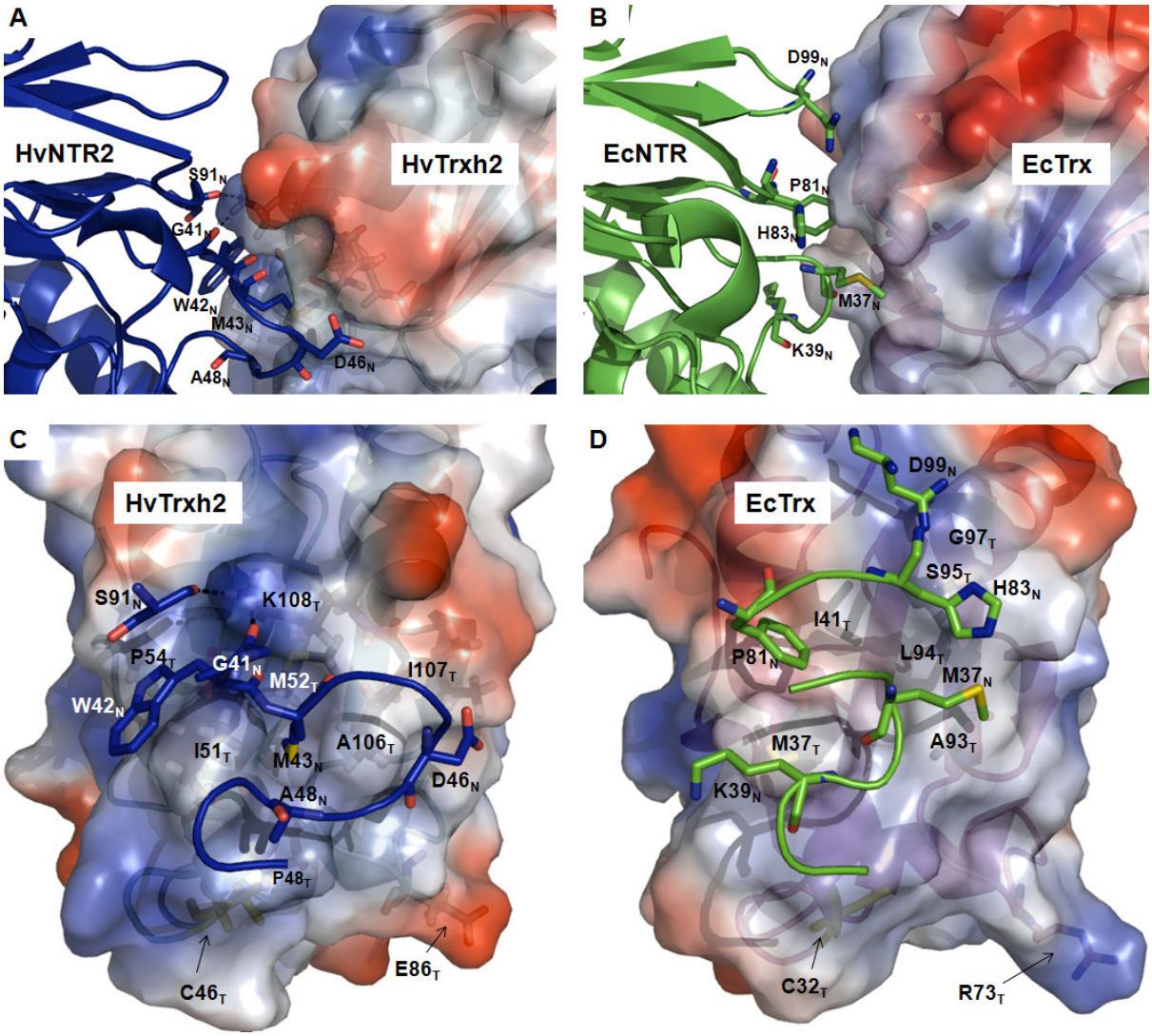

Figure 5. Residues involved in interactions between Trx and the FAD domain of NTR in complexes of HvNTR2 (dark blue):HvTrxh2 ((**A**) and (**C**)) and EcNTR (green):EcTrx ((**B**) and (**D**), pdb 1F6M, Lennon *et al.,* 2000). Residues from NTR and Trx are marked with 'N' and 'T', respectively. The surfaces of the Trxs are shown as electrostatic surface potential plots, where blue is positive and red negative electrostatic potential. In (**C**) and (**D**) the active site cysteine (C32 in HvTrxh2 and C46 in EcTrx) and a residue involved in binding to the NADPH domain (R73 in EcTrx and E86 in HvTrxh2) are marked with arrows. The images were generated using the software PyMOL (Delano, 2002).

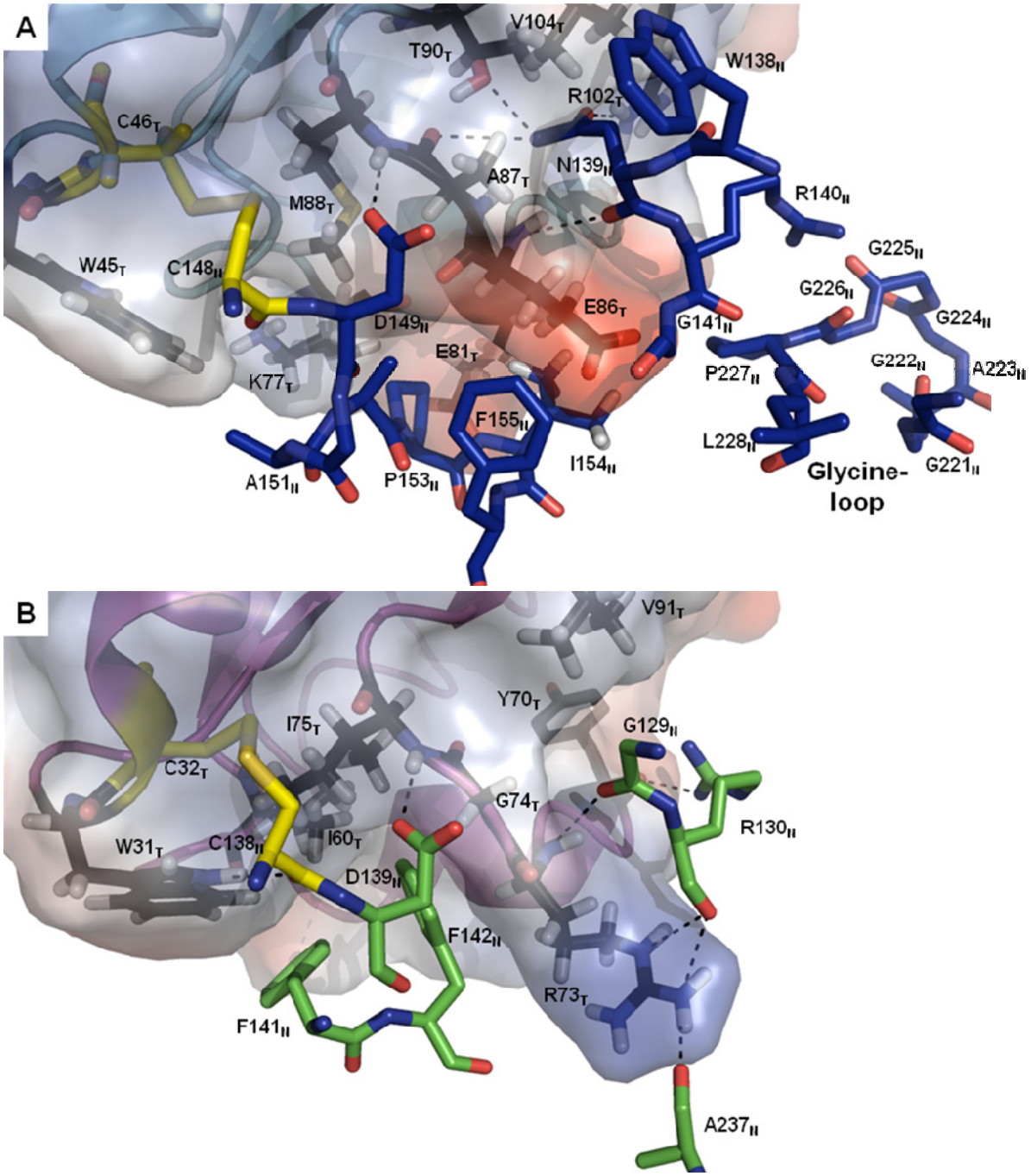

Figure 6. Comparison of residues involved in the interactions between of Trx and the NADPH domain of NTR in (**A**) the modelled complex of HvNTR2 (dark blue):HvTrxh2 and (**B**) EcNTR (green):EcTrx (pdb 1F6M, Lennon *et al.,* 2000). The Trxs are shown as electrostatic surface potential plots, where red is negative and blue positive. The active site cysteines are in yellow. In (**A**) the position of the Glycine-loop, $_{221}$GGAGGGPL$_{228}$, is shown (see also Figure 2 for its position in the structure).

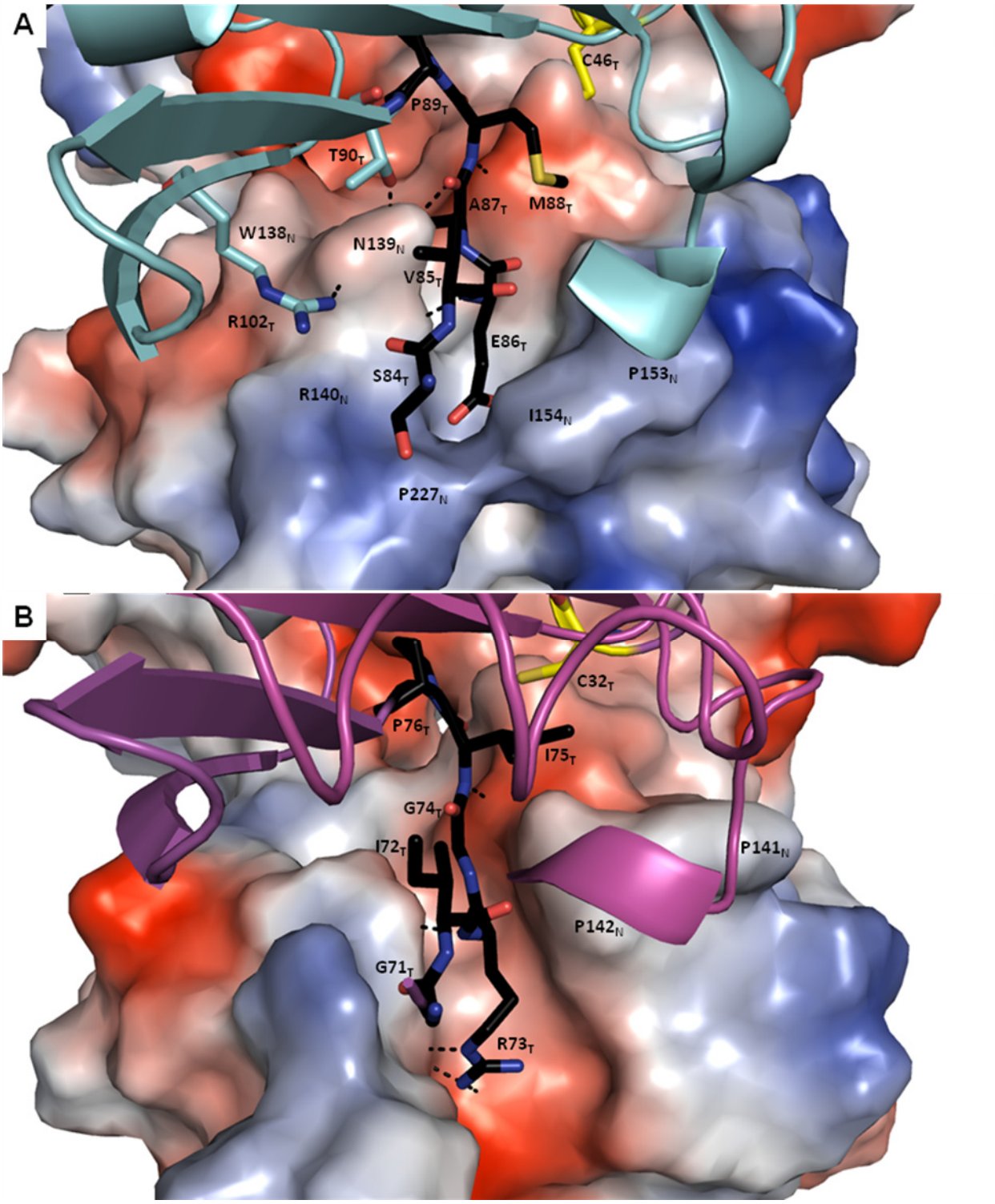

Figure 7. Comparison of the Trx binding surfaces in the NADPH domain of NTR in (**A**) the modelled complex of HvNTR2:HvTrxh2 (cyan) and (**B**) EcNTR:EcTrx (magenta, pdb 1F6M, Lennon *et al.,* 2000). The surfaces of the NTRs are shown as electrostatic surface potential plots, where red is negative and blue positive. Residues 23—29 and 80—83 of HvTrxh2 as well as 68-70 of EcTrx are omitted for clarity. Residues from the bound *cis*-proline-loop in Trx are shown in black. The active site cysteines in Trxs are in yellow.

Table 1. Kinetic parameters for the activity of wild-type and mutants of HvNTR2 in reactions with wild-type (wt) and mutant HvTrxh2 and AtTrxH3. Some reactions were too slow to be used to determine K_m and V_{max} marked by n.d. (not detectable). Instead the slope of the reaction [A_{412} s^{-1} μM^{-1}] is given as a relative percentage (last column) of the initial slope (slope for the very lowest substrate concentrations) of HvNTR2wt/HvTrxh2wt.

Wild-type

HvNTR2	HvTrxh2	K_m [µM]	k_{cat} [s^{-1}]	k_{cat}/K_m [M^{-1} s^{-1}]	k_{cat}/K_m [%]	initial slope [%]
wt	wt	1.17 ± 0.04	8.0 ± 0.10	(6.80 ± 0.25) · 10^6	100 ± 4	100
wt	HvTrxh1	1.23 ± 0.08	12.1 ± 0.20	(9.84 ± 0.66) · 10^6	145 ± 10	151
wt	AtTrxh3	0.80 ± 0.05	4.8 ± 0.09	(6.00 ± 0.39) · 10^6	88 ± 6	91
wt	EcTrx	149 ± 13	9.4 ± 0.38	(6.31 ± 0.61) · 10^4	0.9 ±0.1	1.0
AtNTR-B	AtTrxh3	0.48 ± 0.03	5.9 ± 0.10	(1.23 ± 0.08) · 10^7	181 ± 11	177
AtNTR-B	wt	60 ± 7	8.5 ± 0.48	(1.40 ± 0.18) · 10^5	2.1 ±0.3	2.0

FAD-domain mutants

HvNTR2	HvTrxh2	K_m [µM]	k_{cat} [s^{-1}]	k_{cat}/K_m [M^{-1} s^{-1}]	k_{cat}/K_m [%]	initial slope [%]
wt	I51G	15.5 ±0.7	15.9 ± 0.3	(1.03 ± 0.05) · 10^6	15 ± 1	23
M43A	wt	16.0 ± 0.8	11.4 ± 0.2	(7.13 ± 0.39) · 10^5	11 ± 1	15
M43A	I51G	n.d.	n.d.	n.d.	-	0.4
M43A	AtTrxh3	14.1 ± 1.2	14.8 ± 0.6	(1.05 ± 0.10) · 10^6	16 ± 1	15
M43A	EcTrx	n.d.	n.d.	n.d.	-	0.03
W42A	wt	45.7 ± 4.0	10.4 ± 0.4	(2.28 ± 0.22) · 10^5	3.3 ± 0.3	3.8
W42A	I51G	n.d.	n.d.	n.d.	-	0.5
W42A	AtTrxh3	2.4 ± 0.2	10.4 ± 0.4	(4.24 ± 0.41) · 10^6	62 ± 6	61
W42A	EcTrx	n.d.	n.d.	n.d.	-	0.016
W42A/M43A	wt	n.d.	n.d.	n.d.	-	0.09
W42A/M43A	I51G	n.d.	n.d.	n.d.	-	0.3
W42A/M43A	AtTrxh3	30.5 ± 3.4	11.0 ± 0.6	(3.61 ± 0.44) · 10^5	5.3 ± 0.6	5.5
W42A/M43A	EcTrx	n.d.	n.d.	n.d.	-	0.002
Δ42-47	wt	n.d.	n.d.	n.d.	-	0.06
Δ42-47	AtTrxh3	54.3 ± 5.2	15.3 ± 1.0	(2.82 ± 0.32) · 10^5	4.1 ± 0.5	4.9
Δ42-47	EcTrx	n.d.	n.d.	n.d.	-	0.0
wt	G47P	1.4 ± 0.1	7.9 ± 0.3	(5.49 ± 0.56) · 10^6	73 ± 8	77
Δ42-47	G47P	n.d.	n.d.	n.d.	-	0.0
W42A/M43A	G47P	n.d.	n.d.	n.d.	-	0.0
N45A_D46A	wt	2.2 ±0.2	7.3 ± 0.2	(3.30 ± 0.27) · 10^6	49 ± 4	47
N45A_D46A	AtTrxh3	4.2 ±0.6	10.7 ± 0.7	(2.55 ± 0.38) · 10^6	38 ± 6	37
N45A_D46A	EcTrx	n.d.	n.d.	n.d.	-	0.2
AtNTR-B	I51G	n.d.	n.d.	n.d.	-	0.1
AtNTR-B	G47P	n.d.	n.d.	n.d.	-	1.3

NADPH-domain mutants						
HvNTR2	**HvTrxh2**	**K_m [µM]**	**k_{cat} [s^{-1}]**	**k_{cat}/K_m [M^{-1} s^{-1}]**	**k_{cat}/K_m [%]**	**Initial slope [%]**
wt	E86A	0.57 ± 0.03	5.3 ± 0.1	(9.23 ± 0.50) · 10^6	137 ± 7	131
N139A	wt	0.68 ± 0.04	4.2 ± 0.1	(6.18 ± 0.37) · 10^6	91 ± 5	89
N139A	E86A	0.41 ± 0.01	4.2 ± 0.04	(1.02 ± 0.26) · 10^7	151 ± 4	128
R140A	wt	3.43 ± 0.27	5.1 ± 0.1	(1.49 ± 0.25) · 10^6	22 ± 2	22
R140A	E86A	1.60 ± 0.20	2.6 ± 0.1	(1.63 ± 0.21) · 10^6	24 ± 3	27
G225R_G226D_P227V	AtTrxh3	0.73 ± 0.07	3.9 ± 0.1	(5.34 ± 0.53) · 10^6	79 ± 8	79
G225R_G226D_P227V	wt	1.05 ± 0.06	1.8 ± 0.03	(1.71 ± 0.25) · 10^6	25 ± 1	32
G225R_G226D	AtTrxh3	0.67 ± 0.03	5.0 ± 0.1	(7.46 ± 0.35) · 10^6	110 ± 5	116
G225R_G226D	wt	1.28 ± 0.06	8.1 ± 0.1	(6.33 ± 0.31) · 10^6	93 ± 5	98
G222D_A223G_G224E	AtTrxh3	0.52 ± 0.04	5.0 ± 0.1	(9.62 ± 0.76) · 10^6	141 ± 11	133
G222D_A223G_G224E	wt	1.46 ± 0.06	7.9 ± 0.1	(5.41 ± 0.23) · 10^6	80 ± 3	82

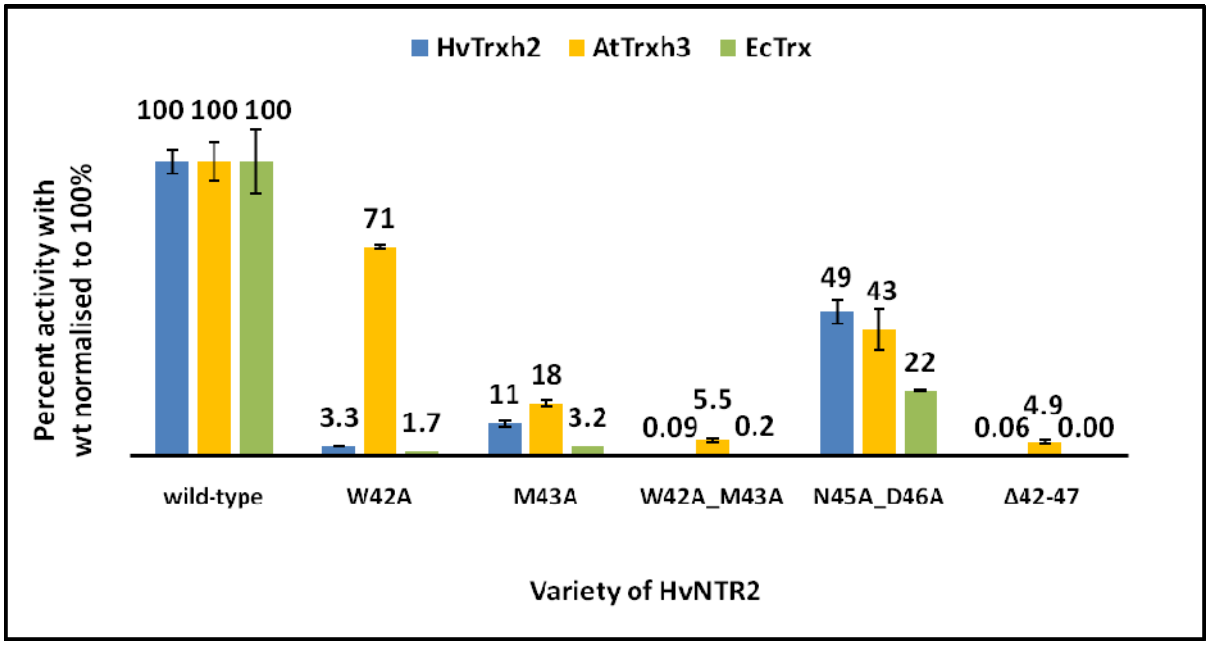

Figure 8. Relative k_{cat}/K_m. The values for the activity of HvNTR2wt with the three different substrates HvTrxh2, AtTrxh3 and EcTrx were all set to 100%. The activities of different mutants of HvNTR2 are shown relative to these.

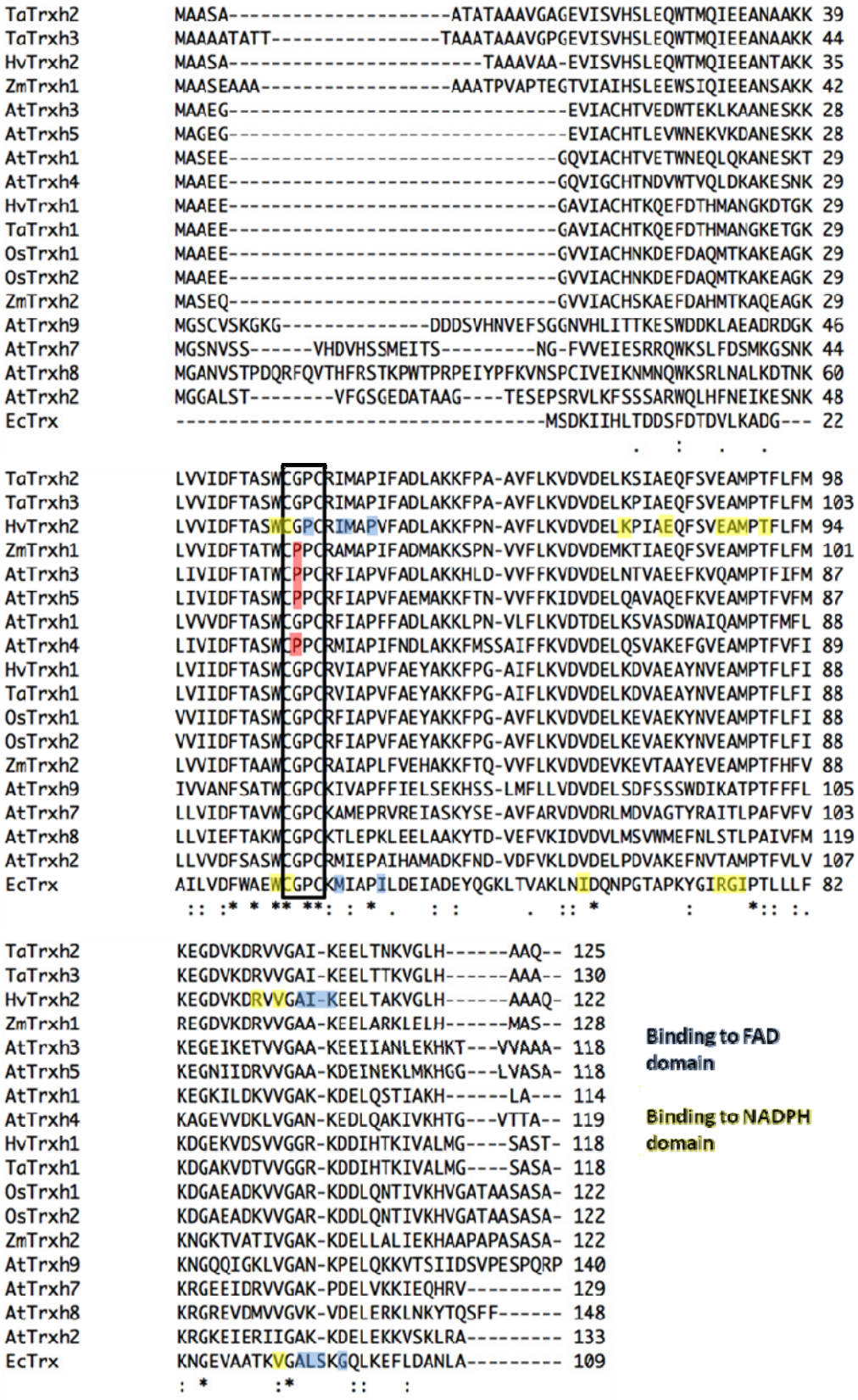

Figure 9. Multiple sequence alignment of selected thioredoxins from plants and from *E. coli*. The residues in HvTrxh2 which were predicted to bind to the FAD domain and the NADPH domain in the modelled complex of HvNTR2:HvTrxh2 are marked in blue and yellow, respectively. For EcTrx the residues interacting with EcNTR in the complex of EcNTR:EcTrx (pdb accession number 1F6M) were determined using LIGPLOT (Lennon *et al.*,

2000). The active site is boxed. In some of the sequences, the classical active site CGPC is replaced by the sequence CPPC (first proline marked in red). The sequences were aligned using Clustal-W2 (Thompson *et al*., 1994). The Trxs and their accession numbers in parentheses are TaTrxh1 (Q8GVD3), TaTrxh2 (Q9LDX4) and TaTrxh3 (Q7FT21) from *Triticum aestivum* (wheat), HvTrxh1 (Q7XZK3) and HvTrxh2 (Q7XZK2) from *Hordeum vulgare* (barley), ZmTrxh1 (Q4W1F7) and ZmTrxh2 (Q4W1F6) from *Zea mays* (maize), OsTrxh1 (Q0D840) and OsTrxh2 (A2YIW7) from *Oryza sativa* (rice) and AtTrxh1 (P29448), AtTrxh2 (Q38879), AtTrxh3 (Q42403), AtTrxh4 (Q39239), AtTrxh5 (Q39241), AtTrxh7 (NP_176182), AtTrxh8 (NP_177146) and AtTrxh9 (Q9C9Y6) from *Arabidopsis thaliana* (Mouse-ear cress), and EcTrx (P0AA25**)** from *E. coli*.

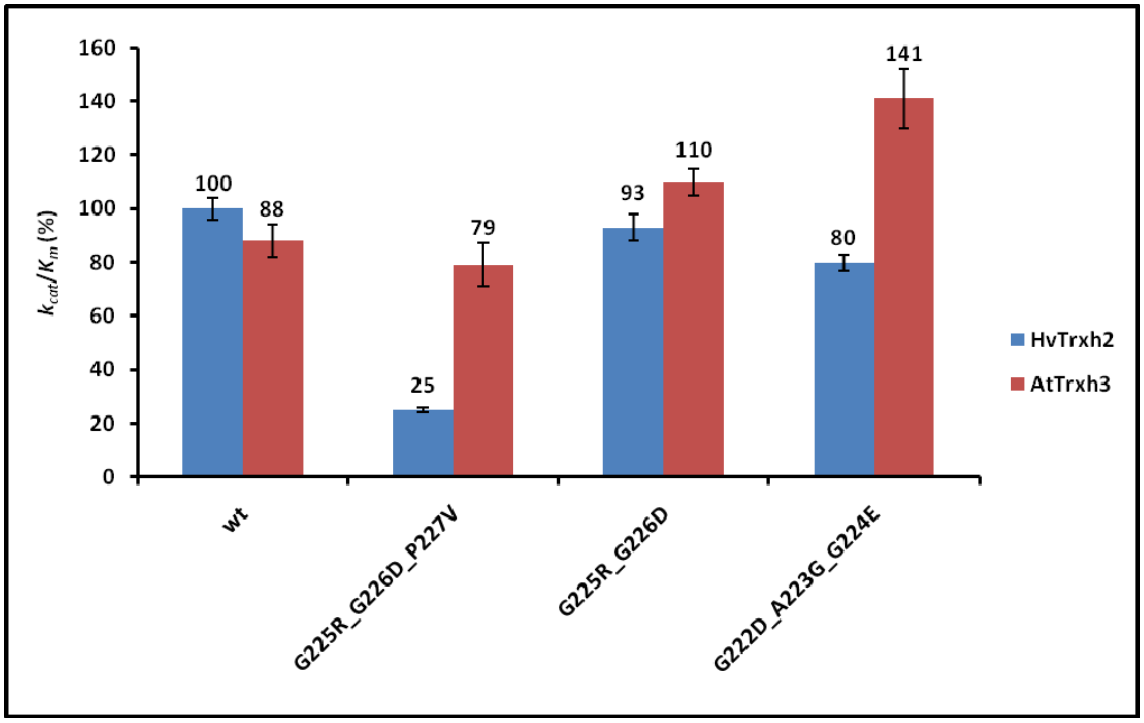

Figure 10. Relative values for k_{cat}/K_m. The value for the activity of HvNTR2wt with the HvTrxh2 was set to 100%. The activities of different mutants of HvNTR2 with either HvTrxh2 or AtTrxh3 are shown relative to these.

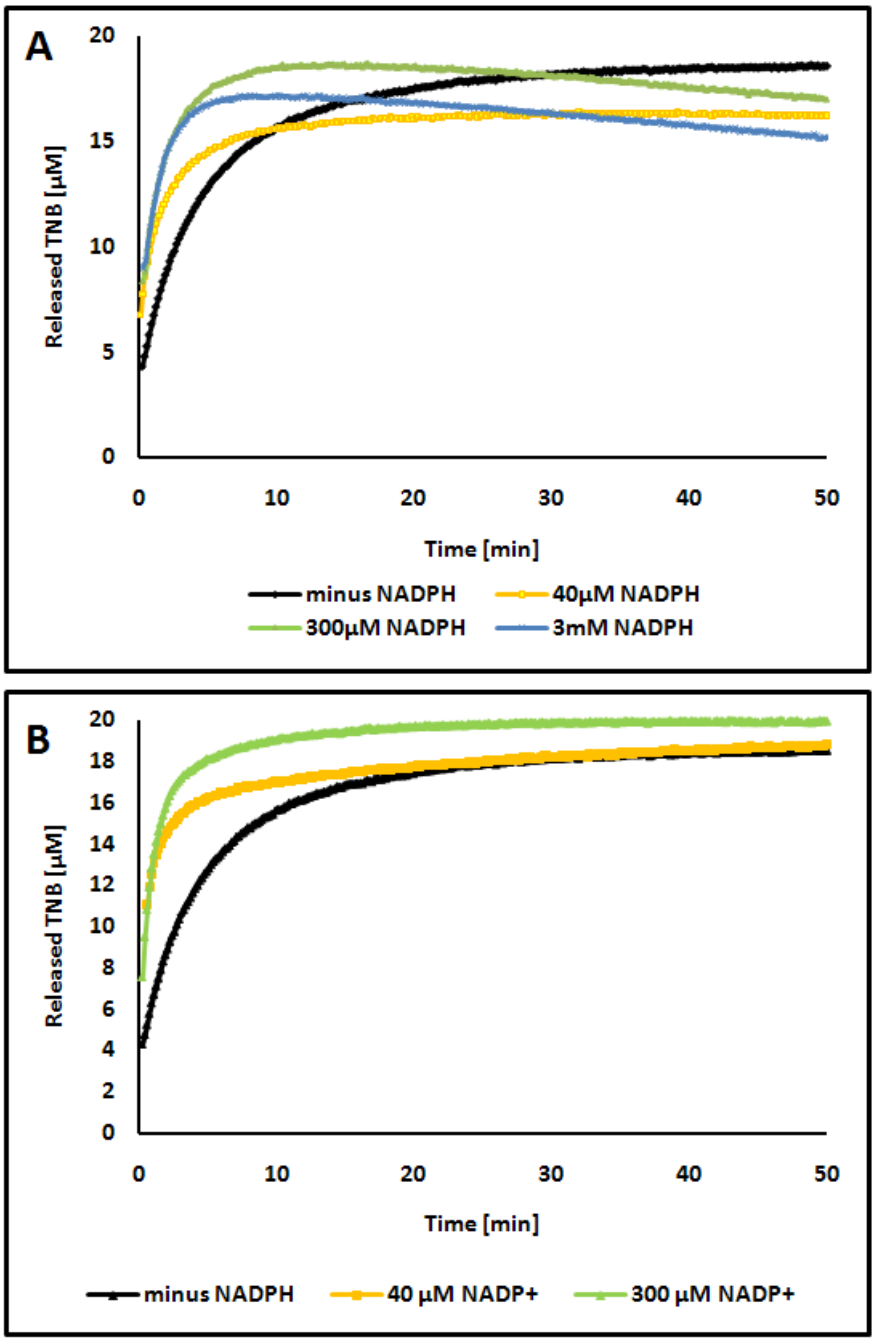

Figure 11. Complex formation. Release of TNB followed at A_{412} upon reaction of 30µM HvNTR2_C145S with 20µM HvTrxh2_C49S-TNB (black lines). (**A**) Addition of NADPH initially increased the rate of the complex formation but ended at lower absorbance than without NADPH, which may be due to reduction of FAD. (**B**) Addition of NADP+ increases the reaction rate.

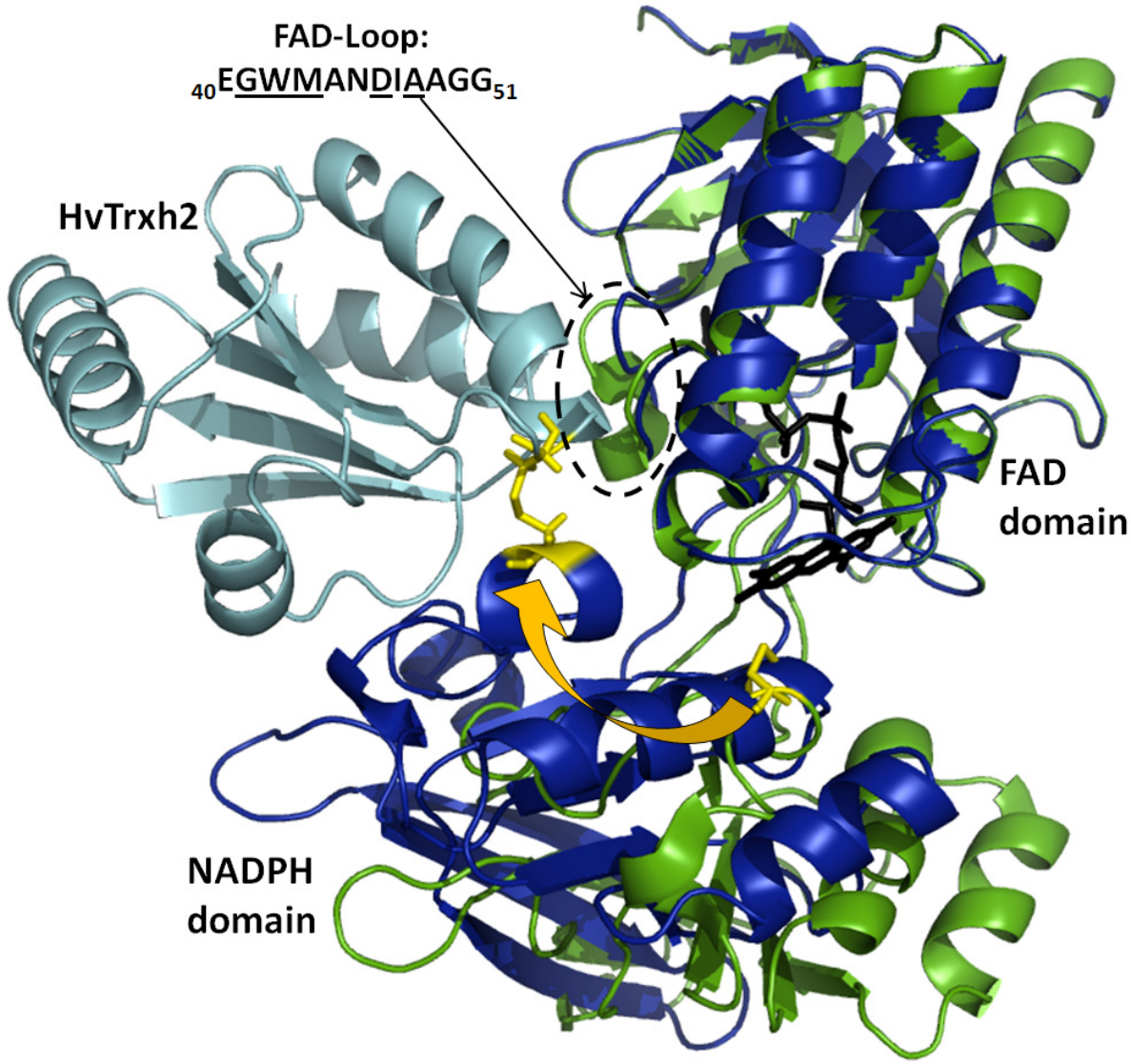

Figure 12. Superposition of the FAD domains of the modelled complex of HvNTR2 (dark blue):HvTrxh2 (cyan) and of the crystal structure of HvNTR2 (green, pdb accession 2WHD). The FAD-loop is circled and the active site cysteines are in yellow. The orange arrow indicates how the active site cysteines of HvNTR2 are brought in proximity to the active site cysteines of HvTrxh2, when HvNTR2 changes from FO to FR conformation.

Appendix G

Molecular Recognition in NADPH-Dependent Plant Thioredoxin Systems—Catalytic Mechanisms, Structural Snapshots and Target Identifications

PER HÄGGLUND,*[,1] KRISTINE GROTH KIRKENSGAARD,* KENJI MAEDA,* CHRISTINE FINNIE,* ANETTE HENRIKSEN[†] AND BIRTE SVENSSON*

**Enzyme and Protein Chemistry, Department of Systems Biology, Technical University of Denmark, DK-2800 Kgs. Lyngby, Denmark*
[†]Protein Chemistry Group, Carlsberg Laboratory, Gamle Carlsberg Vej 10, DK-2500 Valby, Denmark

[1]Corresponding author: Email: ph@bio.dtu.dk

Advances in Botanical Research, Vol. 52 0065-2296/09 $35.00

DOI: 10.1016/S0065-2296(09)52015-0

ABSTRACT

NADPH-dependent thioredoxin systems (NTS) control enzymatic activities and provide reducing equivalents to metabolic pathways in all types of organisms, from bacteria to mammals. In these redox systems, thioredoxin reduces disulfide bonds in target proteins and receives electrons from NADPH via thioredoxin reductase (NTR). Plant NTS were first discovered in wheat seeds some 30 years ago and were demonstrated to play a key role in the seed germination process. Since then, NTS have been identified in a large variety of photosynthetic organisms, and an organelle-specific pattern for their cellular localization is established. The last decade has witnessed a remarkable expansion of the knowledge about these systems and novel molecular architectures, catalytic mechanisms and target proteins have been revealed. In general, these findings have provided a wealth of information about the physiological role and molecular mechanisms of plant NTS, and this chapter will highlight some of the recent developments in this area.

ABBREVIATIONS

BASI	barley α-amylase/subtilisin inhibitor
DHAR	dehydroascorbate reductase
FO	flavin-oxidizing
FR	flavin-reducing
Grx	glutaredoxin
GR	glutathione reductase
GSH	glutathione
IAM	iodoacetamide
ICAT	isotope-coded affinity tags
mBBr	monobromobimane
MSR	methionine sulfoxide reductase
NTR	NADPH-dependent thioredoxin reductase
NTS	NADPH-dependent thioredoxin systems
TCEP	tris(2-carboxyethyl)phosphine
TNB	2-nitro-5-thiobenzoate
Trx	thioredoxin
4-VP	4-vinylpyridine

I. INTRODUCTION

Protein thiol groups are highly reactive and may undergo oxidative modifications under stress conditions. Furthermore, reversible thiol modifications are utilized for electron transfer in a range of enzymatic processes and redox signalling pathways. Therefore, control of intracellular thiol oxidation

is essential and in general maintained by the NADPH-dependent thioredoxin (Trx) and glutaredoxin (Grx) systems present in all kingdoms of life (Holmgren, 1989). Trx and Grx reduce disulfides in target proteins and receive reducing equivalents from NADPH via the flavoenzyme thioredoxin reductase (NTR) and glutathione reductase (GR), respectively. Trx is reduced directly by NTR, whereas GR donates electrons to the tripeptide glutathione (GSH), which in turn reduces Grx (Fig. 1). Examples of cross-talk between these NADPH-dependent systems include reduction of Trx by Grx (Gelhaye *et al.*, 2003; Koh *et al.*, 2008), Grx by NTR (Johansson *et al.*, 2004) and GSH by Trx (Kanzok *et al.*, 2001). The physiological significance of these overlapping interactions is underpinned by the non-viable phenotype of *Escherichia coli* and *Saccharomyces cerevisiae* double knock-out mutants lacking both systems, while single knock-out mutants are viable (Muller, 1996; Prinz *et al.*, 1997). Trx and Grx play key roles in many cellular processes, and targets can be divided into three categories: (i) enzymes, such as ribonucleotide reductase and methionine sulfoxide reductase (MSR) that depend on Trx/Grx as suppliers of reducing equivalents, (ii) redox-regulated transcription factors and enzymes (e.g. chloroplastic malate dehydrogenase) that are activated/deactivated through disulfide reduction and (iii) proteins such as T7 DNA polymerase that incorporate Trx/Grx as subunits of protein complexes (Arnér and Holmgren, 2000).

Plants have evolved advanced redox control systems that are remarkable in terms of complexity and diversity. For example, *Arabidopsis thaliana* contains more than 20 Trx genes that are grouped into categories (Trx-f,-m,-h,-o,-x,-y and -s) based on sequence similarity (Meyer *et al.*, 2002). A similar range of Trx genes has been found in other model organisms, such as rice (Nuruzzaman *et al.*, 2008). Trx-f and Trx-m are the most well-characterized categories of plant Trxs, and play important roles in the

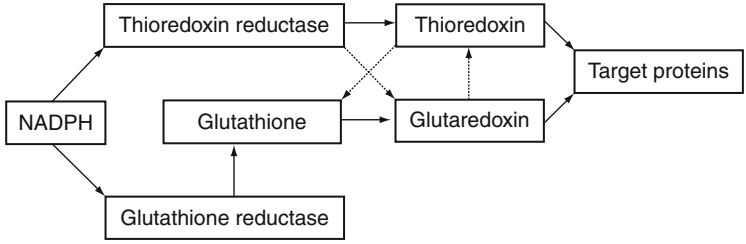

Fig. 1. NADPH-dependent redox systems. Solid arrows represent the general pathways for electron transfer and dotted arrows represent alternative pathways for reduction of Trx by Grx (Gelhaye *et al.*, 2003; Koh *et al.*, 2008), Grx by NTR (Johansson *et al.*, 2004) and GSH by Trx (Kanzok *et al.*, 2001).

regulation of key enzymes in the Calvin cycle and pentose phosphate pathway (Buchanan and Balmer, 2005). These chloroplastic Trxs are reduced by light via ferredoxin and ferredoxin:thioredoxin reductase in a unique thioredoxin system recently reviewed elsewhere (Schürmann and Buchanan, 2008). This chapter addresses the current knowledge of catalytic mechanisms and molecular recognition in NADPH-dependent thioredoxin systems (NTS) from plants with focus on recent data from proteome analyses and structural investigations. A very recent review has summarized data concerning NTR in plants (Jacquot *et al.*, 2009).

II. COMPONENTS OF NADPH-DEPENDENT Trx SYSTEMS IN PLANTS

A. Trx

1. Trx-h

Trx-h was the first NTR-dependent Trx to be discovered in plants and its name derives from its heterotrophic origin as opposed to the previously characterized chloroplastic Trxs (Johnson *et al.*, 1987; Suske *et al.*, 1979). Trx-h comprises the largest and most diverse group of plant Trxs. For example, *A. thaliana* contains at least eight Trx-h isoforms. The h isoforms show differential time and tissue-specific expression patterns (Cazalis *et al.*, 2006; Reichheld *et al.*, 2002). Although h-type Trxs are considered to be mainly cytosolic, some Trx-h are apparently translocated to other compartments (Fig. 2). For example, Trx-h has been isolated from the nucleus of

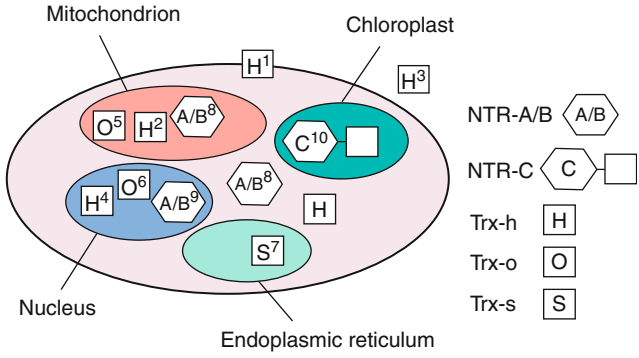

Fig. 2. A schematic cell illustrating locations of different components from NTS based on the following references: [1]Shi and Bhattacharyya, 1996; [2]Gelhaye *et al.*, 2004; [3]Juárez-Díaz *et al.*, 2006; [4]Serrato *et al.*, 2001; [5]Laloi *et al.*, 2001; [6]Marti *et al.*, 2009; [7]Alkhalfioui *et al.*, 2008; [8]Reichheld *et al.*, 2005; [9]Pulido *et al.*, 2009; [10]Serrato *et al.*, 2004.

cells in developing wheat seeds (Serrato and Cejudo, 2003; Serrato *et al.*, 2001). Furthermore, Trx-h transport to phloem sieve tubes is shown in many plant species, including rice and maize (Ishiwatari *et al.*, 1995, 1998; Santandrea *et al.*, 2002). Trx-h can be subdivided into three groups based on sequence similarity (Gelhaye *et al.*, 2005). In short, subgroup I contains several well-characterized cytosolic Trxs, and some members harbour a RKDD motif implicated in cell-to-cell transport (Fig. 3). Subgroup II contains proteins with N-terminal extensions that are translocated to mitochondria, the plasma membrane, or the extracellular matrix (Gelhaye *et al.*, 2002, 2004; Juárez-Díaz *et al.*, 2006; Shi and Bhattacharyya, 1996). Trx-h from subgroup III are exceptional as they are reduced by the GSH/Grx system and not by NTR (Gelhaye *et al.*, 2003; Juttner *et al.*, 2000; Koh *et al.*, 2008).

The first physiological functions ascribed to Trx-h were related to the germination of cereal seeds. Trx-mediated disulfide bond reduction was demonstrated to facilitate germination by (i) inactivating small proteinaceous inhibitors of proteolytic and amylolytic enzymes, (ii) activating hydrolytic enzymes, such as thiocalsin and pullulanase and (iii) enhancing the solubility of storage proteins (Besse *et al.*, 1996; Kobrehel *et al.*, 1991, 1992). Indeed, overexpression of Trx-h in barley seeds results in an accelerated germination rate, an increase in gibberellic acid concentration, and an increased α-amylase release from the aleurone layer (Cho *et al.*, 1999; Wong *et al.*, 2002). Trx-h isoforms display different temporal and spatial distributions in cereal seed tissues indicating that they may have different roles during seed germination (Cazalis *et al.*, 2006; Maeda *et al.*, 2003; Shahpiri *et al.*, 2008).

The role of Trx-h in oxidative stress resistance has been investigated in complementation studies with yeast mutants deprived of endogenous Trxs (Bréhélin *et al.*, 2000; Mouaheb *et al.*, 1998). It was concluded that Trx-h acts as an electron donor for MSR as judged by the ability of several *A. thaliana* Trx-h to restore growth on methionine sulfoxide as sole sulphur source. This was confirmed in a later study that described the mode of regeneration of plant MSR of the A type (Rouhier *et al.*, 2007). The *A. thaliana* Trx-h isoforms appear to have at least partially non-redundant functions as two isoforms, *At*Trxh2 and *At*Trxh3, confer a different extent of tolerance to hydrogen peroxide (Bréhélin *et al.*, 2000; Mouaheb *et al.*, 1998). In this context, it is interesting to note that *At*Trxh3 has been demonstrated to interact directly with peroxiredoxin *in vivo* (Verdoucq *et al.*, 1999) and also *in vitro* (Rouhier *et al.*, 2002). In addition, Trx-h plays a key role in pollen self-incompatibility by inhibiting an S-locus receptor kinase in *Brassica oleracea* (Bower *et al.*, 1996; Cabrillac *et al.*,

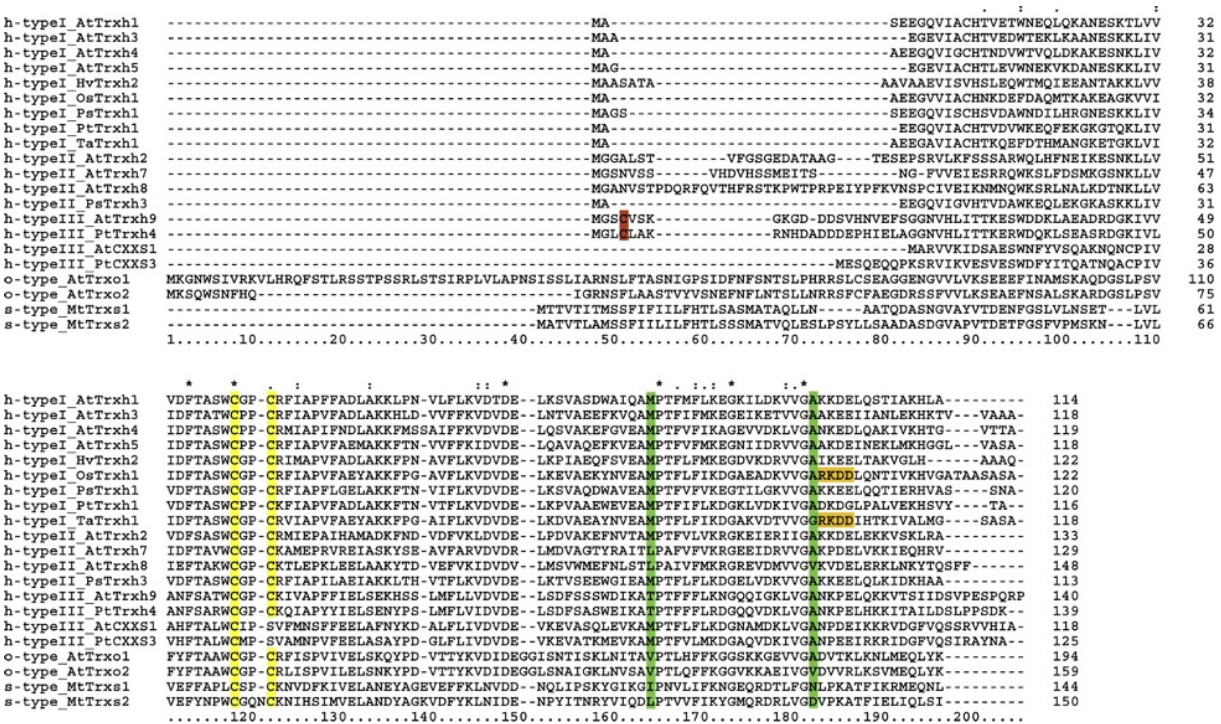

Fig. 3. Multiple sequence alignment of Trx-h, Trx-o and Trx-s. The catalytic cysteines in the CXXC motif and a third cysteine implicated in the catalytic mechanism of class III h-type Trxs are highlighted in light and dark gray (yellow and red in the web version), respectively. Residues aligned with barley *Hv*Trxh2 M88 and A106 implicated in target recognition are in dark gray (green in the web version). The RKDD motif implicated in cell-to-cell transport is highlighted in mid gray (orange in the web version). *At*Trxh1 (P29448); *At*Trxh3 (Q42403); *At*Trxh4 (Q39239); *At*Trxh5 (Q39241); *Hv*Trxh2 (Q7XZK2); *Os*Trxh1(Q0D840); *Ps*Trxh1 (Q9AR82); *Pt*Trxh1 (B9GRI3)); *Ta*Trxh1 (Q8GVD3); *At*Trxh2 (Q38879); *At*Trxh7 (NP_176182); *At*Trxh8 (NP_177146); *Ps*Trxh3 (Q8GUR9); *At*Trxh9 (Q9C9Y6); *Pt*Trxh4 (P85801); *At*CXXS1 (NP_172620); *Pt*CXXS3 (EEE85494); *At*Trxo1 (AAC12840); *At*Trxo2 (AF396650); *Mt*Trxs1 (A9RAA5); *Mt*Trxs2 (A9RAA6). The sequences were aligned using CLUSTAL-W (Thompson *et al.*, 1994).

2001). Other processes associated with Trx-h include sulphate assimilation (Bréhélin *et al.*, 2000), cell cycle regulation (Mouaheb *et al.*, 1998), DNA damage repair (Sarkar *et al.*, 2005) and pathogen interactions (Sweat and Wolpert, 2007).

2. *Trx-o and Trx-s*

The o-type Trxs have N-terminal transit peptides (Fig. 3), and *At*Trxo1 from *A. thaliana* has been localized in mitochondria (Laloi *et al.*, 2001), while *Ps*Trxo1 from garden pea (*Pisum sativum*) was recently reported to be present in the nucleus (Marti *et al.*, 2009). So far the physiological importance of Trx-o is not well defined, but it has been shown to interact with the mitochondria-specific peroxiredoxin PrxIIF (Barranco-Medina *et al.*, 2008) and to activate the alternative oxidase that acts as an electron acceptor in the electron transport chain under oxidative stress conditions (Marti *et al.*, 2009).

Recently, two Trx sequences that did not match the hitherto described Trx types were isolated from *Medicago truncatula* (Alkhalfioui *et al.*, 2008). The genes contained N-terminal signal peptides (Fig. 3), and it was shown that the proteins were translocated to the endoplasmic reticulum (Fig. 2). The proteins appear to be specifically expressed in *M. truncatula* grown in symbiosis with the nitrogen-fixing bacterium *Sinorhizobium meliloti* and were assigned to a new Trx type, coined as Trx-s. These proteins seem to be unique to *M. truncatula* since no orthologs were identified in other plant species (Alkhalfioui *et al.*, 2008). Notably, only one of the two proteins (*Mt*Trxs1) is reduced by *M. truncatula* NTR and both proteins lack disulfide reductase activity in the insulin-based Trx assay (Holmgren, 1979).

B. NTR

1. *NTR-A/B*

Even though NTS in plants were described 30 years ago, it was not until 1994 that the first gene encoding a plant NTR was isolated from *A. thaliana* (Jacquot *et al.*, 1994). The protein was named NTR-B, and later the highly similar NTR-A was isolated from mitochondrial fractions (Laloi *et al.*, 2001). The *A. thaliana* genes encoding NTR-A and NTR-B are transcribed in short and long versions, and the products of the longer transcripts are translocated to mitochondria. It has been concluded that NTR-B is the major mitochondrial form, while NTR-A is most abundant in the cytoplasm (Reichheld *et al.*, 2005). Remarkably, *ntra ntrb* knock-outs in *A. thaliana* are

viable and fertile but hypersensitive to buthionine sulfoximine, an inhibitor of glutathione biosynthesis (Reichheld *et al.*, 2007). Highly similar NTR-A and NTR-B orthologs have also been identified in several other plant species, for example, barley (Shahpiri *et al.*, 2008) and wheat (Serrato *et al.*, 2002). Wheat NTR has been demonstrated to co-localize with Trx-h in the nucleus (Pulido *et al.*, 2009).

Enzyme kinetics analyses suggest that both NTR-A and NTR-B are efficient electron donors for Trx-h and Trx-o (Laloi *et al.*, 2001). Furthermore, NTR-B shows similar affinity for four out of five tested *A. thaliana* Trx-h isoforms, and two forms of barley Trx-h (*Hv*Trxh1 and *Hv*Trxh2) are reduced at a comparable rate by the two endogenous NTR-A/B orthologs, *Hv*NTR1 and *Hv*NTR2 (Rivera-Madrid *et al.*, 1995; Shahpiri *et al.*, 2008). Taken together, these results could suggest that NTRs have rather broad specificities for Trxs or that the variations between NTR-A/B and Trx isoforms within a species are relatively conservative (Table I). However, cross-species comparisons reveal that interactions between NTRs and Trxs are highly species-dependent and that NTR–Trx interactions are specific (Table I). For example, barley NTR has a hundred-fold reduced affinity (increased K_M) for *E. coli* Trx when compared to endogenous Trx-h (Shahpiri *et al.*, 2008). Besides the capacity to transfer electrons to oxidized Trx, NTR has been demonstrated to activate 1-Cys peroxiredoxin in a Trx-independent manner (Pulido *et al.*, 2009).

2. NTR-C

NTR-C was recently isolated from rice and *A. thaliana* (Serrato *et al.*, 2004). This protein has a different architecture, with an N-terminal domain similar to NTR-A/B and a Trx-like domain in a C-terminal extension. Noticeably, this molecular architecture seems to be found mainly among plants, but recurs in the pathogenic bacterium *Mycobacterium leprae* (Wieles *et al.*, 1995a,b). NTR-C is localized in chloroplasts and acts as an efficient electron donor to 2-Cys peroxiredoxin (Alkhalfioui *et al.*, 2007a; Moon *et al.*, 2006). If either the NTR or Trx domain is removed, the capacity to reduce 2-Cys peroxiredoxin is lost indicating that NTR-C functions as a complete NTS in a single polypeptide chain. In *A. thaliana*, *ntrc* knock-outs show severe growth inhibition, oxidative stress sensitivity, perturbed chlorophyll biosynthesis and lower rate of photosynthesis (Pérez-Ruiz *et al.*, 2006; Serrato *et al.*, 2004; Stenbaek *et al.*, 2008).

TABLE I
Interactions between NTRs and Trxs from different sources measured as K_M in enzyme kinetics assays with Trxs in varying concentrations as substrates for NTRs

NTR	Trx	K_M (μM)
A. thaliana NTRA[a]	*A. thaliana* Trxo1	2.6
A. thaliana NTRA[a]	*A. thaliana* Trxo2	1.8
A. thaliana NTRA[a]	*A. thaliana* Trxh3	2.8
A. thaliana NTRB[a]	*A. thaliana* Trxo1	2.2
A. thaliana NTRB[a]	*A. thaliana* Trxo2	2.1
A. thaliana NTRB[a]	*A. thaliana* Trxh3	3.0
A. thaliana NTRB[b]	*A. thaliana* Trxh1	2.0
A. thaliana NTRB[b]	*A. thaliana* Trxh2	0.8
A. thaliana NTRB[b]	*A. thaliana* Trxh3	0.7
A. thaliana NTRB[b]	*A. thaliana* Trxh4	20
A. thaliana NTRB[b]	*A. thaliana* Trxh5	1.6
A. thaliana NTRB[c]	*C. reinhardtii* Trx-h	1.6
A. thaliana NTRB[c]	*C. reinhardtii* Trx-m	5.8
A. thaliana NTRB[c]	*E. coli* Trx	81
H. vulgare NTR1[d]	*H. vulgare* Trxh1	1.2
H. vulgare NTR1[d]	*H. vulgare* Trxh2	1.8
H. vulgare NTR2[d]	*H. vulgare* Trxh1	1.1
H. vulgare NTR2[d]	*H. vulgare* Trxh2	1.3
H. vulgare NTR2[d]	*E. coli* Trx	107
A. thaliana NTRB[d]	*H. vulgare* Trxh1	25
A. thaliana NTRB[d]	*H. vulgare* Trxh2	27
T. aestivum NTR[e]	*T. aestivum* Trx-h	7.6
T. aestivum NTR[e]	*E. coli* Trx	36

[a]Laloi *et al.* (2001)
[b]Rivera-Madrid *et al.* (1995)
[c]Jacquot *et al.* (1994)
[d]Shahpiri *et al.* (2008)
[e]Serrato *et al.* (2002)

III. STRUCTURAL SNAPSHOTS AND CATALYTIC MECHANISMS

A. Trx

1. Catalytic mechanisms

Trx reduces protein disulfides through a dithiol/disulfide exchange reaction involving two thiol groups in a conserved C_NXXC_C motif (Figs. 3 and 4). The cysteine residue at the N-terminal end of this motif (C_N) has a perturbed, low thiol-pK_a value and the deprotonated thiolate form acts as a nucleophile and attacks a protein disulfide to transiently form an intermolecular disulfide bond (Kallis and Holmgren, 1980). The thiol group of the other active-site

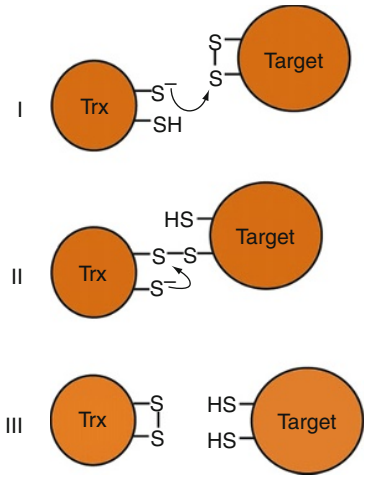

Fig. 4. Catalytic mechanism of Trx. (i) The N-terminal cysteine (C_N) in the Trx redox-active C_NXXC_C motif makes a nucleophilic attack on the target disulfide bond and forms an intermolecular Trx-target disulfide intermediate. (ii) The disulfide is attacked by the C-terminal cysteine (C_C). (iii) The reduced target protein and oxidized Trx is released.

cysteine residue (C_C) subsequently attacks this disulfide bond, resulting in the release of the reduced target protein and oxidized Trx. An aspartic acid residue (D26 in *E. coli* Trx) is proposed to act as a general acid/base catalyst for the protonation/deprotonation of the C_C thiol group during Trx oxidoreduction (Chivers and Raines, 1997; Menchise *et al.*, 2001). A tryptophan residue at the immediate N-terminal side of the CXXC motif (Fig. 3) is conserved, and also suggested to be important for efficient catalysis (Krause and Holmgren, 1991; Krimm *et al.*, 1998).

In most plant Trxs, the C_NXXC_C motif is CGPC, but in some h-type Trxs from subgroup I it is replaced by CPPC (Fig. 3). This substitution of glycine with proline appears not to change the redox potential or the overall protein disulfide reductase activity of Trx (Behm and Jacquot, 2000; Bréhélin *et al.*, 2004; Rivera-Madrid *et al.*, 1995), but it nevertheless influences certain biological functions, such as sulphate assimilation (Bréhélin *et al.*, 2000). In the recently described s-type Trx from *M. truncatula*, the active-site motif is either CSPC (*Mt*Trxs1) or CGQNC (*Mt*Trxs2). Finally, some h-type Trxs from subgroup III lack one of the catalytic cysteines (CXXS) and consequently are not to be considered as 'true' Trxs according to the mechanism described above (Fig. 4). Indeed, Trxs with this type of CXXS motif show Grx-like activity (Gelhaye *et al.*, 2003).

2. 3D structures

Trxs are small proteins of ~12 kDa that display highly conserved 3D structures with a central five-stranded β-sheet surrounded by four α-helices in a $\beta\alpha\beta\alpha\beta\alpha\beta\beta\alpha$ topology (Holmgren *et al.*, 1975). The 3D structure of Trx includes the so-called Trx-fold ($\beta\alpha\beta\alpha\beta\beta\alpha$) (Martin, 1995), which also appears in other redox proteins with different functions, including glutathione transferase, Grx and protein disulfide isomerase. The active-site C_NXX_C motif is located at the N-terminus of α2 and the preceding loop (Fig. 5A). In accordance with the catalytic mechanism, the catalytic C_N is exposed to the solvent, while C_C is buried and inaccessible. The conserved aspartic acid residue proposed to act as a general acid/base during catalysis is located further toward the protein interior. The solvent accessible surface surrounding C_N is composed of hydrophobic and uncharged residues that form a shallow groove, suggested to act as a target-binding site (Eklund *et al.*, 1984).

3D structures have been determined for several plant Trx-h, including barley *Hv*Trxh1 and *Hv*Trxh2 (Fig. 5A), *A. thaliana At*Trxh1, poplar *Pt*Trxh1 and *Pt*Trxh4 (Fig. 5B), and *Chlamydomonas reinhardtii* Trxh1 (Coudevylle *et al.*, 2005; Koh *et al.*, 2008; Maeda *et al.*, 2008;

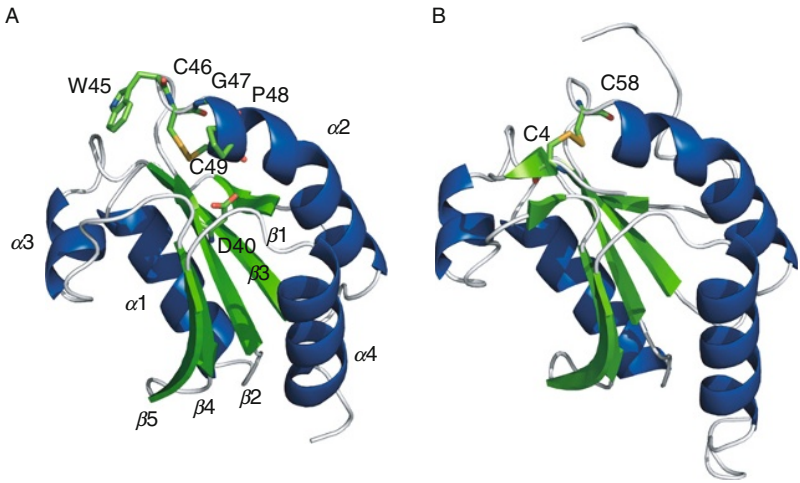

Fig. 5. (A) The structure of *Hv*Trxh2 from barley (h-type Trx from subclass I) in the oxidized form (Maeda *et al.*, 2008). The two conserved redox-active cysteines in the $_{45}$WCGPC$_{49}$ motif are connected by a disulfide bond. D40 corresponds to the aspartic acid residue proposed to act as a general acid/base during catalysis. β-Strands and α-helices are labelled. (B) The structure of a $C_C \rightarrow S$ mutant of *Pt*Trxh4 from poplar (h-type Trx from subgroup III) in the oxidized form (Koh *et al.*, 2008). A disulfide bond is formed between C58 (C_N) and C4 (C_{NT}) conserved in the N-terminal part of Trx-h from subgroup III.

Mittard *et al.*, 1997; Peterson *et al.*, 2005). In general, the overall molecular architectures and topologies of these proteins are similar to Trxs from non-photosynthetic organisms (Katti *et al.*, 1990; Weichsel *et al.*, 1996). The structures of *A. thaliana At*Trxh1 and barley *Hv*Trxh2 in the reduced and oxidized forms revealed no major redox-induced structural changes although few residues sequentially close to the CGPC motif do change conformation (Maeda *et al.*, 2008; Peterson *et al.*, 2005). Dimers of barley *Hv*Trxh1 are formed in the crystal lattice and the Trx–Trx interface is stabilized by three backbone–backbone hydrogen bonds in a pattern that resembles the intermolecular contacts observed in Trx-target complexes as described below (Maeda *et al.*, 2008).

The recently reported structure of the poplar *Pt*Trxh4 sheds light on the observed Grx-dependent activity of Trx-h from subgroup III (Gelhaye *et al.*, 2003; Koh *et al.*, 2008). In the oxidized wild-type protein, a disulfide is formed between the two cysteines in the C_NXXC_C motif. In a $C_C \rightarrow S$ mutant, however, a disulfide is formed between C_N and a conserved cysteine in the N-terminal part of Trx-h from subgroup III (Figs. 3 and 5B). Based on these structures and biochemical data, a novel catalytic mechanism was suggested (Koh *et al.*, 2008). The proposed reaction pathway is initiated as described above for 'classical' Trx, that is, a target disulfide bond is reduced and a C_N–C_C disulfide is formed in Trx (Fig. 6). Then the C_N–C_C disulfide is attacked by the third N-terminal cysteine (C_{NT}) and the C_{NT}–C_N disulfide is formed (Fig. 5B). Reduction of this disulfide is proposed to proceed through glutathionylation of C_{NT} as supported by experimental evidence for a GSH-mixed disulfide of C_{NT} *in vitro* (Koh *et al.*, 2008). Finally, the glutathione is released from C_{NT} by Grx.

3. Thioredoxin-target complexes

As described above, Trx and its target proteins are linked with a disulfide bond as an intermediate in the catalytic cycle of disulfide reduction (Fig. 4). This intermediate can be trapped by an approach based on site-directed mutagenesis of CXXC that was originally developed for NTR–Trx complex formation (Veine *et al.*, 1998, Wang *et al.*, 1996). Briefly, the thiol group of C_C in the Trx C_NXXC_C motif is removed through a $C \rightarrow S$ mutation to generate a mutant capable of performing the initial nucleophilic attack on the target disulfide but lacking the ability to reduce the intermolecular disulfide (Fig. 7). To facilitate the formation of a Trx-target complex, a $C \rightarrow S$ mutation is also introduced in one of the cysteines from the target disulfide bond, and the remaining single cysteine is activated by reaction with Ellman's reagent (5,5'-dithiobis-2-nitrobenzoic acid; DTNB) yielding a 2-nitro-5-thiobenzoate (TNB) conjugate that is subsequently replaced by the

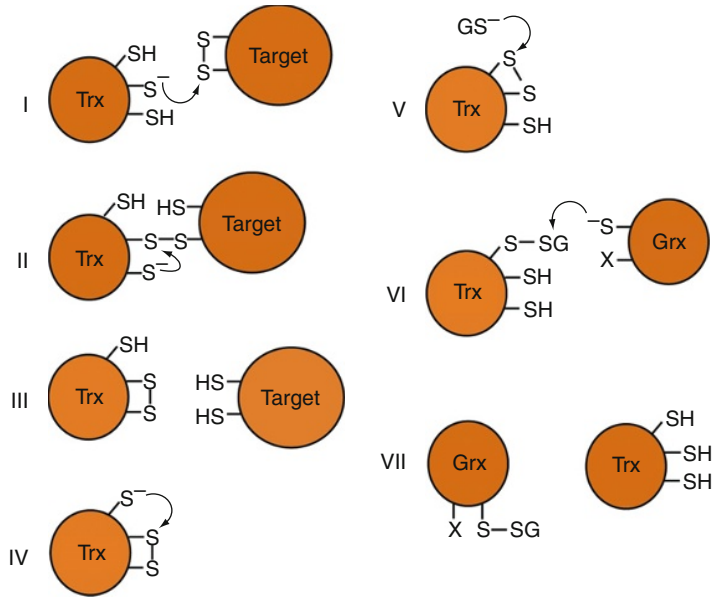

Fig. 6. Catalytic mechanism of h-type Trxs from subgroup III as proposed by Koh *et al.* (2008). (i–iii) As in 'classical' Trx, the pathway is initiated by the nucleophilic attack of C_N on the target disulfide bond followed by the release of the resulting Trx-target disulfide bond by C_C. (iv) The C_N–C_C disulfide is then reduced by the third N-terminal cysteine (C_{NT}) and a C_{NT}–C_N disulfide is formed. (v) C_{NT} is attacked by reduced glutathione (GS^-) and finally (vi) the glutathione is released from C_{NT} by Grx.

C_N thiol of the Trx mutant (Fig. 7). The release of TNB can be monitored at 412 nm. This approach has been successfully applied to obtain high yields of products for structure determination of Trx-target complexes from different biological systems (Chartron *et al.*, 2007; Li *et al.*, 2007; Maeda *et al.*, 2006; Qin *et al.*, 1995, 1996).

The only Trx-target structure from a plant source so far is the complex between barley h-type Trx (*Hv*Trxh2) and an α-amylase/subtilisin inhibitor (BASI) involved in the barley seed germination process (Maeda *et al.*, 2006). The structure reveals a relatively small interaction area of 762 $Å^2$. In the *Hv*Trxh2–BASI interface, C_N in *Hv*Trxh2 (C46) is conjugated to the BASI target cysteine (C148), and the neighbouring D146 and W147 are positioned into a shallow hydrophobic groove of *Hv*Trxh2 (Fig. 8). The residues in D146-C148 are exposed in an extended backbone conformation and form numerous van der Waals interactions and three hydrogen bonds to *Hv*Trxh2 in a manner resembling the interactions in an anti-parallel β-sheet. The hydrogen bond partners in *Hv*Trxh2 are M88 and A106 positioned in two

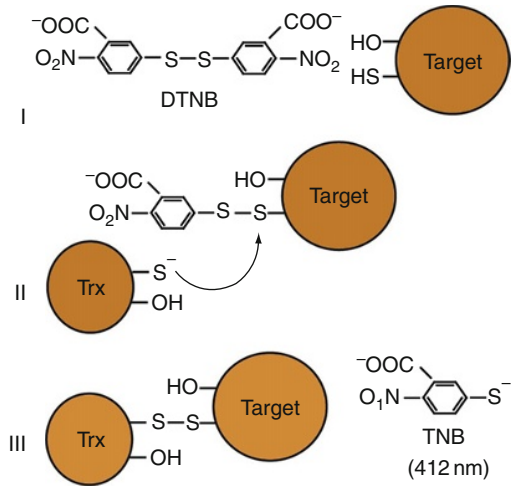

Fig. 7. A strategy to form Trx-target complexes adapted from Wang *et al.* (1996). (i) Single cysteine (C→S) mutants of target disulfides are activated by TNB conjugation. (ii) The activated target disulfide is attacked by C_N in a single cysteine (C→S) Trx mutant that lacks C_C. (iii) A kinetically stable intermolecular Trx-target disulfide in formed and the reaction can be monitored spectrophotometrically by following the release of TNB at 412 nm.

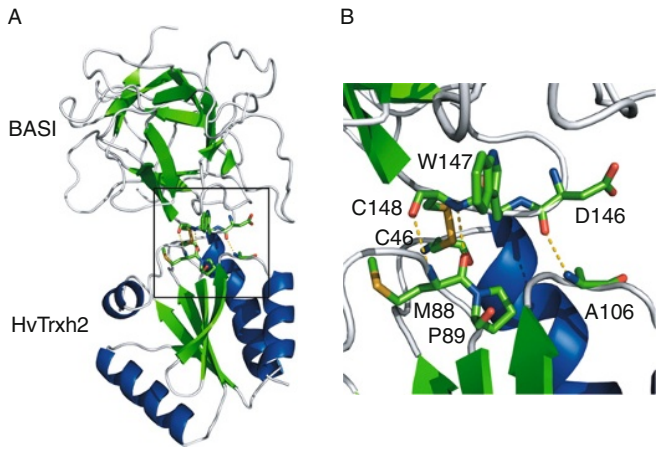

Fig. 8. The crystal structure of *Hv*Trxh2-S-S-BASI (Maeda *et al.*, 2006). (i) Overall structure of *Hv*Trxh2-S-S-BASI in cartoon display with β-strands and α-helices in green and blue, respectively. (ii) Close up view of the interaction between *Hv*Trxh2 and BASI. The segment $_{146}$DWC$_{148}$ of BASI and C$_{46}$, $_{88}$MP$_{89}$ and A$_{106}$ of *Hv*Trxh2 are shown in stick representation. Carbon, oxygen, nitrogen and sulphur are shown in green, red, blue and yellow, respectively. Intermolecular hydrogen bonds are shown as dashed yellow lines.

loops that form the shallow groove surrounding the active site. M88 and A106 form backbone-backbone hydrogen bonds to C148 and D146 in BASI, respectively (Fig. 8). Remarkably, the hydrogen bond pattern involving M88 and the target cysteine C148 appears to be conserved in disulfide bonded protein–protein complexes involving Trxs and other related redox proteins, suggesting that Trx-like proteins share this common molecular feature involved in the recognition of target proteins (Chartron *et al.*, 2007; Li *et al.*, 2007; Qin *et al.*, 1995, 1996; Rozhkova *et al.*, 2004). Indeed the importance of the residue corresponding to M88 in several Trx-like proteins has recently been validated by biochemical data (Ren *et al.*, 2009). M88 is conserved among h-type Trxs from subgroup I and is replaced by similar large hydrophobic residues in other plant Trx isoforms (Fig. 3). A106 is also fairly well conserved among plant Trxs.

B. NTR

1. Catalytic mechanisms

NTR (E.C. 1.8.1.9) transfers electrons from NADPH to the oxidized CXXC motif in Trx via a bound FAD and a redox-active C_NXXC_C motif (Fig. 9). Briefly, the reduced C_C in the NTR C_NXXC_C motif attacks the oxidized CXXC motif in Trx resulting in a covalent NTR–Trx intermediate that is subsequently reduced by C_N from the C_NXXC_C motif in NTR (Veine *et al.*, 1998). The now oxidized CXXC motif in NTR is in turn reduced by FAD, which receives reducing equivalents from NADPH. In the 'flavin-oxidizing' state (FO), FAD is positioned for transfer of electrons to the oxidized NTR disulfide and separated by a distance of 17 Å from NADPH. In this state, the C_NXXC_C motif is buried and inaccessible to Trx (Fig. 9). A large domain rearrangement is needed to expose the active-site cysteines to Trx, and to position the FAD isoalloxazine rings in close proximity of the NADPH nicotinamide ring for electron transfer (Fig. 9). The latter conformation is referred to as the 'flavin-reducing' (FR) conformation (Fig. 9) and the FO to FR conformational change is most likely the rate-limiting step of the reaction (Lennon and Williams, 1997). It is not yet known if this catalytic mechanism also applies to the recently described NTR-C.

2. 3D structures

NTR is a member of the family of pyridine nucleotide-disulfide oxidoreductases (Pai, 1991) that contain two Rossman-type nucleotide-binding domains binding FAD and NADPH, respectively. NTR from higher eukaryotes are relatively rigid homodimeric proteins ($\geq$ 55 kDa) that have an additional C-terminal domain at the subunit interface (Manstein *et al.*, 1988;

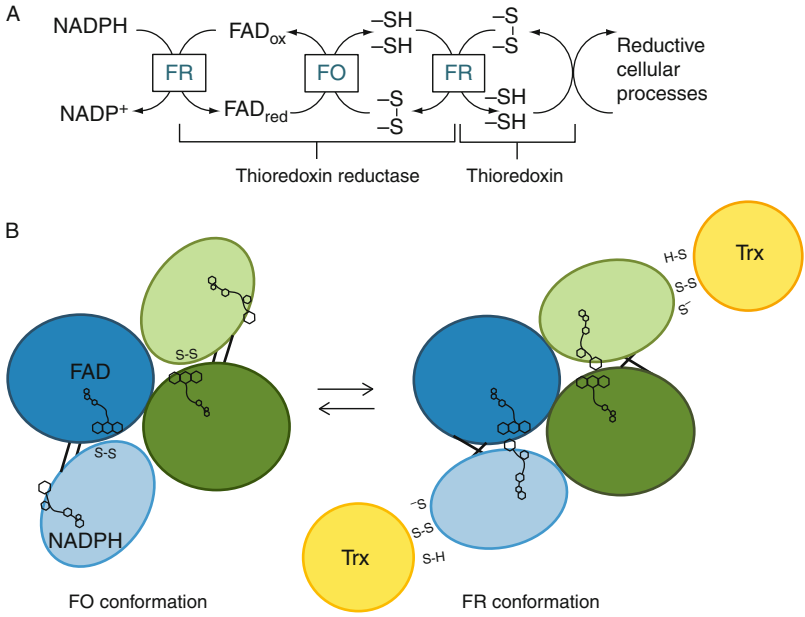

Fig. 9. (A) The catalytic mechanism of NTR. Reducing equivalents are transferred from NADPH to a tightly bound FAD in NTR. From FAD, the electrons are transferred to a CXXC in the enzyme and subsequently to the oxidized target CXXC disulfide in Trx. In order to catalyze the entire reaction, NTR needs to shift between two conformations, the FO and FR conformation. The electron transfers linked to each conformation are indicated. (B) The two conformations as proposed by Waksman *et al.* (1994) are shown schematically. The two subunits of the NTR dimer are shown in blue and green, respectively. The darker coloured ovals symbolize the FAD domains, while the lighter coloured show the NADPH domains. Disulfides and dithiols are indicated as S–S and S–H, respectively. The black lines connecting the two domains symbolize the anti-parallel β-sheet around which a 66° rotation occurs to bring NTR from the FO to the FR conformation. The rotation position of the nicotinamide ring in proximity of the flavin ring system and the CXXC dithiol is brought to the surface of the protein, where it can interact with thioredoxin (shown in yellow). Adapted from Waksman *et al.* (1994).

Waksman *et al.*, 1994; Williams *et al.*, 2000). NTRs from prokaryotes, yeast and plants ($\sim$35 kDa) are also homodimeric proteins, but each NTR subunit only contains the core of two Rossman-type nucleotide-binding domains. The structures of *E. coli* NTR in the FO and FR conformations revealed that the FAD domain needs to undergo a 66° rotation relative to the NADPH domain in order to switch from one conformation to the other (Lennon *et al.*, 2000).

The *A. thaliana* NTR-B in the FO conformation (Dai *et al.*, 1996) and recently the A/B-type barley *Hv*NTR2 (Kirkensgaard *et al.*, 2009) are the

only crystal structures available for plant NTRs. These structures show the same overall homodimeric molecular organization as displayed in other low-molecular-weight NTR structures (Akif *et al.*, 2005; Gustafsson *et al.*, 2007; Kuriyan *et al.*, 1991; Lennon *et al.*, 1999, 2000; Ruggiero *et al.*, 2009; Waksman *et al.*, 1994; Zhang *et al.*, 2009; pdb: 2q7v, unpublished data). *At*NTR-B is shown superimposed on the structure of *E. coli* NTR (Waksman *et al.*, 1994) in Fig. 10. Each subunit of the homodimeric protein contains the composite FAD domain made from the C- and N-terminal regions of the polypeptide and the central NADPH domain carrying the redox-active CXXC motif. Each domain has a central five-stranded parallel β-sheet.

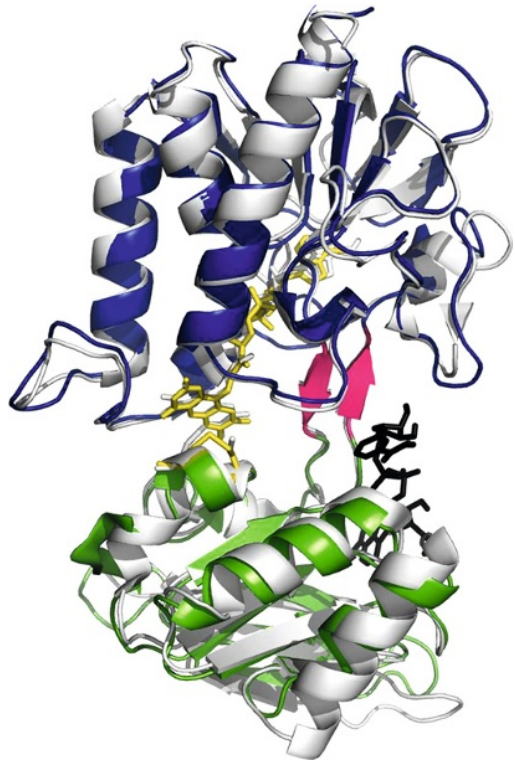

Fig. 10. Superposition of one subunit of the functionally dimeric NTRs from *A. thaliana* (pdb: 1vdc, shown in blue/green) and *E. coli* (shown in white, pdb: 1tdf). The enzymes consist of two domains with similar Rossman-folds. One domain (blue) binds FAD (yellow sticks) and the other domain (green) binds NADPH. The two domains are connected by two anti-parallel β-strands (pink). The structures are in the FO conformation, having FAD in close proximity of the redox-active CXXC motif (yellow sticks) from the NADPH domain. The *E. coli* structure was crystallized in the presence of $NADP^+$ (black).

The central sheet in the FAD domain is flanked by a four-stranded β-sheet on one side and three α-helices on the other. In the NADPH domain, the central sheet has a three-stranded β-sheet on one side and two α-helices plus an extra short helix containing the redox-active motif on the other. Two anti-parallel β-strands ($\beta9 + \beta18$) form a hinge between the two domains (Fig. 10), which are otherwise separated by a broad cleft with only few inter-domain contacts. In *At*NTR-B, there are hydrogen bonds from T53 in the FAD domain to W140 and N141 in the NADPH domain. Hydrogen bonds are found in the same regions in *Ec*NTR, but the residues involved in the inter-domain interactions are not conserved and the relative position of interacting residues are shifted by one or two residues in the sequence. Hence, G129 and R130 from the NADPH domain are hydrogen bonded with T47 and E48 in the FAD domain, respectively.

An alignment of plant NTR sequences shows that both T53 and W140 are strictly conserved within this group, whereas N141 is only conserved among the NTRs of the A/B type and replaced by a serine in the C-type (Fig. 11). The loop containing W140 and N141 is one of the variable loops in plant NTRs, and the consequences of the sequence variation for inter-domain interactions are hard to predict for C-type NTRs. The relative orientation of the FAD and NADPH domains is not the same among NTR structures. For example, the NADPH domains of *At*NTR-B and *S. cerevisiae* Trr1 (Zhang *et al.*, 2009) must be rotated by 8° to overlay the corresponding *Ec*NTR domain, when the respective FAD domains are superimposed. The *Mycobacterium tuberculosis* NTR domains have to be rotated by 11° for superposition with *Ec*NTR domains (Akif *et al.*, 2005). It is not clear if this variation in domain packing reflects a general flexibility of NTRs, or if it could be relevant for the reaction mechanism and the transformation between the FO and FR states. Two conserved arginines (R190 and R195 in *At*-B) impose NADPH over NADH specificity to short chain NTRs by donating hydrogen bonds to the 2′-phosphate of NADPH (Gustafsson *et al.*, 2007). The NADPH/NADH diphosphate is positioned by hydrogen bonds donated by conserved R, I and S/T amino acid residues.

As stated earlier, enzyme kinetics analyses suggest species-dependent interactions between plant NTRs and Trxs (Table I). Such specificity determinants are likely to reside in loop regions, where the major differences between plant NTR structures have been observed (Kirkensgaard *et al.*, 2009). For example, the group of monocot A/B type NTRs are characterized by an [H/Y]-F-[S/P/A]-G-S-D-[T/A] loop between strand $\beta9$ and $\beta10$, while the corresponding loop in dicot NTRs can be extended by four residues and have a [S/N/P]-F-[T/V/A]-G-S-[G/E]-[E/K/T/D]-[G/A]-[N/P/S]-[G/N]-G motif (Fig. 11). Another loop segregating the monocot and dicot NTRs of

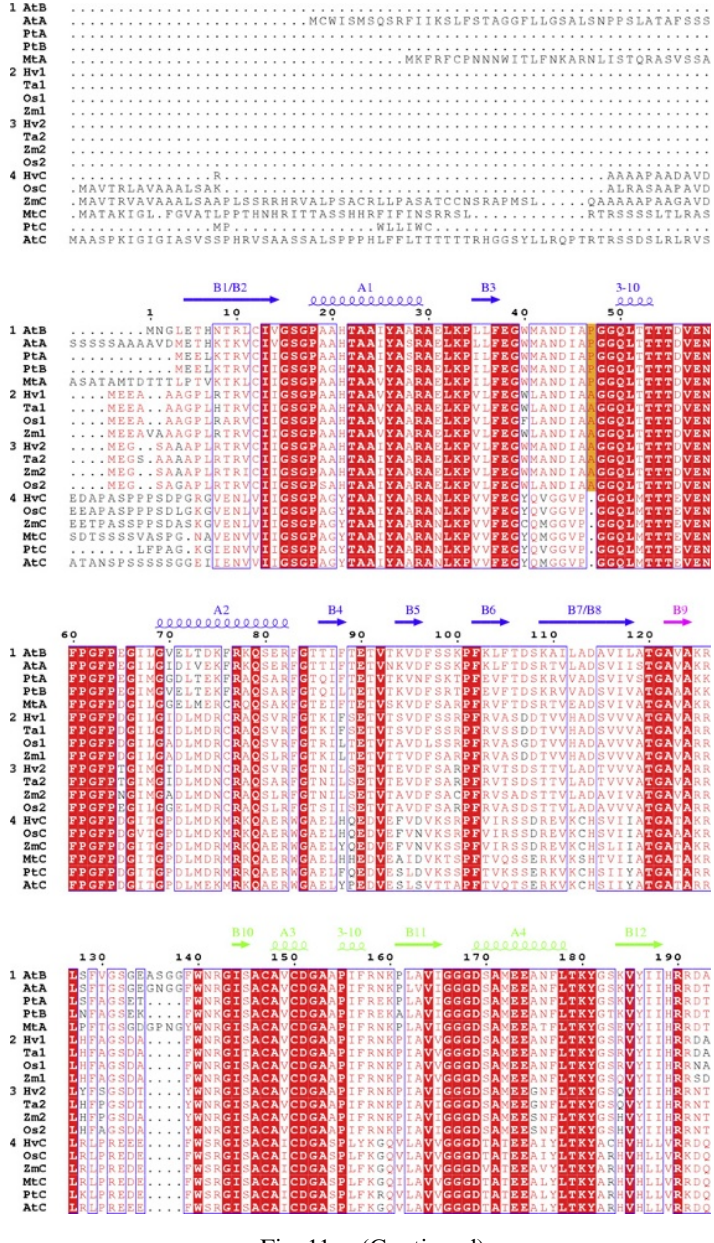

Fig. 11. (Continued)

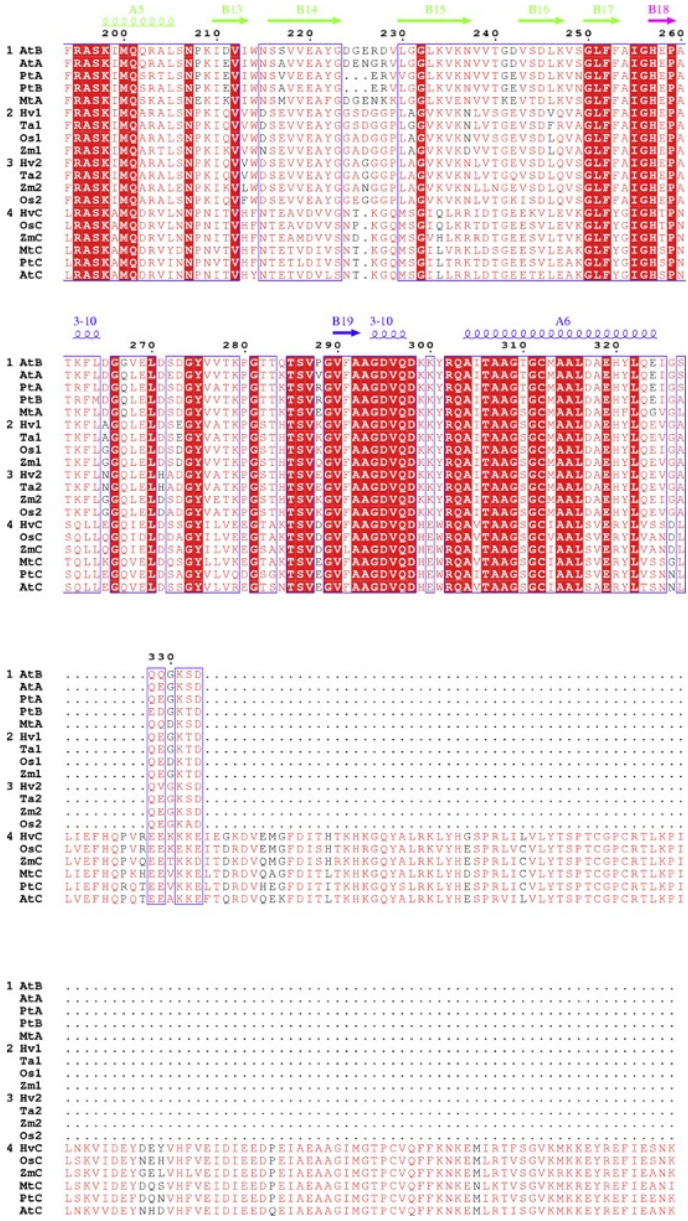

Fig. 11. (Continued)

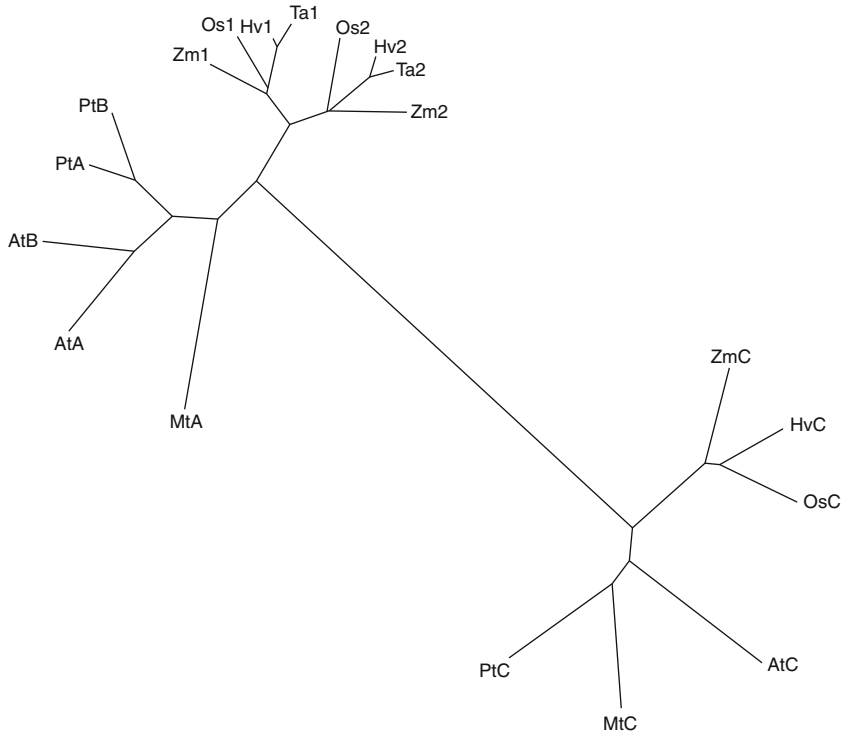

Fig. 11. Alignment of plant NTRs. The NTRs and their accession numbers in parentheses are *Hv*NTR1 (EU314717), *Hv*NTR2 (EU250021) and *Hv*NTRC from *Hordeum vulgare* (barley); *Ta*NTR1 (Q8VX47) and *Ta*NTR2 (TC297680) from *Triticum aestivum* (wheat); *Os*NTR1 (Q69PS6), *Os*NTR2 (Q6ZFU6) and *Os*NTRC (Q70G58) from *Oryza sativa* (rice); *Zm*NTR1 (EU966898), *Zm*NTR2 (BT054285) and *Zm*NTRC (BT037345) from *Zea mays* (maize); *At*NTRA (Q39242), *At*NTRB (Q39243) and *At*NTRC (O22229) from *Arabidopsis thaliana* (Mouse-ear cress); *Pt*NTRA (AC149479), *Pt*NTRB (XM_002317595) and *Pt*NTRC (XM_002308899) from *Populus trichocarpa* (western balsam poplar) and *Mt*NTRA and *Mt*NTRC from *Medicago truncatula* (Barrel Medic, legume). Residues strictly conserved have a dark gray background (red in the web version), residues well conserved within a group according to the Risler matrix (Risler *et al.*, 1988) are indicated by dark gray letters (red in the web version), residues conserved between groups are boxed and residues conserved within a group, but showing significant differences between groups, have a light gray background (orange in the web version). The secondary structure of *At*NTR-B was added using ESPript, and coloured according to domain; dark gray (blue in the web version) is the FAD domain (B1-B8 and B19-A6), (light gray) (green in the web version) the NADPH domain (B10-B17) and medium gray (pink in the web version) the β-sheets functioning as a link between the two. The sequences where aligned using CLUSTAL-W (Thompson *et al.*, 1994), and fall into three main groups, which can be characterized as dicotyledon A/B type (group 1), monocotyledon A/B type (group 2 and 3), and chloroplastic C-type (group 4). Monocotyledons appear to always have two NTRs of the A/B-type, which can be phylogenetically subgrouped (group 2 and 3). The alignment is followed by the phylogentic tree produced by the same CLUSTAL-W analysis and is illustrated in TreeView.

the A/B type is the loop between strand β14 and β15. This loop appears more flexible in monocots, where the G-G-[A/E/S]-[N/G/D]-G-G-P-L-[A/G] motif is found. The corresponding loop is variable in both length and sequence in dicots with no clear sequence motif. Both of these loops are likely to face and interact with the Trx substrate (Kirkensgaard *et al.*, 2009). A third loop placed between strand β3 and a short 3_{10}-helix, which is only present in plant and yeast NTR structures, is predicted to bind to Trx (Zhang *et al.*, 2009). This loop is strictly conserved in dicots with the sequence E-G-W-M-A-N-D-I-A-P-G-G. In monocots, the proline in this loop is exchanged with an alanine and the loop sequence is more variable: E-G-[W/F]-[M/L]-A-N-D-I-A-A-G-G. The C-type NTRs have a quite different sequence motif: E-G-[Y/C]-Q-[M/V]-G-G-V-P-G-G.

IV. IDENTIFICATION OF Trx TARGETS BY PROTEOMICS APPROACHES

A. PROTEOMICS TECHNIQUES APPLICABLE AT THE PROTEIN IDENTIFICATION LEVEL

Proteome analysis involves polyacrylamide gel-based or chromatographic multidimensional separation of protein mixtures, combined with highly sensitive mass spectrometry for protein identification and characterization. As such, proteomics enable parallel analysis and identification of many proteins in complex mixtures and has been applied with success for *in vitro* identification of Trx target proteins. Broadly, two approaches have been applied: (i) labelling of thiol groups released by Trx treatment of protein extracts followed by detection of labelled proteins on 2D gels and (ii) affinity isolation of proteins binding to immobilized active-site mutants of Trx.

1. Labelling approaches

A method was developed using the thiol-specific fluorescent probe monobromobimane (mBBr) to label free thiol groups in protein extracts treated with recombinant Trx prior to their separation by 2D gel electrophoresis (Yano *et al.*, 2001). Labelled proteins were visualized on 2D gels by UV-illumination, and comparison with protein extracts without Trx treatment demonstrated the appearance of additional fluorescent 2D gel spots containing putative Trx target proteins. Using this procedure, five potential target proteins were identified by Edman degradation in peanut seed extracts (Yano *et al.*, 2001). Similar procedures have also been applied together with mass spectrometry to identify five targets in barley embryo and 23 targets in the

starchy endosperm of mature wheat seeds (Marx *et al.*, 2003; Wong *et al.*, 2003). The same strategy applied in parallel with a method based on a C→S mutated-Trx affinity column led to the identification of 111 putative Trx target proteins in germinating *M. truncatula* seeds (Alkhalfioui *et al.*, 2007b). In a related procedure, mBBR was replaced with a more sensitive Cy5 maleimide dye, which resulted in the identification of 16 putative *Hv*Trxh1 and *Hv*Trxh2 target proteins in mature barley seeds or seeds after 72 h germination (Maeda *et al.*, 2004). Other thiol-specific reagents have also been used, for example target proteins have been radio-labelled by alkylation with ^{14}C-iodoacetamide or biotinylated by reaction with thiol-reactive biotin derivatives (Marchand *et al.*, 2006). The latter approach enables affinity isolation of labelled proteins on immobilized avidin.

2. Affinity isolation approaches

The two-step catalytic mechanism of Trx (Fig. 4) has been exploited to trap target proteins in an intermolecular disulfide complex with an immobilized Trx, where the active-site CXXC has been replaced by CXXS through site-directed mutagenesis. Non-targets are washed away, and the target proteins can subsequently be released from the mutant Trx by addition of a strong reducing agent, such as DTT. This methodology has been used for the identification of putative target proteins from mitochondrial (Balmer *et al.*, 2004) and cytosolic extracts (Alkhalfioui *et al.*, 2007b; Marchand *et al.*, 2006; Wong *et al.*, 2004; Yamazaki *et al.*, 2004).

B. TECHNIQUES FOR IDENTIFICATION OF TARGET DISULFIDE BONDS

Information of specific target sites in target proteins can provide insight into molecular details of target recognition. Determination of specific target disulfides can be achieved by analysing mass spectra of peptides from proteolytically digested target proteins conjugated with different thiol-reactive reagents. For example, iodoacetamide (IAM) and 4-vinylpyridine (4-VP) were used to identify target disulfides in mature barley seed extract (Maeda *et al.*, 2005). Samples were incubated ± barley Trx-h followed by labelling of accessible thiol groups with IAM. Prior to the second dimension in 2D gel electrophoresis, protein thiol groups were reduced and the remaining free cysteines labelled with 4-VP. Thus, cysteines from target disulfides are labelled with IAM in the Trx-treated sample and with 4-VP in a control without Trx. Cysteines labelled with the two forms of modifications have different masses and are thus are distinguished in mass spectra. This procedure was used to analyse proteins in 2D-gel spots that were indicated to contain target proteins on the basis of Cy5 maleimide labelling patterns (Maeda *et al.*, 2004). By comparing samples

incubated in the presence or absence of Trx, nine disulfides in eight proteins were identified as Trx-h targets.

A quantitative proteomics approach for site-specific identification of target disulfides was recently developed (Hägglund *et al.*, 2008). In this method, IAM-based isotope-coded affinity tag (ICAT) reagents were used. The ICAT reagents react with free thiol groups and are available with nine either 'light' (^{12}C; $ICAT_L$) or 'heavy' (^{13}C; $ICAT_H$) carbon atoms. The isotopically labelled ICAT reagents are identical except for a mass difference of 9 Da, and are therefore compatible with quantitative mass spectrometric detection. Basically, two identical samples of protein extract were incubated in the presence (+ Trx) or absence (− Trx) of Trx (Fig. 12). Subsequently, IAM was added to quench the Trx activity and block cysteine thiols released from the target disulfides, followed by complete reduction of remaining protein disulfides by tris(2-carboxyethyl)phosphine (TCEP) under denaturing conditions in SDS. The samples were ICAT-labelled (+ Trx, $ICAT_L$; − Trx, $ICAT_H$), mixed in a 1:1 ratio and digested by trypsin. Cysteine-containing peptides are isolated by avidin affinity chromatography and analyzed by mass spectrometry. Because non-target disulfide bonds remain intact until the TCEP reduction, they give rise to identical amounts of thiol groups available for ICAT labelling in the ± Trx samples and $ICAT_H/ICAT_L$ peptide ratios of 1 are expected when the samples are mixed 1:1. In contrast, cysteine residues released from Trx target disulfide bonds are blocked by IAM and hence do not undergo $ICAT_L$-labelling in the + Trx sample. Peptides carrying Trx-targeted residues will thus exhibit $ICAT_H/ICAT_L$ ratios >1. The method was applied to identify targets of barley *Hv*Trxh1 in protein extracts of 48 h germinated barley seed embryo.

C. EXAMPLES OF TARGET PROTEINS

Several proteomics studies of Trxs from different organisms, tissues, and organelle extracts have provided over 400 putative Trx-target proteins that were recently compiled into a comprehensive list (Montrichard *et al.*, 2009). Some examples of targets from NTS are described below.

1. Seed germination

As previously stated, Trx-h plays an important role in the germination of cereal seeds by facilitating release of storage reserves through reduction of disulfide bonds in storage proteins, hydrolytic enzymes, and their inhibitors (Besse *et al.*, 1996; Kobrehel *et al.*, 1991, 1992). Storage proteins identified as target proteins include hordeins and globulins from barley and globulins, glutenins, and avenins in wheat (Hägglund *et al.*, 2008; Marx *et al.*, 2003;

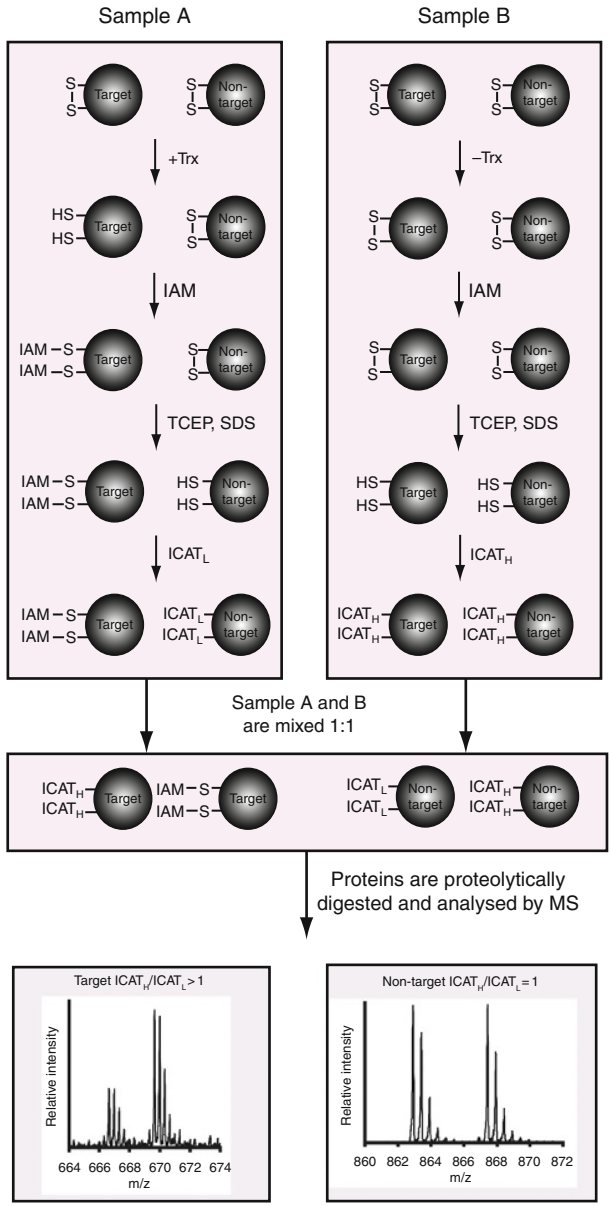

Fig. 12. An approach for the identification of target protein disulfides using ICAT-labelling. Two identical samples of protein extract were incubated in the presence (+ Trx) or absence (– Trx) of Trx and IAM was added to quench Trx activity and block cysteine thiols. Proteins were denatured by SDS and remaining disulfides were reduced by TCEP. The samples were ICAT-labelled (+ Trx, $ICAT_L$; – Trx, $ICAT_H$), mixed in a 1:1 ratio, digested with trypsin and analysed by mass spectrometry. $ICAT_H$/$ICAT_L$ peptide ratios of 1 are expected for non-targets and peptides carrying Trx-targeted residues are expected to show $ICAT_H$/$ICAT_L$ ratios >1.

Wong *et al.*, 2004). Several inhibitors of α-amylases and proteases have been identified, including the barley α-amylase/subtilisin inhibitor (BASI) that has been structure-determined in complex with barley *Hv*Trxh2 (Fig. 8). The specific disulfide target in BASI was determined to be C144-C148 by the IAM/4-VP labelling approach described above (Maeda *et al.*, 2005).

2. Redox control

Dehydroascorbate reductase (DHAR) participates in redox control mediated through the ascorbate–glutathione cycle in higher plants. DHAR has been identified as a Trx-h target in *A. thaliana* and wheat (Marchand *et al.*, 2004, 2006; Wong *et al.*, 2004). The cysteine proposed to be the catalytic residue in DHAR (Dixon *et al.*, 2002) was identified as a target for barley h-type Trx using ICAT labelling (Hägglund *et al.*, 2008). Other examples of putative Trx-targeted redox proteins include 1-Cys peroxiredoxin (Hägglund *et al.*, 2008; Maeda *et al.*, 2004, Marx *et al.*, 2003; Wong *et al.*, 2004), 2-Cys peroxiredoxin (Alkhalfioui *et al.*, 2007b; Marchand *et al.*, 2006) and ascorbate peroxidase (Marchand *et al.*, 2004, 2006; Yamazaki *et al.*, 2004).

3. Amino acid metabolism

Several enzymes involved in amino acid metabolism have been identified to be targets, including adenosylhomocysteinase (Hägglund *et al.*, 2008), alanine aminotransferase (Balmer *et al.*, 2004; Marchand *et al.*, 2004, 2006; Wong *et al.*, 2004), aspartate aminotransferase (Balmer *et al.*, 2004), aspartate-semialdehyde dehydrogenase (Hägglund *et al.*, 2008) and glutamine synthetase (Alkhalfioui *et al.*, 2007b; Lemaire *et al.*, 2004; Marchand *et al.*, 2004, 2006; Yamazaki *et al.*, 2004). One of the target cysteines in adenosylhomocysteinase was identified (Hägglund *et al.*, 2008) and represents a conserved residue previously demonstrated to be essential for enzymatic activity and positioned near the active site in the ortholog from human placenta (Yuan *et al.*, 1996).

4. Carbohydrate metabolism

Enolases from plants were demonstrated to be redox sensitive *in vitro*, and suggested to be regulated by Trx (Anderson *et al.*, 1998). Indeed, enolase has been identified as a target of Trx-h in several proteomics surveys (Alkhalfioui *et al.*, 2007b, Hägglund *et al.*, 2008; Lemaire *et al.*, 2004; Wong *et al.*, 2004). Furthermore, one of the target cysteines identified by the ICAT labelling approach (Hägglund *et al.*, 2008) is suggested to form a regulatory disulfide bond (Anderson *et al.*, 1998). Other targets involved in carbohydrate metabolism include fructose bisphosphate aldolase (Marchand *et al.*, 2004, 2006; Yamazaki *et al.*, 2004), malate dehydrogenase (Alkhalfioui *et al.*, 2007b;

Balmer *et al.*, 2004; Marchand *et al.*, 2004; Yamazaki *et al.*, 2004) and succinyl-CoA ligase (Balmer *et al.*, 2004; Hägglund *et al.*, 2008).

V. SUMMARY AND PERSPECTIVES

Thanks to the outstanding research achievements in recent years, it is becoming increasingly apparent that plant NTS make use of a remarkable multitude of molecular mechanisms for control of cysteine oxidation. The recently discovered chloroplastic NTR-C represents a truly novel NTS with NTR and Trx functionalities fused into a single protein. Little is as yet known about the structure and catalytic mechanism of NTR-C, and this is unquestionably a highly prioritized target for future research efforts. Another topic which deserves attention, is the molecular basis for specific Trx–NTR interactions. Despite the large number of high-resolution structures of Trxs and NTRs from plants and other organisms, surprisingly little biochemical data is available regarding the molecular recognition of Trxs by NTR.

Proteomics studies have identified numerous proteins with different functions that are targeted by Trx *in vitro*. Furthermore, the recent application of quantitative proteomics to identify specific target disulfides has revealed site-specific targets that are candidates for further investigations. However, the biological relevance of the putative targets must be validated by other means. In this respect, recent developments of proteomics methods aimed at measuring *in vivo* redox states hold a great promise for the future. For example, an ICAT labelling strategy has been developed to identify oxidized cysteines in the proteome of *E. coli* mutants lacking Trx (Leichert *et al.*, 2008). It will indeed be a great challenge for the future to transfer this technology to plant systems, given the large number of NTR and Trx genes present in these organisms.

ACKNOWLEDGEMENTS

The Danish Technical Research Council (STVF, grant no. 26-03-0194), the Carlsberg Foundation and the Center for Advanced Food Studies (LMC) are acknowledged for financial support. K. G. K. holds a Ph.D. scholarship from the Technical University of Denmark.

REFERENCES

Akif, M., Suhre, K., Verma, C. and Mande, S. C. (2005). Conformational flexibility of *Mycobacterium tuberculosis* thioredoxin reductase: Crystal structure and normal-mode analysis. *Acta Crystallographica Section D* **61**, 1603–1611.

Alkhalfioui, F., Renard, M. and Montrichard, F. (2007a). Unique properties of NADP-thioredoxin reductase C in legumes. *Journal of Experimental Botany* **58**, 969–978.

Alkhalfioui, F., Renard, M., Vensel, W. H., Wong, J., Tanaka, C. K., Hurkman, W. J., Buchanan, B. B. and Montrichard, F. (2007b). Thioredoxin-linked proteins are reduced during germination of *Medicago truncatula* seeds. *Plant Physiology* **144**, 1559–1579.

Alkhalfioui, F., Renard, M., Frendo, P., Keichinger, C., Meyer, Y., Gelhaye, E., Hirasawa, M., Knaff, D. B., Ritzenthaler, C. and Montrichard, F. (2008). A novel type of thioredoxin dedicated to symbiosis in legumes. *Plant Physiology* **148**, 424–435.

Anderson, L. E., Li, A. D. and Stevens, F. J. (1998). The enolases of ice plant and *Arabidopsis* contain a potential disulphide and are redox sensitive. *Phytochemistry* **47**, 707–713.

Arnér, E. S. J. and Holmgren, A. (2000). Physiological functions of thioredoxin and thioredoxin reductase. *European Journal of Biochemistry* **267**, 6102–6109.

Balmer, Y., Vensel, W. H., Tanaka, C. K., Hurkman, W. J., Gelhaye, E., Rouhier, N., Jacquot, J. P., Manieri, W., Schürmann, P., Droux, M. and Buchanan, B. B. (2004). Thioredoxin links redox to the regulation of fundamental processes of plant mitochondria. *Proceedings of the National Academy of Sciences of the United States of America* **101**, 2642–2647.

Barranco-Medina, S., Krell, T., Bernier-Villamor, L., Sevilla, F., Lázaro, J. J. and Dietz, K. J. (2008). Hexameric oligomerization of mitochondrial peroxiredoxin PrxIIF and formation of an ultrahigh affinity complex with its electron donor thioredoxin Trx-o. *Journal of Experimental Botany* **59**, 3259–3269.

Behm, M. and Jacquot, J. P. (2000). Isolation and characterization of thioredoxin h from poplar xylem. *Plant Physiology and Biochemistry* **38**, 363–369.

Besse, I., Wong, J. H., Kobrehel, K. and Buchanan, B. B. (1996). Thiocalsin: A thioredoxin-linked, substrate-specific protease dependent on calcium. *Proceedings of the National Academy of Sciences of the United States of America* **93**, 3169–3175.

Bower, M. S., Matias, D. D., Fernandes-Carvalho, E., Mazzurco, M., Gu, T., Rothstein, S. J. and Goring, D. R. (1996). Two members of the thioredoxin-h family interact with the kinase domain of a Brassica S locus receptor kinase. *Plant Cell* **8**, 1641–1650.

Bréhélin, C., Mouaheb, N., Verdoucq, L., Lancelin, J. M. and Meyer, Y. (2000). Characterization of determinants for the specificity of *Arabidopsis* thioredoxins h in yeast complementation. *Journal of Biological Chemistry* **275**, 31641–31647.

Bréhélin, C., Laloi, C., Setterdahl, A. T., Knaff, D. B. and Meyer, Y. (2004). Cytosolic, mitochondrial thioredoxins and thioredoxin reductases in *Arabidopsis thaliana*. *Photosynthesis Research* **79**, 295–304.

Buchanan, B. B. and Balmer, Y. (2005). Redox regulation: A broadening horizon. *Annual Review of Plant Biology* **56**, 187–220.

Cabrillac, D., Cock, J. M., Dumas, C. and Gaude, T. (2001). The S-locus receptor kinase is inhibited by thioredoxins and activated by pollen coat proteins. *Nature* **410**, 220–223.

Cazalis, R., Pulido, P., Aussenac, T., Pérez-Ruiz, J. M. and Cejudo, F. J. (2006). Cloning and characterization of three thioredoxin h isoforms from wheat showing differential expression in seeds. *Journal of Experimental Botany* **257**, 2165–2172.

Chartron, J., Shiau, C., Stout, C. D. and Carroll, K. S. (2007). 3'-Phosphoadenosine-5'-phosphosulfate reductase in complex with thioredoxin: A structural snapshot in the catalytic cycle. *Biochemistry* **46**, 3942–3951.

Chivers, P. T. and Raines, R. T. (1997). General acid/base catalysis in the active site of *Escherichia coli* thioredoxin. *Biochemistry* **36**, 15810–15816.

Cho, M. J., Wong, J. H., Marx, C., Jiang, W., Lemaux, P. G. and Buchanan, B. B. (1999). Overexpression of thioredoxin h leads to enhanced activity of starch debranching enzyme (pullulanase) in barley grain. *Proceedings of the National Academy of Sciences of the United States of America* **96**, 14641–14646.

Coudevylle, N., Thureau, A., Hemmerlin, C., Gelhaye, E., Jacquot, J. P. and Cung, M. T. (2005). Solution structure of a natural CPPC active site variant, the reduced form of thioredoxin h1 from poplar. *Biochemistry* **44**, 2001–2008.

Dai, S., Saarinen, M., Ramaswamy, S., Meyer, Y., Jacquot, J. P. and Eklund, H. (1996). Crystal structure of *Arabidopsis thaliana* NADPH dependent thioredoxin reductase at 2.5 Å resolution. *Journal of Molecular Biology* **264**, 1044–1057.

Dixon, D. P., Davis, B. G. and Edwards, R. (2002). Functional divergence in the glutathione transferase superfamily in plants. Identification of two classes with putative functions in redox homeostasis in *Arabidopsis thaliana*. *Journal of Biological Chemistry* **277**, 30859–30869.

Eklund, H., Cambillau, C., Sjöberg, B. M., Holmgren, A., Jörnvall, H., Höög, J. O. and Brändén, C. I. (1984). Conformational and functional similarities between glutaredoxin and thioredoxins. *EMBO Journal* **3**, 1443–1449.

Gelhaye, E., Rouhier, N., Laurent, P., Sautière, P. E., Martin, F. and Jacquot, J. P. (2002). Isolation and characterization of an extended thioredoxin h from poplar. *Physiologia Plantarum* **114**, 165–171.

Gelhaye, E., Rouhier, N. and Jacquot, J. P. (2003). Evidence for a subgroup of thioredoxin h that requires GSH/Grx for its reduction. *FEBS Letters* **555**, 443–448.

Gelhaye, E., Rouhier, N., Gerard, J., Jolivet, Y., Gualberto, J., Navrot, N., Ohlsson, P. I., Wingsle, G., Hirasawa, M., Knaff, D. B., Wang, H. Dizengremel, P. *et al.* (2004). A specific form of thioredoxin h occurs in plant mitochondria and regulates the alternative oxidase. *Proceedings of the National Academy of Sciences of the United States of America* **101**, 14545–14550.

Gelhaye, E., Rouhier, N., Navrot, N. and Jacquot, J. P. (2005). The plant thioredoxin system. *Cellular and Molecular Life Sciences* **62**, 24–35.

Gustafsson, T. N., Sandalova, T., Lu, J., Holmgren, A. and Schneider, G. (2007). High-resolution stuctures of oxidized and reduced thioredoxin reductase from *Helicobacter pylori*. *Acta Crystallographica Section D* **63**, 833–843.

Hägglund, P., Bunkenborg, J., Maeda, K. and Svensson, B. (2008). Identification of thioredoxin disulfide targets using a quantitative proteomics approach based on isotope-coded affinity tags. *Journal of Proteome Research* **7**, 5270–5276.

Holmgren, A. (1979). Thioredoxin catalyzes the reduction of insulin disulfides by dithiothreitol and dihydrolipoamide. *Journal of Biological Chemistry* **254**, 9627–9632.

Holmgren, A. (1989). Thioredoxin and glutaredoxin systems. *Journal of Biological Chemistry* **264**, 13963–13966.

Holmgren, A., Söderberg, B. O., Eklund, H. and Brändén, C. I. (1975). Three-dimensional structure of *Escherichia coli* thioredoxin-S2 to 2.8 Å resolution. *Proceedings of the National Academy of Sciences of the United States of America* **72**, 2305–2309.

Ishiwatari, Y., Honda, C., Kawashima, I., Nakamura, S., Hirano, H., Mori, S., Fujiwara, T., Hayashi, H. and Chino, M. (1995). Thioredoxin h is one of the major proteins in rice phloem sap. *Planta* **195**, 456–463.

Ishiwatari, Y., Fujiwara, T., McFarland, K. C., Nemoto, K., Hayashi, H., Chino, M. and Lucas, W. J. (1998). Rice phloem thioredoxin h has the capacity to mediate its own cell-to-cell transport through plasmodesmata. *Planta* **205**, 12–22.

Jacquot, J. P., Rivera-Madrid, R., Marinho, P., Kollarova, M., Le Maréchal, P., Miginiac-Maslow, M. and Meyer, Y. (1994). *Arabidopsis thaliana* NADPH thioredoxin reductase. cDNA characterization and expression of the recombinant protein in *Escherichia coli*. *Journal of Molecular Biology* **235**, 1357–1363.

Jacquot, J. P., Eklund, H., Rouhier, N. and Schürmann, P. (2009). Structural and evolutionary aspects of thioredoxin reductases in photosynthetic plants. *Trends in Plant Science* **14**, 336–343.

Johansson, C., Lillig, C. H. and Holmgren, A. (2004). Human mitochondrial glutaredoxin reduces *S*-glutathionylated proteins with high affinity accepting electrons from either glutathione or thioredoxin reductase. *Journal of Biological Chemistry* **279**, 7537–7543.

Johnson, T. C., Wada, K., Buchanan, B. B. and Holmgren, A. (1987). Reduction of purothionin by the wheat seed thioredoxin system. *Plant Physiology* **85**, 446–451.

Juárez-Díaz, J. A., McClure, B., Vázquez-Santana, S., Guevara-García, A., León-Mejía, P., Márquez-Guzmán, J. and Cruz-García, F. (2006). A novel thioredoxin h is secreted in *Nicotiana alata* and reduces S-RNase *in vitro*. *Journal of Biological Chemistry* **281**, 3418–3424.

Juttner, J., Olde, D., Langridge, P. and Baumann, U. (2000). Cloning and expression of a distinct subclass of plant thioredoxins. *European Journal of Biochemistry* **267**, 7109–7117.

Kallis, G. B. and Holmgren, A. (1980). Differential reactivity of the functional sulfhydryl groups of cysteine32 and cysteine35 present in the reduced form of thioredoxin from *Escherichia coli*. *Journal of Biological Chemistry* **255**, 10261–10265.

Kanzok, S. M., Fechner, A., Bauer, H., Ulschmid, J. K., Muller, H. M., Botella-Munoz, J., Schneuwly, S., Schirmer, R. and Becker, K. (2001). Substitution of the thioredoxin system for glutathione reductase in *Drosophila melanogaster*. *Science* **291**, 643–646.

Katti, S. K., LeMaster, D. M. and Eklund, H. (1990). Crystal structure of thioredoxin from *Escherichia coli* at 1.68 Å resolution. *Journal of Molecular Biology* **212**, 167–184.

Kirkensgaard, K., Hägglund, P., Finnie, C., Svensson, B. and Henriksen, A. (2009). Crystal structure of *Hordeum vulgare* NADPH-dependent thioredoxin reductase 2. Unwinding the reaction mechanism. *Acta Crystallographica section D* **65**, 932–941.

Kobrehel, K., Yee, B. C. and Buchanan, B. B. (1991). Role of the NADP/thioredoxin system in the reduction of alpha-amylase and trypsin inhibitor proteins. *Journal of Biological Chemistry* **266**, 16135–16140.

Kobrehel, K., Wong, J. H., Balogh, A., Kiss, F., Yee, B. C. and Buchanan, B. B. (1992). Specific reduction of wheat storage proteins by thioredoxin h. *Plant Physiology* **99**, 919–924.

Koh, C. S., Navrot, N., Didierjean, C., Rouhier, N., Hirasawa, M., Knaff, D. B., Wingsle, G., Samian, R., Jacquot, J. P., Corbier, C. and Gelhaye, E. (2008). An atypical catalytic mechanism involving three cysteines of thioredoxin. *Journal of Biological Chemistry* **283**, 23062–23072.

Krause, G. and Holmgren, A. (1991). Substitution of the conserved tryptophan 31 in *Escherichia coli* thioredoxin by site-directed mutagenesis and structure–function analysis. *Journal of Biological Chemistry* **266**, 4056–4066.

Krimm, I., Lemaire, S., Ruelland, E., Miginiac-Maslow, M., Jacquot, J. P., Hirasawa, M., Knaff, D. B. and Lancelin, J. M. (1998). The single mutation Trp35–>Ala in the 35–40 redox site of *Chlamydomonas reinhardtii* thioredoxin h affects its biochemical activity and the pH dependence of C36–C39 ^{1}H–^{13}C NMR. *European Journal of Biochemistry* **255**, 185–195.

Kuriyan, J., Krishna, T. S. R., Wong, L., Guenther, B., Pahler, A., Williams, C. H., Jr. and Model, P. (1991). Convergent evolution of similar function in two structurally divergent enzymes. *Nature* **352**, 172–174.

Laloi, C., Rayapuram, N., Chartier, Y., Grienenberger, J. M., Bonnard, G. and Meyer, Y. (2001). Identification and characterization of a mitochondrial thioredoxin system in plants. *Proceedings of the National Academy of Sciences of the United States of America* **98**, 14144–14149.

Leichert, L. I., Gehrke, F., Gudiseva, H. V., Blackwell, T., Ilbert, M., Walker, A. K., Strahler, J. R., Andrews, P. C. and Jakob, U. (2008). Quantifying changes in the thiol redox proteome upon oxidative stress *in vivo*. *Proceedings of the National Academy of Sciences of the United States of America* **105**, 8197–8202.

Lemaire, S. D., Guillon, B., Le Marechal, P., Keryer, E., Miginiac-Maslow, M. and Decottignies, P. (2004). New thioredoxin targets in the unicellular photosynthetic eukaryote *Chlamydomonas reinhardtii*. *Proceedings of the National Academy of Sciences of the United States of America* **101**, 7475–7480.

Lennon, B. W. and Williams, C. H. (1997). Reductive half-reaction of thioredoxin reductase from *Escherichia coli*. *Biochemistry* **36**, 9464–9477.

Lennon, B. W., Williams, C. H., Jr. and Ludwig, M. (1999). Crystal structure of reduced thioredoxin reductase from *Escherichia coli*: Structural flexibility in the isoalloxazine ring of the flavin adenine dinucleotide cofactor. *Protein Science* **8**, 2366–2379.

Lennon, B. W., Williams, C. H., Jr., and Ludwig, M. L. (2000). Twists in catalysis: Alternating conformations of *Escherichia coli* thioredoxin reductase. *Science* **289**, 1190–1194.

Li, Y., Hu, Y., Zhang, X., Xu, H., Lescop, E., Xia, B. and Jin, C. (2007). Conformational fluctuations coupled to the thiol-disulfide transfer between thioredoxin and arsenate reductase in *Bacillus subtilis*. *Journal of Biological Chemistry* **282**, 11078–11083.

Maeda, K., Finnie, C., Østergaard, O. and Svensson, B. (2003). Identification, cloning and characterization of two thioredoxin h isoforms, HvTrxh1 and HvTrxh2, from the barley seed proteome. *European Journal of Biochemistry* **270**, 2633–2643.

Maeda, K., Finnie, C. and Svensson, B. (2004). Cy5 maleimide labeling for sensitive detection of free thiols in native protein extracts: Identification of seed proteins targeted by barley thioredoxin h isoforms. *Biochemical Journal* **378**, 479–507.

Maeda, K., Finnie, C. and Svensson, B. (2005). Identification of thioredoxin h-reducible disulphides in proteomes by differential labelling of cysteines: Insight into recognition and regulation of proteins in barley seeds by thioredoxin h. *Proteomics* **5**, 1634–1644.

Maeda, K., Hägglund, P., Finnie, C., Svensson, B. and Henriksen, A. (2006). Structural basis for target protein recognition by the protein disulphide reductase thioredoxin. *Structure* **14**, 1701–1710.

Maeda, K., Hägglund, P., Finnie, C., Svensson, B. and Henriksen, A. (2008). Crystal structures of barley thioredoxin h isoforms HvTrxh1 and HvTrxh2 reveal features involved in protein recognition and possibly in discriminating the isoform specificity. *Protein Science* **17**, 1015–1024.

Manstein, D. J., Massey, V., Ghisla, S. and Pai, E. F. (1988). Stereochemistry and accessibility of prosthetic groups in flavoproteins. *Biochemistry* **27**, 2300–2305.

Marchand, C., Le Maréchal, P., Meyer, Y., Miginiac-Maslow, M., Issakidis-Bourguet, E. and Decottignies, P. (2004). New targets of *Arabidopsis* thioredoxins revealed by proteomic analysis. *Proteomics* **4**, 2696–2706.

Marchand, C., Le Marechal, P., Meyer, Y. and Decottignies, P. (2006). Comparative proteomic approaches for the isolation of proteins interacting with thioredoxin. *Proteomics* **6**, 6528–6537.

Marti, M. C., Olmos, E., Calvete, J. J., Diaz, I., Barranco-Medina, S., Whelan, J., Lazaro, J. J., Sevilla, F. and Jimenez, A. (2009). Mitochondrial and nuclear localization of a novel pea thioredoxin: Identification of its mitochondrial target proteins. *Plant Physiology* **150**, 646–657.

Martin, J. L. (1995). Thioredoxin—A fold for all reasons. *Structure* **3**, 245–250.

Marx, C., Wong, J. H. and Buchanan, B. B. (2003). Thioredoxin and germinating barley: Targets and protein redox changes. *Planta* **216**, 454–460.

Menchise, V., Corbier, C., Didierjean, C., Saviano, M., Benedetti, E., Jacquot, J. P. and Aubry, A. (2001). Crystal structure of the wild-type and D30A mutant thioredoxin h of *Chlamydomonas reinhardtii* and implications for the catalytic mechanism. *Biochemical Journal* **359**, 65–75.

Meyer, Y., Vignols, F. and Reichheld, J. P. (2002). Classification of plant thioredoxins by sequence similarity and intron position. *Methods in Enzymology* **347**, 394–402.

Mittard, V., Blackledge, M. J., Stein, M., Jacquot, J. P., Marion, D. and Lancelin, J. M. (1997). NMR solution structure of an oxidised thioredoxin h from the eukaryotic green alga *Chlamydomonas reinhardtii*. *European Journal of Biochemistry* **243**, 374–383.

Montrichard, F., Alkhalfioui, F., Yano, H., Vensel, W. H., Hurkman, W. J. and Buchanan, B. B. (2009). Thioredoxin targets in plants: The first 30 years. *Journal of Proteomics* **72**, 452–474.

Moon, J. C., Jang, H. H., Chae, H. B., Lee, J. R., Lee, S. Y., Jung, Y. J., Shin, M. R., Lim, H. S., Chung, W. S., Yun, D. J., Lee, K. O. and Lee, S. Y. (2006). The C-type *Arabidopsis* thioredoxin reductase ANTR-C acts as an electron donor to 2-Cys peroxiredoxins in chloroplasts. *Biochemical and Biophysical Research Communications* **348**, 478–484.

Mouaheb, N., Thomas, D., Verdoucq, L., Monfort, P. and Meyer, Y. (1998). *In vivo* functional discrimination between plant thioredoxins by heterologous expression in the yeast *Saccharomyces cerevisiae*. *Proceedings of the National Academy of Sciences of the United States of America* **95**, 3312–3317.

Muller, E. G. D. (1996). A glutathione reductase mutant of yeast accumulates high levels of oxidized glutathione and requires thioredoxin for growth. *Molecular Biology of the Cell* **7**, 1805–1813.

Nuruzzaman, M., Gupta, M., Zhang, C., Wang, L., Xie, W., Xiong, L., Zhang, Q. and Lian, X. (2008). Sequence and expression analysis of the thioredoxin protein gene family in rice. *Molecular Genetics and Genomics* **280**, 139–151.

Pai, E. F. (1991). Variations on a theme: the family of FAD-dependent NAD(P)H-(disulfide)-oxidoreductases. *Current Opinion in Structural Biology* **1**, 796–803.

Pérez-Ruiz, J. M., Spínola, M. C., Kirchsteiger, K., Moreno, J., Sahrawy, M. and Cejudo, F. J. (2006). Rice NTRC is a high-efficiency redox system for chloroplast protection against oxidative damage. *Plant Cell* **18**, 2356–2368.

Peterson, F. C., Lytle, B. L., Sampath, S., Vinarov, D., Tyler, E., Shahan, M., Markley, J. L. and Volkman, B. F. (2005). Solution structure of thioredoxin h1 from *Arabidopsis thaliana*. *Protein Science* **14**, 2195–2200.

Prinz, W. A., Åslund, F., Holmgren, A. and Beckwith, J. (1997). The role of the thioredoxin and glutaredoxin pathways in reducing protein disulfide bonds in the *Escherichia coli* cytoplasm. *Journal of Biological Chemistry* **272**, 15661–15667.

Pulido, P., Cazalis, R. and Cejudo, F. J. (2009). An antioxidant redox system in the nucleus of wheat seed cells suffering oxidative stress. *Plant Journal* **57**, 132–145.

Qin, J., Clore, G. M., Kennedy, W. M., Huth, J. R. and Gronenborn, A. M. (1995). Solution structure of human thioredoxin in a mixed disulfide intermediate complex with its target peptide from the transcription factor NF kappa B. *Structure* **3**, 289–297.

Qin, J., Clore, G. M., Kennedy, W. P., Kuszewski, J. and Gronenborn, A. M. (1996). The solution structure of human thioredoxin complexed with its target from Ref-1 reveals peptide chain reversal. *Structure* **4**, 613–620.

Reichheld, J. P., Mestres-Ortega, D., Laloi, C. and Meyer, Y. (2002). The multigenic family of thioredoxin h in *Arabidopsis thaliana*: Specific expression and stress response. *Plant Physiology and Biochemistry* **40**, 685–690.

Reichheld, J. P., Meyer, E., Khafif, M., Bonnard, G. and Meyer, Y. (2005). AtNTRB is the major mitochondrial thioredoxin reductase in *Arabidopsis thaliana*. *FEBS Letters* **579**, 337–342.

Reichheld, J. P., Khafif, M., Riondet, C., Droux, M., Bonnard, G. and Meyer, Y. (2007). Inactivation of thioredoxin reductases reveals a complex interplay between thioredoxin and glutathione pathways in *Arabidopsis* development. *Plant Cell* **19**, 1851–1865.

Ren, G., Stephan, D., Xu, Z., Zheng, Y., Tang, D., Harrison, R. S., Kurz, M., Jarrott, R., Shouldice, S. R., Hiniker, A., Martin, J. L. Heras, B. *et al.* (2009). Properties of the thioredoxin fold superfamily are modulated by a single amino acid residue. *Journal of Biological Chemistry* **284**, 10150–10159.

Risler, J. L., Delorme, M. O., Delacroix, H. and Henaut, A. (1988). Amino acid substitutions in structurally related proteins. A pattern recognition approach. Determination of a new and efficient scoring matrix. *Journal of Molecular Biology* **204**, 1019–1029.

Rivera-Madrid, R., Mestres, D., Marinho, P., Jacquot, J. P., Decottignies, P., Miginiac-Maslow, M. and Meyer, Y. (1995). Evidences for five divergent thioredoxin h sequences in *Arabidopsis thaliana*. *Proceedings of the National Academy of Sciences of the United States of America* **92**, 5620–5624.

Rouhier, N., Gelhaye, E. and Jacquot, J. P. (2002). Glutaredoxin-dependent peroxiredoxin from poplar: Protein–protein interaction and catalytic mechanism. *Journal of Biological Chemistry* **277**, 13609–13614.

Rouhier, N., Kauffmann, B., Tete-Favier, F., Palladino, P., Gans, P., Branlant, G., Jacquot, J. P. and Boschi-Muller, S. (2007). Functional and structural aspects of poplar cytosolic and plastidial type a methionine sulfoxide reductases. *Journal of Biological Chemistry* **282**, 3367–3378.

Rozhkova, A., Stirnimann, C. U., Frei, P., Grauschopf, U., Brunisholz, R., Grütter, M. G., Capitani, G. and Glockshuber, R. (2004). Structural basis and kinetics of inter- and intramolecular disulfide exchange in the redox catalyst DsbD. *EMBO Journal* **23**, 1709–1719.

Ruggiero, A., Masullo, M., Ruocco, M. R., Grimaldi, P., Lanzotti, M. A., Arcari, P., Zagari, A. and Vitagliano, L. (2009). Structure and stability of a thioredoxin reductase from *Sulfolobus solfataricus*: A thermostable protein with two functions. *Biochimica et Biophysica Acta* **1794**, 554–562.

Santandrea, G., Guo, Y., O'Connell, T. and Thompson, R. D. (2002). Post-phloem protein trafficking in the maize caryopsis: zmTRXh1, a thioredoxin

specifically expressed in the pedicel parenchyma of *Zea mays* L., is found predominantly in the placentochalaza. *Plant Molecular Biology* **50**, 743–756.

Sarkar, N., Lemaire, S., Wu-Scharf, D., Issakidis-Bourguet, E. and Cerutti, H. (2005). Functional specialization of *Chlamydomonas reinhardtii* cytosolic thioredoxin h1 in the response to alkylation-induced DNA damage. *Eukaryotic Cell* **4**, 262–273.

Schürmann, P. and Buchanan, B. B. (2008). The ferredoxin/thioredoxin system of oxygenic photosynthesis. *Antioxidants & Redox Signaling* **10**, 1235–1274.

Serrato, A. J. and Cejudo, F. J. (2003). Type-h thioredoxins accumulate in the nucleus of developing wheat seed tissues suffering oxidative stress. *Planta* **217**, 392–399.

Serrato, A. J., Crespo, J. L., Florencio, F. J. and Cejudo, F. J. (2001). Characterization of two thioredoxins h with predominant localization in the nucleus of aleurone and scutellum cells of germinating wheat seeds. *Plant Molecular Biology* **46**, 361–371.

Serrato, A. J., Pérez-Ruiz, J. M. and Cejudo, F. J. (2002). Cloning of thioredoxin h reductase and characterization of the thioredoxin reductase-thioredoxin h system from wheat. *Biochemical Journal* **367**, 491–497.

Serrato, A. J., Pérez-Ruiz, J. M., Spínola, M. C. and Cejudo, F. J. (2004). A novel NADPH thioredoxin reductase, localized in the chloroplast, which deficiency causes hypersensitivity to abiotic stress in *Arabidopsis thaliana*. *Journal of Biological Chemistry* **279**, 43821–43827.

Shahpiri, A., Svensson, B. and Finnie, C. (2008). The NADPH-dependent thioredoxin reductase/thioredoxin system in germinating barley seeds: Gene expression, protein profiles and interactions between isoforms of thioredoxin h and thioredoxin reductase. *Plant Physiology* **146**, 789–799.

Shi, J. and Bhattacharyya, M. K. (1996). A novel plasma membrane-bound thioredoxin from soybean. *Plant Molecular Biology* **32**, 653–662.

Stenbaek, A., Hansson, A., Wulff, R. P., Hansson, M., Dietz, K. J. and Jensen, P. E. (2008). NADPH-dependent thioredoxin reductase and 2-Cys peroxiredoxins are needed for the protection of Mg-protoporphyrin monomethyl ester cyclase. *FEBS Letters* **582**, 2773–2778.

Suske, G., Wagner, W. and Follmann, H. (1979). NADPH thioredoxin reductase and a new thioredoxin from wheat. *Zeitschrift für Naturforschung* **34**, 214–221.

Sweat, T. A. and Wolpert, T. J. (2007). Thioredoxin h5 is required for victorin sensitivity mediated by a CC-NBS-LRR gene in *Arabidopsis*. *Plant Cell* **19**, 673–687.

Thompson, J. D., Higgins, D. G. and Gibson, T. J. (1994). CLUSTAL W: Improving the sensitivity of progressive multiple sequence alignment through sequence weighting, position-specific gap penalties and weight matrix choice. *Nucleic Acids Research* **22**, 4673–4680.

Veine, D. M., Mulrooney, S. B., Wang, P. F. and Williams, C. H., Jr. (1998). Formation and properties of mixed disulfides between thioredoxin reductase from *Escherichia coli* and thioredoxin: Evidence that cysteine-138 functions to initiate dithiol-disulfide interchange and to accept the reducing equivalent from reduced flavin. *Protein Science* **7**, 1441–1450.

Verdoucq, L., Vignols, F., Jacquot, J. P., Chartier, Y. and Meyer, Y. (1999). *In vivo* characterization of a thioredoxin h target protein defines a new peroxiredoxin family. *Journal of Biological Chemistry* **274**, 19714–19722.

Waksman, G., Krishna, T. S. R., Williams, C. H., Jr. and Kuriyan, J. (1994). Crystal structure of *Escherichia coli* thioredoxin reductase refined at 2 Å resolution. Implications for a large conformational change during catalysis. *Journal of Molecular Biology* **236**, 800–816.

Wang, P.-F., Veine, D. M., Ahn, S. H. and Williams, C. H., Jr. (1996). A stable mixed disulfide between thioredoxin reductase and its substrate, thioredoxin: Preparation and characterization. *Biochemistry* **35**, 4812–4819.

Weichsel, A., Gasdaska, J. R., Powis, G. and Montfort, W. R. (1996). Crystal structures of reduced, oxidized, and mutated human thioredoxins: Evidence for a regulatory homodimer. *Structure* **4**, 735–751.

Wieles, B., van Noort, J., Drijfhout, J. W., Offringa, R., Holmgren, A. and Ottenhoff, T. H. (1995a). Purification and functional analysis of the *Mycobacterium leprae* thioredoxin/thioredoxin reductase hybrid protein. *Journal of Biological Chemistry* **270**, 25604–25606.

Wieles, B., van Soolingen, D., Holmgren, A., Offringa, R., Ottenhoff, T. and Thole, J. (1995b). Unique gene organization of thioredoxin and thioredoxin reductase in *Mycobacterium leprae*. *Molecular Microbiology* **16**, 921–929.

Williams, C. H., Arscott, L. D., Muller, S., Lennon, B. W., Ludwig, M. L., Wang, P. F., Veine, K. B. and Schirmer, R. H. (2000). Thioredoxin reductase two modes of catalysis have evolved. *European Journal of Biochemistry* **267**, 6110–6117.

Wong, J. H., Kim, Y. B., Ren, P. H., Cai, N., Cho, M. J., Hedden, P., Lemaux, P. G. and Buchanan, B. B. (2002). Transgenic barley grain overexpressing thioredoxin shows evidence that the starchy endosperm communicates with the embryo and the aleurone. *Proceedings of the National Academy of Sciences of the United States of America* **99**, 16325–16330.

Wong, J. H., Balmer, Y., Cai, N., Tanaka, C. K., Vensel, W. H., Hurkman, W. J. and Buchanan, B. B. (2003). Unraveling thioredoxin-linked metabolic processes of cereal starchy endosperm using proteomics. *FEBS Letters* **547**, 151–156.

Wong, J. H., Cai, N., Balmer, Y., Tanaka, C. K., Vensel, W. H., Hurkman, W. J. and Buchanan, B. B. (2004). Thioredoxin targets of developing wheat seeds identified by complementary proteomic approaches. *Phytochemistry* **65**, 1629–1640.

Yamazaki, D., Motohashi, K., Kasama, T., Hara, Y. and Hisabori, T. (2004). Target proteins of the cytosolic thioredoxin in *Arabidopsis thaliana*. *Plant and Cell Physiology* **45**, 18–27.

Yano, H., Wong, J. H., Lee, Y. M., Cho, M. J. and Buchanan, B. B. (2001). A strategy for the identification of proteins targeted by thioredoxin. *Proceedings of the National Academy of Sciences of the United States of America* **98**, 4794–4799.

Yuan, C. S., Ault-Riche, D. B. and Borchardt, R. T. (1996). Chemical modification and site-directed mutagenesis of cysteine residues in human placental *S*-adenosylhomocysteine hydrolase. *Journal of Biological Chemistry* **271**, 28009–28016.

Zhang, Z., Bao, R., Zhang, Y., Yu, J., Zhou, C.-Z. and Chen, Y. (2009). Crystal structure of *Saccharomyces cerevisiae* cytoplasmic thioredoxin reductase Trr1 reveals the structure basis for species-specific recognition of thioredoxin. *Biochimica Biophysica Acta* **1794**, 124–128.

Appendix H

Oral and poster contributions

Danscatt (Danish Centre for the use of Synchrotron X-ray and Neutron facilities) annual meeting, June 2nd—3rd 2009, DTU Chemistry. **Poster presented**: **"Reaction Mechanism of Barley Thioredoxin Reductase".**

Protein.DTU, 3rd workshop, March 16th 2010, Technical University of Denmark. **Poster presented: "Reaction Mechanism of Barley Thioredoxin Reductase".**

WORKSHOP for PhD students and Postdocs: Redox modifications and proteomics, June 17th 2010, KU-LIFE. **Oral presentation: "Role of barley thioredoxin reductase"**.

LMC PROTEIN REDOX NETWORK SYMPOSIUM: Novel techniques for analysis of protein redox modifications, June 18th 2010, KU-LIFE. **Poster presented:" Reaction mechanism of NADPH-dependent thioredoxin reductase (NTR) from Barley ".**

Meeting for FTP project, A Quantitative Redox Proteomics and Protein Engineering "Tool Box" for Applications of Thioredoxin in Food Biotechnology, August 20th 2010, Technical University of Denmark. **Oral presentation: "Recognition of thioredoxin isoforms by thioredoxin reductase"**.

Conference: ICCBM13 - 13th International Conference on the Crystallization of Biological Macromolecules, Dublin, September 12th—16th 2010. **Poster presented: "Crystal Structure of NADPH-dependent thioredoxin reductase (*Hv*NTR2) from Barley".**

CoLuAa XIX, Crystallography meeting, November 4th—5th 2010. **Poster presented and oral poster presentation: "Reaction mechanism of NADPH-dependent thioredoxin reductase (NTR) from Barley".**

Protein.DTU, 4th workshop, November 12th 2010. **Presented poster and short oral poster presentation: "Reaction mechanism of NADPH-dependent thioredoxin reductase (*Hv*NTR) from Barley".**

Plant Biotech Denmark, March 3rd—4th 2011, KU-Life. **Poster presented: "Reaction mechanism of NADPH-dependent thioredoxin reductase (*Hv*NTR) from Barley".**

Protein.DTU, 5th workshop, June 9th 2011. **Presented poster and short oral poster presentation: "Homology model of a complex between NADPH-dependent thioredoxin reductase (NTR) and thioredoxin from barley".**

Protein Redox Network Workshop "BIOLOGICAL REDOX REGULATION AND FOOD ANTIOXIDANTS". June 20th 2011. **Oral presentation: "Homology model of a complex between NADPH-dependent thioredoxin reductase (NTR) and thioredoxin from barley"**.

Protein Redox Network Symposium "BIOLOGICAL REDOX REGULATION AND FOOD ANTIOXIDANTS". June 21st 2011. **Poster presented: "Homology model of a complex between NADPH-dependent thioredoxin reductase (NTR) and thioredoxin from barley"**

Reaction Mechanism of Barley Thioredoxin Reductase

Kristine Groth Kirkensgaard[a,b], Per Hägglund[b], Christine Finnie[b], Birte Svensson[b] and Anette Henriksen[a#].
[a]Carlsberg Laboratory, Valby, Denmark, and [b]Technical University of Denmark, Lyngby, Denmark. [#]E-mail: anette@crc.dk

Protein disulfides and seed germination

Many seed proteins containing a disulfide (-S-S-) group undergo redox changes during seed development and germination. The proteins are synthesized in the reduced (-SH) state, become oxidized to the disulfide state during seed maturation and are converted back to the reduced state during the germination process. The reduction of disulfides increases solubility, protease susceptibility, heat stability and it changes the activity of enzymes.

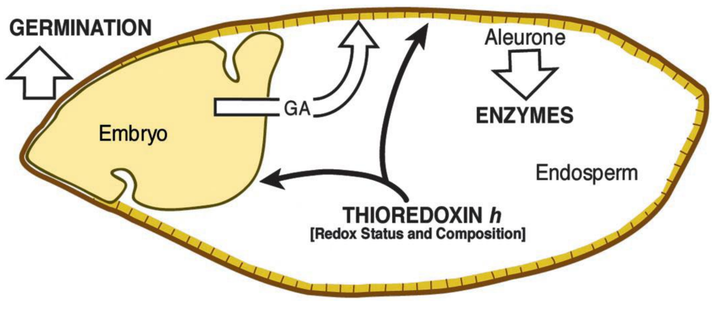

Thioredoxin h plays a role in the communication between the starchy endosperm, the embryo and the aleurone layer that promotes germination and enhances the activity of hydrolytic enzymes.

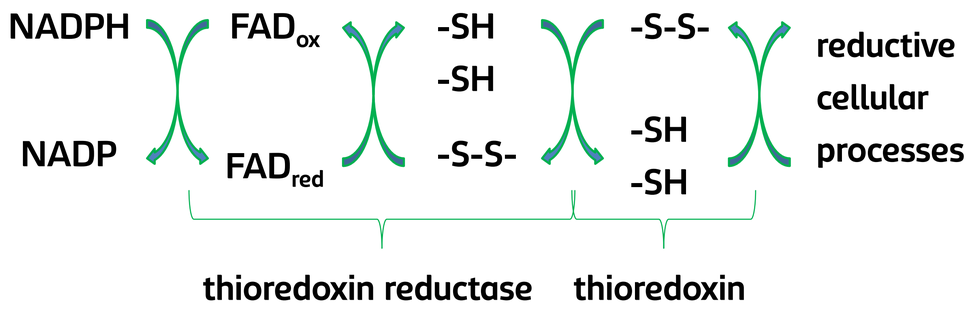

Barley NTR and the reaction mechanism

In the crystal structure of barley NTR (coloured), the two domains responsible for FAD and NADPH binding respectively are trapped in a not previously observed domain arrangement.

The relative domain orientation is different from that observed in oxidized *Arabidopsis* NTR (white). The amino acids involved in inter domain contacts in the oxidized NTR molecules are the same amino acids, which binds to Trx. The structure of barley NTR does not provide enough space in the NADPH binding site to enable NADPH binding.

The NTR reaction scheme can account for these observation if NTR-Trx interaction is required for breakage of inter domain contacts in the NTR FO conformation and the binding/release of $NADPH/NADP^+$ is assumed to only involve the FR conformation.

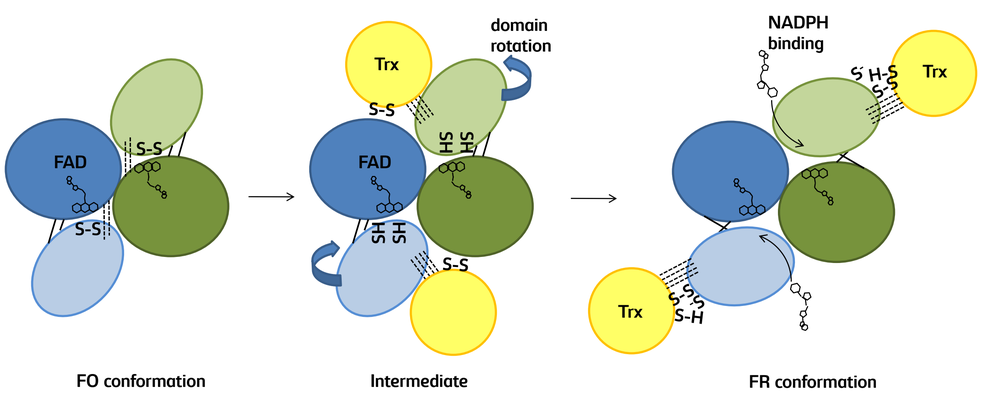

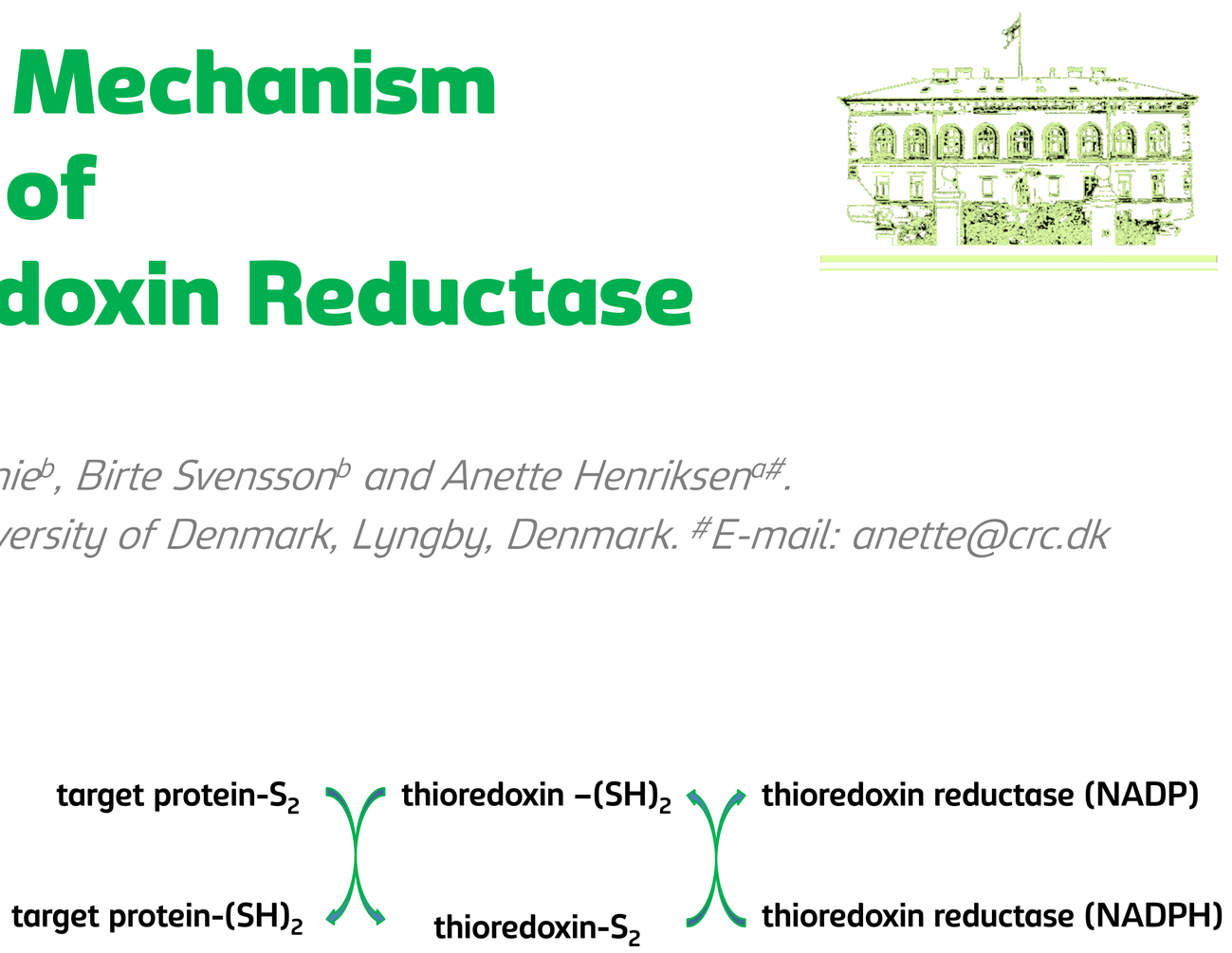

Thioredoxins

Plant Thioredoxins (Trx's) are small (~ 13 kDa) globular proteins that catalyze these thiol-disulfide exchange reactions. The activity of the thioredoxins is dependent on the activity of the thioredoxin reductases (NTR's).

The Trx/NTR system was originally identified as the system able to transfer reducing equivalents to ribonucleotide reductase. In most organisms it is in fact the only way to produce the deoxyribonucleotides needed for cell division. Later, the thioredoxin driven disulfide dithiol exchange reactions were shown to play major roles in plant growth, development and response to environmental constraints including both biotic and abiotic stress.

Thioredoxin reductase

The reduction of thioredoxin requires the presence of two cofactors, FAD and NADPH and a protein scaffold that orient the thioredoxin and the cofactors for a stepwise exchange of reducing equivalents.

In order to catalyze the entire reaction, NTR needs to swap between two conformations, the flavin oxidizing (FO) and flavin reducing (FR) conformation.

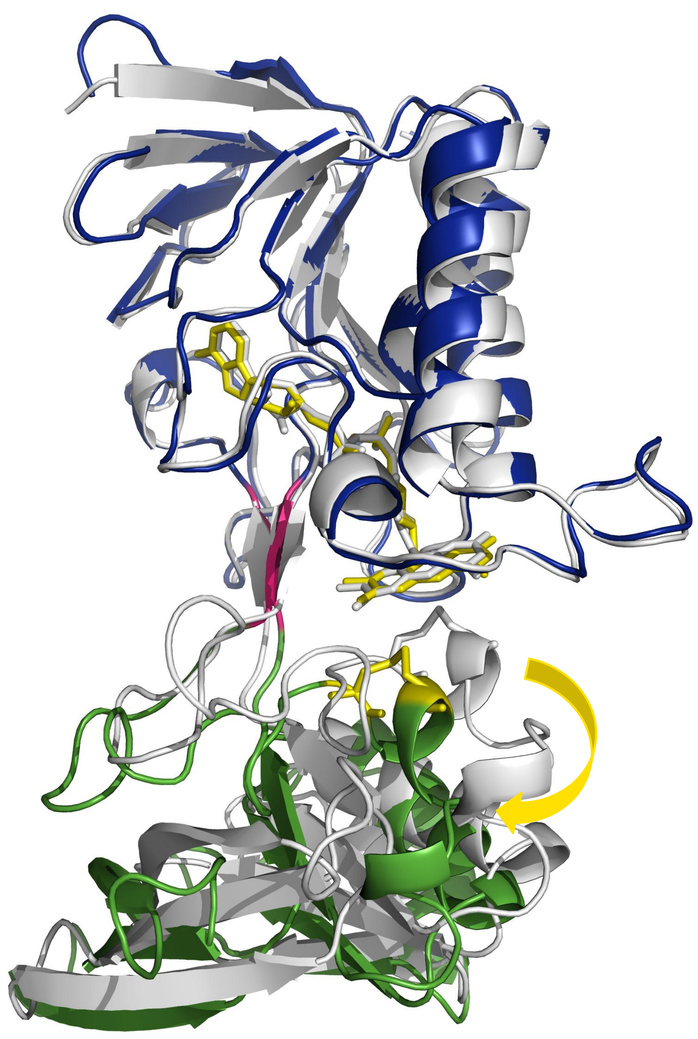

Reaction Mechanism of NADPH-dependent Thioredoxin Reductase (*Hv*NTR2) from Barley

Kristine Groth Kirkensgaard[a,b,#], *Per Hägglund*[a], *Christine Finnie*[a], *Birte Svensson*[a] *and Anette Henriksen*[b].

[a] *Enzyme and Protein Chemistry, Department of Systems Biology, Technical University of Denmark, DK-2800 Kgs. Lyngby, Denmark.*

[b] *Carlsberg Laboratory, DK-2500 Valby, Denmark.* [#]*E-mail: kgk@bio.dtu.dk*

Protein disulfides and seed germination

Many seed proteins containing a disulfide (-S-S-) group undergo redox changes during seed development and germination. The proteins are synthesized in the reduced (-SH) state, become oxidized to the disulfide state during seed maturation and are converted back to the reduced state during the germination process. The reduction of disulfides increases solubility, protease susceptibility, heat stability and it changes the activity of enzymes.

Thioredoxins and thioredoxin reductase

Plant Thioredoxins (Trx's) are small (~13kDa) globular proteins that catalyze these thiol-disulfide exchange reactions (Figure 1). The activity of the thioredoxins is dependent on the activity of the thioredoxin reductases (NTR's) (for a review see [1]).

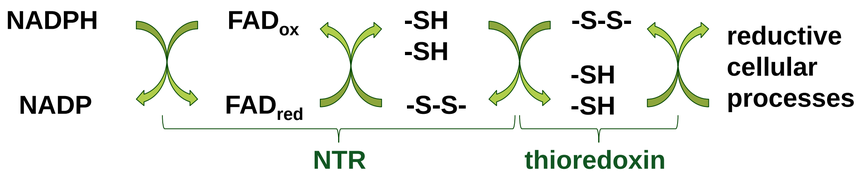

Figure 1 Reaction catalyzed by NADPH-dependent thioredoxin reductase (NTR). Reducing equivalents are transferred from NADPH to FAD bound to NTR. From FAD they are transferred to a disulfide bond in the NADPH domain of NTR and further to a disulfide in thioredoxin (Trx). Hereafter Trx can reduce other proteins.

The reduction of thioredoxin requires the presence of two cofactors, FAD and NADPH, and NTR that orients the thioredoxin and the cofactors for a stepwise exchange of reducing equivalents (Figure 1). In order to catalyze the entire reaction, NTR needs to swap between two conformations, the flavin oxidizing (FO) and flavin reducing (FR) conformation (Figure 4). We have solved the structure of one NTR isoform (*Hv*NTR2) from barley to 2.6Å (Figure 2) [2]. It consists of two domains, the FAD and the NADPH binding domains, and so far all previously solved low-molecular-weight NTRs were found to be in one of two conformations; the flavin oxidizing (FO) or the flavin reducing (FR) conformation. To obtain the latter, one domain has to rotate 66° relative to the other. Only by covalently binding NTR to Trx, the FR can be stabilized for characterization [3].

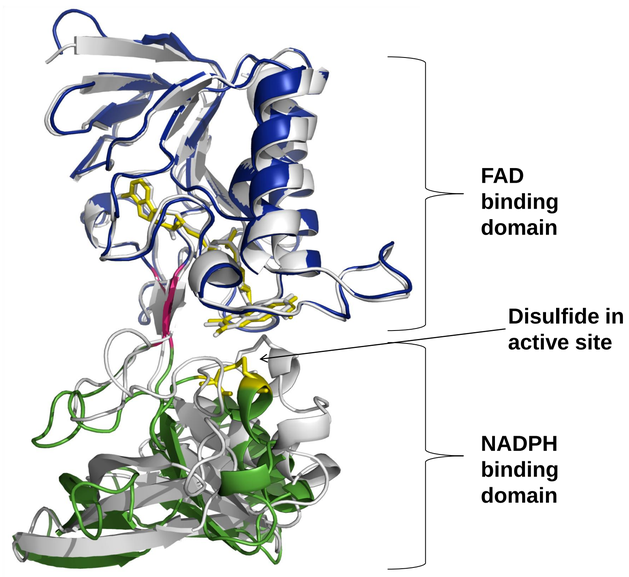

Figure 2 Superposition of the FAD domain of *Hv*NTR2 (blue) and NTR from *Arabidopsis thaliana* (*At*NTR-B, white, pdb accession: 1vdc). The NADPH domains (green) were not included in the superposition. The *Hv*NTR2 FAD and the disulfide bridge are shown in yellow and the β-strand linker in pink.

Barley NTR and the reaction mechanism

In the crystal structure of *Hv*NTR2 (Figure 2, colored), the two domains responsible for FAD and NADPH binding respectively are trapped in a not previously observed domain arrangement. The relative domain orientation is different from that observed in NTR from *Arabidopsis thaliana* (white) in the FO conformation [4]. The amino acids involved in inter domain contacts in the oxidized NTR molecules (corresponding to Gly129 and Arg130 in NTR from *E. coli*) are the same amino acids, which binds to Trx, as judged from a structure of NTR from *E. coli* covalently bound to Trx (Figure 3) [3]. The structure of barley NTR does not provide enough space in the conserved NADPH binding site to enable NADPH binding.

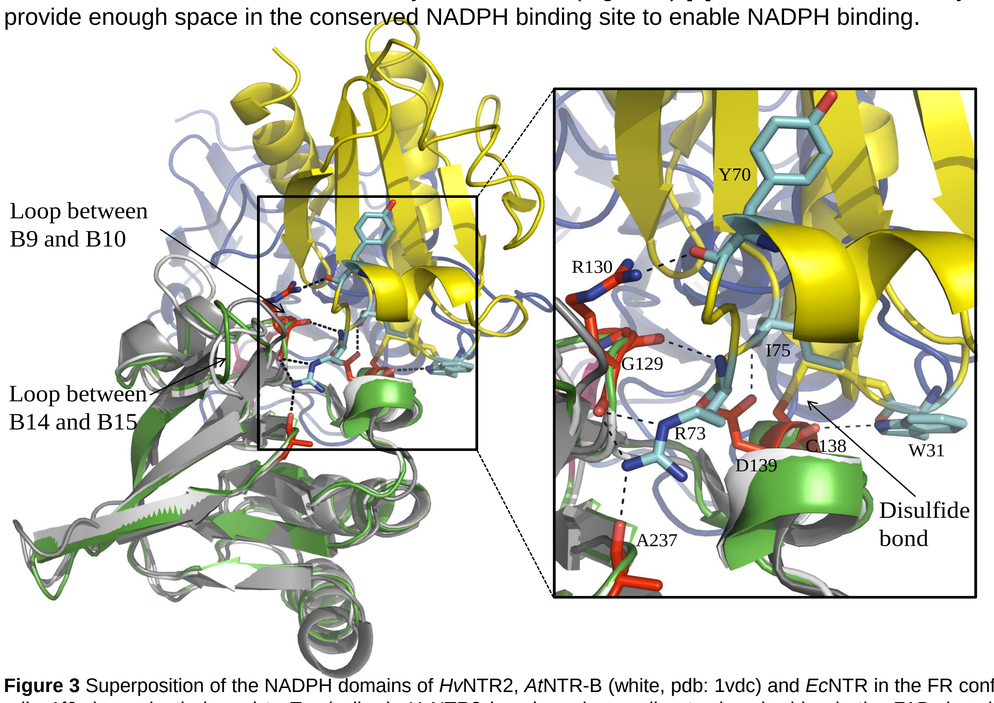

Figure 3 Superposition of the NADPH domains of *Hv*NTR2, *At*NTR-B (white, pdb: 1vdc) and *Ec*NTR in the FR conformation (grey, pdb: 1f6m) covalently bound to Trx (yellow). *Hv*NTR2 is coloured according to domain; blue is the FAD domain, green is the NADPH domain and pink is the β-sheet linker between the two domains.

The NTR reaction scheme can account for these observation if NTR-Trx interaction is required for breakage of inter-domain contacts in the NTR FO conformation and the binding/release of NADPH/$NADP^+$ is assumed to only involve the FR conformation (Figure 4).

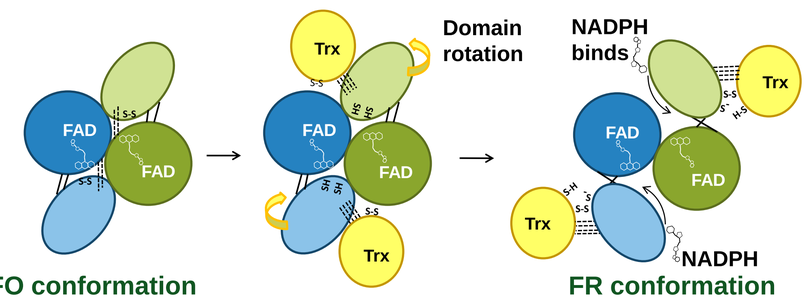

Figure 4 The NTR reaction scheme modified to take the observation of differences in inter-domain interactions and lack of space for NADPH binding in the *Hv*NTR2 crystal structure into account. Hydrogen bonds are shown by dotted lines. Trx interaction is required for breakage of inter domain contacts in the FO conformation and NADPH/$NADP^+$ is assumed not to bind during domain re-orientation.

As seen on Figure 3 a loop between β-sheets B14 and B15 is placed close to the binding site of Trx. The structure of *Hv*NTR2 reveals a loop, which is predicted to be flexible due to many glycine residues. An alignment of different plant NTRs (Figure 5) shows that this loop is conserved in monocots, but with small variations between isoforms which may lead to preference for a specific Trx isoform.

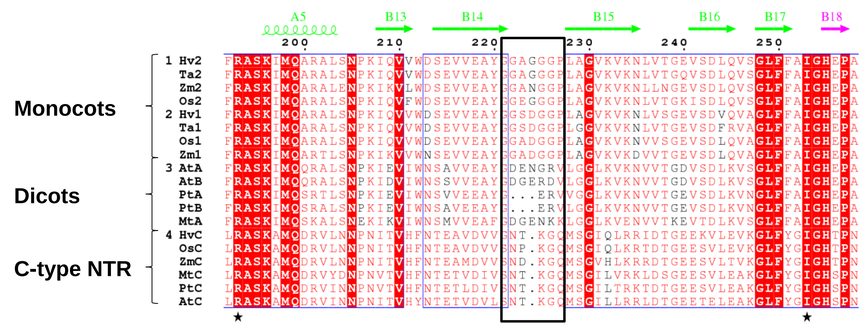

Figure 5 Part of an alignment between different NTRs from plants reveals a glycine-rich loop (boxed) in monocots. Hv = barley, Ta = wheat, Zm = mays, Os = rice, At = *Arabidopsis thaliana,* Pt = poplar and MT = *Medicago truncatula* (Barrel Medic, legume)

To investigate the role of the glycin loop mutants have been made in this as well as deletion of another loop (WMANDI, see Figure 5) conserved in plants. Changing residues in the glycin loop to the corresponding residues in *A. thaliana* decreased the Km about two-fold for *At*trxH3 and slightly increased the Km for *Hv*trxH1 and H2. Deleting the WMANDI loop rendered *Hv*NTR2 almost unable to react with *Hv*trxH1/H2 but for unknown reasons it can still react with *At*trxH3 (data not shown).

Complex model

A complex of *Hv*NTR2 bound to *Hv*trxH2 was made by aligning the two separate domains with the corresponding domains of the *Ec*NTR-*Ec*trx complex (pdb 1f6m [3]) using Coot. *Hv*trxH2 from a complex (pdb 2iwt [5]) was used. Homology modelling , energy minimization and model evaluation was performed using MOE (Figure 6A) and the contacts mapped using Ligplot (Figure 6B). Among other thing is seen that the residue equivalent to Arg140 is central in the binding in *E. coli* is not as important here. Asn139 seems to have taken over this role.

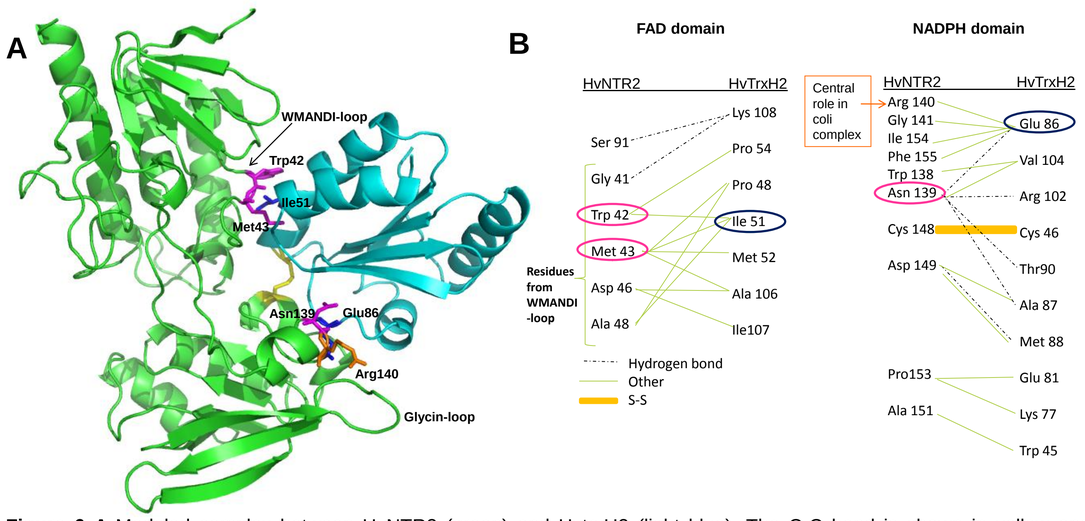

Figure 6 A Modeled complex between HvNTR2 (green) and HvtrxH2 (light blue). The C-C bond is shown in yellow and the residues we plan to examine by site directed mutagenesis are shown in magenta if belonging to HvNTR2 and in dark blue from HvtrxH2. **B** Predicted interactions between HvNTR2 and HvtrxH2 found by using Ligplot on the model. Color code like in **A**.

Future and ongoing work

Different mutations of the residues shown in Figure 6 will be examined to validate the model. Furthermore a complex between *Hv*NTR2 and *Hv*trxH2 has been produced by covalently linking single Cys→Ser mutants of the two protein. The complex has been subjected to crystallization trials but so far without any hits.

References

[1] Hägglund, P., Kirkensgaard, K., Maeda, K., Finnie, C., Henriksen, A. & Svensson, B. (2009) Molecular Recognition in NADPH-Dependent Plant Thioredoxin Systems – Catalytic Mechanisms, Structural Snapshots and Target Identifications. Chapter 15 *in* Oxidative stress and redox regulation in plants. J-P, Jacquot (Ed.). pp. 461-495. Advances in botanical research **52**, Burlington: Academic Press

[2] Kirkensgaard, K.G., Hägglund, P., Finnie, C., Svensson, B. & Henriksen, A. (2009) Structure of *Hordeum vulgare* NADPH-dependent thioredoxin reductase 2. Unwinding the reaction mechanism. *Acta Cryst.* **D65**, 932-941.

[3] Lennon, B. W., Williams, C. H., Jr. & Ludwig, M. L. (2000) Twists in catalysis: alternating conformations of Escherichia coli thioredoxin reductase. *Science* **289**, 1190-1194.

[4] Dai, S., Saarinen, M., Ramaswamy, S., Meyer, Y., Jacquot, J. P. & Eklund, H. (1996) Crystal structure of *Arabidopsis thaliana* NADPH dependent thioredoxin reductase at 2.5 Å resolution. *J. Mol. Biol.* **264**, 1044-1057.

[5] Maeda, K., Hagglund, P., Finnie, C., Svensson, B., Henriksen, A (20006) Structural basis for target protein recognition by the protein disulfide reductase thioredoxin *Structure* **14**, 1701- 1710.

Crystal Structure of NADPH-dependent Thioredoxin Reductase (*Hv*NTR2) from Barley

Kristine Groth Kirkensgaard[a,b,#], *Per Hägglund*[a], *Christine Finnie*[a], *Birte Svensson*[a] *and Anette Henriksen*[b].

[a] *Enzyme and Protein Chemistry, Department of Systems Biology, Technical University of Denmark, DK-2800 Kgs. Lyngby, Denmark.*

[b] *Carlsberg Laboratory, DK-2500 Valby, Denmark.* [#]*E-mail: kgk@bio.dtu.dk*

Protein disulfides and seed germination

Many seed proteins containing a disulfide (-S-S-) group undergo redox changes during seed development and germination. The proteins are synthesized in the reduced (-SH) state, become oxidized to the disulfide state during seed maturation and are converted back to the reduced state during the germination process. The reduction of disulfides increases solubility, protease susceptibility, heat stability and it changes the activity of enzymes.

Thioredoxins and thioredoxin reductase

Plant thioredoxins (Trx's) are small (~13kDa) globular proteins that catalyze these thiol-disulfide exchange reactions (Figure 1). The activity of the thioredoxins is dependent on the activity of the NADPH-dependent thioredoxin reductases (NTR's) (for a review see [1]).

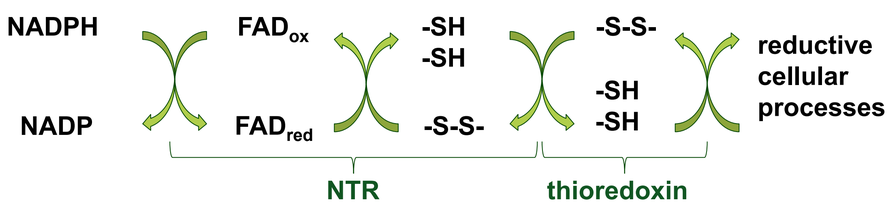

Figure 1 Reaction catalyzed by NADPH-dependent thioredoxin reductase (NTR). Reducing equivalents are transferred from NADPH to FAD bound to NTR. From FAD they are transferred to a disulfide bond in the NADPH domain of NTR and further to a disulfide in thioredoxin (Trx). Hereafter Trx can reduce other proteins.

The reduction of thioredoxin requires the presence of two cofactors, FAD and NADPH, and NTR that orients the thioredoxin and the cofactors for a stepwise exchange of reducing equivalents (Figure 1).

Crystallizing thioredoxin reductase from barley

We have crystallized and solved the structure of one NTR isoform (*Hv*NTR2) from barley: Initial crystal screening experiments were carried out using the PEG6000 grid-screen (Hampton Research) and the hanging drop vapour diffusion method. Drops of 2.0 µL protein solution were mixed with 2.0 µL reservoir solution and equilibrated over a reservoir of 500 µL. Yellow needle clustes (Figure 2A) were detected in 5% (w/v) PEG6000 (Fluka) and 0.1 M citrate-buffer pH 4.0 after four days of incubation at 22°C.

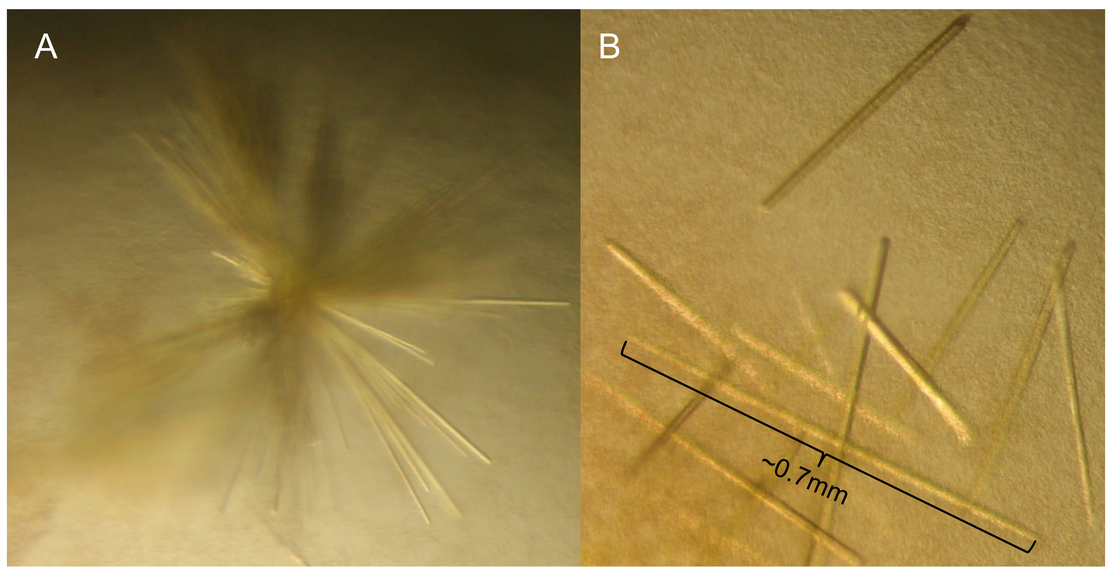

Figure 2 Yellow needle cluster and needles of NADPH-dependent thioredoxin reductase isoform 2 (*Hv*NTR2) from barley. **A)** Crystals where grown in 5% (w/v) PEG6000 (Fluka) and 0.1 M citrate-buffer pH 4.0 for four days at 22°C. **B)** Crystal grown 12 days at 25°C in 2% (w/v) PEG400 and 0.1 M citrate-buffer pH 3.5.

Further optimization included screening of the effect of the PEG molecular weight, the temperature and pH. Longer separate needles (Figure 2B) where obtained by increasing the temperature to 25°C and using 2% (w/v) PEG400 and 0.1 M citrate-buffer pH 3.5. Fine tuning of crystallization conditions included screening of the PEG concentration as well as using the Hampton Research additive screen. When optimized it consisted of 24% (w/v) PEG400, 2% Jeffamine M-600, 0.1 M citrate-buffer pH 3.5, a protein concentration of 5.7 mg mL^{-1} and an incubation temperature of 25°C. These conditions gave bright yellow crystals with hexagonal morphology within a week (Figure 3). The diameter of the crystals could reach 0.18 mm. The crystals were flash-frozen directly from the drop without using additional cryo-protectants.

Solved structure

The structure of *Hv*NTR2 from barley was solved to 2.6Å (Figure 4) [2]. It consists of two domains, the FAD and the NADPH binding domains, and so far all previously solved low-molecular-weight NTRs are found to be in one of two conformations; the flavin oxidizing (FO) or the flavin reducing (FR) conformation. To obtain the latter, one domain rotates 66° relative to the other.

Figure 3 Hexagonal crystals of NADPH-dependent thioredoxin reductase isoform 2 (*Hv*NTR2) from barley. Crystals where grown in 24% (w/v) PEG400, 2% Jeffamine M-600, 0.1 M citrate-buffer pH 3.5, a protein concentration of 5.7 mg mL^{-1} and an incubation temperature of 25°C for a week.

Only by covalently binding NTR to Trx, the FR is stabilized for characterization [3]. The *Hv*NTR2 structure may be an intermediate of the FO and FR conformation but was closest to the FO conformation.

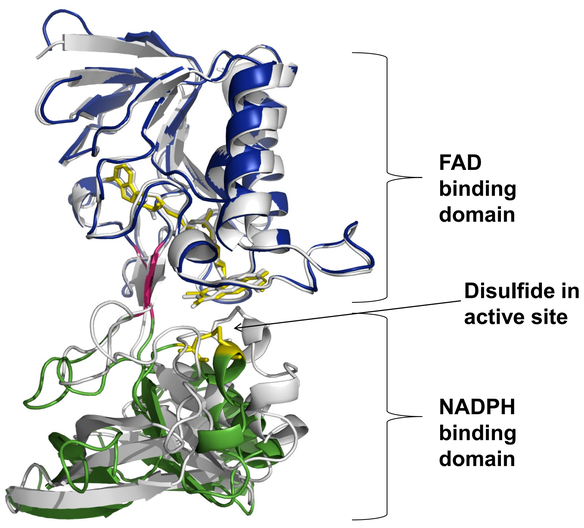

Figure 4 Superposition of the FAD domain of *Hv*NTR2 (blue) and NTR from *Arabidopsis thaliana* (*At*NTR-B, white, pdb accession: 1vdc). The NADPH domains (green for *Hv*NTR2 and white for *At*NTR-B) were not included in the superposition. The *Hv*NTR2 FAD and the disulfide bridge are shown in yellow and the β-strand linker in pink.

Attempts to crystallize the other isoform

Attempt have been made to crystallize the other isoform of NTR (HvNTR1), which has 88.6% sequence identity to HvNTR2. Screening has been done using the PEG6000 grid-screen, the Ammonium sulphate grid-screen and Crystal screen 1 and 2 (all from Hampton). Furthermore Hampton index screen, a salt screen and others where set up by robot, but this as well as attempts to seed with crystals of HvNTR2 have so far not given any results.

Conclusion

An isoform of NADPH-dependent thioredoxin reductase from barley (*Hv*NTR2) was crystallized using the PEG6000 grid-screen (Hampton Research) and fine tuned using the Hampton Research additive screen. The bright yellow hexagonal crystals diffracted to 2.6Å. Attempts to crystallize the other isoform (*Hv*NTR1) has so far not given any results.

References

[1] Hägglund, P., Kirkensgaard, K., Maeda, K., Finnie, C., Henriksen, A. & Svensson, B. (2009) Molecular Recognition in NADPH-Dependent Plant Thioredoxin Systems – Catalytic Mechanisms, Structural Snapshots and Target Identifications. Chapter 15 *in* Oxidative stress and redox regulation in plants. J-P, Jacquot (Ed.). pp. 461-495. Advances in botanical research **52**, Burlington: Academic Press

[2] Kirkensgaard, K.G., Hägglund, P., Finnie, C., Svensson, B. & Henriksen, A. (2009) Structure of *Hordeum vulgare* NADPH-dependent thioredoxin reductase 2. Unwinding the reaction mechanism. *Acta Cryst.* **D65**, 932-941.

[2] Lennon, B. W., Williams, C. H., Jr. & Ludwig, M. L. (2000) Twists in catalysis: alternating conformations of Escherichia coli thioredoxin reductase. *Science* **289**, 1190-1194.

[3] Dai, S., Saarinen, M., Ramaswamy, S., Meyer, Y., Jacquot, J. P. & Eklund, H. (1996) Crystal structure of *Arabidopsis thaliana* NADPH dependent Thioredoxin reductase at 2.5 Å resolution. *J. Mol. Biol.* **264**, 1044-1057.

Reaction Mechanism of NADPH-dependent Thioredoxin Reductase (*Hv*NTR2) from Barley

Kristine Groth Kirkensgaard[a,b,#], *Per Hägglund*[a], *Christine Finnie*[a], *Birte Svensson*[a] *and Anette Henriksen*[b].

[a] *Enzyme and Protein Chemistry, Department of Systems Biology, Technical University of Denmark, DK-2800 Kgs. Lyngby, Denmark.*

[b] *Carlsberg Laboratory, DK-2500 Valby, Denmark.* [#]*E-mail: kgk@bio.dtu.dk*

Protein disulfides and seed germination

Many seed proteins containing a disulfide (-S-S-) group undergo redox changes during seed development and germination. The proteins are synthesized in the reduced (-SH) state, become oxidized to the disulfide state during seed maturation and are converted back to the reduced state during the germination process. The reduction of disulfides increases solubility, protease susceptibility, heat stability and it changes the activity of enzymes.

Thioredoxins and thioredoxin reductase

Plant Thioredoxins (Trx's) are small (~13kDa) globular proteins that catalyze these thiol-disulfide exchange reactions (Figure 1). The activity of the thioredoxins is dependent on the activity of the thioredoxin reductases (NTR's) (for a review see [1]).

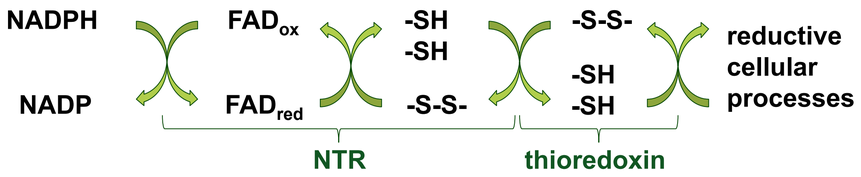

Figure 1 Reaction catalyzed by NADPH-dependent thioredoxin reductase (NTR). Reducing equivalents are transferred from NADPH to FAD bound to NTR. From FAD they are transferred to a disulfide bond in the NADPH domain of NTR and further to a disulfide in thioredoxin (Trx). Hereafter Trx can reduce other proteins.

The reduction of thioredoxin requires the presence of two cofactors, FAD and NADPH, and NTR that orients the thioredoxin and the cofactors for a stepwise exchange of reducing equivalents (Figure 1). In order to catalyze the entire reaction, NTR needs to swap between two conformations, the flavin oxidizing (FO) and flavin reducing (FR) conformation (Figure 4). We have solved the structure of one NTR isoform (*Hv*NTR2) from barley to 2.6Å (Figure 2) [2]. It consists of two domains, the FAD and the NADPH binding domains, and so far all previously solved low-molecular-weight NTRs were found to be in one of two conformations; the flavin oxidizing (FO) or the flavin reducing (FR) conformation. To obtain the latter, one domain has to rotate 66° relative to the other. Only by covalently binding NTR to Trx, the FR can be stabilized for characterization [3].

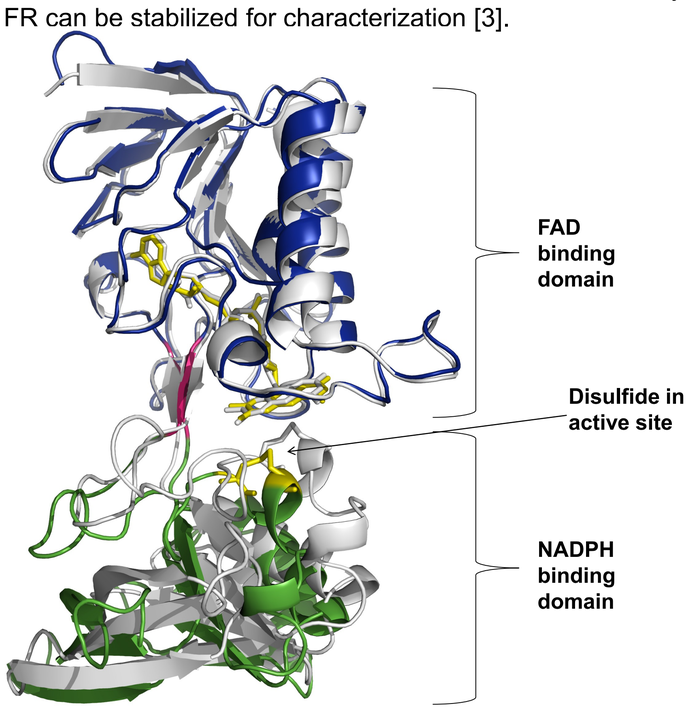

Figure 2 Superposition of the FAD domain of *Hv*NTR2 (blue) and NTR from *Arabidopsis thaliana (At*NTR-B, white, pdb accession: 1vdc). The NADPH domains (green) were not included in the superposition. The *Hv*NTR2 FAD and the disulfide bridge are shown in yellow and the β-strand linker in pink.

Barley NTR and the reaction mechanism

In the crystal structure of *Hv*NTR2 (Figure 2, colored), the two domains responsible for FAD and NADPH binding respectively are trapped in a not previously observed domain arrangement.

The relative domain orientation is different from that observed in NTR from *Arabidopsis thaliana* (white) in the FO conformation [4]. The amino acids involved in inter domain contacts in the oxidized NTR molecules (corresponding to Gly129 and Arg130 in NTR from *E. coli*) are the same amino acids, which binds to Trx, as judged from a structure of NTR from *E. coli* covalently bound to Trx (Figure 3) [2]. The structure of barley NTR does not provide enough space in the conserved NADPH binding site to enable NADPH binding.

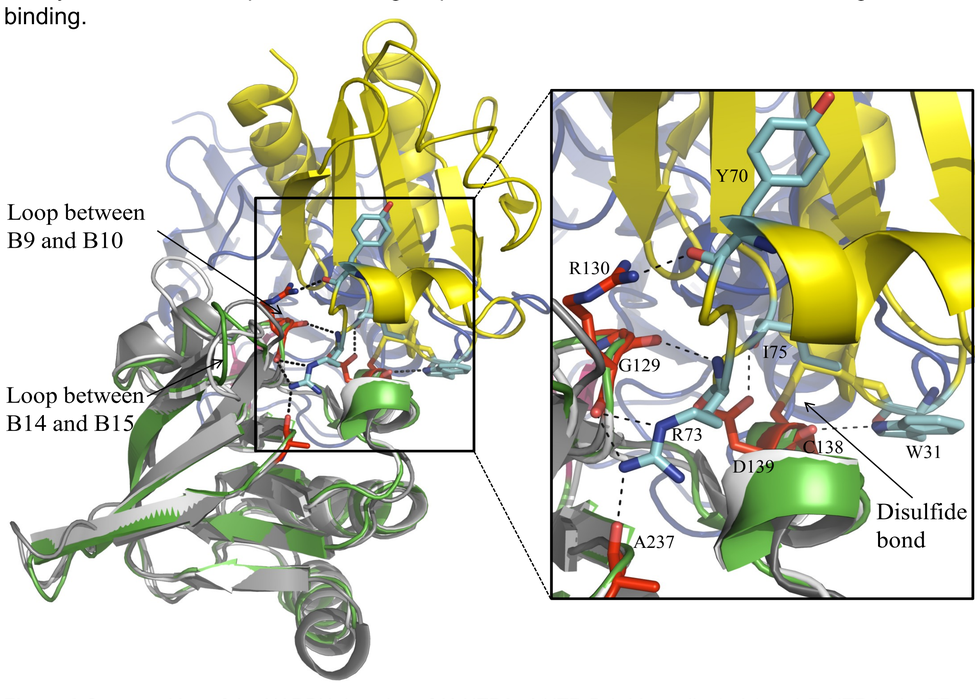

Figure 3 Superposition of the NADPH domains of *Hv*NTR2, *At*NTR-B (white, pdb: 1vdc) and *Ec*NTR in the FR conformation (grey, pdb: 1f6m) covalently bound to Trx (yellow). *Hv*NTR2 is coloured according to domain; blue is the FAD domain, green is the NADPH domain and pink is the β-sheet linker between the two domains.

The NTR reaction scheme can account for these observation if NTR-Trx interaction is required for breakage of inter-domain contacts in the NTR FO conformation and the binding/release of NADPH/NADP$^+$ is assumed to only involve the FR conformation (Figure 4).

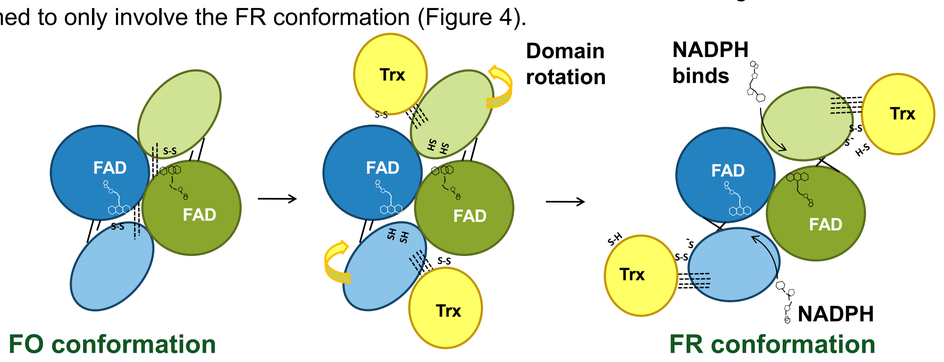

Figure 4 The NTR reaction scheme modified to take the observation of differences in inter-domain interactions and lack of space for NADPH binding in the *Hv*NTR2 crystal structure into account. Hydrogen bonds are shown by dotted lines. Trx interaction is required for breakage of inter domain contacts in the FO conformation and NADPH/NADP$^+$ is assumed not to bind during domain re-orientation.

As seen on Figure 3 a loop between β-sheets B14 and B15 is placed very close to the binding site of Trx. The structure of *Hv*NTR2 reveals a loop, which is predicted to be flexible due to many glycine residues. An alignment of different plant NTRs (Figure 5) shows that this loop is conserved in monocots, but with small variations between isoforms which may lead to their preference for a specific Trx isoform.

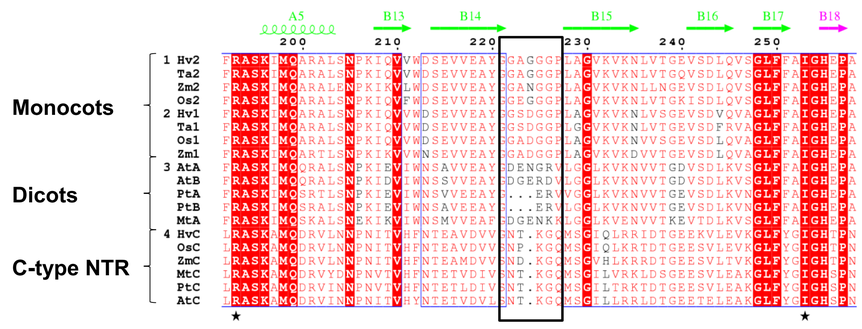

Figure 5 Part of an alignment between different NTRs from plants reveals a glycine-rich loop (boxed) in monocots. Hv = barley, Ta = wheat, Zm = mays, Os = rice, At = *Arabidopsis thaliana,* Pt = poplar and MT = *Medicago truncatula* (Barrel Medic, legume)

Conclusion

The same amino acids that form interdomain contacts (conserved glycine and arginine residues, see Figure 6) in NTR are involved in binding to Trx: Together with an alanine the glycine and arginine provide five hydrogenbonds to Trx. Two loops and these residues form an area which may be able to select and bind the right Trx isoform before a conformational shift. This binding would break the inter-domain hydrogen bonds and thereby facilitate the conformational shift. After a 66°rotation of one domain the bound Trx meets yet another loop which may position it for reduction.

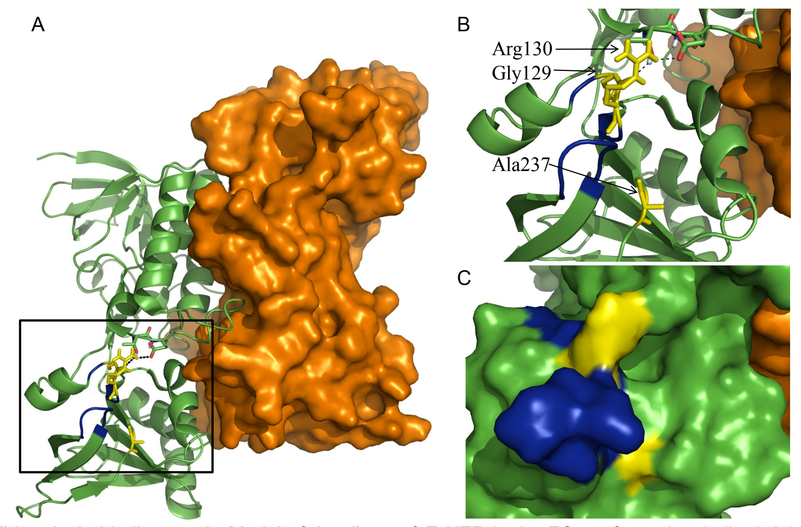

Figure 6 (A) Thioredoxin binding patch. Model of the dimer of *Ec*NTR in the FO conformation (pdb: 1tde), where one subunit is shown in green and the water-accesible surface of the other in orange. Residue Gly129 and Arg130 in the NADPH binding domain form the only hydrogen bonds to the FAD domain in the flavin oxidizing (FO) conformation. These residues together with Ala237 also provide five of the hydrogen bonds formed upon binding with Trx. These residues are shown in yellow and the two loops possibly providing selectivity towards Trx are shown in blue. (B) Close-up of residues. (C) Same as B shown as surface.

Future and ongoing work

We have constructed NTRs that are mutated in the glycine-loop shown in Figure 5 as well as in 2 other loops which may be involved in the recognition of a specific Trx isoform. The activity of these mutants will be tested to examine the role of the loops.

A complex between *Hv*NTR2 and one Trx isoform is in preparation by covalently linking single Cys→Ser mutant of the two protein. The purified complex will be subjected to crystallization trials and biochemical characterization.

References

[1] Hägglund, P., Kirkensgaard, K., Maeda, K., Finnie, C., Henriksen, A. & Svensson, B. (2009) Molecular Recognition in NADPH-Dependent Plant Thioredoxin Systems – Catalytic Mechanisms, Structural Snapshots and Target Identifications. Chapter 15 *in* Oxidative stress and redox regulation in plants. J-P, Jacquot (Ed.). pp. 461-495. Advances in botanical research **52**, Burlington: Academic Press

[2] Kirkensgaard, K.G., Hägglund, P., Finnie, C., Svensson, B. & Henriksen, A. (2009) Structure of *Hordeum vulgare* NADPH-dependent thioredoxin reductase 2. Unwinding the reaction mechanism. *Acta Cryst.* **D65**, 932-941.

[2] Lennon, B. W., Williams, C. H., Jr. & Ludwig, M. L. (2000) Twists in catalysis: alternating conformations of Escherichia coli thioredoxin reductase. *Science* **289**, 1190-1194.

[3] Dai, S., Saarinen, M., Ramaswamy, S., Meyer, Y., Jacquot, J. P. & Eklund, H. (1996) Crystal structure of *Arabidopsis thaliana* NADPH dependent thioredoxin reductase at 2.5 Å resolution. *J. Mol. Biol.* **264**, 1044-1057.

Homology model of a complex between NADPH-dependent thioredoxin reductase (NTR) and thioredoxin from barley

Kirkensgaard, K.G.[a,b,#], *Shahpiri, A.*, *Hägglund, P.*[a], *Finnie, C.*[a], *Henriksen, A.*[b] *and Svensson, B.*[a]

[a] *Enzyme and Protein Chemistry, Department of Systems Biology, Technical University of Denmark, DK-2800 Kgs. Lyngby, Denmark.*
[b] *Carlsberg Laboratory, DK-2500 Valby, Denmark.*
[c] *Department of Agriculture Biotechnology, College of Agriculture, Isfahan University of Technology, Isfahan, Iran.* [#]*E-mail: kgk@bio.dtu.dk*

Thioredoxins and thioredoxin reductase

Thioredoxins (Trx's) are protein disulfide reductases that regulate the intracellular redox environment by catalyzing thiol-disulfide exchange reactions. Furthermore they participate in a large number of cellular processes including DNA synthesis, oxidative stress response and apoptosis. They are present in several isoforms in plants of which the cytosolic Trx h isoforms are reactivated by specific NADPH-dependant thioredoxin reductases (NTRs) (reviewed in [1]). NTRs catalyze the reduction of a redox-active disulfide bond in Trx using NADPH as reductant and FAD as cofactor (see Figure 1).

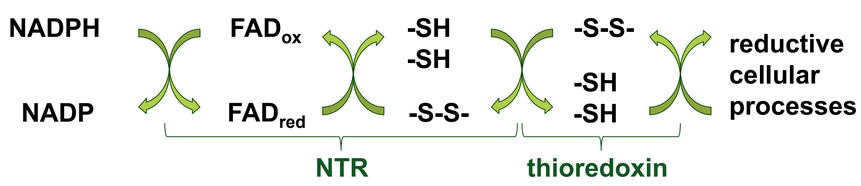

Figure 1 Reaction catalyzed by NADPH-dependent thioredoxin reductase (NTR).

NTR is a homodimer, where each monomer consists of two domains, the FAD and the NADPH binding domains (see Figure 2A). It can shift between two conformations; the flavin oxidizing (FO) or the flavin reducing (FR) conformation. To obtain the latter, one domain has to rotate 66° relative to the other. Only by covalent binding of NTR to Trx can the FR conformation be stabilized for characterization [3]. We have solved the structure of one NTR isoform (*Hv*NTR2) from barley to 2.6Å (Figure 2A) [2].

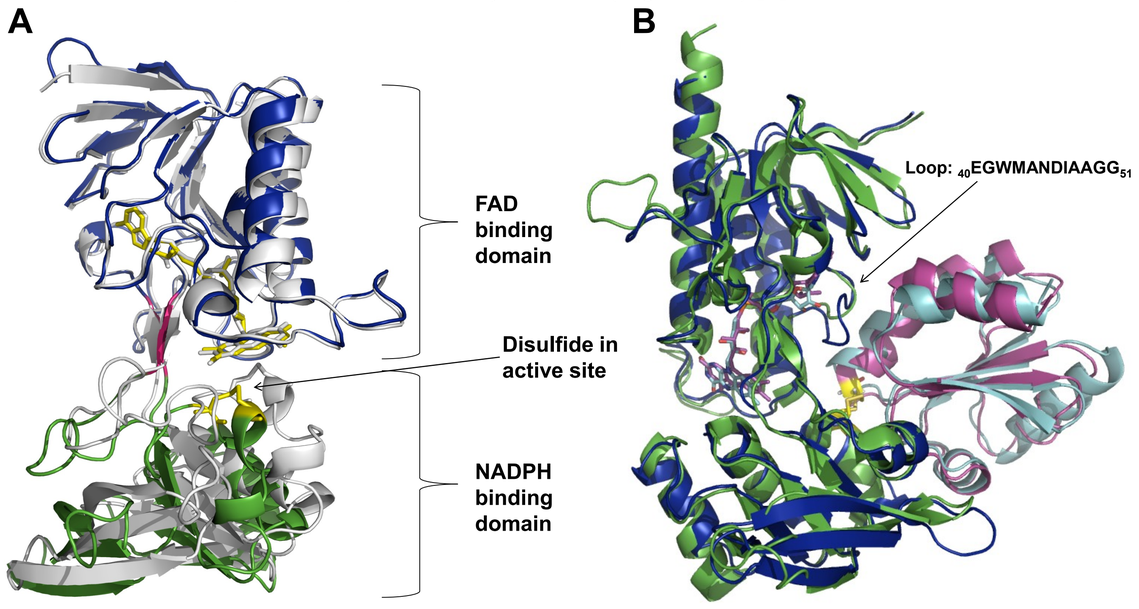

Figure 2 Structure of *Hv*NTR2 from barley. A) FAD domain (blue) of the crystal structure of *Hv*NTR2 (pdb accession 2whd, [2]) superposed to *At*NTR-*B* from *Arabidopsis thaliana (*white, pdb accession 1vdc [4]). **B**) A model of a complex between *Hv*NTR2 (dark blue) in the FR conformation bound covalently to *Hv*TrxH2 (cyan). The model is superposed with the crystal structure of *Ec*NTR (green) bound to *Ec*Trx (magenta) (pdb accession 1f6m, [3]).

Complex model

A complex of *Hv*NTR2 bound to *Hv*trxH2 was made (Figure 2B) by superposing the two separate domains with the corresponding domains of the *Ec*NTR-*Ec*trx complex (pdb 1f6m [3]) using the program *Coot*. *Hv*trxH2 from pdb accession 2iwt [5] was used. Homology modelling, energy minimization and model evaluation was performed using the program *MOE,* and the possible contacts were determined using *Ligplot* (Figure 3).

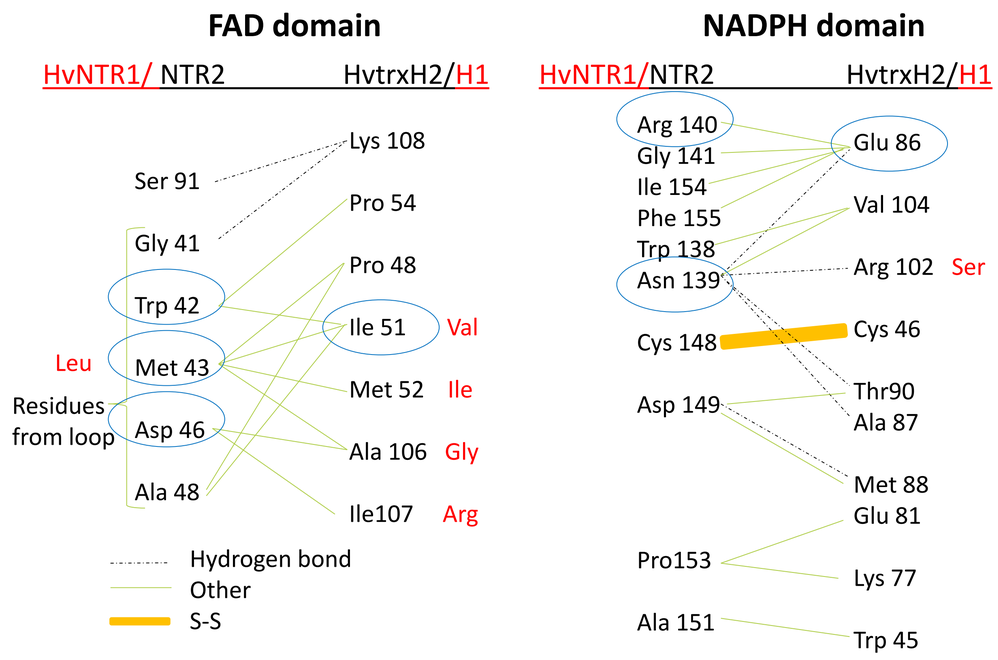

Figure 3: Possible interactions found using *Ligplot* on the model of a complex between *Hv*NTR2 and *Hv*trxH2. In red is shown the corresponding residue in *Hv*NTR1 or *Hv*trxH1 in the case they are not the same. Circled residues have been examined by kinetics on mutants.

For the FAD domain all but one of the residues involved in binding Trx are located in a loop with the sequence $_{40}$EGWMANDIAAGG$_{51}$ (interacting residues are underlined). This loop is semi-conserved in some bacteria like *Clamydia* as well as eukaryotic LMW NTRs from e.g. plants, yeast, amoebas and fungi. The corresponding loop is five residues shorter in *Ec*NTR and has a totally different sequence. Therefore, the only available crystal structure of a complex does not provide any information regarding how NTRs from these organisms bind Trx to the FAD domain. The model presented here suggests how this loop binds Trx mainly by hydrophobic contacts (see Figure 4A+C). W42, M43 and D46 protrude from the surface; M43 is buried in a groove on the surface of Trx, whereas W42 and D46 are bound to each side.

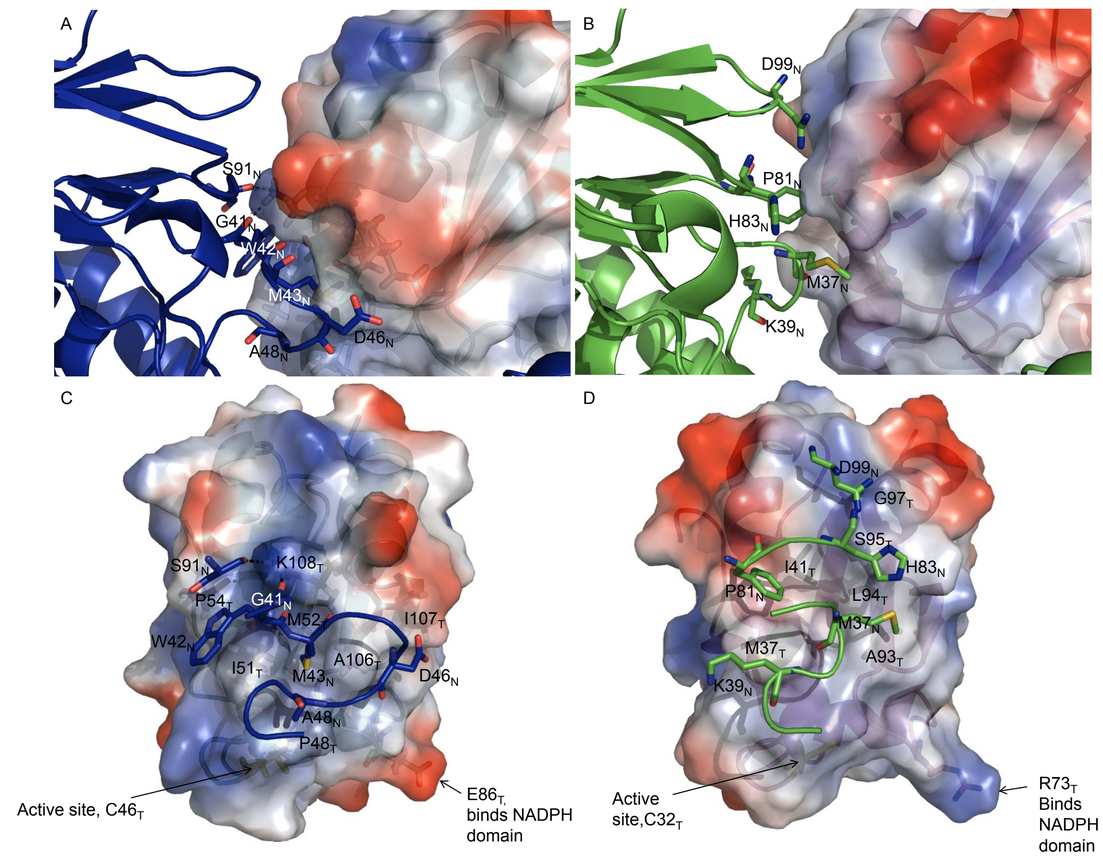

Figure 4: Comparison of the binding to the FAD domain in complexes of **A+C**) *Hv*NTR2(dark blue):*Hv*TrxH2 and **B+D**) *Ec*NTR(green):*Ec*TrxA (pdb 1f6m, [3]). The surfaces of the Thioredoxins are shown with charge distribution.

Residues involved in binding of Trx

Based on the model a number of mutants were constructed and examined using enzyme kinetics (Figure 5). It is seen that *Ec*TrxA is a poor substrate for *Hv*NTR2 compared to *Hv*TrxH2 and Trx from *Arabidopsis thaliana*, *At*TrxH3. However, when scaling the data it seems that the loop binds *Hv*NTR2 and *Ec*TrxA in a similar manner: They depend mainly on W42 and M43, and deletion of part of the loop (Δ42-47) leads to an almost total loss of activity. Binding of *At*TrxH3 is not very dependent on W42, and deletion of the loop still gives 5% activity. This may be due to a stronger binding elsewhere.

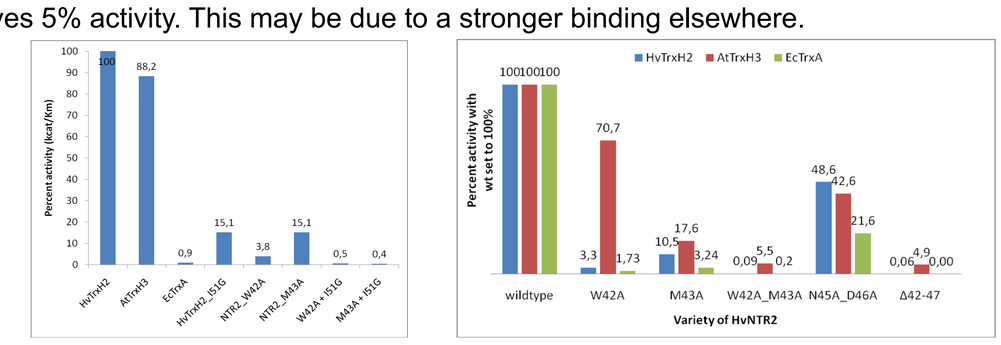

Figure 5: Relative values for k_{cat}/K_m. Left: The activity of *Hv*NTR2/*Hv*TrxH2 was set to 100%. Right: The values for the activity of *Hv*NTR2wt with the three different substrates *Hv*TrxH2, *At*TrxH3 and *Ec*TrxA were all scaled to 100%. The activity of different mutants of *Hv*NTR2 are shown relative to these.

Conclusions

- We have made a model of *Hv*NTR2 from barley bound to *Hv*TrxH2
- The model predicts that mainly a large loop is responsible for binding one of the domains (the FAD binding domain).
- This loop is found in eukaryotic LMW NTRs, but not in the only available crystal structure of a complex (from *E.coli*). Therefore, the model provides new insight to how these NTRs bind Trx.
- The residues Trp42 and Met43 from the loop are essential in binding *Hv*Trx2. Ile51 from Trx is bound between these.
- Even though NTR from *Arabidopsis thaliana* has the same sequence of the loop it apparently binds in a different manner.

References

[1] Hägglund, P., Kirkensgaard, K., Maeda, K., Finnie, C., Henriksen, A. & Svensson, B. (2009) Molecular Recognition in NADPH-Dependent Plant Thioredoxin Systems – Catalytic Mechanisms, Structural Snapshots and Target Identifications. Chapter 15 *in* Oxidative stress and redox regulation in plants. J-P, Jacquot (Ed.). pp. 461-495. Advances in botanical research **52**, Burlington: Academic Press

[2] Kirkensgaard, K.G., Hägglund, P., Finnie, C., Svensson, B. & Henriksen, A. (2009) Structure of *Hordeum vulgare* NADPH-dependent thioredoxin reductase 2. Unwinding the reaction mechanism. *Acta Cryst.* **D65**, 932-941.

[3] Lennon, B. W., Williams, C. H., Jr. & Ludwig, M. L. (2000) Twists in catalysis: alternating conformations of Escherichia coli thioredoxin reductase. *Science* **289**, 1190-1194.

[4] Dai, S., Saarinen, M., Ramaswamy, S., Meyer, Y., Jacquot, J. P. & Eklund, H. (1996) Crystal structure of *Arabidopsis thaliana* NADPH dependent thioredoxin reductase at 2.5 Å resolution. *J. Mol. Biol.* **264**, 1044-1057.

[5] Maeda, K., Hagglund, P., Finnie, C., Svensson, B. & Henriksen, A (20006) Structural basis for target protein recognition by the protein disulfide reductase thioredoxin. *Structure* **14**, 1701-1710.